Erzbildende Prozesse in hydrothermalen Ganglagerstätten, Schwarzwald, SW-Deutschland

Dissertation

der Mathematisch-Naturwissenschaftlichen Fakultät
der Eberhard Karls Universität Tübingen
zur Erlangung des Grades eines
Doktors der Naturwissenschaften
(Dr. rer. nat.)

vorgelegt von
Dipl. Min. Benjamin Florian Walter
aus Baden-Baden

Tübingen
2016

Gedruckt mit Genehmigung der Mathematisch-Naturwissenschaftlichen Fakultät der Eberhard Karls Universität Tübingen.

Tag der mündlichen Qualifikation:	26.04.2016
Dekan:	Prof. Dr. Wolfgang Rosenstiel
1. Berichterstatter:	Prof. Dr. Gregor Markl
2. Berichterstatter:	PD. Dr. Thomas Wenzel

Danksagung

Ich möchte mich zu Beginn bei Prof. Dr. Gregor Markl für die Vergabe und Betreuung der Dissertation herzlich bedanken. Für Fragen und Probleme jeglicher Art hatte Prof. Dr. Gregor Markl stets ein offenes Ohr. Ohne seine ständige konstruktive Kritik wäre diese Arbeit nie zustande gekommen. Auch für die zeitnahe Bearbeitung meiner Manuskripte bin ich ihm zu besonderem Dank verpflichtet. Das ist nicht selbstverständlich und ich weiß das sehr zu schätzen.

Bei PD. Dr. Thomas Wenzel möchte ich mich herzlich für die Zweitbetreuung bedanken. PD. Dr. Thomas Wenzel hat mit seinem analytischen Feingespür signifikant zum Gelingen dieser Arbeit beigetragen. Ebenfalls ganz besonders möchte ich PD. Dr. Michael Marks und Dr. Udo Neumann für die konstruktive Kritik, viele Diskussionen, Ratschläge und Unterstützung danken. Dank dieser konnten viele Aspekte dieser Arbeit erst herausgearbeitet werden. Dr. Horst Hann gilt ebenfalls ein ganz besonderer Dank für viele Hinweise, Ratschläge, Diskussionen über die regionale Geologie und Kontakte zum LGRB. Bei Prof. Dr. Paul Bons möchte ich mich ganz herzlich für viele Diskussionen über die hydraulischen Eigenschaften der Fluide bedanken. Prof. Dr. Adrian Immenhauser gilt mein Dank für die hervorragende Zusammenarbeit im Bereich der Mg-Isotopen und Oilfieldbrines. Bei Prof. Dr. Christoph Heinrich und Dr. Markus Wälle möchte ich mich für die Hilfe und Diskussion während der LA-ICPMS Analytik an Fluideinschlüssen bedanken. Für unerlässliche Hinweise zur regionalen Geologie möchte ich mich herzlich bei Dr. Edgar Nitsch vom LGRB bedanken.

Für die Durchführung und Hilfe der Analytik dieser Arbeit bedanke ich mich bei PD Dr. Thomas Wenzel, PD. Dr. Michael Marks, Dr. Markus Wälle, Prof. Dr. Adrian Immenhauser, Mathias Burisch, Dr. Melanie Keuper, Dr. Heinrich Taubald, Bernd Steinhilber und Gabi Stoschek. Indra Gill-Kopp, Simone Schafflick und Peer Jeiseke danke ich für die Probenpräparation.

Auch meinen Kollegen Maguerita Duchoslav, Maximilian Keim, Stefan Kreißl, Rainer Babiel, Johannes Giebel, Petya Atamasova und ganz besonders Mathias Burisch möchte ich mich für die vielen Diskussionen und die gute Arbeitsatmosphäre bedanken. Den Koautoren meiner Publikationen Prof. Dr. Gregor Markl, PD. Dr. Michael Marks, Mathias Burisch, Prof. Dr. Adrian Immenhauser, Prof. Dr. Paul Bons, Dr. Tobias Fußwinkel, Dr. Anna Geske, Prof. Dr. Christoph Heinrich und Dr. Markus Wälle bin ich für die tolle Zusammenarbeit dankbar. Ich möchte auch meiner Diplomarbeitskollegin Olga Apukthina ganz besonders danken. Zusammen haben wir die Grundlagen für diese Dissertation gelegt. Danke dafür!

Mein ganz besonderer Dank gilt meinen Eltern Gerhard Walter und Hildegart Walter, die mir das Studium ermöglichten. Ebenso gilt mein Dank meiner Tante Ingrid Walter, die mich immer unterstützt hat. Besonders möchte ich mich bei Mathias Burisch, Dr. Horst Hann, Dr. Melanie Keuper, Petya Atamasova, Maximilian Keim und meiner Freundin Fabienne Fischer für das Korrekturlesen dieser Arbeit bedanken. Weiterhin gilt mein besonderer Dank Fabienne Fischer und Julia Oser für Ihre unendliche Geduld und unermüdliche Motivation vor allem in den letzten Monaten. Danke!

Kurzzusammenfassung

Der Schwarzwald in SW-Deutschland ist ein exhumierter Grundgebirgsblock, in dem die hydrothermale Geschichte eines Bergbaugebietes über geologisch lange Zeiträume studiert werden kann. Postmagmatische bis tief hydrothermale Mineralisationen decken einen Zeitraum von über 320 Ma ab und variieren mineralogisch mit dem Bildungsalter. Jedoch werden viele Prozesse der hydrothermalen Gangbildung bis heute nicht hinreichend verstanden. Als Ziel dieser Studie soll ein detaillierteres Bild vom Zusammenspiel von Metallquellen, Erzfällungsmechanismen und der Gangmineralogie entwickelt werden. Die ersten bekannten Mineralisationen sind karbonischen Alters und liegen als Quarz-Turmalin-Gänge vor, welche an karbonische Intrusionen gebunden sind. Sie wurden aus niedrigsalinaren, volatilreichen und hochtemperierten Fluiden ausgefällt. Im Perm führten abkühlende, spät-metamorphe, niedrigsalinare und ebenfalls hochtemperierte Fluide zur Fällung von Quarz-Gängen. Ab der Trias-Jura-Grenze können Quarz-Hämatit-Gänge beobachtet werden, welche alternierende primäre Abfolgen von niedrig- und hochsalinaren, mitteltemperierten Fluiden beinhalten. Im Jura und in der Kreide treten ausschließlich hochsalinare, niedrig- bis mitteltemperierte Fluide in Verbindung mit einer starken Pb-Zn-Cu-Ag-, U-Bi-Co-Ni-As- oder Fe-Mn-Vererzung der Fluorit-Baryt-Quarz-(Karbonat)-Gänge auf, die mit der Öffnung des Nordatlantiks assoziiert sind. An die Öffnung des Oberrheingrabens sind die Gänge des post-kretazischen Zeitraumes gebunden, deren Fluide und Mineralisationen eine große Variabilität in Fluidchemie, Bildungstemperatur und Vererzung aufzeigen.

Für das erstmalige Auftreten der hochsalinaren Lösungen an der Trias-Jura-Grenze wird eine Evaporationsrestlauge aus den Triassischen Muschelkalkhaliten vorgeschlagen, was niedrige Ca/(Na+Ca) -Molverhältnisse und niedrige Cl/Br -Massenverhältnisse im Fluid anzeigen. In der Obertrias führen eindringende Formationswässer in die Muschelkalkevaporite zur Bildung einer hochsalinaren Salzauflösungslauge, die ebenso niedrige Ca/(Na+Ca) -Molverhältnisse aber hohe Cl/Br -Massenverhältnisse im Fluid hat. Diese wird ebenfalls, wie auch die hochsalinare Restlauge, durch Austrocknungs- beziehungsweise Vertonungsprozesse ins kristalline Grundgebirge gezogen. Durch die Fernwirkung der Nordatlantiköffnung im Jura etablierten sich tiefreichende Störungsstrukturen, in welchen sich die modifizierten Evaporitlaugen mischen und zur Bildung der weiträumigen Vererzung führen. Die Fluidchemie variiert nicht nur mit der stratigraphischen Tiefe, sondern auch mit der Paläotopographie des Muschelkalkes. In topographischen Senken wurden Halitformationen gefällt, während auf den Schwellen in erster Linie Sulfate ausgefällt wurden. Basierend auf unterschiedlichen Ca/(Na+Ca) -Molverhältnissen und Cl/Br -Massenverhältnissen im Fluid können paläotopographische Begebenheiten des erodierten Deckgebirges in heute exhumierten Bereichen rekonstruiert werden. Qualitativ werden diese Mischungsverhältnisse über Metallvariationen im Fluid angezeigt. Weitere Belege für eine binäre Mischung zwischen einer silikatischen Quelle (Grundgebirge) und einer karbonatischen Quelle (Muschelkalk) zeigen auch die $\delta^{26}Mg_{Karbonat}$ -Isotopien hydrothermaler Gangartkarbonate an.

Durch den späteren Grabenbruch im post-kretazischen Zeitraum wurden eine Vielzahl unterschiedlicher Aquifere kurzgeschlossen, was zu einer Multi-Komponenten-Fluidmischung und damit zu einer großen Variabilität in der Fluidchemie und in den Vererzungen führte. Fluidmischungsmodellierungen legen den Schluss nahe, dass die im post-kretazischen Zeitraum dominierenden Baryt-Gänge aus einer Vielzahl verschiedener Aquifer-Endgliedskombinationen gefällt werden konnten. In den Resultaten der Modellierungen sind die gemischten Fluide stets an Sulfiden stark untersättigt, was zu der Interpretation führt, dass für eine kogenetische Sulfidfällung im Gang ein Reduktionsmittel wie CH_4 oder H_2S benötigt wird.

Untersuchungen der Fluidchemie mit dem Rb/Cs -Wegsamkeitsindikator (Tonmineral/Fluid Wechselwirkungen) legen nahe, dass die stark vererzten Gangartgenerationen in hydrothermalen Adern mit einer Neuetablierung von Wegsamkeiten im Grundgebirge einhergehen. Entlang dieser neuen Wegsamkeiten werden Feldspäte und Glimmer vertont, wodurch Metalle in das Fluid gebracht werden.

Weitere wichtige Fluide sind hochsalinare Ölfeldlaugen, welche möglicherweise als Reduktionsmittel für die Sulfidfällung in Erzgängen in Frage kommen. Sie zeigen, abhängig vom Ölgehalt, die Tendenz, Wegsamkeiten offen zu halten. Mit zunehmendem Ölgehalt im Fluid ist eine Trennschicht an der Fluid-Gesteins-Grenzschicht wahrscheinlich, welche das Zement- und/oder Tonmineral-Wachstum hemmt.

Abstract

The Schwarzwald in Southwest Germany is an exhumed basement block, where the hydrothermal history of a mining district can be studied over geological long time. Post-magmatic up to low-temperature hydrothermal veins were formed over a period of 320 Ma and show systematic mineralogical variations with formation age. However, numerous processes are still not addressed very well. The goal of this study is to develop a detailed contribution concerning the provenance of metals, ore forming processes and vein mineralogy.

The oldest reported mineralization, are quartz-tourmaline veins formed in Carboniferous and precipitated from a low salinity, volatile-rich and high-temperature fluid. During the Permian quartz-veins were formed from late metamorphic, low salinity, high -temperature fluids. At the Triassic-Jurassic boundary the first occurrence of quartz-hematite-veins can be recognized, showing alternating primary sequences of high salinity and low salinity fluids. In the Jurassic-Cretaceous period high salinity and low to intermediate temperature fluids predominate and occur in fluorite-barite-quartz-(carbonate)-veins in conjunction with large scale Pb-Zn-Cu-Ag-, U-Bi-Co-Ni-As- or Fe-Mn ores. The veins of the Jurassic-Cretaceous period are related to the opening of the North-Atlantic. In contrast, the veins of the post-Cretaceous period are formed during opening of the Upper Rhinegrabenrift. The fluids and the veins of this period show large variations in fluid chemistry, formation temperatures and mineralization.

For the first occurrence of the high salinity brines at the Triassic-Jurassic boundary a bittern brine, derived from the Muschelkalk halite formation, is suggested, which is supported by low Ca/(Na+Ca) mole ratios and low Cl/Br mass ratios. In Upper Triassic the infiltration of formation fluids into the Muschelkalk halite layers leads to the formation of a high salinity halite dissolution brine with also low Ca/(Na+Ca) mole ratios but high Cl/Br mass ratios. Both brines were drawn into the crystalline basement by a hydraulic head triggered by desiccation processes. The opening of the North Atlantic in Jurassic leads to the establishment of deep creeping, large faults as a remote effect, where the modified evaporite derived brines were mixed and the large-scale ore mineralizations were formed. The fluid chemistry shows variations with stratigraphic depth and paleotopography. In depressions halite was precipitated in contrast to topographic heights where dominantly sulphates were formed. Based on variations in Ca/(Na+Ca) mole ratios and Cl/Br mass ratios in the fluid, it is possible to reconstruct paleo-topographic features of today eroded sedimentary cover facies. In contrast, the metals in the fluid show variations with stratigraphic depth and therefore have the capacity for a qualitative mixing ratio tracer. Further evidence for a binary mixing between a silicate source (crystalline basement) and a carbonate source (Muschelkalk) is given by $\delta^{26}Mg_{carb}$ isotopes of hydrothermal gangue carbonates.

In post-Cretaceous time, the breakup of the Upper Rhinegraben leads to a shortcut of many different aquifers and to a multi-component fluid mixing. Hence the post-Cretaceous veins show a large variability in fluid chemistry and mineralogy. Fluid mixing modelling give evidence, that the dominantly barite veins in the post-Cretaceous period can be precipitated from many different aquifer-endmember combinations. In these models, the mixed fluids are strongly undersaturated with respect to sulphides. Hence, for cogenetic sulphide precipitation in e.g. barite veins, a reduction phase like CH_4 or H_2S seems to be required.

Investigations of the fluid chemistry with respect to pathway information leads to the interpretation that ore-rich gangue generations in hydrothermal veins are related to the breakup of new pathways in the crystalline basement. In these new established pathways mica and feldspars get altered and metals are released to the fluid. Oilfieldbrines might be important as reduction phase for sulphide precipitation in hydrothermal veins. They show, depending on their oil content, the tendency to keep pathways open. With increasing oil content in the fluid, presumably a separating layer occurs at the water-rock interface, that inhibits cement and clay mineral growth.

Inhaltsverzeichnis

1. Einleitung

1a. Allgemeine Einleitung

Hydrothermale Fluide aus dem Grundgebirge werden von vielen Autoren (Russell et al., 1981; Gleeson et al., 2001; Muchez et al., 2005; Derome et al. 2007; Heijlen et al., 2003; 2008; Leach et al., 2010; Wilkinson, 2010; Boiron et al., 2010; Pfaff et al. 2010, Aquilina et al., 2011; Fußwinkel et al., 2013) als die wichtigste Metallquelle für hydrothermale Erzlagerstätten angesehen, zu denen in erster Linie MVT-Pb-Zn-Lagerstätten (Heijlen et al., 2001; 2003; Pfaff et al., 2010; Aquilina et al., 2011), hydrothermale Irish-type Pb-Zn-Ganglagerstätten (Russell et al., 1981; Wilkinson, 2010; Fußwinkel et al., 2013), an Diskordanzen gebundene U-Vererzungen (Derome et al., 2007; Boiron et al., 2010) und in metamorphen Settings anzutreffende Cu-Vererzungen (Muchez et al., 2005; Heijlen et al., 2008) zu zählen sind. In den letzten Jahren konnten durch Fluideinschluss-Studien in Verbindung mit stabilen sowie radiogenen Isotopensystemen (e.g. Wilkinson et al., 2010; Stoffell et al., 2008) an vielen Lokalitäten weltweit das kristalline Grundgebirge als dominierendes Fluidreservoir der metallreichen Fluide herausgearbeitet werden (e.g. Dixon et al., 1990; Goldhaber et al., 1995). Den unterschiedlichen kontinentalen Grundgebirgsfluiden ist eine sehr hohe Salinität und mittel bis relativ hohe Temperatur gemein (Frape & Fritz, 1987; Edmunds & Savage, 1991; Pauwels et al., 1993, Emmermann et al., 1995; Fritz, 1997; Stober & Bucher, 1999; Yardley, 2005; Bucher & Stober 2010).

Der Transport und die Mobilität von Metallen in hydrothermalen Lösungen hängen in erster Linie von den Konzentrationen der Liganden, der Temperatur, dem pH-Wert der Lösung und von deren Redox-Zustand ab (e.g. Gallup 1998; Burisch et al., eingereicht). Daher werden auch heiße, reduziertere, hochsalinare, hydrothermale Grundgebirgsfluide als wichtige Metallquelle gesehen. Manche dieser Fluide können hohe Konzentrationen von hunderten bis tausenden ppm an Pb, Zn und anderen Buntmetallen führen. Sie werden durch seismisches Pumpen oder die Entwässerung tiefer Krustenstockwerke mobilisiert (Sibson et al. 1995, Staude et al. 2009, Bons et al., 2014) und in seichtere Krustenstockwerke transportiert (e.g. Yardley, 2005)

Verschiedene Prozesse, wie zum Beispiel Fluidabkühlung, Phasentrennung durch Aufkochen, Fluidmischung und Fluid-Gesteins-Wechselwirkung, können zur Ausfällung einer Phase aus einer hydrothermalen Lösung führen (Barnes 1997, Seward & Barnes 1997).

Für die Bildung von MVT- und hydrothermalen Ganglagerstätten wird als wichtigster Prozess für die Sulfidfällung die Fluidmischung eines heißen, hochsalinaren, reduzierten, hochmineralisierten Grundgebirgsfluides mit einem stagnierenden, oxidierten, sulfatreichen oder schwefelreichen Formationswasser angesehen (Wilkinson et al., 2005; Pfaff et al., 2010; Leach et al., 2010). Darauf deuten Stabile Isotopensysteme (e.g. Goldhaber et al., 1995; Wilkinson, 2010; Staude et al., 2011; Ströbele et al. 2012), Mikrothermometrie, LA-ICPMS- und Crush-Leach Studien (Cl/Br-Systematiken) (Heijlen et al., 2001, Schwinn et al. 2006; Stoffell et al., 2008; Boiron et al., 2010; Wilkinson, 2010; Richard et al., 2011; Fußwinkel et

al., 2013) sowie Paläohydrogeologische Modellierungen hin (Raffensperger & Garven, 1995; Garven et al., 1999; Staude et al., 2011; Pfaff et al., 2010).

Jedoch erklären die bisherigen Fluidmigrations- und Erzfällungsmodelle nur Teilaspekte des komplexen Zusammenwirkens von regionaler Geologie und Tektonik, Hydraulik, Quellaquiferen, Wegsamkeiten, Metalltransportmechanismen, Fluidchemie, Erzfällungsprozessen und Mineralisationstypen. Daher wurde im Zuge dieser Arbeit in Form mehrerer Einzelstudien auf folgende Fragestellungen besonders eingegangen:

1. Ist es möglich Gangbildungen aus Fluidmischungen chemisch sowie hydraulisch zu erklären und einen entsprechenden Mechanismus für Fluid-Versenkung, Fluid-Aufstieg und Fluid-Mischung zu definieren? (Studie 1)
2. Kann eine allgemeingültige Systematik der hydrothermalen Mineralisationen unter Berücksichtigung aller chemischen, strukturellen und hydraulischen Vorkenntnisse sowie deren Variationen mit der Zeit eingeführt werden? (Studie 2)
3. Können verschiedene erzbildende Quellreservoire entschlüsselt und verstanden werden? (Studie 2 und 3)
4. Was für Informationen werden in hydrothermalen Erzgängen archiviert und welche Aufschlüsse über heute erodierte Deckgebirgsbereiche werden übermittelt? (Studie 3)
5. Welche Aquifere und Formen der Fluidmischung spielen bei der Erzbildung im gesamten Schwarzwald nach dem Grabenbruch die entscheidende Rolle? (Studie 4)
6. Sind in archivierten Fluideinschlüssen hydrothermaler Erzgänge Informationen über Fluidwegsamkeiten in der Wurzelzone hydrothermaler Mineralisationen vorhanden? (Studie 5)
7. Wie wichtig sind die Definition und das Studium neuer Isotopensysteme und wie aussagekräftig ist das Mg-Isotopensystem für das Verständnis erzbildender Prozesse im hydrothermalen Mileau? (Studie 6)
8. Welchen Einfluss haben Ölfeldlaugen auf die Gesteins-Wasser-Wechselwirkungen entlang von Wegsamkeiten und bei der Fällung von Mineralisationen? (Studie 7)

1b. Geologische Entwicklung des Schwarzwaldes seit der Variszischen Gebirgsbildung

Der Schwarzwald besteht aus exhumiertem, variszischem Grundgebirge (Kalt et al. 2000) mit einer sedimentären Deckgebirgsauflage. Das Grundgebirge wird durch die Zone von Badenweiler-Lenzkirch unterteilt, welche als Sutur den Südschwarzwälder Gneiskomplex vom Zentralschwarzwälder Gneiskomplex trennt und ein Teil des Moldanubikums bildet. Die Subduktion war hierbei nach Norden gerichtet (Hann et al., 2003). Im Nordschwarzwald trennt die, nach Süden abtauchende, Zone von Baden-Baden-Gaggenau das Moldanubikum im Süden vom Saxothuringikum im Norden (Geyer and Gwinner, 2011). Die Paragneise des Grundgebirges sind lokal mit Orthogneisen und Amphiboliten durchsetzt. Die einzelnen geologischen Einheiten des Grundgebirges wurden im Karbon durch Kollisionsvorgänge im

Rahmen der variszischen Orogenese akkretiert, deformiert, metamorphosiert und häufig migmatisiert (Geyer & Gwinner, 2011 und beinhalteter Referenzen).

Die Gneise wurden von Graniten intrudiert, die heute ca. 50% des aufgeschlossenen Schwarzwaldes ausmachen. Die großen Granitplutone sind überwiegend S-Typ-Granite, welche postkollisional, im Zuge des postorogenen Kollapses der Varisziden (335 bis 315 Ma), aufstiegen und platznahmen (Todt, 1976; Altherr et al., 2000; Hann et al., 2003).

Nach der Einebnung der Varisziden kam es zur Ablagerung und Bildung erster Sedimente (Arkosen, Kohleflöze und Caliche) und rhyolitischer Vulkanite im Perm, welche das verbliebene Relief verfüllten (Schaltegger, 2000; Nitsch & Zedler, 2009; Geyer & Gwinner 2011). Die Rotliegendsedimente (redbeds) sind mit großen Mächtigkeiten bis 400 m nur in wenigen Trögen relativ geringer Ausdehnung (wenige km) zu finden. Sie bestehen aus bevorzugt unreifen, klastischen Sedimenten (Nitsch & Zedler, 2009; Geyer & Gwinner, 2011). Typischerweise beginnt die Sedimentation direkt auf der Erosionsfläche des Kristallins mit Gesteinen der unteren Trias.

In der unteren Trias fand die Schüttung der terrestrischen Buntsandsteinformation statt, welche heute aus Sandsteinen, Konglomeraten und Tonsteinen besteht. Diese Schüttung wird heute als postorogene, variszische Molasse angesehen (Ziegler, 1990). Die Mächtigkeiten betragen nach Geyer & Gwinner (2011) im Nordschwarzwald 400 Meter, während im Südschwarzwald lediglich eine Mächtigkeit von unter 50 Meter ermittelt wurde. Ab der mittleren Trias (Muschelkalk) wurden im flachen, epikontinentalen Muschelkalkmeer zyklisch Kalksteine, Tonsteine und Evaporite mit homogenen Mächtigkeiten zwischen 160 m und 220 m gebildet (Rupf & Nitsch 2008). In der Mittleren Trias wurden in topographischen Senken bis zu 100 m mächtige Halitformationen abgelagert (Rupf & Nitsch 2008). Die obere Trias (Keuper) war geprägt durch die Schüttung bevorzugt klastischer Sedimente und der Fällung von Evaporitserien (vor allem Gips). Die Mächtigkeiten nehmen von ca. 300 m im Nordschwarzwald bis zu 100 m im Südschwarzwald ab (Rupf & Nitsch 2008). Im Jura kam es zur Bildung einer lokal bis 1000 m mächtigen Ablagerung von klastischen Sedimenten und Karbonaten auf dem flachen Kontinentalschelf des Thethysozeanes (Geyer & Gwinner, 2011). Diese Sedimentationsvorgänge in Trias und Jura führten zu einer maximalen Deckgebirgsauflage von 1200 m Mächtigkeit im Südschwarzwald und 1900 m im Nordschwarzwald (Rupf & Nitsch 2008). In der Kreidezeit unterlag das Gebiet der Hebung, was sich in einer stratigraphischen Lücke und dem Fehlen kreidezeitlicher Sedimente in SW-Deutschland wiederspiegelt.

Durch das überregionale Stressfeld der alpinen Orogenese wurden ab dem Paläozän (Geyer & Gwinner, 2011) Riftingprozesse in Südwestdeutschland induziert, die zur Bildung des Oberrheingrabens im Paläogen führten (Schwarz & Henk 2005). Im Zuge der Grabenbildung wurden während des gesamten Paläogens auf der topographischen Breite des Südschwarzwaldes bis zu 5000 m (Rupf & Nitsch 2008; Geyer & Gwinner, 2011) klastische und chemische Sedimente (Gips, Anhydrit, Dolomit, Salze) im zeitweise marin gefluteten Graben abgelagert und ausgefällt (Geyer & Gwinner, 2011 und beinhalteter Referenzen). Mit

der Absenkung des Grabens begann die asymmetrische Hebung der Grabenschultern. Diese führte zu einer Exhumierung bis in die Buntsandsteinformation im Nordschwarzwald. Im Südschwarzwald ist das Deckgebirge komplett erodiert und das Grundgebirge bis ca. 2000 m Tiefe unter der Deckgebirgsdiskordanz exhumiert (Rupf & Nitsch 2008, Walter et al., 2015). Im Mittel- und Nordschwarzwald sind Buntsandsteinreste auf allen höheren Bergen noch erhalten.

1c. Hydrothermale Mineralisationen

Im Schwarzwald wurden über die letzten 320 Ma hinweg bis in die heutige Zeit kontinuierlich hydrothermale Mineralisationen gebildet. Basierend auf einer intensiven Bearbeitung der Schwarzwälder Vererzungen in den letzten zehn Jahren mit Mikrothermometrie (Baatartsogt et al., 2006; Staude et al., 2009, Fußwinkel et al., 2013; Walter et al., 2015), Spurenelementsystematiken in Erzphasen (Pfaff et al., 2011; Staude et al., 2012a), stabilen und radiogenen Isotopensystemen (Staude et al., 2010, 2012b, Ströbele et al., 2012; Walter et al., 2015), Seltene Erden Elemente (SEE)-Verteilung in Fluoriten (Schwinn & Markl, 2005), geochemischen Studien an modernen Thermal- und Mineralwässern, Laugungsexperimenten an Grundgebirgs- und Deckgebirgsgesteinen (Burisch et al., eingereicht), modernen hydraulischen Modellen und Detailstudien der regionalen Geologie konnten tiefgreifende Prozesse der hydrothermalen Zirkulation und Erzfällung dechiffriert werden (Stober and Bucher, 1999a, 1999b, 2004, 2005a, 2005b, 2007, 2014, 2015a, 2015b; Stober et al., 1999, He et al., 1999, Bucher et al., 1999, 2009; Bucher and Stober, 2000, 2002, 2010, Ludwig et al., 2011, Stober 2011, 2013; Göb et al., 2013).

Basierend auf den Arbeiten von Behr and Gerler (1987), Behr et al., (1987), Staude et al., (2009), Pfaff et al. (2009, 2010) und Walter et al. (2015) konnte eine neue Klassifikation in fünf Hauptphasen der hydrothermalen Gangbildung etabliert werden:

(i) karbonische Quarz-Turmalin-Gänge mit geringen W- und Sn-Vererzungen
(ii) permische Quarz-Gänge mit Sb- und Au-Vererzungen
(iii) unvererzte Quarz-Hämatit-Gänge der Trias-Jura-Grenze
(iv) jurassisch-kretazische Fluorit-Baryt-Quarz-(Karbonat)-Gänge mit Pb-Zn-Cu-Ag-, U-Bi-Co-Ni-As- oder Fe-Mn-Vererzung
(v) post-kretazische Baryt ± Quarz ± Karbonat ± Fluorit Gänge mit Pb ± Zn ± Ag ± Cu ± Ni ± Co ± Bi ± U ± As Erzen

Die karbonischen Quarz-Turmalin-Gänge (i) mit geringen Wolframit-, Scheelit- und/oder Kassiteritvererzungen (Marks et al., 2013) treten ausschließlich im Gneisdach variszischer Granitintrusionen auf. Die Gänge haben ein NW-SO-Streichen, was typisch für die karbonische/permische Hauptstressrichtung ist (Geyer & Gwinner 2011, und beinhalteter Referenzen). Sie gehören als post-magmatisch-pneumatolytische beziehungsweise hoch-hydrothermale Bildungen der variszischen magmatischen Aktivitätsphase an. Sauerstoffisotopien an Quarz und Turmalin deuten auf Bildungstemperaturen bis 550°C hin

(Marks et al., 2013). Mikrothermometrisch finden sich vorwiegend niedrigsalinare, volatilreiche, hochtemperierte Fluide mit niedrigen Cl/Br-Verhältnissen (siehe Anhang 2).

Die permischen Quarz-Gänge (ii) führen gelegentlich äußerst geringe Sb±Au-Vererzungen. Die Gänge wurden aus einem niedrigsalinaren, hoch temperierten, spät-metamorphen Grundgebirgsfluid durch Abkühlung ausgefällt. Es handelt sich hierbei vermutlich um Fluide der abkühlenden variszischen Orogenese (Staude et al., 2009; Wagner & Cook, 2000; Walter et al., 2015) mit ebenfalls niedrigen Cl/Br-Massenverhältnissen (Siehe Anhang 2).

Die Quarz-Hämatit-Gänge (iii) der Trias-Jura Grenze (Brander 2000) zeigen erstmalig ein hochsalinares Fluid (>20wt.% NaCl+$CaCl_2$) auf den primären Wachstumszonen der Quarze, welches mit niedrigsalinaren Fluiden alterniert (<5wt.% NaCl+$CaCl_2$). Das primäre NW-SO -Streichen dieser Gänge zeigt eine Anlegung der Strukturen noch vor der Drehung des Hauptstressregimes auf N-S als Fernwirkung durch die Öffnung des Nordatlantiks an.

Die Gänge der Gruppe (iv), haben sich während der Jurassisch-Kretazischen Extensionsphase aus der Mischung von ausschließlich hochsalinaren, niedrig- bis mitteltemperierten Fluiden (>20wt.% NaCl+$CaCl_2$) gebildet. Sie führen erstmalig größere Vererzungen in Fluorit-Baryt-Quarz-(Karbonat)-Gängen mit Pb-Zn-Cu-Ag-, U-Bi-Co-Ni-As- oder Fe-Mn-Vererzungen. Diese Vererzungen sind entweder bevorzugt auf neu entstandenen N-S -streichenden Störungsstrukturen beziehungsweise auf reaktivierten NW-SO -streichenden Brüchen zu finden (Wernicke & Lippolt, 1993; 1997; Meyer et al., 2000; Werner et al., 2002; Pfaff et al., 2009; Staude et a., 2009; 2011; 2012a, 2012b; Werner 2011; Fußwinkel et al., 2013; Walter et al., 2015).

Die Ganggruppe (v) zeigt die größte Vielfalt an Mineralisationstypen und Fluiden. Es handelt sich um Baryt ± Quarz ± Karbonat ± Fluorit-Gänge mit Pb ± Zn ± Ag ± Cu ± Ni ± Co ± Bi ± U ± As –Erzen (Metz et al., 1957, Staude et al., 2009; 2011; 2012a; Walter et al., 2015). Mikrothermometrisch ist das gesamte Spektrum an Salinität (0-26wt.% NaCl+$CaCl_2$) mit Temperaturen von >50 bis <300°C zu finden. Die Gänge dieses Typs sind an Strukturen gebunden, welche sich im Zuge der Oberrheingrabenöffnung bildeten oder an ältere Strukturen, die durch Strike-Slip Tektonik eine Reaktivierung erfuhren. Die große Variabilität dieser Gänge wird als der Effekt einer Multi-Komponenten Fluidmischung interpretiert, welche durch das gegeneinander Versetzen verschiedener Aquifere im Zuge des Grabenbruches bedingt ist (Walter et al., 2015).

2. Einzelstudien

Für die wissenschaftliche Bearbeitung der acht Fragestellungen im Kapitel 1.a wurden mehrere Einzelstudien angefertigt, welche im Anhang 1-7 zu finden sind. Die Reihenfolge der Studien ist nicht chronologisch, sondern baut inhaltlich aufeinander auf.

2a. Mobilisierung und Erzfällung durch hydrothermale Lösungen

In den letzten Jahren konnten weltweit zahlreiche Studien in vielen verschiedenen Lagerstättentypen und Bezirken Fluidmischung als einen der wichtigsten hydrothermalen Erzfällungsprozesse identifizieren. Mikrothermometrie (in erster Linie Halogenverhältnisse), stabile und radiogene Isotopensysteme, Mineralchemie und -texturen sowie Modellierungen konnten chemische Belege für einen Mischungsprozess verschiedener Fluide aus unterschiedlichen Quellen liefern (Raffensperger & Garven, 1995; Garven et al., 1999; Goldhaber et al., 1995, Heijlen et al., 2001, Wilkinson et al., 2005; Schwinn et al. 2006; Stoffell et al., 2008; Boiron et al., 2010; Pfaff et al., 2010; Leach et al., 2010; Wilkinson, 2010; Staude et al., 2011; Ströbele et al. 2012, Richard et al., 2011; Fußwinkel et al., 2013). Die am häufigsten zitierten Modelle gehen von einer Mischung aus, die aus einem heißen, hochsalinaren Grundgebirgsfluid und einem kälteren, niedrig bis hochsalinaren Fluid aus den sedimentären Deckgebirgsschichten besteht (e.g. Heijlen et al., 2001, Wilkinson et al., 2005; Schwinn et al. 2006; Stoffell et al., 2008; Boiron et al., 2010; Pfaff et al., 2010; Leach et al., 2010, Wilkinson, 2010; Staude et al., 2009; Ströbele et al. 2012, Richard et al., 2011; Fußwinkel et al., 2013). Dies gilt für Gebiete, in denen ein magmatischer Motor für die Fluidzirkulation ausgeschlossen werden kann, was zum Beispiel bei den jurassisch-kretazischen Mineralisationen im Schwarzwald der Fall ist. Zu jener Zeit war das Gebiet des Schwarzwaldes von einem flachen Epikontinentalmeer bedeckt (Geyer & Gwinner, 2011 und beinhalteter Referenzen). Aufgrund des flachen Reliefs kann zudem topographisch angetriebener Fluidfluss ausgeschlossen werden. Obwohl die chemischen Belege für eine großräumige Fluidzirkulation und Fluidmischung eindeutig erscheinen, ist es physikalisch fraglich, wie zwei Fluide annähernd gleicher Dichte in Abwesenheit von Magmatismus und Topographie tief versenkt werden konnten, um sich erst dann zu mischen. Details zu den physikalischen Problemen mit den traditionellen Fluidzirkulationsmodellen sind im Anhang 1 (Bons et al., 2014) ausführlich erläutert.

In der Studie 1 (Anhang 1) wird ein neues Modell vorgeschlagen, welches erstmalig konsistent für alle physikalischen und chemischen Beobachtungen und Parameter ist: Hierbei wird die abwärts gerichtete Fluidmigration von Fluidaufstieg und Mischung zeitlich entkoppelt. Die Fluide des jurassisch-kretazischen Zeitraumes sind alle hochsalinar und folgen einem permischen, niedrigsalinaren Fluid, worauf in den Studien 2 und 3 im Anhang im Detail eingegangen wird. Basierend auf den niedrigsalinaren Fluiden im Perm kann davon ausgegangen werden, dass es vor dem Jura noch keine hochsalinaren Fluide im Grundgebirge gab. Seit dem Jura wurde das Grundgebirge mit hochsalinaren Fluiden unterschiedlicher Chemie (für Details Anhang 1-3) aber fast identischer Dichte geflutet (e.g. Staude et al., 2009 und beinhalteter Referenzen. Basierend auf Austrocknungsprozessen durch Vertonungsreaktionen im kristallinen Grundgebirge wird signifikant Wasser verbraucht (Stober & Bucher, 2004; Bons & Gomez-Rivas, 2013). Dies ist bedingt durch die externen Fluide, welche nicht im Gleichgewicht mit dem Mineralbestand stehen. Ein hydraulischer Sog entsteht, welcher wiederum höher liegende Aquifere nach unten nachzieht. Hierbei gelangen

die ältesten Fluide in die größte Tiefe und es entsteht eine Fluidstratigraphie im kristallinen Grundgebirge. Durch extensionale Krustenausdünnung oder Erosion kam es zur Dekompression der physikalisch äquilibrierten Aquifere. Dies führte zum Fluidaufstieg durch Rissfortpflanzung, was nach der Verbindung vieler kleiner Risse zu den tiefgreifenden Kluftsystemen führte, in denen heute die Vererzungen sitzen. Während des Aufstieges mischten sich die Fluide mehrerer Stockwerke, was zur Fällung von Gangarten und Erzmineralen führte.

Zusammenfassend wird mit dieser Studie ein neuer chemisch und physikalisch konsistenter Prozess vorgeschlagen, welcher zuerst Fluide durch Vertonungsprozesse nach unten bringt. Später führt die Dekompression während der Krustenausdünnung oder Erosion zum Überdruck, damit zum Fluidaufstieg und letztendlich zur Mischung. Die Studie ist unter folgendem Titel publiziert: *Bons, P. D., Fusswinkel, T., Gomez-Rivas, E., Markl, G., Wagner, T., & Walter, B. (2014). Fluid mixing from below in unconformity-related hydrothermal ore deposits. Geology, 42(12), 1035-1038.*

2b. Chemische Modifikation der Grundgebirgsfluide im Schwarzwald

Aus früheren Studien sind zahlreiche verschiedene Fluidtypen im Schwarzwald bekannt, welche typisch für bestimmte Mineralisationen in einer definierten Bildungszeit sind (e.g. Behr & Gerler, 1987; Baatartsogt et al., 2006; Staude et al., 2009, 2010, 2011, 2012a, 2012b; Pfaff et al., 2010, 2011). Es stellte sich daher die Frage, durch welche Prozesse sich die Fluide im Grundgebirge verändern und ob eine allgemeingültige Systematik der hydrothermalen Mineralisationen eingeführt werden kann, in der alle chemischen, strukturellen, temporären und hydraulischen Vorkenntnisse berücksichtigt werden. Weiterhin stellt sich die Frage, ob verschiedene erzbildende Quellreservoire entschlüsselt und verstanden werden können.

Um die überregionale Fluidentwicklung im Arbeitsgebiet zu entschlüsseln, wurden die Erzgänge bekannten Alters als natürliche Fluidarchive herangezogen. Somit konnten diejenigen Fluide, welche zum jeweiligen Zeitpunkt der Gangbildung in der Oberkruste vorhanden waren, aufgenommen werden. Deren systematische Variationen mit der Zeit führten zu einem Fluidentwicklungsmodell über 320 Ma, auf welches im Folgenden eingegangen wird (Anhang 2):

Wie bereits in der Einführung beschrieben, handelt es sich bei den frühesten Mineralisationen um Adern, welche im Karbon (i) bevorzugt als Quarz-Turmalin-Gänge mit wenig W- und Sn-Erzen auftreten und stets an Granitkörper gebunden sind (Marks et al., 2013). Der Gangtyp (i) wurde aus niedrigsalinaren, volatilreichen und hochtemperierten Fluiden ausgefällt. Im Perm (ii) führten abkühlende spät-metamorphe, niedrigsalinare und ebenfalls hochtemperierte Fluide zur Fällung von Quarz-Gängen mit geringen Sb- und Au-Vererzungen (Wagner and Cook, 2000). Ab der Trias-Jura-Grenze (iii) können gering vererzte Quarz-Hämatit-Gänge (Brander 2000) beobachtet werden, welche alternierende primäre Abfolgen von niedrig- und hochsalinaren, mitteltemperierten Fluiden beinhalten. Mit der Ganggruppe der jurassisch-

kretazischen Gänge (iv) treten erstmalig ausschließlich hochsalinare, niedrig bis mitteltemperierte Fluide in Verbindung mit einer starken bevorzugt Pb-Zn-Cu-Ag-, U-Bi-Co-Ni-As- oder Fe-Mn-Vererzung der Gänge auf (Behr & Gerler, 1987; Baatartsogt et al., 2006; Staude et al., 2009, 2010, 2011, 2012a, 2012b). Die Gänge des post-kretazischen Zeitraumes (v) sind an die Öffnung des Oberrheingrabens gebunden und zeigen eine große Variabilität in Fluidchemie, Bildungstemperatur und Vererzung (Staude et al., 2009).

Die volatilreichen, niedrigsalinaren, hochtemperierten Fluide des Karbons werden als spätmagmatische Fluide angesehen und zeigen niedrige molare Ca/(Na+Ca) Verhältnisse und Cl/Br Massenverhältnisse im Fluid. Die Gänge des Perm sind ebenfalls niedrigsalinar und hochtemperiert, jedoch ausschließlich H_2O-NaCl-Fluide mit niedrigen Cl/Br Massenverhältnissen. Sie werden als abkühlende metamorphe Fluide in der Spätphase der variszischen Gebirgsbildung angesehen (Wagner & Cook, 2000). Entscheidend für die Fluidentwicklung bis hin zu lagerstättenbildenden Fluiden ist das erstmalige Auftreten der hochsalinaren Lösungen an der Trias-Jura-Grenze. Als Quelle für die hochsalinaren Fluide wird eine Evaporationsrestlauge aus den Triassischen Muschelkalkhaliten vorgeschlagen, auf die niedrige molare Ca/(Na+Ca)-Verhältnisse und niedrige Cl/Br-Massenverhältnisse im Fluid hindeuten. Diese Lösung wurde durch Interaktion mit den Feldspäten und Glimmern des kristallinen Grundgebirges modifiziert. Am Ende der Trias führen eindringende Formationswässer in die Muschelkalkevaporite zur Bildung einer Salzauflösungslauge, welche ebenfalls, wie auch die Restlauge, ins kristalline Grundgebirge gezogen wird (Fußwinkel et al., 2013; Bons et al., 2014). Diese Salzauflösungslauge ist gekennzeichnet durch ebenfalls niedrige Ca/(Na+Ca)-Molverhältnisse und hohe Cl/Br Massenverhältnisse im Fluid. Angetrieben wird dieser Prozess durch Austrocknungs- beziehungsweise Vertonungsprozesse (Bons et al. 2014, Anhang 1). Erst durch das Öffnen tiefreichender Störungsstrukturen im Jura konnten sich die modifizierten Evaporitlaugen mischen und zur Bildung der weiträumigen Vererzung führen (Fußwinkel et al., 2013; Bons et al., 2014).

Durch die Öffnung des Oberrheingrabens wurde eine Vielzahl unterschiedlicher Aquifere kurzgeschlossen. Dies führte ebenfalls zur Fluidmischung und bedingte eine große Variabilität in den Vererzungen, der Salinität, der Ca/(Na+Ca)-Molverhältnisse, der Cl/Br-Massenverhältnisse und der Bildungstemperaturen im gemischten Fluid.

Ein Vergleich zum Harz und Spessart, wo schon seit der frühen Trias hohe Salinitäten in Erzgängen auftreten, zeigt, dass es sich dort wahrscheinlich um Zechsteinrestlösungen handelt, welche zu einem früheren Zeitpunkt das Grundgebirge mit hochsalinaren Lösungen fluteten (Lüders et al., 1993; Fußwinkel et al., 2013).

Die Quintessenz aus der Studie im Anhang 2 ist somit, dass für eine großräumige hydrothermale Vererzung wahrscheinlich zwei Parameter vorhanden sein sollten: Zum Einen sollte eine oberflächliche Evaporitfällung stattgefunden haben, welche erstmalig hohe Salinitäten im Grundgebirge schafft. Zum Anderen wird die Fluidmischung mindestens eines hochsalinaren, metallreichen Aquifers mit weiteren Fluidreservoiren benötigt. Die Studie ist unter folgendem Titel publiziert: *Walter, B.F., Burisch, M., & Markl, G., (2016) Long-term*

chemical evolution and modification of continental basement brines – a field study from the Schwarzwald, SW Germany.

2c. Rekonstruktion erodierter Sedimentfazies und Metall-Quellen im Jura und in der Kreidezeit

In der Studie im Anhang 3 handelt es sich um eine Detailstudie, welche das angesprochene Fluidentwicklungsmodell aus Studie 2 für den jurassisch-kretazischen Zeitraum (Ganggruppe iv) weiter verfeinern soll. Dabei sollen besonders Faziesunterschiede der einzelnen Reservoire, welche durch die Paläotopographie bedingt sind, berücksichtigt werden (Geyer & Gwinner, 2011). Es stellt sich hierbei die Frage, was für Informationen in hydrothermalen Erzgängen archiviert und welche Aufschlüsse über heute erodierte Deckgebirgsbereiche übermittelt werden.

Wie bereits in Studie 2 erörtert, führte eine detaillierte Betrachtung der Erzgänge des Juras und der Kreide zu der Erkenntnis, dass sich zur Zeit der Gangbildung wahrscheinlich eine tiefsitzende, modifizierte Evaporationsrestlauge mit einer spättriassischen Halitauflösungslauge mischte (siehe Fluidchemie-Beschreibung im letzten Kapitel).

Im Gegensatz zum vereinfachten Model in Studie 2 ist in der hier vorliegenden Studie neu, dass die Fluidchemie nicht nur mit der stratigraphischen Tiefe, sondern auch mit der Paläotopographie in der Zeit des Muschelkalkes zu variieren scheint. Muschelkalk-Salze wurden ausschließlich in topographischen Senken gefällt, während auf den Schwellen in erster Linie Sulfate abgelagert wurden (Geyer and Gwinner, 2011 und beinhalteter Referenzen). Somit können basierend auf Ca/(Na+Ca)- molaren Verhältnissen und Cl/Br-Massenverhältnissen im Fluid paläotopographische Begebenheiten in heute exhumierten Bereichen rekonstruiert werden. Fluide, die an der Salzausfällung beteiligt sind, zeigen einen niedrigen Ca-Gehalt im Fluid und niedrige Cl/Br-Massenverhältnisse. Im Gegensatz dazu haben Salz auflösende Fluide ebenfalls einen niedrigen Ca-Gehalt aber hohe Cl/Br-Massenverhältnisse. Fluide, die mit Sulfat agieren, sind Ca-dominiert und zeigen niedrige Cl/Br-Massenverhältnisse. Während die Evaporationsrestlauge das gesamte Grundgebirge flutete, zeigen die Sulfat- und die Halitauflösungslauge genau die Faziesbereiche der Salz- und der Sulfatfazies des mittleren Muschelkalkes und somit die Paläotopographie an.

Die Metalle im Fluid scheinen jedoch in erster Linie mit der stratigraphischen Tiefe zu variieren. Dies lässt sich mit einem zunehmenden Grundgebirgsanteil im gemischten Erzfluid bei zunehmender Bildungstiefe erklären. Pb, Zn, Ag und W scheinen bevorzugt aus dem Kristallinaquifer zu stammen (Burisch et al., eingereicht), während für Cu, Ni, Co und Bi eine Quelle in den Rotliegend- und Buntsandsteinsedimenten wahrscheinlich ist (e.g. Koziy et al., 2009). Eine weitere Zn-Quelle könnte der Muschelkalk darstellen, worauf Variationen in Pb/Zn-Massenverhältnissen des gemischten Fluids hindeuten. Die Ergebnisse dieser Studie

sind in dem Manuskript mit dem folgenden Titel eingereicht: *Walter, B.F., Burisch, M., Marks M.A.W., & Markl G. (eingereicht zu Chemical Geology) Major element and trace metal systematics of fluid inclusions in hydrothermal veins: metal provenance and the reconstruction of eroded sedimentary units.*

2d. Multi-Komponentenfluidmischung im post-kretazischen Zeitraum

Eine weitere Beobachtung dieser Arbeit ist die mineralogische Variabilität der Erzgänge entlang des Schwarzwaldrandverwerfungs-Systems. Hierbei können eine Vielzahl unterschiedlichster Gangtypen auf der großen Grabenrandverwerfung beobachtet werden, welche eine unklare Systematik mit den Nebengesteinen der vorgelagerten Kippschollen zu bilden scheinen (Metz et al., 1957, Bliedner & Martin 1986). Diese Beobachtung kann auf alle Gänge der Ganggruppe (v) ausgeweitet werden, welche mit der Öffnung des Oberrheingrabens in Verbindung stehen. Die deutliche Vielfalt an Erzgängen des post-kretazischen Zeitraumes zeigt einen klaren Unterschied zur jurassisch-kretazischen Ganggruppe (iv).

Somit stellt sich die Frage, was die deutliche Variabilität bewirkt und welche Aquifere und Formen der Fluidmischung die entscheidende Rolle bei der Erzbildung im gesamten Schwarzwald nach und während dem Grabenbruch spielen. Die Arbeit von Staude et al. (2009) und die Studie 2 im Anhang zeigt bereits, dass die Fluide des post-kretazischen Zeitraumes eine deutliche Variabilität in der Salinität im Gegensatz zu den Gängen der Jura-Kreidezeit haben. Die jurassisch-kretazischen Gänge wurden ausschließlich aus gemischten hochsalinaren Fluiden ausgefällt. Studie 4 beleuchtet den Unterschied im Bildungsprozess und der beteiligten Quellaquifere zwischen der Ganggruppe (v) und der Ganggruppe (iv). Darauf basierend soll die Genese der post-kretazischen Gangbildung (v) verstanden werden.

Auf Grundlage von Mikrothermometrie, Crush-Leach-Analysen und LA-ICPMS (laser ablation inductively coupled plasma mass spectrometry) an einzelnen Fluideinschlüssen, konnten Multi-Komponenten Fluidmischungen auf der Skala des gesamten Lagerstättenbezirkes, einer Lokalität und auf der Skala einer Wachstumszone als wichtigster Unterschied zur binären Fluidmischung im Jura und in der Kreide festgestellt werden.

Auf der Skala des gesamten Schwarzwaldes scheint für vererzte Gänge immer eine hochmineralisierte Grundgebirgsfluidquelle nötig zu sein, worauf hohe Metallgehalte und Cl/Br-Verhältnisse hindeuten. Wie auch in der Jura- und Kreidezeit spielt bei der Gangbildung das hochsalinare Muschelkalkaquifer als weiteres Mischungsendglied eine sehr wichtige Rolle. Die Mischung dieser zwei hochsalinaren Aquifere ergibt den horizontalen, hochsalinaren Mischungstrend in Abbildung 5E der Studie 2 und Abbildung 5C der Studie 6. Im Gegensatz zu den jurassisch-kretazischen Gängen treten noch weitere niedrigsalinare Aquifere, zum Beispiel Formationswässer oder meteorische Fluide, hinzu. Diese niedrig

mineralisierten Wässer können das hochsalinare Fluid bei der Mischung stark verdünnen. Basierend auf Fluidchemievariationen in Verbindung mit Metallgehalten, scheinen die Hauptmetallquellen identisch mit denen der Ganggruppe (iv) zu sein. Pb, Zn, Ag, Sb und W kommen wahrscheinlich bevorzugt aus dem Grundgebirge, während die Quellen von Cu und Bi wohl bevorzugt in sedimentären Anreicherungen im Buntsandstein und Rotliegenden zu finden sind (Koziy et al., 2009; Burisch et al., eingereicht).

Auf der Skala einer Lokalität können sowohl Veränderungen der Bildungstemperaturen wie auch der Salinität über mehrere Wachstumszonen hinweg beobachtet werden. Im Detail können komplexe Abfolgen von hoch-, mittel- und niedrigsalinaren Fluiden mit unterschiedlichen Temperaturen, teilweise Sulfat- oder CO_2-führend, detektiert werden. Diese zeigen unsystematische Veränderungen in den Mischungsverhältnissen und beteiligten Aquiferen an.

Betrachtet man die Variationen einzelner Fluideinschlüsse auf einer Wachstumszone, können für viele Fluideinschlussvergesellschaftungen mindestens drei Fluidendglieder festgestellt werden. Daher kann von einer Multi-Komponentenmischung auf einer einzelnen Wachstumszone ausgegangen werden. Diese Mischung tritt bevorzugt zwischen einem sulfatreichen Fluid mit hohen Cl/Br-Massenverhältnissen, einem metallreichen, hochsalinaren Fluid mit niedrigem Cl/Br-Massenverhältnissen und einem gering mineralisiertem Wasser mit ebenfalls niedrigen Cl/Br-Massenverhältnissen auf. Bei ersterem handelt es sich vermutlich um ein Formationswasser, das zweite Fluid entspricht einer hochsalinaren Grundgebirgslauge (Fußwinkel et al., 2013, Bons et al., 2014). Bei dem dritten scheint es sich um ein gering-mineralisiertes meteorisches Fluid zu handeln. Eine auf Diffusion beruhende Modellrechnung deutet auf Wachstumsraten der primären Wachstumszonen im Bereich von Sekunden bis maximal Stunden hin.

Für viele Mineralisationen ist jedoch eine genaue Quellenzuordnung nicht möglich. Dies wird auf eine Instabilität, eine sogenannte chemische Modifikation der einzelnen Aquifere, durch Wasser-Gesteinswechselwirkung, mit der Zeit zurückgeführt. Eindringende niedrig-mineralisierte, meteorische Wässer führen zur Vertonung beziehungsweise zur Laugung der Aquifergesteine. Dies wiederum resultiert mit der Zeit in einer Verschiebung der Aquifersignaturen.

Um dennoch Aussagen über mögliche beteiligte Aquifere treffen zu können, wurden verschiedene Mischungsszenarien diverser Aquiferkombinationen durchgeführt (Pauwels et al., 1993; Göb et al., 2014). Diese Modellierungen zeigen drei Resultate auf: (i) Durch fast jede Kombination moderner Aquifere mit einer Grundgebirgslauge können Barytgänge ausgefällt werden. Dieses Resultat wird durch Beobachtungen im Gelände sehr stark unterstützt(Metz et al., 1957, Bliedner & Martin 1986). (ii) Zur Fluoritübersättigung (und anschließender Fällung) führte ausschließlich die Kombination aus Grundgebirgslauge und hochsalinarem Buntsandsteinformationswasser. Fluoritgänge des post-kretazischen Zeitraumes haben zudem meistens auch hohe Cl/Br -Verhältnisse, was einen Einfluss durch Muschelkalkformationswasser wahrscheinlich macht (Fußwinkel ret al., 2013; Bons et al.,

2014 und beinhalteter Referenzen). Folgt man dem Modell in Studie 1, dann sollte das Muschelkalkaquifer stratigraphisch über dem Buntsandsteinformationswasser im Kristallin sitzen, was wiederum einen Einfluss von Buntsandsteinformationswasser für die Genese der post-kretazischen Fluoritgänge als wahrscheinlich macht. (iii) Sulfide (Galenit, Sphalerit) sind sehr stark untersättigt, da alle beteiligten känozoischen Aquifere oxidiert sind. Um die gängige Textur kogenetischer Sulfide mit Sulfaten in den Erzgängen erklären zu können (Metz et al., 1957; Staude et al., 2012 und beinhalteter Referenzen), wird eine externe Methanzufuhr als Reduktionsmittel vorgeschlagen, was für kurze Zeit lokal die Stabilität des Fluids vom Sulfat ins Sulfidprädominanzfeld verschiebt.

Zusammenfassend kann für die Gänge des post-kretazischen Zeitraumes festgehalten werden, dass der Grabenbruch die hohe Komplexität der post-kretazischen Vererzung hervorgerufen hat. Bei der entstandenen, sehr komplexen geologischen, Situation wurden neue Wegsamkeiten zwischen Aquifere verschiedenster chemischer Zusammensetzung und physikalischer Parameter geschaffen, welche miteinander wechselwirken konnten. Eine vorläufige Manuskriptversion ist im Anhang 5 mit dem folgenden Titel zu finden: *Walter, B.F., Burisch, M., Fußwinkel, T., Marks, M.A.W., Wälle, M., Heinrich, C., Apukhtina, O.B., Markl, G. (in Vorbereitung) Multi-reservoir fluid mixing processes in rift-related hydrothermal vein-type deposits.*

2e. Reaktivierung von Fluidwegsamkeiten in den Wurzelzonen der Erzgänge und ihre Bedeutung für die Erzfällung

Bis heute sind die Bedeutung der Wegsamkeiten in den Wurzelzonen und ihr Einfluss auf Erzfluide nur unzureichend erforscht. Metalle und weitere Spurenelemente werden bevorzugt durch Wasser-Gesteins-Wechselwirkungen in Anwesenheit einer hochsalinare Lauge mobilisiert (Burisch et al., eingereicht). Dieses hochsalinare Fluid steht im chemischen Disäquilibrium mit den Mineralen des kristallinen Grundgebirges. Es stellt sich daher die Frage, ob in archivierten Fluideinschlüssen hydrothermaler Erzgänge Informationen über Fluidwegsamkeiten in der Wurzelzone hydrothermaler Mineralisationen vorhanden sind und ob Veränderungen entlang der Wegsamkeiten, zum Beispiel Vertonung von Feldspäten und Glimmern, einen Einfluss auf die Erzfluide haben.

Um Aussagen über die nicht zugänglichen Wurzelbereiche unterhalb der hydrothermalen Erzgänge treffen zu können, wurde eine Mikrothermometrie- und LA-ICPMS -Detailstudie (Anhang 5) an dem Brandenberg Fluorit-Baryt-Quarz-Gang mit Pb- und Zn-Vererzung durchgeführt. Dieser Gang wird als repräsentativ für viele jurassisch-kretazischen Erzgänge angesehen (vergleiche auch Metz et al., 1957). Besonderes Augenmerk lag auf den fluidmobilen Elementen (Rb, Cs, Li, W, Ba, Zn, Pb und Sr), welche bevorzugt durch das Auflösen von Feldspat- und Glimmer ins Fluid gelangen (Göb et al., 2013 und beinhalteter Referenzen). Ergänzend wurde der Cl/Br-Quellindikator herangezogen, um Effekte der

Fluidmischung und der Quelle eindeutig von den Wegsamkeitsinformationen im gemischten Erzfluid trennen zu können (Fußwinkel et al., 2013; Bons et al., 2013 und beinhalteter Referenzen).

Eine signifikante Abnahme der Spurenelemente vom paragenetisch alten Fluorit zum jungen Quarz wurde beobachtet. Dies kann als ein Effekt von fortschreitender Vertonung entlang der Fluidwegsamkeiten in der Wurzelzone der Vererzungen angesehen werden kann. Dadurch könnten durch fortschreitende Alteration der primären Mineralvergesellschaftung, welche die Metalle in Spuren beinhaltet, nach einer Zeitspanne keine neuen Metalle ins Fluid mehr abgegeben werden. Folglich würden jüngere Fluidschübe, sofern sie ältere, offene Wegsamkeiten benutzen, mit der Zeit an Metallen verarmen. Dies hätte direkten Einfluss auf die Erzfällung während der Fluidmischung und würde vermutlich zu einer geringeren Erzfällung in der neuen Gangartgeneration führen. Erst wenn neue Wegsamkeiten geöffnet werden und neues, unalteriertes Material zur Vertonung zur Verfügung steht, sind jene Fluidschübe wieder reicher an Spurenelementen und Metallen.

Um den Effekt der Vertonung zu monitoren, wurde hierbei das Rb/Cs-Massenverhältnis herangezogen. Das Rb/Cs -Verhältnis im Fluid wird stark durch die Vertonung von Feldspäten und Biotiten gesteuert (Aquilina et al., 1997; Göb et al., 2013, und beinhalteter Referenzen), da dieses während der Alteration fraktioniert. Während bevorzugt Rb in Tonmineralen eingebaut wird, zeigt Cs eher die Tendenz, sich adsorbtiv an die Tonmineraloberflächen anzulagern. Hierbei sind Rb/Cs -Verhältnisse <2 typisch für Fluide, welche mit frischen unalterierten Feldspäten und Biotiten interagieren, während Rb/Cs-Verhältnisse von ~2 einem Fluid entsprechen, welches im Gleichgewicht mit Tonmineralen steht. Der Bereich zwischen 2 und 5 ist nicht aussagekräftig. Rb/Cs -Verhältnisse >5 zeigen eine Auflösung von Tonmineralen an (Aquilina et al., 1997; Göb et al., 2013 und beinhalteter Referenzen).

Die Verbindung vom Rb/Cs -Verhältnis mit der systematischen Abnahme der Metalle und weiterer Spurenelemente zeigt für die niedrigen Gehalte im jungen Quarz ein Fluid an, welches im Gleichgewicht mit Tonmineralen stand (Göb et al., 2013) und somit wahrscheinlich eine bereits vertonte Wegsamkeit benutzte. Basierend auf diesen Beobachtungen konnte somit ein Modell für das zyklische Auftreten von Vererzungen innerhalb einer Mineralisation entworfen werden:

Meteorische/Formationswässer haben ein Rb/Cs -Verhältnis von ~2 (Stadium I). Das Verhältnis bleibt konstant, bis sich eine neue Kluft öffnet und eine große Menge unalterierte Biotite und Feldspäte (Oberfläche) zur Verfügung stehen und vertont werden. Dies führt im Fluid zu einer signifikanten Abnahme des Rb/Cs- Verhältnisses (Stadium II) in der Kluft bei gleichzeitig starker Zunahme der Metallgehalte. In Stadium III nimmt die Verfügbarkeit des frischen Materials stark ab. Zudem werden weniger Metalle ins Fluid entlassen und das Rb/Cs -Verhältnis nimmt ab. Wenn alles frische Material verbraucht ist (Stadium IV), gibt es vier Möglichkeiten, welche alle in der Anfangssituation für einen neuen Zyklus enden und im Detail in Anhang 6 beschrieben werden. Die Resultate und Interpretationen dieser Studie sind

im Anhang mit dem folgenden Titel zu finden: *Burisch, M., Walter, B.F., Wälle, M., & Markl, G. (eingereicht zu Chemical Geology) Tracing fluid migration pathways in the upper brittle part of the crust: a fluid inclusion – LA-ICPMS study in a hydrothermal vein from the Schwarzwald mining district, Germany.*

2f. Kalibrierung von Mg-Isotopen in hydrothermalen Karbonaten als Quell- und Mischungsverhältnisanzeiger.

Das Magnesiumisotopensystem ist ein neues, nicht traditionelles System. In Anlehnung an Studien von Wasseranalysen im Karst, in denen klare Fraktionierungssignaturen im Fluid zwischen silikatischer (+1‰) und karbonatischer (-5‰) Verwitterung beobachtet werden (Buhl et al., 2007; Immenhauser et al., 2010; Riechelmann et al., 2012; Mavromatis et al., 2014), sollten diese Ergebnisse auf ein hydrothermales System übertragen werden (Studie 6 im Anhang). Es stellt sich hierbei die Frage, wie wichtig die Definition und das Studium neuer Isotopensysteme in der Lagerstättenkunde sind und wie aussagekräftig das Mg-Isotopensystem für das Verständnis erzbildender Prozesse im hydrothermalen Mileau sein kann. Weiterführende Arbeiten konnten die hohe Komplexität des Isotopensystems demonstrieren. Diese Komplexität wird durch drei Hauptfaktoren begründet. Sie wird erstens durch selektiven Mg-Entzug während Verwitterungsprozessen verursacht (Bolou-Bi et al., 2010; Li et al., 2010; Tipper et al., 2010; Riechelmann et al., 2012; Geske et al., 2015). Zweitens wird sie durch Fraktionierungen während Tonmineralbildungen bedingt, da hierbei die verschiedenen Isotope strukturell oder adsorptiv gebunden werden (Higgins and Schrag, 2010; Opfergelt et al., 2012; Wimpenny et al., 2014a, 2014b). Drittens spielen auch kinetische Effekte zwischen Mg^{2+} in Lösung und verschiedensten Mg-Senken ($\Delta^{26}Mg_{Fluid\text{-}Karbonat}$; Li et al., 2014a, b) eine signifikante Rolle.

Um $\delta^{26}Mg_{Karbonat}$-Verhältnisse auch in einem tiefen hydrothermalen System erstmalig anwenden zu können, müssen mehrere grundsätzliche Fragen geklärt werden:

- Korrelieren $\delta^{26}Mg_{Karbonat}$-Verhältnisse im Erzgang mit $\delta^{26}Mg_{Wirtsgestein\text{-}}$Signaturen und prägen diese dem jeweiligen Quellaquifer eine identische oder variable Signatur auf?
- Welche Rolle spielt die Mineralogie der hydrothermalen Karbonate und überlagert diese bekannte strukturelle Fraktionierung mögliche Quellinformationen?
- Spielen die Fluidtemperatur und die Salinität eine Rolle bei der Fraktionierung?

Hierfür wird das Magnesiumisotopensystem an dem bisher sehr gut verstandenen Gebiet des Schwarzwalds kalibriert. Wie in Kapitel 3 erwähnt, gibt es eine große Anzahl an früheren Studien, die bereits ein in sich schlüssiges Gesamtbild der komplexen und vielfältigen hydrothermalen Gangbildungsprozesse anzeigen. In diese Resultate und Modelle können die Ergebnisse der $\delta^{26}Mg_{Karbonat}$ -Studie eingehängt werden

Nachdem die oben genannten Fragen hinreichend beantwortet werden konnten, ist eine Klärung der folgenden Forschungsziele möglich:

- Identifizierung und Charakterisierung verschiedenster hydrothermaler Karbonate im geologischen Kontext
- Identifikation der $\delta^{26}Mg_{Wirtsgestein}$-Signaturen der beteiligten Aquifere
- Bedeutung von Gesteins-Wasser-Wechselwirkungen, Karbonatmineralogie, Fluidchemie, Salinität, Temperatur und Mischungsverhältnisse auf die $\Delta^{26}Mg_{Fluid-Karbonat}$-Verhältnisse

Die Resultate dieser Studie (Anhang 6) legen nahe, dass es sich bei der tiefen, langanhaltenden, hydrothermalen Alteration im kristallinen Grundgebirge um einen eher kongruenten Prozess handelt. Im Gegensatz dazu stehen oberflächennahe Verwitterungsprozesse, bei welchen kinetische Fraktionierungen die Quellsignatur viel deutlicher überlagern. Basierend auf einer kontinuierlichen Verschiebung der Mischungsverhältnisse mit der stratigraphischen Bildungstiefe jurassisch-kretazischer Gänge (siehe Anhang 3) kann auf eine Quellaquifer-kontrollierte $\delta^{26}Mg_{Karbonat}$-Signatur im gemischten Erzfluid geschlossen werden. Frühere Studien an Fahlerzen, Sphaleriten, Sr-, C-, O- und Pb-Isotopen konnten ebenfalls eine Veränderung der Mischungsverhältnisse belegen (Staude et al., 2010; 2011; 2012; Pfaff et al., 2011; Ströbele et al., 2012).

Wichtig ist hierbei eine Überprüfung des geologischen Settings auf überprägende Prozesse wie Dolomitisierung, diagenetische Lösung und Fällung, inkongruente Verwitterung, etc. Diese letztgenannten Prozesse können alle einen signifikanten Einfluss auf die $\delta^{26}Mg_{Karbonat}$-Signaturen haben. Da diese im hydrothermalen System des Arbeitsgebietes vernachlässigt werden können, ist es möglich, die beteiligten Reservoire am gemischten Fluid zu identifizieren.

Weiterhin wurden die Daten auf einen mineralogischen Einfluss auf die $\delta^{26}Mg_{Karbonat}$-Signaturen überprüft. Hierbei wurde festgestellt, dass die mineralogisch bedingte Fraktionierung zwischen Niedrig-Mg-Kalzit und Dolomit einen signifikanten Einfluss auf die $\delta^{26}Mg_{Karbonat}$-Signatur auch im hydrothermalen System haben kann. Da jedoch mehrere Datenpunkte sowohl des Dolomits als auch des Niedrig-Mg-Kalzits über den gesamten Isotopenshift streuen, scheint eine mineralogische Fraktionierung möglich, aber nicht dominant, und überlagert somit nicht die Quellinformationen. Weiterhin zeigen die Daten, dass eine systematische Fraktionierung mit der Salinität und Temperatur unwahrscheinlich ist, da auch in diesen Fällen Daten über den gesamten Isotopenshift streuen.

Nachdem die verfälschenden Einflüsse auf $\delta^{26}Mg_{Karbonat}$ und $\delta^{26}Mg_{Fluid}$ eingegrenzt werden konnten, sind folgende Quellreservoire für die Fluidmischung am wahrscheinlichsten: Das kristalline Grundgebirge mit einer Signatur von $\delta^{26}Mg_{Fluid}$ -0,2 ‰, welches sich mit dem Muschelkalkformationswasser mit $\delta^{26}Mg_{Fluid}$ -3,5 ‰ mischte. Eine binäre Mischung dieser beiden Aquifere kann alle vorhandenen Datenpunkte erklären und deckt sich perfekt mit den definierten Quellen früherer Arbeiten. Eine erste grobe Semiquantifizierung ergab einen deutlich höheren Grundgebirgsanteil ($\delta^{26}Mg_{Karbonat}$-Werte näher dem silikatischen Endglied)

im gemischten Fluid der stratigraphisch tiefliegenden Gottesehremine im Gegensatz zur Wenzelgrube, welche sich unmittelbar unterhalb der Grundgebirgs-Deckgebirgs-Diskordanz befindet. Die prozentualen Verhältnisse decken sich mit denen der früheren Arbeiten, insbesondere mit den Sr-Isotopen von Staude et al. (2011). Die größere Ungenauigkeit im Mg-Isotopensystem ist im Gegensatz zu anderen Isotopensystemen in erster Linie der noch ungenauen Fraktionierungsgleichung zwischen Karbonat und Fluid geschuldet. Mit zunehmenden Kenntnissen im Mg-Isotopensystem werden sich auch die Genauigkeiten in der quantitativen Anwendung verbessern. Die Studie konnte einen Beitrag zu den Grundlagen leisten und ist unter folgendem Titel publiziert: *Walter, B. F., Immenhauser, A., Geske, A., & Markl, G. (2015). Exploration of hydrothermal carbonate magnesium isotope signatures as tracers for continental fluid aquifers, Schwarzwald mining district, SW Germany. Chemical Geology, 400, 87-105.*

2g. Erkenntnisse von Wasser-Öl-Übergangszonen in sedimentären Becken auf Fluidwegsamkeiten und die Mobilität von hochsalinaren Ölfeldlaugen.

Die Studien 1-6 betrachten wässrig-salinare, polare Fluide in der kontinentalen Oberkruste. Fluide gänzlich anderer Art sind Kohlenwasserstoffe, wie Öle und damit assoziierte, stark reduzierte, hochsalinare Ölfeldlaugen, die besonders auch in CH_4 und HS angereichert sind (Sverjensky, 1984, 1987; Carpenter et al., 1974). Wie in der Studie 4 ausgeführt, werden hochsalinaren Ölfeldlaugen eine mögliche Bedeutung als Reduktionsmittel bei der Erzfällung zugeschrieben. Weiterhin kann die Ölmigration auch entscheidend für das ökonomische Potenzial eines Reservoirs sein. Daher ist es naheliegend, die Bewegung dieser Fluide in einer kontinentalen Oberkruste zu studieren. Es stellt sich hierbei die Frage, welchen Einfluss Ölfeldlaugen auf die Gesteins-Wasser-Wechselwirkungen entlang von Wegsamkeiten und bei der Fällung von Mineralisationen haben, worauf in dieser Studie eingegangen werden soll (Anhang 7). Zeit bedingte Variationen in der Fluidchemie und den physikalischen Bedingungen sind besonders gut in sich versenkenden sedimentären Becken zu finden. Variationen sind in solchen Becken deutlich einfacher zu interpretieren als in einem tektonisch intensiv überprägten Gebiet wie in einem Grabenbruchsystem. Deshalb wird für diese Studie auf ein Erdölreservoir zurückgegriffen.

Besonders interessant ist hierbei die chemische, physikalische Variation des Fluids mit der Zeit (Versenkungstiefe) an der Öl-Wasser-Grenze in einer Erdölfalle, da dort wechselnde Fluide am wahrscheinlichsten archiviert werden können. Für die Studie wurde ein 5 Meter langes Bohrkernstück aus einem karbonatischen Erdölreservoir von Nurlatsky in der Republik Tatarstan (Russische Föderation) gewählt. Eine detaillierte Studie der Zementphasen in der Übergangszone ermöglicht Rückschlüsse auf die folgenden Fragen:

- Was ist die Beziehung zwischen Karbonatdiagenese und der Öl-Migration beziehungsweise können ausgefällte Zementphasen die Wegsamkeiten für das Öl abdichten?

- Ist die Öl-Migration ein einmaliges Ereignis oder gibt es mehrere Phasen der Ölbewegung über längere diagenetische Zeiträume?
- Wurden die diagenetischen Fluide während der Öl-Migration archiviert und können sie in eine Vormigrationsphase, eine Migrationsphase und in eine Postmigrationsphase physikalisch/chemisch unterschieden werden?

Basierend auf Petrographie, Texturen, C- und O-Isotopen können 5 Stadien der Karbonatbildung (sedimentär bis hochdiagenetisch) unterschieden werden. Kathodolumineszensaufnahmen belegen in der 4. Kalzitgeneration Öleinschlüsse. Nach moderner Vorstellung wird Öl als mikroskopisch kleine Tröpfchen (Emulsion) in wässrig-salinaren Fluiden transportiert. Im Gegensatz zu den anderen Kalzitgenerationen ist die Phase 4 stark korrodiert und die Poren mit einem dünnen schwarzen Ölfilm überzogen. Dies liefert texturelle Anhaltspunkte, dass sich das Wasser-Öl-Verhältnis in der Phase 4 zu einem höheren Ölgehalt hin verschiebt und damit graduell die Zementation unterbunden wird. Details hierzu werden in der Studie 7 beschrieben. Diese Erkenntnisse decken sich mit silikatischen Reservoiren, bei denen die Quarzzementation zum Erliegen kommt, wenn das Fluid die Porenräume nicht mehr erreicht (Worden et al., 1998 und beinhalteter Referenzen). Somit kann die Frage 1 differenziert mit nein für hohe Öl-Wasser-Verhältnisse und mit ja für niedrige Öl-Wasser-Verhältnisse im diagenetischen Fluid beantwortet werden.

Basierend auf der Petrographie der Zementphasen und der Öleinschlüsse ist ein einmaliges Öl-Migrationsereignis anzunehmen. Die Fluidchemie und die Homogenisierungstemperatur zeigen deutlich, dass die Fluide der Ölmigrationsphase deutlich Na-dominierter und höher temperiert sind als die Fluide der Postmigrationsphase, welche wieder auf dem normalen diagenetischen Temperaturgradient eines versinkenden Beckens liegen. Beides kann für die Fluide in der Kalzitgeneration 4 als Quellindikator für die tieferliegenden silikatreicheren Erdölmuttergesteine gesehen werden, aus denen das Öl in das Karbonat-Karstaquifer migrierte.

Zusammenfassend zeigt diese Studie einen deutlichen Zusammenhang zwischen diagenetischer Zementation und Wasserchemie. Während bei wässrig-salinaren Fluiden eine diagenetische Verschließung der Wegsamkeiten wahrscheinlich ist, zeigen unpolare Fluide wie Erdöl eine Tendenz Wegsamkeiten offen zu halten.

Transferiert man diese Ergebnisse in den Schwarzwald, scheint es durchaus möglich, dass zirkulierende Ölfeldlaugen im kristallinen Grundgebirge des Schwarzwaldes einen gewissen Einfluss auf die Sulfidfällung haben könnten, da auch Öl und Ölfeldlaugen in Graniten, wie beispielsweise auf Sumatra oder in Kansas (USA), bekannt sind (Rich, 1931; Koning & Darmono, 1984). Weiterhin war der jurassische Posidonienschiefer, welcher generell auch als Erdölmuttergestein eine Rolle spielt, vor der Exhumierung flächendeckend über SW-Deutschland vorhanden (Geyer & Gwinner, 2011 und beinhalteter Referenzen). Möglicherweise wurden Ölfeldlaugen aus dem Posidonienschiefer wie auch die Fluide des darunterliegenden Muschelkalkes durch Vertonung im tiefen Grundgebirge nachgezogen. Auch diese Interpretation kann mit dem „mixing from below“-Modell in der Studie 1 in

Einklang gebracht werden (Bons et al., 2014). Die Resultate dieser Studie sind im Anhang 7 zu finden und unter folgendem Titel publiziert: *Kolchugin A.N., Immenhauser, A., Walter, B.F., Morozov, V.P., (im Druck) Diagenesis of the palaeo-oil-water transition zone in a Lower Pennsylvanian carbonate reservoir: constraints from cathodoluminescence microscopy and isotope geochemistry.*

3. Schlussfolgerungen

Nach über zehn Jahren der intensiven Erforschung der hydrothermalen Mineralisationen mit moderner Analytik gehört der Schwarzwald in SW-Deutschland zu den am besten verstandenen Lokalitäten der hydrothermalen, an Diskordanzen gebundenen, Ganglagerstätten. Im Zuge dieser Arbeit konnte ein physikalisch und chemisch stimmiges Modell erstellt werden, bei welchem der Fluidfluss nach unten von der Fluidmischung im Erzgang zeitlich entkoppelt wurde. Durch Vertonungsreaktionen im kristallinen Grundgebirge wird Wasser verbraucht und es entsteht eine Sogwirkung, wodurch Fluide, die höher in der Stratigraphie vorhanden sind, nach unten gezogen werden konnten. Eine Exhumierung oder Krustenausdünnung führt dazu, dass die Fluide des Porenraumes einen Überdruck erfahren, der sich dann in Form von Rissbildung äußert, in welchen die Fluide nach oben entweichen. Viele dieser Risse verbinden sich und es entstehen Kluftsysteme, in denen sich beim Aufstieg verschiedene Aquifere mischen. Dies führt zur Ausfällung der Erze.

Weiterhin zeigen die Ergebnisse dieser Arbeit an, dass für eine hydrothermale Buntmetallvererzung das Grundgebirge wahrscheinlich erst einmal mit hochsalinaren Fluiden geflutet werden musste. Hierbei wurden die Feldspäte und Glimmer zu Tonmineralen alteriert und damit einhergehend gelangen Metalle ins Fluid. Die Resultate der Studie legen daher nahe, dass Evaporitfällung an der Oberfläche wichtig für die Bildung hydrothermaler Ganglagerstätten mit Buntmetallen sein kann.

Neben der Evaporitfällung ist die Fluidmischung die zweite, wichtige Voraussetzung für die Gangbildung. Eine Fluidmischung zweier oder mehrerer Reservoire unterschiedlichen Chemismuses und Oxidationszustandes wird vorausgesetzt, um eine Verschiebung der Mineralstabiliäten zu erzeugen, worauf viele der hydrothermalen Minerale übersättigt und somit ausgefällt werden.

Die wichtigsten Mischungsendglieder sind die Fluide des kristallinen Grundgebirges, des Buntsandsteines und der verschiedenen Muschelkalkfazies. Darauf deuten stabile Mg-Isotopien an hydrothermalen Gangartkarbonaten, die Fluidchemie und Fluidmischungsmodellierungen hin. Die genannten Reservoire decken sich ebenfalls mit den Ergebnissen früherer Studien im Arbeitsgebiet. Eine detaillierte Betrachtung der Fluidchemie erlaubt Rückschlüsse auf die Paläotopographie in heute erodierten Strata, da die unterschiedlichen Fazies eigene Fingerabdrücke im gemischten Erzfluid hinterlassen. Cl/Br -

Massenverhältnisse und molare Ca/(Na+Ca) -Verhältnisse variieren mit der Fazies des Deckgebirges, während die Metalle und Spurenelemente mit der stratigraphischen Tiefe des Mischungsprozesses zu variieren scheinen. Mit der Tiefe der Mineralisationen ist eine Zunahme an Pb+Zn+Sb+Ag+W zu erkennen, bei gleichzeitiger Abnahme von Cu+Bi. Dies führt zu der Interpretation, dass die erste Elementcharge dominierend dem Grundgebirge entstammt, während die zweite aus dem Deckgebirge eingetragen wurde.

Eine wichtige Erkenntnis dieser Arbeit liegt in der Untersuchung der Bedeutung von Wegsamkeiten auf Erzfluide und schließlich auf die Vererzung selbst. Bewegt sich das hydrothermale Fluid in einer neu geöffneten Kluft, werden die Kluftwände vertont und dadurch Metalle freigesetzt. Nutzt das Fluid eine bereits vorhandene und damit schon alterierte Wegsamkeit, ist die Metallaufnahme deutlich geringer, was mit vererzten und erzfreien Ganggenerationen korreliert.

Weiterhin wird im Zuge dieser Arbeit auf die mögliche Bedeutung von reduzierenden Fluiden, wie Ölfeldlaugen oder Methan, hingewiesen. Da die an der Fluidmischung beteiligten Aquifere für eine Sulfidfällung zu oxidiert sind, wird für eine kogenetische Sulfidfällung, beispielsweise in Barytgängen, ein Reduktionspartner benötigt. Dieser verschiebt die Stabilität des Fluides kurzzeitig ins Sulfidprädominanzfeld und ermöglicht somit eine kurzzeitige Fällung von kogenetischen Sulfiden und Sulfaten. Da Quarz-Wachstumskalkulationen der Studie 5 nahelegen, dass es sich bei der Fluidmischung um sehr kurze Ereignisse handelt, ist auch ein kurzzeitiger Zustrom eines reduzierten Fluides möglich. In Frage kämen hierfür Formationswässer des Posidonienschiefers, der als wichtiges Erdölmuttergestein bekannt ist. Diese würden, wie die restlichen Fluide, nach dem „mixing from below“ -Modell mit nach unten gezogen werden. Nach der Öffnung von Klüften könnten sie ebenfalls an der Fluidmischung partizipieren. Zumal haben Ölfeldlaugen je nach Ölgehalt die Tendenz, Wegsamkeiten offen zu halten, indem sie die Zementation in einer Wegsamkeit unterbinden. Eine weitere Möglichkeit für die Methanbildung wäre eine Graphitoxidation im Nebengestein.

Die Erkenntnisse und deren Interpretationen können über den Schwarzwald hinaus für weitere Lagerstättenbezirke von Bedeutung sein. Zunehmende Kenntnisse auf dem Gebiet der hydrothermalen Gangmineralisationen werden langfristig auch Beachtung in der Lagerstättenexploration finden. So ist der Nordschwarzwald beispielsweise ein höffigeres Gebiet als der Südschwarzwald. Im Südschwarzwald wurden durch die asymmetrische Exhumierung sehr wahrscheinlich ca. zwei Kilometer Gangmächtigkeit erodiert. Jedoch ist in den Gängen des Nordschwarzwaldes mit einer steigenden Sulfidführung bei zunehmender Tiefe zu rechnen. Eine zunehmende Erzführung im Gang findet sich beispielsweise auf den tiefsten Sohlen der Grube Käfersteige im Nordschwarzwald. Dieses Beispiel zeigt das langfristige ökonomische Potential von Grundlagenstudien an, wie sie auch die hier vorgelegte Arbeit darstellt.

4. Literatur

Altherr, R., Holl, A., Hegner, E., Langer, C., Kreuzer, H., 2000. High-potassium, calc-alkaline I-type plutonism in the European Variscides: northern Vosges (France) and northern Schwarzwald (Germany). Lithos, 50(1): 51-73.

Aquilina, L., Pauwels, H., Genter, A., and Fouillac, C., 1997, Water-rock interaction processes in the Triassic sandstone and the granitic basement of the Rhinegraben: Geochemical investigation of a geothermal reservoir.: Geochimica et Cosmochimica Acta, v. 61, p. 4281-4295.

Aquilina, L., Boulvais, P., Mossmann, J.-R., 2011. Fluid migration at the basement/sediment interface along the margin of the southeast basin (France): implications for Pb–Zn ore formation. Mineralium Deposita 46, 959-979.

Baatartsogt, B., Wagner, T., Taubald, H., Mierdel, K., Markl, G., 2006. Hydrogen isotope determination of fluid inclusion water from hydrothermal fluorite: The results depend on the extraction technique. Chemical Geology, 1-21.

Barnes, H.L., 1997. Geochemistry of Hydrothermal Ore Deposits. John Wiley & Sons, Inc., 3.Aufl.

Behr, H.J., Gerler, J., 1987. Inclusions of sedimentary brines in post-Variscan mineralizations in the Federal Republic of Germany—a study by neutron activation analysis. Chemical Geology, 61, 65-77.

Behr, H.J., Horn, E.E., Frentzel-Beyme, K., Reutel, C., 1987. Fluid inclusion characteristics of the Variscan and post-Variscan mineralizing fluids in the Federal Republic of Germany. Chemical Geology, 61, 273-285.

Bliedtner M., Martin M. 1986. Erz- und Minerallagerstätten des Mittleren Schwarzwaldes. LGRB, Freiburg

Boiron, M.C., Cathelineau, M., Richard, A., 2010. Fluid flows and metal deposition near basement/cover unconformity: lessons and analogies from Pb-Zn-F-Ba systems for the understanding of Proterozoic U deposits. Geofluids 10, 270-292.

Bolou-Bi, E.B., Poszwa, A., Leyval, C., Vigier, N., 2010. Experimental determination of magnesium isotope fractionation during higher plant growth. Geochimica et Cosmochimica Acta, 74(9): 2523-2537.

Bons, P.D., Elburg, M.A., Gomez-Rivas, E., 2012. A review of the formation of tectonic veins and their microstructures. Journal of Structural Geology, 43: 33-62.

Bons, P.D., and Gomez-Rivas, E., 2013, Gravitational fractionation of isotopes and dissolved components as a first-order process in hydrothermal crustal fluids: Economic Geology and the Bulletin of the Society of Economic Geologists, v. 108, p. 1195–1201,

Bons, P. D., Fusswinkel, T., Gomez-Rivas, E., Markl, G., Wagner, T., and Walter, B., 2014, Fluid mixing from below in unconformity-related hydrothermal ore deposits: Geology, p. 1035-1038

Bucher, K., and Stober, I., 2000. The composition of groundwater in the continental crystalline crust. In *Hydrogeology of crystalline rocks* (pp. 141-175). Springer Netherlands.

Bucher, K., and Stober, I., 2002. Water-rock reaction experiments with Black Forest gneiss and granite. In *Water-Rock Interaction* (pp. 61-95). Springer Netherlands.

Bucher, K., and Stober, I., 2010, Fluids in the upper continental crust: Geofluids, v. 10, no. 1-2, p. 241-253.

Bucher, K., Zhu, Y., and Stober, I., 2009. Groundwater in fractured crystalline rocks, the Clara mine, Black Forest (Germany). *International Journal of Earth Sciences*, *98*(7), 1727-1739.

Buhl, D., Immenhauser, A., Smeulders, G., Kabiri, L., Richter, D.K., 2007. Time series δ^{26}Mg analysis in speleothem calcite: Kinetic versus equilibrium fractionation, comparison with other proxies and implications for palaeoclimate research. Chemical Geology, 244: 715-729.

Burisch, M., Marks, M., Novak, M., Markl, G., submitted to Chemical Geology. The importance of temperature and cataclastic deformation for halogen (F, Cl, Br) systematics and metal transport capacities of continental basement brines – an experimental approach

Brander, T., 2000. U/HE-chronologische Fallstudien an Eisen- und Manganerzen. Dissertation. Heidelberg.

Carpenter, A.B., Trout, M.L., Pickett, E.E., 1974. Preliminary report on the origin and chemical evolution of lead-and zinc-rich oil field brines in central Mississippi. Economic Geology, 69(8): 1191-1206.

Derome, D., Cathelineau, M., Fabre, C., Boiron, M.-C., Banks, D.A., Lhomme, T., Cuney, M., 2007. Paleo-fluid composition determined from individual fluid inclusions by Raman and LIBS: Application to mid-proterozoic evaporitic Na–Ca brines (Alligator Rivers Uranium Field, northern territories Australia). Chemical Geology, 237(3-4): 240-254.

Dixon, P.R., LeHuray, A.P., and Rye, D.M., 1990, Basement geology and tectonic evolution of Ireland as deduced from Pb isotopes: Geological Society of London Journal, v. 147, p. 21–132

Edmunds, W.M., Savage, D., 1991. Geochemical characteristics of groundwater in granites and related crystalline rocks. Applied Groundwater Hydrology, a British Perspective (eds Downing RA, Wilkinson WB): 199-216.

Emmermann, R., Althaus, E., Giese, P., Stöckhert, B., 1995. KTB Hauptbohrung results of geoscientific investigation in the KTB field laboratory, final report: 0-9101 m. KTB Report, 95-2: E.

Fußwinkel, T., Wagner, T., Wälle, M., Wenzel, T., Heinrich, C., Markl, G., 2013. Fluid mixing forms basement-hosted Pb-Zn deposits: Insight from metal and halogen geochemistry of individual fluid inclusions. Geology 41, 679-682.

Frape, S., Fritz, P., 1987. Geochemical trends for groundwaters from the Canadian Shield. Geological Association of Canada Special Papers, 33, 19-38.

Fritz, P., 1997. Saline groundwater and brines in crystalline rocks: the contributions of John Andrews and Jean-Charles Fontes to the solution of a hydrogeological and geochemical problem. Applied Geochemistry, 12: 851-856.

Gallup, D.L., 1998. Geochemistry of geothermal fluids and well scales, and potential for mineral recovery. Ore geology reviews, 12(4): 225-236.

Garven, G., Appold, M.S., Toptygina, V.I., Hazlett, T.J., 1999. Hydrogeologic modeling of the genesis of carbonate-hosted lead-zinc ores. Hydrogeology Journal 7, 108-126.

Geske, A., Lockier, S., Dietzel, M., Richter, D.K., Buhl, D., Immenhauser, A., 2015, Magnesium isotope composition of sabkha pore fluids and related (Sub-) Recent stoichiometric dolomites, Abu Dhabi (UAE). Chemical Geology, 393-394: 112-124

Geyer, O. F., and Gwinner, M. P., 2011, Geologie von Baden -Württemberg. – 5., völlig neu bearbeitete Auflage, Stuttgart, Schweizerbart`sche Verlagsbuchhandlung (Nägele u. Obermiller), 627 p.:

Gleeson, S.A., Wilkinson, J.J., Stuart, F.M., Banks, D.A., 2001. The origin and evolution of base metal mineralising brines and hydrothermal fluids, South Cornwall, UK. Geochimica et Cosmochimica Acta, 65, 13, 2067-2079.

Göb, S., Loges, A., Nolde, N., Bau, M., Jacob, D.E. Markl, G., 2013. Major and trace element compositions (including REE) of mineral, thermal, mine and surface waters in SW Germany and implications for water-rock interaction. Applied Geochemistry, 33: 127-152.

Goldhaber, M.B., Church, S.E., Doe, B.R., Aleinikoff, J.N., Brannon, J.C., Podosek, F.A., Mosier, E.L., Taylor, C.D., and Gent, C.A., 1995, Lead and sulfur isotope investigation of Paleozoic sedimentary rocks from the southern midcontinent of the United States: Implications for paleohydrology and ore genesis of the southeast Missouri lead belts: Economic Geology and the Bulletin of the Society of Economic Geologists, v. 90, p. 1875–1910, doi: 10.2113 /gsecongeo .90.7.1875.

Hann, H.P., Chen, F., Zedler, H., Frisch, W., Loeschke, J., 2003. The Rand Granite in the southern Schwarzwald and its geodynamic significance in the Variscan belt of SW Germany. International Journal of Earth Science, 92: 821-842.

He, K., Stober, I., and Bucher, K., 1999, Chemical evolution of thermal waters from limestone aquifers of the Southern Upper Rhine Valley: Applied geochemistry, v. 14, no. 2, p. 223-235.

Heijlen, W., Banks, D.A., Muchez, P., Stensgrad, B.M., Yardley, B.W.D., 2008. The nature of mineralizing fluids of the Kipushi Zn-Cu deposit, Katanga, Democratic Repubic of Congo: quantitative fluid inclusion analysis using laser ablation ICP-MS and bulk crush-leach methods. Economic Geology, 103: 1459-1482.

Heijlen, W., Muchez, P., Banks, D.A., 2001. Origin and evolution of high-salinity, Zn–Pb mineralising fluids in the Variscides of Belgium. Mineralium Deposita, 36: 165-176.

Heijlen, W., Muchez, P., Banks, D. A., Schneider, J., Kucha, H., & Keppens, E., 2003. Carbonate-hosted Zn-Pb deposits in Upper Silesia, Poland: origin and evolution of mineralizing fluids and constraints on genetic models. Economic Geology, 98(5): 911-932.

Higgins, J.A., Schrag, D.P., 2010. Constraining magnesium cycling in marine sediments using magnesium isotopes. Geochimica et Cosmochimica Acta, 74: 5039-5053.

Immenhauser, A., Buhl, D., Niedermayr, A., Riechelmann, D., Dietzel, M., Schulte, U., 2010. Magnesium-isotope fractionation during low-Mg calcite precipitation in a limestone cave – Field study and experiments. Geochimica et Cosmochimica Acta, 74(15): 4346-4364.

Kalt, A., Altherr, R., Hanel, M., 2000. The Variscan basement of the Schwarzwald. Eur. J. Mineral., Beih., 12: 1-43.

Koning, T., Darmono, F. X., 1984. The geology of the Beruk Northeast Field, Central Sumatra: oil production from Pre-Tertiary basement rocks.

Koziy, L., Bull, S., Large, R., and Selley, D., 2009, Salt as a fl uid driver, and basement as a metal source, for stratiform sediment-hosted copper deposits: Geology, v. 37, p. 1107–1110, doi:10.1130/G30380A.1

Leach, D.L., Bradley, D.C., Husten, D., Pisarevsky, S.A., Taylor, R.D., Gardoll, S.J., 2010. Sediment-hosted lead-zinc deposits in Earth history. Economic Geology, 105: 593-625.

Li, S.-L., Liu, C-.G., Li, J., Lang, Y.C., Ding, H., Li, L., 2010. Geochemistry of dissolved inorganic carbon and carbonate weathering in a small typical karstic catchment of Southwest China: Isotopic and chemical constraints. Chemical Geology, 277(3): 301-309.

Li, W., Beard, B.L., Li, C., Johnson, C.M., 2014a. Magnesium isotope fractionation between brucite [Mg $(OH)_2$] and Mg aqueous species: Implications for silicate weathering and

biogeochemical processes. Earth and Planetary Science Letters, 394: 82-93.

Li, W.-Y., Teng, F.-Z., Wing, B.A., Xiao, Y., 2014b. Limited magnesium isotope fractionation during metamorphic dehydration in metapelites from the Onowa contact aureole, Maine. Geochem. Geophys. Geosyst. 15, 408 - 415.

Lüders V, Gerler J, Hein U, Reutel C (1993) Chemical and thermal development of ore-forming solutions in the Harz Mountains: a summary of fluid inclusion studies. Monogr Ser Miner Depos, 30, 117–32.

Ludwig, F., Stober, I., and Bucher, K. (2011). Hydrochemical groundwater evolution in the bunter sandstone sequence of the Odenwald mountain range, Germany: a laboratory and field study. *Aquatic geochemistry*, *17*(2), 165-193.

Marks, M.A., Marschall, H.R., Schühle, P., Guth, A., Wenzel, T., Jacob, D.E., Barth, M. Markl, G., 2013. Trace element systematics of tourmaline in pegmatitic and hydrothermal systems from the Variscan Schwarzwald (Germany): The importance of major element composition, sector zoning, and fluid or melt composition. Chemical Geology, 344, 73-90.

Mavromatis, V., Meister, P., Oelkers, E.H., 2014. Using stable Mg isotopes to distinguish dolomite formation mechanisms: A case study from the Peru Margin. Chemical Geology, 1 - 33.

Metz, R., Richter, M., Schürenberg, H., 1957. Die Blei-Zink-Erzgänge des Schwarzwaldes. Beiheft Geologisches Jahrbuch, 29: 277.

Meyer, M., Brockhamp, O., Clauer, N., Renk, A., Zuther, M., 2000. Further evidence for a Jurassic mineralizing event in central Europe: K-Ar dating of hydrothermal alteration and fluid inclusion systematics in wall rocks of the Käfersteige fluorite vein deposit in the northern Black Forest, Germany. Mineral. Dep., 35, 754–761.

Muchez, P., Heijlen, W., Banks, D., Blundell, D., Boni, M., Grandia, F., 2005. 7: Extensional tectonics and the timing and formation of basin-hosted deposits in Europe. Ore Geology Reviews, 27: 241-267.

Nitsch, E., Zedler, H., 2009. Oberkarbon und Perm in Baden-Württemberg. LGRB-Informationen, 22:7-102; Freiburg i.Br.

Opfergelt, S., Georg, R. B., Delvaux, B., Cabidoche, Y. M., Burton, K. W., Halliday, A. N. 2012. Mechanisms of magnesium isotope fractionation in volcanic soil weathering sequences, Guadeloupe. *Earth and Planetary Science Letters*, *341*, 176-185.

Pauwels, H., Fouillac, C., Fouillac, A.M., 1993. Chemistry and isotopes of deep geothermal saline fluids in the Upper Rhine Graben: Origin of compounds and water-rock interactions. Geochimica et Cosmochimica Acta, 57(12): 2737-2749.

Pfaff, K., Hildebrandt, L.H., Leach, D.L., Jacob, D.E., Markl, G., 2010. Formation of the Wiesloch Mississippi Valley-type Zn-Pb-Ag deposit in the extensional setting of the Upper Rhinegraben, SW Germany. Mineralium Deposita, 45, 7, 647-666.

Pfaff, K., Koenig, M.A., Wenzel, T., Ridley, I., Hildebrandt, L.H., Leach, D.L. Markl, G. 2011. Trace and minor element variations and sulfur isotopes in crystalline and colloform ZnS: Incorporation mechanisms and implications for their genesis. Chemical Geology, 286, 3-4, 118-134.

Pfaff, K., Romer, R.L., Markl, G., 2009. U-Pb ages of ferberite, chalcedony, agate, "U-mica" and pitchblende: constraints on the mineralization history of the Schwarzwald ore district. European journal of mineralogy, 21, 817-836.

Raffensperger, J. P., Garven, G., 1995. The formation of unconformity-type uranium ore deposits; 2, Coupled hydrochemical modeling. *American Journal of Science*, *295*(6), 639-696.

Rich, J. L., 1931. Source and date of accumulation of oil in granite ridge pools of Kansas and

Oklahoma. AAPG Bulletin, 15(12), 1431-1452.

Richard, A., Banks, D.A., Mercadier, J., Boiron, M.C., Cuney, M., Cathelineau, M., 2011. An evaporated seawater origin for the ore-forming brines in unconformity-related uranium deposits (Athabasca Basin, Canada): Cl/Br and δ37Cl study of fluid inclusions. GeochimCosmochim Acta 75:2792–2810

Riechelmann, S., Buhl, D., Schröder-Ritzrau, A., Spötl, C., Riechelmann, D.F.C., Richter, D.K., Kluge, T., Marx, T., Immenhauser, A., 2012. Hydrogeochemistry and fractionation pathways of Mg isotopes in a continental weathering system: Lessons from field experiments. Chemical Geology, 300: 109-122.

Rupf, I., Nitsch, E., 2008. Das Geologische Landesmodell von Baden-Württemberg: Datengrundlagen, technische Umsetzung und erste geologische Ergebnisse. LGRB-Information, 21.

Russell, M.J., Solomon, M., Walshe, J.L., 1981. The genesis of sediment-hosted, exhalative zinc + lead deposits. Mineralium Deposita, 16(1): 113-127.

Schaltegger, U., 2000. U–Pb geochronology of the Southern Black Forest Batholith (Central Variscan Belt): timing of exhumation and granite emplacement. *International Journal of Earth Sciences*, *88*(4), 814-828.

Schwarz, M., Henk, A., 2005. Evolution and structure of the Upper Rhine Graben: insights from three-dimensional thermomechanical modelling. International Journal of Earth Science, 94: 732-750.

Schwinn, G., and Markl, G., (2005) REE systematics in hydrothermal fluorite. Chemical Geology, 216, 225-248.

Schwinn, G., Wagner, T., Baatartsogt, B., Markl, G., 2006. Quantification of mixing processes in ore-forming hydrothermal systems by combination of stable isotope and fluid inclusion analyses. Geochimica et Cosmochimica Acta, 70: 965-982.

Seward, T.M., Barnes, H.L., 1997. Metal transport by hydrothermal ore fluids. *Geochemistry of hydrothermal ore deposits*, *3*, 435-486.

Sibson, R.H., 1995. Selective fault reactivation during basin inversion: potential for fluid redistribution through fault-valve action. *Geological Society, London, Special Publications*, *88*(1), 3-19

Staude, S., Bons, P.D., Markl, G., 2009. Hydrothermal vein formation by extension-driven dewatering of the middle crust: An example from SW Germany. Earth and Planetary Science Letters 286, 387-395.

Staude, S., Dorn, A., Pfaff, K., Markl, G., 2010a. Assemblages of Ag-Bi sulfosalts and conditions of their formation: the type locality of schapbachite ($Ag_{0.4}Pb_{0.2}Bi_{0.4}S$) and neighboring mines in the Schwarzwald ore district, southern Germany. Canadian Mineralogist 48, 441-466.

Staude, S., Mordhorst, T., Neumann, R., Prebeck, W., Markl, G., 2010b. Compositional variation of the tennantite-tetrahedrite solid-solution series in the Schwarzwald ore district (SW Germany): The role of mineralization processes and fluid source. Mineralogical Magazine 74, 309-339.

Staude, S., Göb, S., Pfaff, K., Ströbele, F., Premo, W.R., Markl, G., 2011a. Deciphering fluid sources of hydrothermal systems: A combined Sr- and S-isotope study on barite (Schwarzwald, SW Germany). Chemical Geology 286, 1-20.

Staude, S., Göb, S., Pfaff, K., Ströbele, F., Premo, W.R., Markl, G., 2011b. Deciphering fluid sources of hydrothermal systems: a combined Sr-and S-isotope study on barite (Schwarzwald, SW Germany). Chemical Geology 286, 1-20.

Staude, S., Mordhorst, T., Nau, S., Pfaff, K., Brügmann, G., Jacob, D.E., Markl, G., 2012a. hydrothermal carbonates of the Schwarzwald ore district, southwestern Germany:

carbon source and conditions of formation using δ18O, δ13C, 87Sr/86Sr, and fluid inclusions. The Canadian Mineralogist 50, 1401-1434.

Staude, S., Werner, W., Mordhorst, T., Wemmer, K., Jacob, D., Markl, G., 2012b. Multi-stage Ag–Bi–Co–Ni–U and Cu–Bi vein mineralization at Wittichen, Schwarzwald, SW Germany: geological setting, ore mineralogy, and fluid evolution. Mineralium Deposita 47, 251-276.

Stober, I., and Bucher, K., 1999a, Deep groundwater in the crystalline basement of the Black Forest region: Applied Geochemistry, v. 14, p. 237-254.

Stober, I., and Bucher, K., 1999b. Origin of salinity of deep groundwater in crystalline rocks. *Terra Nova-Oxford*, *11*(4), 181-185.

Stober, I., Richter, A., Brost, E., and Bucher, K., 1999. The Ohlsbach Plume–Discharge of deep saline water from the crystalline basement of the Black Forest, Germany. *Hydrogeology Journal*, *7*(3), 273-283.

Stober, I., and Bucher, K.,, 2004, Fluid sinks within the earth's crust: Geofluids, v. 4, p. 143-151.

Stober, I., and Bucher, K., 2005a. The upper continental crust, an aquifer and its fluid: hydaulic and chemical data from 4 km depth in fractured crystalline basement rocks at the KTB test site. *Geofluids*, *5*(1), 8-19.

Stober, I., and Bucher, K., 2005b. Deep-fluids: Neptune meets Pluto. *Hydrogeology Journal*, *13*(1), 112-115.

Stober, I., and Bucher, K., 2007. Hydraulic properties of the crystalline basement. *Hydrogeology Journal*, *15*(2), 213-224.

Stober, I., and Bucher, K., 2014. Permeability and Fluid Flow in the Upper Continental Crust. In *2014 GSA Annual Meeting in Vancouver, British Columbia*.

Stober, I., and Bucher, K., 2015a. Hydraulic conductivity of fractured upper crust: insights from hydraulic tests in boreholes and fluid-rock interaction in crystalline basement rocks. *Geofluids*, *15*(1-2), 161-178

Stober, I., and Bucher, K., 2015b. Significance of Hydraulic Conductivity as Precondition to Fluid Flow in Fractured and Faulted Crystalline Basement and its Impact on Fluid-Rock Interaction Processes. *Significance*, *19*, 25.

Stober, I., 2011. Depth-and pressure-dependent permeability in the upper continental crust: data from the Urach 3 geothermal borehole, southwest Germany. *Hydrogeology Journal*, *19*(3), 685-699.

Stober, I., 2013. Geothermal fluid and reservoir properties in the Upper Rhine Graben, Europe. In Second EAGE Sustainable Earth Sciences (SES) Conference and Exhibition.

Stoffell, B., Appold, M.S., Wilkinson, J.J., McClean, N.A., Jeffries, T.E., 2008, Geochemistry and evolution of Mississippi Valley-Type mineralizing brines from the Tri-State and northern Arkansas districts determined by LA-ICP-MS microanalysis of fluid inclusions: Economic Geology, v. 103, p. 1411-1435.

Ströbele, F., Staude, S., Pfaff, K., Premo, W.R., Hildebrandt, L.H., Baumann, A., Pernicka, E., Markl, G., 2012. Pb isotope constraints on fluid flow and mineralization processes in SW Germany Neues Jahrbuch für Mineralogie-Abhandlungen: Journal of Mineralogy and Geochemistry 189, 287-309.

Sverjensky, D.A., 1984. Oil field brines as ore-forming solutions. Economic Geology, 79(1): 23-37.

Sverjensky, D.A., 1987. The role of migrating oil field brines in the formation of sediment-hosted Cu-rich deposits. Economic Geology, 82(5): 1130-1141.

Tipper, E.T., Gaillardet, J., Louvat, P., Capmas, F., White, A.F., 2010. Mg isotope constraints on soil pore-fluid chemistry: evidence from Santa Cruz, California. Geochimica et Cosmochimica Acta, 74(14): 3883-3896.

Todt, W., 1976. Zirkon U/Pb-Alter des Malsburg-Granits vom Südschwarzwald. Neues Jahrb Mineral Monatsh 12, 532-544.

Wagner, T., Cook, N.J., 2000. Late-Variscan antimony mineralisation in the Rheinisches Schiefergebirge, NW Germany: evidence for stibnite precipitation by drastic cooling of high-temperature fluid systems. Mineralium Deposita, 35, 206-222.

Walter, B.F., Immenhauser, A., Geske, A., Markl, G., 2015. Exploration of hydrothermal carbonate magnesium isotope signatures as tracers for continental fluid aquifers, Schwarzwald mining district, SW Germany. Chemical Geology.

Werner, W., Franzke, H.J., Wirsing, G., Jochum, J., Lüders, V. Wittenbrink, 2002. mit einem Beitrag von B. Steiber: Die Erzlagerstätte Schauinsland bei Freiburg im Breisgau. Bergbau, Geologie, Hydrogeologie, Mineralogie, Geochemie, Tektonik und Lagerstättenentstehung. - Ber. Naturforsch. Ges. Freiburg, 92: 110 S., 26 Abb., 9 Tab., 16 Taf.; Freiburg i. Br.

Werner, W., 2011. Mineralische Rohstoffe. - In: Hann, P. & Zedler, H.: Erläuterungen zum Blatt 8113 Todtnau: 98-115, 3 Abb.; Freiburg i. Br. (LGRB, Hrsg.).

Wernicke, R.S., Lippolt, H.J., 1997. (U+ Th)–He evidence of Jurassic continuous hydrothermal activity in the Schwarzwald basement, Germany. Chemical Geology, 138, 273-285.

Wernicke, R.S., Lippolt, H.J., 1993. Botryoidal hematite from the Schwarzwald (Germany): heterogeneous uranium distributions and their bearing on the helium dating method. Earth and planetary science letters, 114, 287-300.

Wilkinson, J., Eyre, S., and Boyce, A., 2005, Ore-forming processes in Irish-type carbonate-hosted Zn-Pb deposits: evidence from mineralogy, chemistry, and isotopic composition of sulfides at the Lisheen Mine: Economic Geology, v. 100, no. 1, p. 63-86.

Wilkinson, J.J., 2010. A review of fluid inclusion constraints on mineralization in the Irish ore field and implications for the genesis of sediment-hosted Zn-Pb deposits. Economic Geology, 105: 417-442.

Wimpenny, J., Colla, C.A., Yin, Q.-Z., Rustad, J.R., Casey, W.H., 2014a. Investigating the behaviour of Mg isotopes during the formation of clay minerals. Geochimica et Cosmochimica Acta, 128: 178-194.

Wimpenny, J., Yin, Q.-Z., Tollstrup, D., Xie, L.-W., Sun, J., 2014b. Using Mg isotope ratios to trace Cenozoic weathering changes: A case study from the Chinese Loess Plateau. Chemical Geology, 376: 31-43.

Worden, R.H., Heasley, E.C., Barclay, S.A. 1999. The effects of petroleum emplacement on diagenesis: a comparison between sandstone and carbonate reservoirs, in Sciences Geologiques, Strasbourg, Mem, 100.

Yardley, B.W.D., 2005. Metal concentrations in crustal fluids and their relationship to ore formation. Economic Geology, 100: 613-632.

Ziegler, P.A., 1990. Geological Atlas of Western and central Europe.

5. Anhang 1

Bons, P. D., Fusswinkel, T., Gomez-Rivas, E., Markl, G., Wagner, T., & Walter, B. (2014). Fluid mixing from below in unconformity-related hydrothermal ore deposits. Geology, 42(12), 1035-1038.

akzeptiert zur Veröffentlichung	Anzahl der Autoren	Position des Kandidaten in der Autorenliste	Wissen-schaftliche Idee des Kandidaten (%)	Datengenerier-ung des Kandidaten (%)	Analysen und Interpretat-ionen des Kandidaten (%)	Verfassen der Publikation durch den Kandidaten (%)
ja	6	6	10	10	10	10

Geology, published online on 15 October 2014 as doi:10.1130/G35708.1

Fluid mixing from below in unconformity-related hydrothermal ore deposits

Paul D. Bons[1], Tobias Fusswinkel[2], Enrique Gomez-Rivas[1,3], Gregor Markl[1], Thomas Wagner[2], and Benjamin Walter[1]
[1]Department of Geosciences, Eberhard Karls University Tübingen, Wilhelmstrasse 56, 72074 Tübingen, Germany
[2]Department of Geosciences and Geography, University of Helsinki, Gustaf Hällströmin katu 2a, FI-00014 Helsinki, Finland
[3]Department of Geology and Petroleum Geology, School of Geosciences, King's College, University of Aberdeen, Aberdeen AB24 3UE, UK

ABSTRACT

Unconformity-related hydrothermal ore deposits typically form by mixing of hot, deep, rock-buffered basement brines and cooler fluids derived from the surface or overlying sediments. Current models invoking simultaneous downward and upward flow of the mixing fluids are inconsistent with fluid overpressure indicated by fracturing and brecciation, fast fluid flow suggested by thermal disequilibrium, and small-scale fluid composition variations indicated by fluid inclusion analyses. We propose a new model where fluids first descend, then evolve while residing in pores and later ascend. We use the hydrothermal ore deposits of the Schwarzwald district in southwest Germany as an example. Oldest fluids reach the greatest depths, where long residence times and elevated temperatures allow them to equilibrate with their host rock, to reach high salinity, and to scavenge metals. Youngest fluids can only penetrate to shallower depths and can (partially) retain their original signatures. When fluids are released from different levels of the crustal column, these fluids mix during rapid ascent in hydrofractures to form hydrothermal ore deposits. Mixing from below during ascent provides a viable hydromechanical mechanism to explain the common phenomenon of mixed shallow and deep fluids in the formation of hydrothermal ore deposits.

INTRODUCTION

Mixing of fluids from different origins is often invoked for major unconformity-related hydrothermal ore deposits that have formed in a variety of geological contexts, such as the world-class uranium deposits of the Athabasca Basin (Canada) and McArthur River (Australia), and the Pb-Zn(-Ag) deposits of the Irish Midlands, the Alaskan Brooke Range (USA), the Massif Central (France), and Upper Silesia (Poland), among others. Geochemical evidence for fluid mixing comes from stable and radiogenic isotope signatures, mineral composition data, and fluid-inclusion compositions, including halogen ratios (Goldhaber et al., 1995; Staude et al., 2009, 2012; Boiron et al., 2010; Wilkinson, 2010; Kendrick et al., 2011; Fusswinkel et al., 2013). Mesozoic, unconformity-related hydrothermal deposits of the Schwarzwald district in southwest Germany are representative of a large range of deposits where mixing of (1) hot, basement-derived fluids from below and (2) cooler, surface or sediment-derived fluids from above is invoked in the absence of igneous activity to drive fluid circulation (Staude et al., 2009, 2012, and references therein). Fluid circulation driven by topography or igneous activity can be excluded for the Mesozoic deposits in the Schwarzwald (Staude et al., 2009, 2012).

Although the geochemical evidence of mixing processes appears undeniable, it is unclear how the mixing process proceeds physically. Some authors propose fluid-flow trajectories that converge on the ore deposition site, where mixing takes place (e.g., Boiron et al., 2010; Kendrick et al., 2011). This would imply a local low in the hydraulic head field, violating the condition of a divergence-free potential field in the absence of fluid sinks (Bons et al., 2012). Even if such a low would occur by dilation, it would only be transient, as the influx of fluids would quickly raise the local hydraulic head.

Large-scale fluid circulation has been proposed and modeled to explain the infiltration of surface-derived fluids down to mid-crustal levels (e.g., Matthäi et al., 2004; Oliver et al., 2006a; Person et al., 2007). However, these models assumed a hydrostatic background fluid pressure gradient throughout the whole system, necessary to achieve convection, but unrealistic at depths where rocks mainly deform by ductile flow and cannot maintain large differences between hydrostatic fluid pressure and lithostatic pressure (~100 MPa and 270 MPa at 10 km depth, respectively). Compaction and fracture sealing would reduce porosity and permeability at such depths, and fluid pressure would rise. In the models, permeability and porosity are usually kept constant, ignoring these effects. Hydrothermal ore deposits typically show evidence of fluid overpressure, such as repeated fracturing and brecciation (Cox, 2010; Weisheit et al., 2013). Fluid overpressure is difficult to reconcile with a fluid pressure gradient that is overall close to hydrostatic, or with convergent fluid flow.

Hydrothermal fluids are, by definition (Davies and Smith, 2006), hotter than their surroundings. In the case of slow fluid percolation, fluid and matrix temperatures remain in local equilibrium (de Marsily, 1986). The average distance, $\langle x \rangle$, from a perturbation, over which heat diffuses, by conduction alone, over a time interval, Δt, is determined by the thermal diffusivity, here taken as $D_T = 10^{-6}$ m^2/s, through:

$$\langle x \rangle = \sqrt{D_T \Delta t}. \quad (1)$$

Taking, for example, Δt = 800 k.y., as used by Matthäi et al. (2004), gives $\langle x \rangle \approx 5$ km. This means that the elevated temperature found in a hydrothermal deposit should spread over a few kilometers, if duration of fluid flow is on the order of hundreds of thousands of years. For the thermal perturbation to spread over only a few meters, i.e., $\langle x \rangle \approx 1$ m, duration of fluid flow should be on the order of 10 days at most. It follows that flow rates must be more than six orders of magnitude faster than assumed in classical percolative flow models, such as that of Matthäi et al. (2004), and that therefore Darcy flow through porous media does not apply. Instead, flow must occur in short bursts of fracture flow (Bons, 2001; Bons and van Milligen, 2001). Fluid ascent in hydrofractures can potentially reach velocities of meters per second in the case of aqueous fluids (Dahm, 2000). Minimum ascent velocities of >0.01 m/s were estimated for natural veins from the Sanbagawa belt in Japan (Okamoto and Tsuchiya, 2009) and >1 m/s for fluidized hydrothermal breccia pipes from Cloncurry, Australia (Oliver et al., 2006b). With tectonic events leading to hydrothermal activity probably lasting hundreds of thousands of years to even >100 m.y. (Weisheit et al., 2013), and fluid flow events lasting on the order of days, these bursts would occur months, if not years, apart (Bons, 2001).

In summary, brecciation, indicating fluid overpressure (except in the case of implosion breccias), and strong thermal disequilibrium (Wagner et al., 2010; Beaudoin et al., 2014), indicating fast fluid flow, are incompatible with common models of crustal-scale fluid circulation. The hydrothermal ore deposits in the Schwarzwald (Fig. 1A) show clear evidence for fluid mixing (Fusswinkel et al., 2013). Staude et al. (2009) argued that sufficient fluid volumes to produce the deposits could have been released from below the deposits. Here we propose a new model integrating these observations and accounting for transport and mixing in a physi-

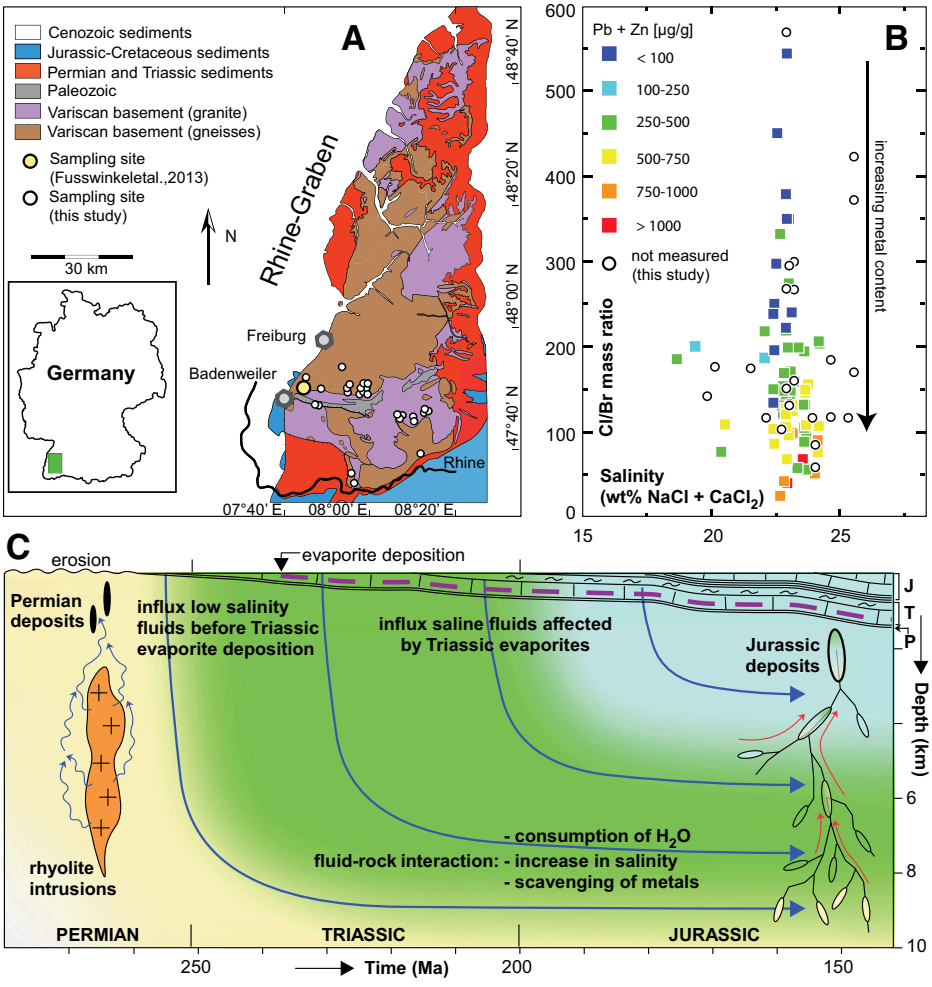

Figure 1. A: Simplified geological map of southern Schwarzwald district in southwestern Germany (modified after Hann and Zedler, 2008), showing locations of study area and sample sites. B: Cl/Br ratios versus salinity of fluid inclusions in hydrothermal veins at localities shown in A. Colored squares are microthermometry and in-situ laser ablation–inductively coupled plasma–mass spectrometry data of fluid inclusions from a single quartz crystal presented by Fusswinkel et al. (2013), showing sample-scale covariation of decreasing metal contents with increasing Cl/Br ratio. Open circles are for microthermometry and crush-leach analyses on gangue minerals from several localities in the Schwarzwald district, encompassing the same range in halogen ratios (see Table DR1 [see footnote 1]). C: Schematic diagram illustrating fluid evolution in Schwarzwald basement and overlying Permian (P), Triassic (T), and Jurassic (J) sediments, from first exhumation in the Permian (left) to Jurassic formation of hydrothermal ore (right). Blue arrows show fluid pathways in space (vertical) and time (horizontal). Oldest fluids (yellow) infiltrated in the Permian and penetrated deepest levels. Triassic (green) and Jurassic (blue) fluids descended less and had shorter residence times. Fractures tapped and mixed fluids from all levels of the crustal column during ore formation.

cally plausible way. Fluids first descended below an unconformity and were later released and expelled upwards, when mixing of fluids with contrasting geochemical signatures occurred.

HYDROTHERMAL SYSTEMS OF THE SCHWARZWALD DISTRICT

The Schwarzwald district in southwest Germany combines a well-known, variable geology with >1000 hydrothermal mineral deposits (Fig. 1A). It consists of Variscan basement (mostly S-type granites and gneisses), which is unconformably overlain by a 1.5-km-thick succession of Permian–Triassic and Jurassic clastic sediments and limestones. Of particular relevance is a 250 Ma, ~100-m-thick evaporite sequence (up to the halite stage) intercalated in the Triassic limestones. Due to Paleogene tectonic tilting, the whole succession is exposed from the Jurassic in the east down to ~2 km below the unconformity in the southwest. The hydrothermal veins occur within both basement rocks and the sedimentary cover. Formation ages indicate hydrothermal activity since Variscan times, peaking in the Jurassic, at which time the area was covered by a shallow sea and no significant tectonic or igneous activity is known (Staude et al., 2009, and references therein).

The deposits are fracture-hosted veins with breccias that indicate repeated fracturing and mineral precipitation. There is no known significant fault activity at the time of ore formation, and the deposits lack evidence for tectonic movements along the fractures. This suggests that space for mineral precipitation was produced by overpressured fluids. Fluid-inclusion studies (Staude et al., 2012, and references therein) demonstrate temperatures of ~150 ± 50 °C for the Jurassic fluids. For veins formed at 2–3 km depth, this is more than 50 °C hotter than the country rock, while fluid pressure may reach 20 MPa in excess of ambient pressure (Baatartsogt et al., 2007).

Geochemical and isotopic data indicate mixing of contrasting fluids that have characteristics of typical basement brines and sedimentary formation waters (Schwinn et al., 2006; Staude et al., 2012; Fusswinkel et al., 2013). Fusswinkel et al. (2013) analyzed a single crystal in a basement-hosted vein mineralization (1 km below the unconformity) of Jurassic age and found evidence for mixing of two distinct fluid end members (Fig. 1B). One is a hot, saline (22 ± 2 wt% NaCl + $CaCl_2$), rock-buffered brine with elevated base metal (Zn, Pb) content and low Cl/Br mass ratios (<100). The other end member is equally saline, is metal poor, and has high Cl/Br ratios that indicate dissolution of halite, for which the only candidates are the Triassic evaporites. The data obtained by laser ablation–inductively coupled plasma–mass spectrometry analysis of individual fluid inclusions show a remarkable variation in fluid composition at the scale of individual growth zones. Such variations could only have been recorded if the different fluids had very little contact time, and therefore flow rates were high, as diffusion would have quickly equalized compositions (cf. Equation 1). Crush-leach and microthermometry analyses on fluid inclusions in gangue minerals in a number of ore deposits confirm that the strongly varying Cl/Br ratios and relatively constant salinities are found throughout the southern Schwarzwald (Fig. 1B; see the GSA Data Repository[1] for methods, and Table DR1 therein).

GETTING FLUIDS DOWN

Following the Variscan orogeny, the crystalline basement of the Schwarzwald was exhumed during the Permian. Fluid inclusions in Permian quartz (± Sb) veins have low (0–5 wt%) salinities and are mostly barren (Staude et al., 2009). This indicates that fluids in the crystalline basement were not yet saline and that the observed

[1]GSA Data Repository item 2014359, crush-leach and microthermometry method and data, is available online at www.geosociety.org/pubs/ft2014.htm, or on request from editing@geosociety.org or Documents Secretary, GSA, P.O. Box 9140, Boulder, CO 80301, USA.

high salinities in Mesozoic fluids must have developed later. The German Continental Deep Drilling Project (KTB) encountered fluid-filled porosity down to a depth of 9 km (Emmermann and Lauterjung, 1997). From this, we infer that the exhumed Schwarzwald basement would have been infiltrated or soaked with fluids from above, down to at least similar depths (~10 km), starting in the Permian.

In the absence of a topographic drive, downflow may have been caused by desiccation of fluids via mineral hydration reactions at depth (Stober and Bucher, 2004; Bons and Gomez-Rivas, 2013), causing a downward flux to replenish consumed H_2O. The source of these fluids was initially surface fluid (rainwater or seawater) and later fluids trapped in pores of the overlying sediments. Desiccation and drawdown would have caused a progressive increase in salinity with depth, which is consistent with the increase in salinity observed at the KTB site (Emmermann and Lauterjung, 1997). The progressive increase in salinity and the corresponding reduction of H_2O activity, near-exhaustive hydration of basement rocks, and/or reduction of porosity and permeability by hydration reactions can slow or even stop the process. Fluid pressure can begin to rise and equilibrate with the lithostatic pressure once it is no longer reduced by H_2O consumption and/or permeability is sufficiently reduced by compaction and sealing. Over time, supra-hydrostatic fluid pressure may thus develop at depth.

Ingression of fluids since late Variscan times would have resulted in fluids increasing in age with depth, with the oldest fluids at the base of the column (Fig. 1C) being ~100 m.y. old by the time of Jurassic ore formation. This is a conceivable residence time for basement fluids (Bottomley et al., 2002; Fehn and Snyder, 2005). These fluids modified their chemistry by reactive interaction with their rock matrix, while higher temperatures at depth allowed for efficient uptake of metals by chloride complexation (Yardley, 2005). This explains the low Na/Ca ratio and elevated Pb and Zn concentrations of the saline deep basement fluid end member in the Schwarzwald (Fig. 1B; Fusswinkel et al., 2013). The deep basement fluids are also characterized by a low Cl/Br ratio, typical of such fluids worldwide (Bucher and Stober, 2010, and references therein), which may be related to bittern ingression (Boiron et al., 2010; Wilkinson, 2010) during deposition of the Triassic evaporites or, alternatively, to leaching of basement rocks (e.g., Bucher and Stober, 2010).

After ca. 250 Ma, fluids entering from above were affected by the Triassic evaporites, which would have given them a high salinity and high Cl/Br ratios (Bucher and Stober, 2010). With older fluids already residing at depth, these new fluids remained at shallower depths, where cooler temperatures inhibited extensive fluid-rock interaction. They could thus preserve their Triassic evaporite signature without significant uptake of metals or exchange of alkalis. These fluids constitute the saline, metal-poor, high Cl/Br, high Na/Ca end member in the Schwarzwald (Fig. 1B). Today, the upper crustal fluid system in the Schwarzwald is still stratified, the uppermost ~2 km being filled by a Ca-HCO_3 water possibly related to carbonate dissolution at shallow depths; below this layer, typical continental Na-Cl brines are still present today (Bucher and Stober, 2010).

FLUID ASCENT AND MIXING

Fluid pressure in the crustal column increases from hydrostatic at the top to close to lithostatic at depth. Reduction of the overburden pressure, i.e., decompression, does not, initially, change the fluid pressure in pores as their volume remains approximately the same (Staude et al., 2009). This can cause the pore fluid pressure to exceed the host rock pressure, leading to the formation of fractures through which fluids can escape. Decompression can result from erosion or thinning of the crust, as well as crustal extension, where reduction of the horizontal stress reduces the pressure, which is the mean of the principal stresses. Staude et al. (2009) showed that decompression by crustal extension and thinning can provide sufficient fluids to produce the Jurassic ore deposits in the Schwarzwald.

Initial microcracks link up, creating ever-bigger fractures in a step-wise fashion, as described for fluids and melt (Bons and van Milligen, 2001). Once these hydrofractures, filled with buoyant fluid, exceed a critical length (on the order of tens of meters) they can become "mobile" by upward tip propagation and ascend rapidly through the crust (Weertman, 1971; Bons, 2001). Fluid is released from different levels of the column and expelled upwards. Deeper fluids ascend through shallower parts of the crust, causing mixing of fluids from various levels. Mixing is expected to be variable, with some batches quickly ascending without much interaction with other fluids, while others may merge and mix with other batches.

We suggest that ascending fluids are arrested at shallow crustal levels where fluid pressure is low, thus allowing fluids to spread into joints and fractures, or discontinuities, such as the post-Variscan unconformity. Bedding may also stop propagation of hydrofractures (Bons, 2001). The arrested fluids are strongly out of equilibrium with the conditions at their final arrest level. Disequilibrium and mixing of fluids with contrasting physicochemical properties cause efficient precipitation of dissolved mineral content to form ore deposits. The heterogeneous fluid signatures reflect the range of fluids sampled in the rock column below, as well as mixing between deep fluids and the high-Cl/Br connate fluids in near-hydrostatic fluid reservoirs at shallow levels. Deposited minerals and metals depend on the lithologies below, especially at depth, where most elements are scavenged.

CONCLUSIONS

Mixing of fluids is common in unconformity-related hydrothermal ore deposits. Using the Schwarzwald district in Germany as an example, we propose that fluids first infiltrate into basement rocks from above. The oldest fluids reach the greatest depth, where these can equilibrate with their host rock and scavenge metals. The youngest fluids carry and maintain the signature of more recent sediments that were deposited on top of the unconformity. Rapidly ascending hydrofractures tap fluids from all levels of the infiltrated rock column, mixing these during ascent. The resulting mineral deposits thus show signatures of both fluid types. Separating fluid descent and ascent in time and mixing fluids during ascent provides a physically viable mechanism that explains the mineralogical and geochemical characteristics of the Schwarzwald ore deposits and may be applicable to many other unconformity-related hydrothermal ores.

ACKNOWLEDGMENTS

This research was partly funded by German Research Foundation (DFG) grant BO 1776/8 and was carried out within the framework of DGMK (German Society for Petroleum and Coal Science and Technology) project 718, funded by the companies ExxonMobil Production Deutschland GmbH, GDF SUEZ E&P Deutschland GmbH, RWE Dea AG, and Wintershall Holding GmbH. Assistance by Simone Kaulfuss, Gabi Stoschek, Sara Ladenburger, Mathias Burisch, and Bernd Steinhilber with sample preparation and crush-leach analyses is gratefully acknowledged. We thank Steve Cox and two anonymous reviewers for their critical comments.

REFERENCES CITED

Baatartsogt, B., Schwinn, G., Wagner, T., Taubald, H., Beitter, T., and Markl, G., 2007, Contrasting paleofluid systems in the continental basement: A fluid inclusion and stable isotope study of hydrothermal vein mineralization, Schwarzwald district, Germany: Geofluids, v. 7, p. 123–147, doi:10.1111/j.1468-8123.2007.00169.x.

Beaudoin, N., Bellahsen, N., Lacombe, O., Emmanuel, L., and Pironon, J., 2014, Crustal-scale fluid flow during the tectonic evolution of the Bighorn Basin (Wyoming, USA): Basin Research, v. 26, p. 403–435, doi:10.1111/bre.12032.

Boiron, M.C., Cathelineau, M., and Richard, A., 2010, Fluid flows and metal deposition near basement/cover unconformity: Lessons and analogies from Pb-Zn-F-Ba systems for the understanding of Proterozoic U deposits: Geofluids, v. 10, p. 270–292, doi:10.1111/j.1468-8123.2010.00289.x.

Bons, P.D., 2001, The formation of large quartz veins by rapid ascent of fluids in mobile hydrofractures: Tectonophysics, v. 336, p. 1–17, doi:10.1016/S0040-1951(01)00090-7.

Bons, P.D., and Gomez-Rivas, E., 2013, Gravitational fractionation of isotopes and dissolved components as a first-order process in hydrothermal crustal fluids: Economic Geology and the Bulletin of the Society of Economic Geologists, v. 108, p. 1195–1201, doi:10.2113/econgeo.108.5.1195.

Bons, P.D., and van Milligen, B.P., 2001, New experiment to model self-organized critical transport and accumulation of melt and hydrocarbons from their source rocks: Geology, v. 29, p. 919–922, doi:10.1130/0091-7613(2001)029<0919:NETMSO>2.0.CO;2.

Bons, P.D., Elburg, M.A., and Gomez-Rivas, E., 2012, A review of the formation of tectonic veins and their microstructures: Journal of Structural Geology, v. 43, p. 33–62, doi:10.1016/j.jsg.2012.07.005.

Bottomley, D.J., Renaud, R., Kotzer, T., and Clark, I.D., 2002, ^{129}I constraints on residence times of deep marine brines in the Canadian Shield: Geology, v. 30, p. 587–590, doi:10.1130/0091-7613(2002)030<0587:ICORTO>2.0.CO;2.

Bucher, K., and Stober, I., 2010, Fluids in the upper continental crust: Geofluids, v. 10, p. 241–253.

Cox, S.F., 2010, The application of failure mode diagrams for exploring the roles of fluid pressure and stress states in controlling styles of fracture-controlled permeability enhancement in faults and shear zones: Geofluids, v. 10, p. 217–233, doi:10.1111/j.1468-8123.2010.00281.x.

Dahm, T., 2000, On the shape and velocity of fluid-filled fractures in the Earth: Geophysical Journal International, v. 142, p. 181–192, doi:10.1046/j.1365-246x.2000.00148.x.

Davies, G.R., and Smith, L.B., 2006, Structurally controlled hydrothermal dolomite reservoir facies: An overview: AAPG Bulletin, v. 90, p. 1641–1690, doi:10.1306/05220605164.

de Marsily, G., 1986, Quantitative Hydrogeology: Groundwater Hydrology for Engineers: San Diego, California, Academic Press, Inc., 440 p.

Emmermann, R., and Lauterjung, J., 1997, The German Continental Deep Drilling Program KTB: Overview and major results: Journal of Geophysical Research, v. 102, p. 18,179–18,201, doi:10.1029/96JB03945.

Fehn, U., and Snyder, G.T., 2005, Residence times and source ages of deep crustal fluids: Interpretation of ^{129}I and ^{36}Cl results from the KTB-VB drill site, Germany: Geofluids, v. 5, p. 42–51, doi:10.1111/j.1468-8123.2004.00105.x.

Fusswinkel, T., Wagner, T., Wälle, M., Wenzel, T., Heinrich, C.A., and Markl, M., 2013, Fluid mixing forms basement-hosted Pb-Zn deposits: Insight from metal and halogen geochemistry of individual fluid inclusions: Geology, v. 41, p. 679–682, doi:10.1130/G34092.1.

Goldhaber, M.B., Church, S.E., Doe, B.R., Aleinikoff, J.N., Brannon, J.C., Podosek, F.A., Mosier, E.L., Taylor, C.D., and Gent, C.A., 1995, Lead and sulfur isotope investigation of Paleozoic sedimentary rocks from the southern midcontinent of the United States: Implications for paleohydrology and ore genesis of the southeast Missouri lead belts: Economic Geology and the Bulletin of the Society of Economic Geologists, v. 90, p. 1875–1910, doi:10.2113/gsecongeo.90.7.1875.

Hann, H.P., and Zedler, H., 2008, Variscan internides: Black Forest (Schwarzwald), *in* McCann, T., ed., The Geology of Central Europe, Variscan Tectonics, Volume 1: Precambrian and Palaeozoic: London, Geological Society of London, p. 599–665.

Kendrick, M.A., Honda, M., Oliver, N.H.S., and Phillips, D., 2011, The noble gas systematics of late-orogenic H_2O–CO_2 fluids, Mt Isa, Australia: Geochimica et Cosmochimica Acta, v. 75, p. 1428–1450, doi:10.1016/j.gca.2010.12.005.

Matthäi, S.K., Heinrich, C.A., and Driesner, T., 2004, Is the Mount Isa copper deposit the product of forced brine convection in the footwall of a major reverse fault?: Geology, v. 32, p. 357–360, doi:10.1130/G20108.1.

Okamoto, A., and Tsuchiya, N., 2009, Velocity of vertical fluid ascent within vein-forming fractures: Geology, v. 37, p. 563–566, doi:10.1130/G25680A.1.

Oliver, N.H.S., McLellan, J.G., Hobbs, B.E., Cleverley, J.S., Ord, A., and Feltrin, L., 2006a, Numerical models of extensional deformation, heat transfer, and fluid flow across basement-cover interfaces during basin-related mineralization: Economic Geology and the Bulletin of the Society of Economic Geologists, v. 101, p. 1–31, doi:10.2113/gsecongeo.101.1.1.

Oliver, N.H.S., Rubenach, M.J., Fu, B., Baker, T., Blenkinsop, T.G., Cleverley, J.S., Marshall, L.J., and Ridd, P.J., 2006b, Granite-related overpressure and volatile release in the mid crust: Fluidized breccias from the Cloncurry District, Australia: Geofluids, v. 6, p. 346–358, doi:10.1111/j.1468-8123.2006.00155.x.

Person, M., Mulch, A., Teyssier, C., and Gao, Y., 2007, Isotope transport and exchange within metamorphic core complexes: American Journal of Science, v. 307, p. 555–589, doi:10.2475/03.2007.01.

Schwinn, G., Wagner, T., Baatartsogt, B., and Markl, G., 2006, Quantification of mixing processes in ore-forming hydrothermal systems by combination of stable isotope and fluid inclusion analyses: Geochimica et Cosmochimica Acta, v. 70, p. 965–982, doi:10.1016/j.gca.2005.10.022.

Staude, S., Bons, P.D., and Markl, G., 2009, Hydrothermal vein formation by extension-driven dewatering of the middle crust: An example from SW Germany: Earth and Planetary Science Letters, v. 286, p. 387–395, doi:10.1016/j.epsl.2009.07.012.

Staude, S., Mordhorst, T., Nau, S., Pfaff, K., Brügmann, G., Jacob, D.E., and Markl, G., 2012, Hydrothermal carbonates of the Schwarzwald ore district, southwestern Germany: Carbon source and conditions of formation using δ^{18}O, δ^{13}C, ^{87}Sr/^{86}Sr, and fluid inclusions: Canadian Mineralogist, v. 50, p. 1401–1434, doi:10.3749/canmin.50.5.1401.

Stober, I., and Bucher, K., 2004, Fluid sinks within the Earth's crust: Geofluids, v. 4, p. 143–151, doi:10.1111/j.1468-8115.2004.00078.x.

Wagner, T., Boyce, A.J., and Erzinger, J., 2010, Fluid-rock interaction during formation of metamorphic quartz veins: A REE and stable isotope study from the Rhenish Massif, Germany: American Journal of Science, v. 310, p. 645–682, doi:10.2475/07.2010.04.

Weertman, J., 1971, Velocity at which liquid-filled cracks move in the Earth's crust or in glaciers: Journal of Geophysical Research, v. 76, p. 8544–8553, doi:10.1029/JB076i035p08544.

Weisheit, A., Bons, P.D., and Elburg, M.A., 2013, Long-lived crustal-scale fluid-flow: The hydrothermal mega-breccia of Hidden Valley, Mt. Painter Inlier, South Australia: International Journal of Earth Sciences, v. 102, p. 1219–1236, doi:10.1007/s00531-013-0875-7.

Wilkinson, J.J., 2010, A review of fluid inclusion constraints on mineralization in the Irish ore field and implications for the genesis of sediment-hosted Zn-Pb deposits: Economic Geology and the Bulletin of the Society of Economic Geologists, v. 105, p. 417–442, doi:10.2113/gsecongeo.105.2.417.

Yardley, B.W.D., 2005, Metal concentrations in crustal fluids and their relationship to ore formation: Economic Geology and the Bulletin of the Society of Economic Geologists, v. 100, p. 613–632, doi:10.2113/gsecongeo.100.4.613.

Manuscript received 25 March 2014
Revised manuscript received 1 September 2014
Manuscript accepted 3 September 2014

Printed in USA

Anhang 2

Walter, B.F., Burisch, M., & Markl, G., (in press) Long-term chemical evolution and modification of continental basement brines – a field study from the Schwarzwald, SW Germany

akzeptiert zur Veröffentlichung	Anzahl der Autoren	Position des Kandidaten in der Autorenliste	Wissen-schaftliche Idee des Kandidaten (%)	Datengenerier-ung des Kandidaten (%)	Analysen und Interpretat-ionen des Kandidaten (%)	Verfassen der Publikation durch den Kandidaten (%)
ja	3	1	40	80	60	50

doi: 10.1111/gfl.12167

GFL | Journal Code | 12167 | Manuscript No. | WILEY | Dispatch: 1.2.16 | No. of pages: 20 | CE: Arockia Raj | PE: Amul

REVIEW

Long-term chemical evolution and modification of continental basement brines – a field study from the Schwarzwald, SW Germany

B. F. WALTER, M. BURISCH AND G. MARKL

Department of Geosciences, Eberhard Karls University Tübingen, Tübingen, Germany

ABSTRACT

Highly saline, deep-seated basement brines are of major importance for ore-forming processes, but their genesis is controversial. Based on studies of fluid inclusions from hydrothermal veins of various ages, we reconstruct the temporal evolution of continental basement fluids from the Variscan Schwarzwald (Germany). During the Carboniferous (vein type i), quartz–tourmaline veins precipitated from low-salinity (<4.5wt% NaCl + $CaCl_2$), high-temperature (≤390°C) H_2O-NaCl-(CO_2-CH_4) fluids with Cl/Br mass ratios = 50–146. In the Permian (vein type ii), cooling of H_2O-NaCl-(KCl-$CaCl_2$) metamorphic fluids (T ≤ 310°C, 2–4.5wt% NaCl + $CaCl_2$, Cl/Br mass ratios = 90) leads to the precipitation of quartz-Sb-Au veins. Around the Triassic–Jurassic boundary (vein type iii), quartz–haematite veins formed from two distinct fluids: a low-salinity fluid (similar to (ii)) and a high-salinity fluid (T = 100–320°C, >20wt% NaCl + $CaCl_2$, Cl/Br mass ratios = 60–110). Both fluids types were present during vein formation but did not mix with each other (because of hydrogeological reasons). Jurassic–Cretaceous veins (vein type iv) record fluid mixing between an older bittern brine (Cl/Br mass ratios ~80) and a younger halite dissolution brine (Cl/Br mass ratios >1000) of similar salinity, resulting in a mixed H_2O-NaCl-$CaCl_2$ brine (50–140°C, 23–26wt% NaCl + $CaCl_2$, Cl/Br mass ratios = 80–520). During post-Cretaceous times (vein type v), the opening of the Upper Rhine Graben and the concomitant juxtaposition of various aquifers, which enabled mixing of high- and low-salinity fluids and resulted in vein formation (multicomponent fluid H_2O-NaCl-$CaCl_2$-(SO_4-HCO_3), 70–190°C, 5–25wt% NaCl-$CaCl_2$ and Cl/Br mass ratios = 2–140). The first occurrence of highly saline brines is recorded in veins that formed shortly after deposition of halite in the Muschelkalk Ocean above the basement, suggesting an external source of the brine's salinity. Hence, today's brines in the European basement probably developed from inherited evaporitic bittern brines. These were afterwards extensively modified by fluid–rock interaction on their migration paths through the crystalline basement and later by mixing with younger meteoric fluids and halite dissolution brines.

Key words: fluid inclusion, fluid mixing, fluid modification, hydrothermal ore, mineralization

Received 17 June 2015; accepted 16 January 2016

Corresponding author: Benjamin F. Walter, Department of Geosciences, Eberhard Karls University Tübingen, Wilhelmstrasse 56, 72074 Tübingen, Germany. Email: benjamin.walter@uni-tuebingen.de. Tel: Xxxxxx. Fax: Xxxxxxxx.

Geofluids (2016)

HIGHLIGHTS

- Reconstruction of the chemical evolution of fluids within the crystalline basement from the Carboniferous till today.
- The influence of the tectonic setting on chemical variations in basement brines.
- Connection of surface related formations of evaporites with the first occurrence of a basement brine.
- Modification of bittern brine by water-rock interaction with crystalline basement rocks.
- Importance of sinking bittern brines for large scale hydrothermal ore deposition.

INTRODUCTION

During the last decades, highly saline, rock-buffered basement brines with >20wt% salinity have been recognized as a common phenomenon worldwide, mainly based on data from deep drilling projects which recovered fluid samples from up to 12 km depth (Frape & Fritz 1987; Pauwels *et al.* 1993; Stober & Bucher 2004; Möller *et al.* 2005; Shouakar-Stash *et al.* 2007). The recognition of these brines stored in basement rocks changed the ideas about fluid flow, water–rock interaction and hydrothermal mineralization in the upper brittle continental crust. Many of these brines are of basinal origin and discharge into the basement (Bons *et al.* 2014 and references therein). Understanding the brines' chemical and physical properties is of scientific and economic interest (e.g. Yardley 2005; Agemar *et al.* 2013).

During formation of epithermal, unconformity-related, hydrothermal ore deposits (Pb, Zn, Cu, Ni, Ag), most authors see deep-seated brines as the provenance of metals. Tectonic processes (e.g. Banks *et al.* 2000; Gleeson *et al.* 2001; Boiron *et al.* 2002; Staude *et al.* 2009) mobilize these brines and form ore deposits due to a change in physiochemical parameters caused by mixing, with other fluids derived from different aquifers (e.g. sedimentary cover) (Fußwinkel *et al.* 2013; Bons *et al.* 2014), cooling (e.g. Wagner & Cook 2000 and references therein) or boiling (e.g. Banks *et al.* 1991 and references therein). Today, there is general consensus about the important influence of highly saline basement brines for ore formation in epithermal, unconformity-related, hydrothermal ore deposits, but the source, formation, mobilization and chemical modification of such fluids are still under debate (e.g. Fritz & Frape 1982; Stober & Bucher 2004; Yardley 2005).

Two different models of basement brine evolution have been proposed: according to the first model, low-salinity fluids are modified by fluid–rock interaction accompanied by desiccation processes (Fritz & Frape 1982; Markl & Bucher 1998; Stober & Bucher 2004). During hydrothermal alteration, feldspars and micas are altered to clay minerals. Therefore, the interstitial water is passively enriched in solutes ('internal source'). In contrast, an alternative model proposes that the high salinity of basement brines was derived from external sources, such as evaporites in the sedimentary cover (e.g. Bottomley *et al.* 1994; Gleeson & Yardley 2002; Bejaoui *et al.* 2014 and references therein). According to this model, the precipitation of halite in shallow marine basins produces near-surface residual brines (bittern brine), which are migrating downwards into the basement ('external source') (e.g. Bons *et al.* 2014 and references therein). This model is supported by mass-balance calculations, which imply that fluid–rock reactions and fluid inclusion leakage alone cannot explain the high salinity in many locations (Savoye *et al.* 1998). Also, experiments by Burisch *et al.* (2015) indicate that fluid–rock interaction alone is not sufficient to produce brines with up to 28wt% with low Cl/Br ratios. For such highly saline fluids with low Cl/Br ratios, an external fluid source seems to be required. Regardless of their source, brines resident in crystalline basement rocks, which we refer to as 'basement brines', represent fluids that have evolved significantly altered by water–rock interaction with their host rocks.

Understanding low-grade metamorphic or hydrothermal processes in the upper brittle crust critically depends on determining the chemical evolution of such basement brines. In this study, we try to reconstruct the chemical history of a basement brine over geologic timescales. This attempt is based on detailed fluid inclusion investigations in minerals from hydrothermal vein-type deposits of different ages in a well-defined area, combined with crush-leach analyses and published analyses of waters from deep drillings. We investigated carefully chosen and well-characterized samples of hydrothermal veins from the Schwarzwald mining district in SW Germany (Staude *et al.* 2009 and references therein). The more or less continuous hydrothermal mineralization over the past 320 million years (Pfaff *et al.* 2009 and references therein) permits construction of a detailed fluid history which can be used to evaluate the controls on basement brine origins and evolution.

GEOTECTONIC SETTING AND MAIN CHARACTERISTICS OF SCHWARZWALD MINERALIZATION

Geotectonic setting

The Schwarzwald comprises exhumed Variscan basement gneisses and granites overlain by Lower Permian to Upper Jurassic sedimentary units (Fig. 1). The paragneiss units are deformed and metamorphosed to dominantly to upper amphibolite grade during Variscan (Carboniferous) collisional processes (Geyer & Gwinner 2011 and references therein). Postcollisional S-type granites, which today form about 50% of the exposed Schwarzwald basement, intruded into the gneisses at 335–315 Ma (Hann *et al.* 2003; Geyer & Gwinner 2011 and references therein). After erosion, during Rotliegend (Permian) times, small sediment traps were filled by proximal red beds (arkoses, conglomerates) (Geyer & Gwinner 2011). During the Lower Triassic, quartzitic Buntsandstein units were deposited, followed by Middle Triassic Muschelkalk limestones, shales and evaporites (gypsum and/or halite). Late Triassic (Keuper) sediments are dominated by clastic sediments and evaporitic units (mainly gypsum) (Geyer & Gwinner 2011). Clastic sediments and carbonates were deposited on the

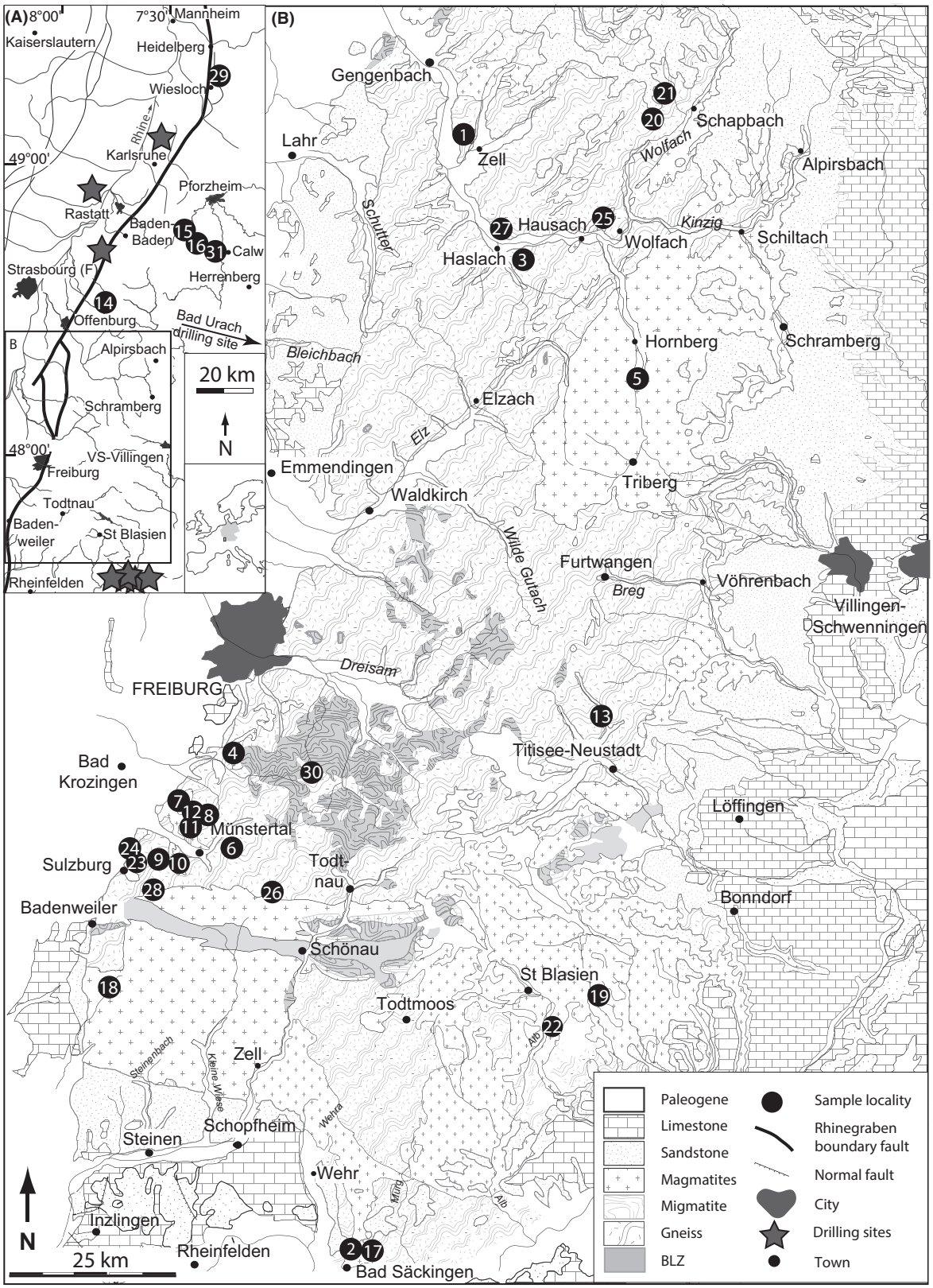

Fig. 1. Geological overview of the Schwarzwald mining district in SW Germany with sample locations. (A) Overview map. (B) Close-up of the Schwarzwald mining district modified after Pfaff *et al.* (2011). Sample localities 1–31 (for more information refer to Table S1 in the electronic supplement).

shallow continental Tethys shelf during Jurassic times, but no sediments formed during the Cretaceous.

The initial break-up of the Upper Rhine Graben during the Paleogene resulted in the deposition of clastic, chemical and evaporitic sediments in the rift valley (Geyer & Gwinner 2011). Simultaneous with rifting, the uplift of the rift shoulders resulted in extensive erosion of the sedimentary overburden formed the erosional window of the basement rocks exposed today.

Hydrothermal vein-type mineralization in the Schwarzwald

Hydrothermal veins formed more or less continuously in basement rocks and their sedimentary cover in SW Germany from about 320 Ma until the present day (Pfaff *et al.* 2009 and references therein; Staude *et al.* 2009; Loges *et al.* 2012). An extensive data set on many different aspects of fluid flow and hydrothermal vein formation exists. This data set includes studies on microthermometry (e.g. Behr & Gerler (1987), Behr *et al.* (1987), Staude *et al.* 2009, 2012a; Fußwinkel *et al.* 2013; Walter *et al.* 2015), trace element distribution in fahlore and sphalerite (Staude *et al.* 2010; Pfaff *et al.* 2011), stable and radiogenic isotopes of O, C, H, S, Sr, Pb, Cu, Fe, Mg (Staude *et al.* 2011, 2012b; Walter *et al.* 2015 and references therein), REE distribution in fluorites (Schwinn & Markl 2005), palaeo-fluid models (Pfaff *et al.* 2010; Staude *et al.* 2011; Fußwinkel *et al.* 2013; Bons *et al.* 2014; Walter *et al.* 2015), geochemistry of modern thermal and mineral waters (Stober & Bucher 1999; Loges *et al.* 2012; Göb *et al.* 2013), leaching experiments on basement and cover rocks (Bucher & Stober 2002; Burisch *et al.* 2015), modern fluid flow models and hydraulic aquifer properties (Stober & Bucher 2005; Bucher & Stober 2010) and the regional geology (Geyer & Gwinner 2011 and references therein). This information is an important prerequisite for the challenging task of deciphering the chemical evolution of a basement fluid.

Following the work of Behr & Gerler (1987); Behr *et al.* (1987); Staude *et al.* (2009); Pfaff *et al.* (2009, 2010); and Walter *et al.* (2015), the hydrothermal veins are subdivided into five formation stages based on structural, mineralogical and microthermometrical arguments (Table 1): (i) Carboniferous, (ii) Permian, (iii) Triassic–Jurassic boundary, (iv) Jurassic–Cretaceous and (v) post-Cretaceous. The general age constraints, chemical and physical characteristics of the different veins and mineralizing fluids are summarized in Table 1.

The Carboniferous veins (i) are quartz–tourmaline veins with trace wolframite, scheelite and cassiterite (Marks *et al.* 2013). These veins occur in close proximity to granitic intrusions and are therefore most likely related to Variscan magmatic activity (Leutwein & Sonet 1974; Marks *et al.* 2013). Oxygen isotope pairs of tourmaline and quartz in those veins indicate temperatures of up to 550°C. Fluid chemistry and temperatures indicate a distinct magmatic fluid component (Marks *et al.* 2013).

The Permian group (ii) comprises mainly very low-grade Sb±Ag±Au-bearing quartz veins. Their precipitation is interpreted to have resulted from cooling of a low-salinity, high-temperature late Variscan metamorphic basement fluid (Staude *et al.* 2009 and references therein; Wagner & Cook 2000).

Veins from the Triassic–Jurassic boundary (iii) are quartz–chalcedony–haematite veins with only minor amounts of barite (Brander 2000). With the exception of rarely occurring pyrite, they contain no ores. The 'Permian veins' of Staude *et al.* (2009) comprise our types (ii) and (iii).

The majority of the hydrothermal veins of the Schwarzwald belong to the Jurassic–Cretaceous group (iv) which comprises variable modal amounts of fluorite, barite, quartz and carbonates with large amounts of either Ag-Bi-Co-Ni-U, Fe-Mn or Pb-Zn-Cu ores (e.g. Mertz *et al.* 1986; Wernicke & Lippolt 1993, 1997; Meyer *et al.* 2000; Werner *et al.* 2002; Pfaff *et al.* 2009; Staude *et al.* 2009, 2011, 2012a,b; Werner 2011; Walter *et al.* 2015). In contrast to the earlier veins, their formation involved a deep-seated highly saline brine (20–28wt% salinity), which was mobilized and mixed with colder formation waters in extensional basin-related fault systems (Staude *et al.* 2009, 2010, 2011, 2012b; ; Fußwinkel *et al.* 2013; Walter *et al.* 2015). In this vein type, no indications of significant fluid cooling and boiling processes were found. This hydrothermal activity was probably related to the opening of the North Atlantic (e.g. Wetzel *et al.* 2003; Pfaff *et al.* 2009; Staude *et al.* 2009).

During Paleogene rifting, Upper Rhine Graben-parallel NE-SW to NNE-SSW-striking fault systems were generated or reactivated. Group (v) mineralization formed in these fault zones (Pfaff *et al.* 2009 and references therein; Staude *et al.* 2012b and references therein) and includes barite, quartz fluorite and/or various carbonates, which precipitated together with Pb and less commonly, As, Zn, Cu, Bi and Ni ores (Staude *et al.* 2009). The variability in mineralogy and fluid chemistry (salinity 1–23wt% NaCl + $CaCl_2$) of these post-Cretaceous veins is interpreted as a consequence of multicomponent, multi-aquifer fluid mixing processes caused by a juxtaposition of different aquifers during opening of the Upper Rhine Graben rift (Walter *et al.* 2015).

Sample material

Samples of fluorite, barite, quartz and carbonates from various Schwarzwald veins were selected based on the following criteria: (1) every mineralization event (i) to (v) is

Table 1 Types of veins and fluid signatures of the Schwarzwald ore district.

Group	Age	Mineralogy	Mineralization	Structural position	Age constraints	Fluid type	Salinity in wt.% ($NaCl + CaCl_2$)	T_h in °C	Na/K mass ratio	Cl/Br mass ratio
i	Carboniferous	Quartz–tourmaline[1]	W-Sn	Spatially associated and genetically related to specific granites	U-Pb age of host granite[2]	H_2O-NaCl±(CO_2±CH_4)†	–*; 0–4†	–*; 130–390°C†	–*; 3.2–5.6†	–*; 48–146†
ii	Permian	Quartz	Sb±Ag±Au	Only in basement rocks (granite and gneiss)	High fluid temperatures >250°C never reached again after Permian times by the SW German basement at shallow depths; comparison with very similar veins from the Taunus[3]	H_2O-NaCl-KCl*,†	<5*; 2–4.5†	150–300°C*; 99–280°C†	–*; 4.2†	–*; 94†
iii	Triassic–Jurassic	Quartz–haematite	Fe	Only in basement rocks (granite and gneiss)	(U-Th)/He age[4]	H_2O-NaCl-KCl† & ^{H_2}O-NaCl-$CaCl_2$†	–*; 0.7–3.3 & 23.3–25.8†	–*; 121–224°C†	–*; 0.3–5.5†	–*; 60–112†
iv	Jurassic–Cretaceous	Fluorite–quartz–barite barite–quartz	Pb-Zn-Cu-Ag & U-Bi-Co-Ni-Ag & Fe-Mn	From >2000 m below the basement/cover unconformity up to the boundary between Lower and Middle Triassic sediments[5]	Rb-Sr and U-Pb age-dating[6]	H_2O-NaCl-$CaCl_2$*,†[,5,6,7,8]	20–28*[,5,6,7,8] 23–26†	50–180°C*[,5,6,7,8] 50–143°C†	–*; 0.8–10.4†	49–824*[,8]; 62–522†
v	Post-Cretaceous	Quartz–barite–fluorite	Pb-Zn-Cu-Ag & Cu-Ni-Bi-Ag	Spatially closely associated with Upper Rhine Graben faults or tributary fault systems	Structural position on Rhine Graben-related faults[6]	H_2O-NaCl-$CaCl_2$± (SO_4±CO_2±HCO_3)*,†[,5,6,7,9,10]	0–25*[,5,7,9]; 5–25†	50–150°C*[,5,6,7, 9]; 66–194°C†	–*; 1.7–8.7†	–*; 2–144†

*Literature data. †This study. References: 1 Marks *et al.* (2013); and references therein; 2 Leutwein & Sonet (1974); 3 Wagner & Cook (2000); 4 Brander (2000); 5 Staude *et al.* (2009); 6 Pfaff *et al.* (2009); and references therein; 7 Walter *et al.* (2015); 8 Fußwinkel *et al.* (2013); 9 Pfaff *et al.* (2010); 10 Pfaff *et al.* (2011).

represented; (2) the age of formation of the sampled vein is known based on radiogenic isotope dating or a combination of structural, mineralogical and fluid inclusion criteria; (3) the veins contain sufficient amounts of gangue minerals in up to centimetre-sized crystals, which show growth zonation. This is important because the fluid inclusions on the growth zones (former crystal surfaces) can be directly related to the fluids present during vein formation; (4) sample locations are distributed over the whole mining district to include mineralization from various depths. The sample numbers are reported in Table S2 in the supplement.

The samples from (i) Carboniferous veins consist of massive, fluid inclusion-rich, milky quartz with brownish tourmaline crystals up to 5 cm (Fig. 2A). The samples from (ii) Permian mineralization show massive, fine-grained grey quartz (coloured by tiny Sb-bearing sulphides) alternating with milky, coarser grained quartz, subhedral to euhedral crystallized in vugs (Fig. 2B). The mineralization of group (iii) are quartz–haematite veins with alternating red, yellow or grey chalcedony and transparent, euhedral quartz generations (Fig. 2C). Breccias are common. Every mineralization sequence starts with a ferriferous chalcedony, which is overgrown by milky and coarse-grained, sometimes euhedral quartz. The younger quartz generations differ in grain size, colour and brecciation style. The youngest quartz generation (Fig. 2C) forms always clear, very coarse-grained, euhedral crystals with many sealed cracks. Late-stage euhedral haematite crystals occur locally in quartz vugs. Group (iv) samples contain coarse-grained quartz,

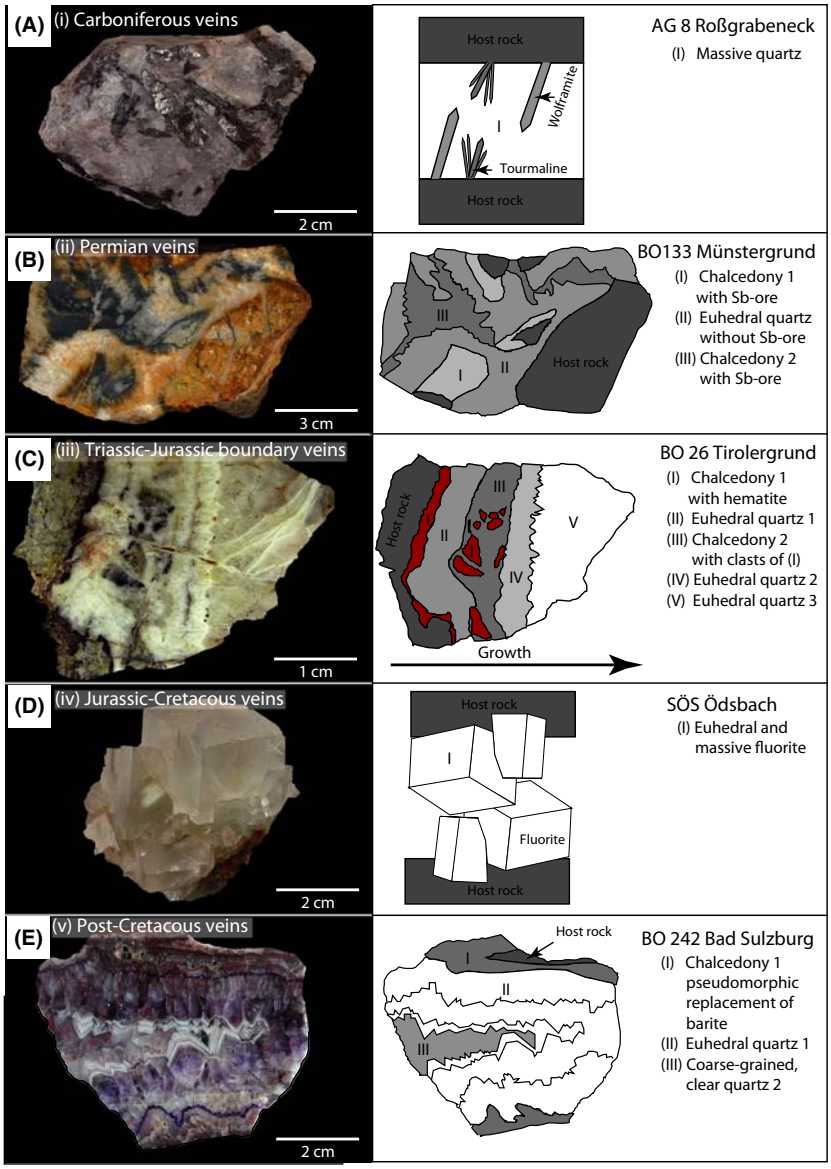

Fig. 2. Photographs and sketches illustrating the various vein types. (A) Carboniferous quartz–tourmaline vein from the Roßgrabeneck near Nordrach; (B) Permian quartz vein with Sb-mineralization from the Münstergrund vein near Staufen; (C) Triassic–Jurassic quartz–haematite vein from the Lattfelsen near Staufen; (D) Jurassic fluorite from the Ödsbach mine near Oberkirch; (E) post-Cretaceous agate–barite vein from the Speichel, Bad Sulzburg.

fluorite, barite and in some cases minor amounts of carbonates with Pb-Zn-Cu ores (Fig. 2D). Their mineralogy is highly variable: some veins consist of exclusively fluorite (e.g. BW255 fl) or quartz (e.g. HM24a); others contain complex sequences of all gangue minerals and ores. Post-Cretaceous veins of group (v) show in many cases textures similar to the Jurassic–Cretaceous ones. Again, pure quartz or fluorite veins as well as complex sequences of alternating gangue minerals can be observed. Many group (iv) and (v) veins show huge crystal sizes (up to many dm, commonly zoned) and the pseudomorphic replacement of barite and rarely fluorite by quartz (Fig. 2E).

Analytical procedure

Microthermometry

For the microthermometric study, samples were cut perpendicular to the longitudinal orientation of the respective vein. Each sample was oriented from early precipitates nucleating on the host rock (rim), to late-stage precipitates facing the commonly open vein centre (vug). The samples were prepared as double-polished thick sections (200–400 μm).

Relative chronological sequences of fluid inclusions (fluid inclusion assemblages (FIA) after Goldstein & Reynolds 1994) were then investigated by optical microscopy. Clearly identified primary (p), pseudo-secondary (ps) and secondary (s) inclusions were identified in addition to isolated inclusions (iso) and clusters of inclusions (c) with no relation to former crystal surfaces or fractures. The 'iso' and 'c' type inclusions provide no clear chronological or genetic information. A detailed explanation is given in Fig. 4 of Walter *et al.* (2015).

Microthermometric investigations were performed using a Linkam (model THMS 600) fluid inclusion stage on a Leica DMLP microscope at Tübingen University. For each inclusion, we measured the ice melting temperature ($T_{m,ice}$), the hydrohalite melting temperature ($T_{m,hh}$) and the homogenization temperature (T_h). For calibration, synthetic H_2O, H_2O-NaCl and H_2O-CO_2 standards were used and only results with a maximum variation of the final melting temperatures of less than 0.1°C were accepted for interpretation; for homogenization temperatures, a variation of up to 1°C was accepted due to poor visibility in some samples. Single measurements with strong deviation in salinity and homogenization temperature within a homogeneous trail are neglected as are data of fluid inclusions in which post-entrapment modification cannot strictly be ruled out.

For the calculation of salinity in the ternary NaCl-$CaCl_2$-H_2O system, the Microsoft Excel-based calculation sheet of Steele-MacInnes *et al.* (2011) was used. The degree of fill was estimated optically based on filling degree tables (Shepherd *et al.* 1985). Pressure correction was done using the formula of Bodnar & Vityk (1994) in combination with estimates on basement and sedimentary overburden based on Geyer & Gwinner (2011). All Th are presented as uncorrected values, because for most of the presented veins hydrostatic conditions can be assumed. As the effect of pressure on the homogenization temperature is highly dependent on the salinity, the correction does not affect the majority of the discussed fluid inclusions. Exceptions are the Carboniferous and the Permian veins, which have lower salinities and are formed under higher pressures. Consequently, the pressure-related effects on Th are discussed in detail in the discussion chapter. The uncertainties of this approach are discussed in Walter *et al.* (2015).

Crush-leach ion chromatography

After careful microthermometric analysis and characterization of the fluid inclusions, samples with only one fluid signature (identical fluid characteristics in p, s, ps and c inclusions) were carefully hand-picked to remove visible impurities. The samples dominantly show primary inclusions, but secondary inclusions cannot be entirely excluded. Samples were only analysed if primary and secondary inclusions showed identical microthermometric behaviour. Two grams per sample (fluorite, quartz, calcite or barite) was separated, heated in a beaker at 60–70°C for 3 hours in concentrated HNO_3 on a sand bath and then washed with ultrapure water twice a day for 7 days. After 2 hours of drying, they were crushed to fine powder and 11 ml of acidulated ultrapure water (pH ~2) was added to suppress the adsorption of Ca^{2+} and other highly charged cations onto surfaces (Köhler *et al.* 2009).

This solution was injected into a Dionex ICS 1000 ion chromatography system at the University of Tübingen (IonPac AS 9-HC 2 mm column for anions; IonPac CS 12-A column for cations). For anions (F, Cl, Br, NO_3, PO_4 and SO_4), the disposable syringe filter CROMAFILE® Xtra RC-20/25 was used; for cations (Li, Na, K, Mg, Ca, Ba, Sr), the disposable syringe filter CROMAFILE® Xtra PVDF-(20/25) was chosen. Blank runs were performed to check for possible contamination. Reference materials were used to monitor the reproducibility and precision of the measurements. The total error was below 20% relative (1 sigma level). Note that the detected NO_3 is related to the acidification of the samples with HNO_3. Absolute elemental fluid concentrations were calculated by normalizing the Cl concentration derived from crush-leach analysis to the Cl concentration derived from microthermometry.

RESULTS

The results reported in Tables 1, 2 and S1 in the electronic supplement clearly show that the five fluid types distinguished in section Hydrothermal vein-type mineralization in the Schwarzwald have distinct chemical compositions.

Table 2 overview of microthermometric results ordered according to fluid petrography (p, s and ps).

Vein type	Fluid type	T first melt in °C	Tm ice in °C	Tm hydrohalite in °C	Salinity (wt % NaCl + $CaCl_2$)	Th °C	Ca/(Na + Ca) in mole
I Carboniferous	A	P ~−21°C	P 0 to −3.3°C	P −21.2°C	P 0 to 5.5	P 148 to 343	P no Ca
		S ~−21°C	S 0 to −3.3°C	S −21.2°C	S 0 to 5.5	S 113 to 389	S no Ca
II Permian	B	Ps not observed	Ps not observed	Ps −21.2°C	Ps not observed	Ps not observed	Ps no Ca
		P ~−21°C	P −0.5 to −3.2	P −21.2°C	P 0.8 to 5.4	P 99 to 264	P no Ca
		S ~−21°C	S −0.2 to −5.1	S −21.2°C	S 0 to 8.2	S 127 to 313	S no Ca
		Ps not observed	Ps not observed	Ps −21.2°C	Ps not observed	Ps not observed	Ps no Ca
III Triassic–Jurassic	B & C	P ~−21°C & ~−50°C	P −0.4 to −24.7	P −21.2 to −25.9	P 0.6 to 25.2	P 98 to 320	P no Ca
		S ~−21°C & ~−50°C	S −0.4 to −22.8	S −21.2 to −25.0	S 0.9 to 23.9	S 125 to 216	S no Ca
		Ps ~−21°C & ~−50°C	Ps −0.4 to −25.0	Ps −21.2 to −25.9	Ps 0.4 to 25.4	Ps 111 to 190	Ps no Ca
IV Jurassic–Cretaceous	CD	P ~−50°C	P −21.2 to −28.5	P −10.4 −26.4	P 22.7 to 27.1	P 50 to 156	P 0.2 to 0.4
		S ~−50°C	S −19.2 to −28.1	S −10.4 −26.5	S 21.2 to 27.1	S 77 to 129	S 0.2 to 0.4
		Ps ~−50°C	Ps −21.8 to −25.2	Ps −19.0 to −24.1	Ps 22.9 to 26.8	ps 115 to 124	Ps 0.2 to 0.4
V post-Cretaceous	CD & DE	P ~−21°C & ~−50°C	P −2.5 to −25	P −21. to −26.6	P 4.5 to 25.2	P 67 to 180S 110 to 165	P no Ca to 0.4
		S ~−21°C & ~−50°C	S −0.7 to −26.3	S −21.2 to −26.4	S 1.0 to 25.1		S no Ca to 0.4
		Ps ~−21°C & ~−50°C	Ps −23.5 to −25.0	Ps −21.2 to −25.0	Ps 23.7 to 24.5	Ps 71 to 131	Ps no Ca to 0.4

Dominantly late magmatic Carboniferous veins of group (i): fluid type (A)

Carboniferous veins contain only one fluid signature (fluid (A)). Type A fluids have homogenization temperatures between 130°C and 389°C. Two maxima at about 250°C and 350°C can be recognized in T_h. Final ice melting temperatures between 0°C and −3.3°C result in a calculated salinity of 0–4wt% ($NaCl_{eq}$) (one outlier at 9wt%). First melting of ice can be recognized at about −11°C. A $CaCl_2$-poor or $CaCl_2$-free system is indicated by hydrohalite melting at the binary H_2O-NaCl eutectic temperature of −21.2°C; the freezing temperature is above the ternary H_2O-NaCl-$CaCl_2$ eutectic temperature of −52°C. In addition, CO_2 can be optically recognized by a double bubble. Further volatile phases detected by Micro-Raman are CH_4 and N_2. The degree of fill depends on the volatile content: The liquid-rich volatile-poor inclusions show a degree of fill above 0.8. The volatile-rich inclusions have ratios of 0.5–0.8. Hence, in Carboniferous veins an H_2O-NaCl-CO_2-CH_4 fluid was present. Br was only detected in five samples which resulted in a Cl/Br mass ratio of 48 and 146. Na/K mass ratios are 3.2–5.6.

Permian quartz veins of group (ii): fluid type (B)

Permian quartz veins contain inclusions of a distinct fluid type (B). The fluid inclusions of type B freeze in the range −30 to −45°C. First melting can be observed above −20°C which implies a binary NaCl-H_2O or NaCl-KCl-H_2O system. Ice is the last melting phase in the range of −0.3 to −5.1°C, which results in a calculated salinity of 2–4.5wt% $NaCl_{eq}$. Homogenization temperatures range from 99 to 310°C. Within FIA, the salinity and T_h are constant, but these parameters can vary between different trails. The filling degree ranges from 0.8 to 0.95. The crush-leach analyses confirm a NaCl-H_2O fluid with Cl/Br mass ratios of 94 and Na/K mass ratios of 4.2.

Triassic–Jurassic veins of group (iii): alternating type B and C type fluids

Veins of group (iii) contain primary fluid inclusions of type B and a different fluid type (type C), which alternate between different quartz layers in some samples (Fig. 3A). Fluid inclusions containing fluid type C freeze between −70 and −100°C. Homogenization temperatures vary between 121 and 224°C (Fig. 3E). Within each fluid inclusion assemblage, the temperature variation is small. The first melt can be observed around −50°C. Final melting temperatures of ice show variations between −20.2°C and −24.7°C. Final dissolution temperatures of hydrohalite range from −19.7°C to −25.9°C, showing filling degrees between 0.9 and 0.95. Calculated salinities vary between 23.3 and 25.8wt% (NaCl + $CaCl_2$) assuming a NaCl-$CaCl_2$-H_2O system.

Petrographic observations (Fig. 3A) (alternating low- and high-salinity fluid signatures) indicate that, while both fluids were present at the time of sample formation, there is no evidence of mixing to form fluids intermediate in composition between types B and C. Instead, fluid inclusions of this age contain either B or C in alternating layers within a sample. Because crush-leach analyses of these samples cannot resolve the microscopic interlayering of FIA containing type B and type C fluids, they represent mixtures of both fluid types. The two mixed analyses show Na/K mass ratios of 0.3 and 5.5 with Cl/Br mass ratios of 60 and 112 (Fig. 3F). Thus, their element budget is dominated by the high-salinity, high total dissolved solids (TDS) fluids of type C.

Jurassic–Cretaceous veins of group (iv): mixed fluid type CD

This vein type shows exclusively high-salinity fluids (Fig. 3B,D–F). The inclusions freeze between −70 to −100°C. First melting can be detected above −50°C implying a ternary NaCl-$CaCl_2$-H_2O system with a eutectic temperature at −52.0°C. Ice and hydrohalite are last melting phases. The final melting temperature of ice is in the range of −19.1° to −27.1°C, of hydrohalite between −10.4° to −26.4°C, which records a salinity of 23–26wt% (NaCl + $CaCl_2$). Homogenization temperatures vary from 50 to 143°C. Within single trail, salinity and T_h are almost constant, but they vary between different trails within one sample. The degree of fill is constant at 0.95.

Crush-leach analyses confirm a NaCl-$CaCl_2$-H_2O fluid. Important element mass ratios for later discussions, regarding, for example, fluid mixing and fluid source, are Na/K between 0.8 and 10.4 and Cl/Br mass ratios between 62 and 522. The high Cl/Br mass ratios in this vein type are notable. Most inclusions of fluid type CD are similar in salinity and temperature to type C but vary in Cl/Br mass ratios and show a stronger scatter in salinity, which requires the definition of a mixed fluid type CD, including an additional, high Cl/Br mass ratio reservoir D (Fig. 3F).

Post-Cretaceous veins of group (v): fluid type CD and DE

MicroRaman analysis shows that H_2O is the dominant Raman-active species in the fluid in all trails. In some samples, sulphate can be detected. Based on charge balance calculations, it seems very likely that HCO_3 appears to be present. Individual FIA may show freezing temperatures between −70 to −100°C and/or −30 to −45°C, respectively. Inclusions with low freezing points have eutectic temperatures of −52°C, the others of −21.2°C corresponding to a NaCl-$CaCl_2$-H_2O and a NaCl-H_2O fluid, respectively. All measurements from individual FIA form a cloud rather than a point in the NaCl-$CaCl_2$-H_2O ternary phase diagram of Steele-MacInnes *et al.* (2011), a feature that testifies to Ca/Na variations of single inclusions in individual FIA.

The last species to dissolve is invariably ice. The final melting temperature of ice is in the range of 0 to −27.0°C and for hydrohalite between −21.2 and −26.4°C, which implies a salinity of 5–25wt% (NaCl + $CaCl_2$). Homogenization temperatures are in the range from 66 to 194°C. Within single trails, the salinity and T_h are constant, but they may vary between different trails.

Crush-leach analyses and laser Raman spectroscopy confirm the NaCl-($CaCl_2$)-H_2O fluid with different amounts of SO_4 and HCO_3. Na/K mass ratios vary between 1.7 and 8.7 and Cl/Br mass ratios between 2 and 144. Veins of group (v) contain fluids with a large variation in salinity (Fig. 3E), involving both the CD fluid signature and a mixture of fluid end-member D with a low TDS end-member E.

DISCUSSION

Fluid types in the context of geological setting and time

In the following, the temporal chemical evolution of deep-seated basement brines is placed in a well-defined geological context and the processes that govern this development are discussed. Hydrothermal veins are well suited to this because they contain zoned minerals with large primary inclusions. In contrast, fluid inclusions in basement host rocks (granites and gneisses), which could also record changes in fluid chemistry, cannot be reliably related to a specific event in time.

Reservoir A, fluid type A – from veins of group (i): late magmatic fluids are expelled to the middle and upper crust

The oldest fluids detected in the Schwarzwald basement are those of fluid type A. These fluids with a significant magmatic component (granite age 322 ± 20 Ma; Leutwein & Sonet 1974) are high-temperature, low-salinity NaCl-H_2O or H_2O-CO_2-CH_4 fluids with Na/K mass ratios of 3.2–5.6 and Cl/Br mass ratios around 100. The low Cl/Br ratio in this low-salinity fluid type is most likely of magmatic origin (Irwin & Roedder 1995) or could be derived from water–rock interaction with the surrounding gneisses (Burisch *et al.* 2015). The large range in homogenization temperatures indicates continuous fluid cooling, as the fluid chemistry remains constant with decreasing T_h. Evidence for a change in other parameters is lacking. These 'Variscan fluids' have also been reported by Behr & Gerler (1987) and Behr *et al.* (1987). Veins of group (i) can be exclusively observed in the direct vicinity of magmatic intrusions. Highly differentiated granitic melts like the Variscan intrusions in the Schwarzwald or the Erzgebirge

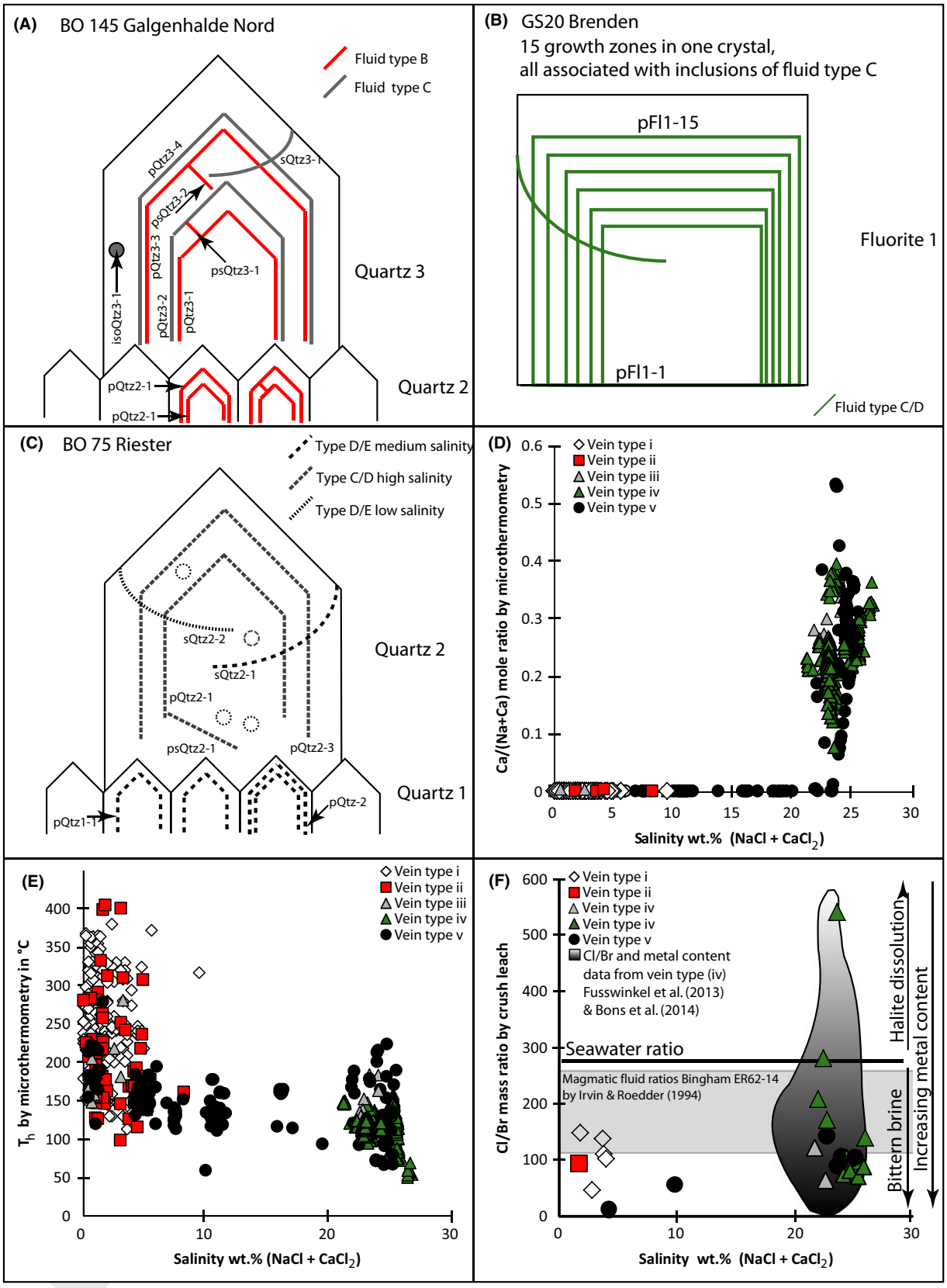

COLOR

Fig. 3. Schematic presentation of the petrological results of fluid inclusion assemblages. (A) Sample BO145 from the Triassic–Jurassic Galgenhalde Nord vein. Note alternating high- and low-salinity fluids on growth zones. (B) Sample GS20 from the Jurassic–Cretaceous Brenden vein; only high-salinity fluids are present. (C) Sample BO75 from the post-Cretaceous Riester vein with alternating, high-salinity, moderate and low-salinity fluids. Some assemblages contain sulphate and/or CO_2; (D) Ca/(Na + Ca) molar ratio (from microthermometry) versus salinity; (E) homogenization temperatures (uncorrected) versus salinity; (F) Cl/Br mass ratio versus salinity. High Cl/Br is typically associated with halite dissolution. Cl/Br mass ratios can be internally derived by WRI with basement rocks or externally by a descending bittern brine.

typically crystallize at shallow depths (Romer *et al.* 2012). As a consequence, we assume a crystallization depth of 1–3 km. The vein geometry can be described as pockets rather than discrete veins. Taking this into account, lithostatic conditions during vein formation can be assumed. Pressure corrections for a lithostatic pressure of 1 kbar (around 3 km depth) increase the uncorrected temperatures in average by 90°C. This indicates a fluid close to thermal equilibrium with two feldspars (Giggenbach 1988), that is with the basement rocks (Fig. 4). As about 50% of the present outcrops in the Schwarzwald consist of granites, we assume that fluid type A (Fig. 5A) was the typical fluid in the middle and upper crust during late Variscan, Carboniferous times.

Reservoir B, fluid type B – from veins of group (ii): the typical late metamorphic basement fluid, when almost no cover rocks are present

Type B fluids are high-temperature, low-salinity H_2O-NaCl-KCl-($CaCl_2$) or H_2O-KCl-NaCl-($CaCl_2$) fluids (Fig. 5B) with a Na/K mass ratio of 0.7–4.2 (Fig. 4), a Cl/Br mass ratio of 70–90 (Fig. 3F) and high homogenization temperatures up to 280°C (Fig. 3E). Such fluids are typical of late metamorphic fluids in cooling orogenies, for example the Rheinisches Schiefergebirge (Germany), the Western Carpathians (Romania) and the Massif Central (France) (Wagner & Cook 2000; Bellot *et al.* 2003). It should be noted that in the Permian, the sedimentary cover consisted of a maximum of some tens of metres of red beds in the whole area (Geyer & Gwinner 2011). Even the deepest Permian veins (2 km below basement/cover unconformity) do not show higher salinity fluid inclusions. The K/Na thermometer of Giggenbach (1988) for sample ML10 records temperatures up to 320°C in good agreement with the measured, uncorrected fluid inclusion homogenization temperatures up to 280°C. Veins from group (ii) can only be recognized within the crystalline basement situated closely below the Permian surface. Breccia geometry indicates hydraulic fracturing (Jébrak 1997). Therefore, pressures between lithostatic and hydrostatic conditions can be assumed. The possible range includes hydrostatic conditions at 1 km (0.1 kbar) up to lithostatic conditions at 2 km depth (0.6 kbar). Pressure corrections for 0.6 kbar for these low-salinity inclusions increase the measured homogenization temperatures in average by 40°C. Hence, the typical basement fluid was of low salinity in the Permian. This also would explain why the Permian veins do not contain metals like Pb and Zn, which are typically mobilized as Cl complexes from the basement (Yardley 2005 and references therein, Burisch *et al.* 2015).

COLOR

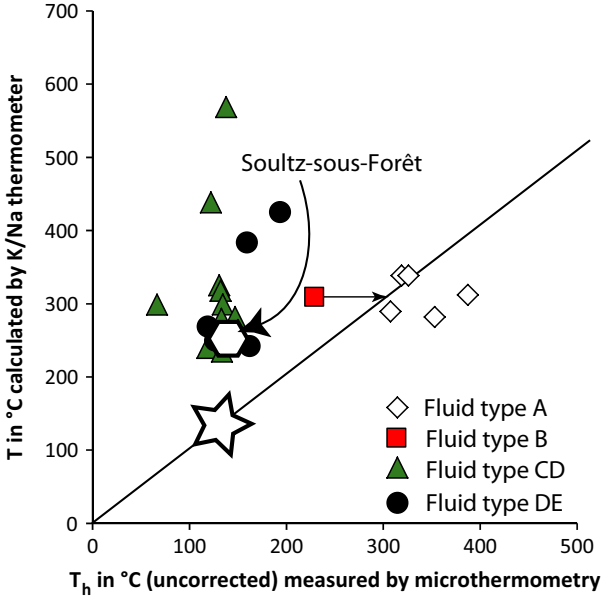

Fig. 4. Temperatures, calculated by the K/Na thermometer of Giggenbach (1988) versus homogenization temperature measured by microthermometry. Fluid samples from the Bad Urach bore-hole (big star), which is situated 80 km, east of the Upper Rhine Graben lies on a 1:1 line. A pressure correction for the type B fluid results in +30°, which shift the uncorrected data point towards the 1:1 line. The Jurassic–Cretaceous and post-Cretaceous veins were not pressure corrected.

Hydrothermal activity at the Triassic–Jurassic boundary: the switch from low to high salinity (reservoir B and C, alternating fluid types B and C)

The first high-salinity fluid inclusions (unmixed fluid type C) in the study area occur in quartz–haematite veins formed at the Triassic–Jurassic boundary, in which euhedral haematite in vugs was age-dated by U-Th/He to 180–200, 202 ± 2 and 235 ± 20 Ma by Brander (2000). The oldest quartz layer in these samples contains type B, the next younger quartz layer containing type C fluid inclusions. Here, fortuitous and unique samples record the transition from an earlier low-salinity regime to a later high-salinity fluid regime (Fig. 5C). The fact that type B fluids can be recognized in younger veins indicates a persistent fluid reservoir in the basement. Hence, fluid type B persisted from the Permian to at least the late Triassic. The

COLOR

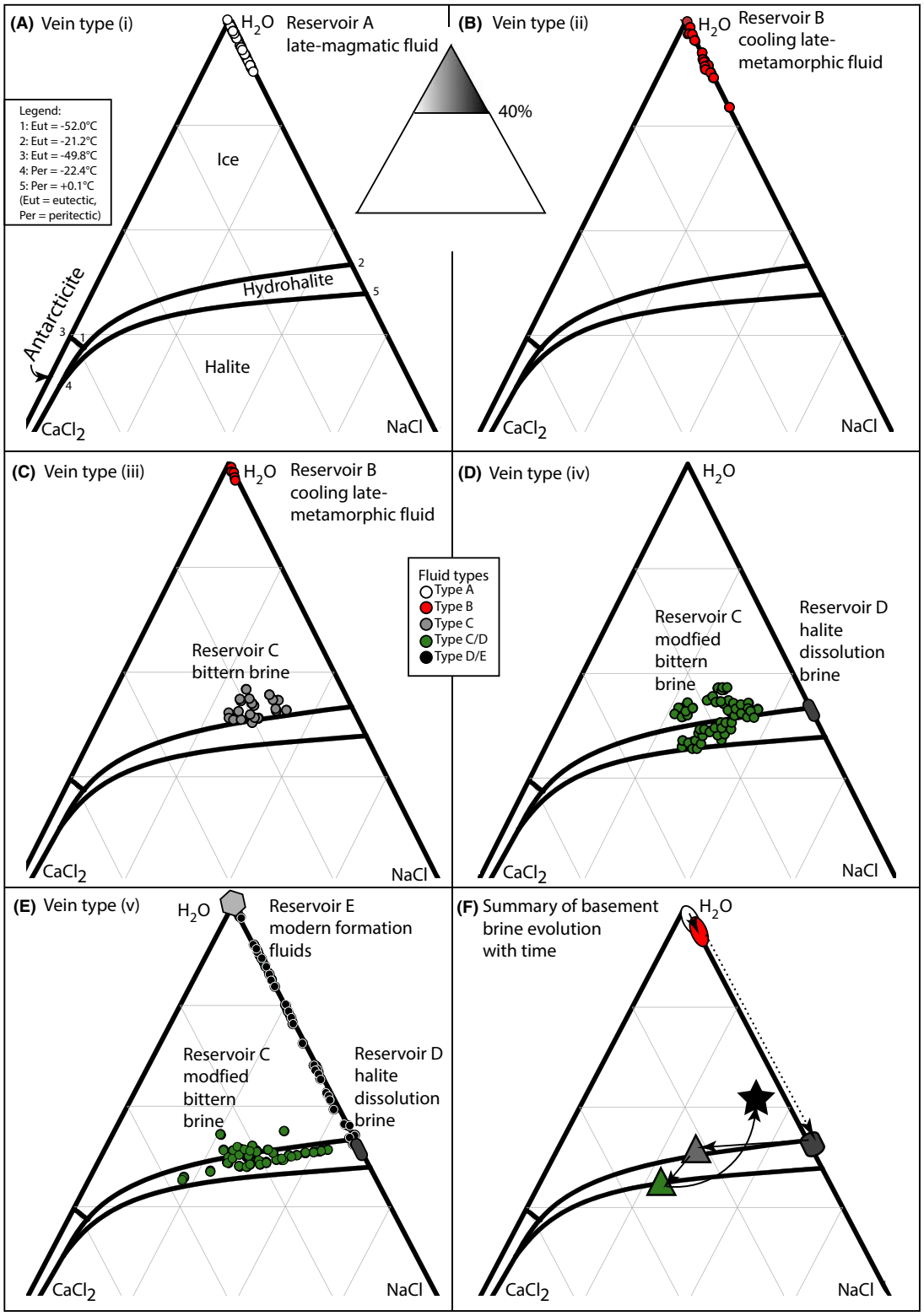

Fig. 5. Phase diagrams of the ternary H_2O-NaCl-$CaCl_2$ fluid system. Note that (F) is a summary of (A) to (E). The colours of the symbols in (F) refer to the different fluid types. Figure (F) summarizes the development from low-salinity fluids in Carboniferous and Permian times to a highly saline, modified bittern brine (basement brine), which formed by descending surficial bittern brines (in middle Triassic), that were modified (Ca increase and metal uptake) by WRI (water rock interactions) with crystalline rocks. The black star illustrates the modern basement brine in the Upper Rhine Graben, showing a distinct dilution by low TDS meteoric/formation fluids.

low Cl/Br mass ratios of 60 and 112 (Fig. 3F) and high salinities (Burisch *et al.* 2015) indicate a bittern brine origin for the type C inclusions.

Reservoir C and D, fluid type CD: mixed, highly saline fluids in a sediment-covered basement

In the Jurassic, large, north–south striking faults through the brittle part of the central European crust opened as a far-field consequence of the opening of the North Atlantic (e.g. Wetzel *et al.* 2003; Pfaff *et al.* 2009; Staude *et al.* 2009 and references therein). At that time and until the upper Cretaceous, mineralization in the Schwarzwald records fluid inclusions of one type: fluid type CD. These contain fluids of very high salinity (Figs 3E and 5D) and intermediate temperature which are interpreted as mixtures of two highly saline brines: one basement-derived with low Cl/Br mass ratios (fluid type C) and one cover-derived fluid with high Cl/Br mass ratio (fluid type D) (Staude *et al.* 2009, 2011, 2012a,b; Fußwinkel *et al.* 2013; Walter *et al.* 2015). Fußwinkel *et al.* (2013) demonstrated that the deep basement brine (reservoir C) with Cl/Br mass ratio of ~80 (inherited from the bittern brine) contained high amounts of dissolved metals, which originated by water–rock interaction with crystalline rocks (specifically, Pb and Zn) (see literature data in Fig. 3F). The second, metal-poor end-member (reservoir D) was proposed to be a Triassic Muschelkalk (limestone) formation fluid with very high Cl/Br mass ratios of >1000 (see literature data in Fig. 3F). The mixed 'ore fluid' (fluid type CD) consequently shows Cl/Br mass ratios between 60 and 820 (Fußwinkel *et al.* 2013 and this study).

The basement brine end-member of fluid type CD is a NaCl-dominated highly saline (21–26wt% NaCl + $CaCl_2$) fluid with a Na/K mass ratio of 0.8–10.4 (Fig. 4). Interestingly, the K/Na thermometer results in temperatures up to 560°C, which are not plausible for the geothermal regime and much higher than T_h (pressure corrected) from microthermometry. This indicates that the mixed CD type fluids are not in chemical equilibrium with their host rocks. This might suggest fast mixing processes during vein formation and fluid inclusion entrapment (see also Bons *et al.* 2014).

Reservoir C, D and E, fluid type CD and DE – from veins of group (v): the influence of the Rhine Graben opening

Vein group (v) occurs either as discrete veins on Rhine Graben-related faults or as younger generations of gangue and ore minerals in the centre of older veins, which are reopened by Neogene strike-slip tectonics. In both cases, fluid inclusions show no clear systematics in Na/K and Cl/Br mass ratios. This is interpreted as a result of mixing during the precipitation processes (Staude *et al.* 2009; Walter *et al.* 2015); in addition to type CD fluids, mixing obviously involved more than two end-members including a low-salinity reservoir E (Fig. 5E). This appears reasonable, as many of the group (v) veins are situated on deep faults where different lithologies of the Mesozoic sedimentary overburden are juxtaposed to the crystalline basement (Walter *et al.* 2015). Figure 3C illustrates the complex sequence of fluid inclusions recording various mixing processes within one crystal.

Most fluid inclusions contain fluid type DE with variable salinities between 0 and 25wt%; rarely the fluid type CD (highly saline) is also present in this vein type. Similar fluids were reported by, for example, Smith *et al.* (1998). Hence, a highly saline end-member exists, which is assigned to the highly saline basement brine, already present as type CD fluids. In most cases, however, only the reservoir D mixed and was diluted by lower salinity fluids from reservoir E. Comparing the fluid inclusion records of vein types (iv) and (v) implies that the reservoirs of fluid type CD were still available in Paleogene times. The fact that ternary C-D-E mixtures are lacking (Fig. 5E) is potentially an effect of fluid stratification. Similar to CD fluids, the K/Na thermometer for type DE yields geologically implausible temperatures of up to 430°C, indicating disequilibrium between rock and fluid, most likely caused by rapid mixing processes.

Modern fluids: The stratification of modern mineral and thermal waters and the modern basement brine

One of the reasons to choose the Schwarzwald as a model region for characterizing the evolution of basement brines is the large amount of data available from numerous deep bore-holes and many thermal and mineral wells in the study area (Fig. 1). More than ten deep drillings and tens of thermal and mineral water wells provide an insight into the recent fluid situation in the Upper Rhine Graben (Soultz-sous-Forêt, NAGRA drillings, Bruchsal, and Bühl; Pearson *et al.* 1989; Pauwels *et al.* 1993) and in the distal undisturbed basement and cover sequence (Urach, KTB, NAGRA drillings: Pearson *et al.* 1989; Stober & Bucher 2004; Möller *et al.* 2005). These data show that present-day fluids in the study area are stratified. Shallow ground waters are weakly mineralized Ca-Na-HCO_3 fluids, chemically controlled by weathering reactions in the subsurface (Bucher & Stober 2010). The sulphate content increases with depth by oxidation of host rock sulphides (Bucher & Stober 2010). The TDS increases further with depth and a high-salinity Na-Ca-Cl fluid is present below about 3 km (Bucher & Stober 2010). The carbonate and chloride fluids apparently do not mix (Bucher & Stober 2010).

The K/Na thermometer applied to fluids from Bad Urach or KTB records a close agreement between calculated and measured temperatures (Stober & Bucher 2004;

Möller *et al.* 2005), which implies equilibrium between fluid and rock (Fig. 4). Also the modern Cl/Br mass ratios of 80–100 (Pearson *et al.* 1989; Stober & Bucher 2004; Möller *et al.* 2005) show no significant admixture of any sedimentary formation fluid which would be expected to result in higher ratios. In contrast, the chloridic fluids derived from the crystalline part of the Soultz-sous-Forêt drill hole record Na-K-temperatures more than 100°C (Fig. 4) above the measured ones (Pauwels *et al.* 1993); their Cl/Br mass ratios up to 255 support an influx of meteoric or formation fluids (Pauwels *et al.* 1993). Hence, in the vicinity of the Rhine Graben, mixing processes affecting the chlorine rich fluids still go on today and lead to a fluid mixture which is not in equilibrium with the crystalline basement. These mixing processes may be driven by topographic fluid flow (Agemar *et al.* 2013).

History and development of the basement brine

Veins of groups (i) and (ii) record low-salinity fluids with significant magmatic or late metamorphic components in thermal equilibrium with the basement rocks (Figs 4 and 5A,B). Around the Triassic–Jurassic boundary, the first highly saline fluids were recorded in group (iii) veins (Fig. 5C). It is important to notable that in the middle Triassic, the study area was, for the first time after the Variscan orogeny, covered by a shallow ocean, in which the evaporate sequence reached halite saturation. This coincided with the occurrence of a high-salinity basement brine (reservoir C) shortly after formation of the evaporates (Fig. 5C,D).

Halite precipitation leads to a decrease in Cl/Br mass ratios in the residual fluid below the seawater ratio of 288 (see seawater evaporation line by McCaffrey *et al.* (1987) in Fig. 6). Hence, the low Cl/Br values of about 80 (mass ratios) and the highly saline basement brine end-member (reservoir C) of mixed type CD fluids may record downward migration of such residual bittern brines (fluid type C, reservoir C) (Fig. 5C and arrow 1 in Fig. 6) into the basement during the Triassic (see Bons *et al.* 2014). The large-scale albitization phenomena (Brockamp *et al.* 2003; Schlegel *et al.* 2007) in the crystalline basement of the central Schwarzwald are very likely related to the influx of such NaCl-rich fluids. Plagioclase dissolution and conversion to albite enriched the originally Ca-poor bittern brine in Ca and in base metals. Rough phase equilibrium calculations show that plagioclase with an X_{An} of 0.3 can shift the fluid to a Ca/(Ca + Na) of up to ~0.7 in the temperature range 30–220°C. Hence, the observed Ca/(Ca + Na) ratios of 0.2–0.3 in the high-salinity type C fluids could

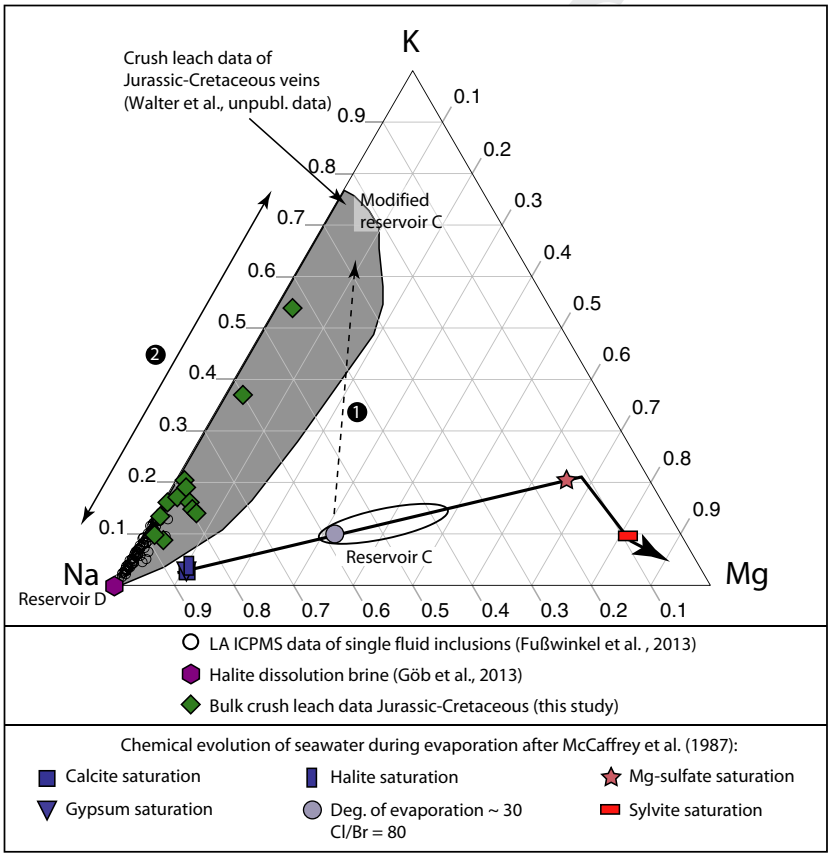

Fig. 6. Ternary diagram showing Na, Mg and K. The dotted arrow (1) indicates the modification of a bittern brine by water–rock interaction, shifting its composition, away from the seawater evaporation line towards higher K and lower Mg. During this process, the breakdown of rock-forming minerals during water–rock interaction modifies the fluid signature and concomitantly leads to increasing metal contents in the fluid. Fluid mixing (2) of a modified bittern brine (low Cl/Br mass ratio, high metal content) and a halite dissolution brine (high Cl/Br mass ratio, low metal content) yields the mixed two-component fluid signature CD.

COLOR

easily be explained by such albitization reactions. Furthermore, the formation of secondary minerals (e.g. chlorite, illite, smectite) as a consequence of biotite breakdown causes a modification of the bittern brine towards higher K and lower Mg concentrations (see arrow 1 in Fig. 6) (Brockamp *et al.* 2003, 2011).

Hence, it seems very plausible that the Jurassic–Cretaceous high-metal, low Cl/Br mass ratios of 'basement brine' reported by Fußwinkel *et al.* (2013) (our type C) is a modified middle Triassic bittern brine (Fig. 6). During the Jurassic and Cretaceous, it was mixed with a halite dissolution brine (NaCl-dominated and high Cl/Br mass ratios, end-member of line 2 in Fig. 6) derived by interaction of meteoric waters with the Muschelkalk evaporites (mixed fluid CD, see Fig. 3F and line 2 in Fig. 6). Early diagenetic dissolution textures in the middle Triassic host rocks reported by Geyer & Gwinner (2011) confirm that such processes indeed took place.

Alteration of feldspars (mainly plagioclase) and micas to clay minerals consumes water and leads to a desiccation process which both increase the salinity and the metal content in a fluid. The basement brine end-member (reservoir C) in type CD fluids would then have formed by a combination of inherited salinity from the middle Triassic Muschelkalk Ocean (Fig. 5D) and a long reaction time with the granitic/gneissic basement. Furthermore, the desiccation process consumes water within the basement, which causes a hydraulic gradient that enables downward migration of the younger (Middle–Upper Triassic) halite dissolution brine (fluid type D) with higher Cl/Br mass ratios (Stober & Bucher 2004; Bons *et al.* 2014). As the topography during the Jurassic and Cretaceous was too flat to drive topographic fluid flow, and as gravitational downward movement of the surface brine is unlikely due to the similar density of the bittern (reservoir C = basement) and the halite dissolution (reservoir D = surface) brines, this 'desiccation suck' (downward migration of brines caused by water consumption at depth; Stober & Bucher 2004; Bons *et al.* 2014) appears the only viable mechanism to bring large amounts of surface water to depth.

The Triassic–Jurassic boundary marks the first occurrence of highly saline basement brines. The group (iii) samples show that two fluids of different salinity were present during the first occurrence of a high-salinity brine (reservoir C, fluid type C), at the Triassic–Jurassic boundary (Fig. 3A and 5C). The low Cl/Br mass ratios are in agreement with a bittern brine origin. The lack of fluids of intermediate salinity shows that no fluid mixing occurred between type B and C fluids, although based on our FIA textural observations (Fig. 3), they intermittently coexisted on scales ranging from regional to individual fractures. This resembles the modern situation, in which NaCl- and Ca-HCO_3 fluids coexist in horizontally stratified reservoirs in SW Germany without any sign of mixing (Bucher & Stober 2010). Later on, this may have changed and type B fluid signature might be modified, by mixing or replacement with the much more saline type C (Fig. 7), so that it can no longer be recognized. Type B fluids were not observed in any younger sample (Figs 5 and 7). Interestingly, no deep-seated low-salinity fluids were found in the deep boreholes of KTB and Kola. If any type B fluid is present today, it would be expected to be just above the

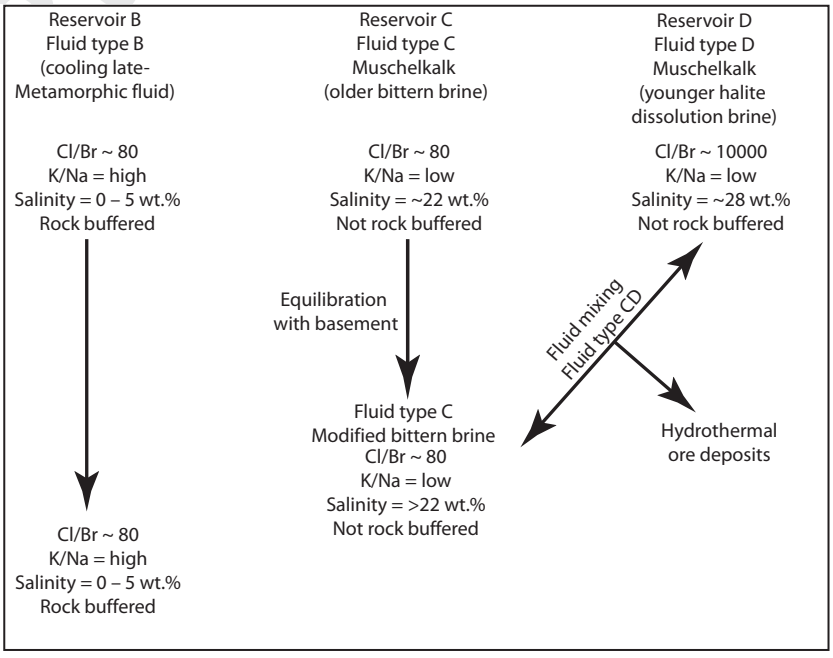

Fig. 7. Summary of fluid reservoirs B, C and D and their influence on hydrothermal ore deposition.

COLOR

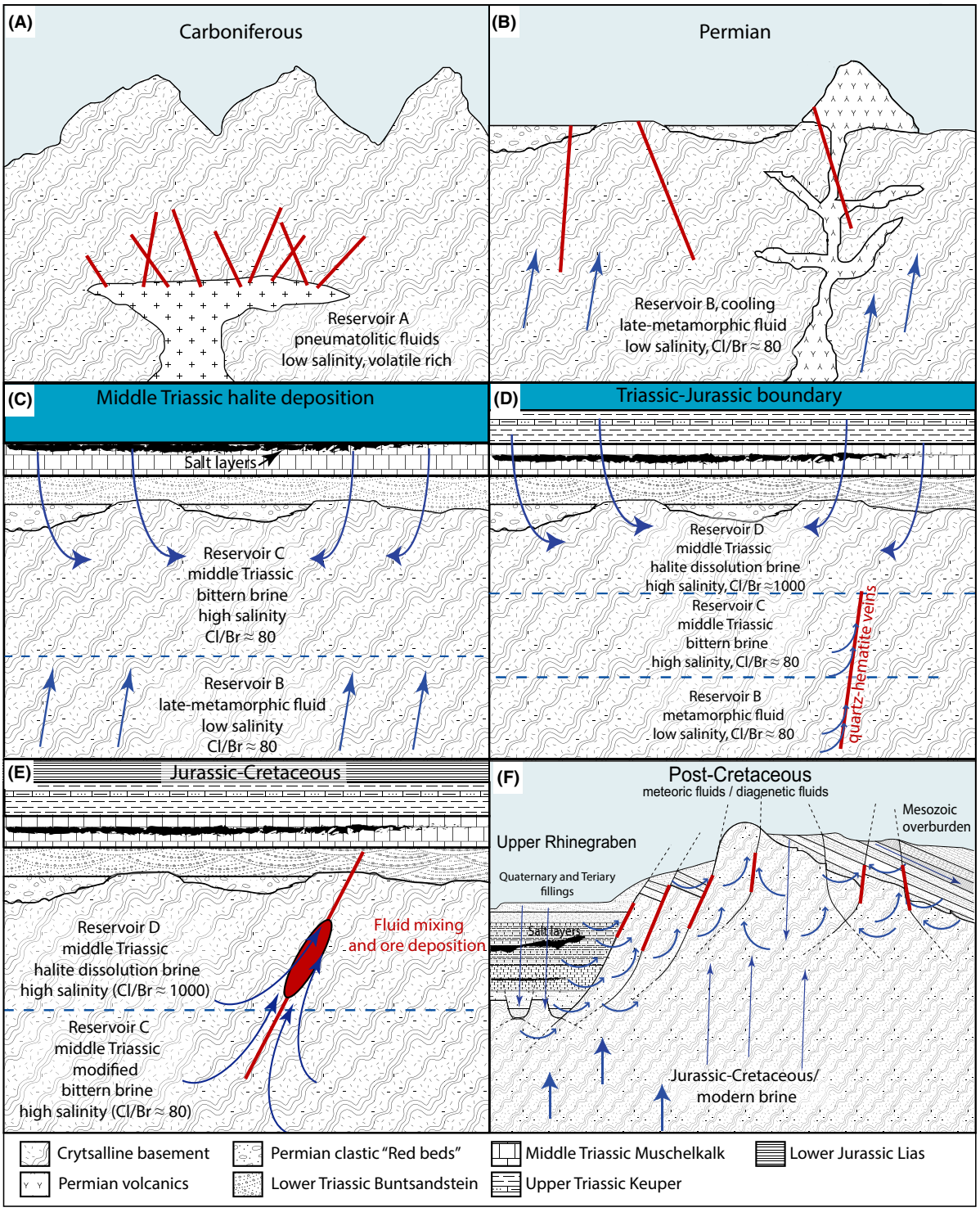

Fig. 8. Schematic crustal sections showing the evolution of the central European basement brine from (A) Carboniferous to (F) post-Cretaceous time. (A) Carboniferous fluids showing exclusively low salinity, volatile rich, high temperature in quartz–tourmaline veins, (B) Permian fluids showing only low salinity, high temperature in quartz veins with Sb-Au mineralization. (C) First deposition of halite in a shallow ocean in the Triassic and subsequently sinking of a bittern brine into the basement. (D) At the Triassic–Jurassic boundary, first dissolution of the halite and formation of a halite dissolution brine that sinks downwards (Bons *et al.* 2014). Furthermore, formation of the Triassic–Jurassic quartz–haematite veins with alternating fluid signatures. (E) Opening of fracture networks as a far-field consequence of the North Atlantic opening and formation of the Jurassic–Cretaceous veins by binary fluid mixing. (F) Multi-component fluid mixing and vein formation in the complex geological environment of the Upper Rhine Graben rift.

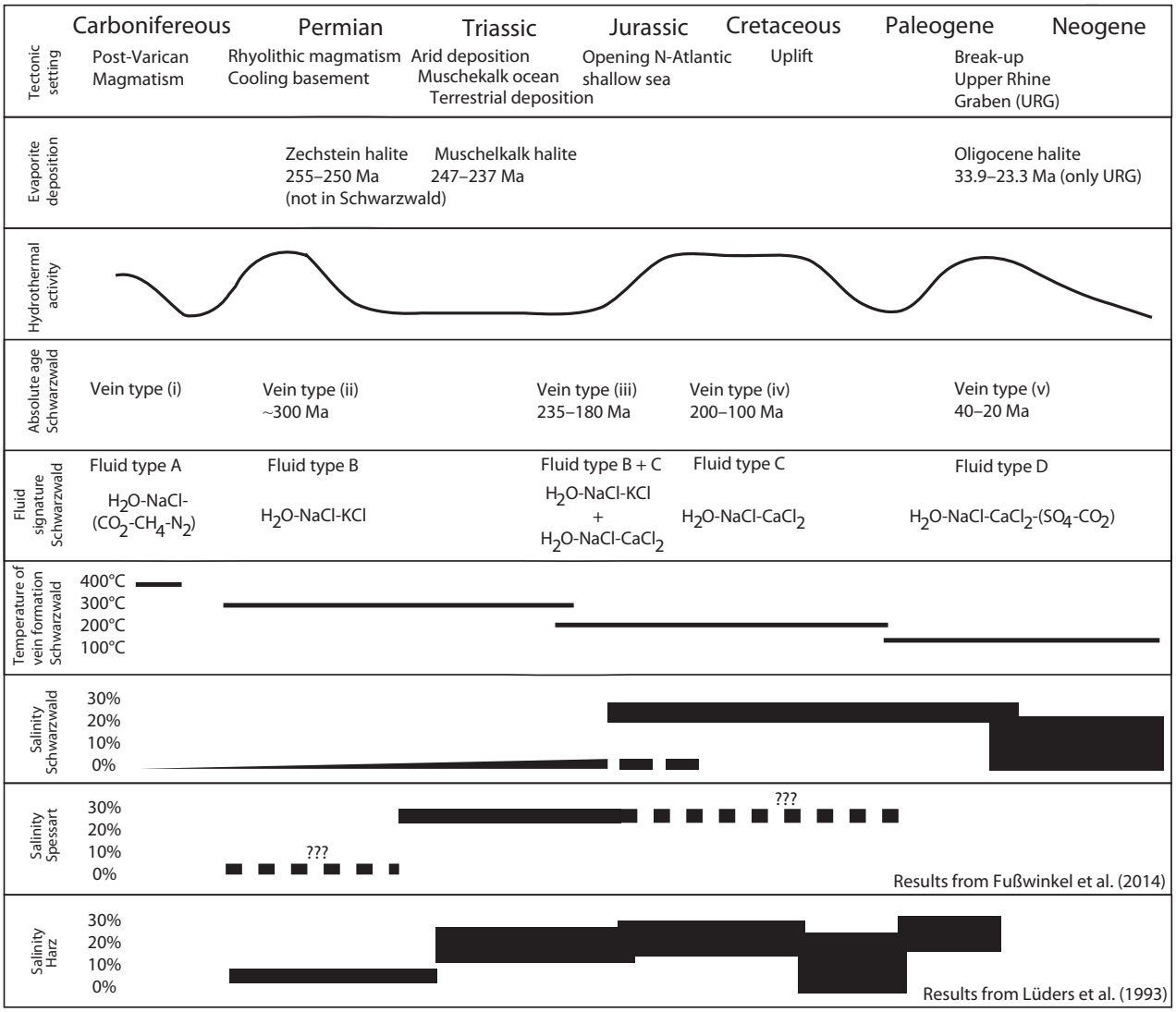

Fig. 9. Temporal comparison of ore precipitation in the Schwarzwald, Harz and Spessart mining districts. Data from Lüders *et al.* (1993) and Fusswinkel *et al.* (2014). Note that the first recognition of a high-salinity basement brine is invariably linked to the formation of halite-bearing evaporites at the surface.

brittle/ductile transition zone (~12–15 km), deep below the depth of the drill holes (<8 km).

As the break-up of the Upper Rhine Graben, various types of meteoric and formation waters (low TDS; Fig. 5E) entered the basement by topographic fluid flow (Agemar *et al.* 2013). The multisource fluids found in Paleogene veins still show a minor component of the highly saline basement brine, which is potential evidence that the fluid stratification in the continental central European basement still prevails until today (Pauwels *et al.* 1993; Bucher & Stober 2010). Diluting the high-salinity NaCl-$CaCl_2$ basement fluids by meteoric and/or formation fluids with low TDS (Pauwels *et al.* 1993) could explain the shift in average salinity from ~23wt% during the Jurassic to ~17wt% today. This modification is also visible in the higher Cl/Br mass ratios of 255 in the modern brine of Soultz-sous-Forêt (Fig. 1) in contrast to the fluids of the Bad Urach and KTB drill holes, which are not proximal to the rift (Fig. 1), showing depleted Cl/Br mass ratios of 80–105.

The history of the basement brine in the context of large-scale ore mineralization

An interesting additional aspect of this study is the relation of brine development and Pb-Zn-Cu-Ag ore deposition in the study area. Before large-scale mixing occurred (Fig. 7), only very low amounts of ore were precipitated in vein types (i), (ii) and (iii), which precipitated from low-salinity fluids A and B and high-

salinity type C (pure end-member fluids). However, as soon as mixing between fluid type C and D occurred, during Jurassic to Paleogene times, massive ore precipitation can be recognized (Fig. 7). The occurrence of high metal concentrations in the mixed CD fluid correlates with the timing of the first percolation of the bittern brine into the crystalline basement. Hence, our data imply in accordance with Fußwinkel *et al.* (2013) that the high-salinity type C bittern brine (modified by fluid–rock reactions in the crystalline basement) was the major carrier of metals. Thus, in the Schwarzwald, the mobilization of metals and the formation of ore deposits are directly linked to and crucially dependent on the formation of evaporites at the surface.

CONCLUSIONS

Upper and middle crustal fluids from SW Germany were investigated by crush-leach analyses of primary fluid inclusions from well-characterized hydrothermal veins of known age. This approach allows the reconstruction of chemical changes and modifications of these fluids over the last 300 Ma (Figs 8 and 9). During the Carboniferous, Permian and Triassic, only dominantly magmatic or metamorphic, high-temperature/low-salinity fluids (probably in equilibrium with their host rock) are recorded. With the beginning of the Jurassic, however, highly saline brines emerge and a subsequent two-component mixing process between basement brine and cover fluid appears to be responsible for their composition during the Jurassic and Cretaceous. Finally, a multicomponent mixing process (basement with various types of cover fluid reservoirs) is necessary to explain the observed variation in fluid compositions related to the onset of Rhine Graben rifting in the Paleogene.

The most striking feature of the reconstruction of the fluid history is the shift from low-salinity to high-salinity fluids around the Triassic–Jurassic boundary (Fig. 9) and its temporal relation to the evaporites at the surface. A comparison of our study area with two other well-studied mineralized regions in central Europe, the Spessart and the Harz mountains (Lüders *et al.* 1993; Fusswinkel *et al.* 2014) indicates that this link between evaporates and high-salinity ore fluids may be also true for other ore districts (of similar type) in central Europe. In contrast to the Schwarzwald, the Spessart and the Harz mountains were covered much earlier by halite-bearing evaporitic sediments during the late Permian. Interestingly, the first high-salinity basement brines in these regions appear in early Triassic veins already. Hence, high-salinity basement fluids emerged in all three regions shortly after the deposition of marine evaporitic halite at the surface. In the Schwarzwald, this happens during the end of the Triassic, in the Spessart and Harz mountains, at the beginning of the Triassic (Fig. 9). Consequently, this suggests that the high salinity in basement brines develops by a combination of external (evaporitic fluids) and internal (desiccation) processes.

ACKNOWLEDGEMENTS

We would like to thank C. Manning and two anonymous reviewers, who helped to improve the manuscript substantially as well as M. Marks and T. Wenzel who helped with many hints and discussions. Furthermore, we would like to thank G. Stoschek and B. Steinhilber for their help with crush-leach analyses and technical support and P. Jeiseke and S. Kaulfuß for sample preparation. This study was supported by the Alfried-Krupp Prize for Young University Teachers of the Krupp Foundation to Gregor Markl and the German Research Foundation (DFG), grant 2135/20-1.

REFERENCES

Agemar T, Brunken J, Jodocy M, Schellschmidt R, Schulz R, Stober I (2013) Untergrundtemperaturen in Baden-Wurttemberg. *Zeitschrift der Deutschen Gesellschaft für Geowissenschaften*, **164**, 49–62.

Banks DA, Davies GR, Yardley BWD, McCaig AM, Grant NT (1991) The chemistry of brines from an Alpine thrust system in the Central Pyrenees: an application of fluid inclusion analysis to the study of fluid behaviour in orogenesis. *Geochimica et Cosmochimica Acta*, **55**, 1021–30.

Banks DA, Giulliani G, Yardley BWD, Cheilletz A (2000) Emerald mineralisation in Columbia: fluid chemistry and the role of brine mixing. *Mineralium Deposita*, **35**, 699–713.

Behr HJ, Gerler J (1987) Inclusions of sedimentary brines in post-Variscan mineralizations in the Federal Republic of Germany—a study by neutron activation analysis. *Chemical Geology*, **61**, 65–77.

Behr HJ, Horn EE, Frentzel-Beyme K, Reutel C (1987) Fluid inclusion characteristics of the Variscan and post-Variscan mineralizing fluids in the Federal Republic of Germany. *Chemical Geology*, **61**, 273–85.

Bejaoui J, Bouhlel S, Sellami A, Braham A (2014) Geology, mineralogy and fluid inclusion study of Oued Jebs Pb–Zn–Sr deposit; comparison with the Bou Grine deposit (diapirs zone, Tunisian atlas). *Arabian Journal of Geosciences*, **7**, 2483–97.

Bellot J-P, Lerouge C, Bailly L, Bouchot V (2003) The Biards Sb-Au–bearing shear zone (Massif Central, France): an indicator of crustal-scale transcurrent tectonics guiding Late Variscan Collapse. *Economic Geology*, **98**, 1427–47.

Bodnar RJ, Vityk MO (1994) Interpretation of microthermometric data for H_2O-NaCl fluid inclusions. In: *Fluid Inclusions in Minerals: Methods and Applications* (eds ?????? ?????), pp. 117–30. ??????, ???????.

Boiron MC, Cathelineau M, Banks DA, Buschaert S, Fourcade S, Coulibaly Y, Michelot JL, Boyce A (2002) Fluid transfer at a basement/cover interface. Part II. Large-scale introduction of chlorine into the basement by Mesozoic basinal brines. *Chemical Geology*, **192**, 121–40.

Bons PD, Fusswinkel T, Gomez-Rivas E, Markl G, Wagner T, Walter BF (2014) Fluid mixing from below in unconformity-related hydrothermal ore deposits. *Geology*, **42**, 1035–8.

Bottomley DJ, Conrad Gregoire D, Raven KG (1994) Saline ground waters and brines in the Canadian Shield: geochemical and isotopic evidence for a residual evaporite brine component. *Geochimica et Cosmochimica Acta*, **58**, 1483–98.

Brander T (2000) U/HE-chronologische Fallstudien an Eisen- und Manganerzen. Dissertation. ???????, Heidelberg.

Brockamp O, Clauer N, Zuther M (2003) Authigenic sericite record of a fossil geothermal system: the Offenburg trough, central Black Forest, Germany. *International Journal of Earth Sciences*, **92**, 843–51.

Brockamp O, Schlegel A, Clauer N (2011) Mesozoic hydrothermal impact on Rotliegende and Bunter immature sandstones of the High Rhine trough and its adjacent eastern area (southern Black Forest, Germany). *Sedimentary Geology*, **234**, 76–88.

Bucher K, Stober I (2002) Water–rock reaction experiments with Black Forest gneiss and granite. In: *Water–Rock Interaction*, Springer, ?????, pp. 61–95.

Bucher K, Stober I (2010) Fluids in the upper continental crust. *Geofluids*, **10**, 241–53.

Burisch M, Marks M, Nowak M, Markl G (2015) ??????. *Goldschmidt Abstracts*, **2015**, 426.

Frape S, Fritz P (1987) Geochemical trends for groundwaters from the Canadian Shield. *Geological Association of Canada Special Papers*, **33**, 19–38.

Fritz P, Frape ST (1982) Saline groundwaters in the Canadian Shield—a first overview. *Chemical Geology*, **36**, 179–90.

Fußwinkel T, Wagner T, Wälle M, Wenzel T, Heinrich C, Markl G (2013) Fluid mixing forms basement-hosted Pb-Zn deposits: Insight from metal and halogen geochemistry of individual fluid inclusions. *Geology*, **41**, 679–82.

Fusswinkel T, Wagner T, Wenzel T, Wälle M, Lorenz J (2014) Red bed and basement sourced fluids recorded in hydrothermal Mn–Fe–As veins, Sailauf (Germany): a LA-ICPMS fluid inclusion study. *Chemical Geology*, **363**, 22–39.

Geyer OF, Gwinner MP (2011) Geologie von Baden - Württemberg. – 5., völlig neu bearbeitete Auflage, Stuttgart, Schweizerbart'sche Verlagsbuchhandlung (Nägele u. Obermiller), 627.

Giggenbach WF (1988) Geothermal solute equilibria. Derivation of Na-K-Mg-Ca geoindicators. *Geochimica et Cosmochimica Acta*, **52**, 2749–65.

Gleeson S, Yardley B (2002) Extensional veins and Pb-Zn mineralisation in basement rocks: the role of penetration of formation brines. In: *Water–Rock Interaction*, Springer, ?????. pp. 189–205.

Gleeson SA, Wilkinson JJ, Stuart FM, Banks DA (2001) The origin and evolution of base metal mineralising brines and hydrothermal fluids, South Cornwall, UK. *Geochimica et Cosmochimica Acta*, **65**, 2067–79.

Göb S, Loges A, Nolde N, Bau M, Jacob DE, Markl G (2013) Major and trace element compositions (including REE) of mineral, thermal, mine and surface waters in SW Germany and implications for water–rock interaction. *Applied Geochemistry*, **????**, ????–????.

Goldstein RH, Reynolds TJ (1994) Systematics of fluid inclusions in diagenetic minerals. *SEPM Short Course Notes*, **31**, 199.

Hann HP, Chen F, Zedler H, Frisch W, Loeschke J (2003) The Rand Granite in the southern Schwarzwald and its geodynamic significance in the Variscan belt of SW Germany. *International Journal of Earth Science*, **92**, 821–42.

Irwin J, Roedder E (1995) Diverse origins of fluid in magmatic inclusions at Bingham (Utah, USA), Butte (Montana, USA), St. Austell (Cornwall, UK), and Ascension Island (mid-Atlantic, UK), indicated by laser microprobe analysis of Cl, K, Br, I, Ba + Te, U, Ar, Kr, and Xe. *Geochimica et Cosmochimica Acta*, **59**, 295–312.

Jébrak M (1997) Hydrothermal breccias in vein-type ore deposits: a review of mechanisms, morphology and size distribution. *Ore Geology Reviews*, **12**, 111–34.

Köhler J, Schönenberger J, Upton B, Markl G (2009) Halogen and trace-element chemistry in the Gardar Province, South Greenland: subduction-related mantle metasomatism and fluid exsolution from alkalic melts. *Lithos*, **113**, 731–47.

Leutwein F, Sonet J (1974) Geochronologische Untersuchungen im Südschwarzwald. *Neues Jahrbuch für Mineralogie – Abhandlungen*, **121**, 252–71.

Loges A, Wagner T, Kirnbauer T, Göb S, Bau M, Berner Z, Markl G (2012) Source and origin of active and fossil thermal spring systems, northern Upper Rhine Graben, Germany. *Applied Geochemistry*, **27**, 1153–69.

Lüders V, Gerler J, Hein U, Reutel C (1993) Chemical and thermal development of ore-forming solutions in the Harz Mountains: a summary of fluid inclusion studies. *Monogr Ser Miner Depos*, **30**, 117–32.

Markl G, Bucher K (1998) Composition of fluids in the lower crust inferred from metamorphic salt in lower crustal rocks. *Nature*, **391**, 781–3.

Marks MA, Marschall HR, Schühle P, Guth A, Wenzel T, Jacob DE, Barth M, Markl G (2013) Trace element systematics of tourmaline in pegmatitic and hydrothermal systems from the Variscan Schwarzwald (Germany): the importance of major element composition, sector zoning, and fluid or melt composition. *Chemical Geology*, **344**, 73–90.

McCaffrey M, Lazar B, Holland H (1987) The evaporation path of seawater and the coprecipitation of Br^- and K^+ with halite. *Journal of Sedimentary Research*, **57**, 928–37.

Mertz DF, Lippolt HJ, Huck KH (1986) K/Ar, Ar-40/Ar-39, and Rb/Sr investigations on the genesis of the Clara vein deposit, Central Black Forest. Jahrestagung Dtsch. *Geophysikalischen Ges. e.V.*, **46**, 235.

Meyer M, Brockhamp O, Clauer N, Renk A, Zuther M (2000) Further evidence for a Jurassic mineralizing event in central Europe: K-Ar dating of hydrothermal alteration and fluid inclusion systematics in wall rocks of the Käfersteige fluorite vein deposit in the northern Black Forest, Germany. *Mineralium Deposita*, **35**, 754–61.

Möller P, Woith H, Dulski P, Lüders V, Erzinger J, Kämpf H, Pekdeger A, Hansen B, Lodemann M, Banks DA (2005) Main and trace elements in KTB-VB fluid: composition and hints to its origin. *Geofluids*, **5**, 28–41.

Pauwels H, Fouillac C, Fouillac A-M (1993) Chemistry and isotopes of deep geothermal saline fluids in the Upper Rhine Graben: origin of compounds and water–rock interactions. *Geochimica et Cosmochimica Acta*, **57**, 2737–49.

Pearson JFJ, Lolcama JL, Scholtis A (1989) Chemistry of waters in the Böttstein, Weiach, Riniken, Schafisheim, Kaisten and Leuggern boreholes: a hydrochemically consistent data set. *NAGRA Technical Report*, **86–19**, 153.

Pfaff K, Romer RL, Markl G (2009) U-Pb ages of ferberite, chalcedony, agate, "U-mica" and pitchblende: constraints on the mineralization history of the Schwarzwald ore district. *European Journal of Mineralogy*, **21**, 817–36.

Pfaff K, Hildebrandt LH, Leach DL, Jacob DE, Markl G (2010) Formation of the Wiesloch Mississippi Valley-type Zn-Pb-Ag deposit in the extensional setting of the Upper Rhinegraben, SW Germany. *Mineralium Deposita*, **45**, 647–66.

Pfaff K, Koenig MA, Wenzel T, Ridley I, Hildebrandt LH, Leach DL, Markl G (2011) Trace and minor element variations and sulfur isotopes in crystalline and colloform ZnS: incorporation mechanisms and implications for their genesis. *Chemical Geology*, **286**, 118–34.

Romer RL, Förster H-J, Kroner U, Müller A, Rötzler J, Seltmann R, Wenzel T (2012) *Granites of the Erzgebirge – Relation of Magmatism to Metamorphic and Tectonic Evolution of the Varsican Orogen*. Scientific Technical Report 12/15, GFZ German Research Centre for Geosciences.

Savoye S, Aranyossy J-F, Beaucaire C, Cathelineau M, Louvat D, Michelot J-L (1998) Fluid inclusions in granites and their relationships with present-day groundwater chemistry. *European Journal of Mineralogy*, **10**, 1215–26.

Schlegel A, Brockamp O, Clauer N (2007) Response of clastic sediments to episodic hydrothermal fluid flows in intramontane troughs: a case study from Black Forest, Germany. *European Journal of Mineralogy*, **19**, 833–48.

Schwinn G, Markl G (2005) REE systematics in hydrothermal fluorite. *Chemical Geology*, **216**, 225–48.

Shepherd TJ, Rankin AH, Alderton DHM (1985) *A Practical Guide to Fluid Inclusion Studies*. Blackie, ??????.

Shouakar-Stash O, Alexeev S, Frape S, Alexeeva L, Drimmie R (2007) Geochemistry and stable isotopic signatures, including chlorine and bromine isotopes, of the deep groundwaters of the Siberian Platform, Russia. *Applied Geochemistry*, **22**, 589–605.

Smith MP, Savary V, Yardley BWD, Valley JW, Royer JJ, Dubois M (1998) The evolution of the deep flow regime at Soultz-sous-Forêts, Rhine Graben, eastern France: evidence from a composite quartz vein. *Journal of Geophysical Research*, **103**, 27223–37.

Staude S, Bons PD, Markl G (2009) Hydrothermal vein formation by extension-driven dewatering of the middle crust: an example from SW Germany. *Earth and Planetary Science Letters*, **286**, 387–95.

Staude S, Dorn A, Pfaff K, Markl G (2010) Assemblages of Ag-Bi sulfosalts and conditions of their formation: the type locality of schapbachite ($Ag_{0.4}Pb_{0.2}Bi_{0.4}S$) and neighboring mines in the Schwarzwald ore district, southern Germany. *Canadian Mineralogist*, **48**, 441–66.

Staude S, Göb S, Pfaff K, Ströbele F, Premo WR, Markl G (2011) Deciphering fluid sources of hydrothermal systems: a combined Sr- and S-isotope study on barite (Schwarzwald, SW Germany). *Chemical Geology*, **286**, 1–20.

Staude S, Mordhorst T, Nau S, Pfaff K, Brügmann G, Jacob DE, Markl G (2012a) Hydrothermal Carbonates of the Schwarzwald ore district, southwestern Germany: carbon source and conditions of formation using $\delta^{18}O$, $\delta^{13}C$, $^{87}Sr/^{86}Sr$, and fluid inclusions. *The Canadian Mineralogist*, **50**, 1401–34.

Staude S, Werner W, Mordhorst T, Wemmer K, Jacob DE, Markl G (2012b) Multi-stage Ag–Bi–Co–Ni–U and Cu–Bi vein mineralization at Wittichen, Schwarzwald, SW Germany: geological setting, ore mineralogy, and fluid evolution. *Mineralium Deposita*, **47**, 251–76.

Steele-MacInnes M, Bodnar RJ, Naden J (2011) Numerical model to determine the composition of H_2O-NaCl-$CaCl_2$ fluid inclusions based on microthermometric and microanalytical data. *Geochimica et Cosmochimica Acta*, **75**, 21–40.

Stober I, Bucher K (1999) Deep groundwater in the crystalline basement of the Black Forest region. *Applied Geochemistry*, **14**, 237–54.

Stober I, Bucher K (2004) Fluids sinks within the earth's crust. *Geofluids*, **4**, 143–51.

Stober I, Bucher K (2005) The upper continental crust, an aquifer and its fluid: hydraulic and chemical data from 4 km depth in fractured crystalline basement rocks at the KTB test site. *Geofluids*, **5**, 8–19.

Wagner T, Cook NJ (2000) Late-Variscan antimony mineralisation in the Rheinisches Schiefergebirge, NW Germany: evidence for stibnite precipitation by drastic cooling of high-temperature fluid systems. *Mineralium Deposita*, **35**, 206–22.

Walter BF, Immenhauser A, Geske A, Markl G (2015) Exploration of hydrothermal carbonate magnesium isotope signatures as tracers for continental fluid aquifers, Schwarzwald mining district, SW Germany. *Chemical Geology*, **400**, 87–105.

Werner W (2011) Mineralische Rohstoffe. In: (eds Hann P, Zedler H) *Erläuterungen zum Blatt 8113 Todtnau*. pp. 98–115, 3 Abb.; Freiburg i. Br. (LGRB, Hrsg.).

Werner W, Franzke HJ, Wirsing G, Jochum J, Lüders V, Wittenbrink ???? (2002) mit einem Beitrag von B. Steiber: Die Erzlagerstätte Schauinsland bei Freiburg im Breisgau. Bergbau, Geologie, Hydrogeologie, Mineralogie, Geochemie, Tektonik und Lagerstättenentstehung. Ber. Naturforsch. Ges. Freiburg, 92: 110 S., 26 Abb., 9 Tab., 16 Taf.; Freiburg i. Br.

Wernicke RS, Lippolt HJ (1993) Botryoidal hematite from the Schwarzwald (Germany): heterogeneous uranium distributions and their bearing on the helium dating method. *Earth and Planetary Science Letters*, **114**, 287–300.

Wernicke RS, Lippolt HJ (1997) (U + Th)–He evidence of Jurassic continuous hydrothermal activity in the Schwarzwald basement, Germany. *Chemical Geology*, **138**, 273–85.

Wetzel A, Allenbach R, Allia V (2003) Reactivated basement structures affecting the sedimentary facies in a tectonically "quiescent" epicontinental basin: an example from NW Switzerland. *Sedimentary Geology*, **157**, 153–72.

Yardley BWD (2005) Metal concentrations in crustal fluids and their relationship to ore formation. *Economic Geology*, **100**, 613–32.

SUPPORTING INFORMATION

Additional Supporting Information may be found in the online version of this article:

Table S1. Results of the microthermometry.

Table S2. Results crush leach and age constrains for the individual samples.

Appendix S1. Supplement analytical uncertainties.

Anhang 3

Walter, B.F., Burisch, M., Marks M.A.W., & Markl G. (submitted to Chemical Geology) Major element and trace metal systematics of fluid inclusions in hydrothermal veins: metal provenance and the reconstruction of eroded sedimentary units

akzeptiert zur Veröffentlichung	Anzahl der Autoren	Position des Kandidaten in der Autorenliste	Wissen-schaftliche Idee des Kandidaten (%)	Datengenerier-ung des Kandidaten (%)	Analysen und Interpretat-ionen des Kandidaten (%)	Verfassen der Publikation durch den Kandidaten (%)
nein	4	1	70	90	60	50

Major element and trace metal systematics of fluid inclusions in hydrothermal veins: metal provenance and the reconstruction of eroded sedimentary units

Benjamin F. Walter*, Mathias Burisch, Michael A.W. Marks, Gregor Markl

Department of Geosciences, University of Tübingen, Wilhelmstrasse 56, 72074 Tübingen, Germany

*Corresponding author: benjamin.walter@uni-tuebingen.de

Keywords: hydrothermal ore; base metals; Cl/Br systematics, fluid mixing, basement brine

Abstract:

Mixing of sedimentary formation fluids with basement-derived brines is an important mechanism for the formation of hydrothermal veins. In this study, we focus on the sources and metal contents of the sediment-derived fluid component in ore-forming processes and present a comprehensive fluid inclusion study on 84 Jurassic hydrothermal veins from the Schwarzwald mining district (SW Germany). Our data reveal differences in the average fluid composition between the northern, central and southern Schwarzwald: average fluids from the northern and southern Schwarzwald are characterized by high salinities (18-26 wt.% $NaCl+CaCl_2$), low Ca/(Ca+Na) ratios (0.1-0.4) and variable Cl/Br ratios (30-1140). In contrast, average fluids from the central Schwarzwald are characterized by even higher salinities (23-27 wt.% $NaCl+CaCl_2$), higher Ca/(Ca+Na) ratios (0.2-0.9) and less variable Cl/Br ratios (40-130).

A comparison of the fluid inclusion data with the regional geology shows a connection between fluid composition and the nature and thickness of the reconstructed (now eroded) sedimentary cover rocks. Compared to the northern and the southern Schwarzwald, where halite precipitation occurred during the middle Triassic, the sedimentary basin in the central Schwarzwald was relatively shallow at this

time and no halite was precipitated. Accordingly, Cl/Br ratios of fluids from the central Schwarzwald provide no evidence for the reaction of a sedimentary brine with halite, whereas those from the northern and southern Schwarzwald do. Instead, elevated Ca/(Ca+Na), high SO_4 contents and relatively low Cl/Br imply the presence of a gypsum dissolution brine during vein formation in the central Schwarzwald which nicely agrees with the reconstructed regional Triassic geology.

Base metal (Pb, Zn, Cu, Ni, Co, Bi) contents and Pb/Zn ratios in hydrothermal fluids show differences with the stratigraphic depth of the hydrothermal deposits, because of a decreasing influence of sedimentary fluids with depth. Further, Pb and Zn contents in the fluids increase with stratigraphic depth, whereas Cu, Ni, Bi and Co contents decrease. This indicates that the major Pb and Zn source is the basement brine, while the major source of Cu, Ni, Bi and Co is the sedimentary overburden. The observed increase of the Pb/Zn ratio with depth is unusual, as Pb and Zn behave geochemically similar in hydrothermal solutions. This effect can be explained by an additional Zn source in the sedimentary aquifer – probably Muschelkalk limestones.

1. Introduction:

Fluid mixing is proposed as a major ore-precipitating process for many hydrothermal ore systems (Duane and De Wit, 1988; Tornos et al., 1991; McCaig et al., 2000; Klemm et al., 2004; Fußwinkel et al., 2013; Bons et al., 2014; Fußwinkel, 2014). Previous studies on hydrothermal ore deposits include combinations of microthermometry, stable and radiogenic isotopes (O-C-H-Sr-Cl-Br-Pb-Zn-Mg), trace element studies on fluids and gangue minerals, and paleo-hydrological modelling (e.g., Kessen et al., 1981; Garven et al., 1999; Bau et al., 2003; Wilkinson et al., 2005b; Shouakar-Stash et al., 2007; Wilkinson, 2010; Pfaff et al., 2011; Staude et al., 2011; Fußwinkel et al., 2013; Walter et al., 2015). In many well-studied mining districts (such as the Alaskan Brooke Range, the South East Basin and the Massif Central in France, the Irish Midlands, the Maestrat basin and the Catalan Coastal Ranges in Spain and Upper Silesia in Poland) mixing of hot, deep-seated fluids from the crystalline basement with cooler, sediment-derived fluids from the overburden has been suggested to be the major process causing hydrothermal mineral precipitation (e.g., Aquilina et al., 2011; Banks et al., 2002; Boiron et al., 2010; Leach et al., 2004). In general, the basement-derived fluids are assumed to represent the

dominant metal source, whereas the sedimentary fluids are typically metal-poor (Banks et al., 2000a, 2002; Boiron et al., 2002; Fußwinkel et al., 2013; Bons et al., 2014). Most previous studies focused on the metal-rich basement fluids, although the importance of a sedimentary fluid component was noticed and attention was drawn to the "fluid from above" (Yardley, 2005; Boiron et al., 2010; Bons et al., 2014; Fusswinkel et al., 2014). However, studying these sedimentary fluids in more detail is difficult, if the former sedimentary aquifers overlying the basement rocks are presently (partly) missing, because they were eroded (e.g. Schwarzwald (Geyer and Gwinner, 2011), Spessart (Wagner et al., 2010), Harz (Lüders and Möller, 1992), Irish Midlands (Wilkinson, 2010)) and the sedimentary overburden may be heterogeneous with respect to thickness and composition on the scale of a mining district.

For our study, which focuses on the fluids from "above", we chose the Schwarzwald mining district in SW Germany, because it is an exceptionally well investigated area and detailed studies on various aspects of regional geology and hydrothermal vein formation in this area are available. These include detailed mineralogical, microthermometric and isotopic investigations on specific ore deposits (e.g. Baatartsogt, 2006, 2007; Fußwinkel et al., 2013; Markl et al., 2006; Pfaff et al., 2010; Schwinn et al., 2006; Staude et al., 2007, 2009, 2010a, 2011a, 2012a, b; Ströbele et al., 2012; Walter et al., 2015a, in press),

stable isotope data (Staude et al., 2011a, 2012a, 2012b; Walter et al., 2015a), trace element data for common ore minerals of the district, such as fahlore and sphalerite (Staude et al., 2010b; Pfaff et al., 2011), age-dating (Pfaff et al., 2009), paleo-hydrological modelling (Pfaff et al., 2010; Staude et al., 2011a; Walter et al., 2015a, in press), studies on the composition of modern thermal, mineral and formation waters (Stober & Bucher 1999, 2010; Möller et al. 1997; Loges et al., 2012; Göb et al., 2013), hydraulic data (Stober & Bucher 2004), detailed studies on the regional geology (Ziegler, 1990, Geyer and Gwinner, 2011) and experimental leaching studies (Bucher and Stober, 2002; Burisch et al., 2015, submitted).

The modern water column in the Schwarzwald shows a distinct compositional stratification with HCO_3^- being the dominant anion at shallow crustal levels (<2 km), while SO_4^{2-} is dominant at intermediate depths and Cl^- at depths >2-3 km. The processes that cause this stratification are,

however, poorly understood (Stober and Bucher, 1999; Frape et al., 2003).

The Cl/Br ratio of fluids is often used as a reservoir tracer (Stober & Bucher, 1999; Boiron et al., 2010; Wilkinson, 2010; Fußwinkel et al., 2013). Deep crustal brines are known to have Cl/Br ratios <100, while halite dissolution brines show Cl/Br ratios higher than that of sea water (288). Halite precipitation in evaporites results in the formation of residual bittern brines, which show successively decreasing Cl/Br ratios (288-34) with increasing degree of evaporation (Frape and Fritz, 1987; McCaffrey et al., 1987; Edmunds and Savage, 1991; Banks et al., 2000b; Stober and Bucher, 2004a; Stober and Bucher, 2004b; Möller et al., 2005; Yardley, 2005). We focus here on the qualitative source information provided by Cl/Br systematics of fluids, in contrast to other contributions, which focus on the formation of low-Cl/Br ratios and the development of high salinities in basement brines (Burisch et al., 2015, submitted; Walter et al., in press). Although water-rock interaction with crystalline rocks can result in low Cl/Br ratios (Bucher and Stober, 2002), Burisch et al. (2015, submitted) showed that fluids with salinities above 20 wt.% and low Cl/Br ratios can only be formed involving an externally derived bittern brine.

2. Regional geology

The Schwarzwald (Fig. 1) mainly consists of mostly metasedimentary gneisses, migmatites and granites, representing a deeply eroded basement window. Gneisses are mostly paragneisses with local occurrences of orthogneisses and amphibolites that were metamorphosed during Variscan (Carboniferous) collisional processes (Geyer and Gwinner, 2011). They were intruded between 335 and 315 Ma by post-collisional granites, which today form about 50% of the exposed Schwarzwald basement (Todt, 1976; Altherr et al., 2000; Hann, 2003). These crystalline basement rocks are covered by a Paleozoic and Mesozoic sedimentary sequence (Geyer and Gwinner, 2011; and references therein).

During Permian times (Rotliegend), local sediment basins (thickness <500m) were filled by redbeds (arkoses, conglomerates; Jenkner, 1986; Nitsch and Zedler, 2009; Geyer and Gwinner, 2011) and rhyolithic volcanism occured locally producing flows and sediments with a maximum thickness of <250m (Geyer and Gwinner, 2011). Early Triassic, quartzitic Buntsandstein units reach a thickness of

≤400m in the northern and <50 m in the southern Schwarzwald. The Buntsandstein is an important aquifer and is locally separated from the Middle Triassic by the Rötton aquitard. Middle Triassic (Muschelkalk) units, including limestones, shales and evaporites (the latter only being present in the Middle Muschelkalk) reach thicknesses of 160 to less than 220 m (Stober & Bucher, 2014) in the area of interest. In paleo-depressions, these units contain a halite-bearing horizon, which will be important for the discussion below. This halite-bearing unit reaches its maximum thickness (about 100 m) in the centres of these depressions whereas in shallower areas its thickness successively decreases. At paleo-topographic heights transitions from halite-dominated to sulphate-dominated horizons occur, where no or little halite is present. In contrast, the Late Triassic (Keuper) units are dominantly composed of clastic sediments and evaporitic gypsum. This unit reaches about 300 m in the north and thins out to less than 100 m in the south (Geyer and Gwinner, 2011). During the Jurassic, an approximately 1000m thick unit of mostly marine carbonates covered the Triassic units.

Exhumation of the area since the late Cretaceous happened asymmetrically to a maximum stratigraphic depth of ~2000m below the basement-cover unconformity in the SW of the Schwarzwald (Rupf and Nitsch, 2008; Geyer and Gwinner, 2011), while in relation to the Upper Rhinegraben Rift in the north, the stratigraphic depth exposed to the present surface is about 100 m above the unconformity. A large displacement fault exists in the Elztal area which is responsible for the observation, that hydrothermal veins exposed at the surface now vary in their formation depth from several 100 meters in the northern to more than 2.5 km in the southern Schwarzwald (Staude et al., 2010; 2011; 2012; Walter et al., 2015). Therefore, hydrothermal veins, formed at the same time, but at different stratigraphic depth are nowadays exposed in the Schwarzwald, which makes this region particularly suited for studying fluid composition changes with depth. Associated with the late Upper Rhinegraben rifting, Paleogene sediments of up to 4000 m thickness occur in the Upper Rhinegraben, including Oligocene halite-bearing evaporites (Stober & Bucher, 2014).

2.1. Hydrothermal veins in the Schwarzwald

More than 1000 mineralized hydrothermal veins are documented in the Schwarzwald mining district (Metz et al., 1957; Bliedner & Martin, 1986; Staude et al., 2009; Markl 2015). The veins consist

dominantly of barite, fluorite, quartz and carbonates besides base and precious metal oxides, sulfides and arsenides (Fe-Mn, Cu-Pb-Zn and Ag-Bi-Co-Ni-U) (Metz et al., 1957). Five distinct maxima of hydrothermal activity and associated vein formation are known beginning with late-Carboniferous quartz-tourmaline veins, Permian quartz veins with rare Sb mineralizations, Triassic-Jurassic quartz-hematite veins, Jurassic-Cretaceous fluorite-barite-quartz-carbonate veins with Pb-Zn-Cu, Fe-Mn and or rarely Ag-Bi-Co-Ni-U ores, to post-Cretaceous quartz-barite-fluorite or carbonate veins with Pb-Zn-Cu-(As) mineralizations (Staude et al., 2012; Pfaff et al., 2009, Walter et al., in press).

Abundant vein mineralization occurred over the Jurassic-Cretaceous period in an extensional tectonic regime related to the break-up of the North Atlantic (Staude et al., 2009). During this time, the sedimentary stack was mostly undisturbed (in contrast to the geological situation in the Tertiary related to the Upper Rhine Graben rifting). As a consequence, the fluid inclusion chemistry can be very well described as a bimodal mixing (Walter et al., 2015). The asymmetric exhumation of the crystalline basement related to the formation of the Upper Rhinegraben during the Tertiary (Geyer and Gwinner, 2011) enables a direct comparison of syn-genetic Jurassic-Cretaceous hydrothermal veins from different crustal levels. Although the large-scale Jurassic topography is assumed to have been flat, exact depth estimations are not possible because the topography probably varied locally, as did the absolute amount of exhumation. Therefore, the difference in stratigraphic depth of formation we are referring to is only of a qualitative to semi-quantitative nature.

For many ore districts, hydrogeological models contradict geochemical models (e.g. Boiron et al., 2010; Kendrick et al., 2011), since the emplacement of a meteoric fluid to great depths followed by mixing with a second fluid on its ascent is difficult to explain from a hydrogeological point of view (e.g. to bring down fluids with similar salinity or density is not possible by gravity-driven infiltration, Bons et al., 2014 and references therein). The major driving force for vertical fluid flow is assumed to be the consumption of water at depth due to alteration of primary minerals (Stober & Bucher 2004).

For the Jurassic-Cretaceous hydrothermal veins of the Schwarzwald district, however, a hydrogeological mixing model is available, which is in perfect agreement with the geochemical and hydrogeological observations in the Schwarzwald mining district (Stober & Bucher, 2004; Bons et al., 2014; Walter et al., in press). Compositional and isotope data for Jurassic-Cretaceous fluid inclusions

169 confirm a binary mixing between a continental basement brine and a sedimentary formation fluid
170 (Pfaff et al., 2010, 2011; Staude et al., 2009; 2010a, 2010b, 2011, 2012a, Ströbele et al., 2012;
171 Fußwinkel et al., 2013; Walter et al., 2015a, Walter et al., in press). The basement brine is typically a
172 hot (120 ± 50°C), highly saline (22±2 wt% NaCl+$CaCl_2$), metal-rich fluid (Zn, Pb) with Cl/Br below
173 150 (Fußwinkel et al., 2013, Walter et al., in press). The sedimentary fluid is equally saline but less
174 metal-rich and partly exhibits high Cl/Br ratios (up to 10.000), indicating the dissolution of halite
175 (Stober and Bucher, 1999; 2014; Stober 2014). The only possibility for developing such high Cl/Br-
176 fluids during the Jurassic was probably interaction with Triassic evaporites, since at that time, the
177 Oligocene salts were not yet deposited and the southern margin of the marine evaporate-bearing
178 Zechstein facies ended in the very northern part of the Schwarzwald (Geyer & Gwinner, 2011 and
179 references therein).
180
181 3. Sample material
182 Samples with centimetre-sized euhedral crystals of fluorite, barite, quartz and carbonates were selected
183 based on the following criteria: (1) veins that formed unambiguously during the Jurassic-Cretaceous
184 (based on structural, chemical and age-dating arguments, see details in Pfaff et al., 2011 and Walter et
185 al., in press), (2) abundant gangue minerals with homogeneous fluid inclusions of high salinity with a
186 maximal variance of ±2 wt.% salinity (NaCl+$CaCl_2$) within a given sample, (3) no detectable overprint
187 by post-Cretaceous low- to high-salinity fluids (see Walter et al., 2015, in press). Samples, which did
188 not strictly meet criterion (3) were excluded, since an overprint by post-Cretaceous fluids, which
189 interacted with Oligocene halite in the Upper Rhinegraben, possibly would have distorted the Jurassic
190 Cl/Br signature. Samples from the Paleogene MVT deposit at Wiesloch are an exception, since they
191 are younger than the Jurassic veins, but they are still older than the Oligocene salt deposits related to
192 the Rhinegraben rift (Pfaff et al., 2010; Geyer and Gwinner, 2011). Therefore, they formed under
193 undisturbed hydrogeological conditions and show Cl/Br systematics almost similar to the Jurassic
194 veins.
195 Only gangue minerals (crystals up to 4cm) without visible impurities were analysed to minimize
196 potential contamination. For Jurassic hydrothermal veins, which consist of more than one gangue

mineral, several co-genetic gangue minerals (quartz, barite, fluorite or calcite) of the same vein were analysed whenever possible.

In most of the veins, silicification of the host rock pre-dates the formation of hydrothermal veins. On the top of these silicified selvages, coarse-grained fluorite and/or barite precipitated. In many veins, this stage was followed by the formation of clear, euhedral, coarse-grained quartz. There are significant differences in vein mineralogy correlating with the geographic and stratigraphic position of the respective veins. Veins from the northern Schwarzwald are either barite-quartz or fluorite-barite veins with Cu-Bi mineralization, veins from the central Schwarzwald are fluorite±barite-(carbonate-quartz) veins with Pb-Zn, Fe-Mn or U-Bi-Co-Ni mineralizations, and veins from the southern Schwarzwald are fluorite-quartz-barite veins with Pb-Zn ores.

Fifty-one veins were analysed in detail by microthermometry (in fluorite, quartz and carbonate) including hydrothermal veins from the northern, central and southern Schwarzwald (Fig. 1) and 84 samples (fluorite, quartz, carbonate and barite) were analysed by means of ion chromatography (IC) and total reflection X-ray fluorescence (TXRF). When possible, several samples of one vein were analysed in order to avoid possible nugget effects and to check the reproducibility of the results. A total of 193 crush leach analyses were performed. For most samples, new heating-freezing experiments were done to characterize the fluid inclusions, but the dataset also includes 20 samples, for which microthermometric and crush leach data already existed from former studies (Staude et al., 2012; Walter et al., 2015, in press). The complete dataset is reported in the electronic supplement.

4. Analytical procedure

4.1 Microthermometry

Cross sections through the hydrothermal veins (perpendicular to the longitudinal extent of the veins) with up to three double polished thick sections (200 to 400µm) of each vein were produced and the chronological sequence of fluid inclusions (fluid inclusion assemblages, FIA, Goldstein and Reynolds, 1994) was determined by optical microscopy. Fluid inclusions were classified as primary (p), pseudo-secondary (ps), secondary (s), isolated inclusions (iso) and clusters of inclusions with no geometrical relation to former crystal surfaces or fractures (c). Microthermometric investigations were performed

using a Linkam stage (model THMS 600). Each fluid inclusion was analysed three times for its final melting temperature of ice ($T_{m,ice}$) and hydrohalite ($T_{m,hh}$) and its homogenization temperature (T_h). The data include only fluid inclusions, for which triple analyses differ less than 0.1°C for $T_{m,ice}$ and $T_{m,hh}$ and 1°C for T_h. Synthetic H_2O, H_2O-NaCl and H_2O-CO_2 standards were used for calibration. Fluid inclusion trails with strong deviation in salinity and homogenization temperature within a homogeneous trail were neglected, since this indicates fluid inclusion alteration by post-entrapment processes. The salinity in the ternary NaCl-$CaCl_2$-H_2O system was calculated according to Steele-MacInnes et al. (2011). For each fluid inclusion the degree of filling was estimated based on filling degree tables (Shepherd et al., 1985; Bakker and Diamond, 2006). A pressure correction (Bodnar and Vityk, 1994) was applied assuming hydrostatic conditions with a depth of the water column inferred from the paleo-depth estimated by (Geyer and Gwinner, 2011). Uncertainties of this approach are discussed in Walter et al. (2015). Since the salinity for the Jurassic-Cretaceous fluid inclusions of the Schwarzwald is invariably high, the pressure correction has only minor effects on the homogenization temperature. Microthermometry of fluid inclusions in barite is difficult, since fluid inclusions are often destroyed during freezing. Therefore, repeated heating of fluid inclusions in barite was not always possible. Consequently, microthermometric data obtained from fluid inclusion in barite were only used for calculating salinities in cases where the data agreed with data of quartz, fluorite or calcite of the same or a related vein. Due to the problematic behaviour of barite, microthermometric data were only used for calculating the salinity, and were excluded from Ca/(Ca+Na) calculations.

4.2 Major, minor and trace element composition of fluid inclusions

From 200 selected samples, containing only one fluid type (which was determined by microthermometry (Tm, Th and Te) prior to crush-leach analysis), about 2g of fluorite, quartz, calcite or barite (grain size of 0.5 to 1 mm) were handpicked avoiding visible impurities. These separates were washed for 3 hours in HNO_3 at 60-70°C (the carbonates were washed in Milli-Q water only). Subsequently, the samples were washed for one week with ultrapure water, changing the water twice a day. These samples were then dried and powdered in an agate mortar. To suppress the adsorption of doubly-charged cations (especially Ca^{2+}), crush leach solutions were acidified with suprapure HNO_3

(Köhler et al., 2009). The loaded solution was injected into a Dionex ICS 1000 ion chromatography systems, equipped with an IonPac AS 9-HC 2mm column for quantification of anions (F, Cl, Br, NO_3, PO_4 and SO_4) and an IonPac CS 12-A column for cations (Li, Na, K, Mg, Ca, Ba, Sr). For injection of the solutions, we used disposable syringe filters CROMAFILE® Xtra RC-20/25 and CROMAFILE® Xtra PVDF-20/25 for anions and cations, respectively (Ladenburger 2012, and Ladenburger et al., 2012). Blank runs were carried out before and after each analysis and defined standard solutions were regularly analyses to monitor the reproducibility and precision of the measurements. Uncertainties were usually smaller than 15% and effective detection limits were generally <10 mg/l. Absolute concentrations were calculated based on the salinity determined by micro thermometry using Cl as internal standard.

The concentrations of several trace metals (Cu, Ni, Co, Pb, Zn, Bi) were determined by Total Reflection X-Ray Fluorescence Spectroscopy (TXRF) using a S2 PICOFOX (Bruker AXS Microanalysis) equipped with a Mo-tube operated with a 50 kV and 600µA. Each 1 ml of the crush-leach solutions (see above) were centrifuged and filtered. Subsequently, 190 µl of the solution were mixed with 10 µl Ga solution with a Ga concentration of 5 mg/l. Three aliquots (10µl) were pipetted onto polished quartz-glass disks and dried at 70°C. The dried sample cakes were then analysed for 1000 s. Effective detection limits for these metals vary with the degree of dilution (based on the crush-leach procedure, see above) and were generally <50 mg/l for Cu, Ni, Pb and Zn and <100 mg/l for Co and Bi. Absolute metal concentrations were obtained by normalizing the measured values to the Cl concentrations determined by microthermometry.

4.3 Analytical uncertainties

Quartz, barite, calcite and fluorite were used for crush leach analyses. A contamination of the leachates by the dissolution of the host minerals is potentially relevant for fluorite (Ca, F), calcite (Ca, Mg?) and barite (Ba, Sr, SO_4). The complete dataset in the electronic supplement includes these elements, but their concentrations in the respective inclusions were excluded from interpretation. Many of our crush-leach solutions contain dissolved carbonate from fluid inclusions (as indicated by the presence of CO_2 based on Raman spectroscopy) and we assume that the positive deviations from

electrical neutrality can be ascribed to carbonate species, as has been done before (e.g. Bottrell et al., 1988; Channer and Spooner, 1991; Banks et al., 2000; Dolnischek et al. 2014). This has, however, no impact on the reliability of Cl and Br data in the crush-leach analyses and especially not on the Cl/Br ratios, nor on the quality of the microthermometric data (Ca-Na variations, salinity or homogenization temperatures).

Crush leach solutions were carefully filtered and centrifuged before analysis to exclude potential contamination because of suspended particles of ore minerals. Some analyses revealed very high metal contents (up to about 55000 mg/l Pb and 52000 mg/l Cu). To evaluate the validity of these analyses we performed calculations using Geochemists Workbench Version 10.0.2. Using the compositions of BW163 and STD2 (table 2 of the electronic supplement), at neutral pH, fO_2 of sulfide stability and 150°C the model shows that these high Pb and Cu concentrations are still well below the saturation of Pb and Cu minerals in these particular solutions (0.7 mol/l Pb (~145 g/l) and 10 mol/l Cu (~635 g/l).

5. Results

We focus our presentation here on the microthermometric data and important element ratios (molar Ca/(Na+Ca); Cl/Br mass ratio, Pb/Zn mass ratio and (Pb+Zn)/(Cu+Ni+Co+Bi)), which will be discussed below. The complete dataset is available as electronic supplement. All investigated fluid inclusions exhibit high salinities (18-28 wt.%, $NaCl+CaCl_2$) with homogenization temperatures (T_h) between 50 and 192°C (Fig. 2A-C; Table 2 of the electronic supplement). Freezing temperatures vary between -70 and -100°C. First melting occurs above -50°C implying a ternary $NaCl-CaCl_2-H_2O$ system with a eutectic temperature at -52.0°C, and ice and hydrohalite as last-melting phases. The final melting temperature of ice is in the range of -9.4° to -36.9°C, of hydrohalite between -2.3° to -50.9°C. The molar Ca/(Ca+Na) ratios were calculated according to Steele-MacInnis et al. (2011) and range from 0.1 to 0.9 (Fig. 2D-F). In a given fluid inclusion trail, salinity and T_h do not significantly vary between individual fluid inclusions, but can vary between different trails within one sample. In the following, we present our data sorted by geographical and stratigraphic position in the basement, starting with the lowermost veins of the southern Schwarzwald.

5.1 Southern Schwarzwald (veins up to 2km below the basement-cover unconformity)

The Jurassic-Cretaceous veins of the southern Schwarzwald show salinities of 18-26 wt.% ($NaCl+CaCl_2$). The Cl/Br ratios are variable (33-1139) and molar Ca/(Na+Ca) ratios range between 0.09 and 0.4. Homogenization temperatures range from 77 to 198°C (weighted average of 140°C), maximum (Pb + Zn) contents are up to 56.000 mg/l and maximum (Cu + Ni +Bi +Co) contents reach 55.000 mg/l (Fig. 3A-D).

5.2 Central Schwarzwald (veins close to the basement-cover unconformity)

The Jurassic-Cretaceous veins of the central Schwarzwald show higher salinities of 23-27 wt.% ($NaCl+CaCl_2$). The Cl/Br ratios show relatively small variations (37-133) with a weighted average around 90. The Ca/(Na+Ca) ratios range between 0.21 and 0.89, much higher than those from southern Schwarzwald fluids. Homogenization temperatures range from 59-159°C (weighted average of 120°C), maximum (Pb +Zn) contents are up to 20.000 mg/l and (maximum Cu + Ni + Bi + Co) contents reach 46.800 mg/l (Fig. 3A-D).

5.3 Northern Schwarzwald and Wiesloch MVT deposit (veins above the basement-cover unconformity)

Two fluid types are observed in the northern Schwarzwald: the first one shows the highest salinities (up to 27 wt.% $NaCl+CaCl_2$) with Ca/(Na+Ca) ratios of 0.24-0.43, very similar to fluids observed in central Schwarzwald veins (see above). The second fluid type exhibits lower salinities (20-24 wt.%. $NaCl+CaCl_2$), variable Cl/Br ratios (up to 340, Pfaff et al., 2010) and lower Ca/(Na+Ca) ratios (0.08-0.21), similar to the fluid observed in southern Schwarzwald veins. Homogenization temperatures range from 52-148°C (weighted average of 110°C), maximum (Pb + Zn) contents up to 6.800 mg/l and maximum (Cu + Ni +Bi +Co) contents of up to 10.020 mg/l (Fig. 3A-D).

6. Discussion

6.1. Ca-Na and Cl-Br variations

The variance in fluid chemistry of Jurassic-Cretaceous hydrothermal veins (Fig. 2A-G) correlates with their geographic/stratigraphic position (including large overlaps) and can be divided into three groups

according to their fluid chemistry. As mentioned before, the emplacement depth of the exposed hydrothermal veins is not continuously increasing from north to south. Hydrothermal veins in the northern and central Schwarzwald, which are at present exposed at the surface, occur in sedimentary and basemenet rocks few hundred meters above and below the basement-cover unconformity, while they are hosted exclusively by crystalline basement rocks far below (>2000 m) the unconformity in the southern Schwarzwald.

Mixing models based on microthermometry, LA-ICPMS analyses of single fluid inclusions, stable and radiogenic isotopes and trace element contents of fahlore and sphalerite (Pfaff et al., 2011; Staude et al., 2012; Fusswinkel et al. 2013) imply that the fraction of sedimentary fluid involved in the formation of a specific mineralization is higher in the central and northern Schwarzwald (where the veins are in proximity to the evaporite-bearing Muschelkalk aquifer) than in the south (where the veins are >2 km below the Muschelkalk aquifer; Pfaff et al., 2011; Staude et al., 2009; 2010b; 2011a; 2012a; 2012b; Ströbele et al. 2012; Walter et al. 2015). However, the distribution of Cl/Br ratios implies that other factors than the stratigraphic depth of formation control the Cl/Br ratio. While high Cl/Br ratios above the sea water ratio (288) occur in the northern Schwarzwald (including the post-Cretaceous Wiesloch MVT deposit), veins from the central Schwarzwald have Cl/Br ratios of 90 ± 30, typical of basement fluids that did not dissolve halite (Frape and Fritz, 1987; Banks et al., 2000b; Stober and Bucher, 2004; Yardley, 2005). On the other hand, veins from the deepest stratigraphic levels in the southern Schwarzwald show again variable Cl/Br ratios above the sea water ratio (up to 1140), possibly indicating the influence of a halite-bearing aquifer in the sedimentary cover (Fig. 2H).

The observed Cl/Br variations can be explained using paleo-topography models for the Permian and Triassic when a topographic high existed in the central Schwarzwald area and halite-bearing evaporites were deposited north, south and East of it. Evaporites in the central Schwarzwald, however, did not significantly exceed the anhydrite stage (Fig. 4; Ziegler, 1990; Hansch & Simon, 2003; Rupf and Nitsch, 2008; Geyer and Gwinner, 2011). Thus, in contrast to the north and the south, the sedimentary fluid in the central Schwarzwald appears to have never interacted with a halite-bearing aquifer. This is in good agreement with elevated Ca/(Ca+Na) and invariably low Cl/Br for fluids in the central Schwarzwald fluid inclusions (Figs 2 & 5). In contrast, the sedimentary fluids in the north and

365 south interacted with halite and as a consequence, fluid inclusions exhibit variable and high Cl/Br (33
366 to 1139) and relatively low Ca/(Ca+Na) ratios of 0.1-0.4 (Figs 2 & 5). In addition to the high
367 Ca/(Ca+Na) and low Cl/Br ratios, hydrothermal fluid inclusion data from the central Schwarzwald
368 show elevated SO_4 contents (Fig. 6A). We suggest that this is because the sedimentary fluid involved
369 in hydrothermal vein formation interacted with anhydrite/gypsum-bearing sediments (Fig. 6B).
370 Sulphide oxidation can be excluded as a dominant source for the observed SO_4^{2-} concentration, since
371 these sulphate-rich fluid inclusions are restricted to the central Schwarzwald: sulphide oxidation would
372 have affected also fluids in the northern and southern Schwarzwald, since sulphides are present
373 everywhere in the crystalline basement rocks
374 As a consequence, it can be assumed that the emanation of the bittern brines (in early Triassic times)
375 was restricted to the north and the south (where halite precipitated). There, the basin was apparently
376 deeper (Fig. 5), since bittern brines only form as a result of halite precipitation (see seawater
377 evaporation line in Fig 7). Therefore, the bittern brine with the inherited low Cl/Br ratio had to
378 percolate a significantly longer distance (vertically and laterally) through the crystalline basement to
379 the central Schwarzwald, compared to the north and south.
380 We assume that the downward migrating fluid (bittern brine or sedimentary fluid) did not significantly
381 mix with other fluids at shallow crustal levels, since the high fracture density and the occurrence of
382 large scale fracture zones enables a fast downward movement in the uppermost part of the crust.
383 Reaching deeper crustal levels, fast vertical fluid movement is promoted by fracture orientation, which
384 is preferably vertical (Brown and Hoek, 1978). With increasing depth, the abundance of well-
385 developed fracture networks decreases, favouring lateral dissemination of fluids, which favours a
386 stratification of fluid in deeper parts of the brittle crust (Fig. 5A). The general driving force for large
387 scale vertical fluid movements are most likely desiccation processes caused by the consumption of
388 H_2O during mineral alteration at depth as described by Stober and Bucher 2004 and Bons et al. 2014.
389 Using the hydraulic conductivity given by Stober and Bucher (2007), average flow velocities around
390 10^{-6} and 10^{-8} m/s (in granite and gneiss, respectively) can be assumed in 4 km depth. A rough estimate
391 of the time that bittern brines need to travel from the surface (north and south) to a depth of 10 km
392 (depth slightly above of brittle-ductile transition) in the central Schwarzwald results in 1000 – 100.000

393 years. Taking into account that the hydraulic conductivity further decreases at depths below 4 km,
394 using an extremely low average fluid velocity of 10^{-10} m/s over the entire rock column, the travel time
395 still does not exceed 9 Ma. This calculation shows that there was sufficient time between the
396 formation and downward migration of bittern brines during evaporite formation in the Triassic and the
397 first occurrence of basement brines with low Cl/Br involved in Jurassic vein formation (Walter et al.,
398 in press).
399
400 *6.2 Salinity variations*
401 In addition to variations in their major element chemistry, salinities of the northern, central and
402 southern Schwarzwald vein fluids are quite variable. Based on the observation that the amount of
403 sedimentary fluid involved in vein formation decreases from north to south, one could expect a
404 gradual increase in the salinity (due to the higher proportion of highly saline basement fluid). This is,
405 however, not the case, since the hydrothermal veins in the southern Schwarzwald show lower salinities
406 than those observed in the northern and central Schwarzwald. According to Bons et al.(2014) and
407 Walter et al. (in press), a layer of a late-metamorphic, low-salinity fluid with low Cl/Br (initially
408 formed during the Permian) is situated below the highly saline basement brine, since this fluid
409 migrated into the basement before the late Triassic bittern brine arrived. According to Bons et
410 al.(2014) and Walter et al. (2015b) this fluid did not mix substantially with the modified bittern brine
411 and therefore the former fluid stratification was preserved. Since the hydrothermal veins in the south
412 formed at greater stratigraphic depths, it is likely that these hydrothermal veins incorporated fluid
413 batches of basement fluids, which include relatively small amounts of late-metamorphic fluids situated
414 stratigraphically below the Jurassic basement brine (Bons et al. 2014). The involvement of small
415 amounts of low-salinity metamorphic fluid batches in hydrothermal vein formation might explain the
416 slightly lower salinity in fluid inclusions from the southern Schwarzwald. This “mixing from below”
417 (Bons et al., 2014) dilutes the deep seated brine’s salinity (Fig. 6), while the halogen signature remains
418 unchanged (low Cl/Br).
419
420 *6.3 Minor and trace element variations*

The trace element concentrations of fluid inclusions of each district show large variations (ES I, Fig. 3). Reasons for the large spread in their absolute concentrations are diverse and include local hydrogeological anomalies, precipitation of ore minerals in deeper parts of the same vein and/or local anomalies of the mixing ratio during ore precipitation. Trace metals are much more affected by these processes than e.g. Cl and Br, which results in complex chemical variations. Based on the maximum and average concentrations of Pb, Zn, Cu, Co, Bi and Ni, two major features are recognized:

(I) A difference in maximum concentrations of Pb and Zn in the deep basement (southern Schwarzwald) to much lower maximum values, around the basement-cover unconformity (central Schwarzwald) (Figs. 3A-C).

(II) A variation in the Pb/Zn ratio with increasing depth of formation (Fig. 3E).

Additionally, field observations (vein and ore mineralogy) not only confirm a decrease of Pb+Zn, but also an increase in Cu+Co+Ni+Bi with decreasing depth (Fig. 3B), advancing the unconformity in the mineralization outcrops. Overlying Triassic redbeds are enriched in Cu+Co+Ni+Bi (Matter et al., 1988a, 1988b). Accordingly, the pre-enriched metals can easily be mobilized by the descending saline sedimentary fluid. The breakdown of feldspar and biotite as a consequence of interaction between the basement fluid and its surrounding rock increases the Pb + Zn (Fig. 3A, B, D) in the basement fluid (Wilkinson et al., 2005a, Yardley 2005, Burisch et al., 2015, submitted, Walter et al., in press). Therefore, the maximum Pb + Zn content increases with stratigraphic depth due to advanced reaction times between fluid and rock. Since Pb and Zn behave geochemically similar (Burisch et al., 2015, submitted), a variation in the Pb/Zn ratio (II) cannot simply be explained by water-rock interaction or fractionation processes. If galena precipitated preferably in deeper veins compared to sphalerite, a fractionation of Pb and Zn would be the consequence, but no observation supports such a mechanism (Metz et al., 1957). Therefore, we suggest an additional source of Zn within the sedimentary cover (Fig. 3A). The prime candidate would be the Muschelkalk which is according to Martin (2009) one of the Zn-richest lithologies in SW Germany, and Zn can easily be leached out of the carbonate rock. Therefore, the decrease in the Pb/Zn ratio is most likely an effect of the basement brine's mixing with an additional Zn-rich, Pb-depleted sedimentary fluid. These arguments are in agreement with the

model of Bons et al. (2014) and further support its validity, because the fluids derived from the Muschelkalk limestone aquifer in the southern Schwarzwald (because the Permian is missing and the Buntsandstein pinches out towards the south) should be the main constituent of the fluid layer right above the "basement brine" in the stratified fluid section during the Jurassic-Cretaceous in the Schwarzwald.

Conclusion

The combination of extensive data from the literature (sections 1 and 2) with a large set of new data of fluid inclusion compositions from discontinuity-related hydrothermal veins of different formation depth allowed us to design a model that explains large-scale lateral and vertical chemical variations. Ore-forming fluids record information about the sedimentary rocks/aquifers from which they originated. Based on detailed regional geology, systematic fluid inclusion analyses of hydrothermal veins can in some cases be used to reconstruct eroded sedimentary units, if there was a recognizable difference in paleo-aquifer chemistry at the time of formation. Careful investigation of base metal contents in such fluids may allow the identification of specific fluid sources and a qualitative estimate of mixing ratios can be deduced from such data. Therefore, base metal variations may have the potential to serve as reservoir tracer in hydrothermal systems.

Trace element differences provide evidence for metal variations governed by the host aquifers of the fluids involved in mixing processes. The sedimentary fluids are in most cases not the dominant source of Pb and Zn, but red-bed fluids appear to be the main source of Cu, Co, Ni and Bi. Limestone-derived fluids may introduce additional Zn, which has a significant impact on the Pb/Zn ratio, but not so much on absolute concentrations in ore-forming fluids.

Acknowledgments:

We would like to thank Ingrid Stober and two anonymous reviewers, whose comments improved this

manuscript substantially. Edgar Nitsch (LGRB) is gratefully acknowledged for invaluably hints of the paleo-topography of the sedimentary cover in SW-Germany. We thank Gabi Stoschek and Bernd Steinhilber for their help with crush-leach analyses. Furthermore we thank S. Kaulfuß and P. Jeiseke for sample preparation. This study was supported by the Alfried-Krupp Prize for Young University Teachers of the Krupp Foundation to Gregor Markl and the German Research Foundation (DFG), grant Ma2135/20-1.

References cited:

Altherr, R., Holl, A., Hegner, E., Langer, C., Kreuzer, H., 2000. High-potassium, calc-alkaline I-type plutonism in the European Variscides: northern Vosges (France) and northern Schwarzwald (Germany). Lithos 50, 51-73.

Aquilina, L., Boulvais, P., Mossmann, J.-R., 2011. Fluid migration at the basement/sediment interface along the margin of the southeast basin (France): implications for Pb–Zn ore formation. Mineralium Deposita 46, 959-979.

Baatartsogt, B., Wagner, T., Taubald, H., Mierdel, K., Markl, G., 2006. Hydrogen isotope determination of fluid inclusion water from hydrothermal fluorite: The results depend on the extraction technique. Chemical Geology, 1-21.

Baatartsogt, B., Schwinn, T., Wagner, T., Taubald, H., Beitter, T., Markl, G., 2007. Contrasting paleofluid systems in the continental basement: a fluid inclusion and stable isotope study of hydrothermal vein mineralizations, Schwarzwald district, Germany. Geofluids 7, 1-25.

Bakker, R.J., Diamond, L.W., 2006. Estimation of volume fractions of liquid and vapor phases in fluid inclusions, and definition of inclusion shapes. American Mineralogist 91, 635-657.

Banks, D., Boyce, A., Samson, I., 2002. Constraints on the origins of fluids forming Irish Zn-Pb-Ba deposits: Evidence from the composition of fluid inclusions. Economic Geology 97, 471-480.

Banks, D., Green, R., Cliff, R., Yardley, B., 2000. Chlorine isotopes in fluid inclusions: determination of the origins of salinity in magmatic fluids. Geochimica et Cosmochimica Acta 64, 1785-1789.

Bau, M., Romer, R.L., Lüders, V., Dulski, P., 2003. Tracing element sources of hydrothermal mineral deposits: REE and Y distribution and Sr-Nd-Pb isotopes in fluorite from MVT deposits in the Pennine Orefield, England. Mineralium Deposita 38, 992-1008.

Behr, H.J., Gerler, J., 1987. Inclusions of sedimentary brines in post-Variscan mineralizations in the Federal Republic of Germany—a study by neutron activation analysis. Chemical Geology, 61, 65-77.

Behr, H.J., Horn, E.E., Frentzel-Beyme, K., Reutel, C., 1987. Fluid inclusion characteristics of the Variscan and post-Variscan mineralizing fluids in the Federal Republic of Germany. Chemical Geology, 61, 273-285.

Bliedtner M., Martin M. 1986. Erz- und Minerallagerstätten des Mittleren Schwarzwaldes. LGRB, Freiburg

Bodnar, R.J., Vityk, M.O., 1994. Interpretation of microthermometric data for H2O-NaCl fluid inclusions. In: De Vivo B, Frezzotti ML (eds) Fluid inclusions in minerals, methods and applications. Virginia Tech, Blacksburg,. 117-130.

Boiron, M.-C., Cathelineau, M., Banks, D.A., Fourcade, S., Vallance, J., 2003. Mixing of metamorphic and surficial fluids during the uplift of the Hercynian upper crust: consequences for gold deposition. Chemical Geology 194, 119-141.

Boiron, M.C., Cathelineau, M., Banks, D.A., Buschaert, S., Fourcade, S., Coulibaly, Y., Michelot, J.L., Boyce, A., 2002. Fluid transfer at a basement/cover interface. Part II. Large-scale introduction of chlorine into the basement by Mesozoic basinal brines. Chemical Geology 192, 121-140.

Boiron, M.C., Cathelineau, M., Richard, A., 2010. Fluid flows and metal deposition near basement/cover unconformity: lessons and analogies from Pb-Zn-F-Ba systems for the understanding of Proterozoic U deposits. Geofluids 10, 270-292.

Bons, P.D., Fusswinkel, T., Gomez-Rivas, E., Markl, G., Wagner, T., Walter, B., 2014. Fluid mixing from below in unconformity-related hydrothermal ore deposits. Geology, 42(12), 1035-1038.

Bottrell, S. H., Yardley, B. W. D., Buckley, F., 1988. A modified crush-leach method for the analysis of fuid inclusion electrolytes. Bulletin de Mineralogie, 111, 279-290.

Brown, E., Hoek, E., 1978. Trends in relationships between measured in-situ stresses and depth, International Journal of Rock Mechanics and Mining Sciences & Geomechanics Abstracts. Elsevier, pp. 211-215.

Bucher, K., Stober, I., 2002. Water-rock reaction experiments with Black Forest gneiss and granite. Water Science and Technology Library 40, 61-95.

Bucher, K., Stober, I. 2010. Fluids in the upper continental crust. Geofluids, 10(1-2), 241-253.

Burisch, M., Marks, M., Novak, M., Markl, G., submitted to Chemical Geology. The importance of temperature and cataclastic deformation for halogen (F, Cl, Br) systematics and metal transport capacities of continental basement brines – an experimental approach

Burisch, M., Marks, M., Nowak, M., Markl, G., 2015. Goldschmidt Abstracts, 2015 426

Duane, M., De Wit, M., 1988. Pb-Zn ore deposits of the northern Caledonides: Products of continental-scale fluid mixing and tectonic expulsion during continental collision. Geology 16, 999-1002.

DeR Channer, D.M., Spooner, E.T.C., 1992. Analysis of fluid inclusion leachates from quartz by ion chromatography. Geochimica et cosmochimica acta, 56(1), 249-259.

Dolníček, Z., René, M., Hermannová, S., Prochaska, W. 2014. Origin of the Okrouhlá Radouň episyenite-hosted uranium deposit, Bohemian Massif, Czech Republic: fluid inclusion and stable isotope constraints. Mineralium Deposita, 49(4), 409-425.

Edmunds, W.M., Savage, D., 1991. Geochemical characteristics of groundwater in granites and related crystalline rocks. Applied Groundwater Hydrology, a British Perspective (eds DowningRA, WilkinsonWB), 199-216.

Frape, S., Blyth, A., Blomqvist, R., McNutt, R., Gascoyne, M., 2003. Deep fluids in the continents: II. Crystalline rocks. Treatise on geochemistry 5, 541-580.

Frape, S., Fritz, P., 1987. Geochemical trends for groundwaters from the Canadian Shield. Geological Association of Canada Special Papers 33, 19-38.

Fußwinkel, T., 2014. Direct evidence for fluid mixing processes during formation of post-Variscan, unconformity-related hydrothermal vein deposits.

Fußwinkel, T., Wagner, T., Wälle, M., Wenzel, T., Heinrich, C., Markl, G., 2013. Fluid mixing forms basement-hosted Pb-Zn deposits: Insight from metal and halogen

geochemistry of individual fluid inclusions. Geology 41, 679-682.
Fusswinkel, T., Wagner, T., Wenzel, T., Wälle, M., Lorenz, J., 2014. Red bed and basement sourced fluids recorded in hydrothermal Mn–Fe–As veins, Sailauf (Germany): A LA-ICPMS fluid inclusion study. Chemical Geology 363, 22-39.
Garven, G., Appold, M.S., Toptygina, V.I., Hazlett, T.J., 1999. Hydrogeologic modeling of the genesis of carbonate-hosted lead-zinc ores. Hydrogeology Journal 7, 108-126.
Geyer, O.F., Gwinner, M.P., 2011. Geologie von Baden -Württemberg. – 5., völlig neu bearbeitete Auflage. Schweizerbart`sche Verlagsbuchhandlung (Nägele u. Obermiller), Stuttgart.
Göb, S., Loges, A., Nolde, N., Bau, M., Jacob, D.E., Markl, G., 2013. Major and trace element compositions (including REE) of mineral, thermal, mine and surface waters in SW Germany and implications for water-rock interaction. Applied Geochemistry.
Goldstein, R.H., Reynolds, T.J., 1994. Systematics of fluid inclusions in diagenetic minerals: SEPM Short Course 31. Society for Sedimentary Geology, 199.
Hann, H.P.,Chen, F., Zedler, H., Frisch, W., Loeschke, J., 2003. The rand granite in the southern Schwarzwald and its geodynamic significance in the variscan belt of SW Germany. International Journal of Earth Sciences 92, 821-842.
Hansch, W. Simon, T., 2003. Das Steinsalz aus dem Mittleren Muschelkalk Südwestdeutschlands. - museo, 20: 152-159
Jenkner, B., 1986. Ein Vorschlag zur Neugliederung des sedimentären Oberrotliegenden in der Baden-Badener Senke und ihrer nordöstlichen Fortsetzung (Nordschwarzwald). Jahrbuch des Geologischen Landesamtes Baden-Württemberg 28, 49-159.
Kendrick, M., Honda, M., Oliver, N., Phillips, D., 2011. The noble gas systematics of late-orogenic H_2O–CO_2 fluids, Mt Isa, Australia. Geochimica et Cosmochimica Acta 75, 1428-1450.
Kessen, K., Woodruff, M., Grant, N., 1981. Gangue mineral 87 Sr/86 Sr ratios and the origin of Mississippi Valley-type mineralization. Economic Geology 76, 913-920.
Klemm, L., Pettke, T., Graeser, S., Mullis, J., Kouzmanov, K., 2004. Fluid mixing as the cause of sulphide precipitation at Albrunpass, Binn Valley, central Alps. Schweizer Mineralogische und Petrologische Mitteilungen 84, 189-212.
Köhler, J., Schönenberger, J., Upton, B., Markl, G., 2009. Halogen and trace-element chemistry in the Gardar Province, south Greenland: subduction-related mantle metasomatism and fluid exsolution from alkalic melts. Lithos, 113(3), 731-747.
Ladenburger, S., 2012. Crush-Leach Analysen an Flüssigkeitseinschlüssen von hydrothermalen Erzlagerstätten des Schwarzwaldes. Unpublished BSc Thesis, Tübingen 134p.
Ladenburger, S., Marks, M., Markl, G. 2012. Analysis of crush leach solutions from hydrothermal ore deposits by combining ion chromatography (IC) and total reflection X-ray fluorescence spectroscopy (TXRF).
Leach, D.L., Marsh, E., Emsbo, P., Rombach, C.S., Kelley, K.D., Anthony, M., 2004. Nature of Hydrothermal Fluids at the Shale-Hosted red Dog Zn-Pb-Ag Deposit, Brooks Range, Alaska. Economic Geology 99, 1449-1480.
Loges, A., Wagner, T., Kirnbauer, T., Göb, S., Bau, M., Berner, Z., Markl, G., 2012. Source and origin of active and fossil thermal spring systems, northern Upper Rhine Graben, Germany. Applied Geochemistry 27, 1153-1169.
Lüders, V., Möller, P., 1992. Fluid evolution and ore deposition in the Harz Mountains (Germany). Eur. J. Mineral. 4, 1053-1068.
Markl, G., Lahaye, Y., Schwinn, G., 2006. Copper isotopes as monitors of redox processes in hydrothermal mineralization. Geochimica et Cosmochimica Acta 70, 4215-4228.
Markl, G. 2015. Schwarzwald - Lagerstätten und Mineralien aus vier Jahrhunderten. Bode Verlag, Salzhemmendorf. Volume I, 672 p

619 Martin, M., 2009. Geogene Grundgehalte (Hintergrundwerte) in den petrogeochemischen
620 Einheiten von Baden-Württemberg. LGRB-Informationen 24, 98.
621 Matter, A., Peters, T.J., Bläsi, H.-R., Meyer, J., Ischni, H., Meyer, C., 1988a.
622 Sondierungsbohrung Weiach Nagra Techn. Ber. 86-01. Nagra, Wettingen, 438pp.
623 Matter, A., Peters, T.J., Bläsi, H.-R., Schenker, F., Weiss, h.-P., 1988b. Sondierungsbohrung
624 Schafisheim. Nagra Techn. Ber. 86-03. Nagra, Baden, 321pp.
625 McCaffrey, M., Lazar, B., Holland, H., 1987. The evaporation path of seawater and the
626 coprecipitation of Br^- and K^+ with halite. Journal of Sedimentary Research 57, 928-
627 937.
628 McCaig, A.M., Tritlla, J., Banks, D.A., 2000. Fluid mixing and receycling during Pyrenean
629 thrusting: Evidence from fluid inclusion halogen ratios. Geochimica et Cosmochimica
630 Acta 64, 3395-3412.
631 Metz, R., Richter, M., Schürenberg, H., 1957. Die Blei-Zink-Erzgänge des Schwarzwaldes.
632 Beiheft Geologisches Jahrbuch 29, 277.
633 Möller, P., Stober, I., Dulski, P., 1997. Seltenerdelement-, yttrium-gehalte und bleiisotope
634 in thermal-und mineralwässern des Schwarzwaldes. Grundwasser, 2(3), 118-132.
635 Möller, P., Woith, H., Dulski, P., Lüders, V., Erzinger, J., Kämpf, H., Pekdeger, A., Hansen,
636 B., Lodemann, M., Banks, D.A., 2005. Main and trace elements in KTB-VB fluid:
637 composition and hints to its origin. Geofluids 5, 28-41.
638 Nitsch, E., Zedler, H., 2009. Oberkarbon und Perm in Baden-Württemberg. . LGRB-
639 Information 22, 7-102.
640 Pfaff, K., Hildebrandt, L.H., Leach, D.L., Jacob, D.E., Markl, G., 2010. Formation of the
641 Wiesloch Mississippi Valley-type Zn-Pb-Ag deposit in the extensional setting of the
642 Upper Rhinegraben, SW Germany. Mineralium Deposita 45, 647-666.
643 Pfaff, K., Koenig, M.A., Wenzel, T., Ridley, I., Hildebrandt, L.H., Leach, D.L., Markl, G.,
644 2011. Trace and minor element variations and sulfur isotopes in crystalline and
645 colloform ZnS: Incorporation mechanisms and implications for their genesis.
646 Chemical Geology 286, 118-134.
647 Pfaff, K., Romer, R.L., Markl, G., 2009. U-Pb ages of ferberite, chalcedony, agate, "U-mica"
648 and pitchblende: constraints on the mineralization history of the Schwarzwald ore
649 district. Eur. J. Mineral. 21, 817-836.
650 Rupf, I., Nitsch, E., 2008. Das Geologische Landesmodell von Baden-Württemberg:
651 Datengrundlagen, technische Umsetzung und erste geologische Ergebnisse. LGRB-
652 Information 21.
653 Schwinn, G., Wagner, T., Baatartsogt, B., Markl, G., 2006. Quantification of mixing
654 processes in ore-forming hydrothermal systems by combination of stable isotope and
655 fluid inclusion analyses. Geochimica et Cosmochimica Acta 70, 965-982.
656 Shepherd, T.J., Rankin, A.H., Alderton, D.H., 1985. A practical guide to fluid inclusion
657 studies. Blackie Glasgow.
658 Shouakar-Stash, O., Alexeev, S., Frape, S., Alexeeva, L., Drimmie, R., 2007. Geochemistry
659 and stable isotopic signatures, including chlorine and bromine isotopes, of the deep
660 groundwaters of the Siberian Platform, Russia. Applied geochemistry 22, 589-605.
661 Staude, S., Bons, P.D., Markl, G., 2009. Hydrothermal vein formation by extension-driven
662 dewatering of the middle crust: An example from SW Germany. Earth and Planetary
663 Science Letters 286, 387-395.
664 Staude, S., Dorn, A., Pfaff, K., Markl, G., 2010a. Assemblages of Ag-Bi sulfosalts and
665 conditions of their formation: the type locality of schapbachite ($Ag_{0.4}Pb_{0.2}Bi_{0.4}S$) and
666 neighboring mines in the Schwarzwald ore district, southern Germany. Canadian
667 Mineralogist 48, 441-466.
668 Staude, S., Göb, S., Pfaff, K., Ströbele, F., Premo, W.R., Markl, G., 2011a. Deciphering fluid
669 sources of hydrothermal systems: A combined Sr- and S-isotope study on barite

(Schwarzwald, SW Germany). Chemical Geology 286, 1-20.
Staude, S., Göb, S., Pfaff, K., Ströbele, F., Premo, W.R., Markl, G., 2011b. Deciphering fluid sources of hydrothermal systems: a combined Sr-and S-isotope study on barite (Schwarzwald, SW Germany). Chemical Geology 286, 1-20.
Staude, S., Mordhorst, T., Nau, S., Pfaff, K., Brügmann, G., Jacob, D.E., Markl, G., 2012a. hydrothermal carbonates of the Schwarzwald ore district, southwestern Germany: carbon source and conditions of formation using δ18O, δ13C, 87Sr/86Sr, and fluid inclusions. The Canadian Mineralogist 50, 1401-1434.
Staude, S., Mordhorst, T., Neumann, R., Prebeck, W., Markl, G., 2010b. Compositional variation of the tennantite-tetrahedrite solid-solution series in the Schwarzwald ore district (SW Germany): The role of mineralization processes and fluid source. Mineralogical Magazine 74, 309-339.
Staude, S., Wagner, T., Markl, G., 2007. Mineralogy, mineral chemistry and fluid evolution of the hydrothermal Wenzel deposit, southern Germany: implications for the formation of Kongsberg-type silver deposits. Canadian Mineralogist 45, 1147-1176.
Staude, S., Werner, W., Mordhorst, T., Wemmer, K., Jacob, D., Markl, G., 2012b. Multi-stage Ag–Bi–Co–Ni–U and Cu–Bi vein mineralization at Wittichen, Schwarzwald, SW Germany: geological setting, ore mineralogy, and fluid evolution. Mineralium Deposita 47, 251-276.
Steele-MacInnes, M., Bodnar, R.J., Naden, J., 2011. Numerical model to determine the composition of H_2O-NaCl-$CaCl_2$ fluid inclusions based on microthermometric and microanalytical data. Geochimica et Cosmochimica Acta 75, 21-40.
Stober, I. 1995. Die Wasserführung des kristallinen Grundgebirges. Ferdinand Enke Verlag.Stober, I., Bucher, K., 1999. Deep groundwater in the crystalline basement of the Black Forest
region. Applied Geochemistry 14, 237-254.
Stober, I., Bucher, K. 1999. Origin of salinity of deep groundwater in crystalline rocks. Terra Nova, 11(4), 181-185.
Stober, I., Bucher, K., 2004. Fluid sinks within the earth's crust. Geofluids 4, 143-151.
Stober, I., Bucher, K., 2007. Hydraulic properties of the crystalline basement. Hydrogeology Journal 15, 213-224.
Stober, I., Bucher, K. 2014. Hydraulic and hydrochemical properties of deep sedimentary reservoirs of the Upper Rhine Graben, Europe. Geofluids.Stober 2014 Geothermal energy
Stober, I. 2014. Hydrochemical properties of deep carbonate aquifers in the SW German Molasse basin. Geothermal Energy, 2(1), 1-20.
Ströbele, F., Staude, S., Pfaff, K., Premo, W.R., Hildebrandt, L.H., Baumann, A., Pernicka, E., Markl, G., 2012. Pb isotope constraints on fluid flow and mineralization processes in SW Germany Neues Jahrbuch für Mineralogie-Abhandlungen: Journal of Mineralogy and Geochemistry 189, 287-309.
Todt, W., 1976. Zirkon U/Pb-Alter des Malsburg-Granits vom Südschwarzwald. Neues Jahrb Mineral Monatsh 12, 532-544.
Tornos, F., Casquet, C., Locutura, J., Collado, R., 1991. Fluid inclusion and geochemical evidence for fluid mixing in the genesis of Ba-F (Pb-Zn) lodes of the Spanish central System. Min. Magazine 55, 225-234.
Wagner, T., Okrusch, M., Weyer, S., Lorenz, J., Lahaye, Y., Taubald, H., Schmitt, R.T., 2010. The role of the Kupferschiefer in the formation of hydrothermal base metal mineralization in the Spessart ore district, Germany: insight from detailed sulfur isotope studies. Mineralium Deposita 45, 217-239.
Walter, B.F., Immenhauser, A., Geske, A., Markl, G., 2015. Exploration of hydrothermal carbonate magnesium isotope signatures as tracers for continental fluid aquifers,

Schwarzwald mining district, SW Germany. Chemical Geology.
Walter, B.F., Burisch, M., Markl, G., in press. The long-term chemical evolution of continental basement brines – a field study from the Schwarzwald, SW Germany. Geofluids, DOI: 10.1111/gfl.12167
Wilkinson, J., 2010. A review of fluid inclusion constraints on mineralization in the Irish ore field and implications for the genesis of sediment-hosted Zn-Pb deposits. Economic Geology 105, 417-442.
Wilkinson, J.J., Eyre, S.L., Boyce, A.J. 2005a. Ore-forming processes in Irish-type carbonate-hosted Zn-Pb deposits: Evidence from mineralogy, chemistry, and isotopic composition of sulfides at the Lisheen mine. Economic Geology, 100(1), 63-86.
Wilkinson, J., Weiss, D., Mason, T., Coles, B., 2005b. Zinc isotope variation in hydrothermal systems: preliminary evidence from the Irish Midlands ore field. Economic Geology 100, 583-590.
Yardley, B.W.D., 2005. Metal concentrations in crustal fluids and their relationship to ore formation. Economic Geology 100, 613-632.
Ziegler, P.A., 1990. Geological Atlas of Western and central Europe.

Figure captions

Fig. 1. Geological map of the Schwarzwald mining district (southwestern Germany) with sample locations. (**A**) Overview map. (**B**) Close-up of the Schwarzwald ore district. The sample localities 1 to 84 refer to Table 2 in the electronic supplement. Map modified after Pfaff et al. (2011)

Fig. 2. General characteristics of the Schwarzwald fluids show: (A) Variations in salinity based on single fluid inclusions. (B) Variations in salinity based on average salinity within individual samples. (C) Variations in homogenization temperatures and salinites. (D) Variations in Ca contents of the fluids based on microthermometry of individual inclusions. (E) Variation in Ca contents based on weighted averages. (F) Moles Ca versus moles Na. (G) Cl/Br (crush leach) versus Ca content (microthermometry) of the fluid. Note correlation of the southern and northern Schwarzwald in Cl/Br. (H) log Cl versus log Br plot. Note analyses of the southern and northern Schwarzwald fall on a mixing line between a bittern brine and a halite dissolution brine.

Fig. 3. (A) Trace metal distribution of Pb and Zn in context of the geographic position respectively the stratigraphic depth. (B) Pb +Zn (assumed to be derived from crystalline basement rocks) versus Cu+Ni+Co+Bi (assumed to be derived from the sedimentary cover). (C) Cl/Br versus (Pb +Zn)/(Cu+Ni+Co+Bi). (D) Pb+Zn versus (Pb +Zn)/(Cu+Ni+Co+Bi). (E) Pb/Zn versus (Pb +Zn)/(Cu+Ni+Co+Bi).

Fig. 4. Map is based on Hansch & Simon (2003) and Geyer and Gwinner (2011, and references therein) illustrating paleo-distribution of Middle-Triassic halite sequence above the today eroded basement complex of the Schwarzwald. The isopache illustrating lines of the same thickness. Furthermore the map shows the paleo-topographic features. Development of the paleo heights and depressions can be recognized since Carboniferous and Permian times. Note correlation of veins with Cl/Br ratios (black dots) with the paleo-occurrence of halite. Furthermore the veins below the paleo heights of the Muschelkalk where no halite was deposited show depleted Cl/Br ratios around 90.

Fig. 5. formation model (A) during Middle Triassic halite deposition in the depressions a bittern brine migrate downwards in the basement and formed a fluid stratified section with the older metamorphic fluid (Walter et al. 2015b). (B) In the depressions (with halite sequences) of the Middle-Late Triassic a halite dissolution brine descend by a hydraulic head (Bons et al., 2014) that is triggered by desiccation processes in the crystalline basement. On the topographic height of the central Schwarzwald a sulfate/carbonate dissolution brine migrate downwards. These younger late Triassic fluids formed a fluid stratified section with the older bittern brine and the deeper seated late metamorphic fluid. (C) During Jurassic-Cretaceous pathways were opened and the fluids of the fluid stratified section ascend and mix in hydrofractures and the hydrothermal veins were precipitated.

Fig. 6. (A) Cl/Br versus SO_4 (crush leach). Note high Cl/Br in the southern and northern Schwarzwald and high SO_4 in the central Schwarzwald for some of the samples. (B) plot illustrates three component mixing in the fluid inclusions. [1] Fußwinkel et al., 2013, [2] Göb et al., 2013

Fig. 7. Plot is based on Walter et al. (in press). The ternary diagram showing Na, K and Mg. The dotted arrow (1) indicates the modification of the bittern brine by water-rock interaction in the crystalline basement, shifting its composition towards higher K and lower Mg. Fluid mixing (2) of the modified bittern brine and younger a halite dissolution brine leads to the mixed fluid signature CD.

Figure 1

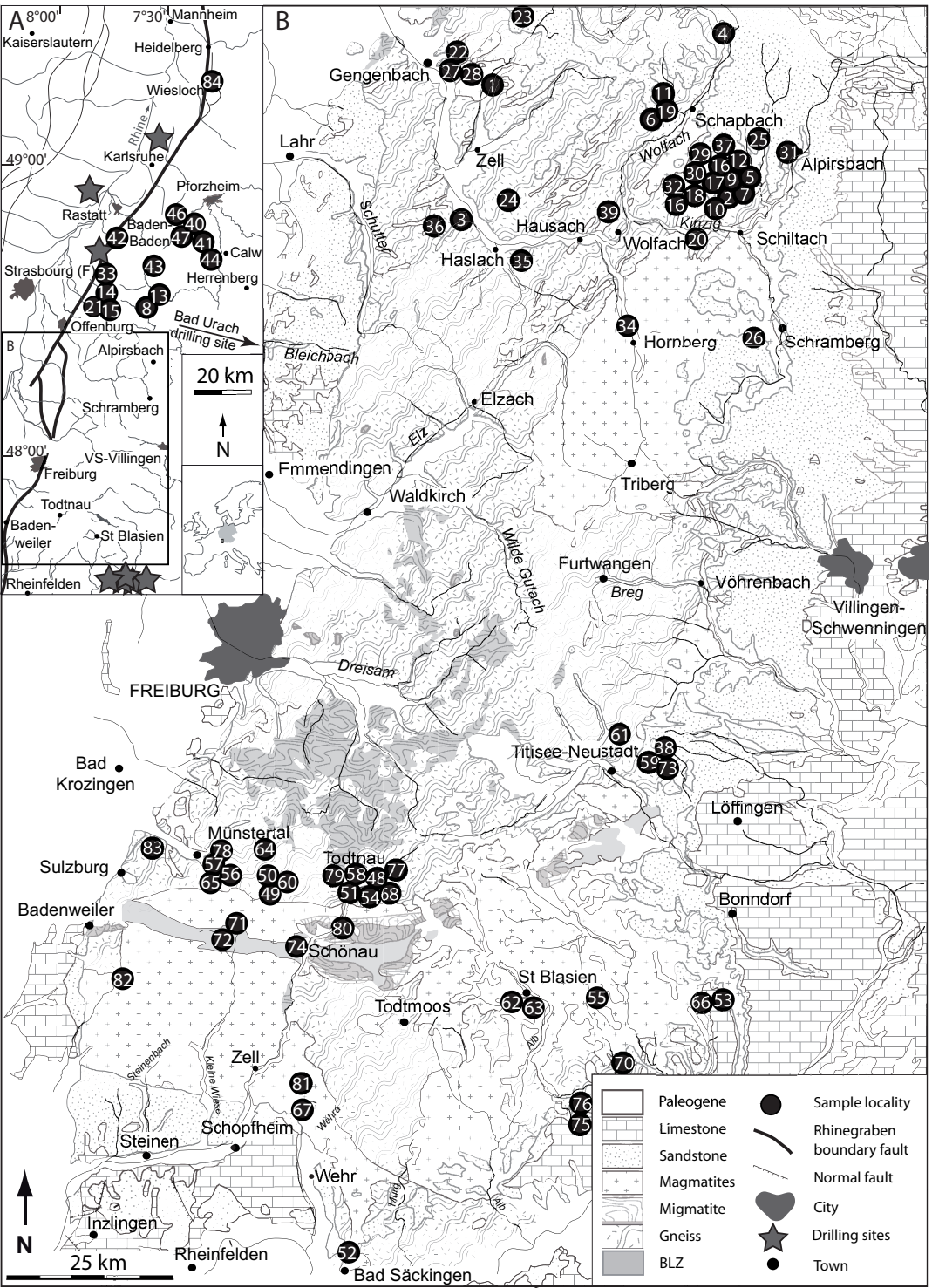
A
B
8°00'
7°30'
Mannheim
Kaiserslautern
Heidelberg
Wiesloch
Rhine
Karlsruhe
49°00'
Pforzheim
Rastatt
Baden
Baden
Calw
Strasbourg (F)
Herrenberg
Offenburg
Bad Urach
drilling site
Alpirsbach
Schramberg
48°00'
VS-Villingen
Freiburg
Todtnau
Baden-
weiler
St Blasien
Rheinfelden
20 km
N
Gengenbach
Lahr
Zell
Schapbach
Wolfach
Alpirsbach
Schiltach
Schutter
Haslach
Hausach
Wolfach
Kinzig
Hornberg
Schramberg
Bleichbach
Elzach
Elz
Emmendingen
Waldkirch
Triberg
Wilde Gutach
Furtwangen
Breg
Vöhrenbach
Villingen-
Schwenningen
Dreisam
FREIBURG
Titisee-Neustadt
Bad
Krozingen
Löffingen
Münstertal
Sulzburg
Todtnau
Bonndorf
Badenweiler
Schönau
St Blasien
Todtmoos
Zell
Steinenbach
Kleine Wiese
Schopfheim
Steinen
Wehra
Wehr
Murg
Alb
Inzlingen
Rheinfelden
Bad Säckingen
25 km
N
Paleogene
Limestone
Sandstone
Magmatites
Migmatite
Gneiss
BLZ
Sample locality
Rhinegraben
boundary fault
Normal fault
City
Drilling sites
Town

Figure 2

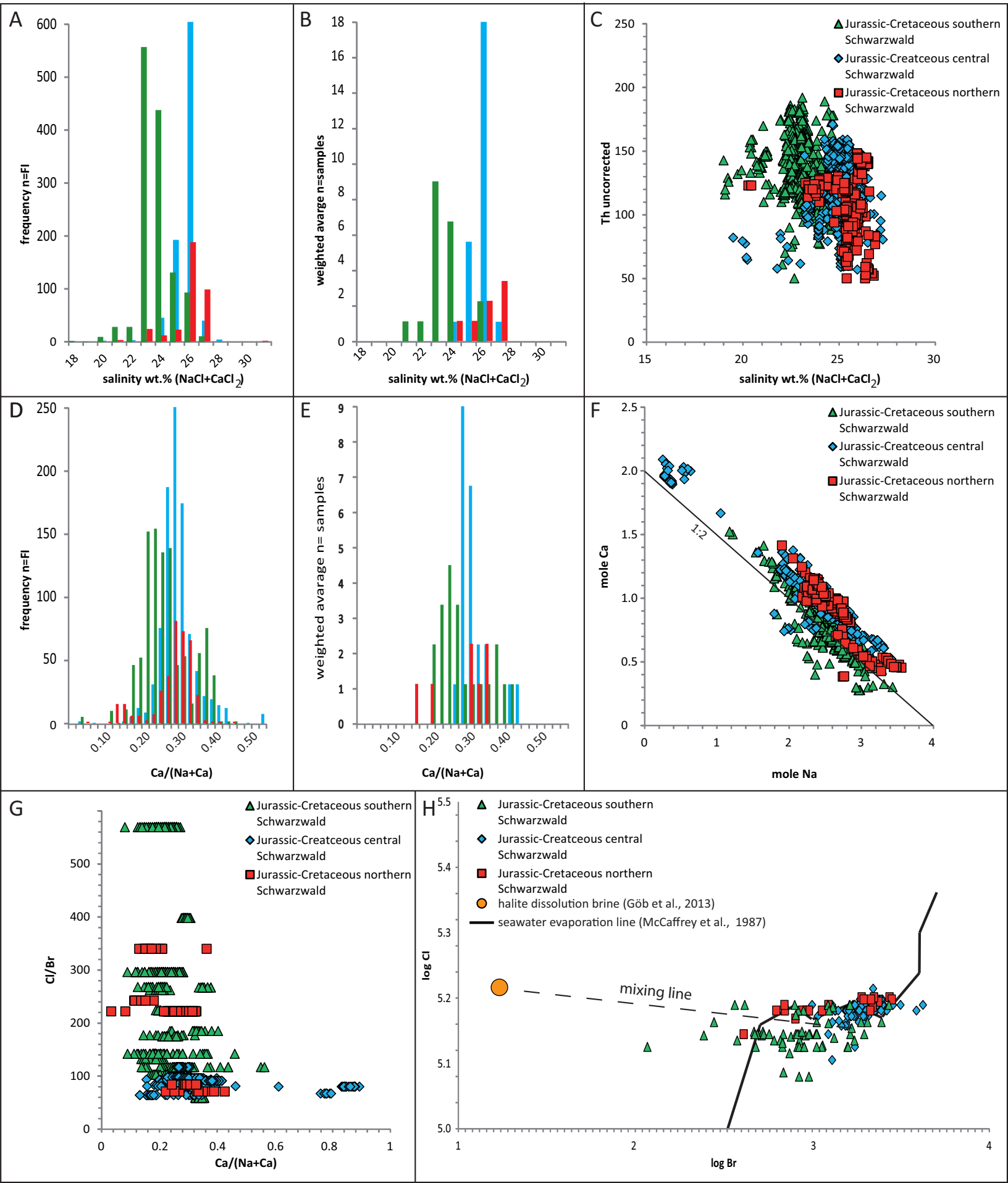
A
frequency n=FI
salinity wt.% (NaCl+CaCl2)
B
weighted avarge n=samples
salinity wt.% (NaCl+CaCl2)
C
Th uncorrected
salinity wt.% (NaCl+CaCl2)
Jurassic-Cretaceous southern Schwarzwald
Jurassic-Creatceous central Schwarzwald
Jurassic-Cretaceous northern Schwarzwald
D
frequency n=FI
Ca/(Na+Ca)
E
weighted avarage n= samples
Ca/(Na+Ca)
F
mole Ca
mole Na
1:2
G
Cl/Br
Ca/(Na+Ca)
H
log Cl
log Br
halite dissolution brine (Göb et al., 2013)
seawater evaporation line (McCaffrey et al., 1987)
mixing line

Figure 3

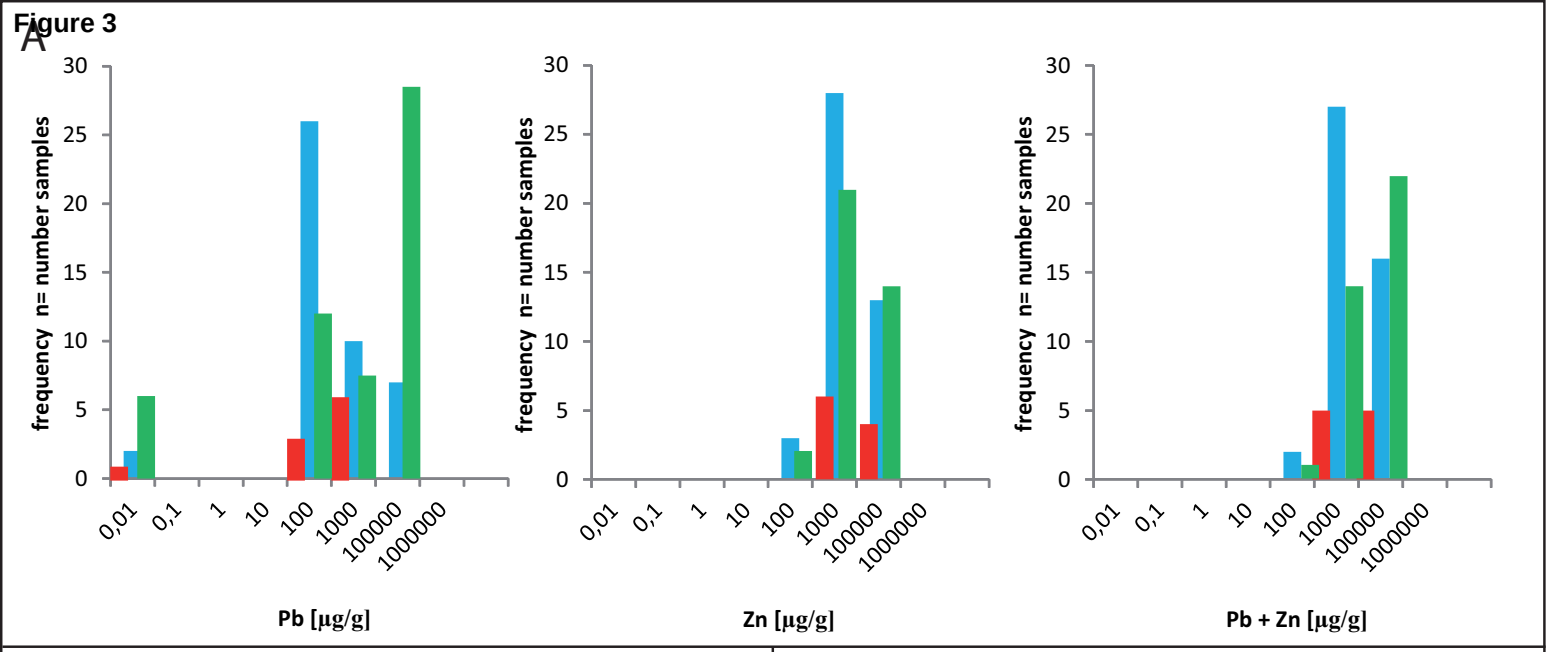
A
frequency n= number samples
Pb [µg/g]
Zn [µg/g]
Pb + Zn [µg/g]
0,01
0,1
1
10
100
1000
100000
1000000

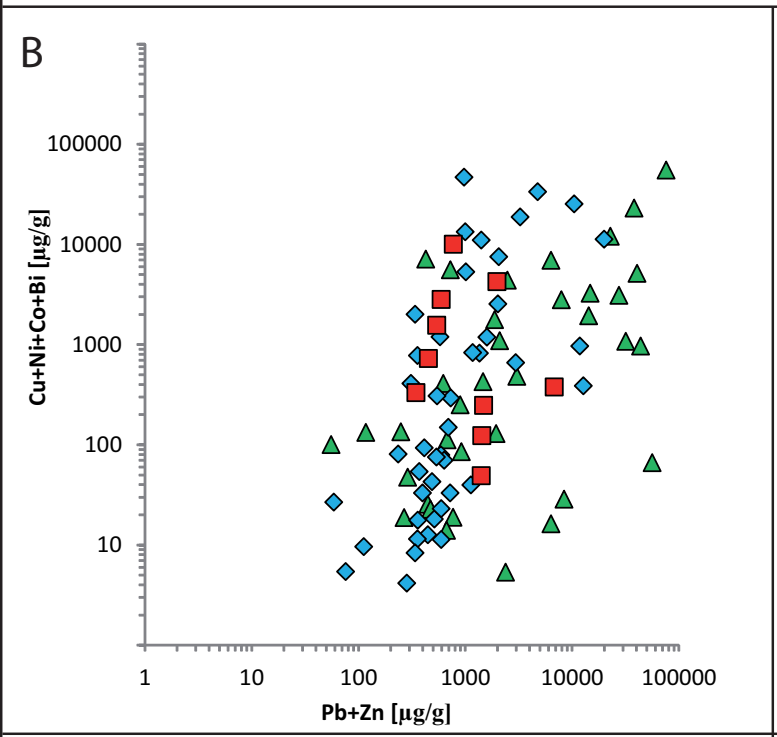
B
Cu+Ni+Co+Bi [µg/g]
Pb+Zn [µg/g]

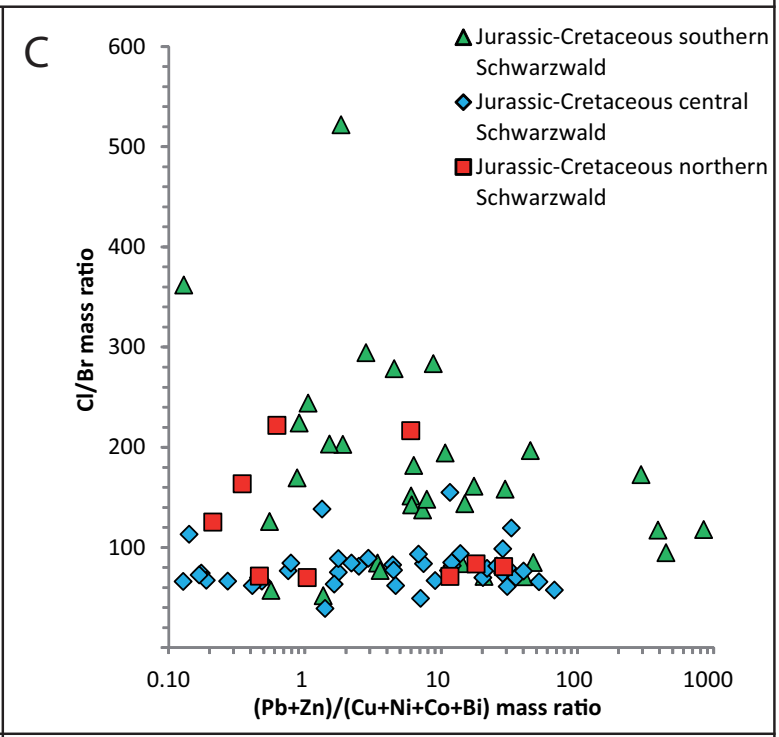
C
Jurassic-Cretaceous southern Schwarzwald
Jurassic-Cretaceous central Schwarzwald
Jurassic-Cretaceous northern Schwarzwald
Cl/Br mass ratio
(Pb+Zn)/(Cu+Ni+Co+Bi) mass ratio

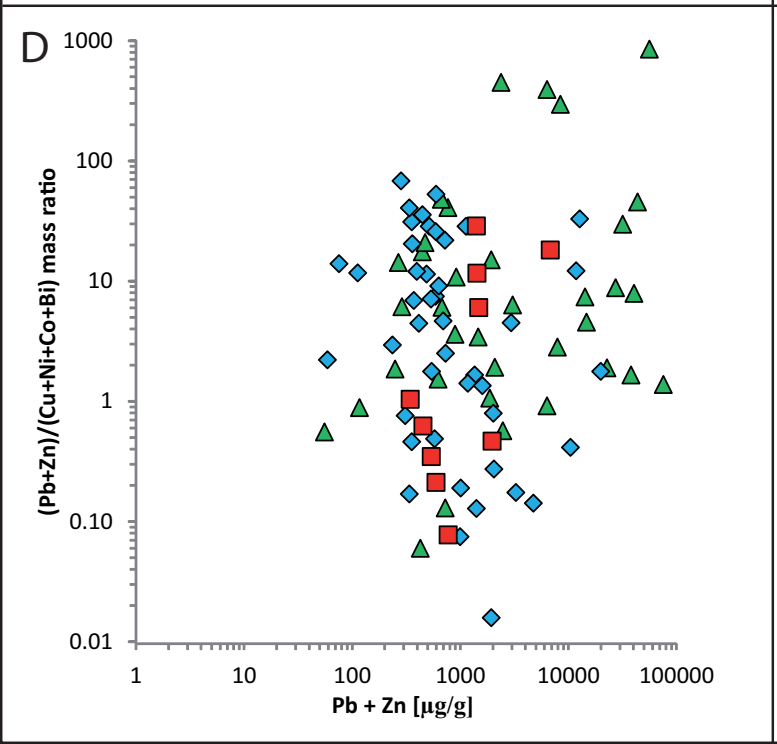
D
(Pb+Zn)/(Cu+Ni+Co+Bi) mass ratio
Pb + Zn [µg/g]

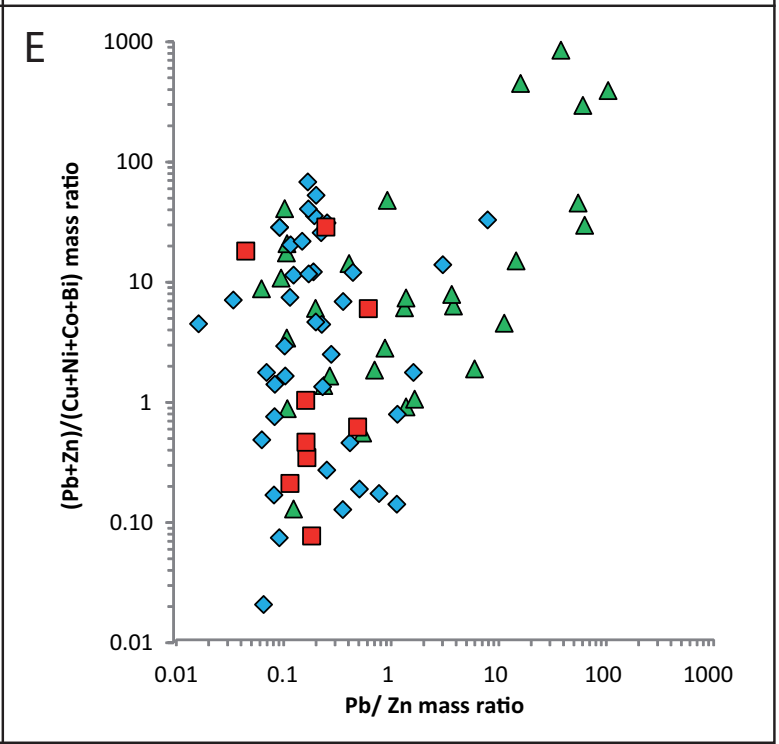
E
(Pb+Zn)/(Cu+Ni+Co+Bi) mass ratio
Pb/ Zn mass ratio

Figure 4

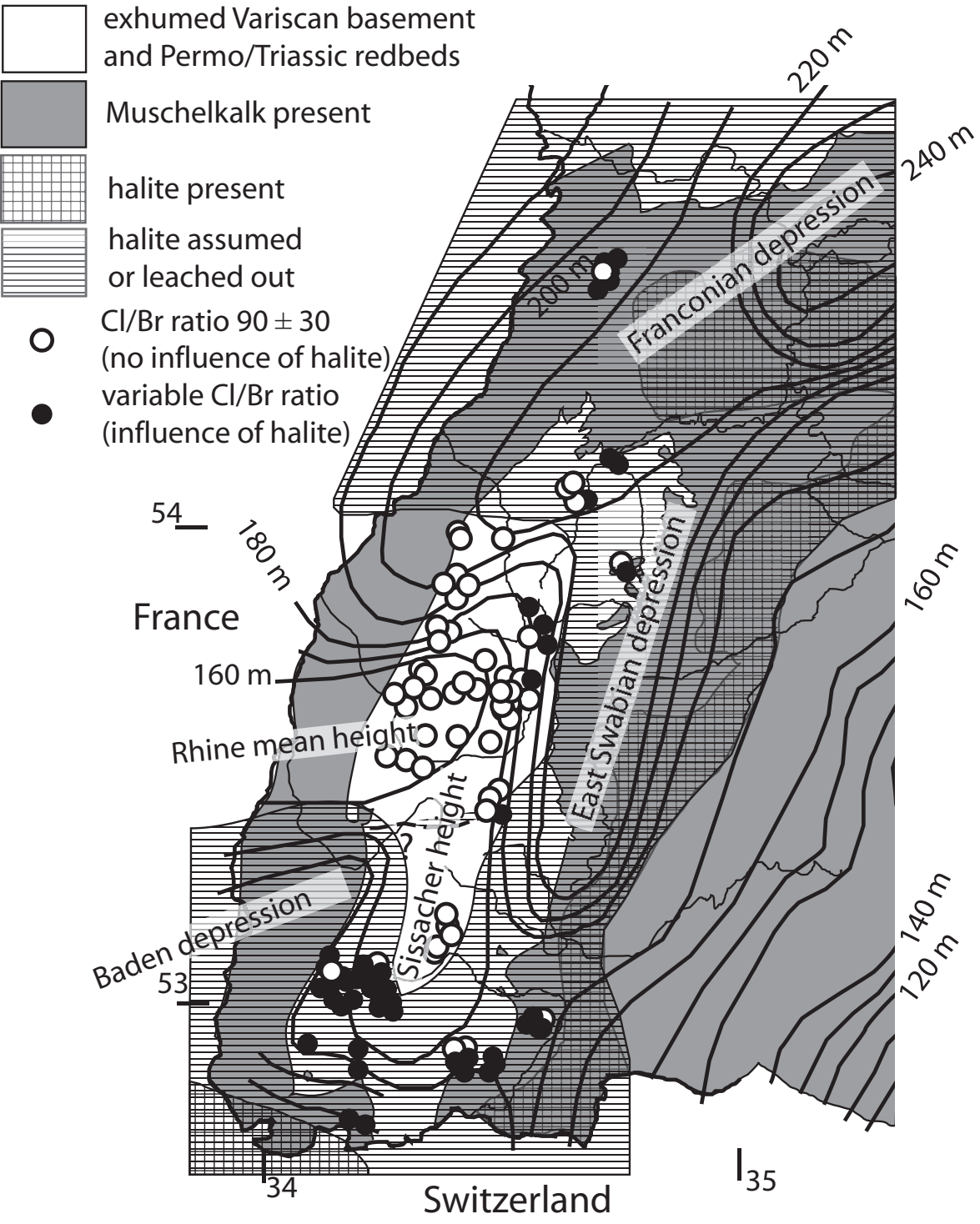
exhumed Variscan basement
and Permo/Triassic redbeds
Muschelkalk present
halite present
halite assumed
or leached out
Cl/Br ratio 90 ± 30
(no influence of halite)
variable Cl/Br ratio
(influence of halite)
220 m
240 m
200 m
Franconian depression
54
180 m
France
160 m
160 m
Rhine mean height
East Swabian depression
Sissacher height
Baden depression
53
140 m
120 m
34
35
Switzerland

Figure 5

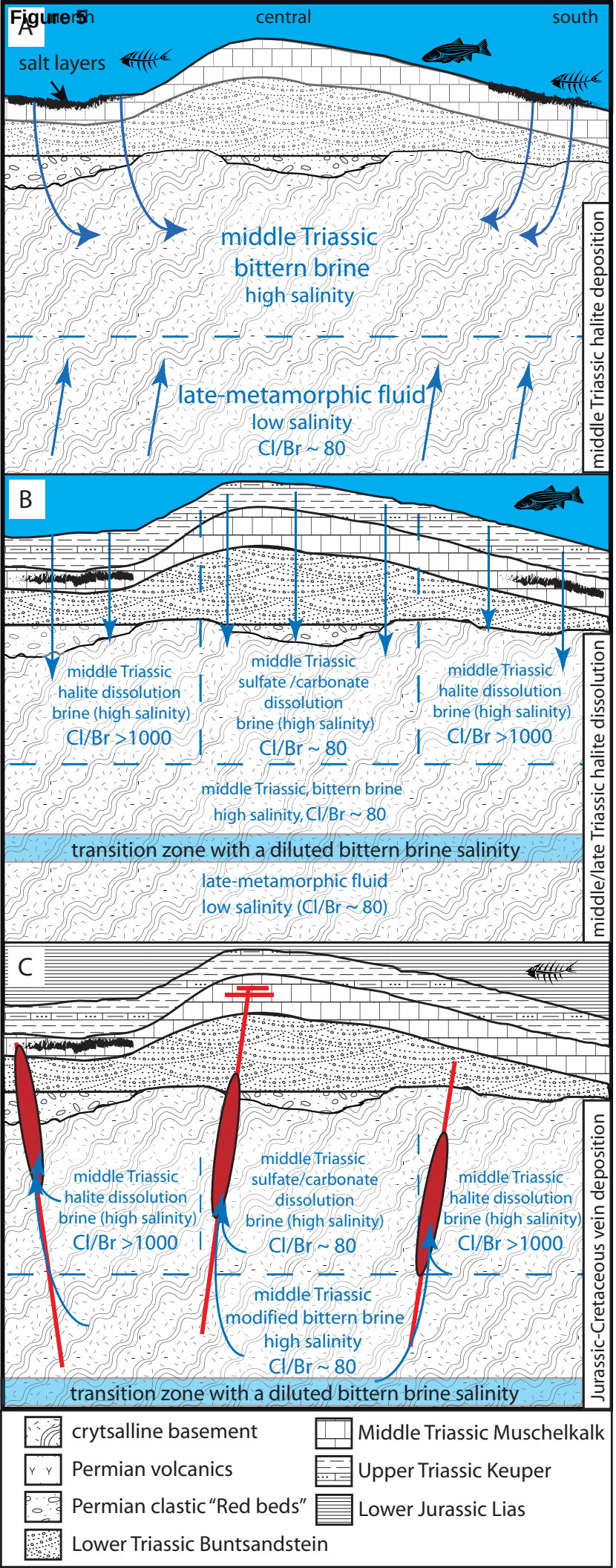
A
north
central
south
salt layers
middle Triassic
bittern brine
high salinity
late-metamorphic fluid
low salinity
Cl/Br ~ 80
middle Triassic halite deposition
B
middle Triassic
halite dissolution
brine (high salinity)
Cl/Br >1000
middle Triassic
sulfate /carbonate
dissolution
brine (high salinity)
Cl/Br ~ 80
middle Triassic
halite dissolution
brine (high salinity)
Cl/Br >1000
middle Triassic, bittern brine
high salinity, Cl/Br ~ 80
transition zone with a diluted bittern brine salinity
late-metamorphic fluid
low salinity (Cl/Br ~ 80)
middle/late Triassic halite dissolution
C
middle Triassic
halite dissolution
brine (high salinity)
Cl/Br >1000
middle Triassic
sulfate/carbonate
dissolution
brine (high salinity)
Cl/Br ~ 80
middle Triassic
halite dissolution
brine (high salinity)
Cl/Br >1000
middle Triassic
modified bittern brine
high salinity
Cl/Br ~ 80
transition zone with a diluted bittern brine salinity
Jurassic-Cretaceous vein deposition
crytsalline basement
Permian volcanics
Permian clastic "Red beds"
Lower Triassic Buntsandstein
Middle Triassic Muschelkalk
Upper Triassic Keuper
Lower Jurassic Lias

Figure 6

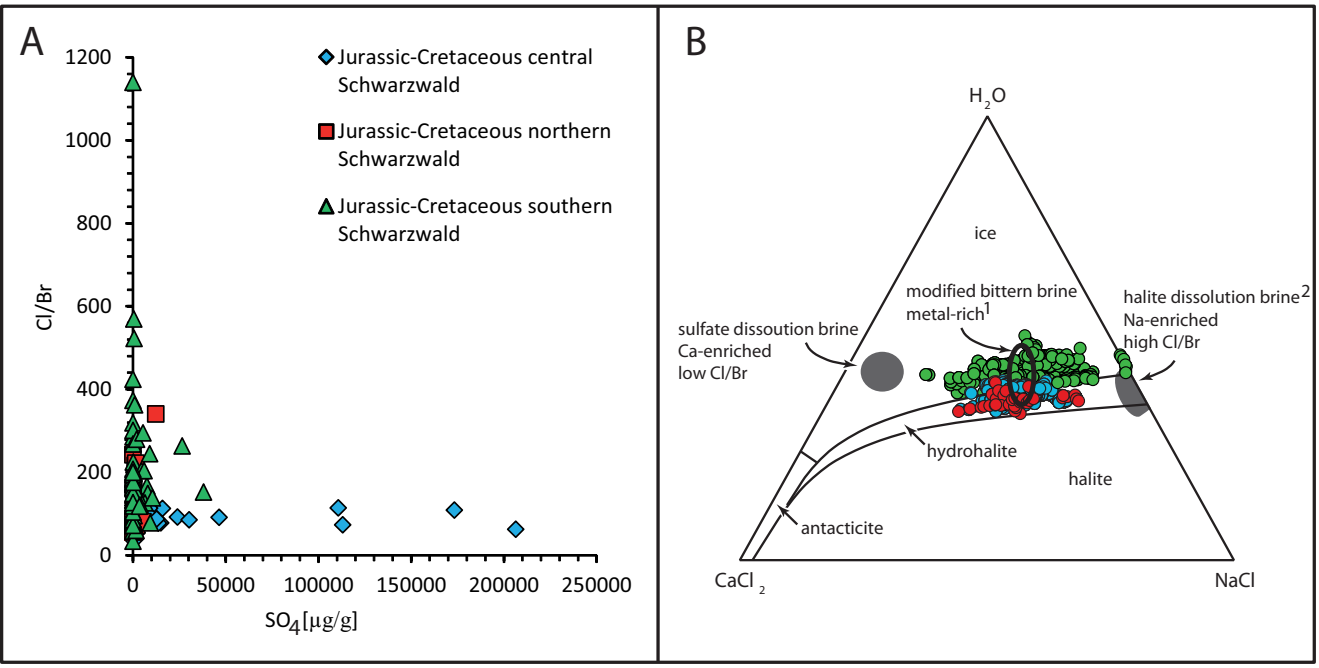
A
1200
1000
800
600
400
200
0
Cl/Br
0
50000
100000
150000
200000
250000
SO4[µg/g]
Jurassic-Cretaceous central Schwarzwald
Jurassic-Cretaceous northern Schwarzwald
Jurassic-Cretaceous southern Schwarzwald
B
H2O
ice
modified bittern brine
metal-rich1
halite dissolution brine2
Na-enriched
high Cl/Br
sulfate dissoution brine
Ca-enriched
low Cl/Br
hydrohalite
halite
antacticite
CaCl2
NaCl

Figure 7

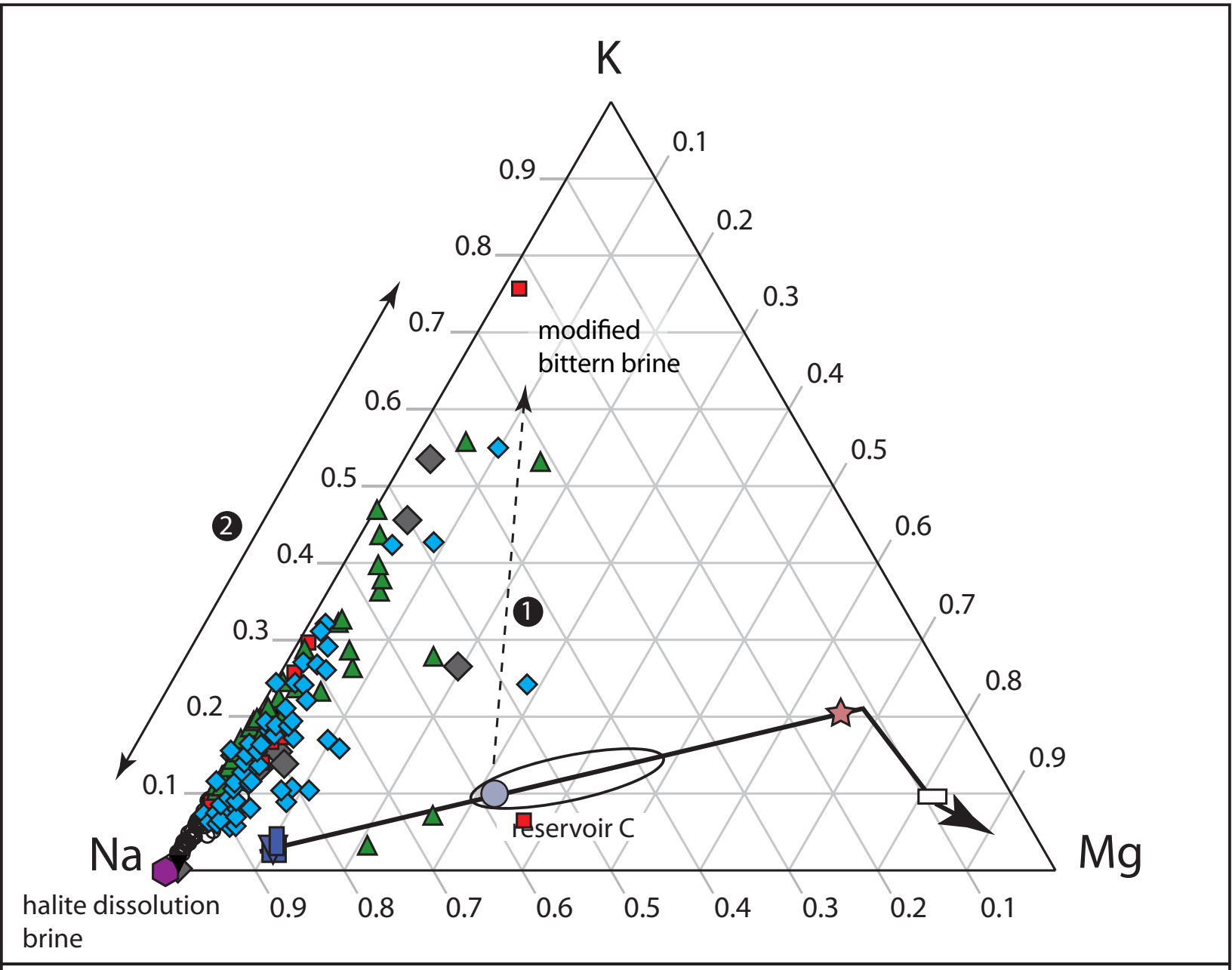

bulk crush leach northern Schwarzwald

bulk crush leach central Schwarzwald

bulk crush leach southern schwarzwald

LA ICPMS data of single fluid inclusions (Fußwinkel et al., 2013)

halite dissolution brine (Göb et al., 2013)

bulk crush leach data Jurassic-Cretaceous (Walter et al., submitted)

chemical evolution of seawater during evaporation after McCaffrey et al. (1987):

calcite saturation

halite saturation

Mg-sulfate saturation

gypsum saturation

deg. of evaporation ~ 30
Cl/Br = 80

sylvite saturation

Anhang 4

Walter, B.F., Burisch, M., Fußwinkel, T., Marks, M.A.W., Wälle, M., Heinrich, C., Apukhtina, O.B., Markl, G. (in prep.) Multi-reservoir fluid mixing processes in rift-related hydrothermal vein-type deposits

akzeptiert zur Veröffentlichung	Anzahl der Autoren	Position des Kandidaten in der Autorenliste	Wissen-schaftliche Idee des Kandidaten (%)	Datengenerier-ung des Kandidaten (%)	Analysen und Interpretat-ionen des Kandidaten (%)	Verfassen der Publikation durch den Kandidaten (%)
nein	8	1	60	90	50	50

Multi-reservoir fluid mixing processes in rift-related hydrothermal vein-type deposits

Benjamin F. Walter, Mathias Burisch, Tobias Fusswinkel, Michael A.W. Marks, Markus Wälle, Christoph Heinrich, Olga B. Apukhtina, Gregor Markl

Abstract

Fluid mixing is an important process during the formation of many hydrothermal vein-type deposits. In this contribution, we present evidence for hydrothermal fluid systems and associated mineralization, in which mineral precipitation is initiated by fluid mixing of more than two fluids. A well investigated natural laboratory, the Schwarzwald mining district (situated at the eastern shoulder of the post-Cretaceous Rhine graben failed rift in SW Germany), has been chosen to investigate such mixing processes on the scale of a large mining district, a single location and a single growth zone within one sample. Based on our observations, we relate the observed diversity of the hydrothermal veins in terms of mineralogy and fluid inclusion chemistry to the disturbed geological environment during ongoing rifting. Literature data on the regional geology, current groundwater reservoirs, formation processes and hydraulic features are augmented by new fluid inclusion analyses from post-Cretaceous, hydrothermal vein minerals including microthermometry, crush leach (IC and TXRF), Microraman and LA-ICPMS data of single fluid inclusions.

Fluid petrography and microthermometry show complex sequences of alternating fluid signatures on different growth zones of one crystal. High (20-26 wt. % $NaCl+CaCl_2$), moderate (5-20 wt. % $NaCl+CaCl_2$) and low salinity (<5 wt. % $NaCl+CaCl_2$), sulfate-bearing and CO_2-bearing primary fluids inclusions may alternate on various growth zones of one single crystal. Such variations are observed abundantly in minerals from different localities. Bulk crush leach analyses show significant variations in major element composition of the trapped fluids, which can generally be described in the Na-K-Ca-Cl-SO_4-HCO_3-system. These variations are caused by mixing of fluids from different aquifers and in various proportions. Ancient fluids show chemical similarities to modern groundwater aquifers such as granitic basement, Lower Triassic Buntsandstein sandstones or Middle Triassic

Muschelkalk limestones, which can be directly sampled in today's wells. Single fluid inclusion investigations by LA-ICPMS support this interpretation and show multi-component fluid mixing processes on the scale of single localities and even on the scale of single crystal growth zones. The latter can be used to calculate a maximum duration of mineral growth (before the fluid is homogenized), which implies very short-lived fluid events on the order of seconds to hours.

By defining end member reservoirs, mixing of different fluid signatures in various ratios was calculated; these hydro-chemical calculations show that almost all mixed fluid compositions are saturated with respect to barite. In contrast, fluorite-saturated fluids can only be modelled by mixing of a basement brine with fluids from Triassic sandstone. All fluid mixtures are strongly undersaturated with respect to galena, chalcopyrite and sphalerite, the most commonly observed ore minerals in the hydrothermal veins. As the calculated fluid mixtures are typically relatively oxidized and contain high sulfate/sufide ratios, precipitation of sulfides was most probably related to short-lived reduction events caused by an influx of hydrocarbons or by reactions with graphitic wall rocks.

Structurally, multi-aquifer fluid mixing processes involving aquifers of different chemical and physical constitution are triggered by a major "short-circuit" such as a tectonic rifting event. The Rhinegraben obviously was able to act as such a trigger and thereby initiated the formation of a large number of mineralogically diverse hydrothermal ore deposits.

1. Introduction

The chemical and hydraulic properties of fluids causing the formation of unconformity-related hydrothermal vein type (specifically base-metal) ore deposits are key parameters to understand the genesis of these systems. Most studies are based on a combination of microthermometry (Wilkinson, 2010), stable and radiogenic isotopes (O, C, H, Sr, Cl, Br, Pb and Zn) (Bau et al., 2003; Kessen et al., 1981; Shouakar-Stash et al., 2007; Staude et al., 2011b; Wilkinson et al., 2005), trace element studies of fluids and gangue (Fusswinkel et al., 2013; Pfaff et al., 2011) or paleo-hydrological modelling (Garven et al., 1999). Examples include the Alaskan Brooke Range (Leach et al., 2004), the South East Basin in France (Aquilina et al., 2011), the Irish Midlands (Banks et al., 2002), the Massif Central in France, the Maestrat basin and the Catalan Coastal Ranges in Spain and Upper Silesia in Poland

(Boiron et al., 2010), the St. Lawrence rift in Canada (Carignan et al., 1997) and the Otavi Mountainland in Namibia (Deane, 1995). Numerous workers (e.g. Wilkinson 2010, Fusswinkel et al., 2013, 2014 a, Bons et al., 2014 and references therein, Walter et al., 2015) concluded, that fluid mixing typically takes place between (I) hot, deep-seated fluids from the crystalline basement, and (II) cooler, sediment-derived fluids from the overburden sequence (Staude et al., 2009, 2012 and references therein). Most authors agree that most of the metals are transported by basement brines or deep seated basinal fluids (Fusswinkel et al., 2013; Boiron et al., 2010) and it is this mid-crustal metal-rich fluid most contributions focus on. However, the simplified model of a two-component mixing system can only be applied to undisturbed environments where two distinct source reservoirs are spatially separated, which is often an oversimplified assumption not able to explain the diversity of fluid compositions and mineral assemblages in hydrothermal veins related to rift systems or large scale lineaments (e.g. Yukon Territory, Rio Grande Rift, Illinois, Nova Scotia, Newfoundland, Sardinia (Van Alstine, 1976)). All these examples share the similarity, that more than two aquifers with different chemical properties were involved during vein formation. It is typical of such districts, that veins of different gangue and ore mineral associations are observed within a relatively small area (e.g. Bjørlykke et al., 1990; Van Alstine, 1976; and references therein).

The same holds true for an old mining district in Central Europe bordered by the post-Cretaceous Rhine graben rift, the Schwarzwald mining district in SW Germany (e.g. Metz et al., 1957, Bliedner & Martin, 1986; Baatartsogt et al., 2007; Staude et al., 2009) where veins of different mineral assemblages occur along and in the vicinity (up to 50 km) of the Rhine graben boundary fault. These veins occur in various types of sedimentary and basement host rocks brought into contact during rifting. Accordingly, this work focuses on the following aspects:

- a fundamental study of ore-forming fluids by microthermometry, crush-leach, TXRF and LA-ICPMS analyses in the various types of post-Cretaceous mineralizations across the entire mining district;
- the geochemical characterization of possible source aquifers and their connection to modern formation fluids;
- the links between the various fluid sources/aquifers and the different types of mineralization;

- the details of mixing on the scale of a mining district, a single locality and a single crystal.

The post-Cretaceous samples for this study were carefully chosen based on a large pre-existing dataset on hundreds of samples from the Schwarzwald mining district which have been investigated in the Tübingen group in the last ten years. These data include microthermometry (Baatartsogt, 2007; Fusswinkelet al., 2013; Pfaff et al., 2009; Staude et al., 2009; Staude et al., 2012b), major, minor and trace element compositions of fahlore and sphalerite (Pfaff et al., 2011; Staude et al., 2010b), age-dating (Pfaff et al., 2009, Staude et a., 2012), stable isotope data (O-D-C-S-Sr-Pb-Cu-Fe; Baatartsogt, 2006, 2007; Markl et al., 2006; Schwinn et al., 2006; Staude et al., 2011a; Staude et al., 2012a; Staude et al., 2012b; Ströbele et al., 2012), REE patterns in fluorites and supergene minerals (Göb et al., 2011; Schwinn and Markl, 2005; Loges et al., 2012), paleo-hydrological modelling (Bons et al., 2014; Pfaff et al., 2010; Staude et al., 2011a, Loges et al., 2012), studies on specific deposits like Wittichen, the Wenzel mine, Schapbach, and Wiesloch (Pfaff et al., 2010; Staude et al., 2010a; Staude et al., 2007; Staude et al., 2012b) and on modern thermal and mineral waters (Göb et al., 2013; Loges et al., 2012). A well-described geology of the region (Geyer and Gwinner, 2011; Ziegler, 1990) and many studies on modern water chemistry and hydraulic properties of the different aquifers (Stober and Bucher, 1999a, 1999b, 1999c, 2000, 2004, 2005a, 2005b, 2007; Stober et al., 1999, He et al., 1999, Bucher et al., 2009; Bucher and Stober, 2000, 2002, 2010, Ludwig et al., 2011, Stober 2011) make this region an ideal one for the present complex study.

It is important to realize that today, tectonic activity in the Upper Rhinegraben still goes on (Geyer and Gwinner, 2011), that more than 20 thermal and mineral wells occur along the boundary faults and in their vicinity (Göb et al., 2013) and that the sedimentary rocks present on top of the partially eroded basement and along the graben shoulders are the same as during the onset of rifting in the Paleogene. Hence, it appears reasonable to assume that today's groundwater compositions have at least some similarities to those which formed the hydrothermal veins since the onset of Rhinegraben rifting in Paleogene times. For some of the aquifers (basement, Muschelkalk limestones), this similarity in terms of salinity, Cl/Br ratios and major and minor element composition has been shown in Walter et al. (in press, submitted Jura). This approach thus enables to draw conclusions on ore-forming processes based on the comparison with active water data.

1.1 Regional geology

The Schwarzwald consists of exhumed Variscan basement gneisses and granites covered by Permian to Upper Jurassic sedimentary units (Fig. 1) (Kalt et al., 2000). The paragneiss units of the basement locally contain orthogneisses and amphibolites deformed and metamorphosed during Variscan (Carboniferous) orogeny (Geyer and Gwinner, 2011). The gneisses were intruded by post-collisional S-type granites between 335 and 315 Ma (Altherr et al., 2000; Hann et al.,, 2003; Todt, 1976). During the Rotliegend (Permian), small proximal sediment traps were filled by redbeds (arkoses, conglomerates) (Geyer and Gwinner, 2011; Jenkner, 1986; Nitsch and Zedler, 2009). In the early Triassic, quartzitic Buntsandstein units up to 400m in the northern and <50 m in the southern Schwarzwald were deposited, while middle Triassic (Muschelkalk) limestones and evaporites (halite or gypsum in different facies configurations) reached a thickness of 160 to 220 m. The Late Triassic (Keuper) was dominated by clastic sediments and evaporitic units (mainly gypsum). Their thickness decreases from about 300m in the north to less than 100m in the south (Geyer and Gwinner, 2011). In total, about 1000m of clastic sediments and carbonates were deposited on the shallow continental Tethys shelf during Jurassic times, including organic-rich shales during the lower Jurassic (Lias ε). No sediments were deposited during the Cretaceous.

During the Paleogene, the commencing rifting of the Upper Rhinegraben (Geyer and Gwinner, 2011; Schwarz and Henk, 2005) resulted in the deposition and precipitation of about 400m of clastic and chemical sediments (gypsum, anhydrite, dolomite, Na-K-Mg halides) in the rift valley (Geyer and Gwinner, 2011; Rupf and Nitsch, 2008). The rifting was accompanied by the uplift of the rift shoulders, which was associated with erosional exhumation of the crystalline basement. Uplift and erosion was stronger in the southern relative to the middle and northern Schwarzwald; while in the middle and northern Schwarzwald, the basement-cover unconformity is preserved to the present day, the southern Schwarzwald is eroded to a depth of about 1.5-2km below the former unconformity (Rupf and Nitsch, 2008). This implies that hydrothermal veins visible today in the central Schwarzwald formed at a more shallow stratigraphic depth (about 1 km) than those in the southern Schwarzwald (about 2.5-3 km).

142

143 *1.2 Hydrothermal veins in SW Germany*

144

145 Hydrothermal veins in the Schwarzwald formed more or less continuously in basement rocks
146 and their Permian and Triassic sedimentary cover between about 300 Ma and the present day (Loges et
147 al., 2012; Pfaff et al., 2009; Staude et al., 2009). Based on the work of Walter et al. (2015) and Walter
148 et al. (in press, Jura submitted), the hydrothermal veins are classified in five formation stages based on
149 structural, mineralogical and microthermometric arguments (Table 1): (i) Carboniferous, (ii) Permian,
150 (ii) Triassic-Jurassic; (iv) Jurassic-Cretaceous and (v) post-Cretaceous ones. We will only deal with
151 group (v) in the present contribution.

152 During Paleogene rifting, Upper Rhinegraben-parallel NE-SW to NNE-SSW-striking fault
153 systems were opened or reactivated, resulting in the formation of veins consisting of barite-quartz,
154 various carbonates with or without barite and quartz or barite-quartz-fluorite assemblages mostly with
155 Pb ores; less commonly, As, Zn, Cu, Bi and Ni ores are present (Staude et al., 2009; Ströbele et al.,
156 2012; Werner, 1994). The formation of the Wiesloch MVT-deposit at 23 Ma in the paleo-karst of the
157 Muschelkalk limestones (Pfaff et al., 2010; Ströbele et al., 2012) also belongs to this group of
158 mineralizations (Table 1 and 2).

159

160 *1.3 Modern reservoirs and associated fluids*

161 1.3.1 *Basement*

162 Data from numerous drill holes and wells indicate that today, a fluid stratification exists in the
163 Schwarzwald basement aquifer (Bucher & Stober, 2010):

164 - shallow wells up to some hundred meters depth produce weakly mineralized Ca-Na-HCO_3
165 fluids;
166 - the total salinity increases with depth. At about 3 to 4 km, the fluids change into a CO_2-
167 bearing Ca-Na-HCO_3-SO_4-fluid as an effect of host rock sulfide oxidation. In the transition
168 zone from oxidized to reduced conditions, the sulfate and CO_2 content decreases with
169 increasing chlorinity;
170 - the deepest fluids probed today are high-salinity Na-Ca-Cl fluids typical of basement brines

worldwide. They have, for example, a Cl/Br mass ratio of ~ 90 (e.g. Frape and Fritz, 1987; Bucher and Stober, 2010) and are enriched in P and As (Bucher and Stober, 2010; Edmunds and Savage, 1991; Emmermann et al., 1995; Frape and Fritz, 1987; Frape et al., 1984; Köhler, 1992; Kozlovsky, 1984; Sanjuan et al., 2010).

This fluid stratigraphy is believed to result from the successive sucking of fluids from the surface into the crust over time (Agemar et al., 2013; Bons et al., 2014; Walter et al., 2016).

1.3.2 Sedimentary cover (Permian-Cretaceous)

The different permeabilities of layers in the sedimentary cover rocks result in a fluid stratigraphy. Some of the formations are separated by aquitards (Ufrecht 2006). The most important hydrological circulation/aquifer systems are the lower Triassic Buntsandstein (including Permian redbeds in small sediment traps) and the middle Triassic Muschelkalk (Ufrecht, 2006) with a clay aquitard in between. The aquifer properties differ significantly: in the crystalline basement, the aquifer consists of fractures, in the Buntsandstein sandstones of matrix porosity and the Muschelkalk limestone is a karst aquifer (Geyer and Gwinner 2011 and references therein; Ufrecht 2006). The composition of the fluids from the specific sedimentary strata is presented in the following, beginning with the oldest.

Fluids from Permian redbeds are typically Na-Ca-(K)-Cl fluids with a maximum TDS (total dissolved solids) of 124 g/L (Pauwels et al., 1993). The scarce analyses of redbed fluids from the Schwarzwald (including both Permian and lower Triassic aquifers) show some trace element enrichment of Ni, Cd and U (Köhler, 1992).

Lower Triassic (Buntsandstein) formation waters are Na-Ca-HCO_3-Cl-(SO_4) fluids with a maximum TDS of 207 g/L and Cl/Br ratios of 165-327 (Pauwels et al., 1993, Ludwig et al., 2011). Aquilina et al. (1997a) noted elevated Rb and Cs trace element contents in the Upper Basement and Buntsandstein formation at Soultz-sous-Forêt, which is caused by the dissolution of mica (Pauwels et al., 1993).

Fluids in the middle Triassic (Muschelkalk) limestone-gypsum-halite formation are quite variable, depending of the specific sedimentary facies. Those which interacted with the halite formation are Na-(Ca)-Cl fluids with a TDS up to 246 g/L (Göb et al., 2013; He et al., 1999) and show high chlorinity

and high Cl/Br ratios up to 9900 (Stober and Bucher, 1999), while those from the dolomite and gypsum/anhydrite lithologies are Na-Ca-(Mg)-Cl-HCO_3-SO_4 and Ca-Mg-Na-HCO_3-SO_4-Cl fluids of low to moderate salinity (6 g/L) and a Cl/Br ratio of 25-725 (He et al., 1999; Göb et al., 2013).

Fluids in the upper Triassic (Keuper) clay-, sand- and marlstones are from of the Ca-Na-HCO_3-SO_4-Cl type with low salinity (TDS =<2400 mg/l) and Cl/Br mass ratios of 405-533 (Göb et al., 2013). Köhler (1992) recognized relative trace element enrichments of phosphate and Ba in the fluid. The Keuper rocks are of minor importance as aquifers (Stober and Bucher, 2014).

The Lower Jurassic (Lias) clay formation is an aquitard rather than an aquifer, but pore fluids show a Na-Mg-Ca-Cl-SO_4 composition (Pearson et al., 2003). The organic-rich Posidonia formation (Lias ε) is internationally recognized as a petroleum source rock (Geyer and Gwinner 2011, and references therein) and hence, fluids from this stratum may contain abundant methane and higher hydrocarbons.

In and along the Rhinegraben valley, the Middle Jurassic (Dogger, Hauptrogenstein Fe-rich limestones) contains an important karst aquifer with two different types of fluids: a Na-Ca-Cl and a Ca-Mg-HCO_3-SO_4 water (He et al., 1999). Upper Jurassic strata are very rare in the vicinity of the Rhinegraben and are therefore not considered as important aquifer rocks.

1.3.3 Sediments in the Upper Rhinegraben

The Upper Rhinegraben contains a complex system of chemically and hydraulically variable aquifers (Fig. 2) (Lorenz, 2002). The Paleogene and Quaternary psephitic filling of the Upper Rhinegraben mainly consists of limestones in addition to evaporate sequences of Oligocene age. Organic-rich shales occur locally. At depth, the Upper Rhinegraben is underlain by the strata of the former sedimentary cover discussed above. Hydrothermal sulfates (dominantly anhydrite and gypsum, more rarely barite) derived from more than 400 m thick sulfate-bearing strata in the rift are common in fractures (Lorenz, 2002) and formed from Ca-SO_4-rich fluids partially related to gypsum dehydration. Fluids which have interacted with Oligocene halite are Na-dominated, have a high salinity and high Cl/Br ratios up to 2400 (Stober and Bucher, 1999).

Lorenz (2002) showed complex interactions between formation waters, highly mineralized basement fluids and meteoric waters. Sanjuan et al. (2010) and Lorenz (2002) described a convection system

with a downward flow in the centre and an upward flow at the boundaries of the Rhinegraben. The major upward fluid flow occurs from the deepest point in the centre of the rift towards the west, which follows the asymmetric geometry of the rift (Agemar et al., 2013) (Fig. 2).

In addition to the fluids from the sedimentary cover sequence described above, Ca-Mg-HCO_3-(SO_4) fluids (Geyer and Gwinner, 2011; Köhler, 1992) are known from the psephitic graben filling sediments. Oil field brines are known from the organic-rich shales of the Pechelbronn formation (Otto and Tòth, 1988). Additionally, fluids which interacted with the 600m thick Oligocene gypsum-anhydrite-halite-sylvite formation in the graben are expected to have a $CaSO_4$-NaCl-KCl signature (Borchert, 1959).

2. Sample material

2.1 Samples used for microthermometry, Raman spectroscopy and crush leach analysis

For the general study of the entire mining district, we collected and analysed all representative (mineralogy, volume, fluid chemistry and structural position) and accessible post-Cretaceous, Upper Rhinegraben-related veins in the Schwarzwald (Fig. 3). The diverse mineralogy of these veins (Fig. 4, Table 2) makes it necessary to analyse fluid inclusions in quartz, carbonates, fluorite and barite. If available, euhedral, clear crystals of centimeter size and with visible growth zoning were chosen. Samples with macroscopically visible intergrowths of different gangue and ore minerals were strictly excluded for crush leach analyses.

2.2 Samples used for LA-ICPMS analyses on individual fluid inclusions

To investigate the processes relevant for ore formation on the scale of one deposit, six locations have been selected based on the occurrence of large (<10cm) euhedral quartz crystals with a distinct growth zonation. These six veins are situated in fractures of the Upper Rhinegraben fault system (SSW-NNE trending). The selected quartz samples contain clearly primary fluid inclusions on the growth zones.

Sample TF35 from the Hausbaden mine near Badenweiler (“Quarzriff”) is a typical and representative quartz-barite vein with galena and sphalerite directly situated on the Rhinegraben boundary fault. At this location, crystalline basement rocks are in contact to several tilted blocks of Muschelkalk

limestones, Buntsandstein sandstones or Keuper gypsum-bearing shales. The Tirolergrund and the Wurmbach barren barite-quartz veins (samples BO26 and BO92) crop out about 500m east of the Rhinegraben boundary fault east of Staufen and Ballrechten, respectively, within a paragneiss basement unit. They originally formed around the Triassic-Jurassic boundary, but with a post-Cretaceous overprint (Walter et al., 2016) The Karl-August quartz vein (sample BO66) occurs near Kropbach/Münstertal 2 km to the east of the Rhinegraben boundary fault. It follows a granitic dyke in the paragneiss unit and contains massive sphalerite overgrown by large euhedral quartz crystals. The Riggenbach and Böschlisgrund veins (samples BO29 and BO98) are similar and consist of an early quartz-galena-sphalerite stage followed by later siderite with Cu-Ni ores. Young euhedral large quartz crystals overgrow this paragenetic sequence. The Riggenbach mine is situated in the Münstertal, about 4 km to the East of the Rhinegraben boundary fault, while the Böschlisgrund vein crops out northeast of the town of Sulzburg about 5 km east of the Rhinegraben boundary fault.

The quartz crystals used for the analyses are in four of the six localities the youngest precipitates within the paragenetic sequence of the respective deposit, only the Badenweiler and Böschlisgrund samples contain fluid inclusions in the ore-stage quartz.

3. Methods

3.1 Microthermometry

Up to three double polished thick sections (200 to 400µm) were produced from a cross-section through each vein to determine the chronological sequence of fluid inclusion assemblages (FIA, Goldstein and Reynolds, 1994) by optical microscopy. Fluid inclusions were classified as primary (p), pseudo-secondary (ps), secondary (s), isolated inclusions (iso) and clusters of inclusions with no geometrical relation to former crystal surfaces or fractures (c). Microthermometric investigations were performed using a Linkam stage (model THMS 600). Each fluid inclusion was analysed three times with respect to the final melting temperature of ice ($T_{m,ice}$) and hydrohalite ($T_{m,hh}$) and the homogenization temperature (T_h). The data include only fluid inclusions, for which triple analyses differ less than 0.1°C for $T_{m,ice}$ and $T_{m,hh}$ and less than 1°C for T_h. Synthetic H_2O, H_2O-NaCl and H_2O-CO_2 standards were used for calibration.

Fluid inclusions strongly deviating in salinity and homogenization temperature from a close-by homogeneous trail were neglected, since this may indicate fluid inclusion alteration by post-entrapment processes. The salinity in the ternary SO_4-free NaCl-$CaCl_2$-H_2O system was calculated according to Steele-MacInnes et al. (2011). The volume proportion for each fluid inclusion was estimated based on filling degree tables and reported in the volume proportion notation (Shepherd et al., 1985; Bakker and Diamond, 2006). A pressure correction according to Bodnar and Vityk (1994) was applied, assuming hydrostatic conditions with a depth of the water column inferred from the paleo-depth estimated by (Geyer and Gwinner, 2011). Uncertainties of this approach are discussed in Walter et al. (2015). Since hydrostatic conditions can be assumed and overburden is negligible for the post-Cretaceous veins of interest, the pressure correction has only minor effects on the homogenization temperature.

Microthermometry of fluid inclusions in barite is difficult, since they are easily destroyed during freezing or heating (decrepitation, leakage, necking-down). Consequently, microthermometric data obtained from fluid inclusions in barite were only used for calculating salinities, if the data agreed with data of quartz, fluorite or calcite from the same or a closely related vein, and they were principally excluded from Ca/(Ca+Na) calculations.

3.2 Crush leach IC and TXRF analyses

About 2g of fluorite, quartz, calcite or barite with a grain size of 0.5 to 1 mm were handpicked from 155 selected samples (for which microthermometry had been done before), and visible impurities were removed. It was ascertained that only one fluid type was present in the respective crystals. The separates were washed for 3 hours in HNO_3 at 60-70°C (the carbonates being washed in milliQ water only). Subsequently, the samples were washed for one week with ultrapure water, changing the water twice a day. These pre-treated samples were dried and crushed to fine powder in an agate mortar. To suppress the adsorption of doubly-charged cations (especially Ca^{2+}), crush leach solutions were acidified with suprapure HNO_3 (Köhler et al., 2009). The loaded solution was injected into a Dionex ICS 1000 ion chromatography systems, equipped with an IonPac AS 9-HC 2mm column for quantification of anions (F, Cl, Br, NO_3, PO_4 and SO_4) and an IonPac CS 12-A column for cations (Li,

311 Na, K, Mg, Ca, Ba, Sr). For injection of the solutions, we used disposable syringe filters
312 CROMAFILE© Xtra RC-20/25 and CROMAFILE© Xtra PVDF-20/25 for anions and cations,
313 respectively (Ladenburger 2012 and Ladenburger et al., 2012). Blank runs were carried out before and
314 after each analysis and defined standard solutions were regularly analysed to monitor the
315 reproducibility and precision of the measurements. Uncertainties were usually smaller than 15% and
316 effective detection limits were generally <10 mg/l.
317 The concentrations of several trace metals (Cu, Ni, Co, Pb, Zn, Bi) were determined by Total
318 Reflection X-Ray Fluorescence Spectroscopy (TXRF) using an S2 PICOFOX (Bruker AXS
319 Microanalysis) equipped with a Mo-tube operated with 50 kV and 600µA. For these analyses, each 1
320 ml of the crush-leach solutions (see above) were centrifuged and filtered. Subsequently, 190 µl of the
321 solutions were mixed with 10 µl Ga solution with a Ga concentration of 5 mg/l. Three aliquots (10µl)
322 were pipetted onto polished quartz-glass disks and dried at 70°C. The dried sample cakes were then
323 analyzed for 1000 s. Effective detection limits for these metals vary with the degree of dilution (based
324 on the crush-leach procedure, see above) and were generally <50 mg/l for Cu, Ni, Pb and Zn and <100
325 mg/l for Co and Bi.
326 Quartz, barite, calcite and fluorite were used for crush leach analyses (IC and TXRF). A contamination
327 of the leachates by the dissolution of these host minerals is potentially relevant for fluorite (Ca, F),
328 calcite (Ca) and barite (Ba, Sr, sulfate). The complete dataset in the electronic supplement includes
329 these elements, but their concentrations are excluded from interpretation. Many of our crush-leach
330 solutions contain dissolved carbonate from fluid inclusions (as indicated by the presence of CO_2 based
331 on Raman spectroscopy) and we assume that the positive deviations from electrical electroneutrality
332 can be ascribed to carbonate species, as has been done before (e.g. Bottrell et al., 1988; Channer and
333 Spooner, 1991; Banks et al., 2000; Dolnischek et al. 2014). This has no impact on the quality of Cl and
334 Br data in the crush-leach analyses and especially not on the Cl/Br ratios, nor on the quality of
335 microthermometric data (Ca-Na systematics, salinity or homogenization temperatures). The leaching
336 solutions were filtered and centrifuged before analysis, to exclude contamination by suspended
337 particles of e.g. ore minerals. Several analyses revealed high metal contents of up to 48200 mg/l Pb
338 and 51900 mg/l Cu. To evaluate the validity of these analyses we carried out calculations with

Geochemist Workbench Version 10.0.2. Using the compositions and salinities of BO65 and ML40 (table 2 of the electronic supplement) at neutral pH, an fO_2 in the sulfide stability field and a temperature of 150°C, the calculations show that the Pb and Cu concentrations of all crush-leach analyses are well below the saturation of galena and chalcopyrite (0.7 mol/l (~145 g/l) Pb and 10 mol/l (~635 g/l) Cu).

3.3 LA-ICPMS microanalyses of single fluid inclusions

LA-ICPMS microanalysis of individual fluid inclusions was conducted with a Perkin Elmer Elan 6100DRC quadrupole ICPMS connected to an ETH-GeoLas 193 nm ArF excimer laser system at the ETH Zürich, Switzerland. An energy density of 15-20 J/cm^2 with a laser pulse frequency of 10 Hz, with a variable beam size was used. Analytical and standardization procedures are reported in (Heinrich et al., 2003) and (Seo et al., 2011). Twentyseven elements/isotopes were analyzed: ^{7}Li, ^{11}B, ^{23}Na, ^{24}Mg, ^{32}S, ^{35}Cl, ^{39}K, ^{44}Ca (not quantified in fluorite but used for matrix correction), ^{55}Mn, ^{57}Fe, ^{59}Co, ^{60}Ni, ^{63}Cu, ^{66}Zn, ^{75}As, ^{79}Br, ^{85}Rb, ^{88}Sr, ^{95}Mo, ^{107}Ag, ^{121}Sb, ^{133}Cs, ^{137}Ba, ^{182}W, ^{205}Tl, ^{208}Pb, ^{209}Bi and ^{28}Si for the quartz host correction. The peaks of the analysed elements strictly follow the Na and Cl peaks in the time-resolved LA-ICPMS signals which demonstrates that these element peaks are derived from the solutions and not from the host mineral. For absolute concentrations, the measured concentrations were related to the NaCl salinity determined by microthermometry in the $CaCl_2$-NaCl-H_2O system (Steele-MacInnes et al., 2011). Data reduction was done using the SILLS software package (Guillong et al., 2008). The complete dataset is presented in the electronic supplement.

3.4 Microraman spectroscopy

Microraman measurements were performed to detect and identify volatile phases in representative fluid inclusion assemblages, using a confocal Raman spectrometer Renishaw InVia Reflex at Tübingen University. All measurements were carried out with a laser wavelength of 532nm (green) using a laser output of 50%. The use of a 50% objective results in a numerical aperture of 0.55 with an opening angle of 66.7°. The slit diaphragm was regulated and corrected automatically. The focus diameter was approximately 2µm, the measurement time was 30 seconds with a three-rate

accumulation. To correct any influence from the matrix, measurements in the host mineral were performed under identical conditions and orientation. As far as possible (depending on inclusion size), separate measurements focussing on liquid and on vapour were done. For qualitative evaluation, the Raman database for fluid inclusions of (Frezzotti et al., 2012) was used.

3.5 Cathodoluminescence (CL) microscopy

Cathodoluminescence (CL) microscopy studies of different hydrothermal phases were performed to obtain additional qualitative information on the fluid petrography of fluid inclusion assemblages. Furthermore, replacement textures of barite and anhydrite were studied. We used a 'hot cathode' CL microscope (type HC1-LM) at Tübingen university with an acceleration voltage of the electron beam of typically ~14 kV and a beam current density of ~9 μA mm^{-2} on the sample surface.

4. Results

4.1. Classification of fluid signatures

A detailed petrography (optical microscopy and microthermometry) of fluid inclusion assemblages (FIAs) enables the classification of fluid inclusions according to their relative ages (Fig. 5). Characteristic differences between primary and secondary fluid inclusions can be summarized as follows: Primary inclusions on crystal growth zones are typically much smaller (<5-15 μm), than fluid inclusions of secondary and pseudosecondary assemblages (<5-80 μm). These pseudosecondary and secondary inclusions mostly occur on (partly) sealed fractures, which crosscut the primary structures and often exhibit angular shapes.

In general, veins situated directly on the Rhinegraben boundary fault or on conjugated faults show complex, alternating fluid signatures (low, medium and high salinity fluid inclusion assemblages of variable temperatures, table 3) within neighbouring FIA.

Signature A: low salinity, medium to low temperature

Fluid inclusions containing fluid type A (table 3) are recognized in p, s, ps, iso and c fluid inclusion

assemblages. They freeze in the range -30 to -45°C, first melting occurs above -20°C. This implies a binary NaCl-H_2O system with a eutectic temperature of -21.2°C. The final melting temperature of ice is in the range of 0°C to -5°C, which results in a calculated salinity of 0 to 5wt.% (NaCl+$CaCl_2$) (Steele-MacInnes et al., 2011). Homogenization temperatures (Th) range from 50 to 354°C with a conspicuously high abundance of fluid inclusions with Th around 180°C. Within one trail, salinity and T_h is constant, but both may vary between different trails. Fluid inclusions with LV10 to LV1 and sizes of 4 to 40µm can be observed. In most cases, the inclusions are irregularly shaped and occur on (not very well) healed cracks. Microraman analyses show only H_2O, HCO_3^- or CO_3^{2-}, but no SO_4^{2-} in the fluid.

Signature B: high salinity, low to moderate temperature

Type B inclusions (table 3) occur in p, s, ps, iso and c assemblages with freezing temperatures between -70 and -100°C. First melting occurs above -50°C. This implies a ternary NaCl-$CaCl_2$-H_2O system with a eutectic temperature at -52.0°C. Ice and hydrohalite are observed as last dissolving phases. The final melting temperature of ice is in the range of -29.0 to -18.5°C, of hydrohalite between -28.5 and -17.5°C, which implies a salinity of 20 to 26 wt.% (NaCl+$CaCl_2$). Homogenization temperatures are in the range from 70 to 230°C with a Gaussian mean at 130°C. The molar Ca/(Na+Ca) ratio varies between 0.02-0.53. Within one trail, salinity and T_h are constant, but they may vary between different trails. Inclusions have sizes of <5 to 100µm and to -18. Most inclusions are irregularly shaped and occur on primary growth zones and nicely healed fractures. Microraman analyses show H_2O as the only Raman-active species in all FIA

Signature C: variable salinity, low to moderate temperature

Fluid type C (table 3) also occurs as p, s, ps and iso FIAs. Inclusions with freezing point depressions between -70 to -100°C and -30-45°C are observed in numerous samples. In contrast to the previously described groups, two different FIAs occur: one with a eutectic temperature of -21.2 and another with a eutectic temperature of -52°C. Although the Ca/(Na+Ca) molar ratios of these FIA vary, all fluids of intermediate (i.e., between 0.9 and 20 wt.% NaCl+$CaCl_2$) salinity are compiled in fluid group C.

Additionally, the Ca/(Na+Ca) molar ratio may vary within one FIA. In all analysed FIAs, ice is the last dissolving species. The final ice melting temperature is in the range of -2.6 to -18°C, hydrohalite melts between -20.9 and -25.8°C, which results in a calculated salinity of 5 to 20 wt.% ($NaCl+CaCl_2$). Homogenization temperatures vary between 59 and 202°C with a Gaussian peak at 140°C. Molar Ca/(Na+Ca) ratios vary between 0 and 0.3. Within one trail, salinity and T_h are constant, but they may vary between different trails. Inclusions have sizes of <5 to 100µm and LV15 to LV1. Most inclusions are round and occur on primary growth zones and nicely healed fractures. Microraman analyses show in all trails only H_2O as Raman-active species.

Signature D: H_2O-CO_2-(NaCl)

In contrast to the previously described fluid types, type D fluids (table 3) are relatively rare. Only primary and secondary inclusions have been found. The CO_2 phase transition occurs in all inclusions exactly at the -56.8°C triple point. Homogenization of the carbonic liquid into vapour (transition $L_{car}L_{aq}V$ to $L_{aq}V$) occurs between +21.2 to 31°C. For the larger inclusions clathrates have been detected at +4.9 to +5.9°C. The first melting temperature of ice is about -18°C. Final dissolution of ice occurs at -4.7 to -7.6°C, which does not support a pure H_2O-CO_2 fluid; an additional NaCl component seems the most probable one, as Microraman analyses show only CO_2 and H_2O bands. T_h varies between 134 and 219°C and occurs into the vapour phase with L(LV)10 to L(LV)20. Based on the software package "CLATHRATES" (Bakker, 1997) a salinity of maximum 5 wt. % $NaCl_{eq}$ is calculated. The carbonic liquid has a rather low density because it homogenizes into the vapour and total homogenization occurs at low T, too. This points towards very little CO_2 in the bulk inclusion, X_{CO2} of 0.02-0.05.

Signature E: Multi-component system with unknown salinity without CO_2 at moderate temperatures

Secondary and isolated assemblages of this fluid type (table 3) were found in seven samples. First melting occurs above -45°C, freezing point depression ranges from -70 to -100°C. Final ice melting was detected between -10.9 and -15°C, final dissolution of a cubic dark green solid phase (probably sylvite) was reached at +20 to +24°C and a lime green long prismatic solid phase (probably anhydrite)

dissolved at +43° to +63°C (Fig. 6A-D). During repeated heating-freezing cycles, each phase and phase transition could be reproduced in every single run. Microraman analyses verified the presence of dissolved sulfate in the fluid inclusions. Based on the microthermometric and microraman results, this type of fluid obviously has a composition in the NaCl-KCl-$CaSO_4$-H_2O-system. The homogenisation temperature is constant within one trail, but ranges from 98°C to 220°C. The mean is at 130°C. Inclusion sizes vary from <5µm to >100µm with LV10 to LV5.

Signature F: Multi-component system with unknown salinity with CO_2 at moderate temperatures

Type F fluid inclusions (table 3) are of primary and secondary origin. Their most important attribute is a clearly visible double-bubble, which is characteristic of CO_2- or CH_4-bearing fluids. The CO_2 phase transition is visible between -56.4 and -56.8°C. The homogenization of CO_2 liquid into vapour ($L_{car}L_{aq}V$ to $L_{aq}V$) was reached between +21.3 and +31°C. Two types of inclusions are found: One (F1) shows a freezing point depression between -40 and -60°C, final melting of ice from -9.7 to -17.4°C. In many inclusions, an unknown, cubic dark green solid phase dissolves between +22.5 and +24.5°C (probably sylvite). Sometimes, a long prismatic lime green solid phase is observed, melting between +60 and +75.2°C. Hydrohalite nucleation disappears close to the binary eutectic of -21.2°C. Microraman data show CO_2 and sulfate bands. Based on the microthermometric and microraman results, this is an H_2O-CO_2-SO_4-NaCl-KCl fluid. Uncorrected homogenization temperatures vary between 210°C and 307°C with L(LV)10 to L(LV)20.

The second fluid type (F2) shows a freezing point depression below -80° and first melting occurs between -40 and -50°C. Final dissolution of hydrohalite occurs between -23.0°C and -26.0°C and the final ice melting occurs in the range of -0.1°C and -0.8°C. An unknown columnar lime green phase shows a phase transition into liquid at +24 to +27.1°C. The total homogenisation of all vapor species is in the range 140 to 180°C. Clathrates may be observed in some FIAs, finally melting at +5.1°C to +6.3°C. Similar to signature D, a salinity of about 5 wt. % $NaCl_{eq}$ can be calculated. Microraman data show sulfate and CO_2 bands. The carbonic liquid has also a low density based on the homogenization into the vapour phase, with a total homogenization at low T. A small X_{CO2} of 0.02-0.05 in the bulk inclusion can be assumed. Type F2 inclusions probably contain Na-Ca-K-H_2O-SO_4-CO_2 fluids with

L(LV)10 to L(LV)20. Figure 6A-D illustrates the microthermometric observations of this fluid type. Figure 6E and F report the presence of SO_4 in the fluid phase.

Finally, in addition to A, B, C, D, E and F type fluids, most samples contain young FIAs characterized by water-rich, mono-phase liquid inclusions.

4.2 Crush leach IC and TXRF

In total, 155 crush leach analyses of 96 veins were performed. The complete dataset is presented in the electronic supplement (HCO_3 is derived by charge balance). In accordance with the microthermometric results, these analyses record the presence of the following fluid types: Na-Ca-Cl, Ca-Na-Cl, Na-Ca-Cl-HCO_3, Ca-HCO_3, Ca-Na-HCO_3, Ca-Na-SO_4-HCO_3, Ca-K-Mg-Na-HCO_3 and K-Ca-Na-Cl-HCO_3.

Bulk trace element systematics show Cu (b.d.l.-51.920ppm), Zn (b.d.l.-45.130ppm), As (b.d.l.-52.980ppm), Pb (b.d.l.-43.800ppm), U (b.d.l.-12.250ppm), Ni (b.d.l.-8790ppm), Y (b.d.l.-8880ppm), Rb (b.d.l.-7400ppm), Co (b.d.l.-3280ppm), Th (b.d.l.-2250ppm), Tl (b.d.l.-1470ppm), W (b.d.l.-1070ppm) and Bi (b.d.l.-510ppm). Highest Th and U concentrations are found in fluids hosted especially in barite and sometimes in calcite.

In general, there is no systematic dependence of the fluid composition on the proximal host rocks, salinity, homogenization temperatures, vein type or trace element distribution. Cl/Br mass ratios range unsystematically from low to high values, even between adjacent veins, the only exception being the veins of the Badenweiler system: these veins exclusively show high Cl/Br ratios.

4.3 LA-ICP-MS of single fluid inclusions

LA-ICPMS analyses were performed on 110 fluid inclusions from six samples. The results are presented in table 4 and in table ES3 of the supplementary material. Within one FIA, salinity and Ca/(Na+Ca) molar ratio are almost constant, but trace metal concentrations vary.

5. Discussion

The crush-leach and LA-ICPMS results show a large diversity in fluid composition of the post-

Cretaceous veins, but surprisingly, no clear correlation between fluid composition and vein mineralogy exists. Figure 7 shows that both methods render consistent results e. g. in terms of Cl/Br ratios: the bulk Cl/Br ratios derived from crush leach analyses are perfectly within the range of LA-ICPMS data and are interpreted to summarize over small-scale variabilities, thus really providing an average composition of the mixed fluid. In the following sections, we discuss the possible relationship of the observed fluid mixtures in fluid inclusions to the sedimentary aquifers and their formation fluids introduced above. This is done to constrain the fluid sources and the source aquifers involved in vein formation.

5.1 Effects of formation temperature and salinity on vein mineralogy

While there is no recognizable correlation between formation temperature and vein mineralogy (Fig. 8), the fluid salinity appears to have a certain impact on vein mineralogy, particularly on the presence of ore minerals. Metals like Pb and Zn are typically transported as Cl-complexes under the conditions of formation of the Schwarzwald mining district (Yardley, 2005; Burisch et al. Leach and references therein), and hence, it is no surprise that veins with medium to high salinity (chlorinity) fluid inclusions often show significant amounts of galena, sphalerite and fahlore. The large variation in homogenization temperature of the individual fluid signatures is probably an effect of inhomogeneous penetration depth of the sedimentary fluid into the basement.

5.2 Processes of vein formation: Multi-component mixing and the importance of tectonic juxtaposition of diverse lithologies for the aquifers properties

As shown above, the vein mineralogy shows no strict correlation to the fluid inclusion chemistry. Still, fluid mixing has to be the dominant formation process, as fluid cooling alone is not a sufficiently efficient mechanism in this setting to cause the observed amount of hydrothermal mineralization, the diversity of vein mineralogy, the mineral textures and fluid chemistry (Fußwinkel et al., 2013; Bons et al., 2014; Walter et al., 2015, 2016, Jura).

In contrast to the spatially unsystematic variability of fluid chemistry in post-Cretaceous veins, fluid compositions in Jurassic-Cretaceous veins show clear chemical systematics, depending on their depth

535 of formation and the type of sedimentary overburden (Walter et al., 2016, Jura). This difference is
536 consistently described as a two-component mixing in a tectonically undisturbed environment, which
537 prevailed during the Jurassic and Cretaceous. Juxtaposition of various types of aquifers (at least three,
538 possibly more) due to tectonic processes in the Cenozoic requires the consideration of more than two
539 fluid components involved in mixing (see e. g. Fig 6C, 8F in Walter et al., 2015, in press brine). Our
540 multi-aquifer mixing model is capable of explaining the unsystematic variation in major, minor and
541 trace element composition, salinity, formation temperatures and isotopic variations (not further
542 discussed here; see Walter et al., 2015).
543 Fluid ascent may have been triggered by topographic fluid flow or by tectonic opening of confined
544 aquifers in the tectonically disturbed environment of the rift shoulders (Agemar et al., 2013). During
545 earthquakes, pathways opened or were reactivated and the confined aquifers released their fluids. Fluid
546 mixing of two or more aquifers occurred, minerals precipitated in the pathways (partially sealing
547 them) and hence, the ancient pathways are now the mineralized veins.
548
549 ***5.3 Aquifers involved in vein formation***
550
551 *5.3.1 Fluid signature A*
552 The low salinity fluids of group A are dominantly H_2O fluids with minor Na-Ca-Cl-HCO_3
553 components. They are interpreted as weakly mineralized meteoric fluids (see Fig. 9, reservoir 1).
554 Some of the samples containing type A fluid inclusions have K-Ca-Na-Cl-HCO_3 and Na-K-Ca-Cl-
555 HCO_3 signatures in the crush leach analyses, which have to the best of our knowledge no modern
556 analogy. Without exception, this fluid type occurs in veins (Michael im Weiler, Lierbach, Hexenkessel
557 2 and Lattfelsen) very close to Permian rhyolites. We suggest that the extensive alteration of K-
558 feldspar under relatively acidic conditions to gibbsite, pyrophyllite and/or kaolinite, which can be
559 observed in these rhyolites, results in substantial K release to the fluid at the time of alteration which is
560 interpreted also as the time of mineralisation (Brockamp et al., 2003, 2011).
561
562 *5.3.2 Fluid signature B and C Na-Ca-Cl*

563 The medium to highly saline Na-Ca-Cl and Ca-Na-Cl fluid types B and C mainly occur in quartz-
564 barite veins with a Pb-Zn mineralization like Badenweiler, Galgenhalde Nord, Herrenwald or Freiamt
565 (see Table 2). A possible source of these fluids is a mixture of formation waters from the Muschelkalk
566 halite facies (Fig.9, reservoir 2) and highly mineralized basement fluids (Fig. 9, reservoir 3). This
567 assumption is supported by variable Cl/Br mass ratios and high metal contents. Differences in the
568 Na/Ca ratios are probably related to variable mixing ratios (see Walter et al., Jura). The variation from
569 medium to high salinity can be explained by mixing fluid type A as a third component to types B and
570 C, which dilutes the other two components. Increasing amounts of fluid A result in a salinity decrease
571 of the final fluid.
572
573 *5.3.3 Fluid signature D: Ca-(Na)-HCO_3 and Ca-(Na)-SO_4*
574 Fluid signature D shows the largest variation of salinities from 1-26 wt.% ($NaCl+CaCl_2$). Since these
575 fluids have bicarbonate and sulfate as dominant anions, the calculated salinity is imprecise, as these
576 components cannot be accounted for in the salinity calculations (Steele-MacInnes et al., 2011).
577 However, this wide range of salinities reflects a mixing continuum of two or more endmembers. Based
578 on modern fluid stratigraphy in the Schwarzwald basement, one fluid type could be a low salinity,
579 surface- or subsurface-derived fluid residing for some time in the basement, which results in a weak
580 basement brine-like signature. The Ca dominance may be a product of plagioclase alteration which has
581 been invoked as explanation for the low chlorinity fluids with high Ca and bicarbonate content
582 (Bucher & Stober, 2010). The high salinity endmember, bicarbonate-dominated fluids are probably
583 released from a limestone aquifer like the Muschelkalk (Fig. 9, reservoir 2) or the Jurassic
584 Hauptrogenstein (Fig. 9, reservoir 4) where such fluids are present today (He et al., 1999).
585 Fluids with a Ca-(Na)-SO_4 signature occur in sample BW144 from Badenweiler. In this sample,
586 textures clearly indicate the former presence of gypsum or anhydrite (Fig. 10) today replaced by
587 quartz. The investigated fluid inclusions are exclusively hosted in young quartz replacing the sulfate.
588 The same fluid signature could be observed at Schlossberg West and at Calmbach; in both veins,
589 barite is completely pseudomorphed by quartz and sulfides are lacking. Thus, this fluid signature is
590 interpreted as a local phenomenon at or around dissolving sulfates, providing no general source

591 information.

592

593 *5.3.4 Fluid signature E and F: Na-K-Ca-Cl-(SO_4)-(HCO_3), Ca-Na-K-Cl-SO_4-(HCO_3) and Na-Ca-K-*
594 *Cl-SO_4-(HCO_3)*

595 The chemical variability of fluid type E and F makes it difficult to exactly dedicate these fluids to a
596 specific source. These fluid signatures are not sufficiently unique and resemble fluids present in
597 almost all modern sedimentary aquifers (Göb et al., 2013 and references therein). Veins of different
598 mineralogy comprise these signatures, including Fortuna, Pfingstsegen, Galgenhalde, Wurmbach,
599 Schauinsland, Drey, Kammendobel, Erich im Suggental, Katzensteig or Neubulach. Except for
600 Neubulach, all of these veins are situated in the crystalline basement. Low Cl/Br ratios indicate no
601 significant influence of the middle Triassic evaporites. As sulfate occurs in higher concentrations than
602 bicarbonate (if this is present at all), it is most likely that these fluids are derived from intermediate
603 depths of the crystalline basement (Fig. 9, reservoir 5), Triassic Buntsandstein (reservoir 6) and/or the
604 lower or upper Muschelkalk (Fig 9, reservoir 7). High Na/Ca, low Cl/Br ratios and the variation of low
605 to high salinity suggest a strong basement component in the mixed fluid of some of the veins.
606 The source of the Ca-Na-K-Cl-SO_4-(HCO_3) fluid signature is difficult to discern due to the ubiquitous
607 occurrence of chloride, sulfate and bicarbonate in all modern aquifers. Different types of gangue with
608 or without Pb-Zn-(Cu) ores show this fluid signature (e.g. Galgenhalde Nord, Etzenbach, Haidflüh,
609 Lütschenbach, Silbereck, Merzhausen, Neubulach and Schauinsland). Presumably, these fluid
610 signatures are related to different sedimentary formation fluids that were mixed with highly
611 mineralized basement brines.

612

613 *5.3.5 Conclusions on fluid sources*

614 To summarize the chapters above, it seems plausible that most of the fluorite and the majority of the
615 quartz samples have been precipitated from a chloride-rich brine mixed with a bicarbonate-dominated
616 low salinity fluid reservoir (Fig. 11A). A second group of quartz veins precipitated from a Cl-SO_4-
617 HCO_3 fluid. Furthermore, Fig. 11B shows that most quartz and barite precipitated from a Ca-Na fluid
618 with variable Ca/Na ratios. The combination of Figs. 11A, B and F implies that for most veins, the Cl-

619 rich brine endmember is a basement brine, just those with high Cl/Br and high Ca/Na ratios probably
620 involved the halite facies aquifer of the Middle Triassic Muschelkalk.
621
622 *5.3.6 Metal provenance*
623 The post-Cretaceous veins show a large variability in gangue and ore minerals. Furthermore, some
624 veins show a major ore content while other veins are barren. The fluids responsible for formation of
625 highly mineralized and barren veins are chemically similar, so the presence or lack of metal
626 enrichment is unlikely to have been solubility controlled, but rather points towards fluid source rocks
627 and aquifers having exerted a first order control on the fluids' metal budgets. Based on the work of
628 Walter et al. (Jura) and Burisch et al. (Rb/Cs, Leaching), the crystalline basement is the dominant
629 source for Pb and Zn in geologically undisturbed environments (e. g., SW Germany during the
630 Jurassic and Cretaceous). In contrast, the redbeds (Buntsandstein and Rotliegend) are considered as
631 the dominant source for Cu, Co and Bi in the fluid (e.g. Koziy et al., 2009; Hendrickson et al., 2015
632 and references therein). It seems obvious that these metal sources are still important for post-
633 Cretaceous vein formation. However, the juxtaposition of the different aquifers during breakup of the
634 Upper Rhinegraben enabled the participation of more fluid sources.
635 The crush leach data of figure 11C show that almost all samples lie on a mixing line between Cu and
636 Zn. Walter et al. (Jura) explained the same systematic feature in Jurassic veins with depth-depending
637 variations in the fluid mixing ratios. However, these variations with depth cannot be recognized in
638 post-Cretaceous veins. At many localities at the Rhinegraben boundary fault, Buntsandstein units lie
639 next to crystalline basement, and mixing between these two aquifers was easily possible. Hence, also
640 in post-Cretaceous times, the sources of Zn and Cu were identical to the Cu and Zn sources for
641 Jurassic-Cretaceous veins (Walter et al., Jura).
642 Single fluid inclusions show that highest Pb+Zn contents correlate with high salinities and low Cl/Br
643 mass ratios (Fig. 12B)(Fusswinkel et al., 2013). This can be seen as a further argument for a basement
644 brine supplying Pb and Zn.
645 As, W and Sb also show correlations with low Cl/Br ratios (Fig. 12C, D and E). As, W and most likely
646 Sb are typically derived from feldspars in the crystalline basement (Burisch et al., Leaching) and

hence, their source fluid is certainly the basement brine. Furthermore, the Tirolergund vein shows unusually high Tl contents up to 2380ppm, which may be derived from the Permian rhyolite cross-cut by this vein.

An isolated group of calcite and dolomite hosted fluid inclusions (Fig. 11C) shows higher Ni concentrations in contrast to the other fluid inclusions, those are enriched in Zn and Cu in their fluid signatures. These fluids appear as reasonable source fluids for the chalcopyrite-gersdorffite-siderite-barite veins like Hohe Tanne, Riggenbach or Felsenkeller.

Interestingly, figure 11E shows that the fluids trapped in barites of different vein types are enriched in U in contrast to quartz and fluorite gangue generations from the identical veins. Possibly, this observation is related to the oxidation state of the fluid and implies, that the barite-forming fluids were more oxidized (and therefore, enriched in fluid-mobile U^{6+}) than the quartz- and fluorite-forming fluids.

5.3.7 Ore fluid and metal precipitation

The LA-ICPMS data of fluid inclusions show a Gaussian distribution for Pb+Zn with a statistical maximum between 100 and 1000ppb for the Karl August, Riggenbach and Tirolergrund veins. All investigated fluid inclusions are hosted in young quartz crystals, which are not in equilibrium with sphalerite (sphalerite is older and probably belongs to a separate fluid event). The Gaussian mean values indicate that these values are average values of a mixed ore fluid from which sphalerite could potentially, but has not yet precipitated, as a consequence of relative or absolute low sulfide activities.

The Badenweiler and the Böschlisgrund veins, in contrast, show much lower Pb+Zn contents which can be explained by prior precipitation of sulfides: in both veins, the analysed fluid inclusions are hosted in galena-, sphalerite- and chalcopyrite-rich quartz. The same interpretation is suggested for the Ni+Cu, W and for the Sb systematics. As none of these veins contain any Sb- or W-bearing phases, it is plausible that these fluid inclusions show the unchanged, average Sb and W content of the mixed ore fluid, derived from the diluted basement brine.

5.4 Complex mixing processes recorded by various growth zones in a single quartz crystal

675 Some veins show heterogeneous FIAs, i. e. variations of salinity, Ca/Na and homogenization
676 temperatures between adjacent FIAs (e. g., Riggenbach, Fig. 13). Specifically, some of the Münstertal
677 and Sulzburg veins (Katzental, Himmelsehre, Krebsgrund, Karl August; see Fig. 5) show complicated
678 sequences of different fluids on different growth zones in one quartz crystal. Hence, the Karl August
679 data will be discussed in detail (Fig. 14) as a representative case. In this sample, the fluid composition
680 in terms of salinity, sulfate and CO_2 content varies strongly from one growth zone to another. The
681 variability of the fluid inclusion chemistry on a small scale (which also means during a short time
682 period) requires a multi-component fluid mixing, since these variations cannot simply originate from
683 mixing of only two fluids with variable mixing ratios. General aspects of these complex mixtures are:
684 Cl/Br ratios above 150, high salinities and Ca/(Na+Ca) molar ratios of 0.3-0.5 record the involvement
685 of a saline Muschelkalk fluid, while low Cl/Br, high salinities and Ca/(Na+Ca) of 0.1 to 0.3 are typical
686 of deep seated basement brines. Sulfate and CO_2 have, hence, to be derived from at least a third fluid
687 component. These complex multi-component mixtures only occur in close proximity (within few
688 kilometres) to the Rhinegraben boundary fault and it is most plausible, that short-lived tectonic
689 movements established and destroyed various aquifer systems or fluid migration paths, which can be
690 recorded on single growth zones of discontinuously growing quartz.
691
692 *5.5 Complex fluid behaviour recorded by FIAs on one growth zone of a quartz crystal*
693 The physical and chemical details of the complex mixing processes invoked above can be studied in
694 greater detail by investigating various fluid inclusions on one specific growth zone. A primary growth
695 zone in e.g. a euhedral quartz crystal was an exposed surface during its formation and different fluid
696 inclusions on one growth zone should consequently record the same fluid event (Van den Kerkhof, &
697 Hein 2001, and references therein).
698 Figure 14 illustrates LA-ICPMS results for the Karl-August mine near Kropbach. The heterogeneity of
699 these fluid inclusions in terms of their minor and trace element concentrations within one event of
700 crystal growth can be clearly seen (also taking the analytical error into account). Fusswinkel et al.
701 (2013) and Bons et al (2014) showed that fluid mixing is a geologically fast process and occurs on the
702 order of minutes to hours. These short time intervals result in trapping of heterogeneous fluid batches

or schlieren on the µm scale (Fig. 15). During trapping, the fluids are not completely homogenized and therefore show variable mixing ratios on small scales. In the electronic supplement ES 2 we present a calculation of the fractions involved in ternary mixing on one growth zone. The FIAs in the Karl-August mine near Kropbach record ternary mixing ratios (reservoirs 2/3/1) between (81/19/0), (1/5/94) and (2/75/23) on one primary growth zone. These observations imply that the crystallisation of the host quartz is more rapid than the diffusional or turbulent flow equilibration of the fluid components.

The calculation of the time required to homogenize the mixed fluid batches assuming only diffusion as the driving force, consequently yields a minimum growth rate for the host mineral. For a rough assessment of the growth rates of one quartz growth zone, two contiguous fluid inclusions (Ø = ~20 µm) of the FIA pQtz3-5 with a distance of 50µm were selected. One inclusion has a sulfate content of 4000ppm, a Cl content of 81.600ppm, a Cl/Br mass ratio of 100, a salinity of 24wt% and shows a homogenization temperature of 191°C, while the other inclusion has a sulfate content of 15.400ppm, a Cl content of 30.300ppm, a Cl/Br mass ratio of 300, the identical salinity and a homogenization temperature of 131°C.

After fracture formation, fluids from different aquifers enter the fracture and do not completely homogenize for a specific (short) time interval. Two different types of equilibria are considered: thermal equilibration with $DT \approx 10^{-6}$ m^2/s and chemical equilibration $Dm \approx 10^{-9}$ m^2/s. Using these diffusion coefficients in the equation $<X>^2 = D\Delta T$ yields durations of ~2.5s for chemical equilibration and a time for 0.005s for thermal equilibration of the 50 µm distance. Compared to experimental growth rates (e.g. 2 µm/h Okamoto & Sekine, 2011, and references therein), the time intervals based on thermal and chemical diffusion are much smaller. However, the experiments of Okamoto & Sekine (2011) do not consider mixing processes and far-from-equilibrium conditions, which possibly yield much higher growth rates. Alternatively, the observed temperature difference in adjacent fluid inclusions would require a time gap between their trapping or post-entrapment modifications, which both do not seem very plausible considering the textural observations.

5.6 The Rb/Cs ratio and its bearing on the fluid pathways

731 The Rb/Cs ratio is a suitable tracer for fluid pathways because Rb and Cs can be adsorbed to and
732 incorporated into clay minerals that are present along such pathways: Burisch et al. (Rb/Cs, and
733 references therein) and Göb et al. (2013) showed that a fluid Rb/Cs ratio <2 is typical of fluids which
734 interacted with unaltered crystalline rocks, while Rb/Cs ratios of ~2 represent equilibrium conditions
735 during alteration of primary minerals to clay minerals. Rb/Cs ratios >5 indicate water-rock interaction
736 with pre-existing clay minerals (no alteration of primary phases). Most of the measured Rb/Cs ratios
737 (Fig. 16) are below 2 which indicates that new pathways were opened during post-Cretaceous fluid
738 activity, rather than reactivating older fractures. Higher Rb/Cs ratios are present in young FIAs in the
739 Karl August vein. These young growth zones obviously record a reactivation and fluid migration
740 along previous established pathways, while the older quartz generations and growth zones in the same
741 vein show low Rb/Cs ratios.
742
743 *5.7 Temporal and chemical evolution of the aquifers*
744 In contrast to the tectonically undisturbed aquifers during the Jurassic and Cretaceous, post-Cretaceous
745 rocks and their aquifers influence each other by fluid migration from one to another aquifer. For
746 example, Muschelkalk fluids are modified by migrating into the Buntsandstein aquifer, which is
747 indicated by elevated Ca/(Na+Ca) mole ratios and high Cl/Br mass ratios in todays Buntsandstein
748 aquifer fluids (dissolution of halite). Mixing or large scale fluid migration prior to mineralization
749 makes it impossible to distinguish between defined reservoir signatures in the post-Cretaceous veins
750 with the following two exceptions:
751 - Fluid signatures with high Cl/Br and high Ca/(Na+Ca) molar ratios can be related to fluids
752 dissolving halides of the Muschelkalk formation (which are, most plausibly, middle
753 Muschelkalk aquifer fluids).
754 - High salinity and low Cl/Br mass ratios with high metal contents are typical of basement
755 brines.
756 Unfortunately, a more detailed distinction of reservoir signatures from Buntsandstein, Keuper, Jurassic
757 or Tertiary sediments is not possible based on our analyses of mixed fluids in fluid inclusions of the
758 post-Cretaceous veins. However, it is still possible to model different mixing processes and compare

759 them to field observations.

760

761 *5.8 Sources and aquifers: prediction and modelling*

762 *5.8.1 Model setup*

763 To evaluate the influence of the different possible sources on the formation of the mineral veins,
764 existing fluid data (representative of the most important aquifers) of Göb et al. (2013), Pauwels et al.
765 (1993), (Pearson et al. 1989) and Stober and Bucher (2004) were used and combined as input
766 parameters for mixing calculations (table 5). These calculations were designed to model the analyzed,
767 mixed fluids in the fluid inclusions by mixing todays well-defined fluid reservoir signatures, using
768 mixing ratios from 0.1-0.9. For the resulting fluid compositions, saturation indices (SI) for fluorite,
769 barite, quartz, chalcedony, gypsum, anhydrite, sphalerite and galena were calculated. Hydro-chemical
770 calculations were performed with GEOCHEMIST WORKBENCH Version 10.0.2.

771

772 *5.8.2 Saturation indices and precipitation of gangue minerals*

773 Fluid mixing calculations of the basement brine and fluids derived from the Buntsandstein (Fig. 17,
774 table 5) show that it is possible to yield fluids oversaturated with respect to fluorite over a wide range
775 of mixing ratios. Post-Cretaceous fluorite veins are all situated in areas that were once covered by the
776 Buntsandstein formation. Hence, it is likely that fluid mixing of Buntsandstein and crystalline
777 basement brine leads to fluorite precipitation.

778 Furthermore, the calculated saturation indices for different source mixtures indicate that barite can be
779 precipitated from basically all combinations of modern aquifer compositions over a wide range of
780 mixing ratios (Fig. 17, table 5). This is in agreement with field observations: barite-dominated veins
781 are the most common in the post-Cretaceous vein group (in contrast to the Jurassic veins). The
782 occurrence of barite veins is independent of the host rocks, which is also in nice agreement with this
783 model.

784 Many fluids are saturated with respect to gypsum and/or anhydrite (Fig. 17, table 5), but gypsum
785 and/or anhydrite occur rarely. However, pseudomorphic replacement textures of quartz after anhydrite
786 or gypsum can be recognized at some localities (e. g., Badenweiler, Laitschenbach, Laisacker,

787 Lampisweg). Presumably, most of the precipitated gypsum/anhydrite phases were dissolved by later
788 fluid batches or during cooling which explains the discrepancy of the predicted anhydrite/gypsum
789 mineralization (based on this model) and their apparent absence in many veins.
790 Fluid mixtures of basement brine and Buntsandstein brine are close to saturation with respect to quartz
791 and chalcedony (Fig. 17, table 5) which explains the observation that all veins hosted by
792 Buntsandstein in the northern Schwarzwald are quartz- or chalcedony-dominated. Also the "Quarzriff"
793 near Badenweiler occurs, where Buntsandstein is in contact with the basement directly along the
794 Rhinegraben boundary fault.
795
796 *5.8.3 Saturation indices and formation of metal ore minerals*
797 Textures of the mineralized barite veins often show nests of galena that are co-genetic with barite or
798 galena–barite alternations. Based on our calculations, it is unlikely that barite and galena/sphalerite
799 precipitated synchronically during simple mixing, since the log saturation indices for galena and
800 sphalerite are between -120 and -50. This undersaturation may be a consequence of high
801 sulfate/sulfide ratios close to 1.
802 To sum these arguments up: (A) sulfides are typically formed during fluid mixing. (B) The metal
803 source is a deep-seated basement brine (Fusswinkel et al., 2013; Walter et al., brine, Jura). (C) The
804 solubility of sphalerite and galena is very low in the presence of sulfide in fluids. (D) Basement brines
805 are not saturated with respect to galena and sphalerite, due to the low absolute sulphur concentrations
806 in these fluids.
807 Based on these arguments it is unlikely that the metals and the sulfide ions are transported in the same
808 fluid batch. Accordingly, the sulfide (and not dominantly sulfate) is transported in the sedimentary
809 fluid component, galena and sphalerite precipitated upon mixing, or reduction due to methane influx e.
810 g. from shale gas or gas-bearing fluids caused sulfide precipitation (Werner et al., 2002; Markl et al.,
811 submitted).
812 The model shows that barite is produced during mixing of two oxidized fluids, which is in agreement
813 with the fluids recognized in the modern hydrology. An influx of methane (or CH_4- and/or H_2S-
814 bearing fluids (Sverjensky, 1984, 1987; Carpenter et al., 1974)) during mixing and concomitant

oxidation of CH_4 to CO_2 may strongly reduce the fluid, resulting in a substantial decrease of the sulfate/sulfide ratio and subsequent sulfide precipitation. Oilfield brines are strongly reduced and enriched in H_2S and CH_4 and such fluids are locally present in the Paleogene Pechelbronn formation (Otto & Tòth, 1988) and widespread in the Lower Jurassic Lias ε shales (Geyer & Gwinner, 2011). Simple mass balance calculations imply that only very small amounts of methane have to be added to one liter of a fluid contianing 2 ppm Pb or Zn to precipitate galena or sphalerite: ~0.01 mmol and ~0.03 mmol, respectively.

5.9 The relation of post-Cretaceous mineralization fluids to modern thermal wells

The following section focuses on the comparison of the post-Cretaceous fluids/aquifers with modern fluids/aquifers. Modern thermal wells like Baden-Baden show temperatures up to 66°C (Göb et al., 2013) and low TDS up to 4.2 g/L. In contrast to the paleo-fluid systems, fluid mixing is not important in modern wells (Bucher and Stober, 2010). The fluids are released by open fractures and show no seasonal variations in temperature or chemistry. The hydrothermal calcite precipitated from such wells produces sinters with growth-rates of several cm/year (e. g., in Baden-Baden). An artesian upwelling of saline (TDS = 0.2 g/L) thermal waters can be recognized at Ohlsbach, where a saline NaCl-rich brine from depth (>3 km with a TDS 16 g/L) ascends into a gravel aquifer and becomes strongly diluted (Stober et al., 1999).

In contrast, the hydrothermal veins discussed in this work show strong evidence of fluid mixing. Our rough calculation of growth rates suggests ephemeral events of fracture opening, fluid release into the fracture from different crustal levels and aquifers, fluid mixing and vein mineralization that triggers crystal growth and concomittant fracture sealing. S-Isotope data by Schwinn et al. (2006) indicate an equilibration of the metal-rich high-salinity basement brine at 350°C which can be compared to a depth of >5 km. This basement component (which would be necessary for modern ore mineralization to form) is not seen in modern thermal wells. Based on this argumentation it appears that there were (and are?) two different hydrothermal systems present in the Schwarzwald: (i) a relatively shallow system persistent over a long time in open fractures producing constant hydrothermal fluid without a basement brine component and (ii) various short–lived hydrothermal systems in quickly sealed

fractures, involving deep basement brines and producing hydrothermal mineralizations by fluid mixing. The latter system does not appear to be active today, at least not close to the surface, despite of the ongoing seismic activity in SW Germany.

5.10 Analogy of post-Cretaceous veins in the Schwarzwald and the Vosges

There are many similar types of mineralizations east and west of the Rhinegraben, in the Schwarzwald and Vosges mountains (Agard et al., 1975; Hohl 2007). If the rift was perfectly symmetrical and the lithologies east and west of it were identical, one would expect identical fluid types and mineralizations. However, there are differences. In order to show such differences, the mineralization of Hausbaden/Badenweiler (Schwarzwald) and Schlezbourg-Donnerloch/Steinbach (Vosges) were investigated in detail as an example (Gutierrez Lanz, 1985, and references therein). Both veins occur on the respective Rhinegraben boundary faults, both are therefore of post-Cretaceous age, both have macroscopically and microscopically very similar mineral textures, show a dominant massive white quartz phase with minor fluorite and contain galena and some chalcopyrite as main ores. Both veins show multiple episodes of brecciation. Figure 18 A-D illustrates the difference of microthermometric results between Vosges (Steinbach vein) and Schwarzwald (whole database). The fluid inclusions from Steinbach show a distinct range in Fig. 18 and have much higher homogenization temperatures than those of any Schwarzwald vein in the same (low to medium) salinity range.

These significantly higher temperatures in Steinbach cannot be simply explained by a higher geothermal gradient, as Agemar et al. (2013) did not observe significant variations in underground temperature at 2500m b.s.l. (measured in geothermal drillings in the Rhinegraben). However, the Upper Rhinegraben has an asymmetric tilt. The basement-cover uniformity is significantly deeper on the French side of the graben (Beccaletto et al., 2010). Still, today's 150°C isotherm is situated deep below the unconformity and to reach the measured temperatures of 230-250°C, the Steinbach fluid has to be released from a depth deeper than 5km from a crystalline basement reservoir. This reservoir assumption is supported by low Cl/Br ratios and elevated metal concentrations at Steinbach, because the shallower reservoirs show Cl/Br mass ratios of 200 and higher (Pauwels et al., 1993). Furthermore, Pauwels et al. (1993) and Aquilina et al. (1997) calculated reservoir temperatures at 4.5-5km in

Soultz-sous-Forêt (French side of the Rhinegraben, close to the Vosges mountains) in the crystalline basement of 220-260°C, which is in good agreement with the measured temperatures in Steinbach. In summary, the asymmety of the Rhinegraben appears to release hotter fluids in the west, which, however, produce very similar types of mineralizations.

6. Summary and conclusions

The diverse mineralogy of the post-Cretaceous hydrothermal veins in the vicinity of the Rhinegraben in central Europe is the consequence of multi-component fluid mixing processes (Fig. 19) related to the tectonic activity of the post-Cretaceous Rhinegraben rift. These short-lived (in the range of seconds to hours) mixing processes involve numerous different kinds of aquifers including crystalline basement and various sedimentary cover rocks. The interaction of different aquifers is observed on the scales of a district, a location and a single crystal. The most important aquifers involved in mixing are the crystalline basement and the Muschelkalk aquifers. Fluids from the Buntsandstein, Keuper and the various Jurassic aquifers are of minor importance, but may (if involved) locally govern the vein mineralogy. Temperature and salinity variations cannot explain the observed differences in vein mineralogy, although salinity variations are important for metal transport and therefore for the amount of base metal precipitation during fluid mixing.

The chemical composition of the various basement and sedimentary aquifers evolves and changes with time (Walter et al., 2016), which increases the complexity of fingerprinting the fluid sources. Our results imply that the modern thermal wells are fed by a stable, long-living fluid system without much fluid mixing. This system is discontinuously augmented by short-lived fluid mixing events involving a deep-seated brine (which is not normally seen today, with the one exception of the Ohlsbach plume (Stober et al., 1999)) and hydrothermal vein formation, probably caused by tectonics.

A comparative study on a hydrothermal vein from the western, French side of the Rhinegraben rift shows much higher temperatures which are assumed to be an effect of the asymmetric tilt of the Rhinegraben: on the latitude of the southern Schwarzwald the rift is much deeper on the French side (Vosges). Hence it seems plausible that fluid migration by topographic fluid flow reaches higher

depths on the French than on the German side of the rift.

Mixing calculations show that all combinations of modern basement and sediment aquifer fluids result in fluids oversaturated with respect to barite. This is in good agreement with the observation that most of the investigated veins contain abundant barite. Furthermore, all calculated mixed fluids are strongly undersaturated with respect to sulfides. We suggest that the hydrothermal sulfides precipitated during short-lived injections of methane or hydrocarbon-bearing fluids into the hydrothermal fluid system.

7. Acknowledgements

We would like to thank to S. Schafflick for sample preparation in Tübingen. We are grateful to Udo Neumann and T. Wenzel who helped with many hints and discussions. Furthermore, we gratefully acknowledge the help of G. Stoschek and B. Steinhilber with crush leach analyses and technical support. This study was supported by the German Research Foundation (DFG), grant MA2135/20-1.

9. References

Altherr, R., Holl, A., Hegner, E., Langer, C., and Kreuzer, H., 2000, High-potassium, calc-alkaline I-type plutonism in the European Variscides: northern Vosges (France) and northern Schwarzwald (Germany). Lithos, v. 50, p. 51-73.

Agard, J., Fluck, P., Weil, R., Wimmenauer, W., 1975. Geologie des gites minéraux des Vosges et des regions limitrophes. *Mém BRGM*, *87*, 1-189.

Agemar, T., Brunken, J., Jodocy, M., Schellschmidt, R., Schulz, R and Stober, I., 2013. Untergrundtemperaturen in Baden-Württemberg. Zeitschrift der Deutschen Gesellschaft für Geowissenschaften, 164, 49–62.

Aquilina, L., Boulvais, P., and Mossmann, J.-R., 2011, Fluid migration at the basement/sediment interface along the margin of the Southeast basin (France): implications for Pb–Zn ore formation: Mineralium Deposita, v. 46, no. 8, p. 959-979.

Aquilina, L., Pauwels, H., Genter, A., and Fouillac, C., 1997a, Water-rock interaction processes in the Triassic sandstone and the granitic basement of the Rhine Graben: Geochemical investigation of a geothermal reservoir: Geochimica et cosmochimica acta, v. 61, no. 20, p. 4281-4295.

Aquilina, L., Pauwels, H., Genter, A., and Fouillac, C., 1997b, Water-rock interaction processes in the Triassic sandstone and the granitic basement of the Rhinegraben: Geochemical investigation of a geothermal reservoir.: Geochimica et Cosmochimica Acta, v. 61, p. 4281-4295.

Baatartsogt, B., Wagner, T., Taubald, H., Mierdel, K. and Markl, G., 2006. Hydrogen isotope

933 determination of fluid inclusion water from hydrothermal fluorite: The results depend
934 on the extraction technique. Chemical Geology, 1-21.
935 Baatartsogt, B., Schwinn, G., Wagner, T., Taubald, H., Beitter, T., and Markl, G., 2007,
936 Contrasting paleofluid systems in the continental basement: a fluid inclusion and
937 stable isotope study of hydrothermal vein mineralization, Schwarzwald district,
938 Germany.: Geofluids, v. 7, p. 123-147.
939 Bakker, R.J. 1997, Clathrates: Computer programs to calculate fluid inclusion V-X properties
940 using clathrate melting temperatures. Computers & Geosciences, v. 23, 1-18.
941 Banks, D. A., Boyce, A. J., and Samson, I. M. 2002. Constraints on the origins of fluids
942 forming Irish Zn-Pb-Ba deposits: Evidence from the composition of fluid inclusions.
943 *Economic Geology*, *97*(3), 471-480.
944 Bau, M., Romer, R. L., Lüders, V., and Dulski, P., 2003, Tracing element sources of
945 hydrothermal mineral deposits: REE and Y distribution and Sr-Nd-Pb isotopes in
946 fluorite from MVT deposits in the Pennine Orefield, England: Mineralium Deposita,
947 v. 38, no. 8, p. 992-1008.
948 Beccaletto, L., Capar, L., Cruz-Mermy, D., Rupf, I., Nitsch E., Oliviero, G., Elsass, P., Perrin,
949 A., and Stephane, M., 2010, The GeORG project – Geological Potential of the Upper
950 Rhine Graben - Situation, goals and first scientific results. – Abstr., 23ème Réunion
951 des Sciences de la Terre (RST2010), Bordeaux
952 Bjørlykke, A., Ihlen, P. M., Olerud, S., 1990. Metallogeny and lead isotope data from the
953 Oslo Paleorift. *Tectonophysics*, *178*(1), 109-126.
954 Bliedtner, M., and Martin, M., 1986. *Erz- und Minerallagerstätten des Mittleren*
955 *Schwarzwaldes: eine bergbaugeschichtliche und lagerstättenkundliche Darstellung*.
956 Geologisches Landesamt Baden-WürttembergBoiron, M. C., Cathelineau, M., and
957 Richard, A., 2010, Fluid flows and metal deposition near basement/cover
958 unconformity: lessons and analogies from Pb-Zn-F-Ba systems for the understanding
959 of Proterozoic U deposits.: Geofluids, v. 10, p. 270-292.
960 Bons, P. D., Fusswinkel, T., Gomez-Rivas, E., Markl, G., Wagner, T., and Walter, B.F. ,
961 2014, Fluid mixing from below in unconformity-related hydrothermal ore deposits:
962 Geology, p. G35708. 35701.
963 Borchert, H., 1959, Ozeane Salzlagerstätten: Grundzüge der Entstehung und Metamorphose
964 ozeaner Salzlagerstätten sowie des Gebirgsverhaltens von Salzgesteinsmassen, Gebr.
965 Borntraeger.
966 Brockamp, O., Clauer, N., Zuther, M., 2003. Authigenic sericite record of a fossil geothermal
967 system: the Offenburg trough, central Black Forest, Germany. International Journal of
968 Earth Sciences, 92, 843–51.
969 Brockamp, O., Schlegel, A., Clauer, N., 2011. Mesozoic hydrothermal impact on Rotliegende
970 and Bunter immature sandstones of the High Rhine trough and its adjacent eastern
971 area (southern Black Forest, Germany). Sedimentary Geology, 234, 76–88.
972 Bucher, K., and Stober, I., 2000. The composition of groundwater in the continental
973 crystalline crust. In *Hydrogeology of crystalline rocks* (pp. 141-175). Springer
974 Netherlands.
975 Bucher, K., and Stober, I., 2002. Water-rock reaction experiments with Black Forest gneiss
976 and granite. In *Water-Rock Interaction* (pp. 61-95). Springer Netherlands.
977 Bucher, K., and Stober, I., 2010, Fluids in the upper continental crust: Geofluids, v. 10, no. 1-
978 2, p. 241-253.
979 Bucher, K., Zhu, Y., and Stober, I., 2009a. Groundwater in fractured crystalline rocks, the
980 Clara mine, Black Forest (Germany). *International Journal of Earth Sciences*, *98*(7),
981 1727-1739.
982 Bucher, K., Zhu, Y., and Stober, I., 2009b. Groundwater in fractured crystalline rocks, the
983 Clara mine, Black Forest (Germany). *International Journal of Earth Sciences*, *98*(7),

1727-1739.
Burisch, M., Marks, M., Novak, M. and Markl, G., submitted to Chemical Geology. The importance of temperature and cataclastic deformation for halogen (F, Cl, Br) systematics and metal transport capacities of continental basement brines – an experimental approach
Burisch, M., Walter, B.F., Wälle, M., & Markl, G. (submitted to Chemical Geology) Tracing fluid migration pathways in the root zone below unconformity-related hydrothermal veins: insights from trace element systematics of individual fluid inclusions
Carignan, J., Gariépy, C., and Hillaire-Marcel, C., 1997, Hydrothermal fluids during Mesozoic reactivation of the St. Lawrence rift system, Canada: C, O, Sr and Pb isotopic characterization: Chemical Geology, v. 137, no. 1, p. 1-21.
Carpenter, A.B., Trout, M.L. and Pickett, E.E., 1974. Preliminary report on the origin and chemical evolution of lead-and zinc-rich oil field brines in central Mississippi. Economic Geology, 69(8): 1191-1206.
Chaussidon, M., and Jambon, A., 1994. Boron content and isotopic composition of oceanic basalts: geochemical and cosmochemical implications Earth Planet. Sci. Lett., 121, pp. 277–291
Davies, G.R., and Smith, L.B., 2006. Structurally controlled hydrothermal dolomite reservoir facies: An overview: AAPG Bulletin, v. 90, p. 1641–1690,
Deane, J., 1995, The structural evolution of the Kombat deposits, Otavi Mountainland, Namibia: Communications of the Geological Survey of Namibia, v. 10, p. 99-107.
Edmunds, W. M., and Savage, D., 1991, Geochemical characteristics of groundwater in granites and related crystalline rocks: Applied Groundwater Hydrology, a British Perspective (eds DowningRA, WilkinsonWB), p. 199-216.
Emmermann, R., Althaus, E., Giese, P., and Stöckhert, B., 1995, KTB Hauptbohrung results of geoscientific investigation in the KTB field laboratory, final report: 0-9101 m: KTB Report, v. 95-2, p. E.
Frape, S., and Fritz, P., 1987, Geochemical trends for groundwaters from the Canadian Shield: Geological Association of Canada Special Papers, v. 33, p. 19-38.
Frape, S., Fritz, P., and McNutt, R. t., 1984, Water-rock interaction and chemistry of groundwaters from the Canadian Shield: Geochimica et Cosmochimica Acta, v. 48, no. 8, p. 1617-1627.
Frezzotti, M. L., Tecce, F., and Casagli, A., 2012, Raman spectroscopy for fluid inclusion analysis: Journal of Geochemical Exploration, v. 112, p. 1-20.
Fusswinkel, T., Wagner, T., Wälle, M., Wenzel, T., Heinrich, C., and Markl, G., 2013, Fluid mixing forms basement-hosted Pb-Zn deposits: Insight from metal and halogen geochemistry of individual fluid inclusions: Geology, v. 41, p. 679-682.
Garven, G., Appold, M. S., Toptygina, V. I., and Hazlett, T. J., 1999, Hydrogeologic modeling of the genesis of carbonate-hosted lead-zinc ores: Hydrogeology Journal, v. 7, p. 108-126.
Genter, A., Evans, K., Cuenot, N., Fritsch, D., and Sanjuan, B., 2010, Contribution of the exploration of deep crystalline fractured reservoir of Soultz to the knowledge of enhanced geothermal systems (EGS): Comptes Rendus Geoscience, v. 342, no. 7, p. 502-516.
Geyer, O. F., and Gwinner, M. P., 2011, Geologie von Baden -Württemberg. – 5., völlig neu bearbeitete Auflage, Stuttgart, Schweizerbart`sche Verlagsbuchhandlung (Nägele u. Obermiller), 627 p.:
Göb, S., Loges, A., Nolde, N., Bau, M., Jacob, D. E., and Markl, G., 2013, Major and trace element compositions (including REE) of mineral, thermal, mine and surface waters in SW Germany and implications for water-rock interaction: Applied Geochemistry.
Göb, S., Wenzel, T., Bau, M., Jacob, D. E., Loges, A., and Markl, G., 2011, The redistribution

of rare-earth elements in secondary minerals of hydrothermal veins, Schwarzwald, southwestern Germany: The Canadian Mineralogist, v. 49, no. 5, p. 1305-1333.
Guillong, M., Meier, D., Allan, M., Heinrich, C., and Yardley, B., 2008, SILLS: a MATLAB-based program for the reduction of laser ablation ICP-MS data of homogeneous materials and inclusions: Mineralogical Association of Canada Short Course, v. 40, p. 328-333.
Gutierrez Lanz, J.R. (1985): Etude des filons a Pb-Zn-Cu comportant une gangue sulfatee siliciferee de la region de Thann-Watwiller (Vosges sud), Doktorarbeit , Institute National Polytechnique De Lorraine. 321 p.
Hann, H. P. e. A., 2003, The rand granite in the southern Schwarzwald and its geodynamic significance in the variscan belt of SW Germany: International Journal of Earth Sciences, v. 92, p. 821-842.
He, K., Stober, I., and Bucher, K., 1999, Chemical evolution of thermal waters from limestone aquifers of the Southern Upper Rhine Valley: Applied geochemistry, v. 14, no. 2, p. 223-235.
Heinrich, C. A., Pettke, T., Halter, W. E., Aigner-Torres, M., Audétat, A., Günther, D., Hattendorf, B., Bleiner, D., Guillong, M., and Horn, I., 2003, Quantitative multi-element analysis of minerals, fluid and melt inclusions by laser-ablation inductively-coupled-plasma mass-spectrometry.: Geochimica et Cosmochimica Acta, v. 67, p. 3473-3496.
Hendrickson, M. D., Hitzman, M. W., Wood, D., Humphrey, J. D., & Wendlandt, R. F. 2015. Geology of the Fishtie deposit, Central Province, Zambia: iron oxide and copper mineralization in Nguba Group metasedimentary rocks. *Mineralium Deposita*, *50*(6), 717-737.
Hohl, J.-L. (2007): Le grand livre des minéraux d'alsace, La nuée Bleue/DANN, Strasbourg, 237 p.
Jenkner, B., 1986, Ein Vorschlag zur Neugliederung des sedimentären Oberrotliegenden in der Baden-Badener Senke und ihrer nordöstlichen Fortsetzung (Nordschwarzwald): Jahrbuch des Geologischen Landesamtes Baden-Württemberg, v. 28, p. 49-159.
Kalt, A., Altherr, R., and Hanel, M., 2000, The Variscan basement of the Schwarzwald.: Eur. J. Mineral., Beih., v. 12, p. 1-43.
Kessen, K., Woodruff, M., and Grant, N., 1981, Gangue mineral 87 Sr/86 Sr ratios and the origin of Mississippi Valley-type mineralization: Economic Geology, v. 76, no. 4, p. 913-920.
Köhler, W. R., 1992, Beschaffenheit ausgewählter, nicht direkt anthropogen beeinflußter oberflächennaher und tiefer Grundwasservorkommen in Baden-Würtemberg: Tübinger Geowissenschaftliche Arbeiten, v. 10, p. 144.
Kolchugin A.N., Immenhauser, A., Walter, B.F. and Morozov, V.P., (submitted to Marine and Petroleum Geology) Diagenesis of the palaeo-oil-water transition zone in a Lower Pennsylvanian carbonate reservoir: constraints from cathodoluminescence microscopy and isotope geochemistry.
Koziy, L., Bull, S., Large, R., and Selley, D., 2009, Salt as a fl uid driver, and basement as a metal source, for stratiform sediment-hosted copper deposits: Geology, v. 37, p. 1107–1110, doi:10.1130/G30380A.1
Kozlovsky, Y., 1984, The world's deepest well: Scientific American, v. 251, p. 106-112.
Leach, D. L., Marsh, E., Emsbo, P., Rombach, C. S., Kelley, K. D., and Anthony, M., 2004, Nature of Hydrothermal Fluids at the Shale-Hosted red Dog Zn-Pb-Ag Deposit, Brooks Range, Alaska.: Economic Geology, v. 99, p. 1449-1480.
Loges, A., Wagner, T., Kirnbauer, T., Göb, S., Bau, M., Berner, Z., and Markl, G., 2012, Source and origin of active and fossil thermal spring systems, northern Upper Rhine

Graben, Germany: Applied Geochemistry, v. 27, no. 6, p. 1153-1169.
Lorenz, G. D., 2002, Diagenese der känozoischen Sedimente des Oberrheingrabens als Hinweis der tertiären Fluidentwicklung.
Lüders, V., Plessen, B., Romer, R. L., Weise, S. M., Banks, D. A., Hoth, P., Dulski, P., and Schettler, G., 2010, Chemistry and isotopic composition of Rotliegend and Upper Carboniferous formation waters from the North German Basin.: Chemical Geology, v. 276, p. 198-208.
Ludwig, F., Stober, I., and Bucher, K. (2011). Hydrochemical groundwater evolution in the bunter sandstone sequence of the Odenwald mountain range, Germany: a laboratory and field study. *Aquatic geochemistry*, *17*(2), 165-193.
Markl, G., Lahaye, Y., and Schwinn, G., 2006, Copper isotopes as monitors of redox processes in hydrothermal mineralization.: Geochimica et Cosmochimica Acta, v. 70, p. 4215-4228.
Markl, G., Burisch, M. and Neumann, U. (2016)
Martin, M., 2009, Geogene Grundgehalte (Hintergrundwerte) in den petrogeochemischen Einheiten von Baden-Württemberg: LGRB-Informationen, v. 24, p. 98.
Metz, R., Richter, M., and Schürenberg, H., 1957, Die Blei-Zink-Erzgänge des Schwarzwaldes: Beiheft Geologisches Jahrbuch, v. 29, p. 277.
Nitsch, E., and Zedler, H., 2009, Oberkarbon und Perm in Baden-Württemberg. : LGRB-Information, v. 22, p. 7-102.
Otto, C. J., and Toth, J., 1988. Hydrogeological controls and indicators for oil deposits in rift grabens-An example from the Upper Rhine graben, France. *AAPG Bulletin (American Association of Petroleum Geologists);(USA)*, *72*(CONF-8809346--).
Pauwels, H., C., F., and A.C., F., 1993, Chemistry and isotopes of deep geothermal saline fluids in the Upper Rhine Graben: Origin of compounds and water-rock interactions: Geochimica et Cosmochimica Acta, v. 57, no. 12, p. 2737-2749.
Pearson, F. J., Lolcama, J. L., and Scholtis, A., 1989, Chemistry of waters in the Böttstein, Weiach, Riniken, Schafisheim, Kaisten and Leuggern boreholes: a hydrochemically consistent data set: NAGRA Technical Report, v. 86-19, p. 153.
Pearson, F.J., Arcos, D., Bath, A., Boisson, J.-Y., Fernández, A.M., Gäbler, H.-E., Gaucher, E., Gautschi, A., Griffault, L., Hernán, P., and Waber, H.N., 2003. Mont Terri Project - Geochemistry of water in the Opalinus Caly Formation at the Mont 'Terri Rock Laboratory. Berichte des BWG, Serie Geologie, Bern.
Pfaff, K., Hildebrandt, L. H., Leach, D. L., Jacob, D. E., and Markl, G., 2010, Formation of the Wiesloch Mississippi Valley-type Zn-Pb-Ag deposit in the extensional setting of the Upper Rhinegraben, SW Germany: Mineralium Deposita, v. 45, no. 7, p. 647-666.
Pfaff, K., Koenig, M. A., Wenzel, T., Ridley, I., Hildebrandt, L. H., Leach, D. L., and Markl, G., 2011, Trace and minor element variations and sulfur isotopes in crystalline and colloform ZnS: Incorporation mechanisms and implications for their genesis: Chemical Geology, v. 286, no. 3-4, p. 118-134.
Pfaff, K., Romer, R. L., and Markl, G., 2009, U-Pb ages of ferberite, chalcedony, agate, "U-mica" and pitchblende: constraints on the mineralization history of the Schwarzwald ore district.: Eur. J. Mineral., v. 21, p. 817-836.
Rupf, I., and Nitsch, E., 2008, Das Geologische Landesmodell von Baden-Württemberg: Datengrundlagen, technische Umsetzung und erste geologische Ergebnisse.: LGRB-Information, v. 21.
Sanjuan, B., Millot, R., Dezayes, C., and Brach, M., 2010, Main characteristics of the deep geothermal brine (5km) at Soultz-sous-Forêts (France) determined using geochemical and tracer test data: Comptes Rendus Geoscience, v. 342, no. 7, p. 546-559.
Schwarz, M., and Henk, A., 2005, Evolution and structure of the Upper Rhine Graben: insights from three-dimensional thermomechanical modelling.: International Journal

of Earth Science, v. 94, p. 732-750.
Schwinn, G., and Markl, G., 2005, REE systematics in hydrothermal fluorite.: Chemical Geology, v. 216, p. 225-248.
Schwinn, G., Wagner, T., Baatartsogt, B., and Markl, G., 2006, Quantification of mixing processes in ore-forming hydrothermal systems by combination of stable isotope and fluid inclusion analyses.: Geochimica et Cosmochimica Acta, v. 70, p. 965-982.
Seo, J. H., Guillong, M., Aerts, M., Zajacz, Z., and Heinrich, C. A., 2011, Microanalysis of S, Cl, and Br in fluid inclusions by LA–ICP-MS: Chemical Geology, v. 284, no. 1, p. 35-44.
Sverjensky, D.A., 1984. Oil field brines as ore-forming solutions. Economic Geology, 79(1): 23-37.
Sverjensky, D.A., 1987. The role of migrating oil field brines in the formation of sediment-hosted Cu-rich deposits. Economic Geology, 82(5): 1130-1141.
Shouakar-Stash, O., Alexeev, S., Frape, S., Alexeeva, L., and Drimmie, R., 2007, Geochemistry and stable isotopic signatures, including chlorine and bromine isotopes, of the deep groundwaters of the Siberian Platform, Russia: Applied geochemistry, v. 22, no. 3, p. 589-605.
Staude, S., Bons, P. D., and Markl, G., 2009, Hydrothermal vein formation by extension-driven dewatering of the middle crust: An example from SW Germany.: Earth and Planetary Science Letters, v. 286, p. 387-395.
Staude, S., Dorn, A., Pfaff, K., and Markl, G., 2010a, Assemblages of Ag-Bi sulfosalts and conditions of their formation: the type locality of schapbachite ($Ag_{0.4}Pb_{0.2}Bi_{0.4}S$) and neighboring mines in the Schwarzwald ore district, southern Germany.: Canadian Mineralogist, v. 48, p. 441-466.
Staude, S., Göb, S., Pfaff, K., Ströbele, F., Premo, W. R., and Markl, G., 2011a, Deciphering fluid sources of hydrothermal systems: A combined Sr- and S-isotope study on barite (Schwarzwald, SW Germany): Chemical Geology, v. 286, no. 1-2, p. 1-20.
Staude, S., Göb, S., Pfaff, K., Ströbele, F., Premo, W. R., and Markl, G., 2011b, Deciphering fluid sources of hydrothermal systems: a combined Sr-and S-isotope study on barite (Schwarzwald, SW Germany): Chemical Geology, v. 286, no. 1, p. 1-20.
Staude, S., Mordhorst, T., Nau, S., Pfaff, K., Brügmann, G., Jacob, D.E., and Markl, G., 2012 . Hydrothermal carbonates of the Schwarzwald ore district, southwestern Germany: Carbon source and conditions of formation using $\delta^{18}O$, $\delta^{13}C$, $^{87}Sr/^{86}Sr$, and fluid inclusions. The Canadian Mineralogist, 50(5), 1401-1434.
Staude, S., Mordhorst, T., Neumann, R., Prebeck, W., and Markl, G., 2010b, Compositional variation of the tennantite-tetrahedrite solid-solution series in the Schwarzwald ore district (SW Germany): The role of mineralization processes and fluid source.: Mineralogical Magazine, v. 74, p. 309-339.
Staude, S., Wagner, T., and Markl, G., 2007, Mineralogy, mineral chemistry and fluid evolution of the hydrothermal Wenzel deposit, southern Germany: implications for the formation of Kongsberg-type silver deposits.: Canadian Mineralogist, v. 45, p. 1147-1176.
Staude, S., Werner, W., Mordhorst, T., Wemmer, K., Jacob, D., and Markl, G., 2012b, Multi-stage Ag–Bi–Co–Ni–U and Cu–Bi vein mineralization at Wittichen, Schwarzwald, SW Germany: geological setting, ore mineralogy, and fluid evolution: Mineralium Deposita, v. 47, no. 3, p. 251-276.
Steele-MacInnes, M., Bodnar, R. J., and Naden, J., 2011, Numerical model to determine the composition of H2O-NaCl-CaCl2 fluid inclusions based on microthermometric and microanalytical data.: Geochimica et Cosmochimica Acta, v. 75, p. 21-40.
Stober, I., and Bucher, K., 1999a, Deep groundwater in the crystalline basement of the Black Forest region: Applied Geochemistry, v. 14, p. 237-254.

1187 Stober, I., and Bucher, K., 1999b. Origin of salinity of deep groundwater in crystalline rocks.
1188 *Terra Nova-Oxford*, *11*(4), 181-185.
1189 Stober, I., Richter, A., Brost, E., and Bucher, K., 1999c. The Ohlsbach Plume–Discharge of
1190 deep saline water from the crystalline basement of the Black Forest, Germany.
1191 *Hydrogeology Journal*, *7*(3), 273-283.
1192 Stober, I., and Bucher, K.,, 2004, Fluid sinks within the earth's crust: Geofluids, v. 4, p. 143-
1193 151.
1194 Stober, I., and Bucher, K., 2005a. The upper continental crust, an aquifer and its fluid:
1195 hydaulic and chemical data from 4 km depth in fractured crystalline basement rocks at
1196 the KTB test site. *Geofluids*, *5*(1), 8-19.
1197 Stober, I., and Bucher, K., 2005b. Deep-fluids: Neptune meets Pluto. *Hydrogeology Journal*,
1198 *13*(1), 112-115.
1199 Stober, I., and Bucher, K., 2007. Hydraulic properties of the crystalline basement.
1200 *Hydrogeology Journal*, *15*(2), 213-224.
1201 Stober, I., and Bucher, K., 2014. Permeability and Fluid Flow in the Upper Continental Crust.
1202 In *2014 GSA Annual Meeting in Vancouver, British Columbia*.
1203 Stober, I., and Bucher, K., 2015a. Hydraulic conductivity of fractured upper crust: insights
1204 from hydraulic tests in boreholes and fluid-rock interaction in crystalline basement
1205 rocks. *Geofluids*, *15*(1-2), 161-178
1206 Stober, I., and Bucher, K., 2015b. Significance of Hydraulic Conductivity as Precondition to
1207 Fluid Flow in Fractured and Faulted Crystalline Basement and its Impact on Fluid-
1208 Rock Interaction Processes. *Significance*, *19*, 25.
1209 Stober, I., 2011. Depth-and pressure-dependent permeability in the upper continental crust:
1210 data from the Urach 3 geothermal borehole, southwest Germany. *Hydrogeology*
1211 *Journal*, *19*(3), 685-699.
1212 Stober, I., 2013. Geothermal fluid and reservoir properties in the Upper Rhine Graben,
1213 Europe. In *Second EAGE Sustainable Earth Sciences (SES) Conference and*
1214 *Exhibition*.
1215 Ströbele, F., Staude, S., Pfaff, K., Premo, W. R., Hildebrandt, L. H., Baumann, A., Pernicka,
1216 E., and Markl, G., 2012, Pb isotope constraints on fluid flow and mineralization
1217 processes in SW Germany Neues Jahrbuch für Mineralogie-Abhandlungen: Journal of
1218 Mineralogy and Geochemistry, v. 189, no. 3, p. 287-309.
1219 Todt, W., 1976, Zirkon U/Pb-Alter des Malsburg-Granits vom Südschwarzwald: Neues Jahrb
1220 Mineral Monatsh, v. 12, p. 532-544.
1221 Ufrecht, W., 2006, Zur Hydrogeologie der Aquifersysteme Buntsandstein und Muschelkalk
1222 zwischen Neckar und Donau.: Schriftenreihe des Amtes für Umweltschutz, p. 19-48.
1223 Van Alstine, R., 1976, Continental rifts and lineaments associated with major fluorspar
1224 districts: Economic Geology, v. 71, no. 6, p. 977-987.
1225 Van den Kerkhof, A. M., & Hein, U. F. 2001. Fluid inclusion petrography. *Lithos*, *55*(1), 27-
1226 47.
1227 Walter, B.F., Immenhauser, A., Geske, A. and Markl, G., 2015. Exploration of hydrothermal
1228 carbonate magnesium isotope signatures as tracers for continental fluid aquifers,
1229 Schwarzwald mining district, SW Germany. Chemical Geology, 400, 87-105..
1230 Walter B.F., Burisch, M. and Markl, G., submitted to Geofluids.Long-term chemical
1231 evolution and modification of continental basement brines – a field study from the
1232 Schwarzwald, SW Germany
1233 Walter, B.F., Burisch, M., Marks, M.A.W. and Markl, G., submitted to Chemical Geology.
1234 Major element and trace metal systematics of fluid inclusions in hydrothermal veins:
1235 metal provenance and the reconstruction of eroded sedimentary units
1236 Werner, W. F., Hans Joachim, 1994, Tektonik und Mineralisation der Hydrothermalgänge am
1237 Schwarzwaldrand im Bergbaurevier Freiamt-Sexau: Abh. geol. Landesamt Baden-

Württemberg, v. 14, p. 27-98.
Werner, W., Franzke, H.J., Wirsing, G., Jochum, J., Lüders, V., Wittenbrink, 2002. mit einem Beitrag von B. Steiber: Die Erzlagerstätte Schauinsland bei Freiburg im Breisgau. Bergbau, Geologie, Hydrogeologie, Mineralogie, Geochemie, Tektonik und Lagerstättenentstehung. Ber. Naturforsch. Ges. Freiburg, 92: 110 S., 26 Abb., 9 Tab., 16 Taf.; Freiburg i. Br.
Wetzel, A., Allenbach, R., and Allia, V., 2003, Reactivated basement structures affecting the sedimentary facies in a tectonically "quiescent" epicontinental basin: an example from NW Switzerland.: Sedimentary Geology, v. 157, p. 153-172.
Wilkinson, J., 2010, A review of fluid inclusion constraints on mineralization in the Irish ore field and implications for the genesis of sediment-hosted Zn-Pb deposits: Economic Geology, v. 105, no. 2, p. 417-442.
Wilkinson, J., Weiss, D., Mason, T., and Coles, B., 2005, Zinc isotope variation in hydrothermal systems: preliminary evidence from the Irish Midlands ore field: Economic Geology, v. 100, no. 3, p. 583-590.
Yardley, B.W., 2005. 100th anniversary special paper: metal concentrations in crustal fluids and their relationship to ore formation. *Economic Geology*, *100*(4), 613-632.
Ziegler, P. A., 1990, Geological Atlas of Western and Central Europe., Shell Internationale Petroleum Maatschappij B.V.

Figure captions

Fig. 1. Geological map of the rift shoulders and the hydrothermal veins of group (v). GeoRG data after Beccaletto et al. (2010) was used.

Fig. 2. Structural positions of the different aquifers within the Upper Rhinegraben, from surface to 5 km b.s.m. The map is based on GeoRG data after Beccaletto et al. (2010). Note the asymmetric tilt of the rift.

Fig. 3. Geological overview of the Schwarzwald mining district in SW Germany with sample locations. (**A**) Overview map. (**B**) Close-up of the Schwarzwald mining district modified after Pfaff et al. (2011). Sample localities sorted after mineralization type (for more information refer to Table 1 in the electronic supplement).

Fig. 4. Examples of post-Cretaceous hydrothermal veins including different mineral assemblages. (**A**) Segen Gottes fluorite-barite vein near Schnellingen; (**B**) barite-quartz vein

with sphalerite, Schauinsland mine near Freiburg; (**C**) Siderite-chalocopyrite vein, Riggenbach near Staufen; (**D**) barren barite vein, Freudenstadt.

Fig 5. Schematic petrography of fluid inclusion assemblages. Note alternating, high salinity, moderate and low salinity fluids. Some assemblages contain sulfate and/or CO_2.

Fig. 6. **(A-D)** Melting and dissolution behaviour of sulfate bearing fluid inclusions. **(E)** Microraman spectra of SO_4 and CO_2 bearing fluid inclusion from the Riester vein. **(F)** LA-ICPMS signal of a sulfate bearing fluid inclusion from the Karl-August vein near Kropbach. Sulphur is correlating with Na and Cl, clearly indicating that S is present in the liquid phase and not in the host mineral.

Fig. 7. Diagram is illustrating that Cl/Br of crush leach results are a bulk of all single fluid inclusions by LA-ICPMS analyses.

Fig 8. Homogenization temperature versus salinity (microthermometrical data) sorted according to vein mineralogy. There seems to be no correlation between the microthermometric data and vein mineralogy.

Fig 9. Ternary phase diagram of the NaCl-CaCl2-H2O system. Included data is restricted to signatures A-C. The black boxes indicate the reservoir fluid compositions, their numbering is consistent with the numbering used in the text.

Fig 10. Cathodolumenscense and microphotographs (AxPol) of pseudomorphic replacement of quartz after anhydrite.

Fig. 11. Crush leach results (A) SO_4-Cl-HCO_3 system. Note, fluids from fluorite only scatter between Cl and HCO_3. (B) Na-Ca-K system. Most of the data points of barite and quartz showing Na and Ca as dominant cation. All the K rich fluids are of low salinity. (C) Metal distribution in the Ni-Cu-Zn system. All FIAs hosted by fluorite, barite and quartz are Ni poor. In contrast, there is an isolated group of Ni-rich carbonates. (D) illustrates the fluid signatures in the As-Pb-Zn system. Interestingly, almost all barites are Pb-poor. (E) dominantly fluids from barite are enriched in U. (F) Cl/Br versus Cl content.

Fig. 12. LA-ICPMS results of single fluid inclusions from six veins. (A) Cl/Br versus Cu +Ni content. (B) Cl/Br versus Pb + Zn. (C) Cl/Br versus As content. (D) Cl/Br versus W content. (E) Cl/Br versus Sb content. (F) Cl/Br versus B content. For all plots note triangle shape of the data cloud.

Fig. 13. Temporal evolution of fluid mixing. Data of the Riggenbach siderite-quartz-chalocpyrite vein are illustrated. Na/Ca, salinity and T_H vary with time.

Fig. 14. LA-ICPMS results of the Karl August vein near Kropbach. (A) S content versus Cl content. (B) Cl/Br mass ratio versus Pb + Zn content. (C) Cl/Br mass ratio versus Cu +Ni content. Ternary mixing and variation in mixing ratio with time (represented by FIAs) can be observed.

Fig. 15. Schematic illustration of the fluid trapping involving heterogeneous co-existing fluid batches (schlieren).

Fig. 16. Rb vs Cs content. Most of the data points are plotting below a Rb/Cs ratio of <2.

Fig. 17. Mixing model results log SI versus wt.% basementbrine. (A) basement versus Buntsandstein. (B) basement brine versus Muschelkalk (halite facies). (C) basement brine versus Muschelkalk (sulfate facies). (D) basement brine versus Keuper. (E) basement brine versus Hauptrogenstein. (F) basement brine versus crystalline intermediate depth. (G) basement brine versus crystalline shallow depth.

Fig. 18. Microthermometrical results arranged after Schwarzwald (blue) and Steinbach in the Vosges (red). (A) homogenization temperatures versus salinity. (B) Ca/(Na+Ca) mole ratio versus salinity. (C) Ca/(Na+Ca) mole ratio versus homogenization temperatures. (D) mole Ca versus mole Na.

Fig. 19. Schematic crustal sections showing multi-component fluid mixing and vein formation in the complex geological environment of the Upper Rhinegraben rift.

Table 1 Types of veins and fluid signatures of the Schwarzwald ore district modified after Walter et al. (2016, and references therein).

Table 2 Overview of mineralization types in the post-Cretaceous period with some representative localities.

Table 3 fluid characteristica

Table 4 maxium values LA-ICPMS data of single inclusions of six veins

Table 4 Aquiferdata (representative for the most important aquifers) of Göb et al. (2013); Pauwels et al. (1993); (Pearson et al. 1989); Stober and Bucher (2004) were used and combined as input parameter for modelling.

Figure 1

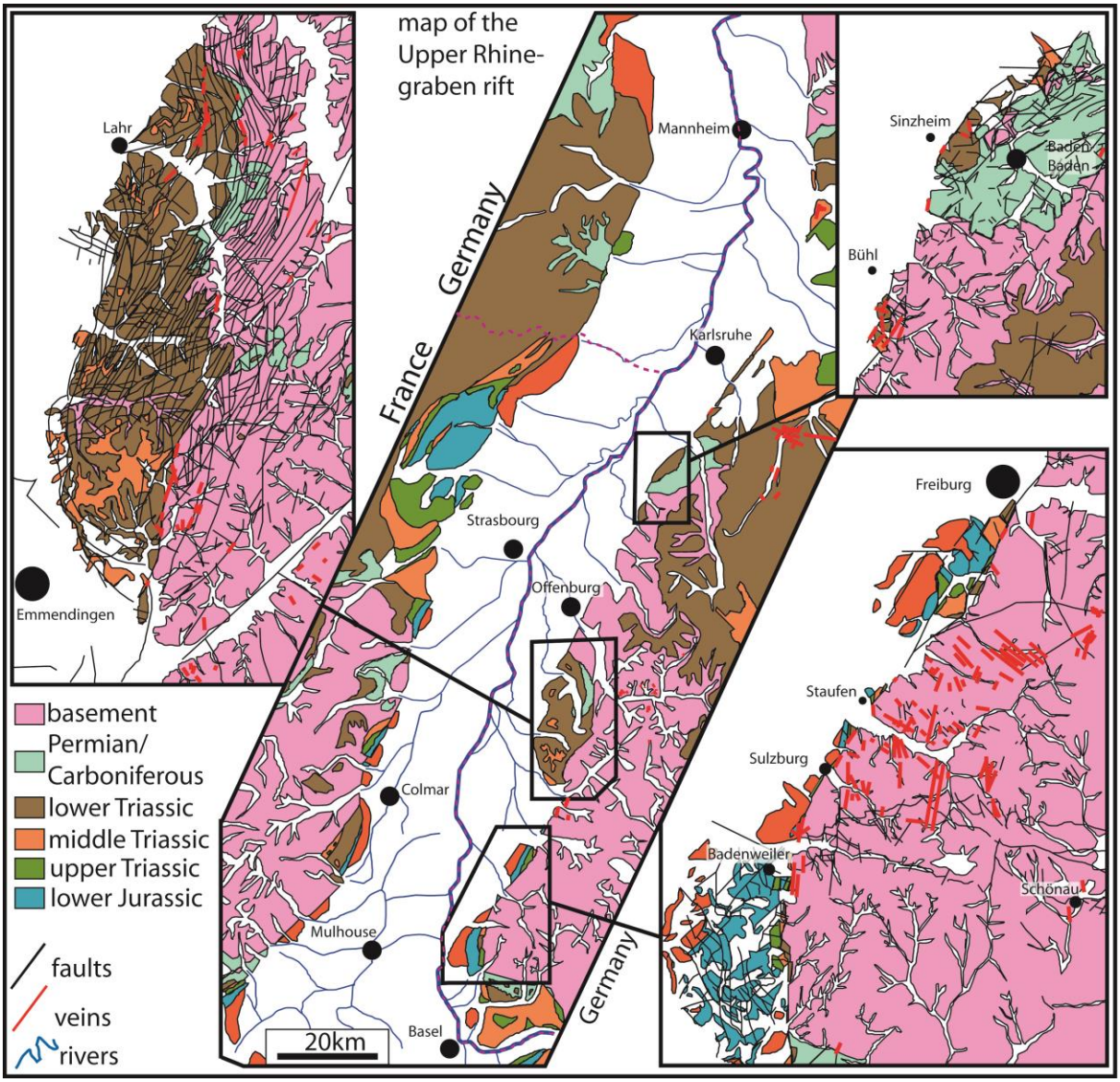
map of the
Upper Rhine-
graben rift
France
Germany
Germany
Lahr
Emmendingen
Mannheim
Karlsruhe
Strasbourg
Offenburg
Colmar
Mulhouse
Basel
Sinzheim
Baden-
Baden
Bühl
Freiburg
Staufen
Sulzburg
Badenweiler
Schönau
basement
Permian/
Carboniferous
lower Triassic
middle Triassic
upper Triassic
lower Jurassic
faults
veins
rivers
20km

Figure 2

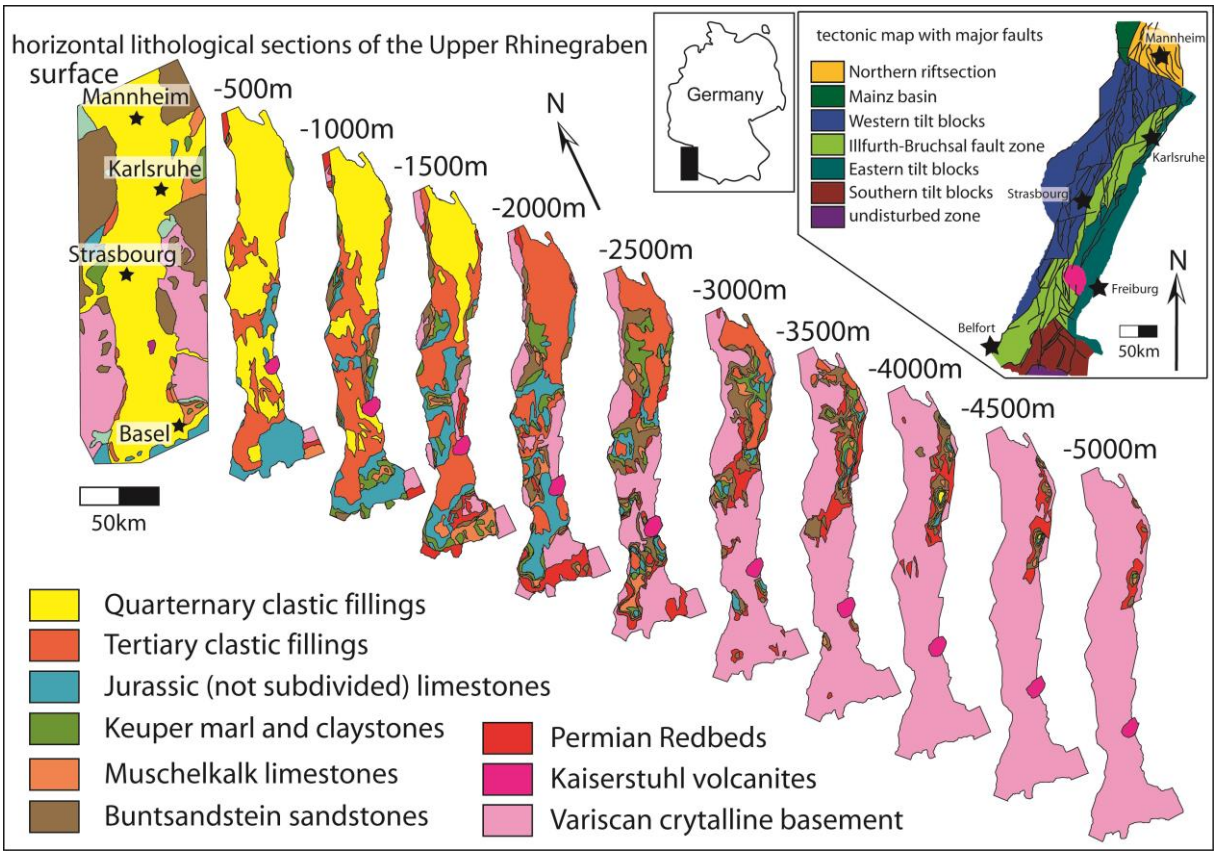
horizontal lithological sections of the Upper Rhinegraben
surface
-500m
-1000m
-1500m
-2000m
-2500m
-3000m
-3500m
-4000m
-4500m
-5000m
N
Mannheim
Karlsruhe
Strasbourg
Basel
50km
Germany
tectonic map with major faults
Northern riftsection
Mainz basin
Western tilt blocks
Illfurth-Bruchsal fault zone
Eastern tilt blocks
Southern tilt blocks
undisturbed zone
Mannheim
Karlsruhe
Strasbourg
Freiburg
Belfort
N
50km
Quarternary clastic fillings
Tertiary clastic fillings
Jurassic (not subdivided) limestones
Keuper marl and claystones
Muschelkalk limestones
Buntsandstein sandstones
Permian Redbeds
Kaiserstuhl volcanites
Variscan crytalline basement

Figure 3

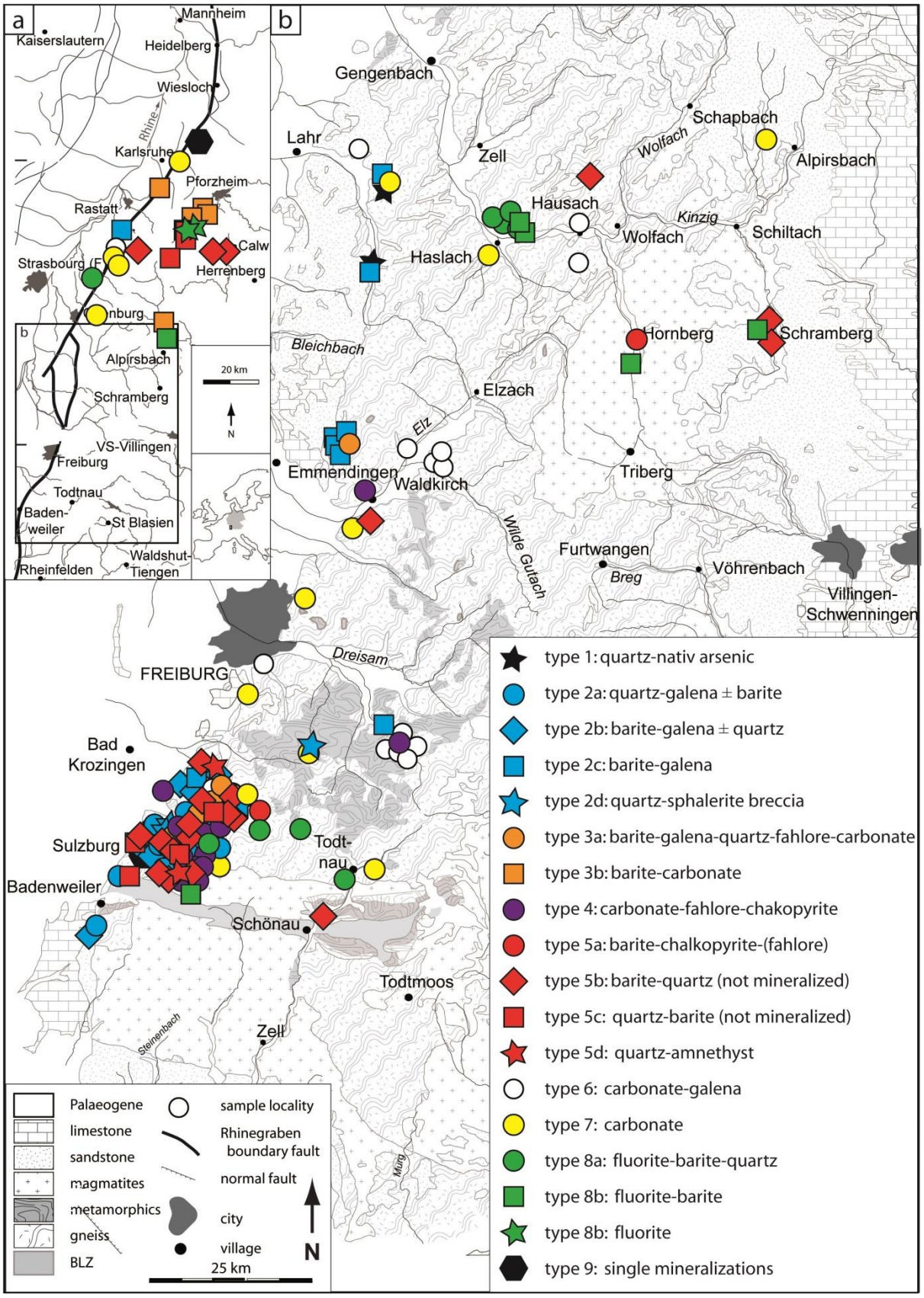
a
b
Mannheim
Kaiserslautern
Heidelberg
Wiesloch
Rhine
Karlsruhe
Pforzheim
Rastatt
Calw
Herrenberg
Strasbourg (F)
Alpirsbach
Schramberg
20 km
N
VS-Villingen
Freiburg
Todtnau
Baden-
weiler
St Blasien
Waldshut-
Tiengen
Rheinfelden
Gengenbach
Lahr
Zell
Schapbach
Wolfach
Alpirsbach
Hausach
Kinzig
Wolfach
Schiltach
Haslach
Hornberg
Schramberg
Bleichbach
Elzach
Elz
Emmendingen
Waldkirch
Triberg
Wilde Gutach
Furtwangen
Breg
Vöhrenbach
Villingen-
Schwenningen
Dreisam
FREIBURG
Bad
Krozingen
Sulzburg
Todt-
nau
Badenweiler
Schönau
Todtmoos
Zell
Steinenbach
Palaeogene
limestone
sandstone
magmatites
metamorphics
gneiss
BLZ
sample locality
Rhinegraben
boundary fault
normal fault
city
village
25 km
N
type 1: quartz-nativ arsenic
type 2a: quartz-galena ± barite
type 2b: barite-galena ± quartz
type 2c: barite-galena
type 2d: quartz-sphalerite breccia
type 3a: barite-galena-quartz-fahlore-carbonate
type 3b: barite-carbonate
type 4: carbonate-fahlore-chakopyrite
type 5a: barite-chalkopyrite-(fahlore)
type 5b: barite-quartz (not mineralized)
type 5c: quartz-barite (not mineralized)
type 5d: quartz-amnethyst
type 6: carbonate-galena
type 7: carbonate
type 8a: fluorite-barite-quartz
type 8b: fluorite-barite
type 8b: fluorite
type 9: single mineralizations

Figure 4

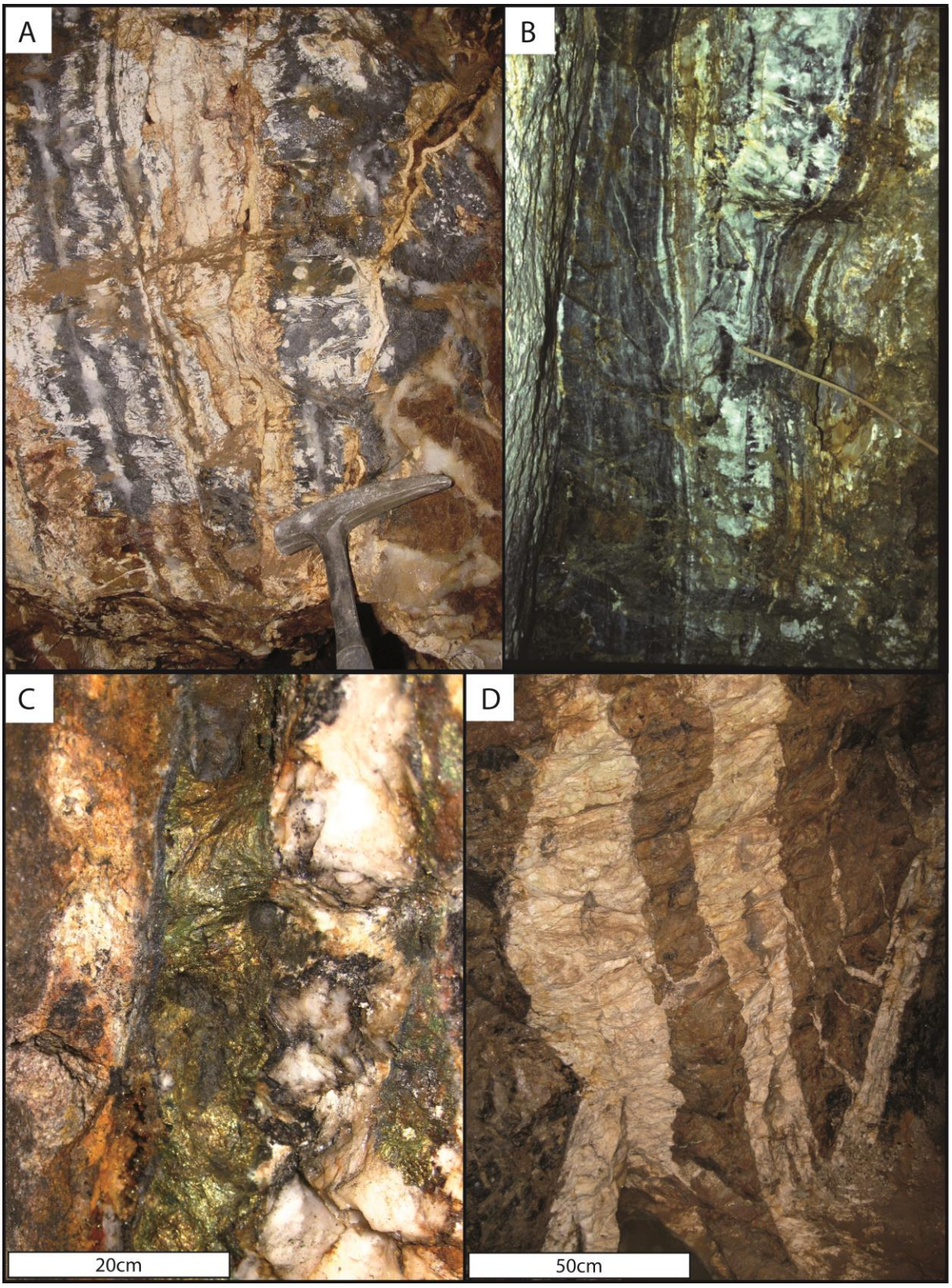

Figure 5

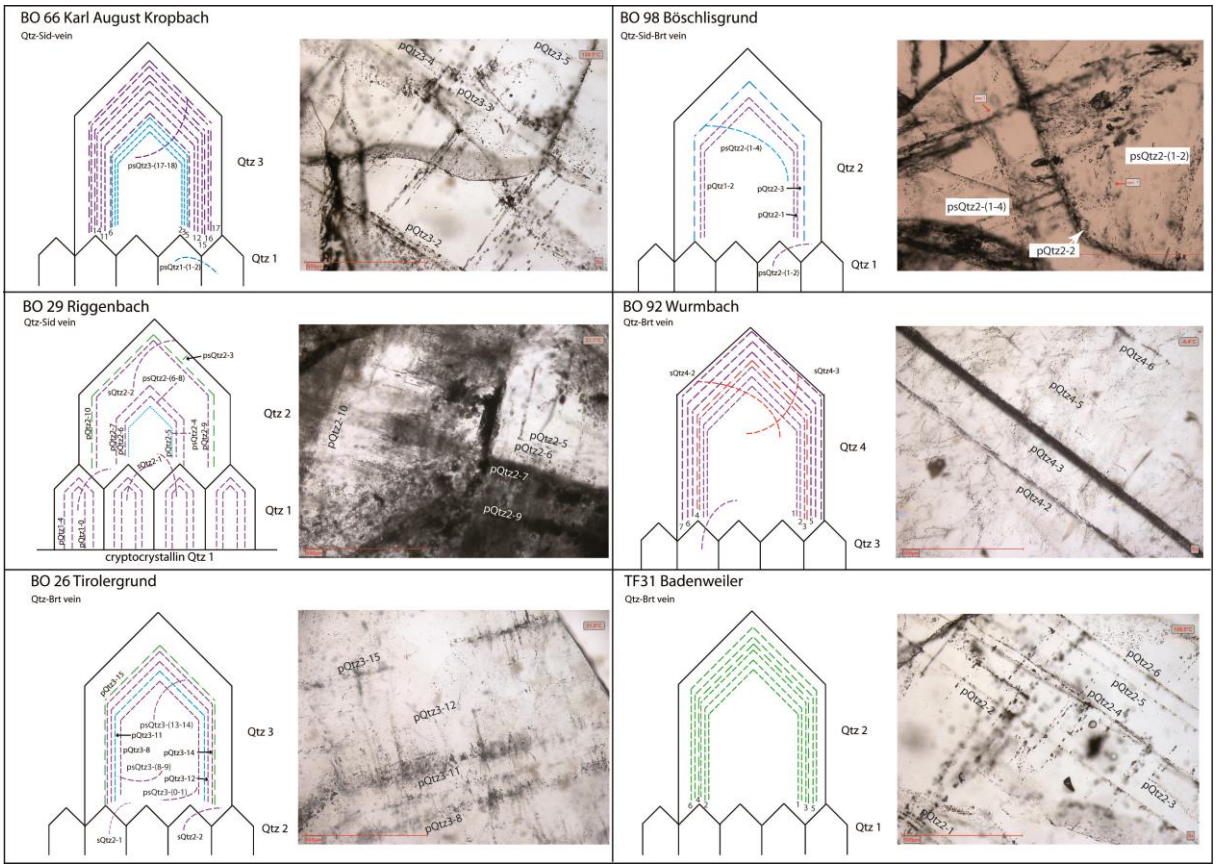
BO 66 Karl August Kropbach
Qtz-Sid-vein
Qtz 3
Qtz 1
psQtz3-(17-18)
psQtz1-(1-2)
pQtz2-4
pQtz3-5
pQtz3-3
pQtz2-2
BO 98 Böschlisgrund
Qtz-Sid-Brt vein
Qtz 2
Qtz 1
psQtz2-(1-4)
pQtz1-2
pQtz2-3
pQtz2-1
psQtz2-(1-2)
psQtz2-(1-2)
psQtz2-(1-4)
pQtz2-2
BO 29 Riggenbach
Qtz-Sid vein
Qtz 2
Qtz 1
cryptocrystallin Qtz 1
psQtz2-3
psQtz2-(6-8)
sQtz2-2
pQtz2-10
pQtz2-5
pQtz2-6
pQtz2-7
pQtz2-9
BO 92 Wurmbach
Qtz-Brt vein
Qtz 4
Qtz 3
sQtz4-2
sQtz4-3
pQtz4-6
pQtz4-5
pQtz4-3
pQtz4-2
BO 26 Tirolergrund
Qtz-Brt vein
Qtz 3
Qtz 2
psQtz3-(13-14)
pQtz3-11
pQtz3-8
pQtz3-14
psQtz3-(8-9)
pQtz3-12
psQtz3-(0-1)
sQtz2-1
sQtz2-2
pQtz3-15
pQtz3-12
pQtz3-11
pQtz3-8
TF31 Badenweiler
Qtz-Brt vein
Qtz 2
Qtz 1
pQtz2-6
pQtz2-5
pQtz2-4
pQtz2-3
pQtz2-1

Figure 6

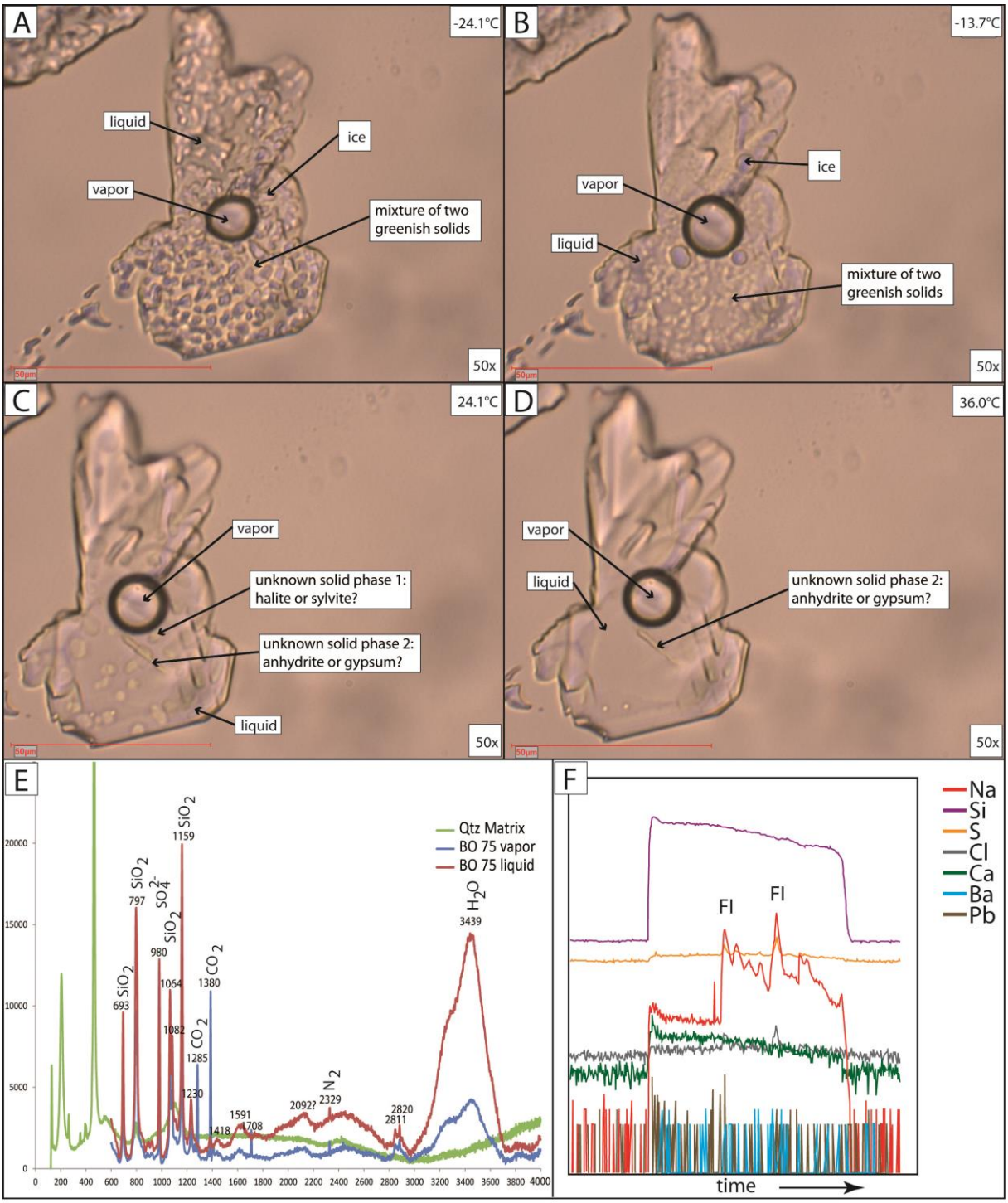
A
-24.1°C
liquid
ice
vapor
mixture of two greenish solids
50x
B
-13.7°C
ice
vapor
liquid
mixture of two greenish solids
50x
C
24.1°C
vapor
unknown solid phase 1: halite or sylvite?
unknown solid phase 2: anhydrite or gypsum?
liquid
50x
D
36.0°C
vapor
liquid
unknown solid phase 2: anhydrite or gypsum?
50x
E
Qtz Matrix
BO 75 vapor
BO 75 liquid
SiO2 693
SiO2 797
SiO2 980
SiO2 1159
SO4 2- 1064
CO2 1082
CO2 1285
CO2 1380
1230
1418
1591
1708
2092?
N2 2329
2811
2820
H2O 3439
F
FI
FI
Na
Si
S
Cl
Ca
Ba
Pb
time

Figure 7

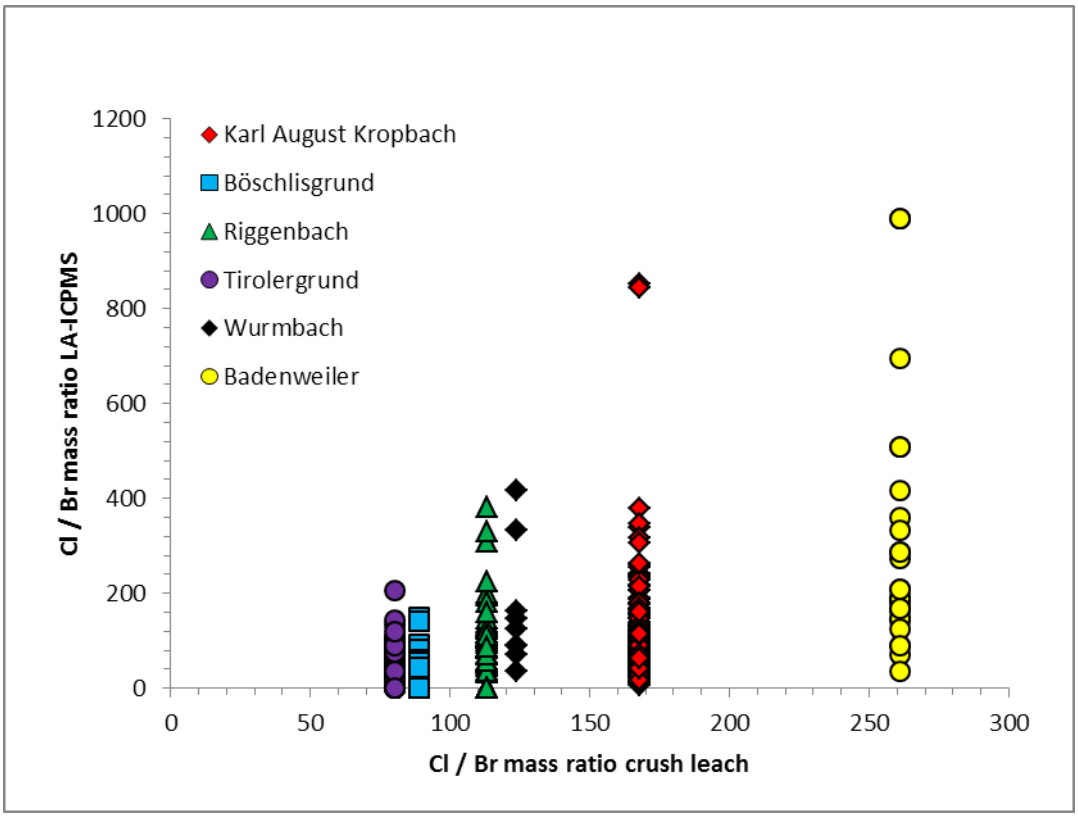
Karl August Kropbach
Böschlisgrund
Riggenbach
Tirolergrund
Wurmbach
Badenweiler
Cl / Br mass ratio LA-ICPMS
Cl / Br mass ratio crush leach
0
200
400
600
800
1000
1200
0
50
100
150
200
250
300

Figure 8

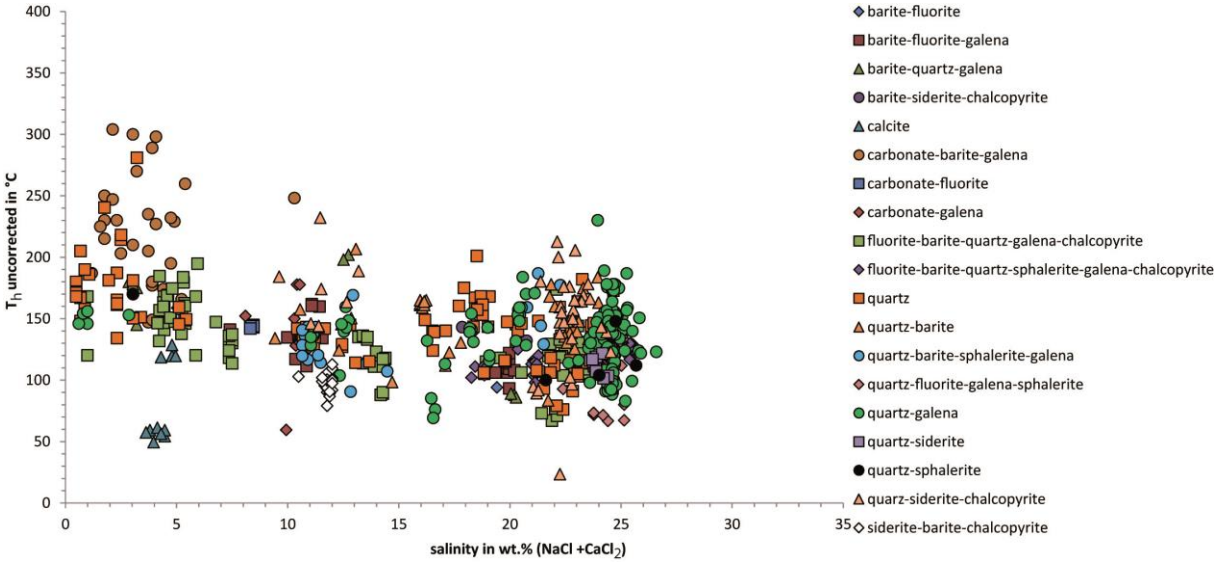
400
350
300
250
200
150
100
50
0
0
5
10
15
20
25
30
35
T_h uncorrected in °C
salinity in wt.% (NaCl +$CaCl_2$)
barite-fluorite
barite-fluorite-galena
barite-quartz-galena
barite-siderite-chalcopyrite
calcite
carbonate-barite-galena
carbonate-fluorite
carbonate-galena
fluorite-barite-quartz-galena-chalcopyrite
fluorite-barite-quartz-sphalerite-galena-chalcopyrite
quartz
quartz-barite
quartz-barite-sphalerite-galena
quartz-fluorite-galena-sphalerite
quartz-galena
quartz-siderite
quartz-sphalerite
quarz-siderite-chalcopyrite
siderite-barite-chalcopyrite

Figure 9

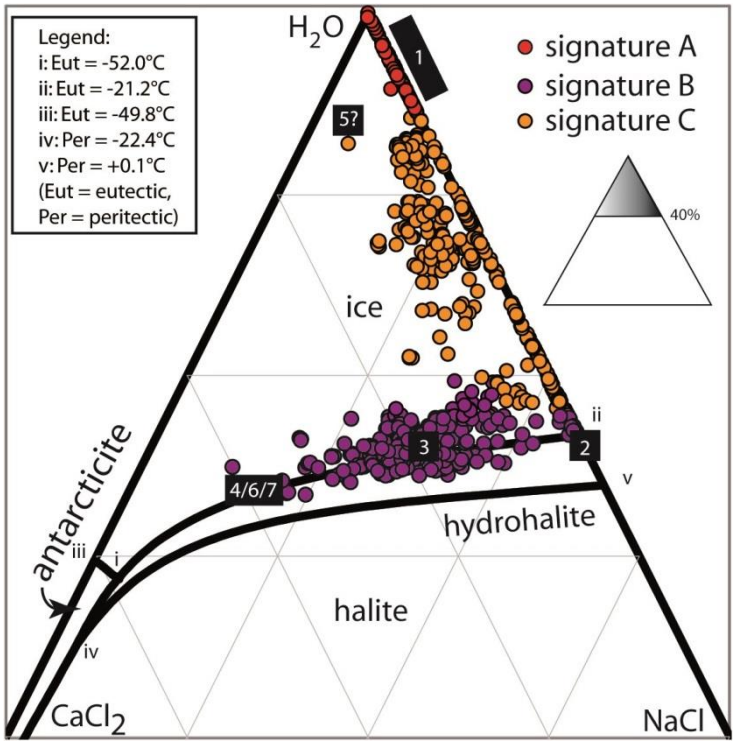
Legend:
i: Eut = -52.0°C
ii: Eut = -21.2°C
iii: Eut = -49.8°C
iv: Per = -22.4°C
v: Per = +0.1°C
(Eut = eutectic,
Per = peritectic)
H2O
signature A
signature B
signature C
40%
1
5?
ice
ii
3
2
v
4/6/7
hydrohalite
antarcticite
iii
i
halite
iv
CaCl2
NaCl

Figure 10

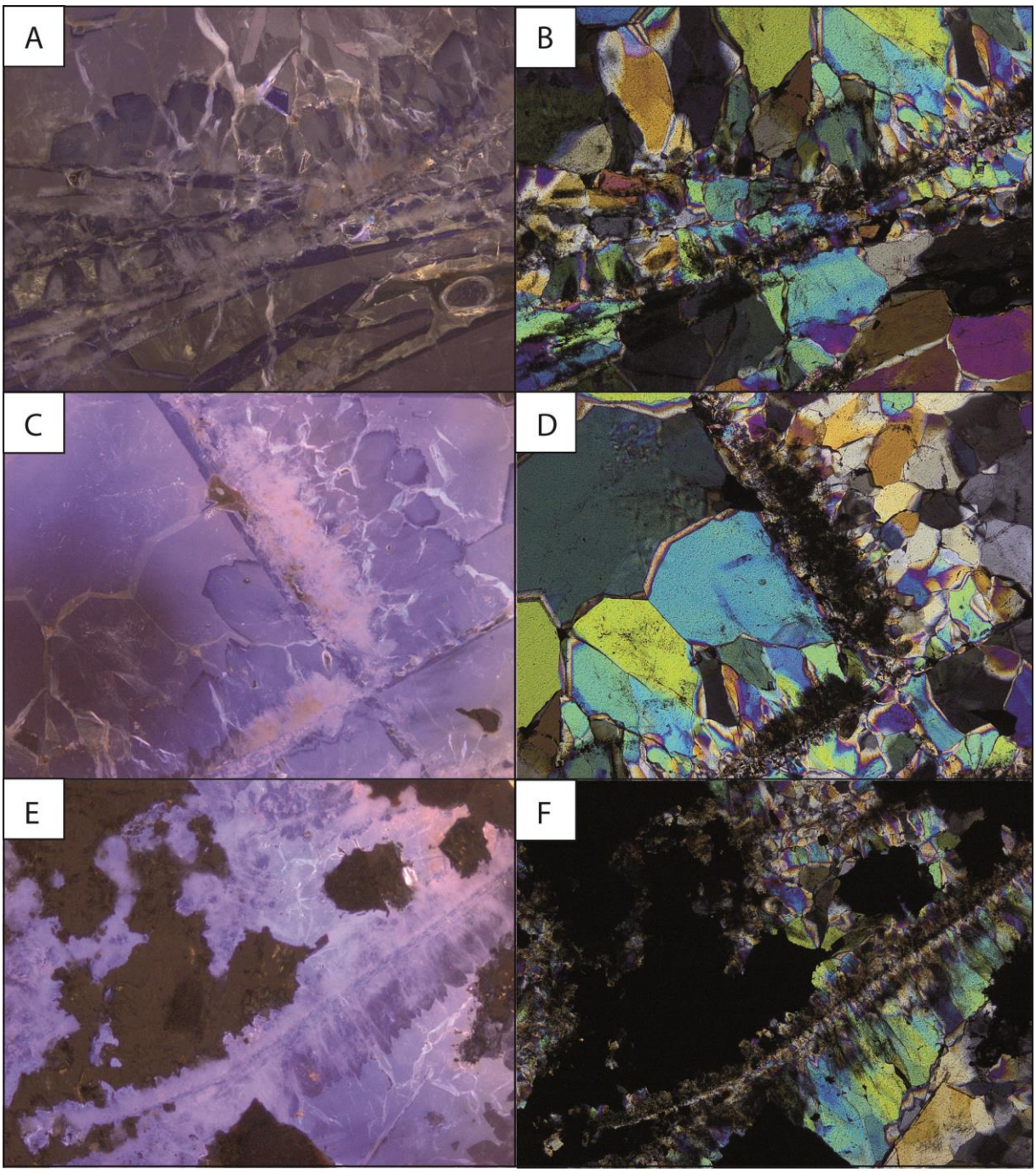

Figure 11

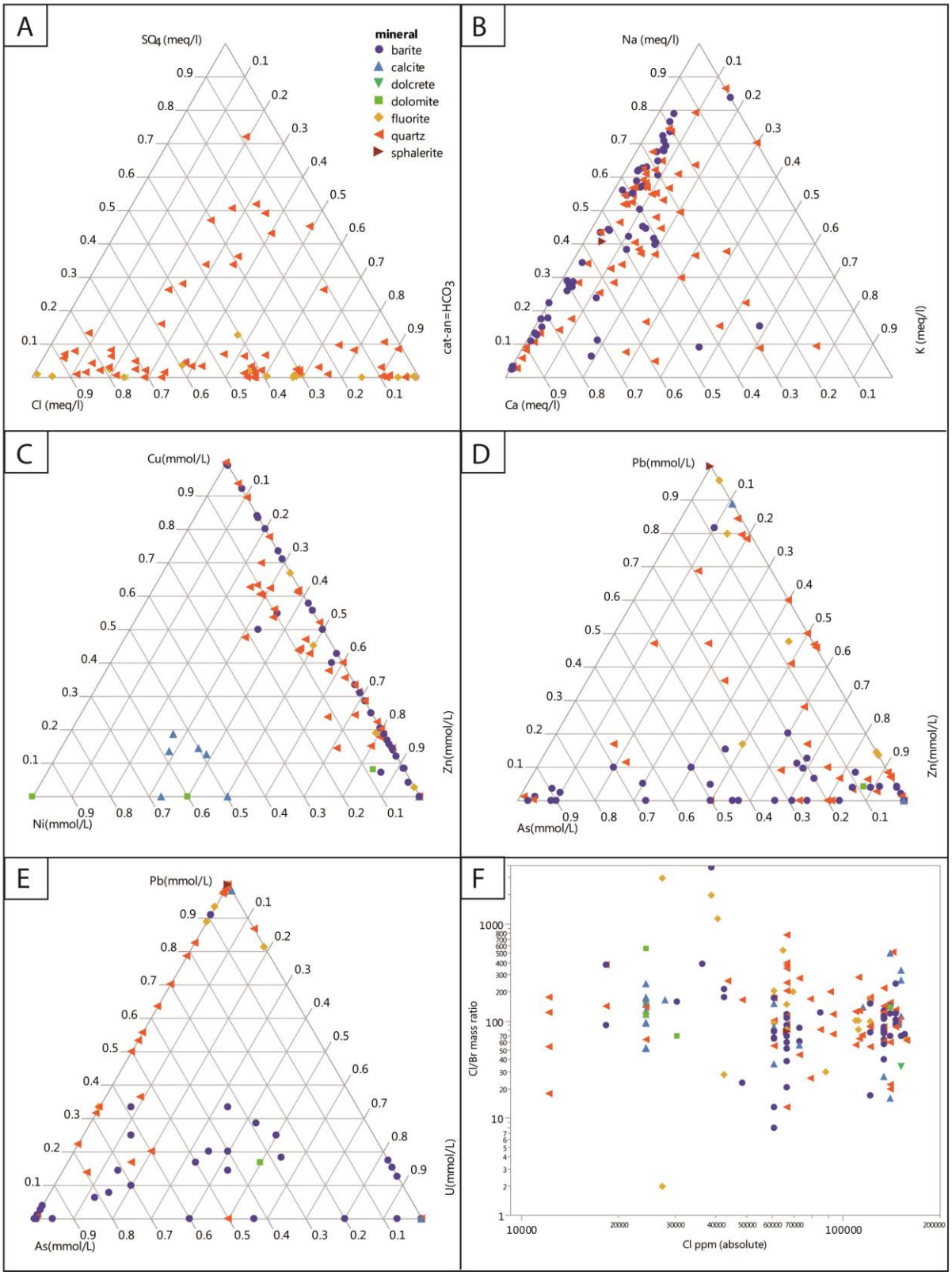
A
SO4 (meq/l)
Cl (meq/l)
cat-an=HCO3
mineral
barite
calcite
dolcrete
dolomite
fluorite
quartz
sphalerite
B
Na (meq/l)
Ca (meq/l)
K (meq/l)
C
Cu(mmol/L)
Ni(mmol/L)
Zn(mmol/L)
D
Pb(mmol/L)
As(mmol/L)
Zn(mmol/L)
E
Pb(mmol/L)
As(mmol/L)
U(mmol/L)
F
Cl/Br mass ratio
Cl ppm (absolute)

Figure 12

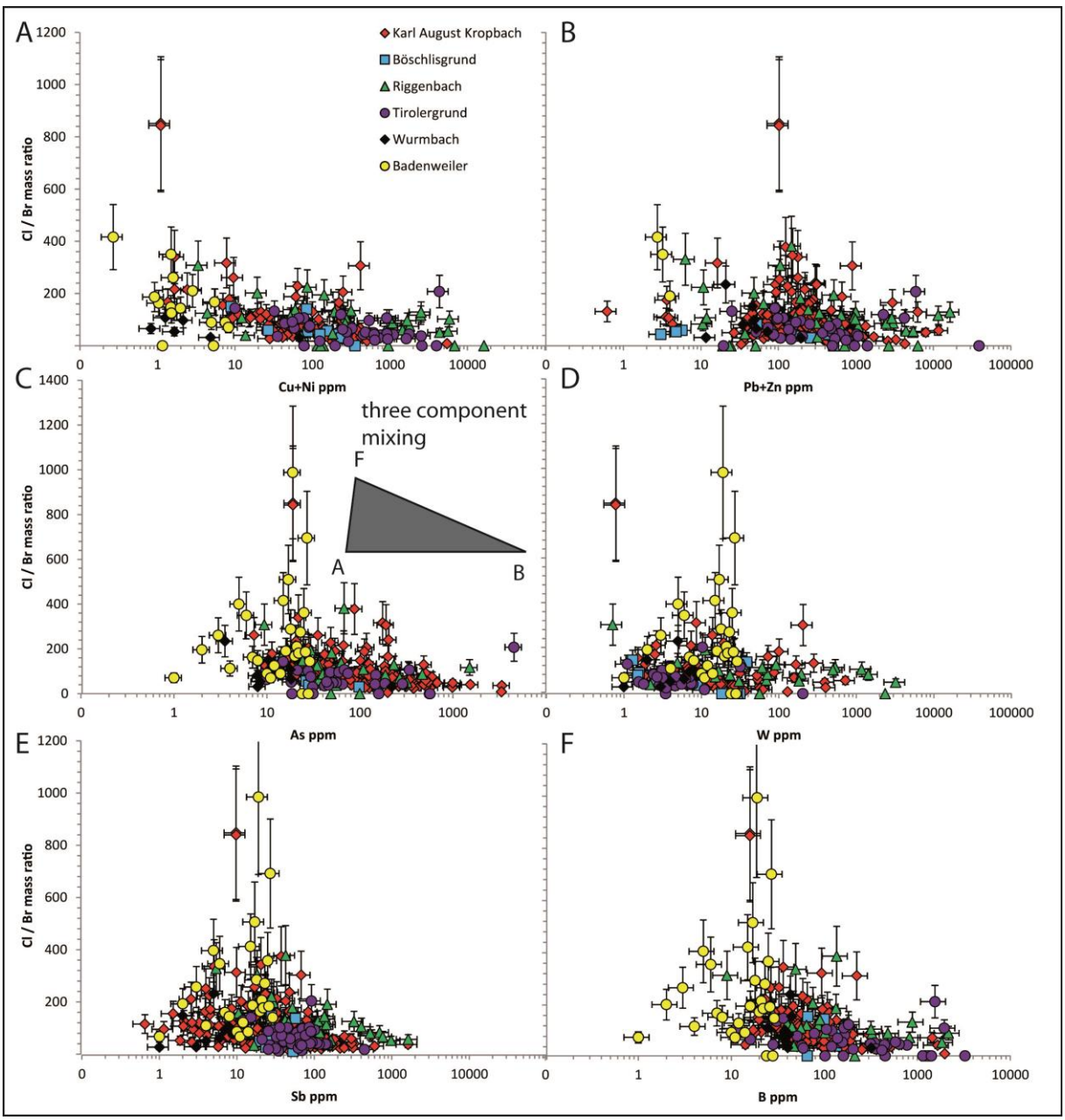
A
B
C
D
E
F
Karl August Kropbach
Böschlisgrund
Riggenbach
Tirolergrund
Wurmbach
Badenweiler
Cl / Br mass ratio
Cu+Ni ppm
Pb+Zn ppm
As ppm
W ppm
Sb ppm
B ppm
three component mixing
F
A
B

Figure 13

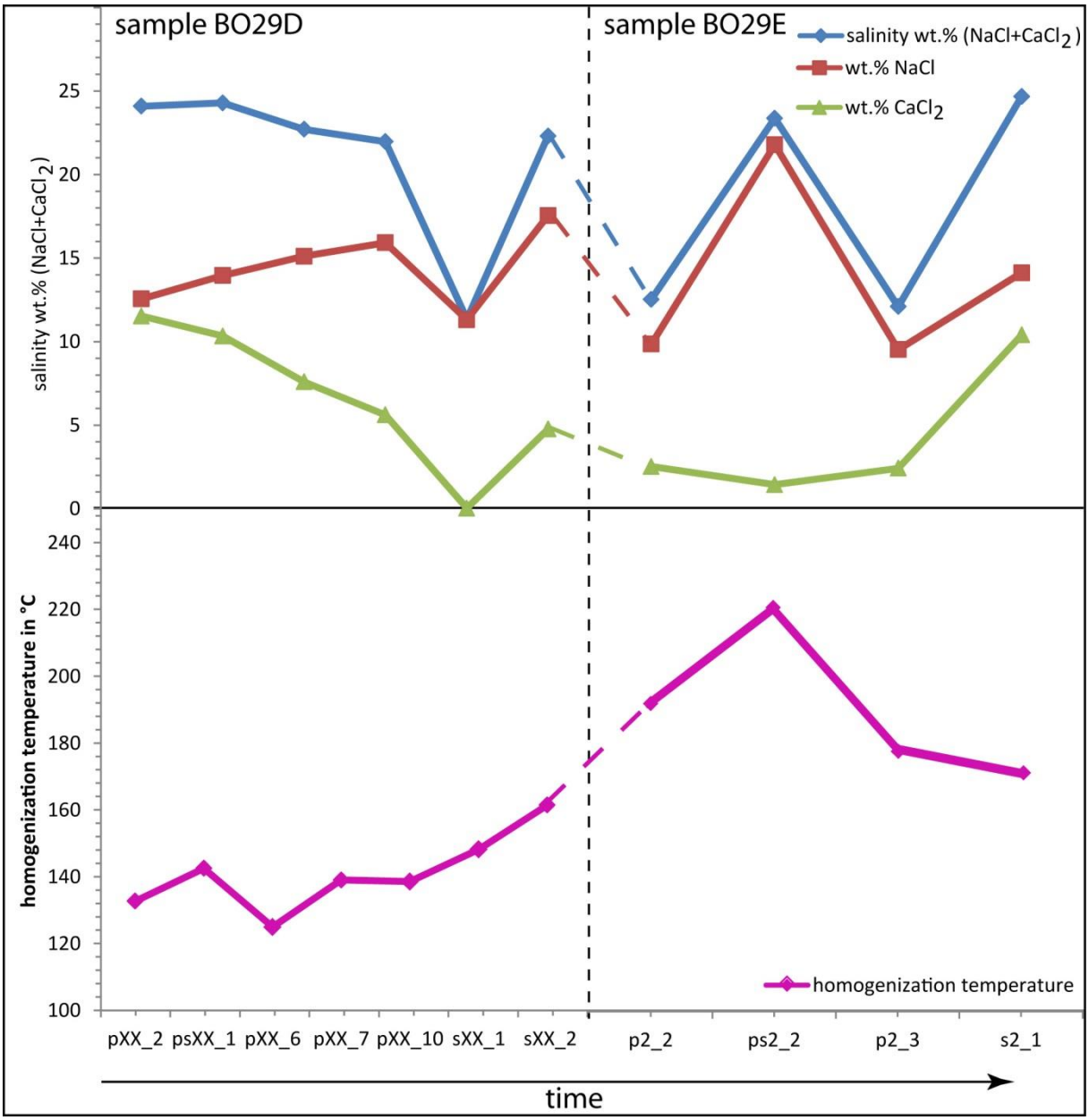
sample BO29D
sample BO29E
salinity wt.% (NaCl+CaCl2)
wt.% NaCl
wt.% CaCl2
salinity wt.% (NaCl+CaCl2)
25
20
15
10
5
0
homogenization temperature in °C
240
220
200
180
160
140
120
100
homogenization temperature
pXX_2
psXX_1
pXX_6
pXX_7
pXX_10
sXX_1
sXX_2
p2_2
ps2_2
p2_3
s2_1
time

Figure 14

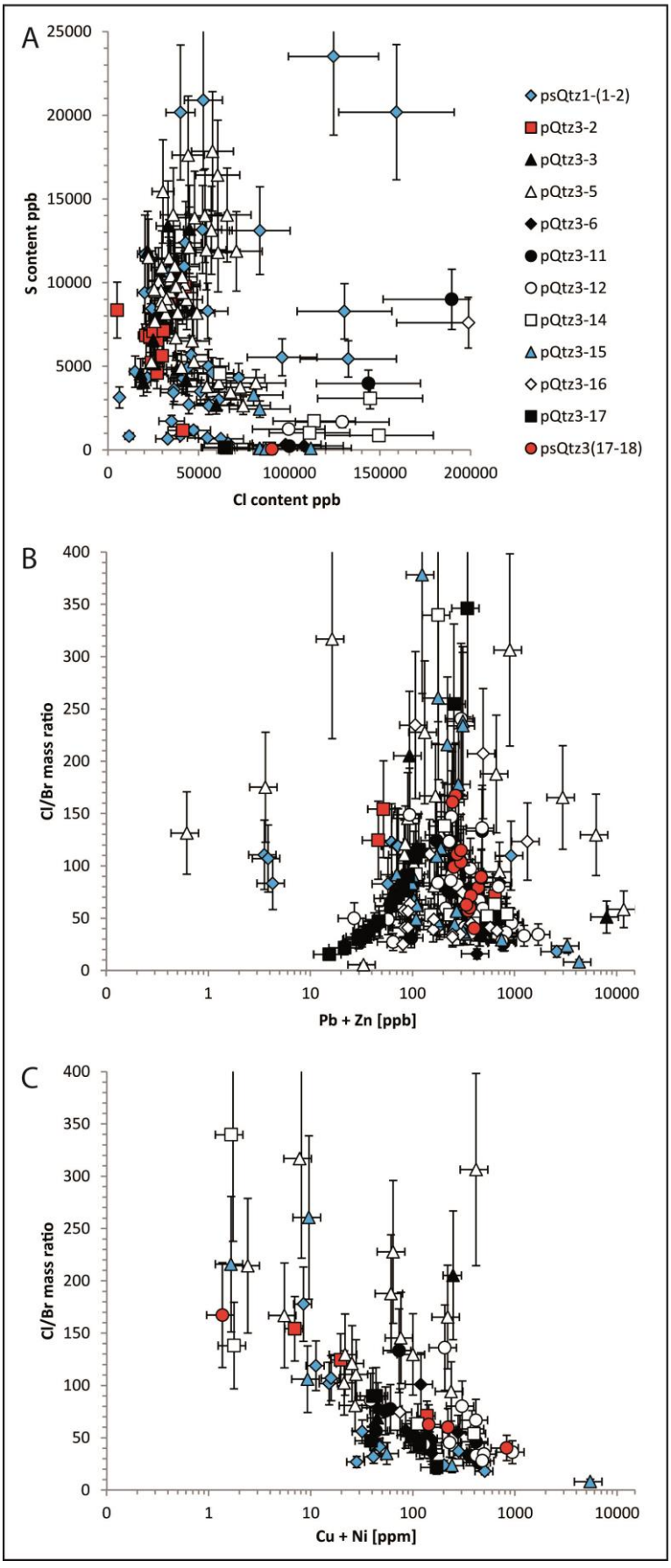
A
S content ppb
Cl content ppb
psQtz1-(1-2)
pQtz3-2
pQtz3-3
pQtz3-5
pQtz3-6
pQtz3-11
pQtz3-12
pQtz3-14
pQtz3-15
pQtz3-16
pQtz3-17
psQtz3(17-18)
B
Cl/Br mass ratio
Pb + Zn [ppb]
C
Cl/Br mass ratio
Cu + Ni [ppm]

Figure 15

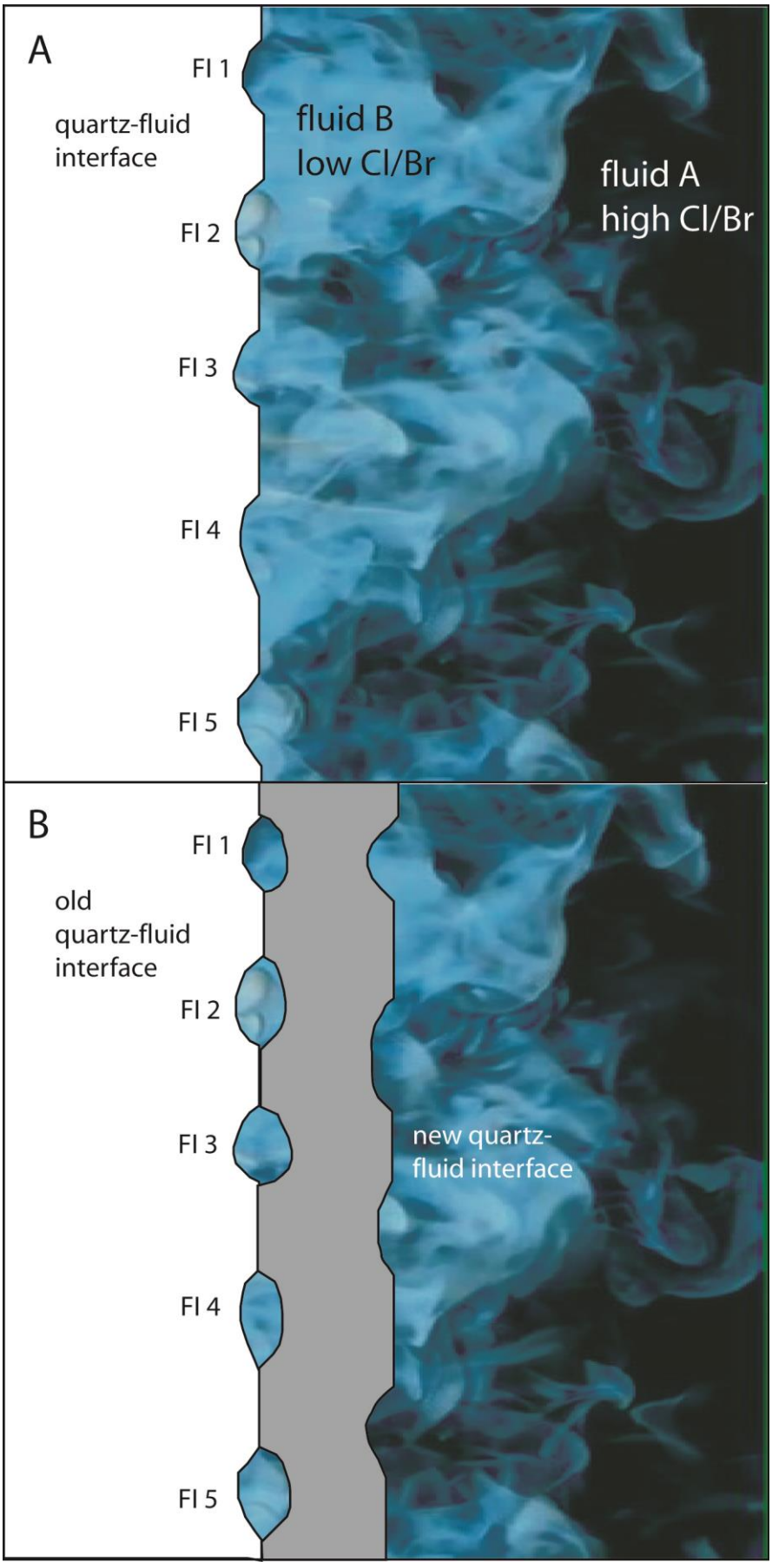
A
FI 1
quartz-fluid
interface
fluid B
low Cl/Br
fluid A
high Cl/Br
FI 2
FI 3
FI 4
FI 5
B
FI 1
old
quartz-fluid
interface
FI 2
FI 3
new quartz-
fluid interface
FI 4
FI 5

Figure 16

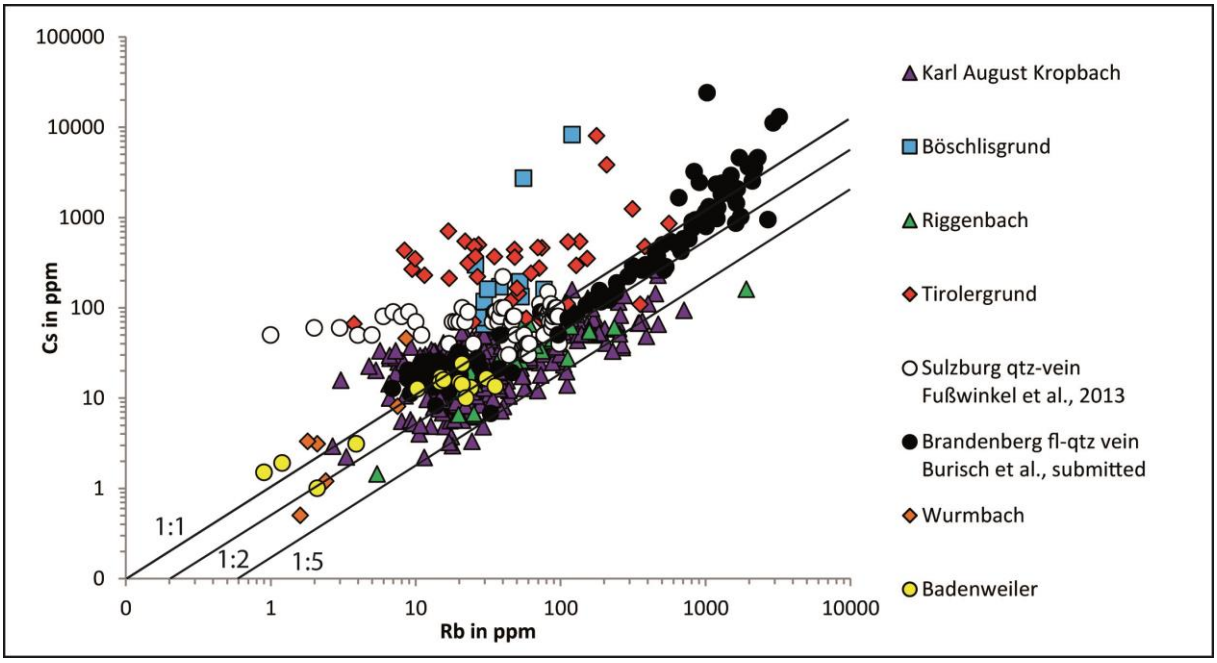
100000
10000
1000
100
10
1
0
Cs in ppm
0
1
10
100
1000
10000
Rb in ppm
1:1
1:2
1:5
Karl August Kropbach
Böschlisgrund
Riggenbach
Tirolergrund
Sulzburg qtz-vein
Fußwinkel et al., 2013
Brandenberg fl-qtz vein
Burisch et al., submitted
Wurmbach
Badenweiler

Figure 17

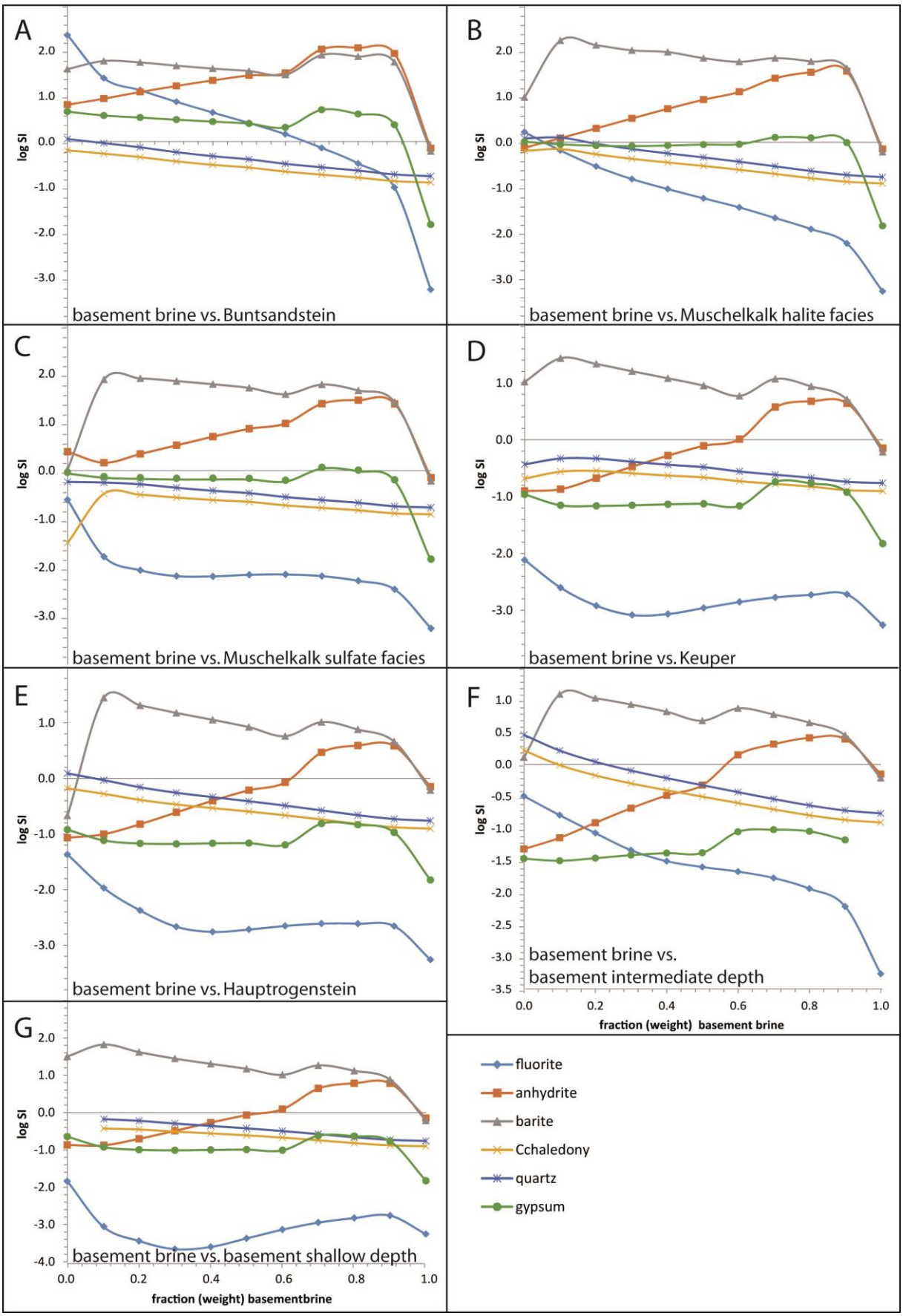
A
log SI
basement brine vs. Buntsandstein
B
log SI
basement brine vs. Muschelkalk halite facies
C
log SI
basement brine vs. Muschelkalk sulfate facies
D
log SI
basement brine vs. Keuper
E
log SI
basement brine vs. Hauptrogenstein
F
log SI
basement brine vs.
basement intermediate depth
fraction (weight) basement brine
G
log SI
basement brine vs. basement shallow depth
fraction (weight) basementbrine
fluorite
anhydrite
barite
Cchaledony
quartz
gypsum

Figure 18

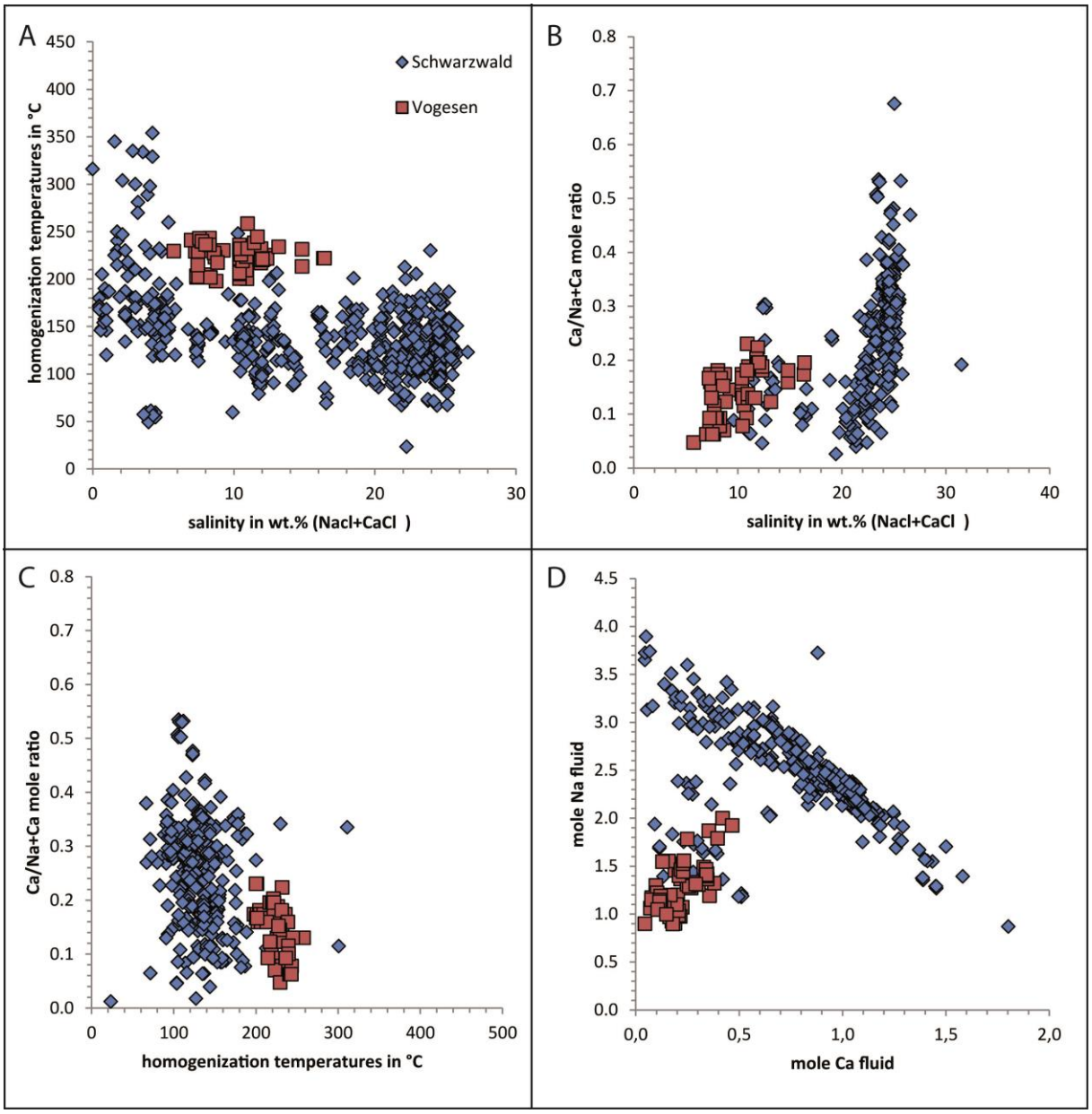
A
homogenization temperatures in °C
salinity in wt.% (Nacl+CaCl)
Schwarzwald
Vogesen
B
Ca/Na+Ca mole ratio
salinity in wt.% (Nacl+CaCl)
C
Ca/Na+Ca mole ratio
homogenization temperatures in °C
D
mole Na fluid
mole Ca fluid

Figure 19

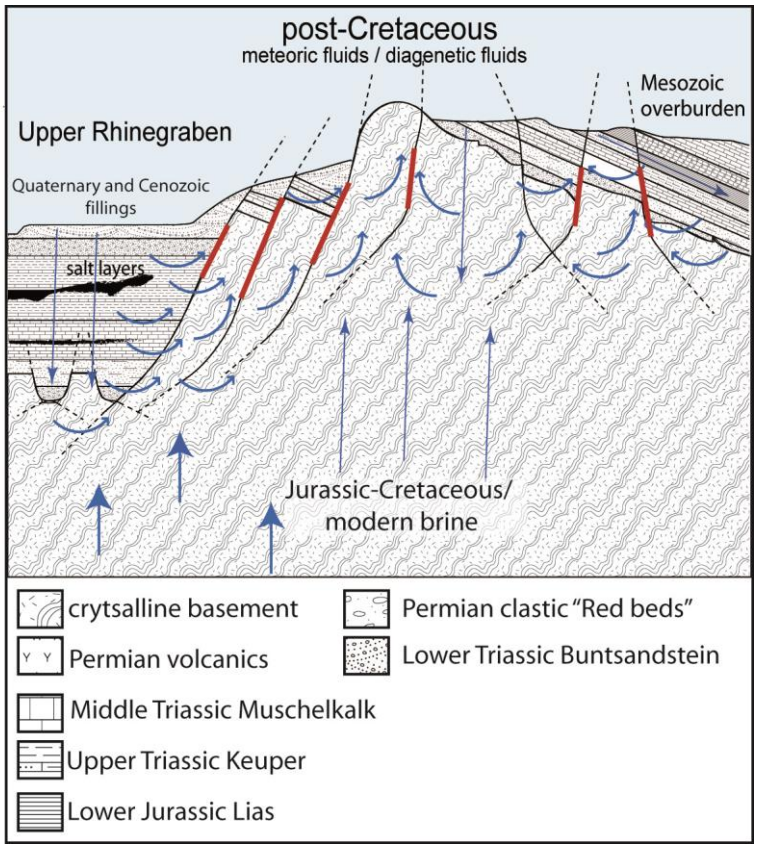
post-Cretaceous
meteoric fluids / diagenetic fluids
Mesozoic overburden
Upper Rhinegraben
Quaternary and Cenozoic fillings
salt layers
Jurassic-Cretaceous/ modern brine
crytsalline basement
Permian clastic "Red beds"
Permian volcanics
Lower Triassic Buntsandstein
Middle Triassic Muschelkalk
Upper Triassic Keuper
Lower Jurassic Lias

group	age	mineralogy	mineralisation	structural position	age constraints	fluid type	salinity in wt.% ($NaCl+CaCl_2$)	T_h in °C	Cl/Br mass ratio
i	Carboniferous	quartz-tourmaline	W-Sn	Spatially associated and genetically related to specific granites	U-Pb age of host granite	H_2O-NaCl±(CO_2±CH_4)	0-4	130-390°C	48-146
ii	Permian	quartz	Sb±Ag±Au	Only in basement rocks (granite and gneiss)	High fluid temperatures >250°C never reached again after Permian times by the SW German basement at shallow depths; comparison with very similar veins from the Taunus	H_2O-NaCl-KCl	<5	99-300°C	94
iii	Triassic-Jurassic	quartz-hematite	Fe	Only in basement rocks (granite and gneiss)	(U-Th)/He age	H_2O-NaCl-KCl & H_2O-NaCl-$CaCl_2$	0.7-3.3 & 23.3-25.8	121-224°C	60-112
iv	Jurassic-Cretaceous	fluorite- quartz-barite barite-quartz	Pb-Zn-Cu-Ag & U-Bi-Co-Ni-Ag & Fe-Mn	From >2000 m below the basement/cover unconformity up to the boundary between Lower and Middle Triassic sediments	Rb-Sr and U-Pb age-dating	H_2O-NaCl-$CaCl_2$	20-28	50-180°C	49-824
v	post-Cretaceous	quartz-barite-fluorite	Pb-Zn-Cu-Ag & Cu-Ni-Bi-Ag	Spatially closely associated with Upper Rhinegraben faults or tributary fault systems	Structural position on Rhinegraben-related faults	H_2O-NaCl-$CaCl_2$± (SO_4±CO_2±HCO_3)	0-25	50-194°C	2-144

Table 1 Types of veins and fluid signatures of the Schwarzwald ore district modified after Walter et al. (2016) and references therein.

Mineralization type	location	calcite	dolomite	siderite	quartz	barite	fluorite	gypsum (pseudomorph)	galena	fahlore	sphalerite	chalcopyrite	pyrite	gersdorffite	native arsenic
Type 1: Quartz-native arsenic	Michael and Silbereckle mine, Lahr-Reichenbach (late stage)				xx	x			x		xx		x		xx
	Josefi mine, Schuttertal (late stage)				xx	x					xx		x		x
Type 2a: Quartz-galena±barite	Badenweiler (Haus Baden, Wilhelminenstollen)				xxx	xxx	xx	x	xxx		x	x			
	Amalie, Grunern			x	xx	x	x		x	x	x	x	x		
	Herrenwald im Münstertal														
	Kropbach West				xx	x			x	x	x		x		
	Wildsbach Ost				xx	x			x	x	x		x		
	Galgenhalde Nord				xxx	x			xx	x	x		x		
	Galgenhalde Süd			x	x	xx			xx	x	x	x	x		
	Prinzbach				xx	xxx			x		x	x			
	Katzental				xxx	x			x	x	x	x			
	Steinebächle (Alsace, France)							x							
	Etzenbach HG				xx	x	x		x	x	x	x	X		
Type 2b: Barite-galena±quartz	Badenweiler (Otto, Karlstollen)														
	Riester and Himmelsehre, Sulzburg				xxx	xxx	xx		xx	x	x		x		
	Bierenstiel					xxx			x		x	x	x		
	St. Gotthardhof, Staufen				x	xxx			x	x	x	x	x		
	Krebsgrund				xx	xxx			x	x	x	x			
Type 2c: Barite-galena	Katzensteig, hSt. Wilhelm (upper levels)				x	xxx	xx	x	xx	x	x	x		x	
	Michael and Silbereckle mine, Lahr-Reichenbach (main stage)				x	xxx			xxx						
	Josefi mine, Schuttertal (main stage)				x	xxx			xxx						
	Segen Gottes mine, Freiamt					xxx			xx	x	x	x			
	Silberloch mine, Freiamt				x	xxx			xx	x					
	Marianne mine, Prinzbach-Emersbach	x		x	x	xxx			xx						
	Freiamt Sexau Schlossberg Gegentrum				x	xxx			xx						
	Lingellöcher			x	xx	xx			x	x	x	x			
	Schwarzhalde				xxx	xx			x		x				
Type 2d: Quartz-spahlerite breccia	Schauinsland	x	x	x	x	xxx			x	x	xx	x			
	Teufelsgrund				xx	x	xx				x				
	Karl August Kropbach			x	xxx					x	xx	x			
	Porphyrbruch Kropbach			x	x	x					xx		x		
	Kropbach Hof			x	xx	x			x	x	x	x	x		
	Unterer Steinbrunnen			xx	xx	xx			x	x	x				
	Laitschenbach			x	xx	x			x	x	x		x		
Type 3a: Barite-galena-quartz-fahlore-carbonate	Prinzbach village			xxx	xxx	xx			xxx	x	x	x			
	Eichhalde near Prinzbach			x	x	xxx			xx	xx		x			
	Caroline mine, Freiamt				x	xxx			x						
	Maria Theresia, Kropbach	x		xx	xx	xx			x	x	x	x	x		
	Ludwig Heinrich, Kropbach			xx	xx	x			x	x	x	x	x		

	Baderskopf			x	x	xxx			xx	x	x	xx	x		
Type 3b: barite-carbonate	Neuenbürg mining district	xx				xx									
	Reutbachklinge (late stage)	xx				xx	x								
	Diersburg-Zunsweiser veins			x		xxx									
	Diersburg-Reichenbach veins			x		xxx									
Type 4: Carbonate-fahlore/chalcopyrite	Rotenbach, Feldberg	xxx	x	x	x				x	xx	x	xx		xx	
	Hohe Tanne, Waldkirch	xx	xx	xx	xx					xx		xx		x	
	Felsenkeller mine, Staufen			xxx	x	x						x		x	
	Riggenbach, Münstertal (late stage)			xxx	x	x				x		xxx		x	
	Süßenbrunn, Münstertal			xxx	xxx	xxx	xx		x	x	x	xxx		x	
	Gabler Gang			x	xxx	xx	xx		x	x	x	x		x	
	Kindler vein near Gabel vein			xx	xx	x	x		x	x	x	x	x		
	Dietzelbach Ost, Münstertal			xx	x	xx			x	x	x	x		x	
	Böschlisgrund, Sulzburg			xx	xxx	x			xx	x	x	xx		x	
	Breitmatt, Münstertal			xx	xxx	x						x			
	Wildsbach Süd, Münstertal			xx	xx	xx			x		x	x	x		
	Laisacker, Münstertal			xx	xxx	x			x	x		xx			
	Karl August Kropbach (crosscutting vein)			xx		x						x	x	x	
	Schlossberg Ost			x	x	xxx	xx				x				
	Schlossberg West			x	x	xxx	x		x	x	x	X			
Type 5a: barite-chalkopyrite (fahlore)	Daniel im Drehs					xxx				x					
	Bad Antogast					xxx									
	Pfaffenbach					xx						x			
	Fuchsloch bei Hornberg				x	xxx						x			
Type 5b: quartz-chalkopyrite	Caroline im Eberbächle			x	xx	xxx						x			
	Silbergründle (late stage)			xx											
	Benedikt im Drehs					xxx						x			
	Gangzug Suggental	x	x	x	xxx	xx			x		x	xx			
Type 5c: barite-(quartz) not mineralized	Dürrer Buck Ost					xx	x								
	Neubulach (late stage)				xxx										
	Haidflüh bei Wembach				x	xx									
	Menzenschwand (late stage)					xx									
	Rammelsbacher Eck				xxx	xxx							x		
	Rammelsbacher Schwerspatgrube				x	xx	xxx								
	Fuchslöcher Martinsmoos					xx	x								
	Tirolergrund (late stage)					xxx									
	Wonnen Süd					xxx									
	Heidenknie					xxx									
	Fohrenberg			x		xx									
	Kohlrain			x		xxx									
	Oberer Steinbrunnen					x									
Type 5d: quartz-(barite) not mineralized	Wurmbach				xxx	x	x								
	Calmbach quarry Würzbach				xxx										
	Calmbach Radstraße				xxx										
	Klosterberg bei Enzklösterle				xxx										
	Speichel				xxx	x							x		

	Speichel Gipfel				xxx	x							x		
	Josefhalden Mitte				xx	x							x		
Type 5e: quartz amethyst	Finkerstal				xxx	x			x	x	x	x	x		
	Amethystgang Dürrer Grund				xx										
	Dottinger Halde				xx										
Type 6: Carbonate-galena	Giesenbächle, Lahr-Reichenbach			xxx	xx	xx			x	x					
	Zähringen		xxx			xx		xx	x		x				
	Bleibach	x	x	xxx	x				xx		xx				
	Bernhard mine, Hausach	xxx	xx	x	x	xxx		xx	xx	x	xx	x			
	Maria Theresia mine, Hausach	x		x		x	x		x	x	x	x	x		
	Silbereck, St. Wilhelm	xxx	x	x	x	x			xx			x			
	Fuchsdobel St. Wilhelm	x		xx	x				x	x	x	xx	x	x	
	Kammendobel		xx			x			x			x	x		
Type 7: Carbonate	Freiburg-Wittnau		xxx										x		
	Hugenwaldtunnel	x	xxx			x			x		x		x		
	Wattkopftunnel, Ettlingen	x	xx	xx	x	x									
	Michael mine, Lahr-Reichenbach (last stage)	x	x									x	x		
	Schauinsland (Late stage)	xxx													
	Artenberg (late stage)	xx													
	Merzhausen		xx										x		
	Lütschenbach	xx	xx												
	Brandenberg (late stage)		xxx												
	Teufelsgrund (late stage)	xx													
	Johann am Burgfelsen (late stage)	x													
	Zähringen	xx													
Type 8a: fluorite-barite-quartz	Aitern														
	Dey bei Schnellingen				x	xxx	xx		x		x	x			
	Anna bei Fahl														
	Teufelsgrund (ore stage1)				x	x	xxx		x	x	xx	x	x		
	Babara am Kinzigsteg				x	xxx	xxx		x						
	Erzengel Gabriel				x	xxx	xxx		x						
	Ludwigs Trost im Kutschbach			x	x	xxx	xxx		x	x					
	Fortuna Gelbach			x	x	xxx	xxx		x	x					
	Segen Gottes Schnellingen				x	xx	xx			x	x	x			
Type 8b: barite fluorite	Gnade Gottes bei Dietental					xx	xx					x			
	Barbara, Urban, Anton and Josef bei Schnellingen				x	xxx	xxx		x						
Type 8c: fluorite	Käfersteige (late stage)						xxx								
	Grunbach (late stage)		x			xx	xxx								
Type 9: Single mineralizations without systematics	Kobaldgrube Sulzburg		x		x	xxx	x		x	x	x	x			
	Rollenbergtunnel Bruchsal	xx	x	x	xx	xx		xx	x	x	x	x	x		x
	Wattkopftunnel Ettlingen	x	x	x	x	x		x	x	x	x		x		

Table 2 locality description

Fluid signature	$T_{m,ice}$ in °C	$T_{m,hh}$ in °C	$T_{m,sylvite}$ in °C	$T_{m,sulfate}$ in °C	$T_{t,CO2}$ in °C	$T_{m,clath}$ in °C	T_f in °C	T_{eut} in °C	Salinity In wt. % (NaCl+ $CACl_2$)	T_h in °C	Volume proportion in %	Fluid signature	volatiles
A	0 to -5	-21.2	-	-	-	-	-30to -45	-21.2	0 to 5	50 to 354	LV10-LV1	H_2O-NaCl-(HCO_3^-, CO_3^{2-})	HCO_3^- or CO_3^{2-}
B	-18.5 to -29.0	-28.5 to -17.5	-	-	-	-	-70 to -100	-52	20-26	70 to 230	LV15 to LV1	H_2O-NaCl-$CaCl_2$	
C	-2.6 to -18.0	-20.9 to -25.8	-	-	-	-	-70 to -100 and -30 to -45	-21.2 and -52	0.9 to 20	59 to 202	LV15 to LV1	H_2O-NaCl-($CaCl_2$)	
D	-4.7 to 7.6	-	-	-	-56.8	4.9 to 5.9		-21.2	<5	134 to 219	L(LV)10 to L(LV)20	H_2O-CO_2-(NaCl)	CO_2
E	-10.9 to -15	-	20 to 24	43 to 63	-	-	-70 to -100	-52	Unknown intermediate	98 to 202	LV10 to LV5	NaCl-KCl-$CaSO_4$-H_2O	SO_4
F1	-9.7 to -17.4	-	22.5 to 24.5	60 to 75.2	-56.4 to -56.8	4.9 to 5.9	-40 to -60	-21.2	Unknown intermediate	210 to 307	L(LV)10 to L(LV)20	H_2O-CO_2-SO_4-NaCl-KCl	CO_2 and SO_4
F2	-0.1 to -0.8	-23 to -26		24 to 27	-56.6 to -56.9	5.1 to 6.3	-80 to -100	-52	~5	140 to 180	L(LV)10 to L(LV)20	NaCl-$CaCl_2$-KCL-H_2O-SO_4-CO_2	SO_4 and CO_2

Table 3 fluid characteristica

Location	Karl August	Böschlisgrund	Riggenbach	Tirolergrund	Wurmbach	Badenweiler
Li (µg/g)	5710	1070	26830	15700	280	3150
B (µg/g)	1660	1250	2160	3260	320	70
S (µg/g)	91620	7990	2930	63800	2750	490
Co (µg/g)	290	630	250	400		
Ni (µg/g)	5150	360	16390	1630		
Cu (µg/g)	3830	10	1870	3980	70	8
As (µg/g)	3370	98	1520	4560	220	440
Br (µg/g)	9760	10050	5890	7540	4290	2230
Rb (µg/g)	470	120	1910	1200	70	36
Sr (µg/g)	3090	1930	2440	2830	1680	450
Mo (µg/g)		970	250	3620		
Sb (µg/g)	3120	103	8420	440	3858	170
Cs (µg/g)	230	8270	320	8000	70	50
Ba (µg/g)	3890	80	13660	1080	350	30
Zn (µg/g)	7170	520	15660	39000	150	70
W (µg/g)	3750	40	3230	205		
Pb (µg/g)	17750	10	980	320	50	56
Ag (µg/g)					10	2
Tl (µg/g)					10	2
Cl/Br min	18	14	45	22	30	70
Cl/Br max	850	150	380	207	235	988

Table 4 maximum values of trace elements in single fluid inclusions

Sample input data	unit	Basement brine	Muschelkalk halite facies	Muschelkalk sulfate facies	Buntsandstein	Keuper	Jura Hauptrogenstein	basement shallow depth	basement intermediate depth
Ca^{2+}	mg/kg	1232	1705	1197	11700	229.3	461.9	429	127.8
Mg^{2+}	mg/kg	164	230.8	166.9	1900	75.75	81.3	149	3.79
Na^{+}	mg/kg	25000	123689	2388	63900	43.62	928	260	802.5
K^{+}	mg/kg	905	25.35	55.65	503	3.04	45.4	14.5	76.84
HCO_3^{-}	mg/kg	29.41	347.8	545.5	2431	564.4	960.7	2110	176.6
SO_4^{2-}	mg/kg	790	4020	1872	5894	320.8	291.4	509	158.7
Cl^{-}	mg/kg	42650	174784	5019	120500	118.7	1758	29	1518
pH		6	6.35	6.4	6.93	6.92	6	5.8	7.02
F^{-}	mg/kg	0.34	3.65	1.85	31	0.43	0.76	0.4	4.09
Ba^{2+}	mg/kg	12.5	b.d.l.	b.d.l.	2.3	0.5	0.01	0.5	0.16
Fe^{3+}	mg/kg	15.1	0.04	12.56	36	0.01	1.22	13	0.15
Li^{+}	mg/kg	44.5	0.85	2.43	41.2	0.03	0.34	0	8.68
Pb^{2+}	mg/kg	2.42	0.01	b.d.l.	b.d.l.	b.d.l.	b.d.l.	12	b.d.l.
U^{4+}	mg/kg	b.d.l.	b.d.l.	b.d.l.	0.59	b.d.l.	b.d.l.	b.d.l.	b.d.l.
Zn^{2+}	mg/kg	0.59	0.2	b.d.l.	0.07	0.04	b.d.l.	10	0.01
Cu^{2+}	mg/kg	0.81	0.1	b.d.l.	b.d.l.	b.d.l.	b.d.l.	b.d.l.	b.d.l.
Co^{2+}	mg/kg	b.d.l.	b.d.l.	b.d.l.	b.d.l.	b.d.l.	b.d.l.	b.d.l.	b.d.l.
Ni^{2+}	mg/kg	b.d.l.	b.d.l.	b.d.l.	0.03	b.d.l.	b.d.l.	b.d.l.	b.d.l.
SiO_2(aq)	mg/kg	93	3.91	8.72	15.14	5.57	7.9	0	58.38
Sr^{2+}	mg/kg	111	32.12	14.63	485	0.43	6.07	0	3.13
O_2(aq)	mg/kg	1.00E-05	4.5	1.3	1.3	0.26	b.d.l.	0.1	b.d.l.
Temperature	C	300	20	20	20	20	28	20	60

Table 5

Anhang 5

Burisch, M., Walter, B.F., Wälle, M., & Markl, G. (submitted to Chemical Geology) Tracing fluid migration pathways in the root zone below unconformity-related hydrothermal veins: insights from trace element systematics of individual fluid inclusions

akzeptiert zur Veröffentlichung	Anzahl der Autoren	Position des Kandidaten in der Autorenliste	Wissen-schaftliche Idee des Kandidaten (%)	Datengenerier-ung des Kandidaten (%)	Analysen und Interpretat-ionen des Kandidaten (%)	Verfassen der Publikation durch den Kandidaten (%)
nein	4	2	40	90	40	40

Tracing fluid migration pathways in the root zone below unconformity-related hydrothermal veins: insights from trace element systematics of individual fluid inclusions

Mathias Burisch*†, Benjamin F. Walter†, Markus Wälle[×], Gregor Markl†

†Department of Geosciences, Eberhard Karls University Tübingen, Wilhelmstrasse 56, 72074 Tübingen, Germany

[×]Institute of Geochemistry and Petrology, ETH Zurich, Clausiusstrasse 25, CH-8092 Zürich, Switzerland

*Corresponding author: mathias.burisch@ifg.uni-tuebingen.de

Keywords: ore mineralization, fluid mixing, Rb/Cs, clay formation, alteration, water-rock interaction

1. **Abstract:**

The temporal evolution of fracture networks (root zones) below hydrothermal veins and their impact on fluid chemistry, vein mineralogy and ore formation is insufficiently understood for unconformity-related hydrothermal veins in regions of extension, such as the common epithermal sediment- and basement-hosted Pb-Zn deposits. As metals and other trace elements are presumably mobilized during water-rock interaction of highly saline brines with crystalline basement rocks, the evolution of these fracture zones seems to play a major role for hydrothermal ore formation.

To shed light on this topic, laser ablation-inductively coupled plasma-mass spectrometry (LA-ICPMS) microanalysis of individual, texturally well-characterized fluid inclusions, hosted in fluorite and quartz of the Jurassic-Cretaceous Brandenberg fluorite-barite-quartz-galena-sphalerite vein were carried out. Fluid mobile elements (Rb, Cs, Li, W, Ba, Zn, Pb, Sr), preferentially released by the alteration of primary rock-forming minerals (process tracer) were analysed as well as the Cl/Br ratio (source tracer) of fluid inclusions in genetically early fluorite and later quartz. A distinct decrease of trace elements within the fluid inclusions with time indicates successive alteration of primary minerals at the fracture wall to clay minerals with consecutive fluid pulses. A maximum concentration of trace elements in the fluid and consequent ore precipitation is associated with the initial phase of formation of a fracture root. Later fluid pulses migrate along pre-existing fractures so that the amount of fresh reactive rock material decreases with each fluid pulse. As a consequence, multiple generations of ore minerals require the formation of new fracture branches in the root zone of hydrothermal veins. Therefore, it seems that cataclastic zones below hydrothermal veins essentially control ore formation, and their tectonically induced dynamics might be one key parameter that governs the temporal interval of ore precipitation.

2. Introduction

The nature of the feeding systems of hydrothermal unconformity-related vein-type deposits and of the detailed relation between active tectonics, fluid flow and mineral precipitation is poorly constrained. Few studies have addressed feeder systems of other hydrothermal systems: Richards et al. (1987) and Everett et al. (1999) describe alteration and concomitant metal depletion of the wall rock in large-scale

fractured root zones below volcanogenic massive sulphide and Irish-type deposits, and Seedorf et al (2008) investigated root zones in porphyry systems and noted the important role of these zones for understanding the genesis of the superimposed ore system. If, however, this interconnected network is a new fracture system related to recent tectonics (which also is responsible for vein opening), or if this system has been active over a long time and discontinuously feeds into reactivated mineralizations, is completely unknown, as yet, no approach has been proposed to distinguish between these two types. This is exactly what we try to address in the present contribution by proposing a new geochemical tool, which allows distinguishing “old” from “new” fracture systems. In contrast to previous studies (e.g. Richards et al. 1987; Seedorff et al. 2008), which are based on direct petrographic investigations of the root zones, this contribution focuses on chemical tracers archived in the fluid inclusions of the hydrothermal veins above the root zones. This approach renders it possible to characterize the temporal evolution of the root zone below a specific hydrothermal vein, even if the actual root zone is not exposed/accessible.

Previous work on epithermal sediment- and basement-hosted unconformity-related vein deposits mainly focused on the chemical and hydraulic processes that cause ore precipitation, especially on fluid mixing (e.g. Russell et al., 1981; Sverjensky, 1981; Gleeson et al., 2001; Muchez et al., 2005; Boiron et al., 2010; Leach et al., 2010; Richard et al. 2011; Bons et al., 2014; Fußwinkel et al., 2013; Walter et al., 2015 and references therein). Most of these studies deal with a combination of microthermometry (Banks et al., 2000; Derome et al., 2007; Wilkinson, 2010; Staude et al., 2012; Fußwinkel et al., 2013; Walter et al., 2015 and references therein), stable and radiogenic isotopes (O-C-H-Sr-Cl-Br-Pb-Zn-Mg) (e.g. Gleeson et al., 2001; Wilkinson et al., 2005; Richard et al., 2011; Walter et al., 2015 and references therein), trace element studies of fluids and gangue (Fußwinkel et al., 2013 and references therein). As shown by numerous workers (e.g. Sverjensky, 1981; Boiron et al., 2010; Gleeson and Yardley, 2002 and references therein) fluid mixing occurs between (I) hot, deep-seated fluids from the crystalline basement, and (II) cooler, sediment-derived fluids from the overburden sequence (e.g. Richard et al., 2011; Staude et al., 2009, 2012; Boiron et al., 2010; Fußwinkel et al., 2013; Walter et al., 2015; Walter et al., 2016 and references therein). Most authors suggest the basement brine to be metal-rich (Boiron et al., 2010; Bons et al., 2014; Fußwinkel et al.,

2013, Wilkinson et al. 2005) in unconformity-related veins.

In contrast to the referred contributions, our study focuses on the temporal evolution of fluid migration paths, which govern the chemical composition (focusing on trace elements) of the basement fluid involved in ore-forming processes. Therefore, we focus on the investigation of one representative and well-characterized Jurassic vein in detail, rather than to compare different localities. Conceptually, we argue as follows: If the fracture system, through which the basement fluid percolates, remains physically unchanged over the whole period of mineral precipitation in a specific vein, microthermometric data should not change significantly over time, while certain chemical tracers (Rb/Cs, Li, W, Pb, Zn) in fluid inclusions of vein minerals should show a systematic variation with time. After initial fracture opening, fresh primary host minerals like feldspar or micas become altered to secondary minerals like e.g. illite or chlorite (Stober and Bucher, 2004; Brockamp, 2005) in non-magmatic epithermal systems. Early fluids should be rich in elements released by primary, but not incorporated into secondary minerals. The absolute concentrations of these elements should successively decrease with increasing fluid-rock interaction, since the amount of primary minerals at the fracture-fluid interface decreases. In contrast, absorption effects of fluid components on secondary mineral surfaces should increase with progressing alteration of the fracture wall.

The Rb/Cs ratio is a suitable tracer for this approach, since both elements typically substitute for K in primary rock-forming minerals, but fractionate during clay mineral formation (Göb et al., 2013 and references therein). Rb is incorporated into the structure of clay minerals, while Cs is adsorbed on clay surfaces (Göb et al., 2013 and references therein), and this difference causes fractionation in the fluid. Hence, the Rb/Cs ratio of a fluid can be modified by alteration of feldspars and biotite to clay minerals (Aquilina et al., 1997; Göb et al., 2013, and references therein). As a consequence, Rb/Cs ratios <2 are typical of fluids, which interacted with unaltered crystalline rocks, while Rb/Cs ratios of ~2 represent equilibrium conditions during alteration of primary minerals to clay minerals. Rb/Cs ratios >5 indicate water-rock interaction with pre-existing clay minerals (no alteration of primary phases) (Göb et al., 2013). Further elements like W, Zn and Pb are released by feldspars (Burisch et al., 2015), Li and Zn by biotites during water-rock interaction (Burisch et al. 2015) and should therefore systematically decrease in the fluid with increasing alteration of the fracture walls.

Epithermal, unconformity-related hydrothermal veins containing Pb-Zn, Fe-Mn, Cu or also Ag ores, occur frequently and widespread in central Europe, where the Variscan basement is exposed and was subjected to extension (Boiron et al., 2010, and references therein). The characteristic mineral assemblage typically consists of fluorite, quartz, sometimes barite, with galena and sphalerite as the most common ore minerals in addition to fahlores, chalcopyrite and other, rarer sulfides and sulf-arsenides. The majority of these veins formed during the Jurassic, when extensional stress regimes related to the opening of the northern Atlantic prevailed (Staude et al., 2009; Boiron et al., 2010; and references therein). Mixing of two highly saline brines, a sedimentary and a deep-seated basement one, across the basement-cover unconformity induced mineral precipitation (Staude et al., 2009, Boiron et al., 2010; Fußwinkel et al., 2013; and references therein).

Interconnected fracture systems in the crystalline basement are the major fluid pathways (e.g. Stober and Bucher 2004 and references therein) for deep-seated brines. They govern both direction and chemistry of a migrating fluid (Richards et al., 1987; Everett et al., 1999; Boiron et al., 2010; Burisch et al. 2015) since along these connected fractures, the reaction surface of fluid and rock is significantly increased. This changes with time: a juvenile fracture provides a large volume of fresh, unaltered minerals, which become successively altered to secondary phases (Jébrak, 1997; Stober&Bucher, 2004; Kendrick&Honda, 2008; Seelig&Bucher, 2010). Later fluid pulses, migrating on the same fracture networks will find less unaltered mineral surfaces that can potentially react. Hence, the spatial and temporal evolution of a fracture zone has a significant impact on the fluid chemistry, and therefore on the ore-forming potential of a basement fluid (Jébrak, 1997). In this contribution, the temporal evolution of fracture networks below unconformity-related hydrothermal veins is indirectly monitored based on chemical data of fluid inclusions in mineralized veins. This study, hence, provides new insight into the relationship between host rock alteration in the root zone and ore deposition at higher stratigraphic levels.

3. Regional geology and hydrothermal mineralizations of the Schwarzwald mining district

The Schwarzwald is an asymmetrically exhumed basement window, dominantly composed of granites

and gneisses. Uplift and erosion was associated with the formation of the Tertiary Upper Rhinegraben Rift.

Before opening of the Rhinegraben the basement rocks were covered by 1.5 km thick Triassic and Jurassic sediments including middle Triassic evaporites (often containing halite) (Geyer and Gwinner, 2011; Walter et al., 2016). The oldest record of hydrothermal activity in the Schwarzwald goes back to 320Ma, but the temporal maximum of vein formation in the area was during the Jurassic-Cretaceous period (Staude et al., 2009). The sedimentary cover was tectonically undisturbed, since the prevailing extensional stress regime did not promote the formation of large-scale faults, tilting or rotation. Vein formation in the Jurassic-Cretaceous was initiated by mixing of two chemically distinct fluids (binary mixing) (Walter et al., 2015 and references therein), including the Brandenberg hydrothermal vein near Todtnau presented in this study. Fußwinkel et al. (2013), Bons et al. (2014), Walter et al. (2015) and Walter et al. (2016) showed that the two fluids involved in mixing are a highly saline, metal-rich basement fluid with low Cl/Br and a highly saline sedimentary fluid with high Cl/Br (halite dissolution). Therefore, the analyzed fluid inclusion composition reflects this mixed fluid. Changes in the proportion of the two fluids can be monitored by Cl/Br ratio of the single inclusions. Comparable deposits can be found in the Erzgebierge (Klemm 1994), the Bohemian Massif (Walther 1982; Ondrus et al. 2003), the Harz (Lüders et al., 1993), France (Boiron et al., 2010), Ireland (Wilkinson et al., 2005) and Morocco (Ahmed et al., 2009; Gasquet et al., 2005), just to name some examples.

4. **Sample material and analytical procedure**

A well-characterized sample containing early fluorite inter-grown with minor amounts of galena (Fig 1B) and overgrown by later euhedral chevron quartz was prepared for detailed texturally resolved fluid inclusion studies (Fig 1A and B). No clay minerals were observed in thin section. Both gangue minerals contain visible growth zones including several generations of petrographically unambiguous fluid inclusion assemblages (FIA). Analysed inclusion sizes range from 20-120µm.

Based on previous studies of our working group (Staude et al., 2009, Walter et al., 2015, and references therein), the Jurassic-Cretaceous Brandenberg vein in the Schwarzwald mining district (latitude: 47.841301; longitude: 7.972786) was selected for such a study (Fig 1A and B), since this

vein shows all characteristics typical of hydrothermal veins of the Jurassic-Cretaceous period in central Europe (Behr & Gerler, 1987; Behr et al., 1987; Baatartsogt et al., 2007; Staude et al., 2009; Boiron et al., 2010; Walter et al., 2016), clear relative age relations of gangue minerals and individual primary and pseudosecondary fluid inclusions sufficiently large for LA-ICPMS analysis of single inclusions. Measurements were done in genetically well-characterized fluorite and quartz.

Microthermometry was performed using a Linkam THMS-600 cooling-heating stage. Synthetic fluid inclusion standards were used for calibration. LA-ICPMS microanalysis of individual fluid inclusions was conducted with a Perkin Elmer Elan 6100DRC quadrupole ICPMS connected to an ETH-GeoLas 193 nm ArF excimer laser system at the ETH Zurich. An energy density of 15-20 J/cm^2 with a laser puls frequency of 10 Hz and a variable beam diameter of 5-30 µm was used. Analytical and standardization procedures are reported in Heinrich et al. (2003) and Seo et al. (2011). LA-ICPMS analyses of single fluid inclusions were performed for 27 elements (Li, B, Na, Mg, S, Cl, K, Ca, Mn, Fe, Co, Ni, Cu, Zn, As, Br, Rb, Sr, Mo, Sb, Cs, Ba, W, Tl, Pb, Bi and Si). Calcium was not quantified in FI hosted by fluorite, but was used for matrix correction. The same holds true for Si in quartz-hosted FI. All peaks signals of the analytes were checked for temporal correlation with the Na and Cl peak signals to preclude signals potentially derived by ablation of the host mineral and to verify that the measured elements are in solution.

Microthermometrically determined Na was used as internal standard, assuming a $CaCl_2$-NaCl-H_2O system (Steele-MacInnes et al., 2011). Since Na concentrations vary less than 0.5 wt.% within one FIA, average values of Na were used for each FIA. Data handling was carried out using the SILLS software package of Guillong et al. (2008). The complete dataset is given in the electronic supplement.

5. **Results**

The data set consists of 215 analyses of single fluid inclusions hosted in fluorite and quartz, including primary (p) and pseudo-secondary (ps) fluid inclusion assemblages (FIA) in the fluorite and exclusively primary FIA in the quartz sample. In contrast to distinct differences in trace element chemistry of FIA in fluorite and quartz, microthermometric data of FIA in both minerals strongly overlap and show the same (narrow) variability (see Fig. 2A and 2B). FIAs in both minerals show a

narrow range of salinities (22.0-24.5wt.%, $NaCl+CaCl_2$) and homogenization temperatures T_h (uncorrected 130-192°C). First melting can be detected at around -50°C, freezing during cooling runs happens at -70 to -100°C, which indicates a ternary $NaCl-CaCl_2-H_2O$ system with a eutectic temperature of -52.0°C. Ice is the last-melting phase. The final melting temperature of ice is in the range of -21.0° to -24.5°C, that of hydrohalite between -21.7° and -25.1°C. The molar Ca/(Ca+Na) ratios range from 0.09-0.28. Within one trail, salinity and T_h are almost constant, but they show small variations between different trails within one sample (Fig 1B).

LA-ICPMS analyses could be performed on 110 fluid inclusions. In the following, mean concentrations are presented. Fluid inclusions in early fluorite have average concentrations of 2030 µg/g Li,, 1280 µg/g Br, 930 µg/g Rb, 350 µg/g Sr, 1150 µg/g Cs, 180 µg/g Ba, 470 µg/g Zn, 310 µg/g W, 280 µg/g Pb and Cl/Br ratios between 20-740, while average concentrations in fluid inclusions hosted by younger quartz have 350 µg/g Li, 1210 µg/g Br, 20 µg/g Rb, 400 µg/g Sr, 20 µg/g Cs, 25 µg/g Ba, 26 µg/g Zn, below detection limit (except one inclusion which has 12 µg/g) W, 20 µg/g Pb and Cl/Br ratios of 38-290 (Fig. 3 A, B, C, D and E). Cl/Br and Sr vary unsystematically, while Rb/Cs, Li, W, Cs, Rb, Ba, Pb and Zn show distinctly different values in early fluorite compared to later quartz.

6. Discussion and conclusions

a. The Cl/Br ratio as source tracer

Fußwinkel et al. (2013) and Walter et al. (2016) showed that the Jurassic hydrothermal veins formed by a strictly binary mixing between a basement brine with low Cl/Br ratios (60-100, Walter et al., 2016 and references therein) and a sedimentary fluid, which has high Cl/Br ratios due to halite dissolution (Cl/Br = 10.000, Stober and Bucher 2004). Fast mineral precipitation led to a large scatter in Cl/Br ratios in one FIA, since during rapid mixing the proportion of each involved fluid component can vary (Fußwinkel et al., 2013).

Although the analysed fluid inclusions show a range in Cl/Br ratios from ~20 to ~700 (Fig 2A), there is no systematic variation in Cl/Br from old to young FI, indicating that the variation of Cl/Br is not caused by a systematic variation of the degree of mixing, but is rather an effect of (unsystematic) rapid

mixing (Fußwinkel et al., 2013). Therefore, the Cl/Br ratio of analysed fluid inclusions implies, that the general mixing ratio does not significantly change from early fluorite to late quartz formation (Fig 2A), which is important for further considerations.

b. Rb/Cs and trace elements

The Rb/Cs ratio and the maximum values of Rb, Cs, Li, Pb+Zn, W and Ba concentrations decrease from early fluorite to late quartz (Fig 2 B, D, E and F). Strontium and Cl/Br do not follow this temporal variation (Fig 2 A and C).

When fluid migration paths are established first ("fracture break-up"), abundant fresh mineral surfaces are present along the fracture walls, reacting immediately with the percolating fluid. Therefore, first generation fracture fluids are enriched in Rb, Cs and other fluid-mobile trace elements released by feldspar (W, Pb, Ba, Zn and Sr) and mica (Li, Zn and Ba). The enrichment of these elements indicates, that the basement fluid involved in fluorite precipitation was governed by the alteration of primary host minerals to clay minerals before it ascended and mixed with a sedimentary fluid. Average Rb/Cs values of FIAs in the fluorite of 1.5 strongly support this argument.

The lower values of Rb, Cs, W, Pb, Zn, Li and Ba in the later quartz indicate that later fluid batches migrated along the same fracture networks, rather than establishing new fracture systems. With each fluid pulse, the abundance of fresh rock material decreases, and therefore causes a decrease in the absolute concentration of trace elements in the ascending fluid. Since Rb is structurally incorporated into clay minerals and Cs is only adsorbed onto surfaces of clay minerals and remaining mica (Göb et al., 2013 and references therein), leaching the absorbed Cs results in lower Rb/Cs ratios compared to alteration of primary rock-forming minerals. This is in agreement with the decrease of Rb/Cs from early fluorite to late quartz. Low Rb/Cs of the quartz shows that the later fluid pulses did not dissolve clay minerals, which would result in high Rb/Cs ratios (typically above 2, Göb et al., 2013). As long as minor amounts of fresh rock material are still available along fracture zones, the Rb/Cs ratio positively correlates with the ratio of fresh/altered rock. As a consequence of progressing alteration, ore (galena) precipitation is associated with early fluorite, since the early generation of basement brine

253 was substantially richer in trace elements like Pb than the following fluid pulses. This is in good
254 agreement with the chemical modification of basement fluids along cataclastic fractures as discussed
255 by Jébrak (1997) and Burisch et al. (2015).
256 Empirical data of granitic and sedimentary fluids (Göb et al., 2013) combined with data of this study
257 were used to model an entire cycle of a hydrothermal fracture zone (Fig. 4). Meteoric/sedimentary
258 fluids have typically Rb/Cs above 2 (3.8 to 21.8, Göb et al., 2013). At some point, after these fluids
259 percolated through the crystalline basement they will obtain steady-state Rb/Cs ratios of around 2
260 (Stage I). This does not change, until new fracture systems open, providing vast amounts of fresh
261 granitic rock material. This drastically decreases the Rb/Cs of the fracture fluid and increases trace
262 metal concentrations tremendously (stage II). In stage III the amount of available fresh rock and
263 released trace metals in the fluid is substantially decreased.
264 Although both Rb and Cs concentrations decrease in stage III, Cs concentrations decrease to a lesser
265 extent and therefore, the Rb/Cs ratio further decreases until no fresh rock is available any more (end of
266 stage III). After all fresh rock is consumed (stage IV), four general possibilities of fracture fluid
267 evolution can be assumed. A) The Rb/Cs of the fluid instantaneously increases to a value of 2, since
268 fluids in equilibrium with granite flood the system. B) Rb/Cs increases slowly towards granitic
269 equilibrium, but before the fluid reaches equilibrium values of 2, new fractures open and a new cycle
270 begins. C) Similar to B), but the fracture fluid reaches equilibrium with the granite before a new cycle
271 starts. D) An externally derived sedimentary fluid (high Rb/Cs) enters the fracture (see Fig. 4).
272 Combining the Rb/Cs ratio with Pb, Zn, W, Li and Ba concentration, this data allows reconstructing
273 the temporal evolution of a fracture network below a hydrothermal vein. This evolution has a major
274 impact on fluid chemistry and therefore ore precipitation. Again, the important role of fluid
275 modification and metal uptake along cataclastic fractures has been shown (see also Burisch et al.
276 2015). After the initial break-up of the fracture network, successive fluid pulses continued to migrate
277 on the same fractures (Jébrak, 1997) during the formation of the Brandenberg vein. Reactivation and
278 concomitant fluid migration along pre-existing fracture zones is associated with successive alteration
279 of the fracture walls. The temporal increase of wall rock alteration has a major impact on fluid
280 chemistry and therefore on the mineralogy of the hydrothermal vein. As a consequence, metal

concentrations are highest in the earliest fluids in a specific fracture system, since large amounts of fresh wall rock are available. Accordingly, the younger quartz generation is barren. This implies that a dynamic fracture network is a substantial requisite for the formation of several ore generations in one hydrothermal vein, where the formation of new migration paths in the root of the hydrothermal vein provides sufficient fresh rock material to allocate the metals to consecutive fluid pulses (Fig. 4). On the other hand, metal and trace element concentrations in static fracture zones decrease in consecutive fluid pulses and show their maximum at the time of early fracture zone generation. These observations agree well with the observations made by Jébrak (1997), which link the stage of ore formation in hydrothermal breccia to the "wear" stage, which is the stage immediately following the initial formation of the breccia.

The conclusions of this contribution can only be applied to hydrothermal ore deposits, in which the metals and other trace elements are dominantly controlled by host rock alteration. As a consequence, these conclusions can only be applied to magmatic systems if the amount of dissolved trace elements derived from water-rock interaction relative to those of magmatic origin can be quantitatively determined.

7. Acknowledgements

We would like to thank Richard Tosdal for constructive comments, that helped to improve the manuscript significantly and S. Kaulfuß for sample preparation. This study was supported by the German Research Foundation (DFG), grant 2135/20-1.

8. References

Ahmed, A.H., Arai, S., Ikenne, M., 2009. Mineralogy and Paragenesis of the Co-Ni Arsenide Ores of Bou Azzer, Anti-Atlas, Morocco. Economic Geology, 104(2): 249-266

Aquilina, L., Pauwels, H., Genter, A., and Fouillac, C., 1997. Water-rock interaction processes in the Triassic sandstone and the granitic basement of the Rhinegraben: Geochemical investigation of a geothermal reservoir.: Geochimica et Cosmochimica Acta, v. 61, p. 4281-4295.

Baatartsogt, B., Schwinn, G., Wagner, T., Taubald, H., Beitter, T., & Markl, G. 2007. Contrasting paleofluid systems in the continental basement: a fluid inclusion and stable isotope study of hydrothermal vein mineralization, Schwarzwald district, Germany. Geofluids, 7(2), 123-147.

Banks, D.A., Green, R., Cliff, R.A., and Yardley, B.W.D., 2000. Chlorine isotopes in fluid inclusions: Determination of the origins of salinity in magmatic fluids: Geochimica et Cosmochimica Acta, v. 64, p. 1785–1789.

Behr, H. J., & Gerler, J. 1987. Inclusions of sedimentary brines in post-Variscan mineralizations in the Federal Republic of Germany—a study by neutron activation analysis. Chemical Geology, 61(1), 65-77.

Behr, H. J., Horn, E. E., Frentzel-Beyme, K., & Reutel, C. 1987. Fluid inclusion characteristics of the Variscan and post-Variscan mineralizing fluids in the Federal Republic of Germany. Chemical Geology, 61(1), 273-285.

Boiron, M. C., Cathelineau, M., and Richard, A., 2010. Fluid flows and metal deposition near basement/cover unconformity: lessons and analogies from Pb–Zn–F–Ba systems for the understanding of Proterozoic U deposits: Geofluids, v. 10, no. 1-2, p. 270-292.

Bons, P. D., Fusswinkel, T., Gomez-Rivas, E., Markl, G., Wagner, T., and Walter, B., 2014. Fluid mixing from below in unconformity-related hydrothermal ore deposits: Geology v. 42(12), p. 1035-1038

Burisch, M., Marks, M., Nowak, M. & Markl, G., 2015. The Effect of temperature and cataclastic deformation on salinity, halogen systematics and metal transport capacities of continental basement brines – an experimental approach: SGA abstract in: Proceedings of the 13th Biennial SGA Meeting, Nancy, France, 5 volumes, 2134 p.

Brockamp, O. C., N, 2005. A km-scale illite alteration zone in sedimentary wall rocks adjacent to a hydrothermal fluorite vein deposite: Clay Minerals, v. 40, p. 245-260.

Derome, D., Cathelineau, M., Fabre, C., Boiron, M.C., Banks, D., Lhomme, T., and Cuney, M., 2007. Paleo-fl uid composition determined from individual fl uid inclusions by Raman and LIBS: Application to mid-Proterozoic evaporitic Na-Ca brines (Alligator Rivers Uranium Field, northern territories Australia): Chemical Geology, v. 237, p. 240–254.

Everett, C., Wilkinson, J., and Rye, D., 1999. Fracture-controlled fluid flow in the Lower Palaeozoic basement rocks of Ireland: implications for the genesis of Irish-type Zn-Pb deposits: Geological Society, London, Special Publications, v. 155, no. 1, p. 247-276

Fußwinkel, T., Wagner, T., Wälle, M., Wenzel, T., Heinrich, C., and Markl, G., 2013, Fluid mixing forms basement-hosted Pb-Zn deposits: Insight from metal and halogen geochemistry of individual fluid inclusions: Geology, v. 41, p. 679-682.

Gasquet, D., Levresse, G., Cheilletz, A., Azizi-Samir, M.R., Mouttaqi, A., 2005. Contribution to a geodynamic reconstruction of the Anti-Atlas (Morocco) during Pan-African times with the emphasis on inversion tectonics and metallogenic activity at the Precambrian–Cambrian transition. Precambrian Research, 140(3): 157-182

Geyer, O. F., and Gwinner, M. P., 2011, Geologie von Baden -Württemberg. – 5., völlig neu bearbeitete Auflage, Stuttgart, Schweizerbart`sche Verlagsbuchhandlung (Nägele u. Obermiller), 627 p.

Gleeson, S.A., Wilkinson, J.A., Stewart, F.M., and Banks, D.A., 2001, The origin and evolution of base metal mineralising brines and hydrothermal fluids, south Cornwall, UK: Geochimica et Cosmochimica Acta, v. 65, p. 2067–2079

Gleeson, S., and Yardley, B., 2002, Extensional veins and Pb-Zn mineralisation in basement rocks: the role of penetration of formation brines, Water-Rock Interaction, Springer, p. 189-205.

Göb, S., Loges, A., Nolde, N., Bau, M., Jacob, D. E., and Markl, G., 2013, Major and trace element compositions (including REE) of mineral, thermal, mine and surface waters in SW Germany and implications for water-rock interaction. Applied Geochemistry, v. 33, p. 127-152.

Guillong, M., Meier, D., Allan, M., Heinrich, C., and Yardley, B., 2008, SILLS: a MATLAB-based program for the reduction of laser ablation ICP-MS data of homogeneous

materials and inclusions: Mineralogical Association of Canada Short Course, v. 40, p. 328-333.

Heinrich, C. A., Pettke, T., Halter, W. E., Aigner-Torres, M., Audétat, A., Günther, D., Hattendorf, B., Bleiner, D., Guillong, M., and Horn, I., 2003, Quantitative multi-element analysis of minerals, fluid and melt inclusions by laser-ablation inductively-coupled-plasma mass-spectrometry. Geochimica et Cosmochimica Acta, v. 67, p. 3473-3496.

Jébrak, M. 1997. "Hydrothermal breccias in vein-type ore deposits: a review of mechanisms, morphology and size distribution." Ore geology reviews **12**(3): 111-134.

Kendrick, M. A., et al. 2008. "New constraints on regional brecciation in the Wernecke Mountains, Canada, from He, Ne, Ar, Kr, Xe, Cl, Br and I in fluid inclusions." Chemical Geology 255(1–2): 33-46.

Klemm, W. 1994. Review of data on the composition of hydrothermal solutions during the Variscan and post-Variscan mineralizations in the Erzgebirge, Germany. Monogr. Series on Mineral Deposits, 31, 61-69.

Leach, D.L., Bradley, D.C., Huston, D., Pisarevsky, S.A., Taylor, R.D., and Gardoll, S.J., 2010, Sediment-hosted lead-zinc deposits in Earth history: Economic Geology and the Bulletin of the Society of Economic Geologists, v. 105, p. 593–625, doi:10.2113/gsecongeo.105.3.593.

Lüders, V., Gerler, J., Hein, U. F., & Reutel, C. H. R. 1993. Chemical and thermal development of ore-forming solutions in the Harz Mountains: a summary of fluid inclusion studies. Monogr Ser Miner Depos, 30, 117-132.

Muchez, P., Heijlen, W., Banks, D., Blundell, D., Boni, M., and Grandia, F., 2005, Extensional tectonics and the timing and formation of basin-hosted deposits in Europe: Ore Geology Reviews, v. 27, p. 241–267

Richard, A., Banks, D. A., Mercadier, J., Boiron, M. C., Cuney, M., & Cathelineau, M. 2011. An evaporated seawater origin for the ore-forming brines in unconformity-related uranium deposits (Athabasca Basin, Canada): Cl/Br and δ 37 Cl analysis of fluid inclusions. Geochimica et Cosmochimica Acta, 75(10), 2792-2810.

Richardson, C., Cann, J., Richards, H., Cowan, J., 1987. Metal-depleted root zones of the Troodos ore-forming hydrothermal systems, Cyprus. Earth and Planetary Science Letters, 84(2): 243-253.

Russell, M.J., Solomon, M., and Walshe, J.L., 1981, The genesis of sediment-hosted exhalative zinc + lead deposits: Mineralium Deposita, v. 16, p. 113–127

Seedorff, E., Barton, M.D., Stavast, W.J., Maher, D.J., 2008. Root zones of porphyry systems: extending the porphyry model to depth. Economic Geology, 103(5): 939-956.

Seelig, U. and K. Bucher 2010. "Halogens in water from the crystalline basement of the Gotthard rail base tunnel (central Alps)." Geochimica et Cosmochimica Acta 74(9): 2581-2595.

Seo, J. H., Guillong, M., Aerts, M., Zajacz, Z., and Heinrich, C. A., 2011, Microanalysis of S, Cl, and Br in fluid inclusions by LA–ICP-MS: Chemical Geology, v. 284, no. 1, p. 35-44.

Staude, S., Bons, P. D., and Markl, G., 2009, Hydrothermal vein formation by extension-driven dewatering of the middle crust: An example from SW Germany.: Earth and Planetary Science Letters, v. 286, p. 387-395.

Staude, S., Werner, W., Mordhorst, T., Wemmer, K., Jacob, D., and Markl, G., 2012, Multi-stage Ag-Bi-Co-Ni-U and Cu-Bi vein mineralization at Wittichen, Schwarz wald, SW Germany: Geological setting, ore mineralogy, and fluid evolution: Mineralium Deposita, v. 47, p. 251–276, doi:10.1007/s00126-011-0365-4

Steele-MacInnis, M., Bodnar, R., and Naden, J., 2011, Numerical model to determine the composition of H_2O–NaCl–$CaCl_2$ fluid inclusions based on microthermometric and

microanalytical data: Geochimica et Cosmochimica Acta, v. 75, no. 1, p. 21-40.
Stober, I., and Bucher, K., 2004, Fluids sinks within the earth´s crust.: Geofluids, v. 4, p. 143-151.
Sverjensky, D. A. 1981. "The origin of a Mississippi Valley-type deposit in the Viburnum Trend, southeast Missouri." Economic Geology 76(7): 1848-1872.
Walter, B. F., Immenhauser, A., Geske, A., and Markl, G., 2015, Exploration of hydrothermal carbonate magnesium isotope signatures as tracers for continental fluid aquifers, Schwarzwald mining district, SW Germany: Chemical Geology.
Walter, B.F., Burisch, M., Markl, G., 2016. The long-term chemical evolution and modification of continental basement brines – a field study from the Schwarzwald, SW Germany. Geofluids accepted, DOI: 10.1111/gfl.12167.
Walther, H. W. 1982. Zur Bildung von Erz-und Minerallagerstätten in der Trias von Mitteleuropa. Geologische Rundschau, 71(3), 835-855.
Wilkinson, J., 2010, A review of fluid inclusion constraints on mineralization in the Irish ore field and implications for the genesis of sediment-hosted Zn-Pb deposits: Economic Geology, v. 105, no. 2, p. 417-442.
Wilkinson, J., Eyre, S., and Boyce, A., 2005b, Ore-forming processes in Irish-type carbonate-hosted Zn-Pb deposits: evidence from mineralogy, chemistry, and isotopic composition of sulfides at the Lisheen Mine: Economic Geology, v. 100, no. 1, p. 63-86.

Figure captions

Fig.1. (A) geological overview map modified after Hann and Zedler (2008) with location of the Brandenberg vein. (B) double-polished thin section. Colours indicate different FIA in quartz and fluorite. (C) Histogram showing the Rb/Cs mass ratio of analyses fluid inclusions. (D) Rb versus Cs concentrations of fluid inclusions in fluorite and quartz. Rb/Cs ratios of 1, 2 and 5 are indicated as dotted lines, suggested by Göb et al. (2013) used as a monitor for host-rock alteration.

Fig. 3. Rb/Cs versus (A) Cl/Br. Although fluorites show a slightly higher variability in Cl/Br ratios, no correlation between Rb/Cs and Cl/br can be observed. (B) Li concentrations are highest in FI hosted by fluorite, which are often associated with elevated Rb/Cs ratios. (C) Sr shows no clear correlation with Rb/Cs, (D) Pb + Zn concentrations positively correlate with Rb/Cs and show a systematic decrease from fluorite to quartz , (E) W concentrations are clearly higher in FI in fluorite. (F) Ba content is highest in FI in fluorite, decreasing significantly in FI in quartz.

Fig. 2 A) Homogenization temperature versus total Salinity and B) C/(Na+Ca) versus total Salinity. Both show that there is no systematic change of the major element chemistry and formation

454 temperature indicating that fluorite and quartz formed under equivalent physio-chemical conditions.

455

456 Fig. 4. Schematic model of the temporal evolution of the fluid's Rb/Cs ratio, within the root zone of a
457 hydrothermal vein. A, B, C and D indicate four general possibilities of a transition from one
458 cycle/fluid-pulse to the following.

Figure_1
Click here to download high resolution image

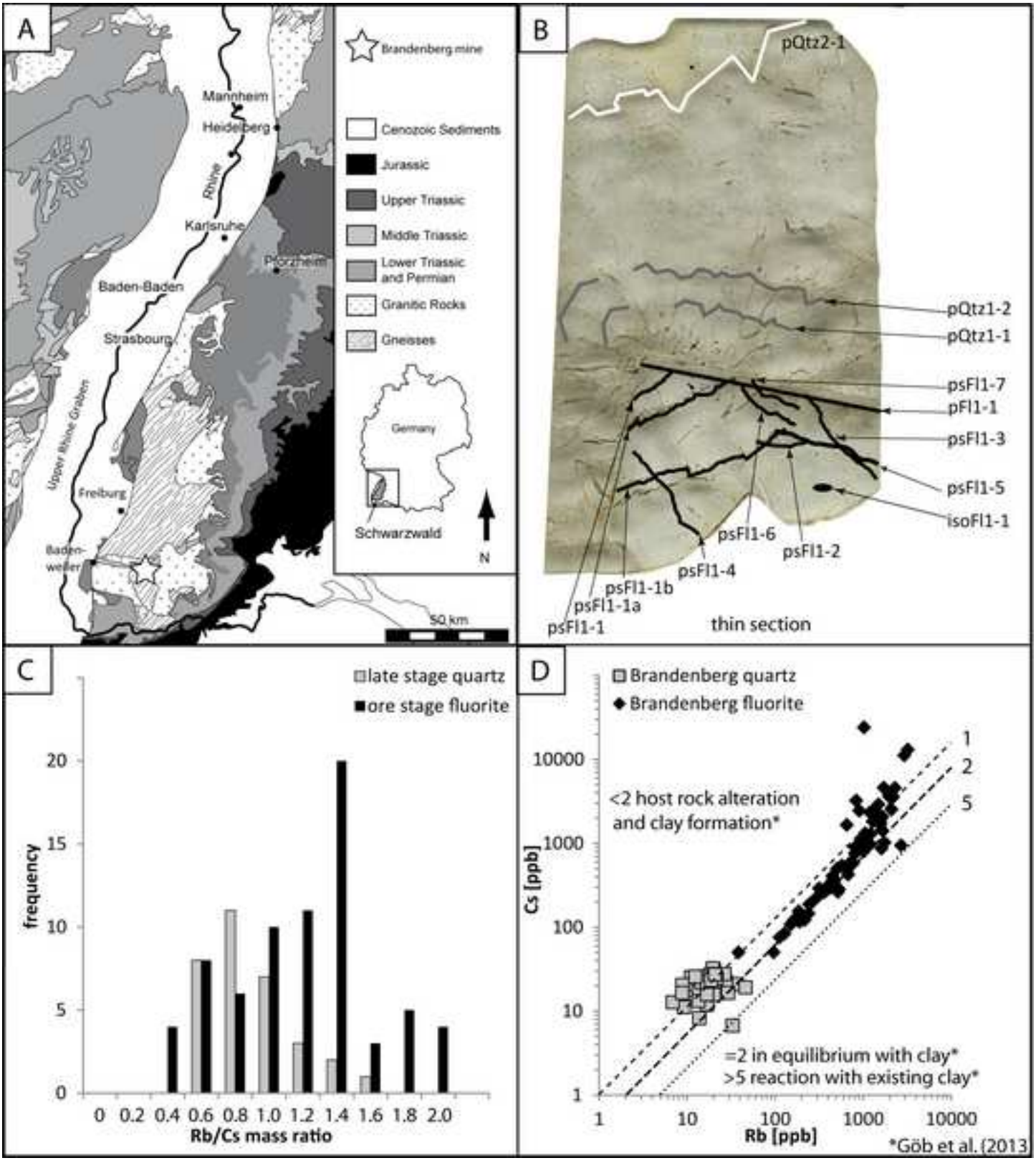

Figure_2

Click here to download high resolution image

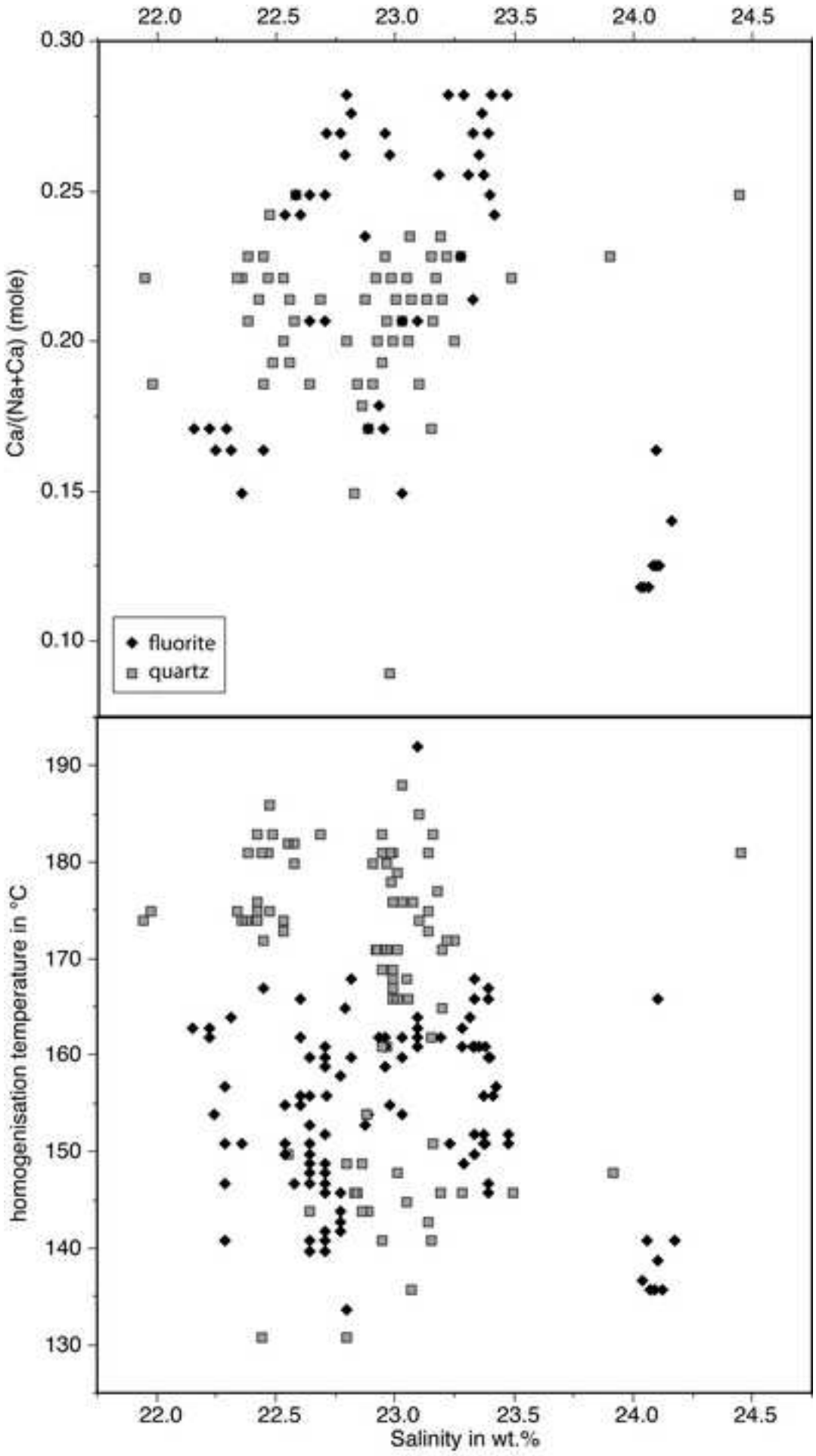

Figure_3
Click here to download high resolution image

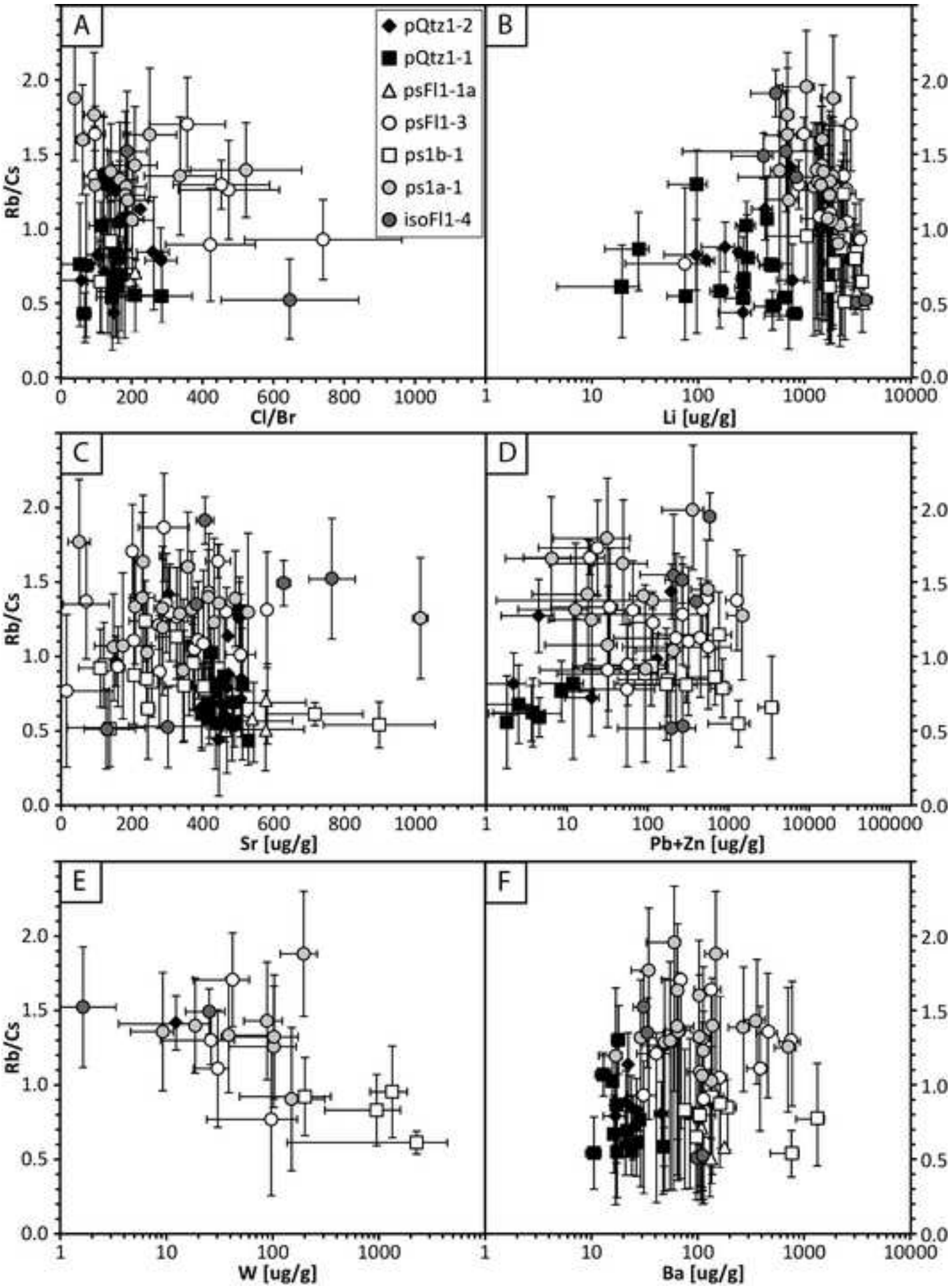

Figure_4
Click here to download high resolution image

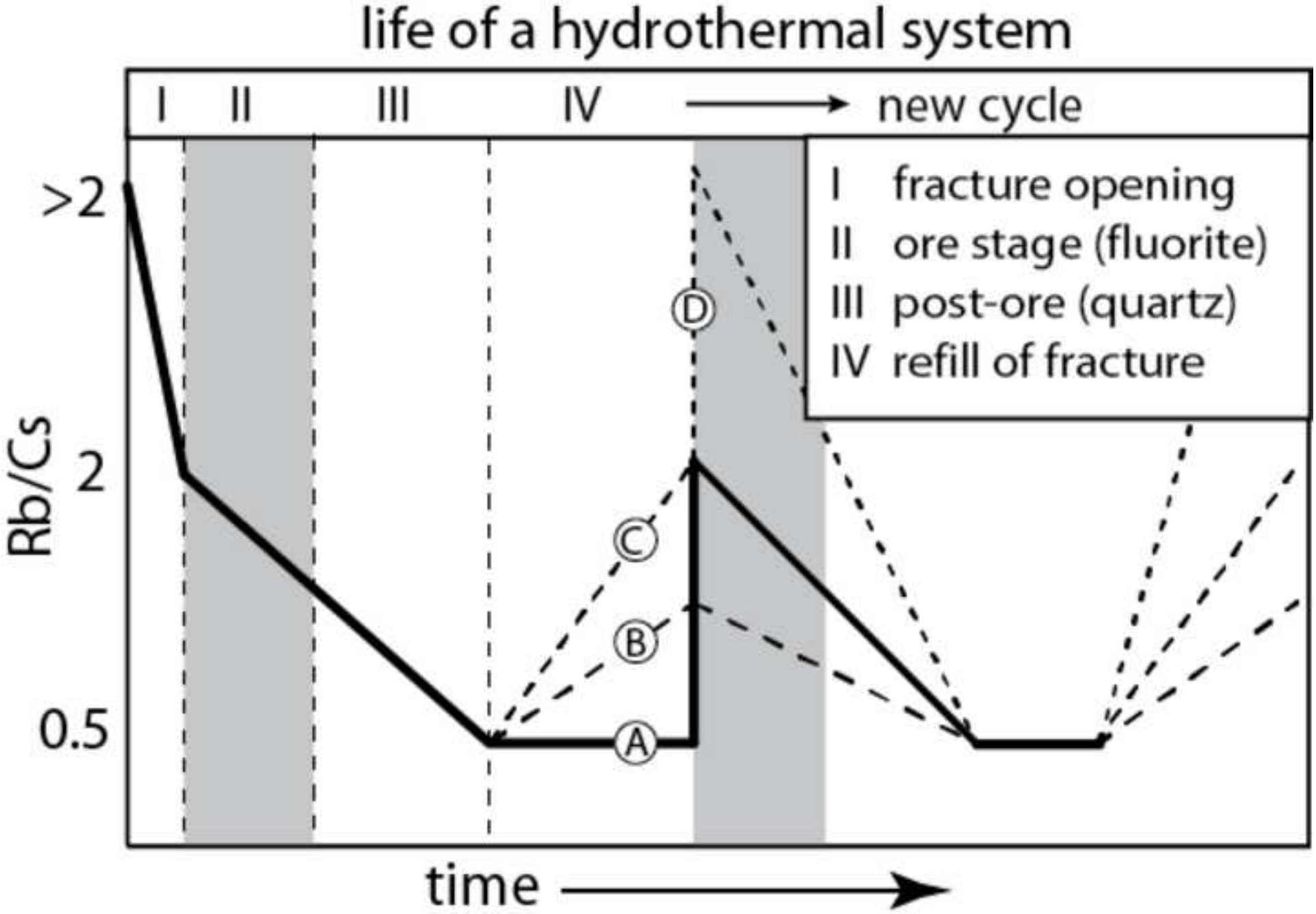

Anhang 6

Walter, B. F., Immenhauser, A., Geske, A., & Markl, G. (2015). Exploration of hydrothermal carbonate magnesium isotope signatures as tracers for continental fluid aquifers, Schwarzwald mining district, SW Germany. Chemical Geology, 400, 87-105.

akzeptiert zur Veröffentlichung	Anzahl der Autoren	Position des Kandidaten in der Autorenliste	Wissen-schaftliche Idee des Kandidaten (%)	Datengenerier-ung des Kandidaten (%)	Analysen und Interpretat-ionen des Kandidaten (%)	Verfassen der Publikation durch den Kandidaten (%)
ja	4	1	50	60	50	70

Chemical Geology 400 (2015) 87–105

Contents lists available at ScienceDirect

Chemical Geology

journal homepage: www.elsevier.com/locate/chemgeo

Exploration of hydrothermal carbonate magnesium isotope signatures as tracers for continental fluid aquifers, Schwarzwald mining district, SW Germany

Benjamin F. Walter [a,*], Adrian Immenhauser [b], Anna Geske [b], Gregor Markl [a]

[a] Department of Geosciences, Universität Tübingen, Wilhelmstr. 56, D-72074 Tübingen, Germany
[b] Ruhr-University Bochum, Institute for Geology, Mineralogy and Geophysics, Universitätsstrasse 150, D-44801 Bochum, Germany

ARTICLE INFO

Article history:
Received 25 June 2014
Received in revised form 3 February 2015
Accepted 6 February 2015
Available online 19 February 2015

Editor Michael E. Böttcher

Keywords:
Schwarzwald mining district
Isotope geochemistry
Magnesium isotopes
Hydrothermal fluids
Carbonates
Fluid mixing

ABSTRACT

The significance of magnesium isotope ($\delta^{26}Mg$) fractionation in the continental hydrothermal domain is poorly explored. Here, a detailed Mg isotope dataset from various aquifer host rocks and corresponding hydrothermal carbonate precipitates from the Schwarzwald mining area in SW Germany is documented and discussed. This study is motivated by the very considerable existing data set on hydrothermal mineralizations in the study area and the excellent regional control of sampling points. Based on structural, mineralogical and microthermometrical arguments, we here subdivide three clusters of veins: (i) Permian, (ii) Jurassic–Cretaceous and (iii) post-Cretaceous (Cenozoic). The focus is on clusters ii and iii and their corresponding, texturally older hydrothermal fluid inclusion-rich, coarse-grained, low-Mg calcite and dolomite–ankerite solid solutions and younger, oscillatory zoned low-Mg calcite and dolomite–ankerite solid solution crystals precipitated from fluids with temperatures between 50 and 350 °C. In terms of their $\delta^{26}Mg$ ratios, three characteristic groups of hydrothermal carbonates can be distinguished: (i) Jurassic–Cretaceous veins ($\delta^{26}Mg = -3.38$ to -0.82‰) in the central Schwarzwald precipitated from fluids containing a significant proportion of sedimentary cover-derived waters. They yield ^{26}Mg-depleted Mg isotope signatures typical of sedimentary carbonate lithologies. (ii) Jurassic–Cretaceous vein carbonates in the southern Schwarzwald precipitated from mainly basement-derived fluids with ^{26}Mg-enriched signatures ($\delta^{26}Mg = -1.22$ to $+0.05$‰). Supporting evidence for the origin of these fluids comes from Sr–C–Pb isotope systematics and trace element compositional variations of fahlore and sphalerite. The Mg isotope variations are controlled by differences in fluid source characteristics dominate over variations exerted by mineralogical differences (where low-Mg calcites are generally, but not in all cases, more depleted in ^{26}Mg compared to dolomite–ankerite solid solutions). (iii) Post-Cretaceous (Cenozoic), Rhinegraben-related veins represent a complex tectonic juxtaposition of different aquifer lithologies. As expected, this phase spans the full range from silicate to carbonate Mg isotope signatures ($+0.45$ to -3.4‰). Magnesium isotope data are supported by textural analyses (optical and cathodoluminescence microscopy), electron microprobe, microthermometry and published radiogenic $^{87}Sr/^{86}Sr$ isotope systematics. Our data are not in agreement with a significant temperature-controlled $\Delta^{26}Mg_{fluid\text{-}calcite}$ and no obvious relation between fluid salinity and hydrothermal carbonate $\delta^{26}Mg$ is found. The results of this study suggest that hydrothermal carbonate magnesium isotope ratios have a significant potential as tracer of hydrothermal fluid sources and corresponding aquifer lithologies.

1. Introduction

Basement-derived, hydrothermal brines represent the dominant fluids and metal sources in vein type and Mississippi valley type (MVT) deposits (Russell et al., 1981; Gleeson et al., 2001; Heijlen et al., 2001; Muchez et al., 2005; Heijlen et al., 2008; Boiron et al., 2010; Leach et al., 2010; Pfaff et al., 2010; Wilkinson, 2010; Fußwinkel et al., 2013). In general, these continental basement brines are characterized by very high salinities of up to 26 wt.%, temperatures between 100 and 350 °C and by their capability to mobilize and transport relatively large amounts of metals including Pb, Cu, Zn, Ag, Co or Ni (Frape et al., 1984; Frape and Fritz, 1987; Kanz, 1987; Edmunds and Savage, 1991; Pauwels et al., 1993; Emmermann et al., 1995; Banks et al., 1996; Fritz, 1997; Stober and Bucher, 1999; Yardley, 2005; Bucher and Stober, 2010).

In the context of hydrothermal mineralizations in basement rocks, the process of mixing of fluids from different sources is of key significance (e.g. Derome et al., 2007; Stoffell et al., 2008; Fußwinkel et al., 2014 and references therein). This is because, in most cases, simple fluid cooling does not suffice to explain the amounts of minerals

* Corresponding author. Tel.: +49 70712973155.
E-mail address: benjamin.walter@uni-tuebingen.de (B.F. Walter).

http://dx.doi.org/10.1016/j.chemgeo.2015.02.009
0009-2541/

precipitated and because the other effective process of mineral precipitation, boiling, is rarely observed in the mineralizations dealt with here. Hot, reducing basement brines cool during their ascent and may then mix with a second fluid of a different source, such as fluids from the sedimentary cover partly sunken into the basement (Bons et al., 2014). This process results in changes of fluid composition and temperature, pH and/or redox conditions, which in turn leads to the precipitation of gangue and ore minerals (Gallup, 1998; Yardley, 2005). In order to trace the migration pathways of fluids and the involvement of various fluid reservoirs in mineralization processes, an advanced understanding of the behavior and reactivity of upper to mid-crustal fluids, typically not considered in the hydrology of near-surface environments, is of importance (Russell et al., 1981; Wilkinson, 2010).

The present study makes use of the very extensive dataset dealing with hydrothermal mineralizations in the Schwarzwald mining district in SW Germany (Baatartsogt et al., 2007; Staude et al., 2009). Available data include: microthermometry (Baatartsogt et al., 2007; Pfaff et al., 2009; Staude et al., 2009, 2012b; Fußwinkel et al., 2013), age-dating (Pfaff et al., 2009), REE-distribution in fluorites and secondary minerals (Schwinn and Markl, 2005; Göb et al., 2011), trace element distribution in fahlore and sphalerite (Staude et al., 2010b; Pfaff et al., 2011), isotope data of a whole suite of elements such as oxygen, deuterium, carbon, sulfur, strontium, lead, copper and iron (Baatartsogt et al., 2006; Markl et al., 2006a,b; Schwinn et al., 2006; Baatartsogt et al., 2007; Staude et al., 2011, 2012a,b; Ströbele et al., 2012) and paleo-hydrological modelling (Pfaff et al., 2010; Staude et al., 2011). Moreover, data from modern thermal and mineral waters (Göb et al., 2013; Loges et al., 2012) and a well-known regional geology (Geyer and Gwinner, 2011 and references therein) contribute to the characterization of this natural laboratory. This uncommonly complete dataset represents the solid foundation and strong motivation for a detailed study of hydrothermal carbonate δ^{26}Mg phases in this mining district.

The starting point for this work comes from the magnesium isotope fractionation pathways in surficial karst domains, a system that is relatively simple when compared to hydrothermal systems. There, cave monitoring of meteoric fluids revealed a clear relation between carbonate versus silicate weathering patterns and related fluid δ^{26}Mg signatures (Buhl et al., 2007; Immenhauser et al., 2010; Riechelmann et al., 2012a,b; Mavromatis et al., 2014). Recent work from other Earth surface settings has, however, revealed a high level of complexity including significant Mg depletion during continental weathering (Bolou-Bi et al., 2010; Li et al., 2010a; Tipper et al., 2010; Riechelmann et al., 2012b; Geske et al., 2015a); the importance of structural and exchangeable Mg in clay minerals and the role of clay minerals as Mg sink (Higgins and Schrag, 2010; Opfergelt et al., 2012; Wimpenny et al., 2014a,b) and the significance of kinetic effects (Mavromatis et al., 2012) between free aqueous Mg^{2+} ions in the fluid and various Mg sinks ($\Delta^{26}Mg_{fluid\text{-}carb}$; Li et al., 2014a,b) to name just some of the factors involved.

This study was guided by a series of questions that have both economic and fundamental significance. These are: Are $\delta^{26}Mg_{carb}$ ratios correlated with the $\delta^{26}Mg_{host\text{-}rock}$ signatures of the specific lithologies through which these fluids circulated (Mg-source fingerprinting)? What is the importance of the mineralogy of the hydrothermal precipitates formed (dolomite–ankerite solid solutions and low-Mg calcites as present in many vein-type deposits)? What is the impact of fluid temperature and salinity on $\Delta^{26}Mg_{fluid\text{-}carb}$? All of these questions are, to the knowledge of the authors, unresolved and published data on δ^{26}Mg signatures of burial realm carbonates precipitated from – or of marine carbonates altered by – hydrothermal phases is limited (Geske et al., 2012; Azmy et al., 2013; Beinlich et al., 2014; Lavoie et al., 2014). This work is performed against a very detailed background dataset of fluid chemistry and temperature as based on fluid inclusion studies and published data. The aims of this paper are: (i) to identify and characterize the Mg-isotope signature of different hydrothermal carbonate phases in their geological and chronological context; (ii) to quantify the Mg isotope signatures of different host rocks from which the involved fluids were derived; and (iii) to discuss the significance and impact of rock-water interaction, carbonate mineralogy, fluid chemistry and salinity, temperature or mixing ratios for $\Delta^{26}Mg_{fluid\text{-}carb}$).

2. Geotectonic setting and main characteristics of Schwarzwald hydrothermal mineralizations

2.1. Geotectonic setting

The Schwarzwald mainly consists of exhumed Variscan basement rocks (mostly gneisses and granites) and is covered by Permian to Upper Jurassic sedimentary units (Fig. 1; Kalt et al., 2000). The paragneiss units of the basement locally contain orthogneisses and amphibolites deformed and metamorphosed during Variscan (Carboniferous) collisional processes (Geyer and Gwinner, 2011). The gneisses were intruded between 335 and 315 Ma by post-collisional S-type granites, which today form about 50% of the exposed Schwarzwald basement (Todt, 1976; Altherr et al., 2000; Hann et al., 2003). After erosion, during Permian times (Rotliegend), small sediment traps were filled by redbeds (arkoses, conglomerates) (Jenkner, 1986; Nitsch and Zedler, 2009; Geyer and Gwinner, 2011). In the Early Triassic, quartzitic Buntsandstein units reaching a thickness of ≤400 m in the northern and <50 m in the southern Schwarzwald were deposited. During the Middle Triassic (Muschelkalk), 160 to 220 m of limestones, shales and evaporites were laid down. In contrast, the Late Triassic (Keuper) was dominated by clastic sediments and evaporitic units (mainly gypsum) the thickness of which decreases from about 300 m in the north to less than 100 m in the south (Geyer and Gwinner, 2011). About 1000 m of clastic sediments and carbonates were deposited on the shallow continental Tethys shelf during Jurassic times. No sediments were deposited during (or are preserved from) the Cretaceous.

During the Paleogene, the Upper Rhinegraben started to break up (Schwarz and Henk, 2005; Geyer and Gwinner, 2011), which resulted in the deposition of about 4000 m of clastic and chemical sediments in the rift valley (gypsum, anhydrite, dolomite, Na–K–Mg halides) (Rupf and Nitsch, 2008; Geyer and Gwinner, 2011). Simultaneously with the rifting, the uplift of the shoulders resulted in extensive erosion of the sedimentary overburden and the basement was exhumed. Uplift and erosion was stronger in the southern relative to the middle and northern Schwarzwald; while in the middle and northern Schwarzwald, the basement-cover unconformity is preserved to the present day, the southern Schwarzwald is eroded to a depth of about 1.5–2 km below the former unconformity (Rupf and Nitsch, 2008). This implies that hydrothermal veins from the central Schwarzwald formed at a depth of about 1 km, while those in the southern Schwarzwald formed at depths of about 2.5-3 km.

2.2. Hydrothermal vein-type mineralization in SW-Germany

Hydrothermal veins formed more or less continuously in basement rocks and their sedimentary cover in SW Germany from about 300 Ma until the present day (Pfaff et al., 2009; Staude et al., 2009; Loges et al., 2012). Following the work of Staude et al. (2009) and Pfaff et al. (2009, 2010), we here subdivide hydrothermal veins in three formation stages according to structural, mineralogical and microthermometrical arguments (Table 1): (i) Permian, (ii) Jurassic–Cretaceous and (iii) post-Cretaceous ones. The Permian group comprises mainly Sb ± Ag ± Au-bearing quartz veins with only minute quantities (if any) of barite or calcite. The precipitation of this group was probably driven by cooling of late-Variscan metamorphic fluids (Baatartsogt et al., 2007; Staude et al., 2009).

Most mineralizations in the Schwarzwald belong to the second, Jurassic–Cretaceous group, and their formation is related to the opening of the North Atlantic (Wetzel et al., 2003; Pfaff et al., 2009). In this context, deep brines were activated and mixed with formation waters in

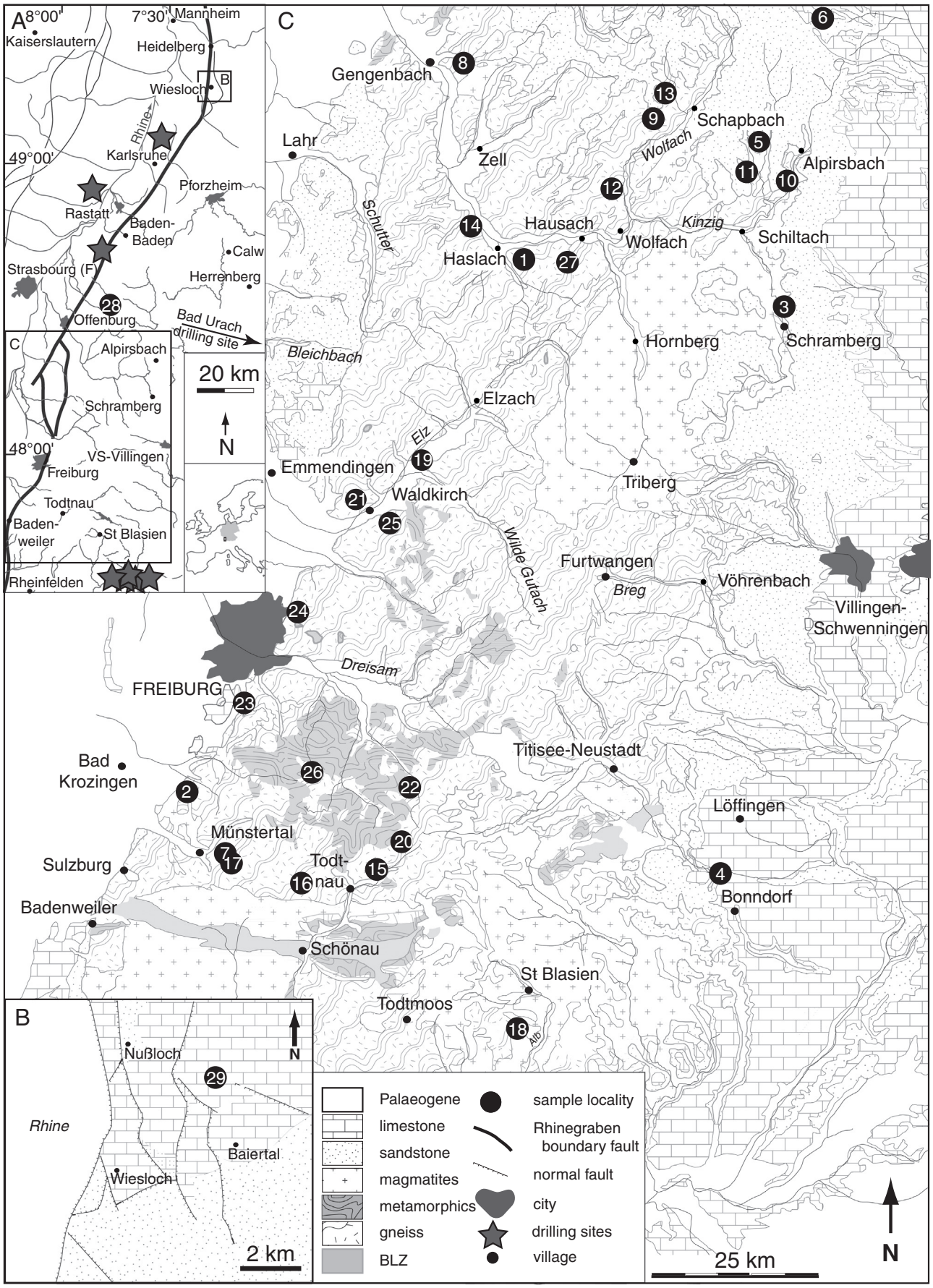

Fig. 1. (A) Overview map of Schwarzwald area and SW Germany with sample locations and indication of different host rock lithologies. (B) The Röder quarry near Wiesloch with the Mississippi valley type (MTV) deposit. (C) Close-up of the Schwarzwald mining district. Sample localities 1 through 29 refer to Table 2. Map based on Pfaff et al. (2011, and references therein).

Table 1
Types of veins and fluid signatures of the Schwarzwald ore district. References: 1: Baatartsogt et al. (2007) 2: Staude et al. (2009), 3: Pfaff et al. (2009), 4: Walter and Apukthina (2012), 5: Pfaff et al. (2010).

Group	Age	Mineralogy	Fluid-type	Salinity wt% ($NaCl + CaCl_2$)	T_h in °C	Mineralisation	Structural position	Formation process	References
1	Permian	Quartz	H_2O–NaCl–KCl	<5	150–300	Sb ± Ag ± Au–Fe	only in granite and gneiss basement rocks	fluid-cooling	1, 2
2	Jurassic-Cretaceous	Fluorite–quartz–barite Barite–quartz	H_2O–NaCl–$CaCl_2$	20–28	50–180	Pb–Zn–Cu–Ag U–Bi–Co–Ni–Ag–Fe–Mn	from more than 2000 m below the basement/ cover discontinuity till redbed sandstones	fluid-mixing	1, 2, 3, 4
3	post-Cretaceous	Quartz–barite–fluorite	H_2O–NaCl–$CaCl_2$	0–25	50–150	Pb–Zn–Cu–Ag Cu–Ni–Bi–Ag	Related to Upper Rhinegraben faults or tributary fault systems	fluid-mixing & fluid-cooling	2, 3, 4, 5,

extensional basin-related fault systems (Staude et al., 2009; Walter and Apukthina, 2012). The Mesozoic veins show variable modal amounts of fluorite, barite, quartz and carbonates (Staude et al., 2009, 2011, 2012a) with either Ag–Bi–Co–Ni–U (Staude et al., 2012a) or Pb–Zn–Cu–Fe–Mn ores (Metz et al., 1957; Staude et al., 2009; 2012b).

In the context of Paleogene rifting, Upper Rhinegraben-parallel NE–SW to NNE–SSW-striking fault systems were opened or reactivated and the third group of mineralization formed: barite-quartz, various carbonates with or without barite and quartz or barite–quartz–fluorite mineralizations were precipitated mainly with Pb ores; less commonly As, Zn, Cu, Bi and Ni ores are present (Werner and Franzke, 1994; Staude et al., 2009; Ströbele et al., 2012). Furthermore, an MVT-deposit formed at 23 Ma in the paleokarst settings of the Muschelkalk limestones near Wiesloch (Pfaff et al., 2010; Ströbele et al., 2012). The characteristics of the different mineralizing fluids are summarized in Table 1.

3. Sample material and petrography

3.1. Sample material

A total of 36 samples (low-Mg calcites n = 9; dolomite-ankerite solid solutions n = 18, siderite n = 1, as well as various lithologies derived from sedimentary-cover units n = 8) from 29 localities in the Schwarzwald area were investigated for their Mg isotope ratios. Details of the analyzed materials are given in Table 2. Here, we only summarize the most salient features. Samples were chosen based on the following criteria: Mg-concentration, lack of alteration features and quantity, availability of supporting data (e.g., geochemical or fluid inclusion data) and parameters such as mineralogy, age and depth of formation or relative chronological position within a paragenetic succession and formation process (fluid mixing, cooling, remobilization). These criteria resulted in the set of samples documented in overview in Fig. 2 and Table 2. It is important to note that Jurassic–Cretaceous veins are derived from various formation depths. Central Schwarzwald samples formed at shallow depths of about 1 km (below basement-cover unconformity), whereas southern Schwarzwald samples formed at greater depths between 2 and 3 km in the crystalline basement.

3.2. Petrography of hydrothermal phases and lithology of aquifer hostrocks

All samples were classified texturally and petrographically in detail by optical and cathodoluminescence microscopy. Please refer to Figs. 2 and 3 for details. Here, the most important charcteristics are summarized. Data obtained (Fig. 3) differentiate between (i) host rock lithologies, (ii) main-stage fluid inclusion-rich, commonly coarser-grained gangue carbonates (low-Mg calcite and dolomite–ankerite) precipitated during the main hydrothermal stage of vein formation. (iii) A paragenetically younger, late-stage phase is present as euhedral, mm- to cm-sized crystals on top of older mineral assemblages.

The coarse-grained marble is rich in fluid and small organic inclusions. It is a rare lithology in some central and southern Schwarzwald paragneiss regions and formed during Variscan metamorphism from presumably sedimentary precursor rocks.

The samples from Buntsandstein and Rotliegend clastic redbed host lithologies (Fig. 2A) display component-supported fabrics with the main grain type being detrital quartz overgrown by secondary quartz cements. A substantial amount of the remaining pore space is occluded by clay as well as low-Mg calcite and dolomite cements that have not been investigated in detail here. The remaining open porosity in these lithologies ranges between 2 and 8% (Demel, 2011).

The contact beween host rock (altered granite and gneiss) and hydrothermal main-stage carbonates (ii) is sharp (Fig. 2F). These main-stage carbonates (low-Mg calcites and dolomite–ankerite solid solutions) are a typically coarse grained gangue and show no significant

Table 2
Sample descriptions and Mg isotope signatures, C and O isotope signatures as based on (ref. 1) Staude et al. (2012a), (ref. 2) Pfaff et al. (2010) and results of microthermometric analysis. Note: = fluid inclusion data from older gangue.

Map	Group	Location	Sample	Mineralogy old = * young = †	Gangue	Ore	δ^{25}Mg	Error	δ^{26}Mg	Error	δ^{13}C VPDB	δ^{18}O VSMOW	Salinity (wt% NaCl + $CaCl_2$)	T_h (uncorr.)	Reference
1	Source	Urenkopf	XSU19	Mg-calcite *	–	–	−2.13	0.02	−4.06	0.04			23.3–24.7	93–115	
2	Source	Grunern	GM1426	Mg-calcite marble *	–	–	−0.57	0.02	−1.05	0.04	−1.1	11.5	0.7–2.0	>175	1
3	Source	Schramberg outcrop B462	SLG14	dolcrete *	–	–	−0.41	0.01	−0.79	0.06	−2.3	22.7	no fi	no fi	1
4	Source	Schattenmühle Wutach	BO88	dolcrete *	–	–	−0.50	0.04	−0.98	0.06	−7.9	16.6	no fi	no fi	1
5	Source	Reinerzau. Staudamm	SRZ3	dolcrete *	–	Ni–U–Co–Pb–Zn–Cu–Bi	−0.67	0.02	−1.28	0.05	−8.2	16	no fi	no fi	1
6	Source	Tigersandstein		bulk	–	–	−0.73	0.02	−1.39	0.03			no fi	no fi	
6	Source	Ecksches Konglomerat	BW148	bulk	–	–	−0.44	0.01	−0.84	0.03			no fi	no fi	
6	Source	Bausandstein	RO7516/B1 CD H17	bulk	–	–	−0.65	0.02	−1.24	0.02			no fi	no fi	
7	Permian	Münstergrund	BO133	dolomite–ankerite *	qtz	Sb	−0.28	0.03	−0.53	0.05	−10.1	16.2	5.1–24.3	118–168	1
8	Jurassic–Cretaceous central	Ohlsbach	TM127a	Mg-calcite *	cc	–	−1.70	0.02	−3.27	0.06	−7.3	13.3	23.2–24.8	142–149	1
9	Jurassic–Cretaceous central	Clara Oberwolfach	TM1	siderite–rhodocrosite*	fl–brt–qtz	Pb–Zn–Cu	−1.56	0.02	−3.01	0.05	−8.5	16.2	24.8 ± 3	123 ± 32	1
10	Jurassic–Cretaceous central	Alpirsbach	SAB28	dolomite–ankerite†	dol	–	−0.28	0.01	−0.54	0.04	−2.8	16.3	no fi	no fi	1
11	Jurassic–Cretaceous central	Sophia Wittichen	SW75	Mg-ankerite*	ank	Ag–Pb–Zn–U	−0.61	0.01	−1.16	0.03	−6.1	19.8	24.9–26.1	74–130	1
11	Sinter	Neu Glück Wittichen	TM96	Mg-calcite		Ag–Pb–Co	−1.86	0.03	−3.61	0.05	−5.6	23.7	no fi	no fi	1
12	Jurassic-Cretaceous central	Wenzel	BW-90	dolomite †	cc-brt	Ag–Pb–Co	−0.43	0.02	−0.82	0.03	−6.8	13.8	no fi	no fi	1
12	Jurassic–Cretaceous central	Wenzel	BW-91	Mg-calcite *	cc-brt	Ag–Pb–Zn	−1.33	0.02	−2.57	0.07	−12	12	23.7–25.3	90–137	1
13	Jurassic-Cretaceous central	Friedrich Christian	BW-92	Mg-calcite †	fl-brt-qtz	Pb–Zn–Cu	−1.76	0.01	−3.38	0.03	−6.2	22	25.5 ± 0.3	120 ± 10	1
14	Jurassic–Cretaceous central	Artenberg quarry	SABG8	Mg-calcite *	cc		−0.55	0.02	−1.02	0.03	−11.6	12.9	24.7–25.9	100–122	1
15	Jurassic–Cretaceous southern	Brandenberg Todtnau	TM162	dolomite–ankerite †	fl–brt–qtz	Pb–Zn	0.01	0.03	0.00	0.05	−0.8	14.8	3.6–5.0	49–57	1
16	Jurassic–Cretaceous southern	Anton Wieden	TM152	dolomite–ankerite †	fl-brt-qtz	Pb-Zn	−0.05	0.02	−0.11	0.02	−1.6	17			
17	Jurassic–Cretaceous southern	Teufelsgrund Münstertal	TM138	dolomite–ankerite †	fl–brt–qtz	Pb–Zn–Ag–Ni–Co	−0.64	0.01	−1.22	0.02	−3.2	16.7	20 ± 1.5	108 ± 12	1
18	Jurassic–Cretaceous southern	Gottesehre Urberg	BO93	Mg-calcite *	cc–fl	Pb–Zn	0.03	0.03	0.05	0.04	−6.2	15.1	22.0–24.1	117–157	1
19	Post-Cretaceous	Bleibach	TM123	dolomite–ankerite *	dol	Pb–Zn	−0.10	0.02	−0.25	0.09	−1.1	14.2	no fi	no fi	1
19	Post-Cretaceous	Bleibach	TM123 rep	dolomite–ankerite *	dol	Pb–Zn	−0.07	0.02	−0.14	0.03	−1.1	14.2	no fi	no fi	1
20	Post-Cretaceous	Silbereck	SN49	dolomite–ankerite *	cc–dol	Cu–Bi	−0.5	0.02	−0.96	0.04	−1.1	17.8	1.5–4.2	147–329	1
21	Post-Cretaceous	Hohe Tanne Waldkirch	SWK8	Mg-calcite †	cc–dol	Cu–Bi	−1.77	0.02	−3.40	0.04	−3.4	22.3	10.5–12.0	79–113	1
21	Post-Cretaceous	Hohe Tanne Waldkirch	SWK5	dolomite–ankerite *	cc–dol	Cu–Bi	−0.13	0.02	−0.21	0.02	−12.6	17.85	10.5–12.0	79–113	1
22	Post-Cretaceous	Immisberg	SN56	dolomite–ankerite *	cc–dol	Cu–Bi	−0.15	0.04	−0.31	0.07	−3.3	13.3	10.1–11.0	248–337	1
23	Post-Cretaceous	Merzhausen Freiburg	TM115	dolomite–ankerite *	dol	–	−1.72	0.03	−3.41	0.06	−4.4	12.2	no fi	no fi	1
24	Post-Cretaceous	Zähringen	TM35	dolomite–ankerite †	dol	–	0.22	0.01	0.45	0.06	−5.4	11.2	no fi	no fi	1
25	Post-Cretaceous	Huggenwaldtunnel Waldkirch	TM34	dolomite–ankerite *	cc–dol	Pb–Zn	−0.74	0.03	−1.43	0.05	−1.7	13.8	no fi	no fi	1
26	Post-Cretaceous	Schauinsland Freiburg	TM106	dolomite–ankerite †	fl–brt–qtz–cc	Pb–Zn	−0.68	0.03	−1.34	0.03	−1.5	15.8	4.3–5.0	119–129	1
27	Post-Cretaceous	Bernhard Hauserbach	TM39	dolomite-ankerite †	dol–brt	Cu–Bi	−0.28	0.02	−0.53	0.01	−2	16.2	no fi	no fi	
28	Post-Cretaceous	Lierbach	TM87	dolomite–ankerite *	dol–ank–cc		−0.70	0.03	−1.34	0.04			no fi	no fi	
29	Post-Cretaceous MVT	Wiesloch Röder quarry	RD100Cc	Mg-calcite *	cc (MVT)	Pb–Zn	−1.47	0.02	−2.79	0.01	0.71	23.8	5.0–11.3	59–178	2
29	Post-Cretaceous MVT	Wiesloch Röder quarry	RD100Dol	dolomite *	cc (MVT)	Pb–Zn	−0.74	0.02	−1.41	0.04	2.92	19.4	5.0–11.3	59–178	2

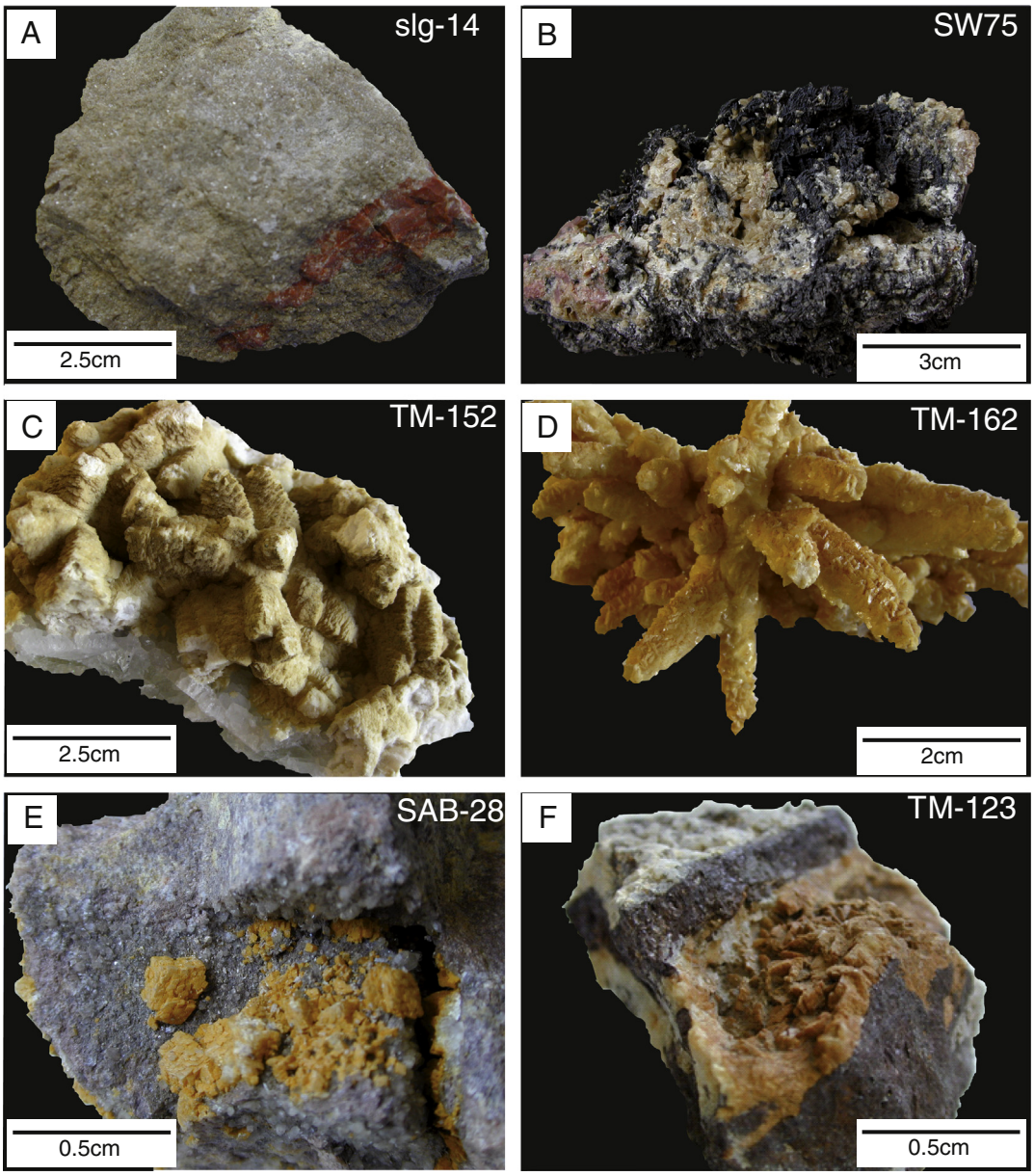

Fig. 2. Images showing hand specimens of (A) Permian dolcretes; (B) Jurassic ankerite-ore intergrowth (paragenetically old) from the Sophia mine in Wittichen; (C) paragentically young dolomite from the (Jurassic) Anton mine in Wieden; (D) pseudomorphic replacements of dolomite–ankerite-solid solutions after hydrothermal gypsum, Brandenberg mine near Todtnau; (E) dolomite–ankerite solid solution single crystals in a redbed cavity from the Alpirsbach quarry; (F) post-Cretaceous dolomite–ankerite vein with sphalerite from Bleibach/Elztal.

zoning. Fluid inclusions are often situated as clusters in the center of the coarse crystals and along cracks which penetrated the carbonates.

Subsequently, towards the center of the hydrothermal veins, low-Mg calcites give way to euhedral, complexly zoned dolomite–ankerite solid solution crystals (iii), which are locally overgrown by euhedral, late-stage calcites (Fig. 3A) and/or tabular barite (Fig. 3F). The zoned dolomite–ankerite phase displays bent crystal surfaces of the saddle type (baroque) that typically precipitate from hydrothermal fluids (Fig. 3F). Where barite is missing, late-stage, small (<150 μm) crystals of euhedral calcite with intrinsic blue luminescence colors and bent crystal surfaces (Fig. 3A) are present that penetrate the carbonates. Locally, growth zones are recognized (Fig. 3B and D) and undulatory extinction is commonly observed. This late-stage phase lacks significant amounts of fluid inclusions. In veins penetrating the late-stage (iii) carbonates, euhedral dolomite-ankerite solid solution crystals are present (Fig. 3B and E). In some samples, hydrothermal carbonates of all phases show brownish Fe-hydroxides on cleavage plains (Fig. 3C).

4. Methods

4.1. Electron microprobe and cathode luminescence analyses

Major, minor and trace element compositions of the investigated samples were analyzed on a JEOL Superprobe JXA-8900RL in wavelength-dispersive mode at the Department of Geosciences, University of Tübingen (Germany). The acceleration voltage was 20 kV with a probe current of 20 nA and a defocused beam diameter of 5 μm. For three high porosity samples we chose an acceleration voltage of 10 kV with a beam diameter of 1 or 2 μm. Counting times on the peak were 16 s for major elements and 8 s on the background. For minor elements, counting times on the peak were 30 s and 15 s on the background. Synthetic and natural standards were used for calibration: Ca, Mg, Si on diopside; Mn on rhodonite; Ba on barite; Fe on hematite and Sr on $SrTiO_3$. Based on the long-term experience with carbonate analyses in Tübingen (>10 years), calibration was done on a diopside

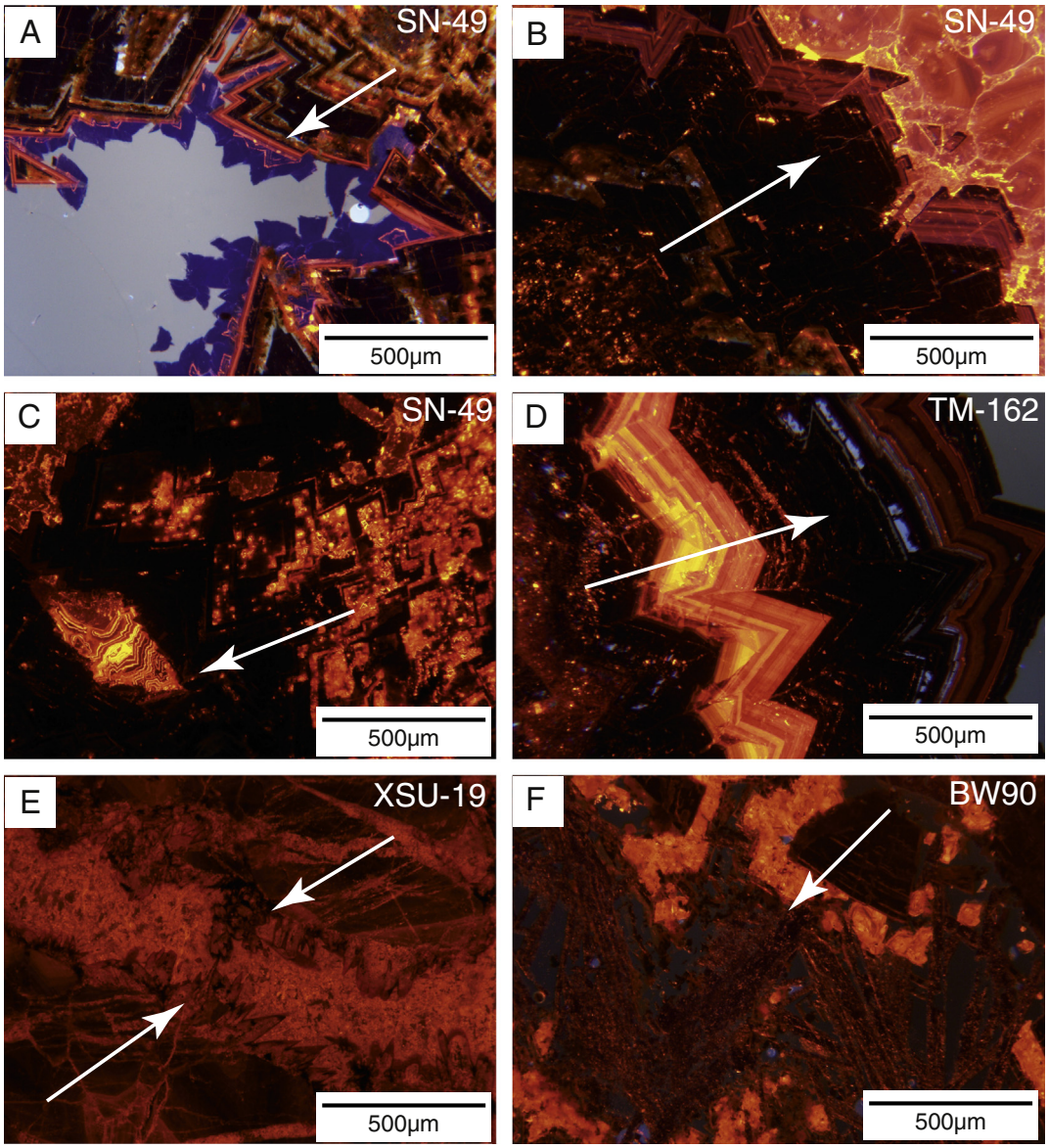

Fig. 3. Cathodoluminescence microphotographs of hydrothermal carbonates. White arrows point in the direction of growth. (A–D) zoned gangue carbonates. Orange color: low-Fe dolomite–ankerite solid solutions, black colors: high-Fe dolomite-ankerite solid solutions, blue: stoichiometric calcites; (E) complex intergrowth of dolomite–ankerite, siderite and low-metamorphic silicates in the calcite veins from the Urenkopf near Haslach; (F) dark and orange dolomite overgrown by sparry barites. (For interpretation of the references to color in this figure legend, the reader is referred to the web version of this article.)

rather than a dolomite standard, because the latter has proven to be quite inhomogeneous.

For the distinction of paragenetic phases, thin sections covered with evaporated gold were analysed using a hot stage cathodoluminescence device of the typ HC1-LM (Lumic) connected to a spectrograph at Bochum University, Germany.

4.2. Microthermometry

For the microthermometric study, samples were cut perpendicular to the orientation of the vein. By doing so, each specific sample was oriented from early precipitates nucleating on the host rock, to later precipitates facing the commonly open vein. The samples were prepared as double polished thick sections (200 to 400 µm).

Relative chronological sequences of fluid inclusions (fluid inclusion assemblages, FIA after Goldstein and Reynolds, 1994) were then established by optical microscopy. Clearly identified primary (p), pseudosecondary (ps) and secondary (s) inclusions were identified in addition to isolated inclusions (iso) with no genetic information, or to clusters of inclusions (c) with no relation to former crystal surfaces or fractures. The cluster assemblages are situated in zones where the low-Mg calcite is porous and altered, which indicates no primary genesis of the trapped fluids. The "iso" and "c" type inclusions provide no clear chronological or genetic information (Fig. 4).

Microthermometric investigations were performed using a Linkam (model THMS 600) fluid inclusion stage on a Leica DLMP microscope at Tübingen University. For each inclusion, the final melting temperature of ice ($T_{m,ice}$) and hydrohalite ($T_{m,hh}$) as well as the homogenization temperature (T_h) were measured. For calibration, synthetic H_2O and H_2O–CO_2 standards were used and only results with a maximal variation of the final melting temperatures of less than 0.1 °C were used for interpretation; for homogenization temperatures, a variation of up to 1 °C was accepted due to their poor visibility in some samples. Single measurements with strong deviation in

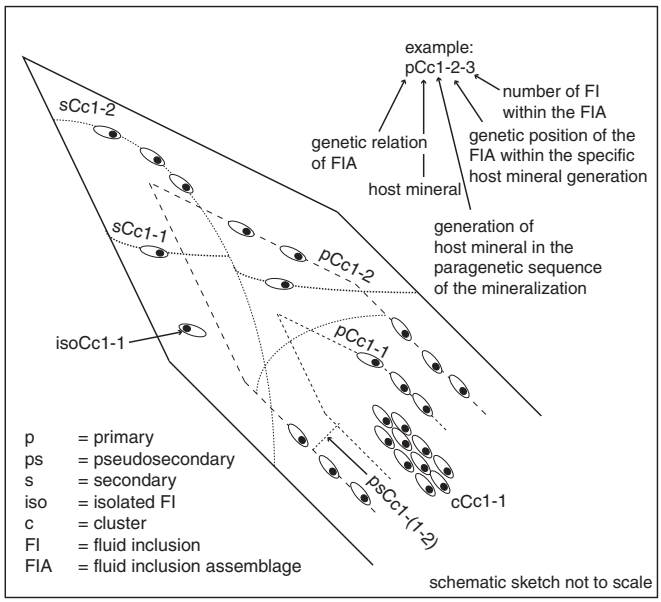

Fig. 4. Sketch showing the explanation of fluid signatures and their genetic relationship. The letters p, s and ps denote primary, secondary or pseudo-secondary fluid inclusions. In addition, each fluid inclusion got three numbers, which report the genetic information. The first number stands for the generation of the hostmineral in which the FIA is observed. The second number reports the relative genetic sequence of the FIA within the hostmineral. The numerical sequence starts in every new generation of the hostmineral at 1. The third number is the number of the measured fluid inclusion within one FIA. The raw data and salinity for each individual fluid inclusion is presented in the electronic supplement.

salinity and homogenization temperature within a homogeneous trail are neglected as are data of fluid inclusions, where post-entrapment modification cannot strictly be ruled out.

For the calculation of salinity in the ternary $NaCl–CaCl_2–H_2O$ system, the Microsoft Excel-based calculation sheet of Steele-MacInnes et al. (2011) was used. The degree of fill was estimated optically based on filling degree tables (Shepherd et al., 1985; Bakker and Diamond, 2006). Pressure correction was performed using the formula of Bodnar and Vityk (1994) in combination with estimates on basement and sedimentary overburden based on Geyer and Gwinner (2011). The uncertainties of this approach are discussed in the Appendix.

4.3. MC–ICP-MS analysis of carbonate magnesium isotope ratios

A growing number of articles describing different procedures and approaches for the separation of various amounts of Mg extracted from silicate- or carbonate-dominated rocks have been recently published (e.g., Tipper et al., 2006; Buhl et al., 2007; Pogge von Strandmann, 2008; Wombacher et al., 2009; Immenhauser et al., 2010; Higgins and Schrag, 2012; Wimpenny et al., 2014a; Beinlich et al., 2014 and references therein). Magnesium isotope analytical work was performed at the Ruhr University Bochum following the method detailed in Geske et al. (2015a,b). Sample digestion and element separation techniques were modified meeting the requirements of specific sample compositions or available sample sizes. With Fe, Mn, K, Na or Si concentration in the lower ppm and upper ppb range the most important issue is blank value and column yield, combined with a highly reproducible and robust discrimination against Ca.

The samples were dissolved in 6 M HCl (supra pure). Subsequently the solution was dried and approximately 250 μl of an 1:1 admixture of HNO_3:H_2O_2 mixture (65% and 31%, respectively) was added. After evaporation until dryness, the samples were re-dissolved applying 1.25 M HCl. Typically 35 μg of Mg passed through the ion exchange columns. The Mg fraction was recovered using BioRad ion exchange resin AG50W-X12 (200 to 400 mesh) and subsequently dried. The average total blank to sample ratio is $2 * 10^{-4}$ (10 ng total blank). Due to the 10 times larger sample size this is considered, compared to the extraordinary low 0.3 ng blank reported by Pogge von Strandmann (2008; blank to signal ratio $6 * {}^{*}10^{-3}$), an acceptable blank value. The column yield for Mg was determined for each column repeatedly using an ICP-OES (Thermo Fisher Scientific iCAP 6500 DUO) and is generally higher than 98%. As a test solution IAPSO seawater was used (diluted 1:1) that underwent the identical chemical preparation procedure as the samples. A convenient gap between the elements Ca, Mg, Na and Fe of > 10 ml could be reproducibly maintained. For the latter the Na tailing on the Mg fraction is less than 0.005‰.

Significant variation in Mg content and availability of sample material necessitated processing samples of considerably different sizes. A potential correlation between sample size and measured Mg delta values was tested analyzing 5 samples (1.5 to 15 mg) of an in-house carbonate standard RUB (Solnhofen Plattenkalk), representing 5 μg to 50 μg Mg. A trend or correlation was not observed for these 5 measurements resulting in mean value for $\delta^{26}Mg = -3.66‰_{DSM3} \pm 0.06$ 2SD and $\delta^{25}Mg = -1.91‰_{DSM3} \pm 0.03$ 2SD, respectively.

The dried Mg fraction was transferred to a 3.5% HNO_3 500 ppb Mg-solution that was analyzed on a Thermo Fisher Scientific Neptune MC–ICP-MS in the isotope laboratory of the Ruhr-University Bochum, Germany. The difference between the Mg concentration of the standard and sample was kept within a 15% limit, which proved minimizing potential isobaric interferences from matrices (Galy et al., 2001). In general the ration of the background signal of the 3.5% HNO_3 with respect to the signal of the sample for the major mass ^{24}Mg was lower than 0.002 (1–2‰ of the sample signal).

A positive effect on signal stability and reduction of matrix interferences was achieved by combining two desolvating systems an ApexIR (ESI) and an Aridus (Cetac) and the low-resolution slit of a Thermo Fisher Scientific Neptune. On average a 500 ppb Mg solution (3.5% HNO_3) resulted in a 25 V signal (10^{11} Ω resistor) for the major mass ^{24}Mg. The spectral interference $^{12}C^{14}N^{+}$ caused by the addition of N_2 via the Aridus was optically resolved at medium resolution. This interference, however, is very stable for the background, the sample and the standard measurement.

Effects described by Chang et al. (2003), who reported a significant influence of Si on the reproducibility of Mg isotope ratios were not observed. In order to test the possible interference of Si, a silicon solution was added to the IAPSO seawater standard. No variation exceeding the analytical error was observed. This is because the amount of Mg separated was 10 times higher than that in their experiment. That may also apply to other matrix inferences reported by Wombacher et al. (2009). The bracketing standard technique was applied to calculate the $\delta^{25}Mg$ and $\delta^{26}Mg$ values. All δ-values presented in this study (Table 1) are based on a sequence of five repeated measurements of the same solution comprising 45 scans for each replicate. The internal precision of each sequence is given as 2 ± SD. As standard reference material (SRM) the DSM3 (Dead Sea Magnesium, provided by A. Galy) was chosen. The other available SRM, the NBS 980, proved to be isotopically heterogonous (Young and Galy, 2004). The reproducibility of the standard measurements was tested against a second, monoelemental solution, the Cambridge1, that does not pass through the chemical procedure. For the year 2008/2009 the mean value for Cambridge1 is $\delta^{25}Mg = -1.34‰_{DSM3} \pm 0.03$ 2SD and $\delta^{26}Mg = -2.58‰_{DSM3} \pm 0.06$ 2SD (n = 129), respectively. In addition two other materials, which passed through an identical chemical separation as the ordinary samples were repeatedly measured in order to verify to external reproducibility of Mg isotope ratios. A) IAPSO seawater ($\delta^{25}Mg = -0.42‰_{DSM3} \pm 0.03$ 2SD, $\delta^{26}Mg = -0.80‰_{DSM3} \pm 0.08$ 2SD, n = 20). B) JCP1 coral ($\delta^{25}Mg = -1.03‰_{DSM3} \pm 0.03$ 2SD, $\delta^{26}Mg = -1.95‰_{DSM3} \pm 0.06$ 2D, n = 9). For details to reference values for these standards, please refer to the detailed Appendix of Geske et al. (2015b).

5. Data reporting

5.1. Electron microprobe analysis

Results of the microprobe analyses are presented in the electronic supplement. The elements above the detection limit are Ca, Mg, Fe, Sr and Mn. All calcite phases studied qualify as low-Mg calcites, i.e. contain less than 4 mol% (~10,500 ppm) Mg, while the Mg carbonates are solid solutions of the dolomite–ankerite–rhodochrosite series. With the exception of sample SW 75, which is closer to an ankerite end-member composition, all other samples are predominantly composed of stoichiometric dolomite and only subordinate amounts of ankerite. Low microprobe totals are the result of highly porous samples and hence represent an analytical bias.

5.2. Petrography and microthermometry of fluid inclusions

The petrography and microthermometry of fluid inclusion assemblages forms an important foundation for the assessment of carbonate magnesium isotope ratios. This is so, because it allows for a subdivision of fluid types from which hydrothermal carbonates precipitated. Nevertheless, in order to properly interpret fluid inclusions, a detailed assessment of their relative age and petrographic relation is required (Fig. 4). The general petrographic observations leading to a subdivision of primary versus secondary inclusions are summarized as follows: Primary inclusions in crystal growth zones are much smaller (<5–15 μm) than comparable younger assemblages (<5–80 μm).

The investigated samples show three different fluid signatures: (i) In some samples, the youngest assemblages are represented by water-rich, monophase inclusions lacking a gas bubble. (ii) Jurassic–Cretaceous veins show petrographically homogeneous sequences of high salinity fluids. (iii) Post-Cretaceous veins are characterized by complex, alternating fluid signatures (low, medium and high salinity fluid inclusion assemblages). Below, we place the different classes of fluid inclusions in their genetic context (Table 1).

5.2.1. Signature A: low salinity, medium to high temperature fluids

Fluid inclusions of this signature contain H_2O–NaCl–(KCl) and are typically observed in the Permian group 1 veins (Staude et al., 2009) but are only found in the one investigated (non-hydrothermal) marble sample. Inclusions appear as secondary or isolated assemblages. The degree of fill varies between 0.80 and 0.95. The size of the fluid inclusions varies between <5 and about 40 μm, they show spherical or negative crystal shapes. Rarely, cubic forms are observed. Freezing point depression is in the range of −40 to −50 °C, which implies an almost pure binary NaCl–H_2O fluid. The last melting phase is ice. Hydrohalite dissolves at the binary eutectic temperature of −21.2 °C. Final melting temperatures of ice are observed between −0.6 °C and −1.3 °C which results in a salinity of 0.7 to 2.0 wt.% NaCl. Homogenization temperatures vary from 175 to >300 °C between different trails.

5.2.2. Signature B: high salinity, low temperature fluids

This type of fluid inclusion, mainly a H_2O–NaCl–$CaCl_2$ phase, is present in samples from numerous localities. Primary inclusions of this type are dominantly found in veins of the Jurassic–Cretaceous group 2 and more rarely in the post-Cretaceous group 3. Secondary inclusion assemblages cut through trails of signature A in veins of the Permian group 1. Freezing occurs between −70 and −100 °C, the first melting is observed between −35° and −50 °C which implies a ternary NaCl–$CaCl_2$–H_2O system. The last melting phases are dominantly ice in the southern Schwarzwald Jurassic–Cretaceous and in post-Cretaceous mineralizations. In contrast, in the central Schwarzwald Jurassic–Cretaceous veins, the last phase dissolving is hydrohalite. Melting temperatures of ice in the southern Schwarzwald veins vary from −19.8 to −24.4 °C, final dissolution temperatures of hydrohalite range from −23.0 to −26.0 °C, which corresponds to salinities between 21.9 and 24.0 wt.% NaCl + $CaCl_2$. Homogenization temperatures vary between 117 and 153 °C. In fluid inclusions from the central Schwarzwald, which contain hydrohalite as the last-melting phase, the final dissolution temperatures of hydrohalite range from −7.5 to −39.1 °C, melting temperatures of ice from −20.7 to −31.1 °C and accordingly, salinities fall in a range of 23.2 to 27.0 wt.% NaCl + $CaCl_2$. Homogenization temperatures in these inclusions range from 57 to 159 °C with a clear maximum at 110–130 °C.

5.2.3. Signature C: variable salinity, low temperature fluid

Fluid inclusions of this type are documented in five samples and also contain H_2O–NaCl–($CaCl_2$) fluids, but are of lower salinity and on average lower temperatures than signature B fluids. In contrast to the other groups, fluid inclusions with two eutectics at −21.2 and −52 °C have been detected. Both types of eutectics occur in one fluid inclusion assemblage (FIA) and so all fluids of intermediate (i.e., between 0.9 and 25 wt.% NaCl + $CaCl_2$) salinity are lumped in group 3. All measurements from a single FIA form a cloud rather than a point in the ternary plot, a feature that testifies to small, but negligible variations of the Ca/Na ratios of single inclusions in one FIA.

Without exception, ice is the last-melting solid. Final melting temperatures of ice range from −2.1 to −24.2 °C. Final dissolution temperatures of hydrohalite only vary between −21.2 and −24.9 °C (only observed in one sample). The range in salinity is considerable and ranges from 3.6 to 25.4 wt.% NaCl + $CaCl_2$. NaCl is dominant. Homogenization temperatures from 50 up to 178 °C with no statistical maximum are found.

5.3. Magnesium-isotope data

Magnesium-isotope data (Table 2) compiled in the context of this study display a significant variability between +0.45 ± 0.06‰ and −4.06 ± 0.04‰. Different hostrock lithologies (i.e., bulk redbed (BW-148, RO7516/B1 CD H17, Tigersandstein), marble (GM1426), greenschist-facies carbonate vein XSU-19 and redbed dolcrete SRZ3, SLG14 and BO88) samples yield δ^{26}Mg ratios between −0.79 ± 0.06‰ and −1.39 ± 0.03‰ with one outlier (sample XSU-19, a greenschist-facies vein carbonate) at −4.06 ± 0.04‰. Samples rd100Cc (−2.79 ± 0.01‰) and rd100dol (−1.41 ± 0.04‰) from the stratiform, carbonate hosted Pb–Zn (MVT) deposit are used as reference for the Muschelkalk limestone source. A Permian dolomite–ankerite sample (BO 133) yields a δ^{26}Mg value of −0.53 ± 0.05‰, but as no other samples were available, we do not consider Permian hydrothermal veins any further.

Texturally older hydrothermal low-Mg calcites from Jurassic–Cretaceous veins yield δ^{26}Mg values of −3.27 ± 0.06‰; 0.05 ± 0.04‰, −2.57 ± 0.07‰ and −1.02 ± 0.03‰ (TM127a, BW-91, BO93, SABG 8). Texturally older hydrothermal dolomite–ankerite solid solutions from Jurassic–Cretaceous veins range between −0.82 ± 0.03‰ and −1.16 ± 0.03‰ (BW90, SW75). In contrast, the texturally younger low-Mg calcite (BW92) from Jurassic-Cretaceous veins, present as euhedral crystals occluding pore space, display a δ^{26}Mg ratio of −3.38 ± 0.03‰. Texturally younger hydrothermal dolomite–ankerite solid solutions range between +0.00 ± 0.05 and −1.22 ± 0.03‰ (TM162, TM152, TM138).

Texturally old, main stage dolomite–ankerite solid solutions (TM123, SN49, SWK5, SN56, TM115, TM34) in post-Cretaceous veins exhibit the largest variation in δ^{26}Mg (−3.41 ± 0.06 to −0.14 ± 0.03‰). The texturally younger low-Mg calcite (SWK8) of this group displays a δ^{26}Mg ratio of −3.40 ± 0.04‰. The texturally younger (late stage) dolomite–ankerite solid solutions (TM35, TM106, TM39) of this group display δ^{26}Mg ratios between −1.34 ± 0.03‰ and +0.45 ± 0.06‰.

6. Interpretation and discussion

6.1. Fluid characterization

The three fluid types defined here are typical of the Schwarzwald mining district (Staude et al., 2009) and similar fluids have been described from many extension-related, hydrothermal mineralizations in general. Low salinity, high temperature fluid type 1 has been described for example from the Erzgebirge and Harz area in Germany, the Massiv Central in France, from Bulgaria or from Cornwall, UK (Lüders and Möller, 1992, 1995; Klemm, 1994b; Boiron et al., 1996, 2003; Gleeson et al., 2001; Kostova et al., 2004).

Fluids that share similarities with the high salinity, low temperature fluid type 2 described here have also been reported from e. g. the Irish Midlands, the Massiv Central and the Ardennes in France, from Asturia in northern Spain and from Upper Silesia in Poland (Heijlen et al., 2001; Banks et al., 2002; Boiron et al., 2010). Fluid types similar to the low temperature fluid type 3 characterized by variable salinities were also previously reported from Upper Silesia in Poland, the Basque-Cantabrian Basin in Spain, the Irish Midlands and the Brook Range of Alaska (Banks et al., 2002; Grandia et al., 2003; Heijlen et al., 2003; Leach et al., 2004).

Low-salinity, high-temperature fluids are interpreted as metamorphic fluids cooling in the last stages of the Variscan orogeny (Staude et al., 2009). Conversely, fluids with elevated salinities and low-temperatures as well as low-temperature fluids with variable salinities are interpreted to represent the mixture of basement brines with formation waters from sediment aquifers (Behr and Gerler, 1987; Klemm, 1994a,b; Lüders, 1994; Baatartsogt et al., 2007; Staude et al., 2012b and references therein). This subdivision is of key significance for the interpretation of hydrothermal carbonate magnesium isotope ratios.

The major difference between the latter two fluid types (Fig. 5B) lies in their range in salinity and their Ca/Na ratios. Specifically, the high salinity, low temperature fluid type 2 is a remarkably homogeneous, highly saline brine with 23 ± 3 wt.% NaCl + $CaCl_2$ salinity and a Ca/Na molar ratio around 0.1 to 0.8. Conversely, the variable salinity, low temperature fluid 3 comprises highly variable salinities between 0.9 and 24.4 wt.% NaCl + $CaCl_2$ and variable Ca/Na molar ratios between 0 and 0.3. This indicates that the high salinity, low temperature fluid 2 represents a binary mixture of largely homogeneous and stable fluid reservoirs, while the variable salinity, low temperature fluid 3 involves possibly more than two and/or possibly transient fluid reservoirs. An advanced understanding of the upper crustal fluid migration and formation of hydrothermal mineral deposits in general requires an assessment of the potentially different fluid reservoirs. As a first step, the raw homogenization temperature data have to be corrected for the pressure they were trapped at. Please refer to the digital Appendix for details on this method.

6.2. Jurassic–Cretaceous versus post-Cretaceous fluid system

Based on microthermometric data, three different fluid types are here subdivided. The two medium-temperature fluid groups agree with the chronological classification of Jurassic–Cretaceous and post-Cretaceous veins. In the case of Jurassic–Cretaceous mineralizations, all fluids are highly saline (>20 wt.%) and all data points plot on a rather coherent trend between an NaCl- and a $CaCl_2$-dominated end member composition (Fig. 5A). We interpret this as a binary mixture of two clearly defined highly saline fluid end members. In the following, a definition of these reservoirs is brought forward. This is performed by comparing data of recent fluids taken from mines in the Schwarzwald area (Fig. 1) to the fluid end member compositions resulting from the microthermometric study.

In the last thirty years, deep seated brines were sampled in SW Germany and close to the German border in the context of continental drilling campaigns. They reached depths up to 4 km in Soultz sous Forêt in France, Bühl, Bruchsal, Urach and in the boreholes of the NAGRA-drilling campaigns in northern Switzerland (Pauwels et al., 1993; Pearson et al., 1989; Stober and Bucher, 2004). These drilling campaigns are spatially distributed over the study area in SW Germany and Alsace (E-France; Fig. 1) and did not only recover direct fluid samples from the various SW German strata (basement rocks, Rotliegend and Buntsandstein redbeds, Muschelkalk etc.), but also recovered samples suitable for fluid inclusion studies. In addition, cored wells in the Permian Rotliegend redbeds of the North German Basin produce fluids, which are believed to be representative of the redbed formation fluids also present in SW Germany at the time of vein formation (Wolfgramm and Seibt, 2003; Lüders et al., 2010). Summing up, these data are generally believed to comprise all important fluid reservoirs present at the time of vein formation during the Jurassic–Cretaceous epochs and during post-Cretaceous times.

Present day, deep basement brines in granites and gneisses in the Schwarzwald area as sampled in mines are NaCl-dominated with Na/Ca ratios between 3.5 and 20 (Pauwels et al., 1993; Pearson et al., 1989; Stober and Bucher, 2004). However, these do not show the high salinities observed in fluid inclusions studied here. This discrepancy may be explained by dilution of a precursor, high-salinity brine by low-salinity water in the context of the formation of the Upper Rhinegraben. This interpretation agrees with previous work (Pauwels et al., 1993), suggesting similar processes at Soultz sous Forêt (Fig. 1). Concluding, based on these data and extensive previous work, it is suggested that the NaCl-dominated fluid end member (Fig. 5D) observed in the fluid inclusion data set presented here, represents a typical continental basement brine. Circumstantial geochemical tracers, such as Cl/Br ratios for the sake of focus not further detailed here, show ratios typical of a basement fluid end member as observed worldwide in many examples.

The $CaCl_2$-dominated end member composition is present in recent redbed (Upper Rotliegend and Buntsandstein) formation fluids and in diagenetic quartz seams in Permian and Lower Triassic sandstones (Pauwels et al., 1993; Wolfgramm, 2002; Wolfgramm and Seibt, 2003; Göb et al., 2013). As mentioned before, we observe a clear difference between central and southern Schwarzwald fluid inclusions. Those from the central Schwarzwald show dominant hydrohalite as the last phase to dissolute, while in those from the southern Schwarzwald ice is the last phase to dissolute under the heating-cooling stage. This pattern, in combination with the fact that all fluids show similar salinities and Na/Ca ratios indicates that similar, but not identical, fluid mixing processes occurred during vein formation.

A plausible explanation for this observation is that differences in sedimentary overburden were of significance. Specifically, in the central Schwarzwald, some hundreds of meters of Permian and Lower Triassic redbed sediments cover the basement top and represent a major fluid reservoir in agreement with previous work by Staude et al. (2010b, 2011, 2012a) or Ströbele et al. (2012). In contrast, in the southern Schwarzwald, redbed sediments pinch out to a stratigraphic thickness of a few tens-of-meters only (Geyer and Gwinner, 2011). Accepting the interpretation of binary fluid mixing, an alternative (non-basement) fluid reservoir is required. We argue that the about 300 m thick Muschelkalk limestones on top of the thin redbed interval represent the most likely fluid reservoir (Göb et al., 2013).

Again, these considerations are of significance for the interpretation of the hydrothermal carbonate δ^{26}Mg ratios. Specifically, from sites in SW Germany, i.e., to the east of the Schwarzwald, Ufrecht (2006) documented that both Buntsandstein- and Muschelkalk-derived fluids mix in drilled wells. Both redbed (Buntsandstein and Rotliegend) and Muschelkalk fluids are commonly enriched in Ca due to leaching of carbonates and/or gypsum (Göb et al., 2013).

In conclusion of the above, the Jurassic–Cretaceous hydrothermal system in the Schwarzwald mining district is characterized by a binary fluid mixing consisting of (i) an NaCl-dominated basement brine and

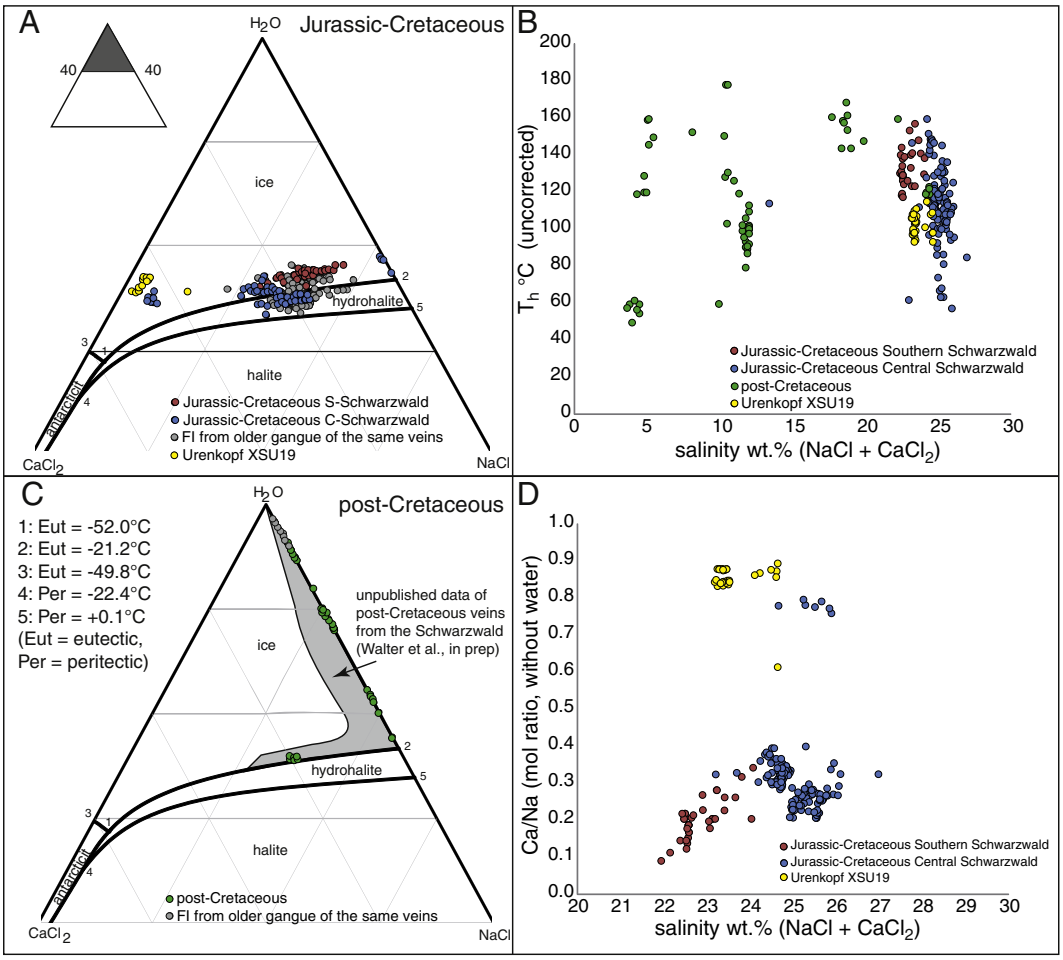

Fig. 5. (A) Fluid inclusion data of Jurassic–Cretaceous hydrothermal carbonates with a binary mixing line between two high salinity end members. (B) Plot of uncorrected homogenization temperatures versus salinity (calculated after Steele-MacInnes et al., 2011). (C) Fluid inclusion data of post-Cretaceous veins show mixing between at least three endmembers. (D) Plot showing Ca/Na molar ratio versus salinity.

(ii) a $CaCl_2$-dominated formation fluid characterized in the central Schwarzwald by redbed- and Muschelkalk-derived waters, in the southern Schwarzwald by Muschelkalk waters alone.

In contrast to the comparably simple, binary trend of Jurassic–Cretaceous fluids, the post-Cretaceous fluids show a far more complex and diverse chemistry (Fig. 5C). In addition to a mixing trend between two high salinity end members, dilution of the Na-rich brine is observed (Fig. 5C). Detailed fluid petrography reveals that low salinity, medium salinity and high salinity fluids alternate and result in complex growth zones within the same crystal. This is considered clear evidence for a multi-component fluid mixing with more than two source reservoirs. Most post-Cretaceous veins are situated on Upper Rhinegraben-related faults basically placing all different SW German sedimentary strata into contact with the adjacent basement rocks (Geyer and Gwinner, 2011). Moreover, it is geologically reasonable to propose that the break-up of the Upper Rhinegraben not only opened pathways in the form of faults and fractures through which mineralizing fluids percolated, but also brought into contact fluid reservoirs from different SW German strata previously hydraulically separated by aquitards. With reference to post-Cretaceous fluids, the data shown here allow to identify at least three end member types: (i) an NaCl-rich, (ii) a $CaCl_2$-rich and (iii) a strongly diluted H_2O-fluid.

Summing up, the following differences between Jurassic–Cretaceous and post-Cretaceous veins are recognized: Jurassic–Cretaceous veins were formed by a binary fluid mixing of two high salinity endmembers, a basement brine and a sedimentary formation fluid from Muschelkalk and Buntsandstein strata. A systematic trend in the mixing ratios is recognized from the deep basement (southern Schwarzwald) to the shallower basement/cover unconformity (central Schwarzwald).

In contrast to the Jurassic–Cretaeous ones, post-Cretaceous hydrothermal carbonates result from multi-component fluid mixing. This pattern is related to the opening of the Upper Rhinegraben rift responsible for the juxtaposition of various lithologies. A clear relation to formation depth is lacking.

Having established the main classes of fluid types in terms of their sources, their hydrochemistry and their age, the Mg isotope signatures of hydrothermal aquifers and carbonate mineralization require attention.

6.3. Constraining magnesium isotope signatures of ancient hydrothermal systems

Here we aim to verify (or falsify) the working hypothesis that $\delta^{26}Mg$ isotope ratios of hydrothermal carbonates represent suitable tracers for different fluid sources and their host rock mineralogies. Water–rock interaction between host rock and hot hydrothermal fluids in the subsurface is significantly more congruent, takes place during prolonged time periods and acts both in tectonically opened and dissolution-widened fluid pathways (Stober and Bucher, 1999 and references therein); it should not be compared with the much more transient and therefore more likely non-equilibrium leaching

in the Earth-surface weathering domain (e.g., Tipper et al., 2006, 2010, 2012; Li et al., 2010a; Riechelmann et al., 2012b; Liu et al., 2014).

Essentially, the interpretation of a fluid-source control on $\delta^{26}Mg_{carb}$ is based on the observation that samples from the central Schwarzwald area are, on average, more depleted in ^{26}Mg relative to those from the southern Schwarzwald region (Fig. 7A). From a more general perspective, controls over $\delta^{26}Mg$ of the resulting hydrothermal carbonate phase can be split into three: (i) factors controlling Mg in the fluid phase, i.e., the initial $\delta^{26}Mg_{fluid}$ overprinted by subsequent fluid–rock interaction. Fluid–rock interaction is controlled for example by silicate (Tipper et al., 2010; Wimpenny et al., 2014a,b) and carbonate dissolution and re-precipitation, bedrock composition or water–rock contact time influencing the completeness of the chemical weathering (Pearce et al., 2012). (ii) The mineralogy of the hydrothermal phase (bond-lengths; Li et al., 2014a,b), reaction kinetics (e.g., Mavromatis et al., 2012) and the fluid properties including temperature or pH but also fluid salinity/oversaturation affecting precipitation rates (Sibley et al., 1994) and fractionation processes. (iii) Later diagenetic processes (Geske et al., 2012). This implies that the working hypothesis brought forward here, i.e., a fluid-source control on $\delta^{26}Mg_{carb}$ must be tested against the above controls. Considering the complexity of the above effects and the fact that only a limited number of these parameters can be quantified in fossil hydrothermal settings, it becomes evident that the discussion can here only focus on the most general, first-order trends in aquifer lithology and hydrothermal carbonate $\delta^{26}Mg$ signatures. Constraining evidence for potential non-equilibrium factors during hydrothermal carbonate precipitation comes from the significant data set on fluid physico-chemical properties discussed above. In a first step, we make use of the supporting data compiled in the context of this study or derived from published work to discuss the impact of vein carbonate mineralogy, fluid temperature and salinity on hydrothermal carbonte $\delta^{26}Mg$.

6.3.1. Significance of vein carbonate mineralogy, fluid temperature and salinity

A first important factor is the mineralogy of hydrothermal carbonates anaylzed. As detailed in Li et al. (2014a,b), the average bond lengths for Mg in different Mg-bearing carbonate minerals affect $\Delta^{26}Mg_{fluid\text{-}carb}$. Essentially, the data set shown here comprises predominantly dolomite–ankerite solid solutions and low-Mg calcites, with one sample consisting of siderite (TM1; Table 2). The Mg elemental composition ranges from <700 to ~8000 ppm (cf. digital Appendix) and hence, calcites qualify as low-Mg calcites. The notion of a mineralogy-dependent fractionation is important as many (but not all) of the low-Mg calcite samples analysed here plot to the more ^{26}Mg-depleted and many (but not all) of the dolomite-ankerite samples plot to the less ^{26}Mg-depleted spectrum of $\delta^{26}Mg_{carb}$ (Fig. 7A).

Along similar lines, many previous authors have shown data indicating that low-Mg calcites are commonly depleted in ^{26}Mg relative to dolomite (Galy et al., 2002; Young and Galy, 2004; Tipper et al., 2006; Buhl et al., 2007; Higgins and Schrag, 2010; Azmy et al., 2013; Geske et al., 2015b). Nevertheless, published work also documents that both mineralogies show a significant overlap in their magnesium isotope range. It is perhaps of interest that often, but not always, biogenic high-Mg calcites plot to the less ^{26}Mg-depleted and biogenic low-Mg calcites to the more depleted spectrum of $\delta^{26}Mg_{carb}$ (Saenger and Wang, 2014). Judging from the data shown here (Fig. 7A) and based on previous work, it is concluded that mineralogy-related $\Delta^{26}Mg_{carb\text{-}fluid}$ is an important control.

Nevertheless, four lines of arguments indicate that mineralogy alone cannot explain the patterns documented in Fig. 7A: (i) Two low-Mg calcite samples are among the least ^{26}Mg-depleted carbonates of this dataset with one (BO93) even showing a positive value of 0.05‰ (Table 2) and another low-Mg calcite showing "typical" dolomite values of −1‰; (ii) one dolomite–ankerite sample (TM115; Mg content of >100,000 ppm) plots among the most ^{26}Mg-depleted values of the data obtained (−3.41‰; Table 2); (iii) the data range of all samples shown is ~4‰. Judging from published work, it is unlikely that a mineralogical control alone accounts for this very significant variability; (iv) finally, the dolomite–ankerite solid solutions represent composites between Mg and CaFe carbonates. The available dataset regarding the bond length-related $\Delta^{26}Mg_{ankerite\text{-}fluid}$ is insufficiently constrained. Summing up, the data shown here suggest that mineralogy is an important, but not the predominant control on $\Delta^{26}Mg_{carb\text{-}fluid}$.

A second important factor known to affect $\Delta^{26}Mg_{carb\text{-}fluid}$ is temperature (Schauble, 2011; Li et al., 2012; Li et al., 2014a,b; Beinlich et al. (2014). These authors discuss data for a wide range of mineralogies including carbonates, oxides or silicates but much of this work is based on theoretical calculations. For example, Li et al. (2012) suggest $\Delta^{26}Mg_{calc\text{-}fluid} > 3‰$ at 100 °C. At present, the temperature-related fractionation kinetics for dolomite is not well constrained. Hydrothermal carbonate $\delta^{26}Mg$ ratios obtained in the context of this study were plotted against fluid inclusion-based temperature reconstructions (Fig. 7B). Most hydrothermal carbonates analyzed here precipitated from fluids with a comparably narrow temperature range of between 100 and 150 °C but they scatter >3‰ in their $\delta^{26}Mg$ signatures (Fig. 7B). Conversely, samples characterized by significantly higher (~300 °C) or lower (~50 °C) fluid temperatures, differ only by <0.3‰ in terms of their magnesium isotope signature (Fig. 7B). The conclusion drawn here is that it seems likely that fluid temperature affected the apparent fractionation (α) between fluid and carbonates but the data shown do not support a dominant temperature control on $\Delta^{26}Mg_{carb\text{-}fluid}$. This tentative conclusion is in agreement with data from natural carbonate depositional settings as documented in Geske et al. (2012), Lavoie et al. (2014) or Li et al. (2014a,b). Concluding, in the view of the authors, it is at present unclear to which degree theoretical calculations or laboratiory experiments apply to complex natural multi-parameter precipitation environments and particularly so in the case of dolomite–ankerite solid solutions.

A third factor that merits attention is fluid salinity and hence, supersaturation. At elevated burial temperatures as reconstructed here, dolomite formation and the rate of dolomitization is influenced by several factors including solution Mg/Ca ratio and degree of fluid supersaturation with respect to dolomite (Sibley et al., 1994). This is important as saturation levels control precipitation rates and precipitation rates are known to affect $\Delta^{26}Mg_{carb\text{-}fluid}$ (Immenhauser et al., 2010). The fluid inclusion dataset obtained here allows for the assessment of salinity (wt% $NaCl + CaCl_2$) versus hydrothermal carbonate $\delta^{26}Mg$ isotope signatures. The reconstructed salinity range reaches from about 5 to more than 25 wt.% and is significant (Fig. 7C). Nevertheless, while hydrothermal carbonates from the Jurassic and Cretaceous of the southern Schwarzwald plot into a narrow salinity range, their Mg isotope signatures scatter over ~4‰ and similar conclusions are drawn for other types of mineralizations. Concluding from the above arguments and the data shown here, it is suggested that at least for the present case study, fluid salinity (precipitation rates) and fractionation patterns between fluid and hydrothermal carbonate are not obvious.

6.3.2. Significance of Mg bearing sheet-silicates

Previous work documents the significance of clay minerals and their bearing on bulk $\delta^{26}Mg$ values. Given that the hydrothermal fluids discussed here have likely been in contact with primary and secondary clay minerals, this process merits discussion. Specifically, secondary clay minerals are often enriched in ^{26}Mg while the corresponding solution is depleted in ^{26}Mg (Tipper et al., 2010; Opfergelt et al., 2012; Wimpenny et al., 2014a and references therein). Modeling data discussed in Wimpenny et al. (2014a) show that in sediments, where the percentage of exchangeable Mg, i.e., Mg adsorbed by electrostratic interaction into the interlayer and surface sites, is >30%, a depletion of −0.5‰ or less of the bulk $\delta^{26}Mg$ value change likely to possible values. Along similar lines, Higgins and Schrag (2010) suggested an enrichment of up to +1.25‰ of clay relative to the precipitating fluid. With reference to the Schwarzwald case

examples, alteration of plagioclase in crystalline basement rock leads to the formation of illite, halloysite and kaolinite. Illites in the hydrothermal systems investigated yield between 0.3 and 3 wt.% Mg^{2+} while halloysites and kaolinites are basically Mg-free. From this it could be concluded that the isotope enrichment of heavy Mg in secondary illite might lead to a ^{26}Mg depletion of the hydrothermal fluid, and considering fractionation of the hydrothermal carbonates in the order of 0.5‰ or less. To quantify the possible influence of illite formation on $\delta^{26}Mg_{hydrothermal\ fluid}$, a mass balance calculation was considered, but this exercise turned out to be pointless due to the 20 variables involved and the siginificance of a factor that, at best, accounts for 10% of the data range observed (Fig. 7A). Moreover, the data shown by Wimpenny et al. (2014a) relate to closed-system behavior, while most workers now agree on an open system behavior for hydrothermal veins in the upper brittle crust (e.g. Bons et al., 2012; Fußwinkel et al., 2013 and references therein). Summing up, the significance of source-sink processes related to exchangeable and structurally bound Mg in secondary clay minerals is not denied but was probably not a major factor controlling $\delta^{26}Mg_{carb}$ ratios in the present data set.

6.4. Crystalline basement and sedimentary cover bulk Mg isotope signatures

Having discussed the significance of carbonate mineralogy, fluid temperature and supersaturation and clay mineral-related source-sink reactions, we now focus on different Mg sources for hydrothermal fluids. The following five principal host rock types are considered: (i) granitic and gneissic basement rocks; (ii) Permian redbed sedimentary rocks; (iii) Buntsandstein quartzitic (redbed) sedimentary rocks; (iv) Muschelkalk limestones and (v) Upper Rhinegraben sedimentary infilling. Sulfur isotope ratios indicate an equilibrium temperature of the basement brine with granitic and gneissic basement aquifer lithologies in the order of 300–350 °C (Schwinn et al., 2006).

In order to test the regional, and hence potentially fluid source-controlled pattern in $\delta^{26}Mg_{carb}$, we assume an average magnesium-isotope value for crystalline rocks from the upper continental crust of −0.2‰ (Li et al., 2010b). The Permian redbed sedimentary rocks in SW Germany are interpreted as terrestrial fill-ups of basin margins. They represent proximal clastic sedimentary rocks consisting of eroded Variscan basement rocks and belong both to the Rotliegend and to the Zechstein (Nitsch and Zedler, 2009) and contain, in places, significant volumes of dolomite and ankerite cements or dolcretes (Geyer and Gwinner, 2011). Carbonate cements are interpreted to have formed during Permian burial diagenesis and hence predated the formation of most hydrothermal veins (Ortlam, 1974; Brockamp et al., 2011). Where pervasively leached by downward percolating fluids or rising basinal brines, these cements have the potential to contribute the isotopically depleted Mg isotope signature typical of carbonates (Immenhauser et al., 2010) to hydrothermal fluids. Recent formation waters (Pearson et al., 1989; Heinl, 2000; Pauwels et al., 1993) and fluid inclusions in diagenetic quartz seams in these sediments (Heinl, 2000) suggest temperatures between 50 and 100 °C for this fluid reservoir. These data agree with our estimates for the Ca-bearing fluid reservoir in Jurassic–Cretaceous and post-Cretaceous times as based on pressure-corrected homogenisation temperatures of fluid inclusions. These represent mixed fluids in Jurassic–Cretaceous hydrothermal mineralizations in the Schwarzwald. The Mg isotope signatures of Permian redbed dolcretes and dolomites analysed in the context of this study (Table 2) range between −0.54 ± 0.04 and −1.28 ± 0.05‰. The redbed carbonate cements (sample Tigersandstein) display more depleted $\delta^{26}Mg$ ratio of = −1.39‰ ± 0.03. We suggest that these values represent a mixture between a ^{26}Mg-enriched clastics-derived Mg source (e.g., biotite) and an isotopically lighter diagenetic carbonate cement precipitated during Permian times in the redbed sediments.

The quartzitic rocks of Early Triassic age ("Buntsandstein") yield low Mg contents (0.03–4.8 wt.% MgO) (Martin, 2009). When present, Mg is contained in sheet silicates (clay minerals and micas) or locally in nodules or calcitic and dolomitic cements (Geyer and Gwinner (2011). Whole rock analyses yield intermediate $\delta^{26}Mg$ signatures of −0.84 ± 0.03 to −1.24‰ ± 0.02. These values suggest an interpretation that is similar to that brought forward for Permian bulk redbed deposits, namely that both carbonates and Mg-bearing clay minerals contribute to the whole-rock values and represent important Mg sources of fluids derived from these units. The values of redbed sedimentary rocks (−0.5 to −1.2‰) and clay-bearing sandstone samples (−0.8 to −1.2‰) as analysed in the context of this study are moderately depleted relative to previously reported values of 0 to −1.2‰ which had been suggested for mainly siliciclastic sediments (e.g., Tipper et al., 2008, 2010; Shirokova et al., 2011). Tipper et al. (2006) showed that, on average, the dissolved $\delta^{26}Mg$ value was about 0.4‰ lighter relative to the siliceous source. Assuming that the redbed $\delta^{26}Mg$ ratios (−0.5 to −1.2‰) are representative, then the dissolved fluid $\delta^{26}Mg$ signature is expectedly in the range of −0.9 to −1.6‰.

Middle Triassic Muschelkalk limestones mainly include low-magnesium calcites and minor amounts of dolomite and contain between 0.02 and 25.1 wt.% MgO (Martin, 2009). The samples analysed in the present study were sampled from the MVT deposit near Wiesloch (Fig. 1) and display $\delta^{26}Mg$ values that are typical of diagenetically stabilized marine limestones (−1 to −3.5‰, e.g., Riechelmann et al., 2012b). Immenhauser et al. (2010) documented that drip waters in karst caves are about 0.5 to 1‰ lighter relative to $\delta^{26}Mg_{soil}$ but about 2‰ enriched in ^{26}Mg relative to the aquifer host limestone. For dolomitic lithologies, we make use of a recently published $\delta^{26}Mg_{dolomite}$ dataset (Geske et al., 2015b) and apply a range in $\delta^{26}Mg$ of between −0.5 and −2.5‰. Note, the typical fields of dolomite and low-Mg calcite $\delta^{26}Mg$ isotope signatures (Fig. 7A) display a significant overlap.

The carbonate-bearing sediments and sedimentary rocks in the Upper Rhinegraben contain dolomite, ankerite, siderite, low-Mg calcite and clay minerals. Locally, Oligocene evaporite units may also contain Mg-bearing halides and sulfates. These rocks may deliver an additional source of Mg to post-Cretaceous hydrothermal fluids. Given the wide lithological range and its regional and stratigraphic variability, a statistically meaningful and representative average Mg isotope signature of fluids that leached these rocks is difficult to obtain.

6.5. Relation between $\delta^{26}Mg_{fluid}$ and $\delta^{26}Mg_{carb}$

Hydrothermal carbonate $\delta^{26}Mg$ isotope ratios found here are not directly representative of their parent fluid $\delta^{26}Mg$ signatures due to various fractionation processes involved and parent fluids are in turn often depleted relative to the bedrock lithology (Tipper et al., 2006; Immenhauser et al., 2010). Nevertheless, the admittedly simplistic concept brought forward here is that leached or dissolved ^{26}Mg-depleted bedrock lithologies will lead to the uptake of isotopically depleted Mg in fluids, which in turn will lead to the precipitation of hydrothermal carbonates that are ^{26}Mg-depleted and vice versa. This concept is probably significant when the $\delta^{26}Mg$ signatures of different source lithologies differ by several permil as it is the case here but becomes mute, where $\delta^{26}Mg$ signatures bedrock are similar. These first-order patterns are likely modulated by secondary order processes such as hydrothermal carbonate mineralogy, fluid temperarture and precipitate rates.

We calculated the relative proportions of the two endmember fluids involved in the formation of two exemplary hydrothermal veins first based on Sr isotope systematics of barites (taken from Staude et al., 2011) and then compared it to the Mg isotope signatures of carbonates from the same and related veins. Hence, these two estimates are complete unrelated analytically, but refer to the same hydrothermal system. The relative proportion of two or more fluids is one parameter only. Perhaps even more important is the relative proportion of the Mg derived from these fluids that determine the mixed $\delta^{26}Mg$ isotope signature.

The Mg content of the bulk lithology of a given hostrock lithology and its solubility must be considered, too. Dolostones, for example, have much higher Mg contents than granites and carbonates are easier to dissolve than silicate minerals (see discussion in Riechelmann et al., 2012b). For a first estimation the absolute Mg content of the modern reservoirs (basement and Muschelkalk) is linked with the estimated $\delta^{26}Mg_{fluid}$ of the source aquifers. As a next step, the two aquifers are mixed with variable mixing ratios. The localities considered in detail are (i) the Wittichen and Wenzel mines, central Schwarzwald. Both of these are situated at the interface between crystalline basement and Permian Rotliegendes sedimentary rocks at a depth of about 1 km. (ii) The Gottesehre mine near Urberg, southern Schwarzwald, which lies about 2 km deeper within crystalline basement (Fig. 1).

Considering the binary fluid mixing as documented in this paper, we correlate the relative proportion of $^{87}Sr/^{86}Sr$ derived from the crystalline basement versus that derived from the overlying sedimentary cover, respectively (see also Staude et al., 2011). Our calculations and the ones of Staude et al. (2011) show that in the case of the central Schwarzwald approximately 10–30% of the fluid was derived from the sedimentary cover (i.e., Middle Triassic Muschelkalk, Lower Triassic Buntsandstein, Permian Rotliegendes) while 70–90% of the palaeo-fluids were derived from the crystalline basement. In the case of the Gottesehre mine near Urberg, most of the hydrothermal fluid (>90%) consisted of crystalline basement fluid and only a subordinate amount (<10%) was derived from sedimentary cover aquifers (Fig. 6A). This difference is in accordance with expectations as the Gottesehre mine lies much deeper in the basement rocks compared to the central Schwarzwald mines (Fig. 6B). It also agrees with previous work (Staude et al., 2012a; Ströbele et al., 2012 and Pfaff et al., 2011) who suggested, based on Sr–C–Pb isotope systematics and trace element compositional variations of fahlore and sphalerite, that southern Schwarzwald fluids are more basement-dominated than those of the central Schwarzwald. In the view of the authors, it is at present not possible to quantify realistic mixing ratios based on Mg isotopes. The main problems include uncertainties in reservoir chemistry and fractionation processes. Nevertheless, a semi-quantitative binary mixing calculation was performed and is documented in the Appendix II. The sample-free gap in Fig. 7A is most likely a consequence of the fact that in the about 30 km between southern and central Schwarzwald samples, no Jurassic–Cretaceous veins are present. Hence, the gap would be a sample bias.

These calculations refer to Jurassic and Cretaceous hydrothermal minerals, while reconstructions for the Cenozoic fluids and resulting mineralization are significantly more complex, as Upper Rhinegraben-related faulting had physically placed different lithologies (and thereby aquifers) in contact (Fig. 6C). The following results from this approach:

(1) Jurassic and Cretaceous hydrothermal carbonates in the southern Schwarzwald region, mainly dolomite–ankerite solid solutions and subordinate low-Mg calcites, reflect depleted ^{26}Mg sources that are mainly silicate (~90%) derived (basement rocks; . 7A). Stratigraphically, the veins sampled are about 1–2 km deeper that those sampled in the central Schwarzwald and located in crystalline basement hostrock. Acknowledging the complex array of leaching, dissolution and precipitation kinetics, differential Mg content and solubility as well as mineralogical control, the resulting hydrothermal carbonate $\delta^{26}Mg$ values are expected to scatter near the less ^{26}Mg depleted end member range as defined by bulk upper continental crust (−0.2‰).

(2) Jurassic and Cretaceous hydrothermal carbonates, mainly low-Mg calcites and subordinate dolomite-ankerite solid solutions, in the central Schwarzwald reflect an admixture of silicate (70–90%) and sedimentary cover (10–30%) derived fluids (Staude et al., 2011) and their corresponding Mg isotope signatures. Assuming the same mixing ratios, relative to silicate bedrock, comparably Mg-enriched nature of cover lithologies and the fact that these are easier to dissolve, it seems plausible that the dissolved Mg is more depleted in ^{26}Mg relative to that of the southern Schwarzwald. Here, a predicted wider range of values spanning the less ^{26}Mg-depleted silica and the more ^{26}Mg-depleted carbonate (Muschelkalk) is to be expected. A shown in Fig. 7A, this is indeed the pattern observed for mainly low-Mg calcites (−3.4 to −0.8‰) while dolomites cluster to the less depleted end member. Dolomite–ankerite solid solutions overlap with the silicate-dominated southern Schwarzwald data.

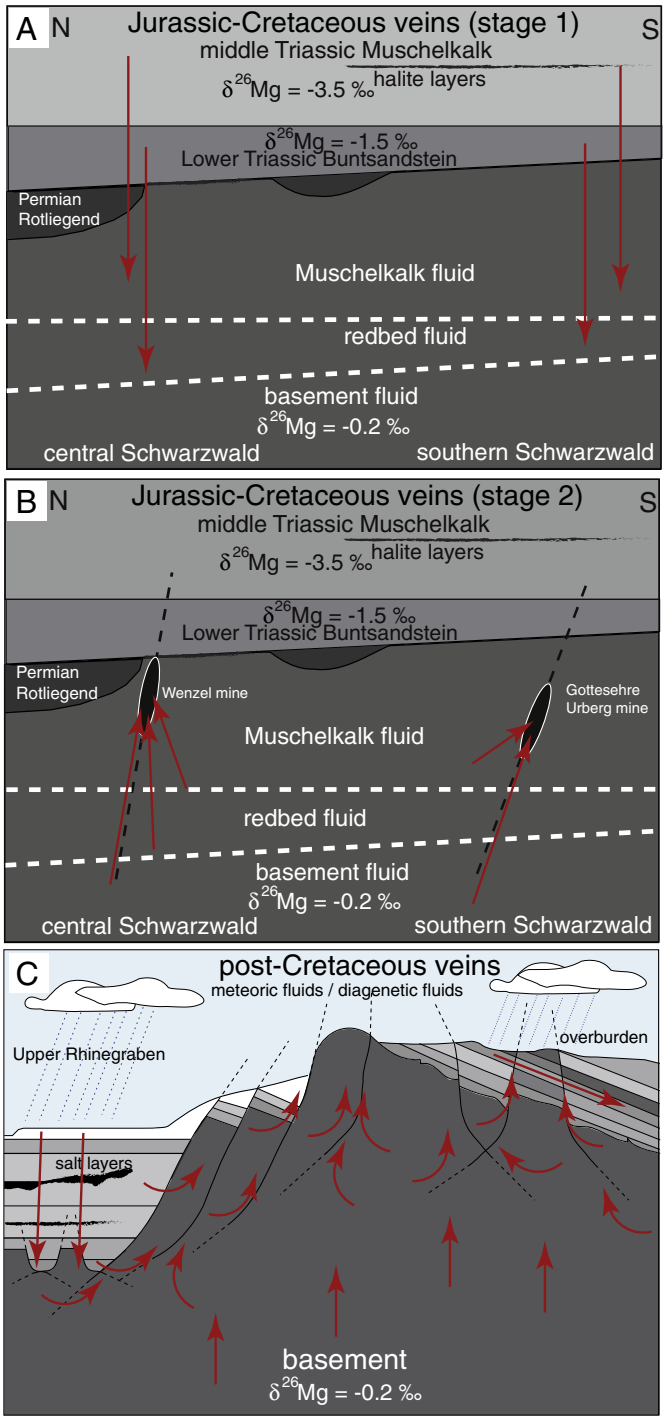

Fig. 6. Formation models of Jurassic–Cretaceous (A and B) and post-Cretaceous (Cenozoic, C) veins. For more details on the Jurassic–Cretaceous fluid mixing process, please refer to Bons et al. (2014). Note complex juxtaposition of different lithologies after Upper Rhinegraben break-up.

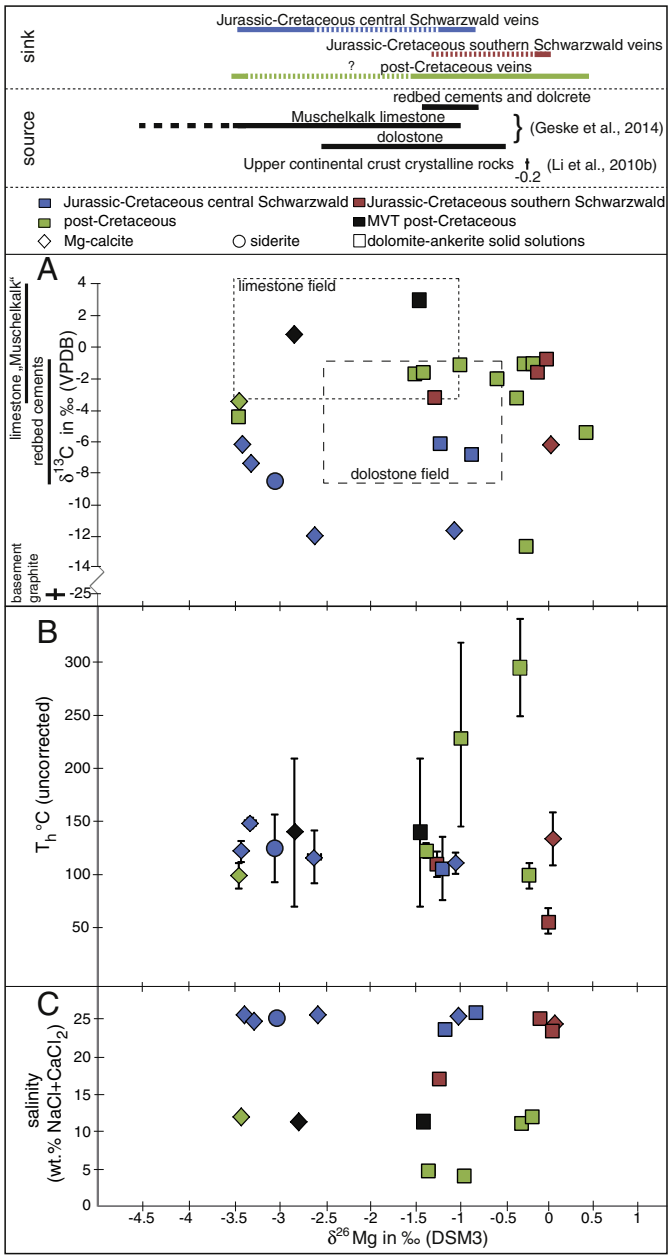

Fig. 7. A) Plot of magnesium versus carbon isotope ratios. Overburden of dolostone, limestone and graphite basement signatures are based on Staude et al. (2012a). Note distinct fields for limestone versus dolostone as based on carbon isotope ratios. Hydrothermal carbonate δ^{26}Mg isotope signatures reflect fluid sources of the dissolved Mg species overprinted in many cases on a lithological control. B) Hydrothermal carbonate magnesium isotope values versus fluid temperature reconstructions (uncorrected). Note lack of correlation. Some δ^{26}Mg could not be plotted due to the lack of fluid inclusion data for some samples. C) Plot showing reconstructed fluid salinity versus hydrothermal carbonate δ^{26}Mg isotope ratios. Note the lack of correlation.

(3) Post-Cretaceous, Upper Rhinegraben-related mineralizations are predicted to reflect the widest, least coherent hydrothermal carbonate δ^{26}Mg ratios, as various lithologies were brought into tectonic contact which were previously hydraulically separated. Accordingly, hydrothermal fluid reservoirs in the various aquifers are expected to have undergone complex mixing patterns (Fig. 7A). Notably, any mineralogical control seems not obvious with most dolomites having δ^{26}Mg values ranging from −3.5 to +0.5‰. The relation of the second cluster to an isotopically more depleted carbonate Mg source is supported by the observation, that both occurrences forming this cluster are situated in the direct vicinity of the Rhinegraben boundary fault, where limestone (Triassic and Jurassic strata) units are juxtaposed to paragneisses of the basement (Fig. 1).

(4) The Mississippi-Valley-Type (MTV) carbonates (black square and diamond in Fig. 7A) show depleted δ^{26}Mg ratios (−1.4 and −2.8‰) typical of carbonate rocks which agrees well with Pfaff et al. (2010) suggesting mixing ratios of 1:9 between an ascending basement fluid and the limestone aquifer.

The results are considered encouraging and support the notion that, at least for the present dataset, hydrothermal carbonate δ^{26}Mg isotope signatures broadly reflect two first order controls: (i) the geochemistry of the leached host aquifer and (ii) carbonate mineralogy. Obviously, these broad, first-order controls are superimposed by smaller-order effects such as fluid temperature that needs more attention.

7. Conclusions

A combined paleo-fluid and Mg isotope study dealing with well-constrained hydrothermal systems in the Schwarzwald mining district in SW Germany is presented. The following conclusions result:

Two different fluid systems are defined based on regional, geochemical and microthermometric data and published work: (i) a Jurassic–Cretaceous fluid system, reflecting a binary mixture between basement- and Muschelkalk-derived fluids and (ii) a post-Cretaceous (Cenozoic) fluid system which involves a complex array of fluid reservoirs.

Based on the Mg isotope signatures of all potential fluid reservoirs (basement rocks and sedimentary cover) as well as of hydrothermal carbonate phases, a relation between Mg source (aquifer rocks) and Mg sink (hydrothermal carbonate) becomes obvious. This control is superimposed on a mineralogical control, with dolomites being – on average – less ^{26}Mg depleted than low-Mg calcites. Magnesium isotope data are in agreement with reconstructed fluid sources as based on published gangue barite $^{87}Sr/^{86}Sr$ ratios. Specifically, the southern Schwarzwald veins of Jurassic and Cretaceous age show less depleted, silicate Mg isotope values compared to the central Schwarzwald Jurassic–Cretaceous veins. This result is in clear agreement with previously published work based on a variety of other tracers and calculations detailed here.

A significant outcome of this study is the observed lack of correlation between fluid temperature, fluid salinity (affecting precipitation rates) and hydrothermal carbonate δ^{26}Mg signatures. These observations are in contrast to theoretical considerations and experimental work regarding the impact of fluid temperature and precipitation rates on $\Delta^{26}Mg_{fluid\text{-}carb}$ and may exemplify the complexity of natural hydrothermal systems. It is here proposed that hydrothermal carbonate δ^{26}Mg signatures represent a first order control and hence a tracer of hydrothermal fluid sources and corresponding aquifer lithologies. Particularly, this is the case where fluids mix that leached/dissolved different aquifer lithologies each with characteristically different bulk δ^{26}Mg signatures.

Acknowledgments

We thank D. Buhl and K. Schauerte in the non-traditional stable isotope laboratory at Bochum for support with the analysis of Mg isotope data. R. Neuser is acknowledged for support in the cathodoluminescence laboratory at Bochum. Furthermore we thank T. Wenzel for help with the electron microprobe analyses and P. Jeiseke and S. Kaulfuß for sample preparation in Tübingen. M. Marks and M. Burisch is thanked for helpful hints and discussions. This study was supported by the Alfried-Krupp Prize for Young University Teachers of the Krupp Foundation to Gregor Markl and the German Research Foundation (DFG), grant 2135/20-1. We acknowledge the very detailed and constructive comments by

Chemical Geology reviewers J. Wimpenny and W-Y. Li and the editorial guidance by M. Böttcher.

Appendix I. Pressure correction

All samples were taken at an altitude between 300 and 1350 m above mean sea level (masl). Due to laterally uplift and variable erosion rates, the present-day erosional profile in the northern and central Schwarzwald exposes stratigraphically higher levels compared to those of the southern Schwarzwald. This differential uplift and erosional patterns are best explained by more pronounced Paleogene uplift of the southern Schwarzwald.

Moreover, the Permian and Mesozoic paleo-topography of what is presently the Schwarzwald area was characterized by sedimentary basins alternating with depositional highs (Geyer and Gwinner, 2011).

Veins in the northern and central Schwarzwald could be sampled either close to the Buntsandstein/Muschelkalk boundary (highest stratigraphic level, e. g. Neuenbürg, Neubulach), close to the Buntsandstein/basement unconformity (intermediate stratigraphic level, e. g. Wittichen, Karneolbank or in the basement not more than about 300 below the basement/cover unconformity (lowest stratigraphic level, e. g. Wenzel, Friedrich-Christian, Artenberg). The total height difference in this area is therefore less than 700 m. In contrast, most samples from the southern Schwarzwald (with exception of the region near the Swiss border) come from basement rocks with not even a close occurrence of sedimentary overburden.

By stratigraphic correlation with the basement-cover unconformity to the east of the southern Schwarzwald, the unconformity is assumed to have been about 1000 m above the Feldberg peak (1493 masl).

Hence, the veins in the vicinity of the Feldberg peak formed approximately 1000 m below the basement/cover unconformity and are the shallowest mineralizations in the southern Schwarzwald. They formed about 700 m below the deepest exposed veins in the central Schwarzwald. The stratigraphically deepest veins formed about 1000 m deeper than the Feldberg veins and hence, about 2000 m below the basement/cover unconformity. Due to the N–S and the W–E tilt during erosive exhumation of the Schwarzwald, each mineralization has to be corrected specifically, according to its depth during formation. We assume hydrostatic pressure conditions in the upper brittle crust, but before being able to apply this, we have to discuss the sedimentary overburden changing with time and location.

Assuming hydrostatic pressure conditions in fact of an open fracture assumption above the brittle ductile transition zone, the differential sedimentary overburden and its changes in time and space require discussion.

This task is most easily performed with respect to the Permian hydrothermal deposits. This is because the Mesozoic sedimentary cover was not yet deposited at that time. Corrections for depth estimates must thus only include basement erosion and, locally, the thickness of Permian volcanic deposits.

In contrast, with respect to Jurassic–Cretaceous and post-Cretaceous veins, an assessment of the former thickness of the Mesozoic sedimentary cover is more difficult due to inherent spatial and temporal changes. For example, the Buntsandstein formation in the northern Schwarzwald exceeds the stratigraphic thickness of the same unit near the German/Swiss border by at least 300 m. In the context of this work, we make use of data published by Rupf and Nitsch (2008) and Geyer and Gwinner (2011) for Permian to the Middle Jurassic Time interval. For Upper Jurassic strata, Rupf and Nitsch (2008) assume a stratigraphic thickness of 500 m for SW Germany while thicknesses of 1200 m for the southern and 1700 m for the northern and central Schwarzwald are proposed. Here, we use these estimates as minimum values in our calculations.

Early Jurassic veins presumably formed under overburdens of 200–400 m. The detailed data used for the stratigraphic reconstruction and the pressure corrections are presented in Table 3 and 4 of the electronic supplement. The pressure corrections for the high salinity fluids in Jurassic-Cretaceous veins are calculated in the range +1° to +5 °C.

Considering the significant error bars in overburden estimates, and the marginal differences in the endmember calculations for lithostatic and hydrostatic conditions the pressure corrections for the *Jurassic–Cretaceous* time is negligible.

Post-Cretaceous veins have not been dated radiometrically. Some early mineralizations within these veins might have formed at depths of 2000 m in the central and at depths of 3200 m in the southern Schwarzwald. Others, however, have formed with almost no overburden such as the mineralization related to the Baden-Baden or Badenweiler thermal wells which exist today.

Rough pressure corrections for low salinity inclusion assemblages show values of more than +40 °C. Depending on the salinity and less on temperatures, the pressure correction of post-Cretaceous fluid inclusions is a really important aspect for interpretation of formation temperature related to isotopic fractionation effects in *post-Cretaceous* veins. In fact of the unknown overburden thickness, the large variations in salinity in contact with the endmember considerations for lithostatic and hydrostatic pressure conditions it is currently not possible to do a realistic pressure correction for *post-Cretaceous* veins.

Appendix II. Semi-quantitative binary mixing model

In Section 6.5, we discussed the potential of Mg isotopes as a qualitative tracer for Mg sources. Interestingly, independent source tracers such as Sr-, Pb- or C-isotopes (Staude et al., 2011; Staude et al., 2012a,b; Ströbele et al., 2012) or the trace element distribution of sphalerite and fahlore (Staude et al., 2010a,b; Pfaff et al., 2011), all lead to very comparable results as also suggested by magnesium isotopes. Awaiting more research, this implies that $\delta^{26}Mg_{calcite}$ ratios are potentially important tracers for fluid Mg sources. Here the main outcome is that Jurassic–Cretaceous veins from the southern Schwarzwald show a dominant influence of fluids derived from the crystalline basement. In contrast, the veins of the central Schwarzwald show a larger proportion of sedimentary fluids originating from above the basement-cover unconformity. Based on these qualitative data, we feel that a quantification of the relative proportion of basement (=silicate) and cover (=limestone) sourced Mg is poorly constrained. Representing an approximatively first-order estimate, we provide a mixing model based on four assumptions:

(I) $\delta^{26}Mg_{fluid\text{-}aquifer}$ is based on best estimates
(II) binary mixing is considered the only mechanism
(III) no kinetic fractionation is assumed during the precipitation of the vein type carbonates
(IV) Mg contents of aquifers are chosen based on measured present-day aquifer data.

Minimum Mg content fluid input data were deduced based on regional datasets of reservoir chemistry as published in Pauwels et al. (1993) and Göb et al. (2013). As present-day reservoirs are diluted compared to the time of formation of the mineralizations, a maximum Mg content of ore-fluids is taken from Yardley (2005). The Jurassic–Cretaceous mixing is bracketed by these two endmembers. Mixing the two fluids (basement- and cover-derived) with their respective Mg contents resulted in the curves illustrated in figure A1A and B.

The estimate of $\delta^{26}Mg_{fluid}$ in the source aquifers is reported in Section 6.3.1. For the crystalline basement a $\delta^{26}Mg_{fluid}$ value of 0 to +1‰ is used, while for the carbonate cover aquifer, a $\delta^{26}Mg_{fluid}$ of −2 to −1‰ is taken. The fields of possible fluid mixing are calculated by the fractionation equations for calcite by Li et al. (2012), which are based on measured Mg-isotopes of the hydrothermal carbonates of the Wenzel (central Schwarzwald) and Urberg (southern Schwarzwald) mines and the median of the measured homogenization temperatures

of their respective fluid inclusion populations. The uncertainties of the fractionation equations are ± 1‰, which results in a large vertical field of a 2‰ shift. The intersection of the $\delta^{26}Mg_{fluid}$ with the curves defined by the Mg-concentrations in the fluids represents the field of possible fluid mixing. See x-axis in figure A1A and B. Please note, the Urberg vein from the southern Schwarzwald shows almost the same mixing ratio (close to basement endmember) as a mixing scenario that can be calculated based on Sr-isotope systematics by Staude et al. (2011).

The Wenzel mine in the central Schwarzwald, in contrast, shows a clear shift to the carbonate reservoir signature. This is in agreement with regional geological data and with the work of Staude et al. (2011) as based on Sr isotope data suggesting a sedimentary cover proportion of 10–30% fluid influx for the Wittichen mining district, which lies at a similar stratigraphic depth as the Wenzel mine. However, due to the curved slope of our mixing line, the field of fluid mixing in the central Schwarzwald basically covers the complete mixing variability from 0–100%. This less than satisfactory result is a consequence of the uncertainties of the fluid compositions and the errors of the fractionation equations. From this it concludes that at present, Mg isotopes should not be applied for quantitative calculations of fluid mixing as long as these uncertainties are not better constrained. With increasing knowledge about the source reservoir composition, decreasing uncertainties in the fractionation equations and more detailed $\delta^{26}Mg_{solid\text{-}solution}$ studies, it is expected that Mg isotopes will become a powerful tool in fluid sourcing.

(See Fig. A1.)

Appendix III. Supplementary data

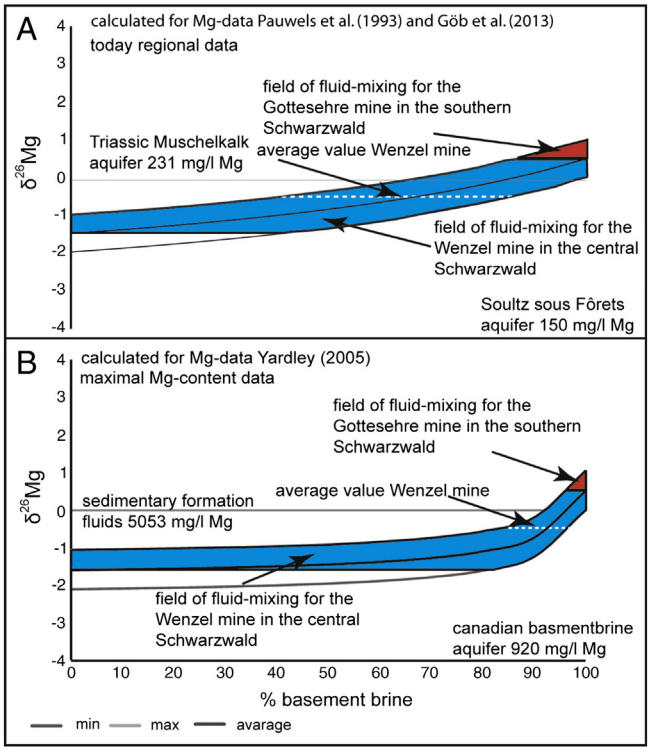

Fig. A1. A & B). Semi-quantitative Mg-isotope mixing model of basement (granite) and sedimentary cover (limestone).

Supplementary data to this article can be found online at http://dx.doi.org/10.1016/j.chemgeo.2015.02.009.

References

Altherr, R., Holl, A., Hegner, E., Langer, C., Kreuzer, H., 2000. High-potassium, calc-alkaline I-type plutonism in the European Variscides: northern Vosges (France) and northern Schwarzwald (Germany). Lithos 50 (1), 51–73.

Azmy, K., Lavoie, D., Wang, Z., Brand, U., Al-Asam, I., Jackson, S., Girard, I., 2013. Magnesium-isotope and REE compositions of Lower Ordovician carbonates from eastern Laurentia: implications for the origin of dolomites and limestones. Chem. Geol. 356, 64–75.

Baatartsogt, B., Wagner, T., Taubald, H., Mierdel, K., Markl, G., 2006. Hydrogen isotope determination of fluid inclusion water from hydrothermal fluorite: the results depend on the extraction technique. Chem. Geol. 1–21.

Baatartsogt, B., Schwinn, G., Wagner, T., Taubald, H., Beitter, T., Markl, G., 2007. Contrasting paleofluid systems in the continental basement: a fluid inclusion and stable isotope study of hydrothermal vein mineralization, Schwarzwald district, Germany. Geofluids 7, 123–147.

Bakker, R.J., Diamond, L.W., 2006. Estimation of volume fractions of liquid and vapor phases in fluid inclusions, and definition of inclusion shapes. Am. Mineral. 91 (4), 635–657.

Banks, D., Odling, N.E., Skarphagen, H., Rohr-Trop, E., 1996. Permeability and stress in crystalline rocks. Terra Nova 8, 223–235.

Banks, D., Boyce, A., Samson, I., 2002. Constraints on the origins of fluids forming Irish Zn–Pb–Ba deposits: evidence from the composition of fluid inclusions. Econ. Geol. 97 (3), 471–480.

Behr, H.J., Gerler, J., 1987. Inclusions of sedimentary brines in post-Variscan mineralizations in the Federal Republic of Germany — a study by Neutron Activation Analysis. Chem. Geol. 61, 65–77.

Beinlich, A., Mavromatis, V., Austrheim, H., Oelkers, E.H., 2014. Inter-mineral Mg isotope fractionation during hydrothermal ultramafic rock alteration — implications for the global Mg-cycle. Earth Planet. Sci. Lett. 392, 166–176.

Bodnar, R.J., Vityk, M.O., 1994. Interpretation of microthermometric data for H_2O–NaCl fluid inclusions. In: De Vivo, B., Frezzotti, M.L. (Eds.), Fluid Inclusions in Minerals, Methods and Applications. Virginia Tech, Blacksburg, pp. 117–130.

Boiron, M.-C., Banks, D., Yardley, B., Noronha, F., Miller, M., 1996. P–T–X conditions of late Hercynian fluid penetration and the origin of granite-hosted gold quartz veins in northwestern Iberia: a multidisciplinary study of fluid inclusions and their chemistry. Geochim. Cosmochim. Acta 60 (1), 43–57.

Boiron, M.-C., Cathelineau, M., Banks, D.A., Fourcade, S., Vallance, J., 2003. Mixing of metamorphic and surficial fluids during the uplift of the Hercynian upper crust: consequences for gold deposition. Chem. Geol. 194 (1), 119–141.

Boiron, M.-C., Cathelineau, M., Richard, A., 2010. Fluid flows and metal deposition near basement/cover unconformity: lessons and analogies from Pb–Zn–F–Ba systems for the understanding of Proterozoic U deposits. Geofluids 10, 270–292.

Bolou-Bi, E.B., Poszwa, A., Leyval, C., Vigier, N., 2010. Experimental determination of magnesium isotope fractionation during higher plant growth. Geochim. Cosmochim. Acta 74 (9), 2523–2537.

Bons, P.D., Elburg, M.A., Gomez-Rivas, E., 2012. A review of the formation of tectonic veins and their microstructures. J. Struct. Geol. 43, 33–62.

Bons, P.D., Fusswinkel, T., Gomez-Rivas, E., Markl, G., Wagner, T., Walter, B., 2014. Fluid mixing from below in unconformity-related hydrothermal ore deposits. Geology 42 (12), 1035–1038.

Brockamp, O., Schlegel, A., Clauer, N., 2011. Mesozoic hydrothermal impact on Rotliegende and Bunter immature sandstones of the High Rhine trough and its adjacent eastern area (southern Black Forest, Germany). Sediment. Geol. 234 (1), 76–88.

Bucher, K., Stober, I., 2010. Fluids in the upper continental crust. Geofluids 10 (1–2), 241–253.

Buhl, D., Immenhauser, A., Smeulders, G., Kabiri, L., Richter, D.K., 2007. Time series $\delta^{26}Mg$ analysis in speleothem calcite: kinetic versus equilibrium fractionation, comparison with other proxies and implications for palaeoclimate research. Chem. Geol. 244, 715–729.

Chang, V.T.-C., Makishima, A., Belshaw, N.S., O'Nions, R.K., 2003. Purification of Mg from low-Mg biogenic carbonates for isotope ratio determination using multiple collector ICP-MS. J. Anal. At. Spectrom. 18 (4), 296–301.

Demel, C., 2011. Geochemische Untersuchungen an der Forschungsbohrung Ro7516/B1 bei Freudenstadt, Nordschwarzwald. Diploma Thesis. University of Tübingen, Germany.

Derome, D., Cathelineau, M., Fabre, C., Boiron, M.-C., Banks, D.A., Lhomme, T., Cuney, M., 2007. Paleo-fluid composition determined from individual fluid inclusions by Raman and LIBS: application to mid-proterozoic evaporitic Na–Ca brines (Alligator Rivers Uranium Field, northern territories Australia). Chem. Geol. 237 (3–4), 240–254.

Edmunds, W.M., Savage, D., 1991. Geochemical characteristics of groundwater in granites and related crystalline rocks. In: Downing, R.A., Wilkinson, W.B. (Eds.), Applied Groundwater Hydrology, a British Perspective, pp. 199–216.

Emmermann, R., Althaus, E., Giese, P., Stöckhert, B., 1995. KTB Hauptbohrung results of geoscientific investigation in the KTB field laboratory, final report: 0–9101 m. KTB Reportp. 95-2 (E.).

Frape, S., Fritz, P., 1987. Geochemical trends for groundwaters from the Canadian Shield. Geol. Assoc. Can. Spec. Pap. 33, 19–38.

Frape, S., Fritz, P., McNutt, R.T., 1984. Water–rock interaction and chemistry of groundwaters from the Canadian Shield. Geochim. Cosmochim. Acta 48 (8), 1617–1627.

Fritz, P., 1997. Saline groundwater and brines in crystalline rocks: the contributions of John Andrews and Jean-Charles Fontes to the solution of a hydrogeological and geochemical problem. Appl. Geochem. 12, 851–856.

Fußwinkel, T., Wagner, T., Wälle, M., Wenzel, T., Heinrich, C.A., Markl, G., 2013. Fluid mixing forms basement-hosted Pb–Zn deposits: insight from metal and halogen geochemistry of individual fluid inclusions. Geology 41, 679–682.

Fußwinkel, T., Wagner, T., Wenzel, T., Wälle, M., Lorenz, J., 2014. Red bed and basement sourced fluids recorded in hydrothermal Mn–Fe–As veins, Sailauf (Germany): a LA-ICPMS fluid inclusion study. Chem. Geol. 363, 22–39.

Gallup, D.L., 1998. Geochemistry of geothermal fluids and well scales, and potential for mineral recovery. Ore Geol. Rev. 12 (4), 225–236.

Galy, A., Belshaw, N.S., Halicz, L., O'Nions, R.K., 2001. High-precision measurement of magnesium isotopes by multiple-collector inductively coupled plasma mass spectrometry. Int. J. Mass Spectrom. 208 (1), 89–98.

Galy, A., Bar-Matthews, M., Halicz, L., O'Nions, R.K., 2002. Mg isotopic composition of carbonate: insight from speleothem formation. Earth Planet. Sci. Lett. 201, 105–115.

Geske, A., Zorlu, J., Richter, D.K., Niedermayr, A., Immenhauser, A., 2012. Impact of diagenesis and low grade metamorphosis on isotope (δ^{26}Mg, δ^{13}C, δ^{18}O and ^{87}Sr/^{86}Sr) and elemental (Ca, Mg, Mn, Fe and Sr) signatures of Triassic sabkha dolomites. Chem. Geol. 332–333, 45–64.

Geske, A., Lockier, S., Dietzel, M., Richter, D.K., Buhl, D., Immenhauser, A., 2015a. Magnesium isotope composition of sabkha pore fluids and related (Sub-) Recent stoichiometric dolomites, Abu Dhabi (UAE). Chem. Geol. 393–394, 112–124.

Geske, A., Goldstein, R.H., Richter, D.K., Buhl, D., Kluge, T., John, C., Immenhauser, A., 2015b. The magnesium isotope (δ^{26}Mg) signature of dolomites. Geochim. Cosmochim. Acta 149, 131–151.

Geyer, O.F., Gwinner, M.P., 2011. Geologie von Baden -Württemberg. – 5, völlig neu bearbeitete Auflage. Schweizerbart'sche Verlagsbuchhandlung (Nägele u. Obermiller), Stuttgart (627 pp.).

Gleeson, S.A., Wilkinson, J.J., Stuart, F.M., Banks, D.A., 2001. The origin and evolution of base metal mineralising brines and hydrothermal fluids, South Cornwall, UK. Geochim. Cosmochim. Acta 65 (13), 2067–2079.

Göb, S., Wenzel, T., Bau, M., Jacob, D.E., Loges, A., Markl, G., 2011. The redistribution of rare-earth elements in secondary minerals of hydrothermal veins, Schwarzwald, southwestern Germany. Can. Mineral. 49 (5), 1305–1333.

Göb, S., Loges, A., Nolde, N., Bau, M., Jacob, D.E., Markl, G., 2013. Major and trace element compositions (including REE) of mineral, thermal, mine and surface waters in SW Germany and implications for water–rock interaction. Appl. Geochem. 33, 127–152.

Goldstein, R.H., Reynolds, T.J., 1994. Systematics of fluid inclusions in diagenetic minerals: SEPM Short Course 31. Soc. Sediment. Geol. 199.

Grandia, F., Canals, À., Cardellach, E., Banks, D.A., Perona, J., 2003. Origin of ore-forming brines in sediment-hosted Zn–Pb deposits of the Basque-Cantabrian Basin, Northern Spain. Econ. Geol. 98 (7), 1397–1411.

Hann, H.P., Chen, F., Zedler, H., Frisch, W., Loeschke, J., 2003. The Rand Granite in the southern Schwarzwald and its geodynamic significance in the Variscan belt of SW Germany. Int. J. Earth Sci. 92, 821–842.

Heijlen, W., Muchez, P., Banks, D.A., 2001. Origin and evolution of high-salinity, Zn–Pb mineralising fluids in the Variscides of Belgium. Mineral. Deposita 36, 165–176.

Heijlen, W., et al., 2003. Carbonate-hosted Zn–Pb deposits in Upper Silesia, Poland: origin and evolution of mineralizing fluids and constraints on genetic models. Econ. Geol. 98 (5), 911–932.

Heijlen, W., Banks, D.A., Muchez, P., Stensgrad, B.M., Yardley, B.W.D., 2008. The nature of mineralizing fluids of the Kipushi Zn–Cu deposit, Katanga, Democratic Repubic of Congo: quantitative fluid inclusion analysis using laser ablation ICP-MS and bulk crush-leach methods. Econ. Geol. 103, 1459–1482.

Heinl, C., 2000. Hydrothermale Alteration des Deckgebirges (Rotliegendes und Buntsandstein) im Offenburger Trog. Schwarzwald, Bremen (72 pp.).

Higgins, J.A., Schrag, D.P., 2010. Constraining magnesium cycling in marine sediments using magnesium isotopes. Geochim. Cosmochim. Acta 74, 5039–5053.

Higgins, J., Schrag, D., 2012. Records of Neogene seawater chemistry and diagenesis in deep-sea carbonate sediments and pore fluids. Earth Planet. Sci. Lett. 357, 386–396.

Immenhauser, A., Buhl, D., Niedermayr, A., Riechelmann, D., Dietzel, M., Schulte, U., 2010. Magnesium-isotope fractionation during low-Mg calcite precipitation in a limestone cave — field study and experiments. Geochim. Cosmochim. Acta 74 (15), 4346–4364.

Jenkner, B., 1986. Ein Vorschlag zur Neugliederung des sedimentären Oberrotliegenden in der Baden-Badener Senke und ihrer nordöstlichen Fortsetzung (Nordschwarzwald). Jahrbuch des Geologischen Landesamtes Baden-Württemberg 28, 49–159.

Kalt, A., Altherr, R., Hanel, M., 2000. The Variscan basement of the Schwarzwald. Eur. J. Mineral. 12, 1–43 (Beih.).

Kanz, W., 1987. Grundwasserfließwege und Hydrogeochemie in tiefen Graniten und Gneisen. Geol. Rundsch. 76 (1), 265–283.

Klemm, W., 1994a. Review of data on the composition of hydrothermal solutions during the Variscan and post-Variscan mineralizations in the Erzgebirge, Germany. Monogr. Ser. Miner. Depos. 31, 61–69.

Klemm, W., 1994b. Chemical evolution of hydrothermal solutions during Variscan and post-Variscan mineralization in the Erzgebirge, Germany. Metallog. Collisional Orogens 150–158.

Kostova, B., Pettke, T., Driesner, T., Petrov, P., Heinrich, C.A., 2004. LA ICP-MS study of fluid inclusions in quartz from the Yuzhna Petrovitsa deposit, Madan ore field, Bulgaria. Swiss Bull. Mineral. Petrol. 84 (1), 25–36.

Lavoie, D., Jackson, S., Girard, I., 2014. Magnesium isotopes in high-temperature saddle dolomite cements in the lower Paleozoic of Canada. Sediment. Geol. 305, 58–68.

Leach, D.L., Marsh, E., Ernbo, P., Rombach, C.S., Kelley, K.D., Anthony, M., 2004. Nature of hydrothermal fluids at the shale-hosted Red Dog Zn–Pb–Ag Deposits, Brooks Range, Alaska. Econ. Geol. 99 (7), 1449–1480.

Leach, D.L., Bradley, D.C., Husten, D., Pisarevsky, S.A., Taylor, R.D., Gardoll, S.J., 2010. Sediment-hosted lead-zinc deposits in Earth history. Econ. Geol. 105, 593–625.

Li, W.-Y., Teng, F.Z., Ke, S., Rudnick, R.L., Gao, S., Wu, F.Y., Chappell, B.W., 2010a. Heterogeneous magnesium isotopic composition of the upper continental crust. Geochim. Cosmochim. Acta 74 (23), 6867–6884.

Li, S.-L., Liu, C.-G., Li, J., Lang, Y.C., Ding, H., Li, L., 2010b. Geochemistry of dissolved inorganic carbon and carbonate weathering in a small typical karstic catchment of Southwest China: isotopic and chemical constraints. Chem. Geol. 277 (3), 301–309.

Li, W., Chakraborty, S., Beard, B.L., Romanek, C.S., Johnson, C.M., 2012. Magnesium isotope fractionation of inorganic calcite under laboratory conditions. Earth Planet. Sci. Lett. 333, 304–316.

Li, W., Beard, B.L., Li, C., Johnson, C.M., 2014a. Magnesium isotope fractionation between brucite [$Mg(OH)_2$] and Mg aqueous species: implications for silicate weathering and biogeochemical processes. Earth Planet. Sci. Lett. 394, 82–93.

Li, W.-Y., Teng, F.-Z., Wing, B.A., Xiao, Y., 2014b. Limited magnesium isotope fractionation during metamorphic dehydration in metapelites from the Onowa contact aureole, Maine. Geochem. Geophys. Geosyst. 15, 408–415.

Liu, X.-M., Teng, F.-Z., Rudnick, R.L., McDonough, W.F., Cummings, M.L., 2014. Massive magnesium depletion and isotope fractionation in weathered basalts. Geochim. Cosmochim. Acta 135, 336–349.

Loges, A., Wagner, T., Kirnbauer, T., Göb, S., Bau, M., Berner, Z., Markl, G., 2012. Source and origin of active and fossil thermal spring systems, northern Upper Rhine Graben, Germany. Appl. Geochem. 27 (6), 1153–1169.

Lüders, V., 1994. Geochemische Untersuchungen an Gangartmineralen aus dem Bergbaurevier Freiamt-Sexau und dem Badenweiler-Quarzriff (Schwarzwald). Abh. geol Landesamt Baden-Württemberg 14, 173–190.

Lüders, V., Möller, P., 1992. Fluid evolution and ore deposition in the Harz Mountains (Germany). Eur. J. Mineral. 4 (5), 1053–1068.

Lüders, V., Möller, P., 1995. Geochemie hydrothermaler Gangmineralisationen des Harzes. Zbl. Geol. Paläont Teil I 9 (10), 1329–1349.

Lüders, V., et al., 2010. Chemistry and isotopic composition of Rotliegend and Upper Carboniferous formation waters from the North German Basin. Chem. Geol. 276 (3), 198–208.

Markl, G., Lahaye, Y., Schwinn, G., 2006a. Copper isotopes as monitors of redox processes in hydrothermal mineralization. Geochim. Cosmochim. Acta 70, 4215–4228.

Markl, G., von Blanckenburg, F., Wagner, T., 2006b. Iron isotope fractionation during hydrothermal ore deposition and alteration. Geochim. Cosmochim. Acta 70, 3011–3030.

Martin, M., 2009. Geogene Grundgehalte (Hintergrundwerte) in den petrogeochemischen Einheiten von Baden-Württemberg. LGRB-Informationen 24, 98.

Mavromatis, V., Pearce, C.R., Shirokova, L.S., Bundeleva, I.A., Prokrovsky, O.S., Benezeth, P., Oelkers, E.H., 2012. Magnesium isotope fractionation during hydrous magnesium carbonate precipitation with and without cyanobacteria. Geochim. Cosmochim. Acta 76, 161–174.

Mavromatis, V., Meister, P., Oelkers, E.H., 2014. Using stable Mg isotopes to distinguish dolomite formation mechanisms: a case study from the Peru Margin. Chem. Geol. 1–33.

Metz, R., Richter, M., Schürenberg, H., 1957. Die Blei-Zink-Erzgänge des Schwarzwaldes. Beih. Geol. Jahrb. 29, 277.

Muchez, P., Heijlen, W., Banks, D., Blundell, D., Boni, M., Grandia, F., 2005. 7: extensional tectonics and the timing and formation of basin-hosted deposits in Europe. Ore Geol. Rev. 27, 241–267.

Nitsch, E., Zedler, H., 2009. Oberkarbon und Perm in Baden-Württemberg. LGRB-Information 22, 7–102.

Opfergelt, S., Georg, R.B., Delvaux, B., Cabidoche, Y.M., Burton, K.W., Halliday, A.N., 2012. Mechanisms of magnesium isotope fractionation in volcanic soil weathering sequences, Guadeloupe. Earth Planet. Sci. Lett. 341, 176–185.

Ortlam, D., 1974. Inhalt und Bedeutung fossiler Bodenkomplexe in Perm und Trias von Mitteleuropa. Int. J. Earth Sci. 63, 850–884.

Pauwels, H., Fouillac, C., Fouillac, A.M., 1993. Chemistry and isotopes of deep geothermal saline fluids in the Upper Rhine Graben: origin of compounds and water–rock interactions. Geochim. Cosmochim. Acta 57 (12), 2737–2749.

Pearce, C.R., Saldi, G.D., Schott, J., Oelkers, E.H., 2012. Isotopic fractionation during congruent dissolution, precipitation and at equilibrium: evidence from Mg isotopes. Geochim. Cosmochim. Acta 90, 1–16.

Pearson, J.F.J., Lolcama, J.L., Scholtis, A., 1989. Chemistry of waters in the Böttstein, Weiach, Riniken, Schafisheim, Kaisten and Leuggern boreholes: a hydrochemically consistent data set. NAGRA Technical Report 86–19, 153.

Pfaff, K., Romer, R.L., Markl, G., 2009. U–Pb ages of ferberite, chalcedony, agate, "U-mica" and pitchblende: constraints on the mineralization history of the Schwarzwald ore district. Eur. J. Mineral. 21, 817–836.

Pfaff, K., Hildebrandt, L.H., Leach, D.L., Jacob, D.E., Markl, G., 2010. Formation of the Wiesloch Mississippi Valley-type Zn–Pb–Ag deposit in the extensional setting of the Upper Rhinegraben, SW Germany. Mineral. Deposita 45 (7), 647–666.

Pfaff, K., Koenig, A., Wenzel, T., Ridley, I., Hildebrandt, L.H., Leach, D.L., Markl, G., 2011. Trace and minor element variations and sulfur isotopes in crystalline and colloform ZnS: incorporation mechanisms and implications for their genesis. Chem. Geol. 286 (3–4), 118–134.

Pogge von Strandmann, P.A.E., 2008. Precise magnesium isotope measurements in core top planktic and benthic foraminifera. Geochem. Geophys. Geosyst. 9 (12).

Riechelmann, S., Buhl, D., Schröder-Ritzrau, A., Riechelmann, D.F.C., Richter, D.K., Vonhof, H.B., Wassenburg, J.A., Geske, A., Spötl, C., Immenhauser, A., 2012a. The magnesium isotope record of cave carbonate archives. Clim. Past 8, 1849–1867.

Riechelmann, S., Buhl, D., Schröder-Ritzrau, A., Spötl, C., Riechelmann, D.F.C., Richter, D.K., Kluge, T., Marx, T., Immenhauser, A., 2012b. Hydrogeochemistry and fractionation pathways of Mg isotopes in a continental weathering system: lessons from field experiments. Chem. Geol. 300, 109–122.

Rupf, I., Nitsch, E., 2008. Das Geologische Landesmodell von Baden-Württemberg: Datengrundlagen, technische Umsetzung und erste geologische Ergebnisse. LGRB-Information 21.

Russell, M.J., Solomon, M., Walshe, J.L., 1981. The genesis of sediment-hosted, exhalative zinc + lead deposits. Mineral. Deposita 16 (1), 113–127.

Saenger, C., Wang, Z., 2014. Magnesium isotope fractionation in biogenic and abiogenic carbonates: implications for paleoenvironmental proxies. Quat. Sci. Rev. 90, 1–21.
Schauble, E.A., 2011. First-principles estimates of equilibrium magnesium isotope fractionation in silicate, oxide, carbonate and hexaaquomagnesium (2+) crystals. Geochim. Cosmochim. Acta 75, 844–869.
Schwarz, M., Henk, A., 2005. Evolution and structure of the Upper Rhine Graben: insights from three-dimensional thermomechanical modelling. Int. J. Earth Sci. 94, 732–750.
Schwinn, G., Markl, G., 2005. REE systematics in hydrothermal fluorite. Chem. Geol. 216, 225–248.
Schwinn, G., Wagner, T., Baatartsogt, B., Markl, G., 2006. Quantification of mixing processes in ore-forming hydrothermal systems by combination of stable isotope and fluid inclusion analyses. Geochim. Cosmochim. Acta 70, 965–982.
Shepherd, T.J., Rankin, A.H., Alderton, D.H., 1985. A Practical Guide to Fluid Inclusion Studies, 239 pp. Blackie Glasgow.
Shirokova, L.S., Mavromatis, V., Bundeleva, I., Pokrovsky, O.S., Bénézeth, P., Pearce, C., Gérard, E., Balor, S., Oelkers, E.H., 2011. Can Mg isotopes be used to trace cyanobacteria-mediated magnesium carbonate precipitation in alkaline lakes? Biogeosci. Discuss. 8, 6473–6517.
Sibley, D.F., Nordeng, S.H., Borkowski, M.L., 1994. Dolomitization kinetics in hydrothermal bombs and natural settings. J. Sediment. Res. 64, 630–637.
Staude, S., Bons, P.D., Markl, G., 2009. Hydrothermal vein formation by extension-driven dewatering of the middle crust: an example from SW Germany. Earth Planet. Sci. Lett. 286, 387–395.
Staude, S., Dorn, A., Pfaff, K., Markl, G., 2010a. Assemblages of Ag–Bi sulfosalts and conditions of their formation: the type locality of schapbachite ($Ag_{0.4}Pb_{0.2}Bi_{0.4}S$) and neighboring mines in the Schwarzwald ore district, southern Germany. Can. Mineral. 48, 441–466.
Staude, S., Mordhorst, T., Neumann, R., Prebeck, W., Markl, G., 2010b. Compositional variation of the tennantite–tetrahedrite solid-solution series in the Schwarzwald ore district (SW Germany): the role of mineralization processes and fluid source. Mineral. Mag. 74, 309–339.
Staude, S., Göb, S., Pfaff, K., Ströbele, F., Premo, W.R., Markl, G., 2011. Deciphering fluid sources of hydrothermal systems: a combined Sr- and S-isotope study on barite (Schwarzwald, SW Germany). Chem. Geol. 286 (1–2), 1–20.
Staude, S., Mordhorst, T., Nau, S., Pfaff, K., Brügmann, G., Jacob, D.E., Markl, G., 2012a. Hydrothermal Carbonates of the Schwarzwald ore district, southwestern Germany: carbon source and conditions of formation using $\delta^{18}O$, $\delta^{13}C$, $^{87}Sr/^{86}Sr$, and fluid inclusions. Can. Mineral. 50 (5), 1401–1434.
Staude, S., Werner, W., Mordhorst, T., Wemmer, K., Jacob, D.E., Markl, G., 2012b. Multistage Ag–Bi–Co–Ni–U and Cu–Bi vein mineralization at Wittichen, Schwarzwald, SW Germany: geological setting, ore mineralogy, and fluid evolution. Mineral. Deposita 47 (3), 251–276.
Steele-MacInnes, M., Bodnar, R.J., Naden, J., 2011. Numerical model to determine the composition of H_2O–NaCl–$CaCl_2$ fluid inclusions based on microthermometric and microanalytical data. Geochim. Cosmochim. Acta 75, 21–40.
Stober, I., Bucher, K., 1999. Deep groundwater in the crystalline basement of the Black Forest region. Appl. Geochem. 14, 237–254.
Stober, I., Bucher, K., 2004. Fluids sinks within the earth's crust. Geofluids 4, 143–151.
Stoffell, B., Appold, M.S., Wilkinson, J.J., McClean, N.A., Jeffries, T.E., 2008. Geochemistry and evolution of Mississippi Valley-Type mineralizing brines from the Tri-State and northern Arkansas districts determined by LA-ICP-MS microanalysis of fluid inclusions. Econ. Geol. 103, 1411–1435.
Ströbele, F., Staude, S., Pfaff, K., Premo, W.R., Hildebrandt, L.H., Baumann, A., Prenicka, E., Markl, G., 2012. Pb isotope constraints on fluid flow and mineralization processes in SW Germany Neues Jahrbuch für Mineralogie-Abhandlungen. J. Mineral. Geochem. 189 (3), 287–309.
Tipper, E., Galy, A., Bickle, M., 2006. Riverine evidence for a fractionated reservoir of Ca and Mg on the continents: implications for the oceanic Ca cycle. Earth Planet. Sci. Lett. 247 (3), 267–279.
Tipper, E.T., Galy, A., Bickle, M.J., 2008. Calcium and magnesium isotope systematics in rivers draining the Himalaya–Tibetan-Plateau region: lithological or fractionation control? Geochim. Cosmochim. Acta 72, 1057–1075.
Tipper, E.T., Gaillardet, J., Louvat, P., Capmas, F., White, A.F., 2010. Mg isotope constraints on soil pore-fluid chemistry: evidence from Santa Cruz, California. Geochim. Cosmochim. Acta 74 (14), 3883–3896.
Tipper, E.T., Lemarchand, E., Hindshaw, R.S., Reynolds, B.C., Bourdon, B., 2012. Seasonal sensitivity of weathering processes: hints from magnesium isotopes in a glacial stream. Chem. Geol. 312, 80–92.
Todt, W., 1976. Zirkon U/Pb-Alter des Malsburg-Granits vom Südschwarzwald. Neues Jb. Mineral. Monat. 12, 532–544.
Ufrecht, W., 2006. Zur Hydrogeologie der Aquifersysteme Buntsandstein und Muschelkalk zwischen Neckar und Donau. Schriftenr. des Amtes für Umweltschutz 19–48.
Walter, B.F., Apukthina, O.B., 2012. Kartierung und geochemische Untersuchungen der hydrothermalen Gangmineralisationen im Untermünstertal und bei Sulzburg im Südschwarzwald. Diploma Thesis. University of Tübingen, Germany.
Werner, W.F., Franzke, H.J., 1994. Tektonik und Mineralisation der Hydrothermalgänge am Schwarzwaldrand im Bergbaurevier Freiamt-Sexau. Abh. geol Landesamt Baden-Württemberg 14, 27–98.
Wetzel, A., Allenbach, R., Allia, V., 2003. Reactivated basement structures affecting the sedimentary facies in a tectonically "quiescent" epicontinental basin: an example from NW Switzerland. Sediment. Geol. 157, 153–172.
Wilkinson, J.J., 2010. A review of fluid inclusion constraints on mineralization in the Irish ore field and implications for the genesis of sediment-hosted Zn–Pb deposits. Econ. Geol. 105, 417–442.
Wimpenny, J., Colla, C.A., Yin, Q.-Z., Rustad, J.R., Casey, W.H., 2014a. Investigating the behaviour of Mg isotopes during the formation of clay minerals. Geochim. Cosmochim. Acta 128, 178–194.
Wimpenny, J., Yin, Q.-Z., Tollstrup, D., Xie, L.-W., Sun, J., 2014b. Using Mg isotope ratios to trace Cenozoic weathering changes: a case study from the Chinese Loess Plateau. Chem. Geol. 376, 31–43.
Wolfgramm, M., 2002. Fluidentwicklung und Diagenese im Nordostdeutschen Becken. Petrographie. Mikrothermometrie und Geochemie stabiler Isotope, Halle-Wittenberg.
Wolfgramm, M., Seibt, A., 2003. Geochemical characteristics of the formation fluid identified during stimulation tests on the Rotliegend geothermal reservoir in the NE German Basin (NEGB). European Geothermal Conference 2003.
Wombacher, F., Eisenhauer, A., Heuser, A., Weyer, S., 2009. Separation of Mg, Ca and Fe from geological reference materials for stable isotope ratio analyses by MC-ICP-MS and double-spike TIMS. J. Anal. At. Spectrom. 24 (5), 627–636.
Yardley, B.W.D., 2005. Metal concentrations in crustal fluids and their relationship to ore formation. Econ. Geol. 100, 613–632.
Young, E.D., Galy, A., 2004. The isotope geochemistry and cosmochemistry of Magnesium. Rev. Mineral. Geochem. 55, 197–230.

Anhang 7

Kolchugin A.N., Immenhauser, A., Walter, B.F., Morozov, V.P., (2016) Diagenesis of the palaeo-oil-water transition zone in a Lower Pennsylvanian carbonate reservoir: constraints from cathodoluminescence microscopy and isotope geochemistry

akzeptiert zur Veröffentlichung	Anzahl der Autoren	Position des Kandidaten in der Autorenliste	Wissen-schaftliche Idee des Kandidaten (%)	Datengenerier-ung des Kandidaten (%)	Analysen und Interpretat-ionen des Kandidaten (%)	Verfassen der Publikation durch den Kandidaten (%)
ja	4	3	20	20	20	20

Marine and Petroleum Geology 72 (2016) 45–61

Contents lists available at ScienceDirect

Marine and Petroleum Geology

journal homepage: www.elsevier.com/locate/marpetgeo

Research paper

Diagenesis of the palaeo-oil-water transition zone in a Lower Pennsylvanian carbonate reservoir: Constraints from cathodoluminescence microscopy, microthermometry, and isotope geochemistry

A.N. Kolchugin [a], A. Immenhauser [b, *], B.F. Walter [c], V.P. Morozov [a]

[a] Kazan Federal University, Institute of Geology and Petroleum Technologies, Russia
[b] Ruhr-University Bochum, Faculty for Geosciences, Institute of Geology, Mineralogy and Geophysics, Germany
[c] Eberhard Karls University Tübingen, Department of Geoscience, Germany

ARTICLE INFO

Article history:
Received 20 July 2015
Received in revised form
11 January 2016
Accepted 13 January 2016
Available online 14 January 2016

Keywords:
Carbonate reservoirs
Diagenesis
Geochemistry
Hydrocarbons

ABSTRACT

Oil-water transition zones in carbonate reservoirs represent important but rarely studied diagenetic environments that are now increasingly re-evaluated because of their potentially large effects on reservoir economics. Here, data from cathodoluminescence and fluorescence microscopy, isotope geochemistry, microthermometry, and X-ray tomography are combined to decipher the diagenetic history of a 5-m-long core interval comprising the oil-water transition zone in a Lower Pennsylvanian carbonate reservoir. The aim is to document the cementation dynamics prior, during, and after oil emplacement in its context of changing fluid parameters. Intergrain porosity mean values of 7% are present in the upper two sub-zones of the oil-water transitions zone but values sharply increase to a mean of 14% in the lower sub-zone grading into the water-saturated portions of the reservoir and a very similar pattern is observed for permeability values. In the top of the water-filled zone, cavernous porosity with mean values of about 24% is found. Carbonate cements formed from the earliest marine to the late burial stage. Five calcite (Ca-1 through 5) and one dolomite (Dol) phase are recognized with phase Ca-4b recording the onset of hydrocarbon migration. Carbon and oxygen cross-plots clearly delineate different paragenetic phases with Ca-4 representing the most depleted $\delta^{13}C$ ratios with mean values of about −21‰. During the main phase of oil emplacement, arguably triggered by far-field Alpine tectonics, carbonate cementation was slowed down and eventually ceased in the presence of hydrocarbons and corrosive fluids with temperatures of 110–140 °C and a micro-hiatal surface formed in the paragenetic sequence. These observations support the "oil-inhibits-diagenesis" model. The presence an earlier corrosion surface between phase Ca-3 and 4 is best assigned to initial pulses of ascending corrosive fluids in advance of hydrocarbons. The short-lived nature of the oil migration event found here is rather uncommon when compared to other carbonate reservoirs. The study is relevant as it clearly documents the strengths of a combined petrographic and geochemical study in order to document the timing of oil migration in carbonate reservoirs and its related cementation dynamics.

1. Introduction

Reservoir oil-water transition zones (Christiansen et al., 2000; Heasley et al., 2000; Byrnes and Bhattacharya, 2006; Carnegie, 2006) are generally described as the intervals from which both oil and water are produced. Following the definition of Fanchi et al. (2002), the top of this interval is the elevation at which water-free oil is produced. The lower limit, although often gradual, is the shallowest depth at which oil-free water is present. In some reservoirs, the entire column is in a transition zone. In the past, oil-water transition zones, ranging in thickness from less than 1 to several 100 m, were considered non-economic and often not cored (Christiansen et al., 2000). More recently, however, oil-water transition zones in reservoir rocks worldwide have been

* Corresponding author.
E-mail address: adrian.immenhauser@rub.de (A. Immenhauser).

http://dx.doi.org/10.1016/j.marpetgeo.2016.01.014
0264-8172/

increasingly re-evaluated and are now considered significant because of their potentially large effects (>30% of the estimated original oil in place) on reservoir economics (Fanchi et al., 2002).

Burial diagenetic processes and products within the interstices of reservoir rocks (shelf carbonates, chalk, clastics etc.) are clearly non-trivial with regard to the processes involved as these take place in the presence of two immiscible fluids, here oil and water (Worden et al., 1998, 1999; Jesenius and Burruss, 1990; Helgeson et al., 1993; Heggheim et al., 2005; Risnes et al., 2003, 2005; Sathar et al., 2012). This holds particularly true in the case of often mixed-wet carbonate reservoirs. This is because hydrocarbons contain abundant polar organic compounds that interact with the carbonate minerals (Ingalls et al., 2004; Hao et al., 2015). As a consequence, work dealing with experimental approaches, field studies and modeling with focus on the relationship between water-saturation, pH, wettability and relative permeability abounds (Christiansen et al., 2000; Morrow and Mason, 2001; Zhang et al., 2007; Sathar et al., 2012; Al-Dhahli et al., 2014).

Considering the potential significance of the oil-water transition zone, however, the number of published case studies dealing specifically with the carbonate diagenetic pathways of rocks in this crucial interval is still remarkably limited (Sellwood et al., 1993; Neilson et al., 1998; Heasley et al., 2000). The comparable scarcity of detailed studies represents an important information gap given the fact that the in-depth analysis of the paragenetic succession at water-oil contacts allows for the assessment of the timing of petroleum migration relative to diagenetic and tectonic events both for carbonate and clastic reservoirs (Burruss et al., 1983; Sellwood et al., 1993; Helgeson et al., 1993; Worden et al., 1998; Cox et al., 2010). Moreover, the comprehensive study of Worden et al. (1998) discusses, albeit from the perspective of clastic reservoirs, two conflicting schools of mind one termed as “oil-inhibits-diagenesis-model”, the other as “oil-does-not-inhibits-diagenesis-model”. The “oil-inhibits-diagenesis” model predicts that early emplacement of oil will inhibit (quartz, clay mineral, or carbonate) cementation and related pressure solution and consequently, reservoir quality is preserved. Conversely, the “oil-does-not-inhibits-diagenesis” model suggests that oil migration and emplacement is no major control of diagenetic pathways and attributes excess porosity to other factors.

This study provides a detailed description and interpretation of carbonate paragenetic phases from core material of a selected Bashkirian (Lower Pennsylvanian, *ca* 323–315 Ma) limestone reservoir in the Volga-Ural region of Russia. The focus is on a 5-m-long core interval representing the palaeo-oil-water transition zone. Paragenetic phases are brought into a temporal, burial, and mechanistic context. Making use of the detailed cement stratigraphy across the oil-water-transition zone documented here, we address the following four main questions:

1. What is the relation between carbonate diagenesis and oil migration? Specifically, does oil emplacement inhibits carbonate cementation or not?
2. Is oil migration assigned to a single paragenetic phase or expanded over a significant portion of the diagenetic pathway of the reservoir rock studied?
3. Are diagenetic fluids during oil emplacement discernible – in terms of their temperature and chemistry – from ambient pore fluids prior to and after oil migration?

The data shown here are significant for the wider understanding of palaeo-oil-water transition zones in carbonate reservoirs in general and highlight the potential of petrographic, microthermometric, and geochemical tools applied studied to these critical reservoir intervals.

2. Geological setting and economic significance

The focus of this study is on Lower Bashkirian limestones from an oil field of the Nurlatsky district in the Republic of Tatarstan (Russian Federation; Fig. 1). The units cored are situated in the Melekesskaya depression located in the south-central part of the vast Precambrian Russian craton (Fig. 1; Hachatryan, 1979). Devonian, Carboniferous, and Lower Permian clastic and shallow water carbonate units, overlaying a weathered Proterozoic basement surface, form the predominant sedimentary succession (Fig. 1; Alekseev et al., 1996; Buggisch et al., 2011). The thickness of the Paleozoic cover reaches about 1900 m. Exposures in this region are only present along major river valleys and are restricted to Neogene and Quaternary rocks.

In terms of its geological setting, the core interval studied is from an oil field located in the eastern part of the East-European carbonate platform, forming portions of the Volga-Ural anticline (Fig. 2; Hachatryan, 1979; Voytovich and Gatiyatullin, 2003). Following Permian sedimentation, the Volga-Ural region experienced a phase of tectonically stability with only minor vertical tectonic movements and very limited sedimentation. From the Neogene onwards, a steady tectonic uplift lead to erosion and the formation of major alluvial depositional systems (thickness up 100–150 m). The main structures of the Volga-Ural anticline were formed as a result of this vertical basement uplift (Hachatryan, 1979; Mkrtchyan, 1980).

Economically significant carbonates reservoir units are concentrated in the Lower Mississippian and the Lower Pennsylvanian, with the Bashkirian units being one of the main carbonate target intervals in the Volga-Ural region (Fig. 3). From a production point of view, significant portions of the Devonian clastic reservoirs rocks are in a late production stage and consequently, the main focus of oil exploration in this region is now on the Carboniferous reservoir rocks. The source rocks of the oil fields in Volga-Ural region (Gordadze and Tikhomirov, 2005; Galimov and Kamaleeva, 2015) are Upper Devonian (Frasnian–Famennian) black shales (Aizenshtat et al., 1998). These units comprise thinly bedded calcareous-siliceous successions with abundant organic matter (Yudina et al., 2002; Gordadze and Tikhomirov, 2005).

3. Depositional environment, stratigraphy, and sedimentology

Accessible data in the international literature with focus on the Carboniferous of the Russian platform are scarce to absent. Here, we provide a brief overview of the facies types found and place our findings in the ramp model of Proust et al. (1998). During the Pennsylvanian and Early Permian, the Russian Platform was characterized in its eastern domains by a large, wave-dominated carbonate ramp and the subsiding foredeep of the Ural Mountains (Proust et al., 1998, Fig. 2). Within this ramp setting, the carbonates studied here were deposited. Based on palaeomagnetic and palaeoenvironmental data, the climate zone assigned to the Melekesskaya depression during Pennsylvanian times was semi-arid and (sub-)tropical (Proust et al., 1998). As recognized in Lower Pennsylvanian sections worldwide (Heckel, 1986; Soreghan and Giles, 1999), the relative sea level fluctuated repeatedly forming hiatal and karstified units on a regional scale. In the short core interval studied here, however, evidence for significant subaerial diagenesis is lacking.

With reference to the middle Carboniferous ramp of the Russian platform, Proust et al. (1998) subdivide inner, mid- and outer ramp facies. The definition used is such that the inner ramp environment is placed permanently above the effective fair-weather wave base, the middle ramp environment is situated between the effective

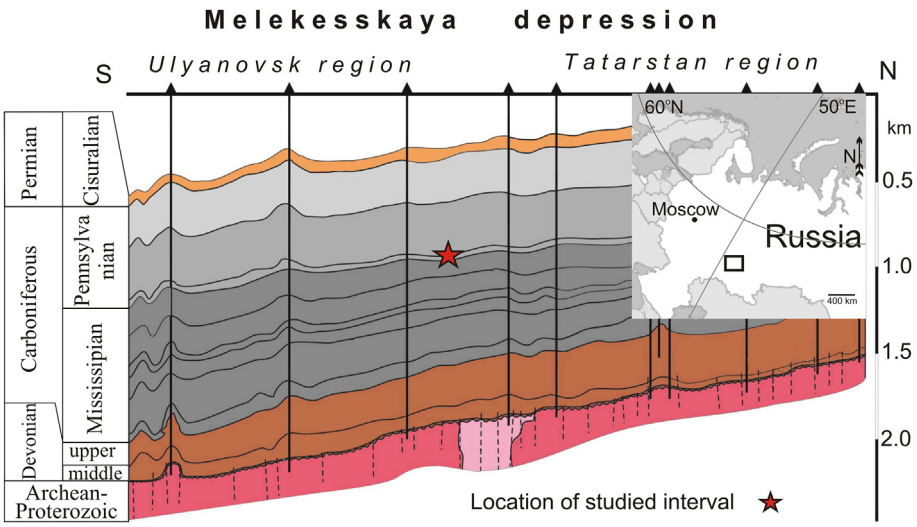

Fig. 1. Transect (south-north) across Melekesskaya depression with indication of main stratigraphic units and approximate indication of study window (modified after Gorunova, 2009). Small inset to upper right indicates position of study area.

storm and fair-weather wave base and the outer ramp is below situated near-permanently below the effective storm wave base with exceptional storm events resulting in wave base orbitals affecting fine-grained seafloor sediments (Immenhauser, 2009). The Bashkirian core portion (Fig. 3) studied in the context of this paper is best assigned a subtidal inner to middle ramp (Halymbadzha, 1962), characterized by normal marine seawater and small coral biostromes affected by occasional storm events. The presence of grainy facies, and specifically superficial ooids facies at some intervals (Fig. 4), points to frequent but not permanent (muddy facies) fair-weather or swell-wave base activity leading to entrainment and winnowing of fine-grained sediment. Evidence for an overall shallow, normal marine depositional setting comes from the overall subtidal mid-ramp biota including brachiopods, benthic foraminifera, crinoids or corals (Fig. 4; Bachtel and Dorobek, 1998; Burchette and Wright, 1992). In terms of the facies associations in the core studied here, these are best assigned to the "subtidal patch-reef and mud-flat lithofacies" of Proust et al. (1998, p. 1178). Small volumes of clastic detrital material are present in core material and include kaolinite in the clay insoluble material suggesting runoff (and/or aeolian transport) from emerged land in the regional vicinity (Kolchugin et al., 2013).

The main facies types found in the only 5-m-long section of Bashkirian core material across the oil-water transition zone studied here are bioclastic grainstones with coated grains and locally oncoidal-ooidal facies, bioclastic algal-foraminiferal packestones and less common, mud- and wackestones with abundant small and unspecified shell debris. In core samples, intact bivalve shells are locally found. At some intervals, coral framestone facies has been cored (Fig. 4E). Stratigraphically, the lower two section meters are characterized by an alternation of pack-to grainstones with two coral framestone intervals. Further upcore, poorly washed grainstones dominate the facies whilst the uppermost section meter is typified by wackestones.

3.1. Oil-water transition zone

Judging from a compilation of available well data, the oil-water transition zones in the stratigraphic interval studied range regionally in thickness from between 2 and 10 m. The present understanding is that the thickness of the transition zone depends on a series of factors that are interrelated in a non-trivial manner: (i) the position of the cored interval on the dome structure in the oil field. The thickness of the transition zone increases towards the dome center and decreases towards the flank of the dome; (ii) the productivity of the reservoir, specifically the thickness of the oil-saturated zone and spatial differences in oil saturation; (iii) the lateral and stratigraphic facies distribution across the oil field, with thicker oil-water transition zones (up to 10 m) in pack-to grainstone facies and stratigraphically thinner transition intervals (2 m and less) in wacke-to mudstone facies.

4. Methods

The core interval studied was drilled in June of 2013 but data sets on density, sonic, wettability, or geochemical data on gas phase CO_2 – now regularly compiled for more recently drilled wells – were either not compiled or are not available due to confidentiality reasons. Consequently, methods applied here focus on cathodoluminescence microscopy, micro-thermometry, and geochemical data complementing data on porosity, permeability, resistivity, and gamma ray (Ali, 1995; Kaufman et al., 1988; Bruckschen et al., 1992; Zeeh et al., 1995; Burley et al., 1989; Ehrenberg et al., 2002; Granier and Staffelbach, 2009; Carpentier et al., 2014). Below methods applied in this study are detailed. Data on resistivity and gamma ray are from the following sources (Gorbachev, 1990; Doveton, 1999; Khalil et al., 2015).

4.1. Isotope geochemistry

Matrix micrite and cement sub-samples were collected from core slabs, using a hand held drill with 1 mm diameter drill bits. The focus was on phase-specific cement data, hence only fabrics that were volumetrically significant enough to mechanically extract enough sample powder were selected. This refers mainly to late diagenetic fabrics. Cement data were complemented by a stratigraphic transect of bulk micrites sampled across the 5-m thick oil-water transition zone. A total of 25 carbon and oxygen isotope analyses were performed at the Ruhr University Bochum, Germany. For the analysis of C and O isotope ratios, between 0.27 and 0.33 mg of sample powder was dried in an oven at 105 °C for 48 h. Phosphoric acid (104%) was added to the sample, in a gasbench and then analyzed with a Finnigan MAT 253. Four repeat samples were analyzed for every sample batch of 48 samples. Adding the

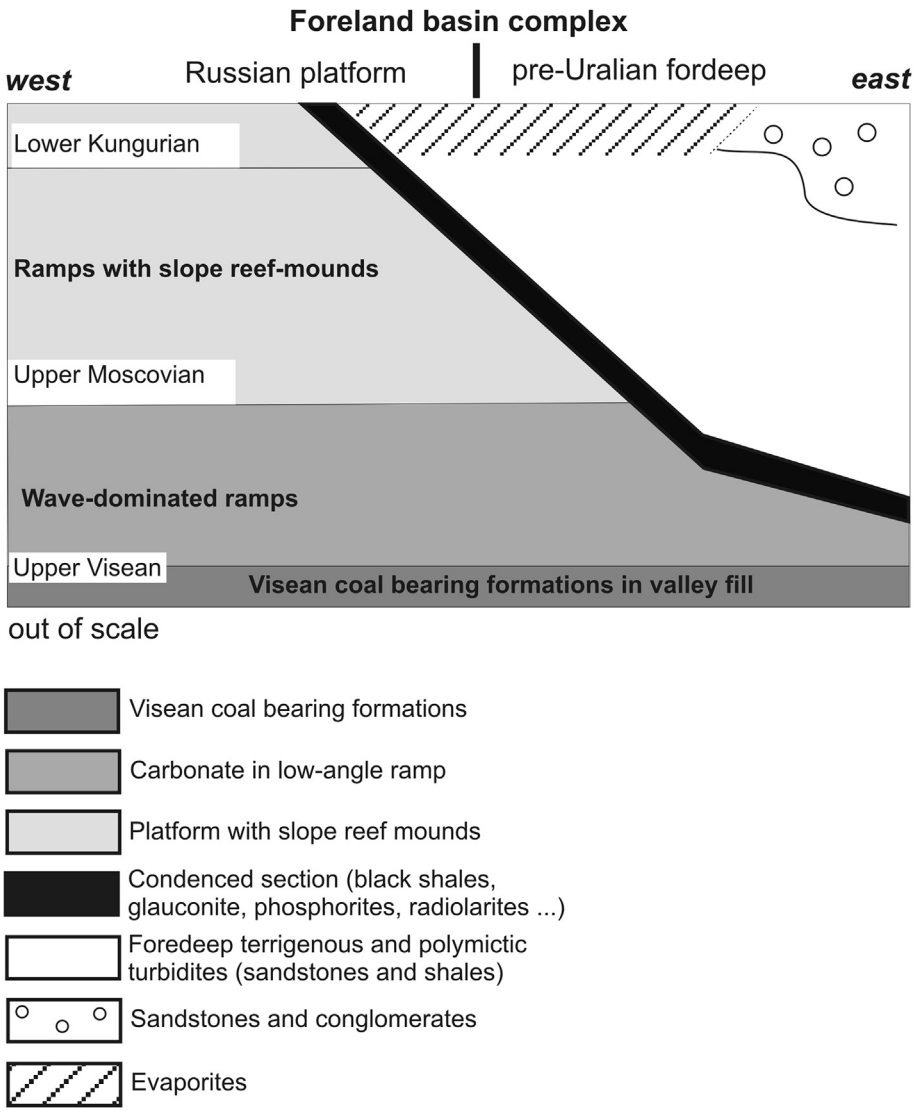

Fig. 2. Simplified scheme of the eastern border of the Russian carbonate platform forming a ramp-like morphology to the east towards the Pre-Uralian fore deep characterized by terrigenous turbidites. The carbonate deposits rest upon Visean terrigenous, coal bearing valley infills. Through time, the mid-Carboniferous carbonate ramp changes into a carbonate platform with a well-defined slope buried by evaporites during the early Kungurian (modified after Proust et al., 1998).

averaged internal standard deviations and the averaged difference of all duplicates suggests a variability of 0.08‰ for carbon and 0.09‰ for oxygen in all samples. Values are expressed in ‰ with respect to the Vienna PDB (V-PDB) standard.

4.2. Cathodoluminescence and fluorescence microscopy

Cathodoluminescence (CL) microscopy examination of different paragenetic phases termed Ca-1 through 5 was performed to obtain qualitative information on the geochemistry and precipitation environment of these fabrics. This was carried out with the 'hot cathode' CL microscope (type HC1-LM) at the Ruhr-University Bochum, Germany. The acceleration voltage of the electron beam is 14 kV and the beam current is set to a level gaining a current density of ~9 μA mm-2 on the sample surface. Refer to Christ et al. (2012) for details on the analytical procedure. Fluorescence (FL) microscopy of hydrocarbon inclusions was performed using a Leica EL6000 instrument using a mercury short-arc reflector lamp.

4.3. Porosity and permeability analysis

The determination of porosity and permeability values was performed on the UltraPoroPerm-500 installation in the uniform integrated module at the Kazan Federal University, Russia. Prior to analysis, full-size core cylinders of 30x50 mm were drilled out of samples. Hydrocarbons were extracted prior to analysis using the method described in Gordadze and Tikhomirov (2005). Pore space of samples was cleaned from oil, bitumen and also (non-diagenetic) salts (extraction). The solvents used included chloroform or ethanol and benzene mixed in a ratio of 1:1. The sample was placed in a cell equipped with a sample holder. A helium gazo-broad porozimeter with a high-precision linear converter of excessive pressure of 0–250 psi (0–17 bars) with a hysteresis less than ±0.11% of a limit of measurements was used. Permeability was measured on nitrogen gas with an atmospheric pressure. The measured porosity range is expressed as 0–40 units of porosity whilst the measured permeability range is expressed as $0.01 \cdot 10^{-3}$ μm^2 to $15 \cdot 10^{-3}$ μm^2.

X-ray tomography investigations were conducted using an industrial x-ray microtomography, Phoenix V|tome|X S 240 (Carl

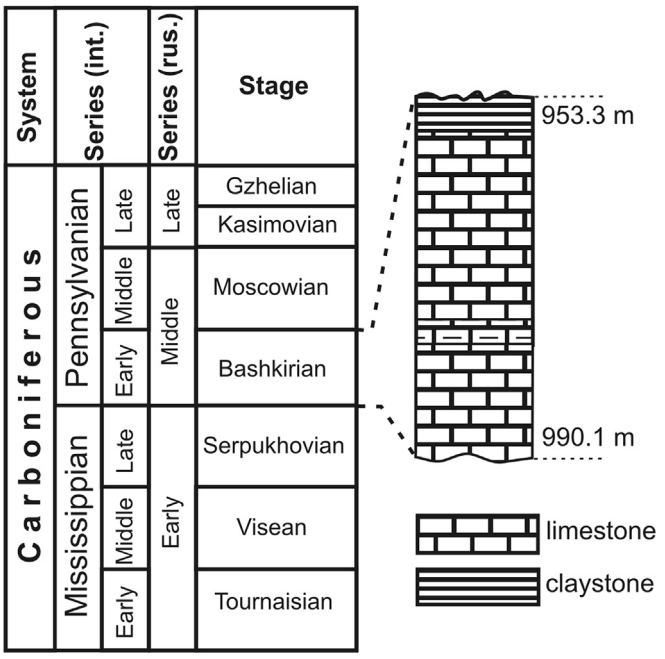

Fig. 3. Stratigraphy and general lithology of Bashkirian stage in the Melekesskaya depression with indication of international and Russian stratigraphic scheme. Note depths refer to absolute depth, i.e. meters below land surface.

Zeiss) at the Kazan Federal University, Russia. The system has two x-ray tubes 1) one being microfocal with maximum accelerating tensions of 240 kV/320 W and 2) one being nanofocal with maximum accelerating tensions of 180 kV/15 W. For the pre-processing of data and the creation of a pore volume model of a sample on the basis of x-ray pictures (projections) the software datos|x reconstruction was used. For data visualization and the analysis of data on elements of the volume image the software of VG Studio MAX 2.1 and Avizo Fire 7.1 was used.

4.4. Microthermometry

Sample C-133 (taken at core meter 1284) was cut perpendicular to the orientation of the idiomorphic Ca-5 generation and prepared as double polished thick section (~200 μm). Paragenetic phases Ca-2 to 4 do not show a preferred orientation of crystal c-axes. Relative chronological sequences of fluid inclusions (fluid inclusion assemblages (FIA) after Goldstein and Reynolds, 1994) were then established and documented by optical microscopy. Clearly identified primary (p), pseudo-secondary (ps) and secondary (s) inclusions were identified. A detailed explanation of fluid petrography terminology is given in Walter et al. (2015, their Fig. 4).

Microthermometric investigations were elaborated using a Linkam (model THMS 600) heating-freezing stage on a Leica DMLP microscope at fluid laboratory at Tübingen University. For each inclusion, we measured the final melting temperature of ice ($T_{m,ice}$), the final hydrohalite dissolution temperature ($T_{m,hh}$), and the homogenization temperature (T_h). For calibration, synthetic H_2O, H_2O–NaCl, and H_2O–CO_2 standards were used and only results with a maximum admissible variation of the final melting temperatures of less than 0.1 °C were used for data interpretation. For homogenization temperatures, a maximum admissible variation of up to 1 °C was accepted due to poor visibility in some samples. A limited number of inclusions and measurements with outlier in salinity and homogenization temperature within a homogeneous trail were disregarded as post-entrapment modification cannot strictly be excluded.

For the calculation of salinity and Ca/(Na + Ca) mole ratios, the Microsoft Excel-based calculation sheet of Steele-MacInnes et al. (2011) for the ternary NaCl–$CaCl_2$–H_2O system was used. The degree of fill was assessed optically with filling degree tables and illustrations of Shepherd et al. (1985). Pressure correction was done using the formula of Bodnar and Vityk (1994) in combination with estimates on sedimentary overburden based on Fig. 1.

5. Results

5.1. Gamma ray and electrical log, porosity, permeability, and oil saturation

Facies patterns data agree well with the gamma ray log data shown in Fig. 5. Essentially, the Bashkirian interval is built by a clean carbonate succession overlain by Moscovian clays. Electrical log data do not cover the full oil-water transition zone but terminate at the oil-water contact (sub-interval II).

The distribution of pore space is irregular both in the oil-saturated productive zone and across the oil-water transition interval (Fig. 5; Table 1). In the oil-saturated zones of the lowermost productive zone, i.e., the top of the core interval studied here, the dominant pore type is intergrain porosity (mean value of total (helium) porosity = 14%). Further down core into the oil-water transition zone intergrain porosity is still recorded but we also observe large cavernous pores and leaching along fractures. At the upper portions of the oil-water transition interval, mean measured values suggested 7–8% porosity whilst at the base of the core, i.e. the lower portion of the oil-water transition zone, porosity values of between 22 and 24% were found and permeability increases rapidly (Fig. 5, Table 1). The down core increase in porosity is well correlated with the increase of large cavernous pore space. Permeability data reveal a very similar overall pattern with values being very low and invariant at the base of the productive zone and across most of the oil-water transition zone (Fig. 5). Please refer to Table 1 for details. Centimetre-sized cavernous pores often connect through nets of leached channels. A prominent case example was studied by means of x-ray tomography and is documented in Fig. 6.

Oil-saturation was determined qualitatively from direct core observation. Oil-saturation is spatially irregular and decreases down core from the reservoir zone towards the water saturated zone. Within the base of the productive zone, limestone intervals with a high degree of oil saturation alternate with such that contain only limited volumes of hydrocarbons in pore space. The aquifer below the oil-water transition zone was not cored.

5.2. Petrography, mineralogy, and cathodoluminescence properties of carbonate cements

Based on rock sample (Figs. 4 and 7 through 9), thin section and cathodoluminescence analysis, the following petrographic succession has been established: (i) Phase Ca-1 (Fig. 10) representing the host sediment is characterized by differential degrees of diagenetic alteration. Very localized, early marine cements are present. This early marine fibrous phase nucleates on recrystallized coral skeletons (Fig. 4E, F) but is not considered any further here due to its volumetrically subordinate nature. The host sediment is commonly orange luminescent. The Ca-1 host sediment substratum is overlain by a non-luminescent early diagenetic, blocky to stubby calcite phase (50–500 μm in thickness) often, but not always, characterized by one to up to ten thin orange to yellow luminescence subzones in its outer portions (Ca-2; Figs. 8 and 9). Ca-2 cement morphologies are euhedral to anhedral depending on the morphology of the pore space they occlude. Phase Ca-2 is common

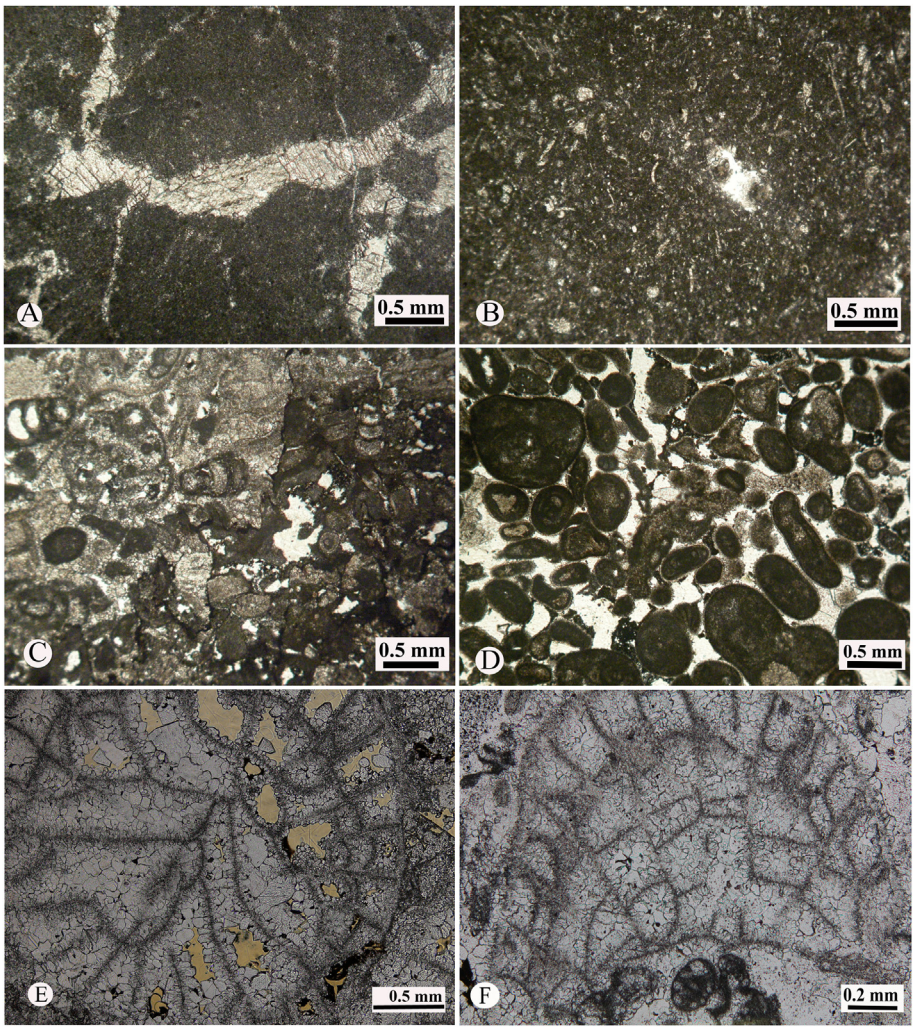

Fig. 4. Thin section images characterizing the different facies types present in the oil-water transition interval studied. (A) Peloidal mudstone with late diagenetic fractures filled by blocky calcite. (B) Fine-grained, argillaceous wackestone with abundant unspecified skeletal debris. (C) Coarse-grained algal, foraminiferal packstone. (D) Oncoidal and ooidal grainstone with composite grains and superficial ooids. (E/F) Coral framestone, note blocky calcite filling recrystallized coral skeletons. Early marine cement phase forms thin, isopachous rim on coral skeletons.

in all Bashkirian samples.

The next diagenetic phase paragenetically (Ca-3) is a dull to bright luminescent, usually blocky calcite (Figs. 8 and 9) with dimensions of some tens to some hundreds of μm depending on the size of the pore space occluded. Luminescence patterns reveal a complex zonation and banding in places. Often the luminescence color changes from bright to darker orange towards the crystal margins. The surfaces of Ca-3 calcite cements are commonly corroded and irregular (Fig. 8B, F). Ca-3 calcites are overlain by a volumetrically insignificant dolomite phase (Dol in Fig. 9F) characterized by a red, mottled luminescence color. Dolomite crystals usually are present as single crystals or as cluster of crystals each with a corroded surface (Fig. 10E and F). In some cases, relictic rhomboedric shapes of dolomite crystals are preserved.

The next fabric is stratigraphically represented by coarse blocky crystals of calcite (Ca-4) and forms one of the volumetrically most significant phases (some hundred μm to 1 cm in diameter; Fig. 7 through 9). Phase Ca-4 has a dark red or dark brown luminescence color often with a darker or lighter brown luminescence zone at its outer crystal margins. Two subtypes are observed. Subtype Ca-4a is a translucent blocky cement phase, whilst subtype Ca-4b is translucent but porous and yields numerous hydrocarbon inclusions ranging in size up to some tens of μm (Fig. 8D). Commonly, the surfaces of calcite phase Ca-4b are corroded (Fig. 8D, F). Subtypes 4a and 4b coexist in some samples. In this case, phase 4b overlies 4a with a sharp and planar boundary (Fig. 8D). Elsewhere, only subphase 4a (Figs. 8B and 9F) or subphase 4b (Fig. 8F) are present.

The paragenetically youngest, often blocky cement phase (Ca-5) is alternating light or dark orange under the cathodoluminescence and displays complex sectorial zoning (Fig. 8F). Crystals are similar in size to phase 4 and reach dimensions of many 100 μm to one cm.

5.3. Microthermometry and fluorescence

Green fluorescence colors of oil inclusions in phase 4 cements were found to be of limited diversity all thin sections studied. Non-oil fluid inclusions were recognized in paragenetic stages 3 through 5 and are document in Figs. 10 and 11. In phase 3 calcites, only liquid monophase fluid inclusions were observed. For calcite generations 4 and 5 detailed microthermometric investigations were performed. Freezing temperatures vary between −70 and −100 °C. First melt can be determined around −50 °C that implies a eutectic at −52 °C that is related to the ternary H_2O–NaCl–$CaCl_2$ system.

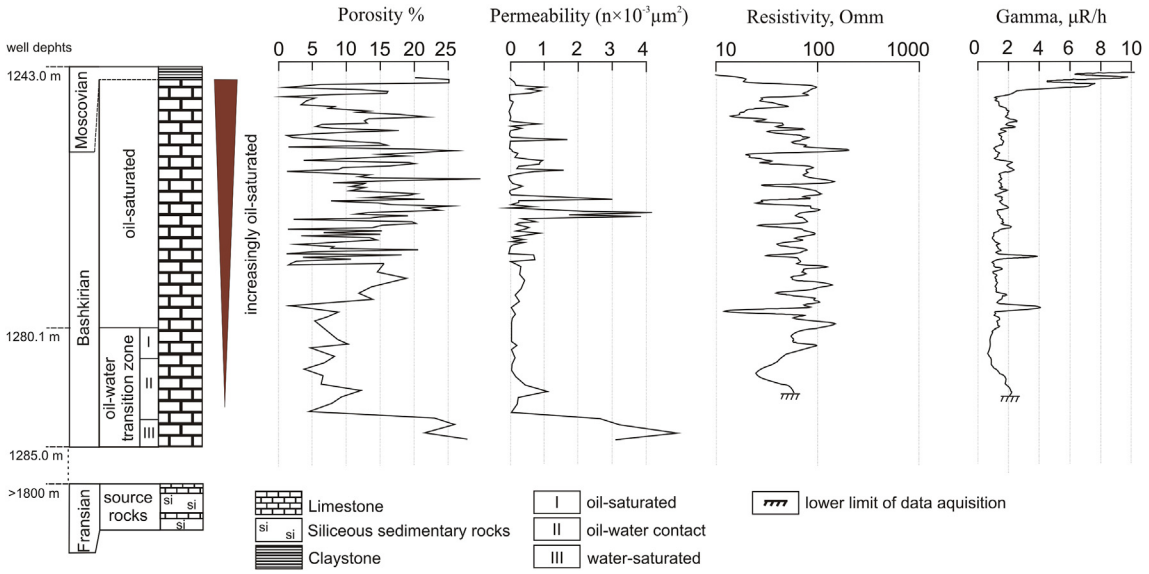

Fig. 5. Schematic geological section of reservoir facies and oil-water transition zone with indication of porosity, permeability, resistivity, and gamma ray data. Transition zone is indicated and subdivided in sub-zones I through III, with I being located at the limit to the overlying productive zone and III at the limit to the underlying water-wet zone. Note, depths are well depths in meters.

Table 1
Porosity-permeability data and type of porosity across the oil-water transition zone.

Zones	Depth, m	Value of open pore space, %	Permeability by gas (n × 10^{-3} μm^2) across layers succession	Type of porosity
Lower part of oil reservoir				
Oil-saturated	1276.5	15.57	0.29	intergrain
	1276.9	14.68	0.27	
	1277.2	18.77	0.40	
	1277.6	13.69	0.30	
	1277.9	12.01	0.12	
	1278.2	13.88	0.24	
	1278.5	2.17	0.01	
	1278.8	8.98	0.11	
	1279	7.47	0.04	
	1279.2	5.69	0.00	
Oil-water contact				
I	1280.1	8.88	0.01	intergrain
	1280.3	10.18	0.16	
	1280.5	5.13	0.01	
	1280.9	8.49	0.10	
	1281.2	7.2	0.03	
	1281.5	4.27	0.01	
	1281.8	6.78	0.13	intergrain and solution-enlarged
II	1282.2	6.52	0.42	
	1282.5	12.15	1.06	
	1282.8	9.56	0.20	
	1283.1	8.06	0.18	
	1283.5	4.78	0.01	
	1283.8	22.75	2.63	cavernous
III	1284.1	25.64	3.21	
	1284.5	21.32	4.89	
	1284.8	27.50	3.10	

Degree of fill shows constant values between 0.9 and 0.95.

For calcite 4, final melting temperature of ice varies from −18.3 to −20.7 °C and final dissolution temperatures for hydrohalite between −22.9 and −24.1 °C, that records a salinity of 20.7–22.2 wt.% (NaCl + $CaCl_2$). Homogenization temperatures vary from 107 to 140 °C (Fig. 10). The molar Ca/(Na + Ca) ranges between 0.13 and 0.21. Based on the ternary system a Ca content of 17000–27000 ppm and a Na content of 55000–67000 ppm can be calculated. Within one single trail, salinity and T_h are almost constant whilst these values vary between different trails.

In contrast for Ca-5 the microthermometric results for the final melting of ice show a variation from −18.8 to −21.9 °C and final dissolution temperatures for hydrohalite in the range of −24.8 and −29.6 °C (Fig. 11). These measurements can be translated into salinities of 20.8–22.7 wt.% (NaCl + $CaCl_2$). The molar Ca/(Na + Ca) ratio show in average a significant higher Ca content in the fluid from 0.26 to 0.53 with a calculated Ca content of 31000–53000 ppm and Na content of 27000–50000 ppm. Homogenization temperatures are in average lower as for Ca-4 and range from 80 to 118 °C (Fig. 10).

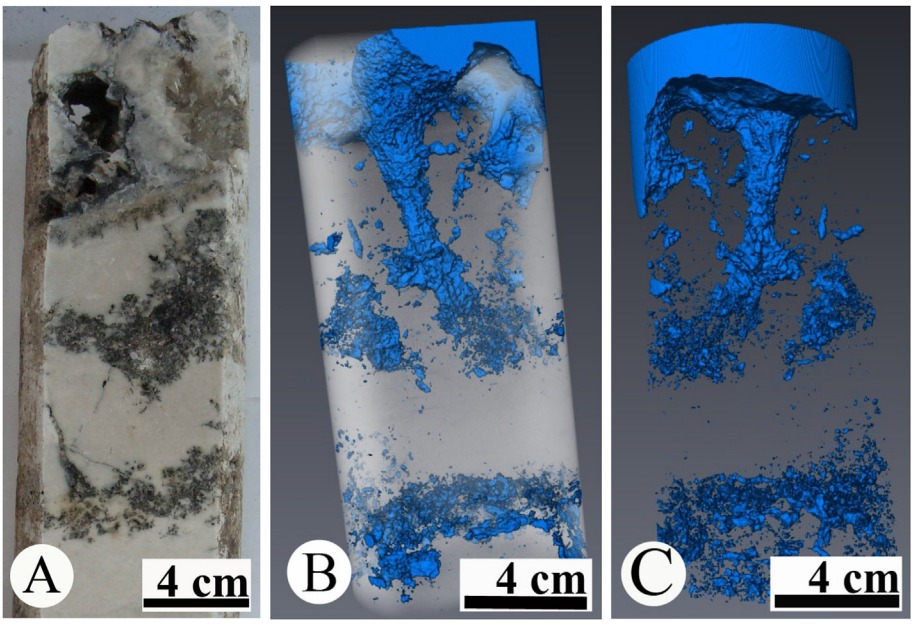

Fig. 6. X-ray tomography of core sample 1284.3–1284.6 m from sub-zone III close to the underlying water-filled interval. A) Photograph of core sample. B) Distribution of pore space in sample (blue). C) Display of pore space. Note cm-sized, spatially connected (cavernous) porosity (For interpretation of the references to color in this figure legend, the reader is referred to the web version of this article.).

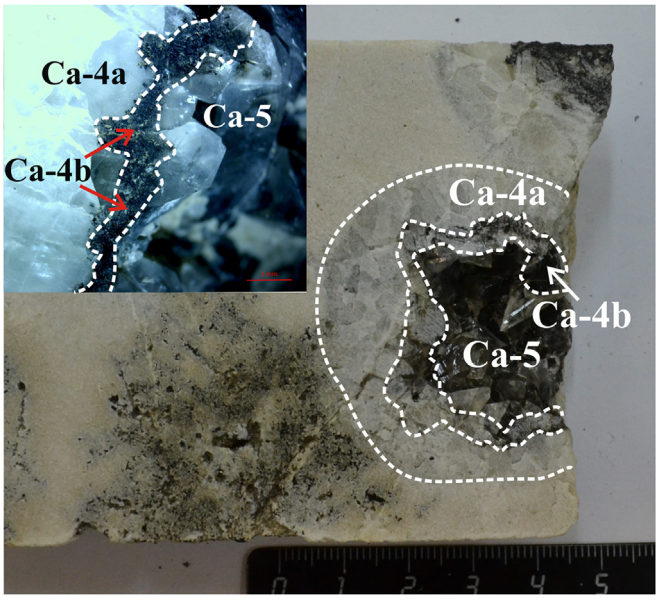

Fig. 7. Core sample and position of selected types of calcite cements Ca-4a, 4b and 5 that represent the volumetrically most important phases. Note black staining by hydrocarbons. Diameter of small upper left inset is 1.5 cm (For interpretation of the references to color in this figure legend, the reader is referred to the web version of this article.).

5.4. Carbon and oxygen isotope data of bulk micrites and carbonate cements

Bulk micrite $\delta^{13}C$ data range from −6.4 to −3.4‰ (n = 16; mean = −5.0‰) whilst $\delta^{18}O$ ratios are between −6.7 and −5.7‰ (n = 16; mean = −6.2‰; Table 2). Essentially, carbon isotope values shift to more negative values from the oil-water contact zone (~-4‰) upcore into the oil saturated zone (~−6‰). Conversely, oxygen isotope data remain comparable invariant across the short core section measured (Fig. 12).

Carbonate cement subsamples were collected from phases Ca-4a, Ca-4b and Ca-5, as these fabrics are volumetrically large enough to allow for the mechanical extraction of sample powder (Fig. 15; Table 3). The scatter of data is significant and ranges from −22.2 to −4.5‰ for carbon and from −6.7 to −4.9‰ for oxygen (Table 3). From carbonate phases Ca-2 and Ca-3, only one bulk sample could be extracted and the resulting values are −4.5‰ for carbon and −6.7‰ for oxygen. The significance of this small data set is unclear. Conversely, data from cement phases Ca-4a and b and Ca-5 are considered significant (Fig. 13). Generally, stage 4 and 5 cements are conspicuously depleted in $\delta^{13}C$ relative to the paragenetically earlier cement phases Ca-2 and 3 and bulk micrite samples, whilst they are similar in their oxygen isotope ratios. Carbon isotope data for Ca-4a cement range between −22.2 and −19.7‰ (n = 4) and represent, with respect to $\delta^{13}C$ the isotopically most depleted cluster in carbon-versus-oxygen isotope cross-plots. Oxygen isotope data of phase Ca-4a range from −4.9 to −5.4‰ (n = 4). Phase Ca-4b is slightly less depleted (−18.3‰), in ^{13}C relative to phase Ca-4a whilst $\delta^{18}O$ ratios are similar (Fig. 13). The paragenetic youngest (Ca-5) cement phase yields $\delta^{13}C$ ratios of between −12.6 and −11.2‰ (n = 3), $\delta^{18}O$ ratios are between −5.4 and −5.1‰ (n = 4) and plot in a specific cluster that is intermediate between bulk micrite and phase Ca-4 samples.

6. Interpretation and discussion

6.1. Cementation dynamics and timing of oil charge

Three subzones are subdivided across the transition zone: Subzone I represents the stratigraphically highest interval (1280.1–1281.8 m) directly beneath the productive, fully oil-saturated zone of the reservoir (Figs. 5 and 12). Subzone III is located in the lower part of oil-water transition zone (1284.1–1284.8 m), i.e. directly above the water-wet zone where oil-filled pores are rare to absent. Subzone II is intermediate in nature (Figs. 5 and 12). This subdivision is - to some degree –

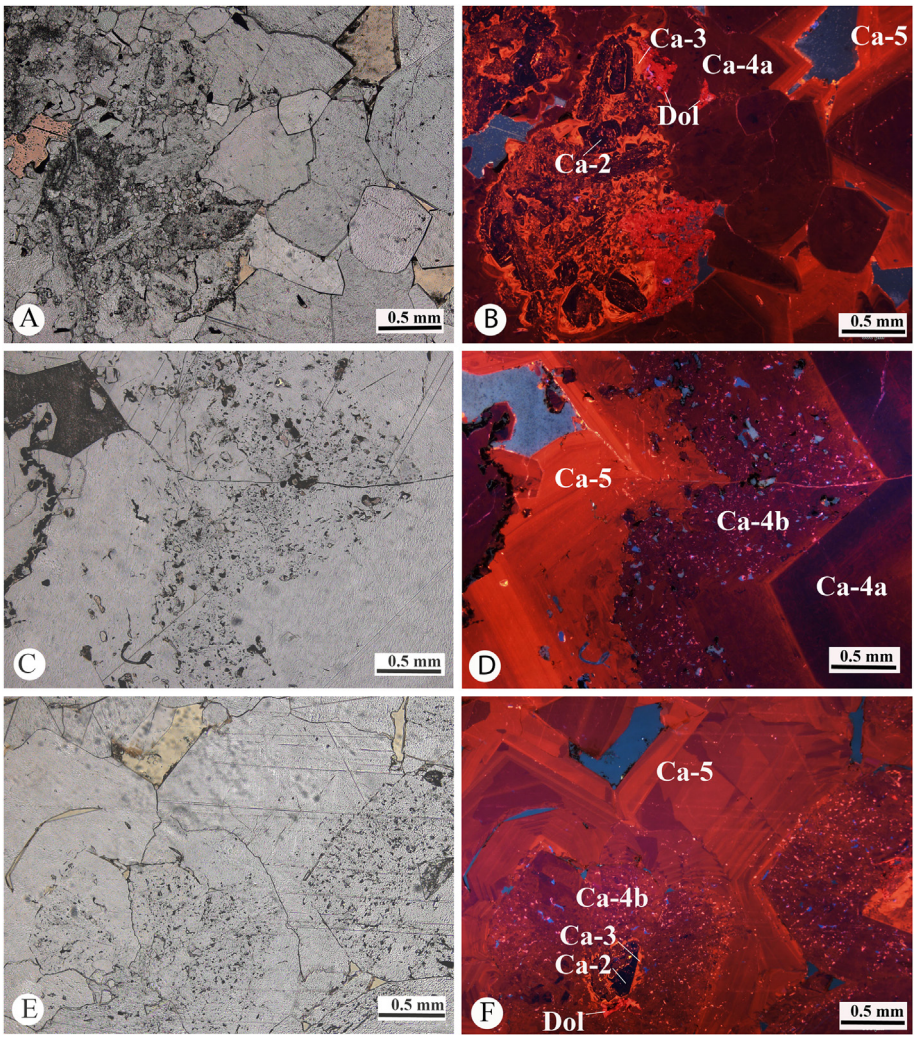

Fig. 8. Cathodoluminescence properties of different paragenetic phases placed against transmitted light photomicrographs. (A/B) Complex intergrowth of different cement types including a dolomite phase (Dol). (C/D) Cement phase Ca-4a, b and 5. Note sharp boundary between phase 4a and 4b and corrosive boundary to overlying phase Ca-5. Ca-4b is interpreted as paragenetic phase coeval to oil migration due to numerous hydrocarbon inclusions. Note complex zoning of phase Ca-5. (E/F) as (C/D), note hydrocarbon inclusions in phase Ca-4b and complex sector zoning of phase Ca-5.

artificial in nature as the boundaries are not sharp but gradual but serves the purpose to simplify the discussion.

The paragenetic succession of carbonate cements observed in thin sections from each of these subzones shares important similarities and differences (Fig. 14A–C). Paragenetic stages Ca-1, 2, and 3, representing the pre-emplacement phase, are present in all samples studied. Ca-1 represents the diagenetically stabilized sediment substratum upon which a series of marine to burial carbonate cements precipitate. The patchy luminescence of Ca-1 reflects the typical admixture of sediment consisting dominantly of magnesian calcites and probably aragonite particles that were later stabilized to diagenetic calcite in the presence of reducing fluid as evidenced by luminescence. Pore space is largely occluded by non-luminescent Ca-2 cements also found as first phase nucleating upon the sedimentary substratum (e.g., Fig. 9B and D). Following previous workers (Bruckschen and Richter, 1994), phase Ca-2 cements are here not considered fully marine in nature but probably represent a shallow burial phase (Kaufmann, 1997) precipitated from modified marine porewaters. In previous work (Walkden and Williams, 1991; Bruckschen et al., 1992; Bruckschen and Richter, 1994; Richter et al., 2003; Swart, 2015), thin yellow luminescent zones (Fig. 9D) in otherwise non-luminescent calcite cements have been interpreted as representing pulsed changes in Eh with transient intervals of sub-oxic fluids leading to the presence of Mn^{2+} incorporated into the crystal lattice (Bruckschen et al., 1992; Richter et al., 2003). Nevertheless, the oxidation stage of the pore fluid, and related to this the presence of Mn^{4+} and Mn^{2+} respectively, is not the only factor that must be considered. Based on experimental work Ten Have and Heijnen (1985), documented that differences in crystal growth rates significantly affect the luminescence patterns of carbonate cements. Moreover, activators other than Mn^{4+} (and quenchers) must be considered.

Similar to Ca-2, cement phase Ca-3 is present throughout all subzones of the water-oil-transition interval. The luminescence patterns of this phase are complicated showing banding and sector zoning (Fig. 9B and 14). In many cases, this phase is corroded at its outer margin pointing to a stage of non-cementation and corrosion between phase Ca-3 and Ca-4 most likely related to a change in pore fluid chemistry (Fig. 15). In several of the thin sections studied, phase Ca-3 is locally overlain by patchy dark-red to orange-brown luminescent, layered dolomite rhombs (Fig. 9F and 14) present throughout subzones I to III (Fig. 15). The precipitation of the dolomite spans the diagenetic stages of early hydrocarbon charge. Evidence for this comes from the inclusions rich-, corroded nature

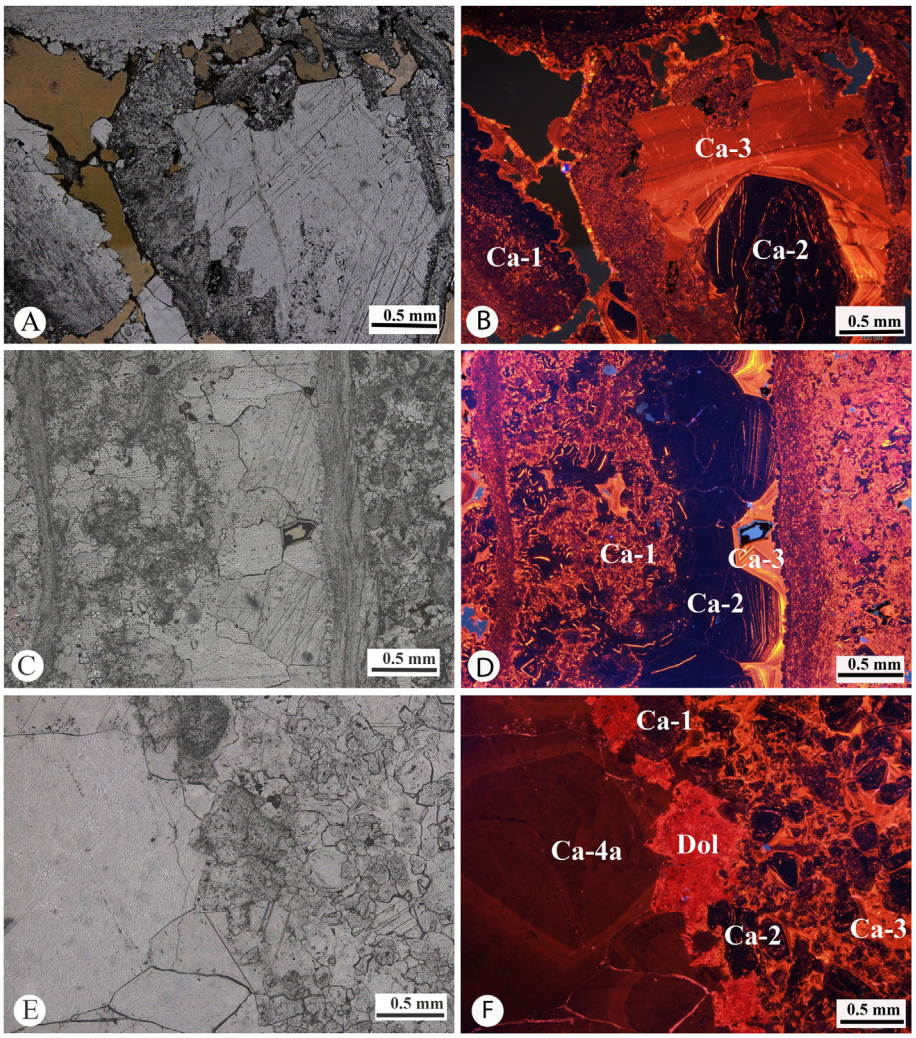

Fig. 9. Cathodoluminescence properties of different paragenetic phases placed against transmitted light photomicrographs. (A/B) Host sediment (Ca-1), non-luminescent blocky spar calcite (Ca-2), and bright orange luminescent blocky spar calcite cement (Ca-3). Note complex zoning of Ca-3. (C/D) Phase Ca-2 and 3 overlaying sediment substratum. Note bright luminescent zones in otherwise non-luminescent Ca-2 phase cements. (E/F) Coarse blocky Ca-4a phase overlying patchy luminescent dolomite cements (Dol) (For interpretation of the references to color in this figure legend, the reader is referred to the web version of this article.).

of the dolomite rhombs and paragenetic position overlying phase Ca-3a calcites. Dolomite precipitation is potentially related to changes in the partial pressure of fluid CO_2 (Morrow, 1982) with the first migration fronts of fluids ahead of the rising hydrocarbons being enriched in CO_2. This notion is in agreement with cement Ca-3 corrosion (Fig. 15).

Dark brown-red luminescent cement phase Ca-4a and b are of key significance for the understanding of the oil charge history of the Bashkirian reservoir facies under study. Based on the microthermometric data compiled here, phase Ca-4a and b cements precipitated from fluids with a salinity range of between 20.7 and 22.2 wt.% (Fig. 10) and a temperature range of between 107 and 140 °C (Fig. 11). The fluid chemistry is in agreement with a non-carbonate source, i.e. the Devonian black shales representing the source rocks (Aizenshtat et al., 1998). According to basin modeling, oil migration in the Volga-Ural region started – depending to the location studied – as early as the Late Triassic and goes on until present time (Kerimov et al., 2014). Several peak intervals of oil migration and accumulation during the Mesozoic and Cenozoic were proposed. Most workers, however, agree that the main oil migration and accumulation phase correlates with an Alpine stage of a tectogenesis. Based on regional data, the Alpine orogenic stage in the Oligocene to early Pliocene (Sharkov et al., 2015) resulted in the formation of the majority of modern structures in the region and triggered most of the oil accumulation in these structures (Ashirov, 1960). Judging from the presence of two corroded internal surfaces (i.e., between phase 3 and 4 and between 4 and 5, Fig. 15) two pluses of ascending corrosive fluids are recorded. These perhaps point to two regionally important fluid migration events resulting from tectonic far-field effects ("squeegee flow", cf. Immenhauser et al., 2007). The latter one of these two events was related to oil emplacement.

In subzone III (Fig. 14C), i.e. the interval that is closest to the water-filled zone, phase Ca-4b is lacking whilst 4a (Fig. 8B and D, 9F) is present. The main difference between Ca-4a and b lies in the presence of abundant oil and bitumen inclusions within phase Ca-4b. The boundary between Ca-4a and b is sharp with luminescent colors gradually turning into brown to black colors with a transition to brown-orange luminescence at the base of phase 4b. In the view of the authors, phase Ca-4b is essentially coeval to initial oil charge from the Devonian source rock into the Bashkirian reservoir facies. Interestingly, subzone III cements of this stage lack oil and bitumen inclusions suggesting spatially localized oil migration as opposed to migration through the bulk lithology. The

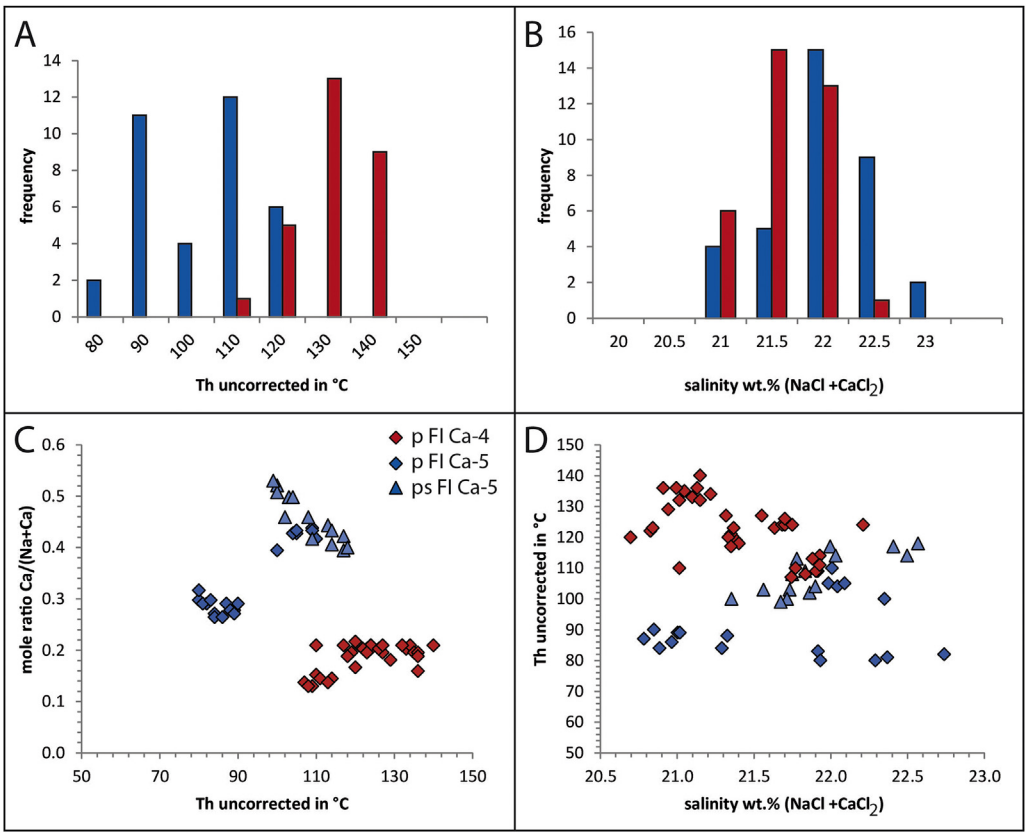

Fig. 10. Homogenization temperatures in cement phases Ca-4 and 5. (A) Histogram of measured homogenization temperatures. (B) histogram of calculated salinities in wt.% (NaCl + $CaCl_2$), (C) homogenization temperatures versus Ca/(Na + Ca) mole ratio, (D) salinity wt.% (NaCl + $CaCl_2$) versus homogenization temperatures. Note systematic variation (A–D) of fluids trapped in Ca-4 (red) and Ca-5 (blue) (For interpretation of the references to color in this figure legend, the reader is referred to the web version of this article.).

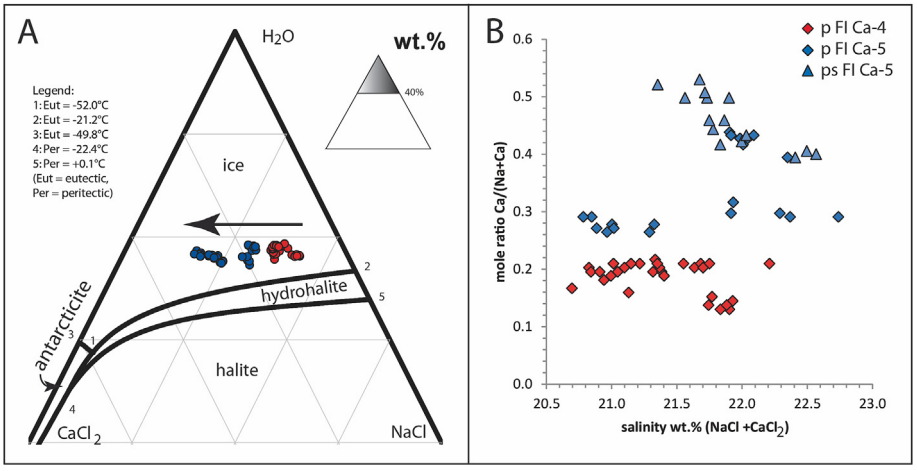

Fig. 11. Fluid salinity in cement phases Ca-4 and 5. (A) Microthermometric results in the ternary NaCl–$CaCl_2$–H_2O phase diagram. (B) salinity wt.% (NaCl + $CaCl_2$) versus Ca/(Na + Ca) mole ratio. Note systematic variation of fluids trapped in cement phases Ca-4 (red) and Ca-5 (blue) (For interpretation of the references to color in this figure legend, the reader is referred to the web version of this article.).

very limited spread of hydrocarbon inclusions fluorescence colors (green, wavelength of 548 nm) implies a single maturity of included oil (see discussion in Sellwood et al., 1993). In subzones I and II, phase Ca-4b is in turn corroded and in all subzones overlain by stage Ca-5 cements with complex luminescence banding and sector zoning (Fig. 8D, F and 14A, B). Based on microthermometric data, stage Ca-5 cements precipitated from fluids with a salinity range of 20.8–22.7 wt.% (Fig. 10), i.e. directly comparable to those of Ca-4 fluids, and a temperature range of 80 though 118 °C (Fig. 11). This fluid temperature range is lower by about 20 °C relative to Ca-5 fluids and judging from the fluid chemistry, these are mainly carbonate hostrock derived (Figs. 13 and 16). It is suggested that the initiation of phase Ca-5 cement precipitation reflects the end of the hydrocarbon migration and the post hydrocarbon stage (Fig. 15).

In comparison to previous studies linking oil charge with cement stratigraphy, the limitation of oil inclusions to one distinct

Table 2
Geochemical data of host matrix micrite bulk samples.

Subzones	Sample name	Well depth, m	$\delta^{13}C$ [‰](VPDB)	$\delta^{18}O$ [‰](VPDB)
I	L122a	1280.2	−6.1	−6.2
	L122a1	1280.3	−6.1	−6.2
	L123a	1280.5	−5.5	−6.3
	L123a	1280.5	−5.5	−6.2
	L124a	1280.7	−6.4	−5.7
	L125a	1281.1	−6.3	−6.3
	L126a	1281.5	−5.1	−5.7
	L127a	1281.8	−4.8	−6.2
II	L128a	1282.2	−4.2	−6.3
	L129a	1282.5	−4.2	−6.7
	L130a	1282.8	−4.5	−6.0
	L130a1	1283.1	−4.4	−6.2
	L132a	1283.5	−4.3	−6.1
	L133a	1283.8	−3.4	−6.2
III	L135a	1284.2	−4.0	−6.4
	L136a	1284.8	−4.3	−6.1

subzone III through I, i.e. towards the oil-saturated zone. It seems likely that this pattern reflects the presence of oil-derived light organic carbon included in the crystal lattice of inorganic calcite phases.

All bulk sediment and cement values are depleted in both ^{13}C (−4 to −23‰) and ^{18}O (−4.7 to −6.7‰) relative to reconstructed marine seawater values for the Bashkirian. Grossman et al. (2002) report Bashkirian brachiopod shell data from the Russian platform and find $\delta^{13}C$ values in the order of +5‰ and $\delta^{18}O$ in the order of −1.5‰. Particularly, the difference of about 10‰ in carbon isotope ratios between reconstructed seawater DIC (+5‰) and measured bulk micrite data (−5‰) is remarkable (Fig. 13). Essentially, phase Ca-2 and 3 plot in the same range in terms of carbon isotope ratios but are more ^{18}O-depleted relative to bulk sediments and other phases. In the absence of evidence for meteoric diagenesis, this may imply dissolution and reprecipitation processes of a formerly shallow marine burial phase in the presence of warm pore

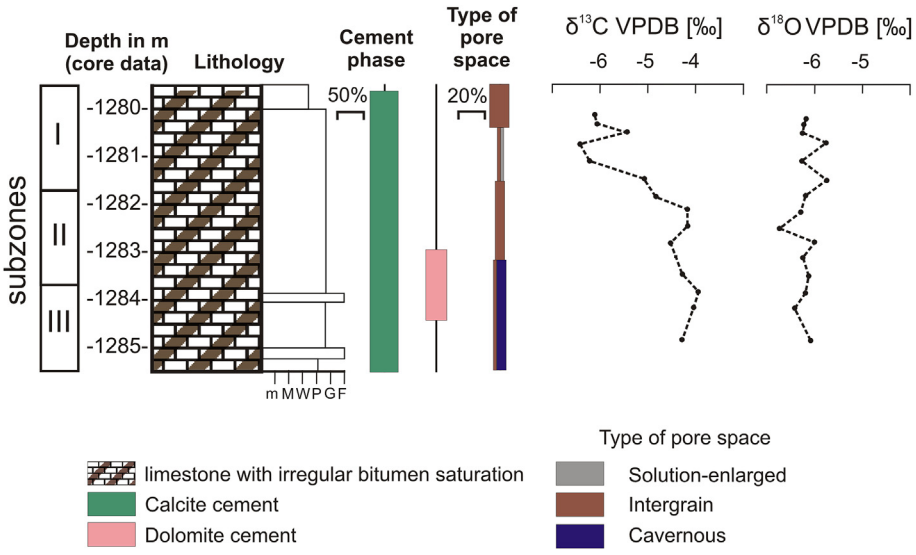

Fig. 12. Detailed geological section across oil-water transition zone with geochemical data, cement types and porosity. Note gradual depletion in ^{13}C from sub-interval III through I. Note, depths are well depths in meters.

paragenetic stage is uncommon (Simo and Lehmann, 2000). From a Cretaceous carbonate field in the U.A.E., Cox et al. (2010) for example, describe not less than 12 subsequent cathodoluminescence zones with oil inclusions. The later notion is in concert with oil charge and cement growth occurring synchronously over very extended time periods. Judging from the data shown here, the Bashkirian oil leg was charged rapidly and perhaps during a comparably brief period triggered by alpine tectonism (Fig. 15 through 17). Having said that, it is conceivable that the corroded surface between phase 4b and 5 (e.g., Fig. 8D) represents a cementation hiatus of unknown duration.

6.2. Carbonate isotope evidence

Carbon and oxygen isotope analyses were obtained from bulk sediments (mainly the fine grained micritic phase; Table 2) as well as from cement phases Ca-4 and 5 (Table 3). Cement volumes of phases Ca-2 and 3 are too small to mechanically separate phase-specific powder samples and hence, these phases were lumped in one analysis. Bulk matrix micrite values are plotted stratigraphically across the palaeo-oil-water transition zone (Fig. 12) and reveal a clear trend to increasingly ^{13}C-depleted values from fluids with a near-marine salinity. In comparison to published $\delta^{18}O$ values of calcite cements in some carbonate reservoirs (~−10 to −14‰; Cox et al., 2010), however, the oxygen isotope values shown here are not remarkably depleted. Using temperature equations for calcite $\delta^{18}O$ (Kim and O'Neil, 1997), a lower formation water temperature limit of 45 °C can be extrapolated but this depends on the choice of the $\delta^{18}O_{fluid}$ and the unknown fluid salinity and must be accepted within geologically reasonable error bars (Fig. 13).

Cement stages Ca 4a and b as well as 5 are less depleted in ^{18}O relative to bulk sediments and altered, early stage cements Ca-2 and 3 whilst they are more depleted in carbon isotope ratios (Fig. 13). The decreasing cement $\delta^{13}C$ with increasing burial depth contrasted by moderately increasing $\delta^{18}O$ is uncommon (Cox et al., 2010). In the view of the authors, slightly less ^{18}O depleted values of cement phases 4 and 5 might either imply a decrease of formation water temperature or, perhaps more likely, an increase of fluid salinity or a combination of both (Steinhauff et al., 1999). The opposing trend, i.e. increasingly ^{13}C depleted values with progressing cementation (Figs. 12, 13 and 16) is perhaps best explained in the context of volumetrically significance volumes of ^{13}C depleted organic matter related to hydrocarbon migration.

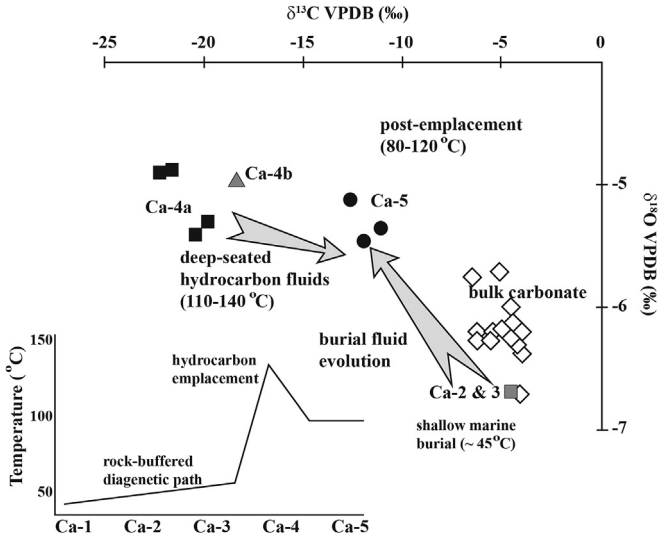

Fig. 13. Cross plot of carbon and oxygen isotope values measured from bulk sediment part of samples and different types of calcite cements with indication of reconstructed fluid palaeotemperature. Note trend to more depleted ^{13}C values of cement phases Ca-4 and 5 relative to bulk sediment. Lower left inset displays schematic temperature history of paragenetic phase Ca-1 through Ca-5. See text for discussion.

Particularly, the most depleted phase 4a is characterized by numerous oil inclusions suggesting that these cements grew in pores that contained both water and oil. It seems likely that organic compounds released ^{13}C-depleted carbon in the precipitating fluid that was then included in the calcite lattice. In agreement with the interpretation brought forward, oil charge took place during the Ca-4a cementation stage and consequently, carbon isotope values of this phase are the most depleted ones. Source rock-derived CO_2 (~−25‰) most likely mixes with rock-derived marine carbon and the resulting data obtained from these carbonate cements precipitated from these fluids lie somewhere on a mixing line between these end members (Fig. 13).

6.3. Porosity and permeability patterns across the oil-water transition

The boundary between subzones II and III, i.e. the transition to the lower portion of the palaeo-oil-water transition zone (Fig. 5) is characterized by a marked increase in porosity from between 5 and 10% to on average 15% (peak values of 25%, Figs. 5 and 17) and permeability. Given that the carbonate facies above the oil-water transition zone is in essence directly comparable to that below, the increase in porosity and permeability is best explained by the differential diagenetic history of the productive zone relative to the oil-water transition interval. Judging from the data available, the syn-oil emplacement phase Ca-4b and particularly the post emplacement phase Ca-5, that occludes significant portion of pore space in subzone I and II of the oil-water transition zone (Fig. 7), is absent in the productive zone above and the water-filled zone beneath explaining the significant increase in porosity and permeability (Fig. 5).

Judging from thin sections and particularly X-ray tomography, the general trend of increasing porosity and permeability in subzone III of the oil-water transition zone is caused by leached channels and a system of connected cavernous porosity (Fig. 6). These channels and cavernous pores are considered the result of non-equilibrium processes in the water filled zone of the transition zone, where hydrocarbons create local changes in the fluid physic–chemical properties with lowered fluid pH and a changing CO_2 regime (Helgeson et al., 1993).

6.4. Did oil emplacement inhibit carbonate cementation?

With regard to carbonate reservoirs, the commonly held view is that calcite cementation in oil saturated carbonate reservoirs is limited or inhibited in the presence of hydrocarbons, displacing burial brines. This is because the transport of dissolved ions and aquo-complexes to the site of, and required for, carbonate cementation demands an aqueous medium, usually burial brines. Cements such as dolomite, kaolinite, quartz, barite, celestine, sphalerite, and galena (Neilson and Oxtoby, 2008) form in the presence of abundant hydrocarbons in the reservoir above the oil-water contact, whereas carbonate cements precipitate in the aquifer below (Heasley et al., 2000; Worden and Heasley, 2000). These concepts can be tested using the data set presented here.

Cement phase 4b is a clear case example of a calcite phase precipitating from pore fluids containing both oil and water (Fig. 8D). Evidence comes from the numerous oil inclusions implying an initial overlap in the timing of oil migration and emplacement and phase 4b cementation. Carbonate fields are, in many cases, only weakly oil-wet (but more often mixed-wet) when compared to clastic reservoirs (Heasley et al., 2000). Essentially, oil films form at the surface of pores and adhere to carbonate surfaces whilst the bulk pore space remains water filled (mixed-wet). Moreover, oil may be transported as micro-droplets (emulsion) in essentially water-wet reservoirs and droplet were attached to the crystallization front to become subsequently built into phase Ca-4b cements. Judging from thin sections, the increasingly inclusion-rich, porous, and corroded nature of these calcites is indicative that the oil-water ratio increased and cementation was gradually retarded. At some stage, cementation ceased (Fig. 15). During peak oil migration, corrosion of carbonate cements took place leading to the formation of a hiatal interval expressed as the irregular interface between phase Ca 4b and phase Ca-5 cements. The subsequent onset of phase 5 is indicative of a significantly decreased oil-water ratio, resulted in cementation fronts that were essentially water wet, and continued cement precipitation (Fig. 15).

The data shown here for a limestone reservoir agree well with the conclusions previously drawn for quartz cementation during oil emplacement (Worden et al., 1998, 1999). These authors suggest that quartz cementation came to a halt when the precipitating fluids were unable to reach the pore space in an oil-wet system. Concluding from the here documented case example, the “oil-does-not-inhibits-diagenesis” model applies as long as the oil-to-water ratio is low. When a threshold limit is passed, the “oil-inhibits-diagenesis” model reasonably describes the formation of a corroded, hiatal surface in the cement succession occluding pore space.

7. Conclusions

(1) A detailed geochemical, cathodoluminescence, fluorescence, and microthermometric analysis of a 5-m-thick palaeo-oil-water transition zone was performed with focus on five calcite (Ca-1 through Ca-5) and one dolomite paragenetic cement phase. Diagenetic environments range from syn-depositional marine to late burial in nature.

(2) The presence of a corrosive micro-hiatal surfaces and numerous oil inclusions in phase Ca-4b cements points to ascending hot fluids with temperatures of 110–140 °C and a salinity range of 20.7–22.2 wt.% related to oil emplacement. Florescence imaging implies a single maturity of included oil. The fluid chemistry is in agreement with a non-carbonate

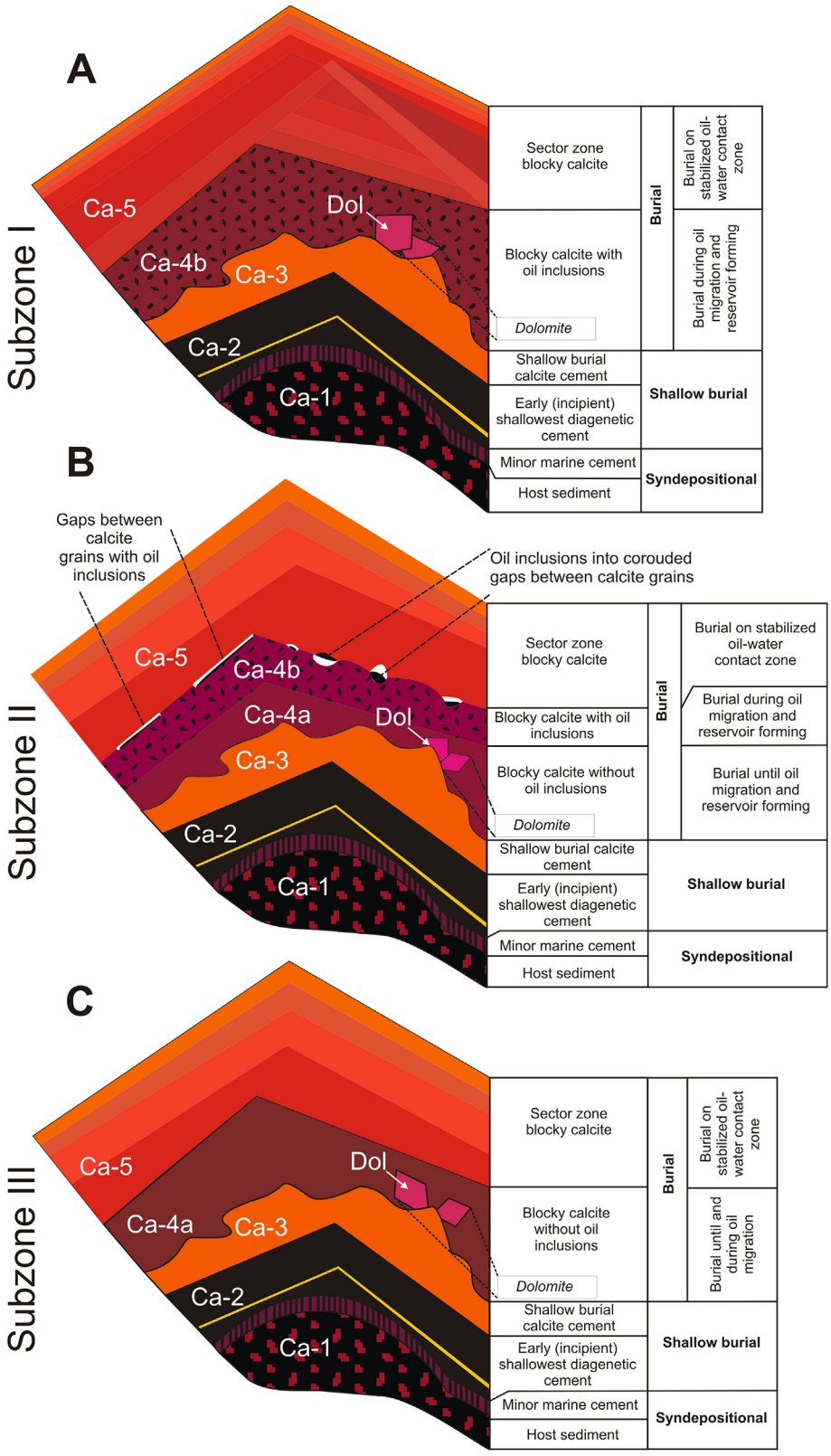

Fig. 14. (A–C). Schematic overview of cement paragenesis in subzones I (A), II (B) and III (C) of oil-water transition zone. See Fig. 12 for relative position of subzones.

source, i.e. the Devonian black shales representing the source rocks.

(3) An earlier corrosive interval, separating stage Ca-3 and 4 and cements lacking hydrocarbon inclusions is best assigned to a first pulse of ascending fluids in advance of the hydrocarbon migration front. Post oil-emplacement cements (Ca-5) reflect cooler fluid temperatures in the order of 80–120 °C and

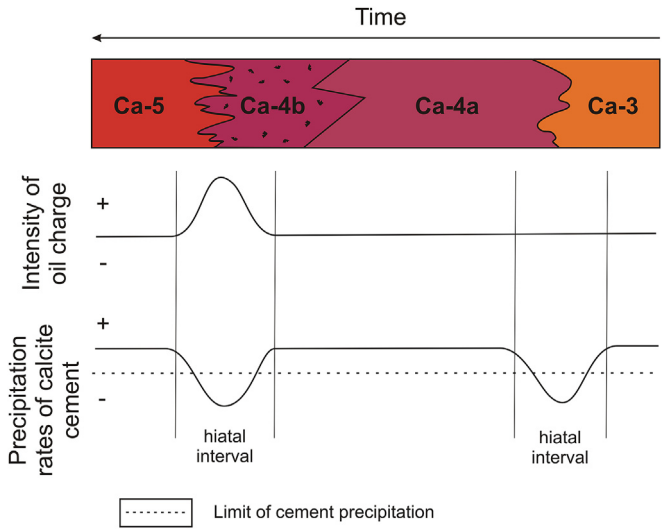

Fig. 15. Conceptual figure placing paragenetic phases versus non-precipitation/leaching leading to formation of micro-hiatal intervals in context to oil charge. Two pluses of ascending corrosive fluids are recorded in micro-hiatal surfaces. Oil charge is related to the second of these corrosive intervals. Note thickness of paragenetic phases is not to scale.

Table 3
Geochemical data of different paragenetic phases.

Sample name	Type of cement	$\delta^{13}C$ [‰](VPDB)	$\delta^{18}O$ [‰](VPDB)
C 130 a	Ca-2 & Ca-3	−4.5	−6.7
C 133 b	Ca-4a	−19.7	−5.3
C 133 d	Ca-4a	−22.2	−4.9
C 133 d	Ca-4a	−21.7	−4.9
C 136 b	Ca-4a	−20.4	−5.4
C 133 c	Ca-4b	−18.3	−5.0
C 135 a	Ca-5	−12.0	−5.4
C 136 a	Ca-5	−11.2	−5.4
C 133 a	Ca-5	−12.6	−5.1

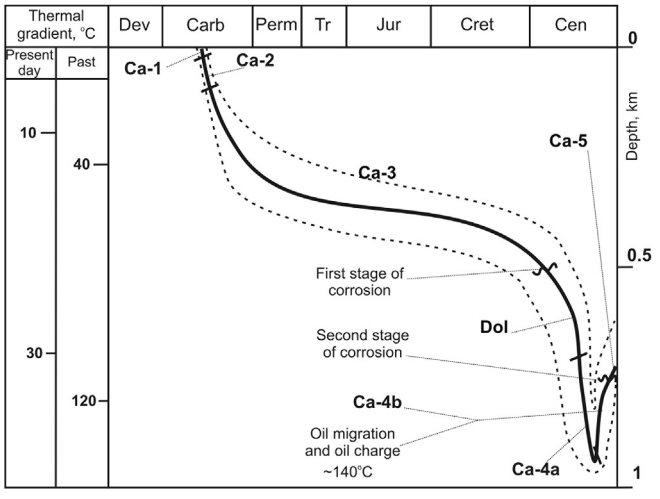

Fig. 16. Schematic temperature–time plot of basin evolution and main paragenetic events recorded in the Bashkirian carbonate rocks studied here. Note, present-day thermal gradients (measured directly in bore holes) differ from those reconstructed for Cenozoic times characterized by pulses of hot ascending fluids triggered by tectonic far-field effects. Assignment of specific paragenetic phases to specific stratigraphic intervals is not well constrained.

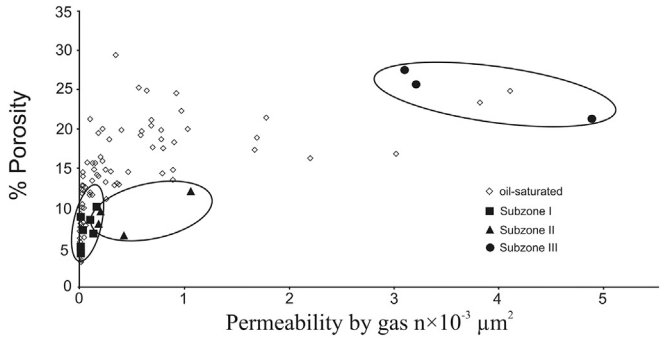

Fig. 17. Cross plot of porosity and permeability measured from oil-saturated core intervals and subzones I, II, III of oil water transition zone.

present day borehole measurements indicate temperatures in the order of about 30 °C.

(4) Porosity and permeability values are highly variable in the productive zone above the oil-water-transition zone but decrease down-core into the transition zone and increase again (up to 25% porosity) towards to water-saturated zoned. Judging from X-ray tomography, the increase in both porosity and permeability at the base of the oil-water transition zone is related to a system of leached channels and a system of connected cavernous porosity.

(5) At an early stage of oil emplacement, hydrocarbons were – in the view of the authors – transported as droplets (emulsion) in essentially water-filled pores and droplets attached to the crystallization front were subsequently built into phase Ca-4b cements. The data shown here support the "oil-inhibits-diagenesis" model but also document that cementation goes on as long as the oil-to-water ratio in mixed wet carbonate reservoirs is below an as yet undefined threshold limit.

Acknowledgments

The authors thank Dr. R. Neuser, Dr. A. Niedermayr and Dr. D. Buhl from the department of Sediment and Isotope Geology, Ruhr University, Bochum, Germany and Dr. E. Korolev from the Kazan Federal University, Russia for technical and scientific support. We acknowledge the experts reviews of K. Hollis and R.H. Worden and the editorial guidance of D.S. Alessi. This study was performed in the context of the Russian Government Program of Competitive Growth of Kazan Federal University.

References

Aizenshtat, Z., Feinstein, S., Miloslavski, I., Yakubson, Z., Yakubson, C.I., 1998. Oil-oil correlation and potential source rocks for oils in paleozoic reservoir rocks in the tataria and perm basins, Russia. Org. Geochem 29, 701–712.

Al-Dhahli, A., Geiger, S., van Dijke, M.I.J., 2014. Impact of pore-scale three-phase flow for arbitrary wettability on reservoir-scale oil recovery. J. Pet. Sci. Eng. 121, 110–121.

Alekseev, A.S., Kononova, L.I., Nikishin, A.M., 1996. The devonian and carboniferous of the Moscow syneclise (Russian platform): stratigraphy and sea-level changes. Tectonophysics 268, 149–168.

Ali, M.Y., 1995. Carbonate cement stratigraphy and timing of diagenesis in a miocene mixed carbonate-clastic sequence, offshore Sabah, Malaysia – constraints from cathodoluminescence, geochemistry, and isotope studies. Sed. Geol. 99, 191–214.

Ashirov, K.B., 1960. About Question of Time of Formation of Oil and Gas Fields in Middle Part of Volga River Region. Geologia nefti i gaza 6. (in Russian).

Bachtel, S.L., Dorobek, S.L., 1998. Mississippian carbonate ramp-to-basin transitions in south-central new Mexico: sequence stratigraphic response to progressively steepening outer-ramp profiles. J. Sed. Res. 68, 1189–1200.

Bodnar, R.J., Vityk, M.O., 1994. Interpretation of microthermometric data for H_2O-NaCl fluid inclusions. Fluid Incl. Min. Methods Appl. 117–130.

Bruckschen, P., Richter, D.K., 1994. Zementstratigraphische grundmuster in marinen

karbonatablagerungen des phanerozoikums – ein abbild der normalen Beckenentwicklung. Zentralbl. Geol. Paläontol. 1993, 959–972.
Bruckschen, P., Neuser, R.D., Richter, D.K., 1992. Cement stratigraphy in triassic and jurassic limestones of the weserbergland (northwestern Germany). Sed. Geol. 81, 195–214.
Buggisch, W., Wang, X., Alekseev, A.S., Joachimski, M.M., 2011. Carboniferous–permian carbon isotope stratigraphy of successions from China (Yangtze platform), USA (Kansas) and Russia (Moscow Basin and Urals). Palaeogeogr. Palaeoclim. Palaeoecol. 301, 18–38.
Burchette, T.P., Wright, V.P., 1992. Carbonate ramp depositional systems. Sed. Geol. 79, 3–57.
Burley, S.D., Mullis, J., Matter, A., 1989. Timing diagenesis in the tartan reservoir (UK North Sea): constraints from combined cathodoluminescence microscopy and fluid inclusions studies. Mar. Pet. Geol. 6, 98–120.
Burruss, R.C., Cercone, K.R., Harris, P.M., 1983. Fluid inclusion petrography and tectonic-burial history of the ali No. 2 well: evidence for timing of diagenesis and oil migration, northern Oman Foredeep. Geology 2, 567–570.
Byrnes, A.P., Bhattacharya, S., 2006. Influence of initial and residual oil saturation and relative permeability on recovery from transition zone reservoirs in shallow-shelf carbonates, SPE/DOE symposium on improved oil recovery. Soc. Pet. Eng. SPE 99736, http://dx.doi.org/10.2118/99736-MS.
Carnegie, A., 2006. Understanding the Pressure Gradients Improves Production from Oil/Water Transition Carbonate Zones, SPE 99240, Presented at the 2006 SPE, DOE. Symposium on Improved Oil Recovery, Tulsa, USA, pp. 22–26.
Carpentier, C., Brigaud, B., Blaise, T., Vincent, B., Durlet, C., Boulvais, P., Pagel, M., Hibsch, C., Yven, B., Lach, P., Cathelineau, M., Boiron, M., Landrein, P., Buschaertf, S., 2014. Impact of basin burial and exhumation on jurassic carbonates diagenesis on both sides of a thick clay barrier (Paris Basin, NE France). Mar. Pet. Geol. 53, 44–70.
Christ, N., Immenhauser, A., Amour, F., Mutti, M., Preston, R., Whitaker, F.F., Peterhänsel, A., Egenhoff, S.O., Dunn, P.A., Agar, S., 2012. Triassic latemar cycle tops - subaerial exposure of platform carbonates under tropical arid climate. Sed. Geol. 265–266, 1–29.
Christiansen, R., Heymans, M., Fanchi, J., 2000. Estimating oil reserves in oil-water transition zones, SPE Asia Pacific conference on integrated modelling for asset Management. Soc. Pet. Eng.
Cox, P.A., Wood, R.A., Dickson, J.A.D., Al Rougha, H.B., Shebl, H., Corbett, P.W.M., 2010. Dynamics of cementation in response to oil charge: evidence from a cretaceous carbonate field. U.A.E. Sed. Geol. 246–254.
Doveton, J.H., 1999. Basics of Oil & Gas Log Analysis, p. 34.
Ehrenberg, S.N., Pickard, N.A.H., Svånå, T.A., Oxtoby, N.H., 2002. Cement geochemistry of photozoan carbonate strata (upper carboniferous-lower permian), finmark carbonate platform, barents sea. J. Sed. Res. 72, 95–115.
Fanchi, J., Christiansen, R., Heymans, M., 2002. Estimating oil reserves of fields with oil/water transition zones. SPE Reserv. Eval. Eng. 5, 311–316. SPE 59352.
Galimov, E.M., Kamaleeva, A.I., 2015. Source of hydrocarbons in the supergiant romashkino oilfield (Tatarstan): recharge from the crystalline basement or source sediments? Eur. Spine J. 24, 95–112.
Goldstein, R.H., Reynolds, T.J., 1994. Systematics of Fluid Inclusions in Diagenetic Minerals: SEPM Short Course 31. Society for Sedimentary Geology, p. 199.
Gorbachev, Y.I., 1990. Geophysical Investigations of Wells. Nedra, p. 398 (in Russian).
Gordadze, G.N., Tikhomirov, V.I., 2005. Geochemical characteristics of oils and dispersed organic matter from the rocks of the central volga-ural basin: hydrocarbon biomarker data. Geochem. Int. 43 (11), 1108–1123.
Gorunova, L.F., 2009. Structure and Assessment of Prospects Oil and Gas Potential of Middle Devonian and Lower Carboniferous Oil Saturated Complexes Melekesskaya Depression. PhD dissertation. Kazan University, p. 150 (in Russian).
Granier, B., Staffelbach, C., 2009. Quick look cathodoluminescence analyses and their impact on the interpretation of carbonate reservoirs. Case study of mid-jurassic oolitic reservoirs in the Paris basin. Carn. Geol. Noteb. Geol. 6, 1–14.
Grossman, E.L., Bruckschen, P., Mii, H.S., Chuvashov, B.I., Yancey, T.E., Veizer, J., 2002. Carboniferous paleoclimate and global change: isotopic evidence from the Russian platform. carboniferous stratigraphy and paleogeography in Eurasia. Inst. Geol. Geochem. Russ. Acad. Sci. 61–71. Urals Branch, Ekaterinburg.
Hachatryan, R.O., 1979. Tectonic Development and Oil-and-gas Potential of the Volga-Kamsky Anticline. Science publications of the University of Kazan, p. 171 (in Russian).
Halymbadzha, V.G., 1962. Middle Carboniferous Rocks North, Central and West Districts Tatar Region. Kazan University press, p. 239 (in Russian).
Hao, F., Hao, F., Zhang, X.F., Wang, C.W., Li, P.P., Guo, T.L., Zou, H.Y., Zhu, Y.M., Liu, J.Z., Cai, Z.X., 2015. The fate of CO_2 derived from thermochemical sulfate reduction (TSR) and effect of TSR on carbonate porosity and permeability, sichuan basin, China. Earth Sci. Rev. 141, 154–177.
Heasley, E.C., Worden, R.H., Hendry, J.P., 2000. Cement distribution in a carbonate reservoir: recognition of a palaeo oil-water contact and its relationship to reservoir quality in the humbly grove field, onshore, UK. Mar. Pet. Geol. 17, 639–654.
Heckel, P.H., 1986. Sea-level curve for the pennsylvanian eustatic marine transgressive-regressive depositional cycles along midcontinent outcrop belt, north-America. Geology 14, 330–334.
Heggheim, T., Madland, M., Risnes, R., Austad, T., 2005. A chemical induced enhanced weakening of chalk by seawater. J. Pet. Sci. Eng. 46, 171–184.
Helgeson, H.C., Knox, A.M., Owens, C.E., Shock, E.L., 1993. Petroleum, oil field waters, and authigenic mineral assemblages: are they in metastable equilibrium in hydrocarbon reservoirs. Geochim. Cosmochim. Acta 57, 3295–3339.
Immenhauser, A., 2009. Estimating palaeo-water depth from the physical rock record. Earth Sci. Rev. 96, 107–139.
Immenhauser, A., Dublyansky, Y.V., Verwer, K., Fleitman, D., Pashenko, S.E., 2007. Textural, elemental and isotopic characteristics of pleistocene phreatic cave deposits (Jabal Madar, Oman). J. Sed. Res. 77, 68–88.
Ingalls, A.E., Aller, R.C., Lee, C., Wakeham, S.G., 2004. Organic matter diagenesis in shallow water carbonate sediments. Geochim. Cosmochim. Acta 68, 4363–4379.
Jesenius, J., Burruss, R.C., 1990. Hydrocarbon-water interactions during brine migration: evidence from hydrocarbon inclusions in calcite cements from danish North sea oil fields. Geochim. Cosmochim. Acta 54, 705–713.
Kaufman, J., Cander, H.S., Daniels, L.D., Meyers, W.J., 1988. Calcite cement stratigraphy and cementation history of the burlington-keokuk formations (mississippian) illinois and missouri. J. Sed. Pet. 58, 312–326.
Kaufmann, B., 1997. Diagenesis of middle devonian carbonate mounds of the mader basin (eastern anti-atlas, Morocco). J. Sed. Res. 67, 945–956.
Kerimov, V.Yu, Osipov, A.V., Lavrenova, E.A., 2014. The hydrocarbon potential of deep horizons in the south-eastern part of the volga-urals oil and gas province. Neft. khozyaystvo Oil Ind. 4, 33–35.
Khalil, M.I., Islam, F., Eunuse, A., 2015. Gamma and resistivity logs for characterization of gondwana coal seams at the northwestern part of Bangladesh. Arab. J. Geosci. 8, 6497–6506.
Kim, S.-T., O'Neil, J.R., 1997. Equilibrium and non-equilibrium oxygen isotope effects in synthetic carbonates. Geochim. Cosmochim. Acta 61, 3461–3475.
Kolchugin, A.N., Morozov, V.P., Korolev, E.A., Eskin, A.A., Gazeeva, F.M., 2013. Typical sections of bashkirian carbonate rocks and structure of oil deposits in southeast part of the Republic of Tatarstan. Neft. Khozyaistvo Oil Ind. 11, 84–86.
Mkrtchyan, O.M., 1980. Regularities of Structural Forms in the East of the Russian Plate. Science pub., p. 134 (in Russian).
Morrow, D.W., 1982. Diagenesis. Dolomite. Pt 2: dolomitization models and ancient dolostones. Geosci. Can. 9, 95–107.
Morrow, N.R., Mason, G., 2001. Recovery of oil by spontaneous imbibition. Curr. Opin. Coll. Interface Sci. 6, 321–337.
Neilson, J.E., Oxtoby, N.H., 2008. The relationship between petroleum, exotic cements and reservoir quality in carbonates – a review. Mar. Pet. Geol. 25, 778–790.
Neilson, J.E., Oxtoby, N.H., Simmons, M.D., Simpson, I.R., Fortunatova, N.K., 1998. The relationships between petroleum emplacement and carbonate reservoir quality: examples from abu dhabi and the amu darya Basin. Mar. Pet. Geol. 15, 57–72.
Proust, J.N., Chuvashov, B.I., Vennin, E., Boisseau, T., 1998. Carbonate platform drowning in a foreland setting: the mid-carboniferous platform in western urals (Russia). J. Sed. Res. 68, 1175–1188.
Richter, D.K., Götte, T., Götze, J., Neuser, R.D., 2003. Progress in application of cathodoluminescence (CL) in sedimentary petrology. Mineral. Pet. 79, 127–166.
Risnes, R., Haghighi, H., Korsnes, R., Natvik, O., 2003. Chalk–fluid interactions with glycol and brines. Tectonophysics 370, 213–226.
Risnes, R., Madland, M., Hole, M., Kwabiah, N., 2005. Water weakening of chalk—mechanical effects of water–glycol mixtures. J. Pet.. Sci. Eng. 48, 21–36.
Sathar, S., Worden, R.H., Faulkner, D.R., Smalley, P.C., 2012. The effect of oil saturation on the mechanism of compaction in granular materials: higher oil saturations lead to more grain fracturing and less pressure solution. J. Sed. Res. 82, 571–584.
Sellwood, B.W., Wilkes, M., James, B., 1993. Hydrocarbon inclusions in late calcite cements: migration indicators in the great oolite group, weald basin, southern England. Sed. Geol. 84, 51–55.
Sharkov, E., Lebedev, V., Chugaev, A., Zabarinskaya, L., Rodnikov, A., Sergeeva, N., Safonova, I., 2015. The caucasian-arabian segment of the alpine-himalayan collisional belt: geology, volcanism and neotectonics. Geosci. Front. 6, 513–522.
Shepherd, T.J., Rankin, A.H., Alderton, D.H.M., 1985. A Practical Guide to Fluid Inclusion Studies. Blackie & Son, Glasgo, p. 239.
Simo, J.A., Lehmann, P.J., 2000. Diagenetic history of pipe creek JR reef, silurian, north-central indiana, U.S.A. J. Sed. Res. 70, 937–951.
Soreghan, G.S., Giles, K.A., 1999. Amplitudes of late pennsylvanian glacioeustasy. Geology 27, 255–258.
Steele-MacInnes, M., Bodnar, R.J., Naden, J., 2011. Numerical model to determine the composition of H_2O-NaCl-$CaCl_2$ fluid inclusions based on microthermometric and microanalytical data. Geochim. Cosmochim. Acta 75, 21–40.
Steinhauff, D.M., Kenneth, R.W., Goldberg, S.A., 1999. Diagenesis by burial fluids, middle Ordovician platform-margin limestones, East Tennessee: relationships to Mississippi valley-type deposits. J. Sed. Res. 69, 1107–1122.
Swart, P.K., 2015. The geochemistry of carbonate diagenesis: the past, present and future. Sedimentology 62, 1233–1304.
Ten Have, T., Heijnen, W., 1985. Cathodoluminescence activation and zonation in carbonate rocks – an experimental approach. Geol. Mijnb. 64, 297–310.
Voytovich, E.D., Gatiyatullin, N.S., 2003. Tectonics of Tatarstan. Kazan University press, p. 132 (in Russian).
Walkden, G.M., Williams, D.O., 1991. The diagenesis of the late dinantian derbyshire-East midland carbonate shelf, central England. Sedimentology 38, 643–670.
Walter, B.F., Immenhauser, A., Geske, A., Markl, G., 2015. Exploration of hydrothermal carbonate magnesium isotope signatures as tracers for continental fluid aquifers, schwarzwald mining district, SW Germany. Chem. Geol. 400, 87–105.
Worden, R.H., Heasley, E.C., 2000. Effects of petroleum emplacement on

cementation in carbonate reservoirs. Bull. Soc. Geol. Fr. 171, 607–620.
Worden, R.H., Oxtoby, N.H., Smalley, P.C., 1998. Can oil emplacement prevent quartz cementation in sandstones? Pet. Geosci. 4, 129–137.
Worden, R.H., Heasley, E.C., Barclay, S.A., 1999. The effects of petroleum emplacement on diagenesis: a comparison between sandstone and carbonate reservoirs. In: Sciences Geologiques, 100. Mem, Strasbourg.
Yudina, A.B., Racki, G., Savage, N.M., Racka, M., Małkowski, K., 2002. The frasnian-famennian events in a deep-shelf succession, subpolar urals: biotic, depositional, and geochemical records. A. Palaeont. Pol. 47, 355–372.
Zeeh, S., Bechstädt, T., McKenzie, J., Richter, D.K., 1995. Diagenesis evolution of the carnian wetterstein platforms of the eastern alps. Sedimentology 42, 199–222.
Zhang, P.M., Tweheyo, M.T., Austad, T., 2007. Wettability alteration and improved oil recovery by spontaneous imbibition of seawater into chalk: impact of the potential determining ions Ca^{2+}, mg (2+), and SO^4_2. Coll. Surf. A Physicochem. Eng. Asp. 301, 199–208.